RECENT ADVANCES IN RADIATION MEDICAL COUNTERMEASURES

EDITED BY: Ales Tichy, Diane Riccobono, Lynnette H. Cary and Christophe Badie

PUBLISHED IN: Frontiers in Pharmacology

frontiers Research Topics

ISSN 1664-8714
ISBN 978-2-83250-349-2
DOI 10.3389/978-2-83250-349-2

About Frontiers

Frontiers is more than just an open-access publisher of scholarly articles: it is a pioneering approach to the world of academia, radically improving the way scholarly research is managed. The grand vision of Frontiers is a world where all people have an equal opportunity to seek, share and generate knowledge. Frontiers provides immediate and permanent online open access to all its publications, but this alone is not enough to realize our grand goals.

Frontiers Journal Series

The Frontiers Journal Series is a multi-tier and interdisciplinary set of open-access, online journals, promising a paradigm shift from the current review, selection and dissemination processes in academic publishing. All Frontiers journals are driven by researchers for researchers; therefore, they constitute a service to the scholarly community. At the same time, the Frontiers Journal Series operates on a revolutionary invention, the tiered publishing system, initially addressing specific communities of scholars, and gradually climbing up to broader public understanding, thus serving the interests of the lay society, too.

Dedication to Quality

Each Frontiers article is a landmark of the highest quality, thanks to genuinely collaborative interactions between authors and review editors, who include some of the world's best academicians. Research must be certified by peers before entering a stream of knowledge that may eventually reach the public - and shape society; therefore, Frontiers only applies the most rigorous and unbiased reviews.
Frontiers revolutionizes research publishing by freely delivering the most outstanding research, evaluated with no bias from both the academic and social point of view. By applying the most advanced information technologies, Frontiers is catapulting scholarly publishing into a new generation.

What are Frontiers Research Topics?

Frontiers Research Topics are very popular trademarks of the Frontiers Journals Series: they are collections of at least ten articles, all centered on a particular subject. With their unique mix of varied contributions from Original Research to Review Articles, Frontiers Research Topics unify the most influential researchers, the latest key findings and historical advances in a hot research area! Find out more on how to host your own Frontiers Research Topic or contribute to one as an author by contacting the Frontiers Editorial Office: frontiersin.org/about/contact

RECENT ADVANCES IN RADIATION MEDICAL COUNTERMEASURES

Topic Editors:
Ales Tichy, University of Defence, Czechia
Diane Riccobono, Institut de Recherche Biomédicale des Armées (IRBA), France
Lynnette H. Cary, Uniformed Services University of the Health Sciences, United States
Christophe Badie, Public Health England, United Kingdom

Citation: Tichy, A., Riccobono, D., Cary, L. H., Badie, C., eds. (2022). Recent Advances in Radiation Medical Countermeasures. Lausanne: Frontiers Media SA. doi: 10.3389/978-2-83250-349-2

Table of Contents

frontiers | Frontiers in Pharmacology

TYPE Editorial
PUBLISHED 13 September 2022
DOI 10.3389/fphar.2022.983702

OPEN ACCESS

EDITED AND REVIEWED BY
Alastair George Stewart,
The University of Melbourne, Australia

*CORRESPONDENCE
Ales Tichy,
ales.tichy@unob.cz

SPECIALTY SECTION
This article was submitted to Translational Pharmacology, a section of the journal Frontiers in Pharmacology

RECEIVED 01 July 2022
ACCEPTED 18 July 2022
PUBLISHED 13 September 2022

CITATION
Tichy A, Ricobonno D, Cary LH and Badie C (2022), Editorial: Recent advances in radiation medical countermeasures. *Front. Pharmacol.* 13:983702. doi: 10.3389/fphar.2022.983702

Editorial: Recent advances in radiation medical countermeasures

Ales Tichy[1]*, Dianne Ricobonno[2], Lynnette H. Cary[3] and Christophe Badie[4]

[1]Department of Radiobiology, Faculty of Military Health Sciences, University of Defence, Hradec Králové, Czechia, [2]Institut de Recherche Biomédicale des Armées (IRBA), Bretigny sur Orge, France, [3]Uniformed Services University of the Health Sciences, Bethesda, MD, United States, [4]Health Security Agency, Didcot, United Kingdom

KEYWORDS

radioprotection, ionizing radiation (IR), growth factors, medical countermeasure, acute radiation syndrome (ARS)

Editorial on the Research Topic
Recent advances in radiation medical countermeasures

We are presenting a topic research study focused on recent advances in radiation medical countermeasures. Unfortunately, the unstable geo-political situation makes this field very current. The majority of the articles deal with the mitigation of ARS. You can start your reading with a review of radioprotective agents summarizing the repurposing approach of previously approved pharmaceuticals (Singh and Seed).

A couple of original articles are engaged with the application of growth factors in rodent models such as IGF-1 treatment for mitigating GIT damage (Pejchal et al.) and an effective combination of pegylated G-CSF and ghrelin (Kiang et al.). Another group applied a polypharmaceutical approach of pegylated triple combination (hG-SCF, mMG-CSF, and hIL-11), and they even potentiated the effect by combination with lisinopril (Gasperetti et al.). Interestingly, lisinopril was studied by Medhora et al., who proposed that radiation increases its bioavailability by vascular regression.

Other authors showed that survival and hematopoietic recovery can be supported by gamma-tocotrienol (Kumar et al.) and in the case of thoracic irradiation, by hyaluronic nanoparticles (Lierova et al.) or RRx-001 (glucose 6-phosphate dehydrogenase inhibitor; Jurgensen et al.). Additionally, Nanduri et al. evaluated the radioprotective potential of secretory extracellular vesicles as it is seen that a plethora of new radioprotective agents is getting forward to regulatory approval.

Two other overview articles bring interesting radiobiological insights. The review of François et al. discussed the possibility to modulate the inflammatory storm associated with COVID-19 pulmonary infection by exposing patients to ionizing radiation at very low doses. Hollingsworth et al. addressed animal model considerations for designing studies and the potential to use the microbiome as a biomarker to assess radiation exposure and predict the outcome.

Last but not least, we would like to draw your attention to further articles on internal contamination (Griffiths et al.), which compared local and systemic DTPA treatment regimens *in*

vivo, and on a novel panel of radiation-responsive biomarkers, which applied an innovative high-throughput proteomics screening approach (Sproull et al.). Finally, Hermann et al. studied the effect of bardoxolone-methyl and successfully radiosensitized oral squamous cancer cells.

As it is seen, our field makes continuous progress forward, and this topic research comprises the latest advances. We hope you will find these articles interesting and the Editorial team wishes you an inspiring tour into the current radiation medical countermeasures.

Author contributions

AT drafted the manuscript. AT, DR, LC, and CB edited the manuscript.

Conflict of interest

The authors declare that the research was conducted in the absence of any commercial or financial relationships that could be construed as a potential conflict of interest.

Publisher's note

frontiers in Pharmacology

ORIGINAL RESEARCH
published: 12 August 2020
doi: 10.3389/fphar.2020.01199

Attenuation of Radiation-Induced Lung Injury by Hyaluronic Acid Nanoparticles

*Anna Lierova[1], Jitka Kasparova[2], Jaroslav Pejchal[3], Klara Kubelkova[4], Marcela Jelicova[1], Jiri Palarcik[5], Lucie Korecka[2], Zuzana Bilkova[2] and Zuzana Sinkorova[1]**

[1] Department of Radiobiology, Faculty of Military Health Sciences, University of Defence, Hradec Kralove, Czechia, [2] Department of Biological and Biochemical Sciences, Faculty of Chemical Technologies, University of Pardubice, Pardubice, Czechia, [3] Department of Toxicology and Military Pharmacy, Faculty of Military Health Sciences, University of Defence, Hradec Kralove, Czechia, [4] Department of Molecular Pathology and Biology, Faculty of Military Health Sciences, University of Defence, Hradec Kralove, Czechia, [5] Institute of Environmental and Chemical Engineering, Faculty of Chemical Technology, University of Pardubice, Pardubice, Czechia

OPEN ACCESS

Edited by:
Diane Riccobono, Institut de Recherche Biomédicale des Armées (IRBA), France

Reviewed by:
Agnès Francois, Institut de Radioprotection et de Sûreté Nucléaire, France
Masoud Najafi, Kermanshah University of Medical Sciences, Iran

***Correspondence:**
Zuzana Sinkorova
zuzana.sinkorova@unob.cz

Specialty section:
This article was submitted to Translational Pharmacology, a section of the journal Frontiers in Pharmacology

Received: *21 April 2020*
Accepted: *23 July 2020*
Published: *12 August 2020*

Citation:
Lierova A, Kasparova J, Pejchal J, Kubelkova K, Jelicova M, Palarcik J, Korecka L, Bilkova Z and Sinkorova Z (2020) Attenuation of Radiation-Induced Lung Injury by Hyaluronic Acid Nanoparticles. Front. Pharmacol. 11:1199. doi: 10.3389/fphar.2020.01199

Purpose: Therapeutic thorax irradiation as an intervention in lung cancer has its limitations due to toxic effects leading to pneumonitis and/or pulmonary fibrosis. It has already been confirmed that hyaluronic acid (HA), an extracellular matrix glycosaminoglycan, is involved in inflammation disorders and wound healing in lung tissue. We examined the effects after gamma irradiation of hyaluronic acid nanoparticles (HANPs) applied into lung prior to that irradiation in a dose causing radiation-induced pulmonary injuries (RIPI).

Materials and Methods: Biocompatible HANPs were first used for viability assay conducted on the J774.2 cell line. For *in vivo* experiments, HANPs were administered intratracheally to C57Bl/6 mice 30 min before thoracic irradiation by 17 Gy. Molecular, cellular, and histopathological parameters were measured in lung and peripheral blood at days 113, 155, and 190, corresponding to periods of significant morphological and/or biochemical alterations of RIPI.

Results: Modification of linear hyaluronic acid molecule into nanoparticles structure significantly affected the physiological properties and caused long-term stability against ionizing radiation. The HANPs treatments had significant effects on the expression of the cytokines and particularly on the pro-fibrotic signaling pathway in the lung tissue. The radiation fibrosis phase was altered significantly in comparison with a solely irradiated group.

Conclusions: The present study provides evidence that application of HANPs caused significant changes in molecular and cellular patterns associated with RIPI. These findings suggest that HANPs could diminish detrimental radiation-induced processes in lung tissue, thereby potentially decreasing the extracellular matrix degradation leading to lung fibrosis.

Keywords: radiation, lung, radiation fibrosis, hyaluronic acid, nanoparticles

INTRODUCTION

Despite the many great advances in the field of radiotherapy, radiation toxicity remains a serious complication in patients receiving such therapy. The lung, in particular, is one of the organs most critically limited by the development of radiation-induced pulmonary injuries (RIPI). The proportion of patients susceptible to RIPI after radiotherapy is as high as 20% (Hanania et al., 2019; Giuranno et al., 2019). The currently accepted model of RIPI has been described as a continuous and multicellular process beginning immediately after insult. Three phases can be recognized within RIPI and also distinguished temporally, these being the latent period, pneumonic phase, and late-fibrotic phase. After irradiation, initial damage induces expression of multiple cytokines and growth factors in specific cell types within lung tissue. This is followed by activation of various signaling pathways and results in the development of subsequent pathophysiological processes. The first manifestation of RIPI is radiation pneumonitis (RP), an acute inflammatory process. RP is characterized by the recruitment of diverse immune cells into the tissue; expression of diverse cytokines, chemokines, and adhesion molecules; and, as a result, edema of the interstitium and alveolar spaces (Schaue et al., 2012; Lierova et al., 2018). The terminating phase, radiation fibrosis (RF), is driven primarily by accumulation of fibroblasts and myofibroblasts, which extensively produce collagen and extracellular matrix (ECM) proteins causing tissue and impaired organ function. Except fibroblast, myofibroblasts may also derive from circulating bone marrow-derived progenitor cells known as fibrocytes or from trans-differentiated epithelial cells (alveolar pneumocytes type I and type II) *via* epithelial–mesenchymal transition (Jang et al., 2013; Lierova et al., 2018; Jin et al., 2020). Recently, the endothelial-to-mesenchymal transition of vascular endothelial cell has been identified also as contributing factor to development of RF (Choi et al., 2015). From another point of view, RF may be perceived as insufficient wound healing characterized by extensive deposition of connective tissue that is followed by destruction of the lung parenchyma to form fibrotic lesions (Straub et al., 2015). Both concepts emphasize the role of transforming growth factor β (TGF-β) and its signaling, but accumulating evidence points to the role of ECM components in the fibrotic process (Wegrowski et al., 1992; Bensadoun et al., 1996; Albeiroti et al., 2015; Collum et al., 2019).

One of the main ubiquitously and naturally occurring moieties in ECM is hyaluronic acid (HA). This linear and negatively charged polysaccharide is widely distributed in many organs and tissues. In lung, HA is present from the time of fetal organ development in the alveolar region, in the basement of bronchiolar and bronchial epithelium, and after insult (bleomycin or hyperoxia) also in perivascular vessels, an area around larger pulmonary arteries. HA plays several important roles in the organization and modification of ECM by binding with cells and other components through specific and nonspecific interaction. It is also regarded as an important signaling molecule and a regulator of inflammatory responses and tissues healing after insult (Singleton and Lennon, 2011; Lauer et al., 2015). HA is unique among other active molecules in that its biological effects depend upon HA fragment size (Cyphert et al., 2015). Under physiological conditions, ECM consists of high-molecular-weight (HMW-HA) HA with an average size range of 1–5 × 10^6 Da. In alveoli, HA is synthesized on cellular surface by hyaluronan synthase 2 (HAS2), and particularly by type II pneumocytes, and it is required for optimal cell survival, maintenance of homeostasis, and self-renewal in healthy lung tissue. The molecule interacts through CD44 receptor on alveolar macrophages (Johnson P. et al., 2018).

HA plays several important roles in the organization and modification of ECM by binding with cells and other components through specific and nonspecific interaction. It is also considered to be an important signaling molecule and regulator of inflammatory response and tissues healing after insult (Dicker et al., 2014). Under certain pathological conditions, including ionizing radiation (IR) and presence of radical oxygen species, HA is a doubled-edge sword in lung tissue. HA is degraded into low-molecular-weight (LMW-HA) bioactive fragments, ranging in size from 2 × 10^4 to 2 × 10^6 Da, with strong pro-inflammatory properties. These particles even may serve as danger-associated molecular patterns and endogenous danger molecules, and they may initiate and perpetuate a noninfectious inflammatory response (Fallacara et al., 2018). Animal models as well as human studies have shown that HA levels rapidly increase in the lung during inflammation and peak with maximum leukocyte infiltration. The tissue homeostasis is restored when HA concentrations decline and its levels return to baseline (Nilsson et al., 1990; Bray et al., 1991; Dentener et al., 2005; Liang et al., 2011). Nevertheless, LMW-HA fragments may strongly augment the inflammatory response. Although LMW-HA interacts *via* CD44, its signaling supports inflammatory cell recruitment, including of T cells, to the injury site (Avenoso et al., 2020). Data from $CD44^{-/-}$ deficient mice have shown increased accumulation of LMW-HA, enhanced pro-inflammatory gene expression, and unremitting inflammation in the lung tissue after intratracheal bleomycin (Teder et al., 2002) or lipopolysaccharide (Liang et al., 2007) treatment, thereby suggesting that CD44 is crucial for successful renewal of homeostasis.

On the other hand, exogenous administration of HA has shown great therapeutic potential. HMW-HA exerts competitive negative feedback on LMW-HA. The molecular weight of HA also affects its affinity for CD44 receptor, and the ratio of LMW-HA/HMW-HA may be important for maintenance of ECM integrity and the final extent of lung injury. This effect has been demonstrated by multiple HMW-HA applications for diverse lung injury modalities, including elastase-induced emphysema, allergic airway inflammatory lung injury, and bleomycin-induced lung damage in mice (Jiang et al., 2005; Cantor, 2007; Johnson C. G. et al., 2018), as well as lipopolysaccharide-induced sepsis and acute lung injury induced by inhalation of fine particulate matter in rats (Liu et al., 2008; Xu et al., 2018). In humans, inhaled HMW-HA improves homeostasis in cystic fibrosis and protects against

disease exacerbations in patients with chronic bronchitis (Venge et al., 1996; Lamas et al., 2016). In recent years, HA has attracted attention as a polymer suitable for drug carrier systems because it can assemble into nanoparticles (NPs) (Hussain et al., 2016; Jeannot et al., 2018).

In the present study, we focus on HA assembled into NPs (HANPs) by intramolecular cross-linking. Two different diameters (123.6 and 86.58 nm) were prepared. The properties of the prepared HANPs were first evaluated *in vitro*. Subsequently, HANPs were administered before irradiation and their effects on the acute and chronic phases of RIPI were analyzed.

MATERIAL AND METHODS

In Vitro Experiments: Nanoparticles Preparation, Characterization, and Irradiation

Simple Cross-Linking Procedure

Hyaluronic acid sodium salt from Streptococcus equi (mol wt 1.5–1.8 MDa, ≤1% protein), adipic acid dihydrazide (AAD), 1-ethyl-3-(3′-dimethylaminopropyl)carbodiimide (EDC), and cellulose dialysis tubing (12,400 Da) were purchased from Sigma-Aldrich (St. Louis, MO, United States). All other chemicals were supplied by Lach-Ner (Neratovice, Czechia) at reagent grade. Hyaluronic acid sodium salt was dissolved in deionized water (prepared using TKA Smart2Pure, Thermo Fisher Scientific, Waltham, MA, United States) to create a 2.5 mg/ml solution. To prepare 5 mg of HANPs, 2 ml of HA solution was used and afterwards 3.4 ml of acetone was added to the solution (15 min incubation, gentle stirring). After the addition of EDC [2.5 mg/75 µl ultrapure water (prepared by TKA Smart2Pure)] and AAD (2.5 mg/75 µl), acetone was added in a stepwise manner (2.03 ml per step) in three repetitions. The total acetone/water ratio was set to 279/80 (w/w) and surplus acetone was then removed by evaporation at 60°C with following dialysis against 0.9% NaCl solution.

Double Cross-Linking Procedure

The cross-linking procedure was repeated using the nanoparticles prepared as described above. After the evaporation of surplus acetone, the addition of EDC (2.5 mg/75 µl ultrapure water) proceeded immediately. Following the same procedure as described above, acetone was again added in a stepwise manner. Finally, the procedure was completed by evaporation of surplus acetone and dialysis against 0.9% NaCl solution. Parameters of the prepared nanoparticles (0.25 mg of HANPs in 1.5 ml 0.9% NaCl) were monitored using dynamic light scattering (DLS; NanoZS, Malvern Instrument, United Kingdom) at 25°C in 0.9% NaCl.

Irradiation

The stability of both types of prepared nanoparticles was investigated. HANPs in concentration 1 mg/ml in 0.9% saline solution were irradiated with a 17 Gy dose. The same dose was later used for thorax irradiation during the *in vivo* experiments. HANPs' properties were analyzed by DLS spectrophotometry prior to irradiation and then 1 day, 1 week, as well as 1 and 2 months after irradiation to assess their stability. The irradiation procedures used a Chisotron ^{60}Co source (Chirana, Prague, Czechia) at a dose rate of 0.32 Gy/min with a target distance of 1 m.

Viability Assay

J774.2 adherent murine macrophages (ATCC®, Manassas, VA, United States) were seeded (7,500 cells/well) on 96-well plates and cultured in 90 µl of Dulbecco's Modified Eagle's Medium with high glucose concentration (DMEM/GlutaMAX™, Gibco, Grand Island, NY, United States) supplemented with 10% fetal bovine serum and 1% antibiotics (150 UI/ml penicillin, and 50 mg/ml streptomycin; all from Sigma-Aldrich) for 24 h at 37°C and 5% CO_2. After incubation, 10 µl of HANPs were dissolved in DMEM without supplements and added to the final concentration ranging from 1 µg/ml to 2 mg/ml. Five replicates were measured per each concentration, and DMEM without supplements was used as negative control group. After 24 h of incubation, cell viability was determined using 4-[3-(4-iodophenyl)-2-(4-nitro-phenyl)-2H-5-tetrazolio]-1,3-benzene sulfonate dye (WST-1, Roche Diagnostics GmbH, Mannheim, Germany). For that determination, 50 µl of WST-1/phosphate-buffered saline (1:4) to final concentration of 0.5 mg/ml was added to each well and plates were incubated for 3 h (37°C, 5% CO_2). Plates were gently mixed and then measured using a Spectronic Helios Gamma microplate reader (Thermo Fisher Scientific) at wavelength 450 nm. WST viability test was performed three times to ensure reproducibility.

In the subsequent experiment, the J774.2 cell line was pre-incubated with HANPs of the same sizes and concentration range for 2 h or 30 min. After incubation, the cells were exposed to a single dose of 4 Gy. Viability was measured 24 h after irradiation using the WST-1 assay, as described above.

In Vivo Experiments: Animals and Irradiation

All experimental animal protocols proceeded under supervision of the Ethics Committee (Faculty of Military Health Sciences, Hradec Kralove, Czechia). Female C57Bl/6 mice aged 12–14 weeks (Velaz, Unetice, Czechia) were kept in an air-conditioned room (22 ± 2°C and 50 ± 10% relative humidity, 12 h light/dark cycle) and allowed access to standard food and tap water *ad libitum*.

In conducting an experiment, mice were randomly divided into four groups. Prior to irradiation, all animals were anesthetized with a combination of Narketan (0.5 ml; Vetoquinol, Prague, Czechia), Rometar (0.16 ml; Bioveta, Ivanovice na Hane, Czechia), and physiological solution (2 ml; B. Braun Melsungen AG, Melsungen, Germany) by intramuscular injection. The first group (control, n = 18) was sham-treated and nonirradiated. Mice from the second group (n = 32) were only irradiated but without application of HANPs. The third and fourth groups (both n = 32) received HANPs of sizes 86.58 nm and 123.6 nm, respectively, by intratracheal instillation. The volume of HANPs was 50 µl in final

concentration of 0.5 mg/ml and was instilled 30 min before irradiation. The anesthetized animals were kept in a Plexiglas box (VLA JEP, Hradec Kralove, Czechia) and received a single dose of irradiation (17 Gy, 0.30 Gy/min, 1 m) to the thoracic region. A local thoracic irradiation was performed in a jig. Head and abdomen were shielded with lead bricks 10 cm thick layer to reduce the dose to surrounding organs.

Tissue Collection and Sample Preparation

Tissue samples were collected on days 113, 155, and 190 post-irradiation, which time points correspond with the periods of significant morphological and/or biochemical alterations of RIPI (Jackson et al., 2010). Six mice per group were euthanized by narcotic gas overdosing at each time point. Directly after euthanasia, venous peripheral blood was drawn from the heart into heparinized syringes (BD Bioscience, Franklin Lakes, NJ, United States) for determination of absolute cell counts and flow cytometry analysis. Additionally, the left lung was perfused with cold phosphate-buffered saline and divided into two parts for cytokine profiling and for flow cytometry. The right lung was dissected and fixed in 10% neutral buffered formalin (Bamed s.r.o., Ceske Budejovice, Czechia) for histological analysis.

Absolute Blood Count and Flow Cytometry Analysis of Peripheral Blood

The heparinized blood from each animal was divided into two parts. A volume of 150 µl was designated for blood count and measured using an ABX Pentra 60 C+ hemoanalyzer (Horiba, Kyoto, Japan). The rest of the blood (200–300 µl) was lysed using EasyLyse™ (Dako, Glostrup, Denmark). The amount of cells in suspension was as determined by Turk's solution (2% acetic acid; Sigma-Aldrich) using a hemocytometer chamber. Cells (5×10^5/100 µl) were marked with two panels of monoclonal antibodies. The first panel was delineated to detect T, B, and NK lymphocytes (CD3ϵ, CD4, CD8, CD19, and NK1.1). The second panel was designed for determination of monocytes and neutrophils (CD11b, F4/80, Ly6C, and Ly6G). The following monoclonal antibodies with fluorochromes for flow cytometry analysis were purchased from BioLegend (San Diego, CA, United States): anti-mouse CD3ϵ–FITC, CD4–BV421, CD19–PE, CD11c–BV421, CD45–APC/Fire™750, F4/80–PE, and from BD Bioscience: CD8–PECy7, CD11b–BV510, Ly6C–FITC, Ly6G–PECy7, and NK1.1–APC.

BCA Protein Assay and Enzyme-Linked Immunosorbent Assay (ELISA) of Cytokines

A sample of the lung determined for protein and cytokine profiling was immediately placed into tubes on ice, weighed, then frozen at −80°C until further analysis. Prior to analysis, the frozen lung tissue was thawed on ice, minced, then lysed with lysis buffer (10 mM TRIS-HCl/pH 8, 150 mM NaCl, 1% Triton X-100, 10% glycerol, 5 mM EDTA, and 1 mM Na_3VO_4) and protease inhibitor cocktail (Roche Diagnostics GmbH). Volume of lysis buffer varied depending on the weight of lung tissue. Each sample was then homogenized using an Ultra Turrax T8 tissue homogenizer (IKA, Werke, Germany) and incubated for 1 h at 4° C while rotating. The lysates were sonicated at 4°C and centrifuged. Supernatants were collected and aliquoted for determination of total protein and cytokine concentrations.

Protein concentration was measured using the Pierce™ BCA Protein Assay Kit (Sigma-Aldrich). Protein level of each sample was measured in triplicate according to the manufacturer's instructions. Briefly, 10 µl samples were added to 190 µl of working reagent and incubated for 30 min at 37°C. Absorbance was then measured at 562 nm using the Spectronic Helios Gamma microplate reader. The actual protein concentrations were calculated from the standard curves generated by calibrator diluents.

Aliquots of supernatants from each animal in the group were pooled together and cytokine profiles were determined from the group sample. Commercially available ELISA kits were used to quantitate mouse cytokines. Cytokine kits for interleukin-1 β (IL-1β), IL-6, CCL2 (MCP-1), CCL4 (MIP-1), CXCL1 (KC), matrix-metalloproteinases-2 (MMP-2), and proMMP-9 (all from LifeSpan BioSciences, Seattle, WA), and TGF-β1 (RayBiotech, Norcross, GA) were performed according to the manufacturers' protocols in triplicates and quantified by comparison with a standard curve using the Spectronic Helios Gamma microplate reader.

Flow Cytometry Analysis of Lung Tissue

The part of the lung tissue intended for flow cytometry analysis was placed into a Petri dish with Iscove's Modified Dulbecco's Medium (IMDM, Gibco) without fetal bovine serum, weighed, minced into small chunks, and enzymatically digested in digestion medium (2 ml IMDM, 2 mg/ml collagenase type IV, and 50 U/ml deoxyribonuclease type IV; all obtained from Sigma-Aldrich) at 37°C for 45 min. After digestion, cells were filtered through a strainer (100 µm; Roche Diagnostics GmbH) to remove tissue debris. The single cell suspensions thus obtained were subsequently centrifuged, counted in a hemocytometer chamber after dilution with Turk's solution (2% acetic acid), and resolved in phosphate-buffered saline for the next analysis. Cell suspension was first processed using Fcγ receptor blocking solution with purified CD16/32 (eBioscience, San Diego, CA). Subsequently, cell suspension (5×10^5 cells/100 µl) was marked with the same two panels of monoclonal antibodies stated above. For better analysis of leukocytes, a common leukocytes marker, CD45, was added to both panels and CD11c was added to the second panel for the detection of alveolar macrophages.

Histology

Formalin-fixed lungs were embedded into paraffin (Paramix, Holice, Czechia) and tissue sections 5 µm thick were cut using a Model SM2000 R microtome from Leica (Heidelberg, Germany). Staining with hematoxylin and eosin (H&E; Merck, Kenilworth, NJ, United States) was performed to determine the air/tissue ratio. To detected collagen fibers in lung parenchyma the histological slides were stained by picrofuchsin using Van Gieson method (DiaPath, Martinengo, Italy). Analysis of stained tissues section was done on a BX-51 microscope

equipped with a DP-72 camera (both from Olympus, Tokyo, Japan) and the Image-Pro 5.1 computer image analysis system (Media Cybernetics Inc., Bethesda, MD, United States) at 200× magnification.

Data Analysis

All data are expressed as mean ± 2× standard error of the mean (SEM), except that the results of cytokine concentration are expressed as mean ± 2× standard deviation (SD). Statistical analysis was performed by one-way ANOVA with *post hoc* Student's *t*-test, Tukey's and Fisher's least significant difference (LSD) tests (WST-1 test and cytokines) or Kruskal–Wallis test with *post hoc* Mann–Whitney *U* test (total protein, flow cytometry, and histology) using STATISTICA 12 software (StataCorp, College Station, TX, United States). Differences were considered significant at $p \leq 0.05$.

RESULTS

Hyaluronic Acid Nanoparticles Stability After Irradiation and Effect on Cell Viability

Two types of HANPs were prepared by covalent cross-linking of HA chains while using AAD as a cross-linking agent. HANPs (size 123.6 ± 0.105 nm) were first prepared by a simple cross-linking method. These HANPs were then used as an initial solution for double cross-linking procedure, the aim being to reduce their size (actual size was 86.58 ± 0.096 nm). Hydrodynamic diameters and polydispersity indices were monitored by DLS. Characteristics of both HANPs are shown **Figure 1A**. To verify the stability of HANPs against irradiation, the HANPs were exposed to IR (17 Gy). We observed no changes in hydrodynamic diameter of HANPs during 60 days after irradiation (**Figure 1B**).

Next, relative viability of the J774.2 cell line after incubation with 86.58 or 123.6 nm HANPs was evaluated using WST-1 assay. **Figure 2A** shows the cell viability of 86.58 nm and 123.6 nm HANPs. The results indicated no significant cytotoxicity of 123.6 nm HANPs (confirmed by all statistical tests). Even at the highest concentration of 2 mg/ml, viability decreased only to 90% and nonsignificant increase in viability of cells compared to the untreated control was found from the 1–50 μg/ml concentrations. On the other hand, one-way ANOVA revealed significant differences between the control and 86.58 nm HANPs-treated groups. In the post-hoc analysis, only Fisher's LSD test showed significantly reduced cell viability at higher concentrations ranging from 1 mg/ml to 2 mg/ml. Supported by these results, we can conclude that no observed cytotoxic effect was detected for 123.6 nm HANPs and cytotoxicity of 86.58 nm HANPs occurred only for concentration 0.5 mg/ml and higher.

The following experiment evaluated the effect of 2 h or 30 min preincubation with HANPs in combination with IR. The cells were exposed to a single dose of 4 Gy. Results are shown in **Figures 2B, C**. Neither concentration nor HANPs size showed a direct influence on radioprotective effect after preincubation. All irradiated cells had significantly decreased

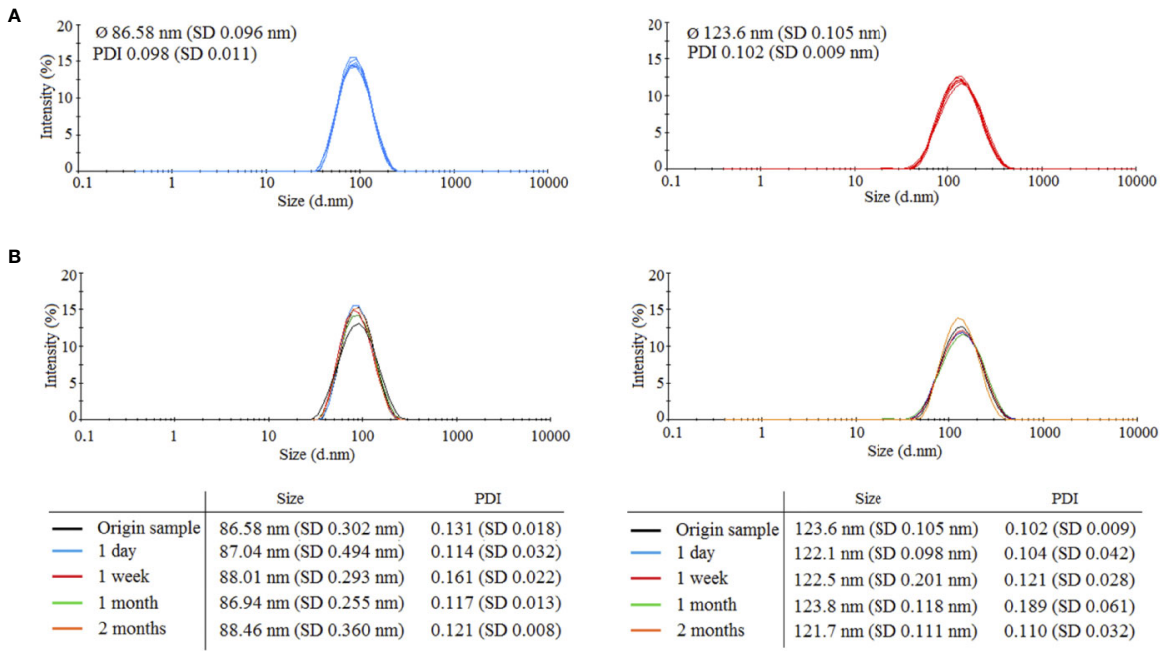

FIGURE 1 | Characteristics of prepared 86.58 and 123.6 nm HANPs. **(A)** Size distribution of synthetized HANPs in 0.9% saline solution as determined by dynamic light scattering (DLS). **(B)** Stability of hyaluronic acid nanoparticles against irradiation by dose 17 Gy. Stability of HANPs was measured by DLS at times 1 day, 1 week, and 1 and 2 months after irradiation.

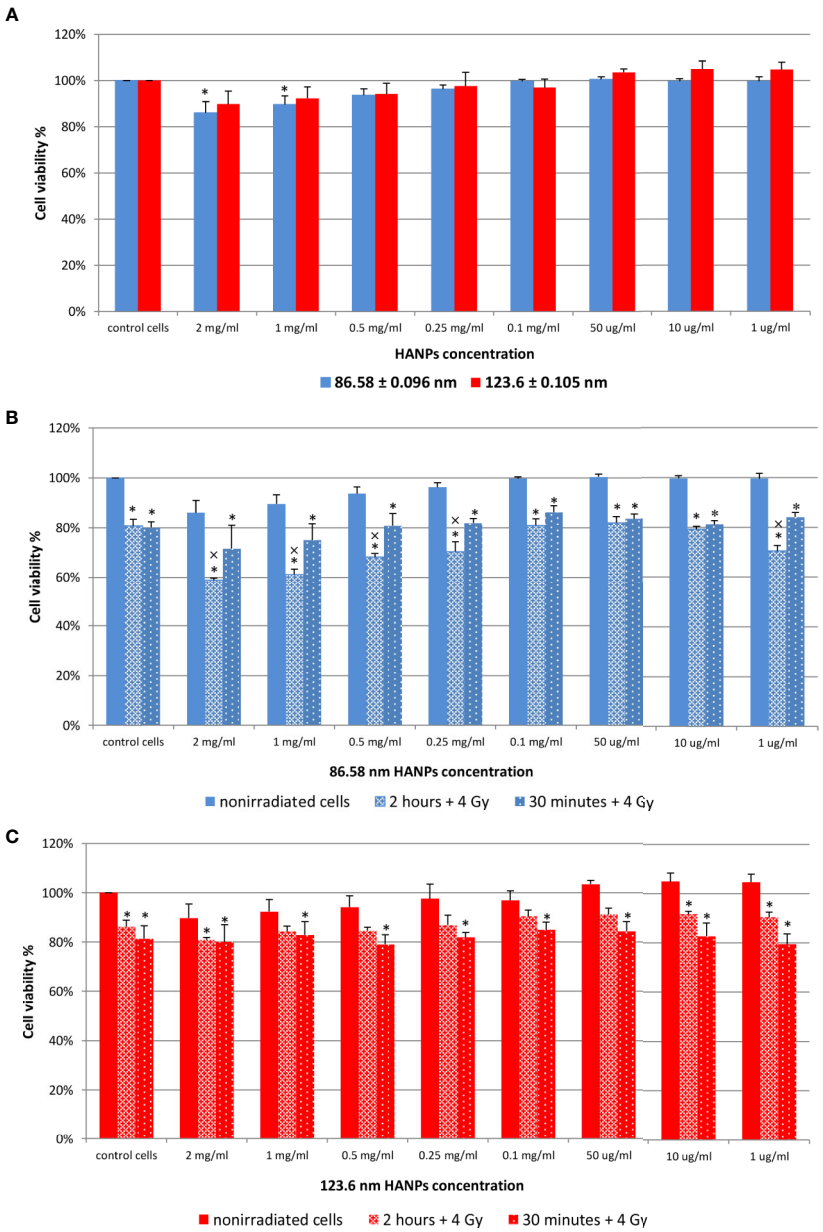

FIGURE 2 | Effect of HANPs on cell viability. **(A)** Concentration-dependent effect on relative viability of J774.2 cell line after 24 h of incubation with 86.58 nm and 123.6 nm HANPs. **(B)** Viability of J774.2 after 2 h or 30 min preincubation with 86.58 nm and **(C)** 123.6 nm HANPs followed by 4 Gy irradiation. Each bar represents the mean ± 2× SEM. Asterisks (*) indicate significance differences at $p \leq 0.05$ in comparison with untreated control and multiplication signs (×) indicate significance differences at $p \leq 0.05$ in comparison with irradiated cells.

viability compared to the nonirradiated control, but differences were observed between groups depending on the size of HANPs and preincubation period used. A response difference was observed for preincubation time intervals when cells were incubated with 86.58 nm nanoparticles (**Figure 2B**). Higher NPs concentration in combination with IR caused significant decrease in cell viability. For concentrations ranging from 2 mg/ml to 0.25 mg/ml and for 1 μg/ml, the differences during 2 h of preincubation were significant not only when compared with untreated controls but also in comparison with irradiated cells. The highest viability of irradiated cells was observed at concentration 0.1 mg/ml for both preincubation intervals. Although the greater cell viability was achieved by 30 min preincubation for 86.58 nm HANPs, it was during longer preincubation that the 123.6 nm HANPs treatment improved the viability of cells (**Figure 2C**). At none of those concentrations of 123.6 nm HANPs used did viability decline in comparison with cells only irradiated, as seen in the case of

86.58 nm HANPs. Also, the greatest viability of irradiated cells was seen at the 0.1 mg/ml concentration point with these NPs. Based on the *in vitro* viability results described here, we decided for *in vivo* experiments to administer the highest possible HANPs concentration not having cytotoxic effect (i.e., 0.5 mg/ml) in experimental mice models *via* intratracheal instillation 30 min before irradiation.

TGF-β and Mediators of Fibrosis Signaling Pathway Are Downregulated by HANPs Treatment

Cytokines have been reported as key features in the pathogenesis of RIPI resulting initially after irradiation and then simultaneously persisting and resolving into tissue damage. To evaluate the effect of HANPs on the inflammation and fibrosis phases in lung tissue, total protein levels and multiple cytokines were measured (**Table 1**). Time-course analysis of total protein levels in lung tissue demonstrated significantly increased level in the partial thoracic irradiated group (17 Gy) during the pneumonitis phase. This finding is consistent with the characteristics of RP, because damage to the integrity of vascular permeability leads to increased protein concentration in alveoli. By contrast, lungs treated with HANPs exhibited decreased levels of total proteins compared with the control group. Only in the group treated with 86.58 nm nanoparticles was a significant degree ($p \leq 0.05$) of decrease observed.

Results from cytokine analysis of the mixed group samples represented the trends in the temporal relationship between groups. At the time point 113 days after irradiation, levels of MCP-1 cytokine were significantly decreased compared to controls and their levels were similar in the irradiated-only group and both groups treated with HANPs. Contrariwise, the cytokine TGF-β significantly increased compared to controls, similarly in the irradiated-only group and both groups treated with HANPs. Cytokines KC and MIP-1 did not change significantly between the 123.6 nm HANPs group and the control, but these cytokines did exhibit decline in comparison with the irradiated-only group. The group treated with 86.58 nm HANPs showed decline compared with the control (significant only in the case of MIP-1) and the 123.6 HANPs groups. Other cytokines during this phase exhibited differences not only compared with the control but also among groups. The level of IL-1β decreased in the irradiated group and in the group treated with 123.6 nm HANPs (by 0.76- and 0.77-fold, respectively) compared to the control. The most significant depression, to 0.67-fold of the control, was in the group treated with 86.58 nm HANPs. This group differed from all the others. The cytokine IL-6 decreased most in the irradiated-only group (0.51-fold). Decrease was observed in both HANPs groups (to 0.64 and 0.70) compared with the control. For the mixed sample of collagen degrading MMP-2 and proMMP-9, however, concentration varied significantly between samples. The proMMP-9 is a precursor of MMP-9, and after insult (including by IR) it is cleaved from the pro- form to the active enzyme form (Atkinson and Senior, 2003). MMP-2 in the irradiated group was increased 1.6-fold while both HANPs irradiated groups showed tendencies to increase only

TABLE 1 | HANPs treatment modulates the concentration of total protein and cytokines in lung tissue lysates.

		Total protein [μg / ml]	IL-1β [pg / ml]	IL-6 [pg / ml]	TGF-β [pg / ml]	MCP-1 [pg / ml]	MIP-1 [pg / ml]	KC [pg / ml]	MMP-2 [pg / ml]	proMMP-9 [pg / ml]
113 day	Control	2.52 ± 0.37	147.01 ± 9.75	102.68 ± 7.27	485.23 ± 18.64	104.37 ± 21.01	55.10 ± 4.94	4.27 ± 0.31	723.86 ± 20.38	13 068.10 ± 440.74
	17 Gy	2.71 ± 0.17 *	111.69 ± 3.30 *	52.03 ± 3.77 *	599.62 ± 49.61*	60.34 ± 8.60 *	34.57 ± 1.32 *	3.56 ± 0.34	1156.67 ± 164.29 *	10 421.42 ± 392.14 *
	86.58 nm + 17 Gy	2.12 ± 0.39 *	98.96 ± 4.40 * ×	65.28 ± 1.54 * ×	633.90 ± 11.76*	63.40 ± 3.14 *	34.50 ± 5.61 *	3.38 ± 0.49	964.61 ± 11.60 *	12 701.03 ± 1604.10 *
	123.6 nm + 17 Gy	2.26 ± 0.28	113.62 ± 2.32 * O	71.54 ± 5.89 *	599.80 ± 31.38*	65.39 ± 12.34 *	50.74 ± 4.32 × O	4.56 ± 0.22 × O	813.24 ± 10.83 * ×	17 438.51 ± 1318.09 * × O
155 day	Control	2.35 ± 0.49	122.58 ± 1.25	96.23 ± 8.63	500.45 ± 30.66	109.89 ± 10.19	51.76 ± 5.05	3.92 ± 0.30	633.28 ± 11.00	9656.51 ± 243.25
	17 Gy	2.23 ± 0.30	111.25 ± 11.29	40.47 ± 3.17 *	602.74 ± 11.92 *	66.61 ± 2.94 *	27.48 ± 2.85 *	3.13 ± 0.13 *	1252.83 ± 3.08 *	8063.81 ± 770.92 *
	86.58 nm + 17 Gy	2.38 ± 0.15	98.06 + 1.00 *	37.54 ± 4.74 *	875.43 ± 5.41 * ×	66.12 ± 6.17 *	28.45 ± 1.66 *	3.13 ± 0.32 *	1285.48 ± 1.47 *×	11 961.83 ± 247.14 *×
	123.6 nm + 17 Gy	2.31 ± 0.33	113.61 ± 3.78 *	45.65 ± 0.94 *	902.99 ± 24.22 * ×	62.23 ± 1.48 *	33.75 ± 3.93 *	3.66 ± 0.24	1027.20 ± 0.93 * × O	20 575.71 ± 1045.02 * × O
190 day	Control	2.46 ± 0.28	86.25 ± 0.93	66.84 ± 5.79	605.49 ± 33.19	110.44 ± 10.81	97.58 ± 6.97	6.26 ± 0.27	557.02 ± 1.92	10 858.00 ± 2044.59
	17 Gy	2.39 ± 0.26	312.35 ± 2.36 *	21.51 ± 2.28 *	904.11 ± 23.49 *	67.88 ± 1.87 *	74.98 ± 2.66 *	5.64 ± 0.15 *	1023.54 ± 1.28 *	5560.84 ± 131.56 *
	86.58 nm + 17 Gy	2.41 ± 0.37	168.17 ± 2.76 *×	–	661.87 ± 38.95 * ×	69.98 ± 4.28 *	87.66 ± 3.18 ×	4.64 ± 0.54 * ×	750.54 ± 0.47 * ×	10 882.15 ± 1949.15 ×
	123.6 nm + 17 Gy	2.01 ± 0.22 *	108.46 ± 1.32 * × O	–	655.50 ± 5.14 * ×	55.23 ± 2.02 *	85.84 ± 2.87 ×	2.91 ± 0.21 * × O	443.57 ± 5.50 * × O	13 804.11 ± 3676.32 ×

Total protein of each sample and cytokine profile of IL-1β, IL-6, TGF-β, MCP-1, MIP-1, KC, MMP-2, and proMMP-9 from mixed group samples were measured in lung tissue. The assays were performed at days 113, 155, and 190 following lung irradiation (17 Gy). Each concentration level is presented as mean ± SD. Asterisks (*) indicate significance differences at p ≤ 0.05 in comparison with untreated control, multiplication signs (×) in comparison with irradiated cells, and small circles (○) in comparison with 85.68 nm HANPs + 17 Gy.

minimally compared to the nonirradiated control (1.33- and 1.12-fold, respectively). Although the concentration of proMMP-9 was decreased in the irradiated group (0.8-fold vs. control), this protein was markedly increased (1.33-fold) relative to the control in the 123.6 HANPs group. The concentration in this group varied significantly in comparison with all other groups at day 113.

At the time point (day 155) for assessing the transition phase between RP and RF, the total protein levels revealed no significant differences among groups. Different trends were observed for the three pro-fibrotic proteins TGF-β, MMP-2, and proMMP-9. Markedly elevated concentrations of the protein TGF-β were observed in both HANPs groups compared to the nonirradiated and also to the 17 Gy irradiated-only group. The MMP-2 concentration increased similarly in both HANPs groups (2.0- and 1.62-fold, respectively) compared to the control, but significant difference in levels of pro MMP-9 versus control was observed between the HANPs groups (1.24-fold in the 86.58 nm HANPs group, but 2.13-fold in the 123.6 nm HANPs group). The trend exhibited in the 123.6 nm HANPs group was higher levels of proMMP-9 and only slight increase in MMP-2. Contrariwise, the trend in 17 Gy-irradiated group and group treated with 86.58 nm HANPs was different, levels of MMP-2 significantly increased and concentration of proMMP-9 increase slightly, even decreased in group only 17 Gy-irradiated. All other cytokines remained similar among all three treatment groups at this time point, which means they were significantly decreased compared with the control.

The time point representing radiation fibrosis (day 190) revealed that total protein levels in the lung treated with 123.6 nm HANPs decreased significantly ($p \leq 0.05$) compared to the control. Also, cytokine concentration trends changed in this phase. Changes were again observed in the pro-fibrotic proteins TGF-β, MMP-2, and proMMP-9, as well as in IL-1β. The levels of IL-6 in both HANPs groups were below the detection limit. The most notable difference was between the 17 Gy-irradiated group and all three other groups. The results showed obvious elevation vis-à-vis the control in TGF-β (1.49-fold), MMP-2 (1.84-fold), and IL-1β (3.62-fold). That was in contrast to the level of proMMP-9, which was decreased relative to the control (0.51-fold) at this time point. The findings therefore reflect that application of HANPs of both sizes prior to irradiation modified the lung environment in a manner that markedly affected pro-fibrotic signaling.

HANPs Changed Leukocytes Proportions in Peripheral Blood

Radiation induces significant alterations in the absolute numbers of peripheral blood leukocytes. The analysis of cell populations in peripheral blood on the flow cytometer revealed changes in the representation of neutrophils as well as of both B and T lymphocytes. The results have shown that significant alternation in proportions of individual cell types depending on irradiation and HANPs treatment (**Figure 3**). At the time point corresponding with RP, day 113, only in the group treated with 86.58 nm HANPs was there a significant increase in total blood leukocyte counts, but the irradiated group and HANPs-treated groups varied significantly in the absolute numbers of their neutrophils and lymphocyte populations. In the 17 Gy partially irradiated group, the overall cell count response occurred prior to the lymphocytes response, mainly reflecting that the number of B lymphocytes had increased significantly compared with the control. By contrast, a significant increase in neutrophil count was identified in the 123.6 nm HANPs group. Significant changes were observed in the experimental group treated with 86.58 nm HANPs, as there was significant increase in all measured leukocyte populations and subpopulations with the exception of $CD8^+$ cytotoxic T lymphocytes (data not shown). These trends were generally comparable with those seen also for the 123.6 nm HANPs group.

At day 155, representing the transition phase, there was—with one exception—decrease in total blood leukocyte counts in all populations and subpopulations compared with the pneumonic phase. The sole exception was significantly increased number of neutrophils in the 17 Gy-irradiated group. Moreover, this group exhibited significantly increased proportions of lymphocytes, and particularly numbers of B lymphocytes, relative to the control group. These values for groups of mice treated with HANPs of both size were similar to those of controls.

At the time point 190 days, however, there was a significant difference between the irradiated-only and HANPs-treated groups. During this fibrotic phase, the irradiated group displayed significant increase in lymphocyte number, represented by both B and T lymphocyte populations (cytotoxic $CD8^+$, as well as helpers $CD4^+$). Absolute numbers of lymphocytes in this group varied significantly not only in comparison to the control but also relative to those for HANPs-treated mice of both NP sizes. The effects observed in these groups were similar to those seen at the day 113 time point, when the cellular response had been more oriented to promoting increase in neutrophil count. Absolute numbers of neutrophils in the 17 Gy-irradiated group were therefore almost identical to those seen in the controls. These observations could suggest a role for HANPs in lymphocytes recruitment and promotion in the different stages of RIPI.

Alterations in Lung Pathology and Leukocyte Infiltration in Lung Tissue From Mice Treated With HANPs

Because a major effect of radiation is injury to the alveolar epithelium and vascularity, the histopathological and cellular responses were analyzed. Histological staining of the lung tissue and analysis of $CD45^+$ leukocyte infiltration was further quantified using flow cytometry of lung cell suspensions. At 113 days post-irradiation, significant decrease in tissue integrity was observed in all groups that had been irradiated. The air/tissue ratio was significantly decreased in all irradiated groups compared with the control (**Figure 5C**). Tissue sections showed markedly thickened alveolar walls, collapsed alveoli, and diffuse accumulation of

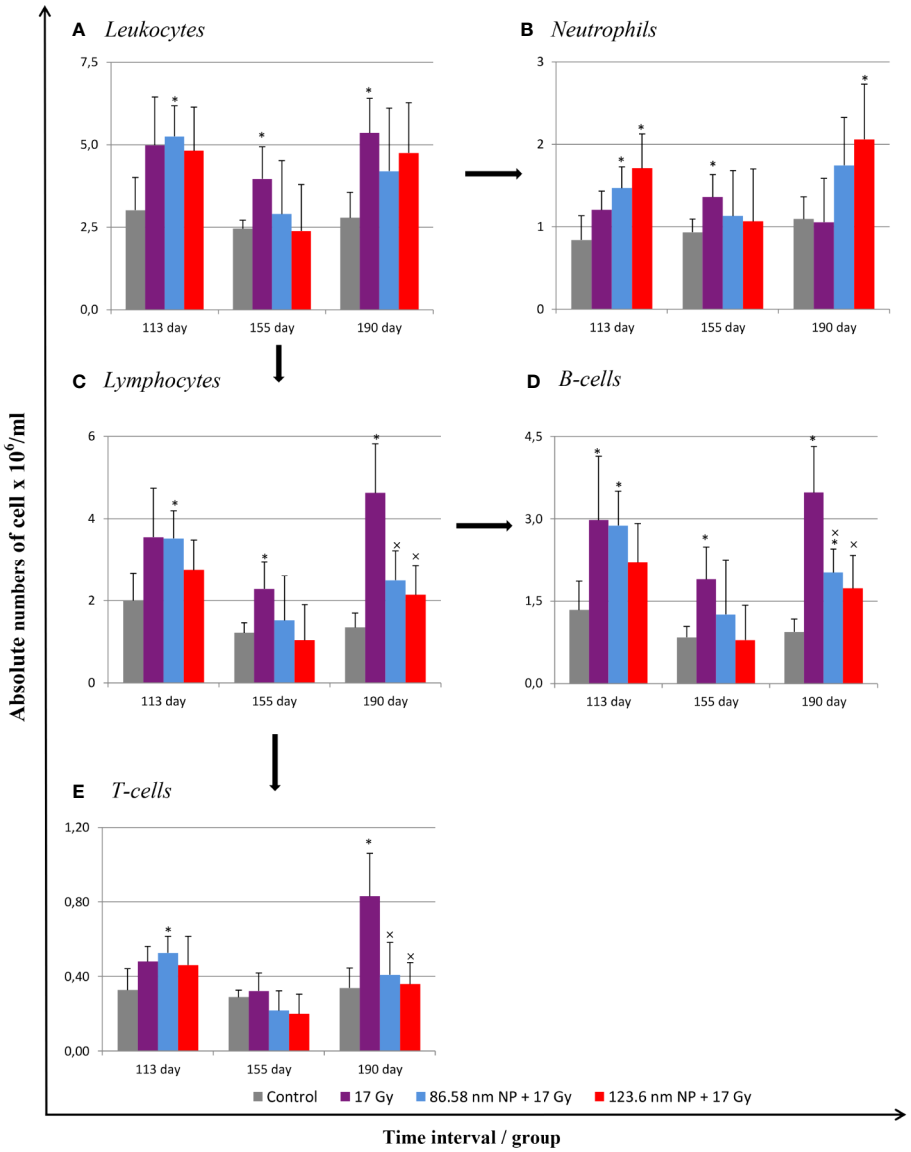

FIGURE 3 | Changes in absolute counts of peripheral blood leukocytes after HANPs and IR treatments. **(A)** Analysis of peripheral blood leukocytes by hemoanalyzer. **(B)** Absolute counts of neutrophils and **(C)** lymphocytes in blood. Flow cytometry analysis of lymphocyte subpopulations of **(D)** B cells and **(E)** T cells. Analyses of peripheral blood were performed at days 113, 155, and 190 following lung irradiation (17 Gy). Each bar represents absolute number of cells presented as mean ± 2× SEM. Asterisks (*) indicate significance differences at $p \leq 0.05$ compared to the control group and multiplication signs (×) compared to the irradiated-only (17 Gy) group.

inflammatory cells (**Figure 5A**). Applications of HANPs did not appear to have prevented damage to lung tissue. Although, deposition of collagen fibers were observed in the group only irradiated with 17 Gy, mainly around capillary vessels (**Figure 5B**). No difference in collagen deposition was seen between HANPs treated groups. Although inflammatory leukocytes infiltration (most especially by the lymphocytes population) was significantly dominant in the irradiated-only group and in the group where 86.58 nm HANPs and IR had been applied (**Figures 4A, C**), the percentage of leukocytes and lymphocytes in the group treated with 123.6 nm and IR, by contrast, did not vary significantly from the control. Moreover, analysis of this group revealed that the leukocytes population most significantly increased in the lung tissue after irradiation was that of neutrophils (**Figure 4B**). Lymphocytes and individual subpopulations play important roles in radiation-induced adverse effects within the lung. Significantly greater presence of B lymphocytes was observed in the irradiation-only group and the treatment using only the smaller-sized HANPs (**Figure 4E**). In the group with partial irradiation there also was recorded increased proportion of T lymphocytes in lung tissue

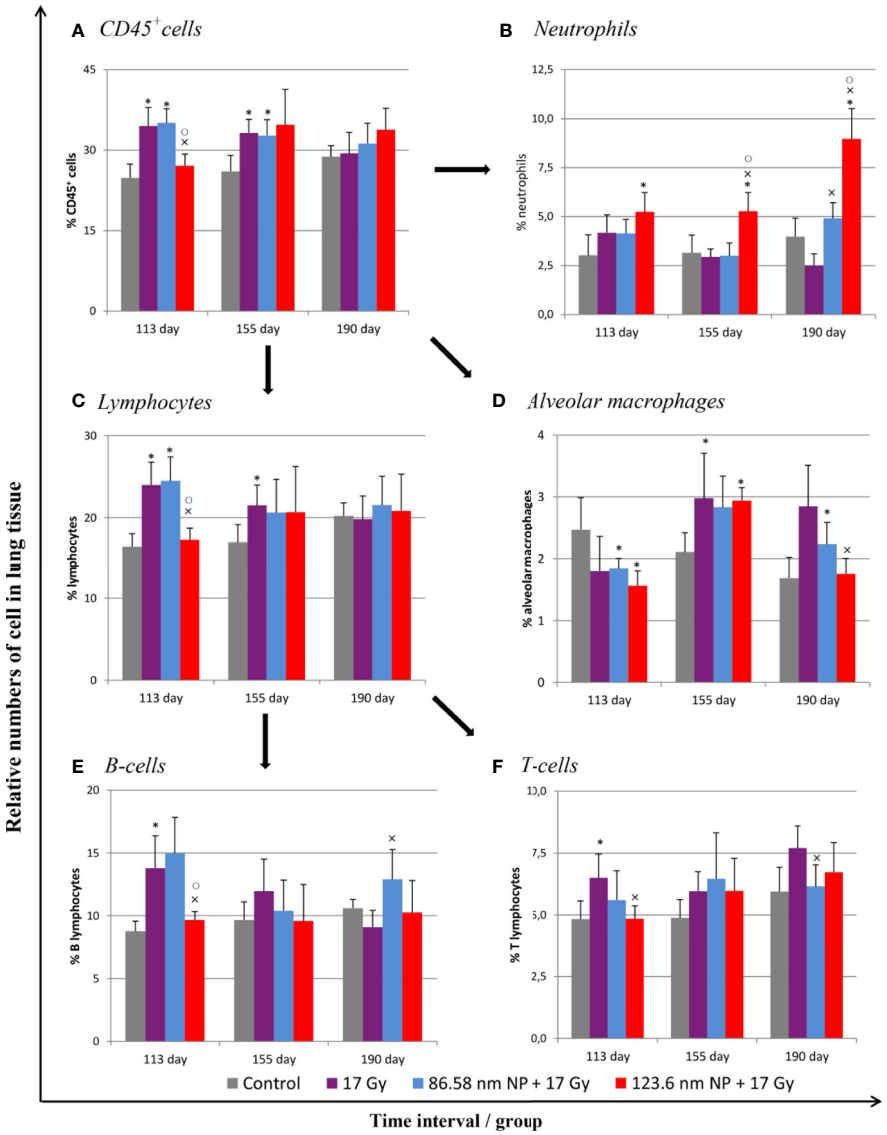

FIGURE 4 | Flow cytometry analysis of lung tissue analysis after irradiation and HANPs application. **(A)** Immunophenotypization of leukocyte infiltration as measured by CD45$^+$ cells, **(B)** neutrophils, **(C)** lymphocytes, and **(D)** alveolar macrophages. The lymphocytes population was subsequently analyzed for percentage representation of **(E)** B cells and **(F)** T cells subpopulations. HANPs were administered by intratracheal instillation prior to irradiation. Samples were prepared at days 113, 155, and 190 following lung irradiation (17 Gy). Each bar represents percentage of positive cells from total viable lung cells presented as mean ± 2× SEM. Asterisks (*) indicate significance differences at $p \leq 0.05$ in comparison with control, multiplication signs (×) in comparison with the irradiated-only (17 Gy) group, and small circles (○) in comparison with the 85.68 nm HANPs + 17 Gy group.

(**Figure 4F**). The group treated with 123.6 nm HANPs and irradiated differed significantly from both other irradiated groups, but it had similar proportions of the various lymphocyte subpopulations as did the control. Another important innate immune cell population present in the alveoli is that of alveolar macrophages. The proportion of these cells decreased markedly after irradiation in the irradiated-only group and significantly in both groups treated with HANPs (**Figure 4D**). Complete cellular response in lung tissue was identical to cell response in peripheral blood during this phase. These data suggest a significant role of 123.6 nm HANPs in modulating lymphocytes response in lung tissue during the RP phase.

At the transition phase, represented by day 155, notable differences were observed between the 17 Gy irradiation and 86.58 nm HANPs treatment groups versus the 123.6 nm HANPs group. Similar to corresponding changes in peripheral blood, albeit with two exceptions, the percentage representations of all leukocyte populations and subpopulations decreased in comparison to the previous phase. The first exception was that the representation of alveolar macrophages in lung tissue was

elevated during the transition phase. The second was that the lymphocyte proportion was slightly elevated due to an increasing of T cells in the 123.6 nm HANPs group. Also, this was the only group within which the numbers of neutrophils and B cells were the same as in the RP phase. On the other hand, the representation of B cells was shown to be most intensively decreased at day 155 (**Figure 4E**). Also, increased collagen deposition was observed in 86.58 nm HANPs treatment groups compared with the 123.6 nm HANPs group.

At the last time point, representing the fibrotic phase, the results manifested the most notable difference in cellular compartments of the irradiated lung between the irradiated-

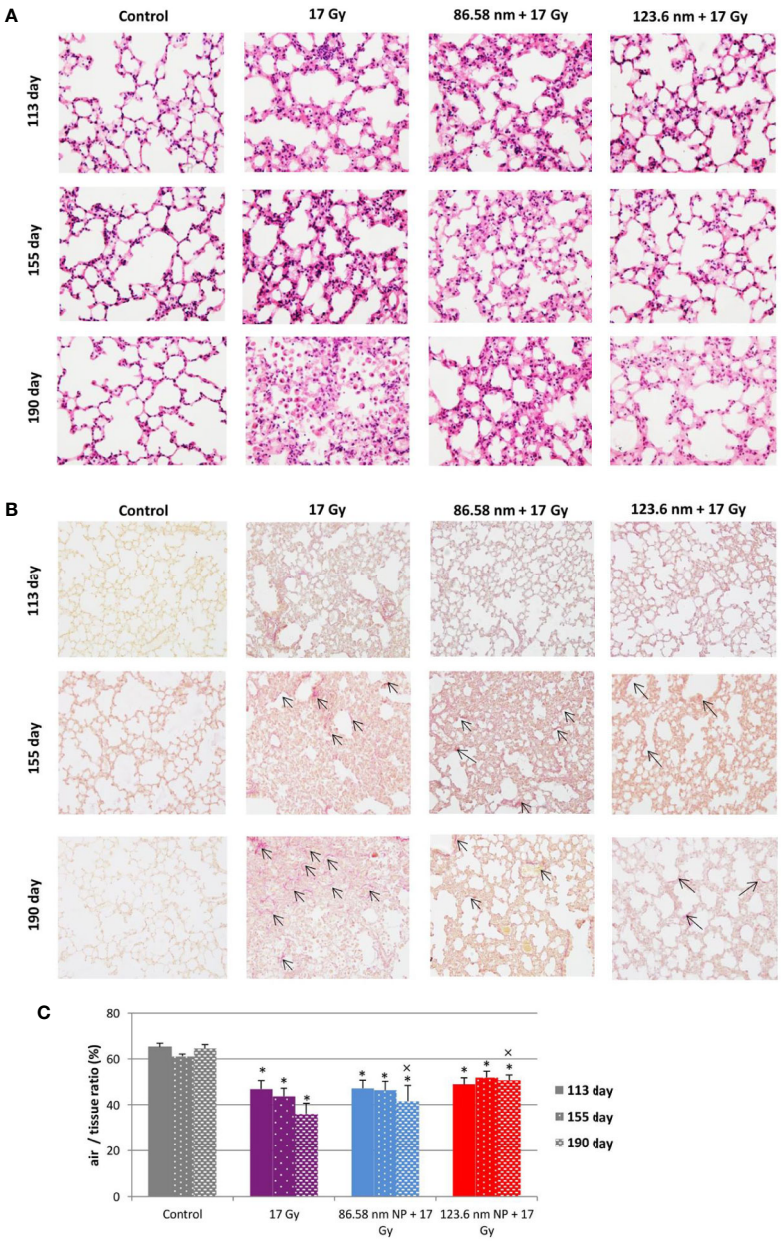

FIGURE 5 | Lung tissue analysis. **(A)** Representative tissue sections of hematoxylin and eosin staining. **(B)** Representative tissue sections of picrofuchsin staining for collagen deposition in lung sections. **(C)** Quantitative analysis of airiness after radiation-induced damage to lung tissue and effect of HANPs treatment. Histology studies of lung tissue were performed at days 113, 155, and 190 following lung irradiation (17 Gy). Each bar represents absolute number of cells presented as mean ± 2× SEM. Original magnification 200×. Arrows indicate presence of collagen. Asterisks (*) indicate significance differences at $p \leq 0.05$ compared to the control group and multiplication signs (×) compared to the irradiated-only (17 Gy) group.

only group and groups treated with HANPs of both sizes. Not only was there observed in the lung tissue section significant improvement of tissue airiness and presence of fibrosis, due to collagen deposition, for the HANPs groups compared with the irradiated-only group (**Figure 5**), but also cellular responses between these groups clearly differed. Significant elevation in percentage numbers was observed in T lymphocyte and alveolar macrophage populations within the group treated with irradiation only. Compared with responses in peripheral blood, however, the representation of B cells was markedly reduced. Despite irradiation, and with neutrophils as the only exception (**Figure 4B**), the HANPs-treated groups showed no significant increase in cell representation during the fibrotic phase. In both HANPs groups the numbers of neutrophils increased significantly compared with the group only irradiated with 17 Gy. The 123.6 nm HANPs group even differed significantly in this population compared to all other groups. The results of our study point to an apparent effect of HANPs on the development of RIPI in both the RP and RF phases. The most evident modulation was observed at the time point representing the onset of RF in the lung tissue.

DISCUSSION

The hyaluronic acid molecule has been investigated intensively since its discovery (Meyer and Palmer, 1934) and to the present day. Due to its versatile properties in relation to its biocompatibility, biodegradability, non-toxicity, non-immunogenicity, and ubiquitous presence, as well as its characteristic metabolism pathways and signaling in organisms, this biopolymer has been used extensively, and especially in controlled-release and targeted drug delivery systems (Mattheolabakis et al., 2015; Huang and Huang, 2018). One of the most critical issues in radiobiology is search for suitable molecules, which can protect/modify response against destructive and damaging outcome of ionizing radiation exposure. Over the last few decades, many natural and synthetic compounds have been investigated for their potential as radioprotectors, mitigators, or therapeutics. In recent few decades, awareness in natural compounds as a potential source of radioprotectors has raised up, due to their ability to provide health benefits, less toxicity and common anti-inflammatory and antioxidant properties (Mun et al., 2018; Khodamoradi et al., 2020). Radioprotective effects to lung tissue have been demonstrated for numerous naturally occurring substances. Genistein, a soy isoflavonoids, provided mitigation of acute and late effects of lung tissue due to reduction of DNA damage in lung fibroblasts (Mahmood et al., 2011) or hesperidin, major flavonoid in lemons and sweet oranges, protected against oxidative stress damage caused by IR exposure by decreasing acute inflammatory pathways (Haddadi et al., 2017). Specifically, flaxseed demonstrated high protective effect against radiation fibrosis, inflammation and oxidative lung damage thought alternation in the TGF-β1 response (Lee et al., 2009). Also, alterations of radiation responses have been observed by endogenous occurring substances. Hormone melatonin significantly prevented against RIPI in the early pneumonic phase *via* a reduction in oxidative stress and the production of cytokines, such as TGF-β1 and TNF- α (Jang et al., 2015).

Although, possibilities for HA's application in radiation biology have been limited since 1950, however, when it was proven that the HA molecule is radiosensitive, resolving in depolarization of primary chain and low fragment productions depending on absorbed dose of irradiation (Schoenberg et al., 1951). To the present day, only a few studies have addressed the potential for HA use in radiation biology. It has been confirmed that exogenous HA may serve as a radioprotective agent through TLR4 interaction in the intestine, that the HA molecule after IR exposure maintained antioxidant activity, that it significantly reduced radiation-induced inflammation and affected tissue hydration in patients with pelvic radiotherapy, and, in one study, that it improved radiation dermatitis (Liguori et al., 1997; Kim et al., 2008; Riehl et al., 2012; Cosentino and Piro, 2018). The present study is the first of its kind to confirm that intramolecularly cross-linked HA in nanoparticle form prevents ionizing radiation defragmentation. The study demonstrated long-term stability of synthetized HANPs after IR. In addition to stability against IR, the 86.58 nm and 123.6 nm HANPs exhibited great stability at various temperatures ranging from −80°C to 60°C, to enzymatic degradation, and to effects of model gastric juice (Kasparova et al., unpublished data). Results of the *in vitro* analysis confirmed that HANPs have no cytotoxic effect on the cell line. Choi et al. (2010) had demonstrated that the binding affinity of HANPs to the CD44 receptor is dependent on the NPs' size. In the present study, we observed that the size of HANPs, but also the preincubation period and the IR insult, contributed to the final effect on cell viability (Choi et al., 2010). Consistent with our results, Gennari et al., (2019) confirmed a size-dependent effect of chitosan/HA nanoparticles on cell uptake and silencing efficiency in macrophages (Gennari et al., 2019). Recent studies of HANPs' biodistribution and stability in organisms have demonstrated the most intensive tissues accumulation to be in liver, tumor, and lungs. Also, improved long-term stability and persistence of nanoparticles in the lung may be achieved by direct lung administration *via* intratracheal instillation (Choi et al., 2009; Kuehl et al., 2016).

Therefore, we decided to use these nanoparticles and investigate their effect on the course of the radiation-induced lung injuries that inevitably still accompany radiation therapy. The complexity of injury and contributions of various molecules and cell types in combination with direct radiation cytotoxicity pose complicated but appealing research challenges. Even though previous studies have not completely comprehended the full scope of the mechanisms involved, new treatment strategies have been employed. The most recent progress has been in nanomedicine. Radioprotective effects in preclinical models have been achieved through administering cerium oxide nanoparticles, manganese superoxide dismutase-plasmid/liposomes complexes, and nanoparticle formulations of Amifostine (Ethyol®) (Pamujula et al., 2005; Carpenter et al., 2005; Colon et al., 2009). Encouraged by these findings, we

decided to test the effect of HANPs in an experimental model of RIPI.

The inflammatory phase of lung disease just after radiation is connected with the immediate response of hyaluronan and its metabolism during the initiation and progression (Li et al., 2000). Among all those molecules and cytokines investigated, TGF-β1 has been implicated as a key cytokine in the initiation, development, and persistence of both RP and RF (Finkelstein et al., 1994; Anscher et al., 1998; Rube et al., 2000). In the lung, TGF-β1 enhances the production of HA and gene expression for HAS2, HAS3, surface receptor CD44, and a receptor for HA-mediated motility (RHAMM) (Li et al., 2015; Ghatak et al., 2017). On the other hand, increased levels of HA in tissue have been shown to regulate response of the cells to TGF-β1 and HA/CD44/TGF-β1interaction is necessary for fibroblast proliferation (Webber et al., 2009; Meran et al., 2011). This reciprocal interaction between HA and TGF-β1 has been reported during tissue inflammation and fibrogenesis. These findings are consistent with our results, which demonstrated the crucial role of HANPs administration on the cytokines and their signaling pathways involved in RIPI. Importantly, TGF-β1 and irradiation are major stimuli that directly modulate the expression of MMP-2 and MMP-9, which are additional significant factors contributing to tissue fibrosis. MMPs are zinc enzymes responsible for the degradation of such ECM components as elastin, collagen, proteoglycans, laminin, and fibronectin during tissue remodeling processes. These processes are highly correlated with the response pattern in the early and late phase of injuries (Haiping et al., 2006). In our study, the increasing trend seen in the levels of these cytokines (TGF-β1, MMP-2, and pro-MMP-9) during courses of RIPI was confirmed only in the irradiated group). Nevertheless, the HANPs treatments significantly regulated the MMP-2 and MMP-9 balance in irradiated lung tissue. That, in turn, significantly affected maintaining the same structural integrity of pulmonary architecture. This was visible also in the histopathological section of lung tissue when compared with tissue from the irradiated group. That comparison was most striking on day 190.

Cytokine response in the tissue results from, but also is an effector of, the subsequent accumulation of immune cells and final tissue response. Our study revealed differential activation of leukocyte and macrophage cell subsets upon treatment. In the irradiated-only group, significant promotion of lymphocytic alveolitis development was apparent and depletion of resident alveolar macrophages was observed during the RP phase. With regard to fibrosis, this group was characterized most prominently by recruitment of macrophages and $CD4^+$ T lymphocytes. These findings, as well as the cytokine profile findings are consistent with those from many other studies (Johnston et al., 2004; Chiang et al., 2005; Park et al., 2017). Lymphocytes have been reported as constituting a prominent feature of post-irradiation lung injury. The role of T lymphocytes has been discussed intensively, especially with regard to the plausible role of regulatory $CD25^+$ lymphocytes (Wirsdörfer and Jendrossek, 2016). Therefore, the impact of B cells on the outcome of RIPI has not remained completely unrevealed. A study by Paun et al. (Paun et al., 2010) identified increased B cell gene expression after irradiation during intervals of RF, thus suggesting a possible new role of B cells in RIPI development. In the lung, B lymphocytes served in antigen presentation and as antibody-secreting plasma cells, but also in producing fibrogenic cytokines. Enhanced HA production has been noted to activate B cells producing these cytokines (Yoshizaki et al., 2008). Increased numbers of B cells were observed in peripheral blood during the present experiment, but only in the irradiated group.

It was predominantly 123.6 HANPs administration that seem to contribute most markedly to neutrophilic response. The possible role of neutrophils in RIPI is controversial. In their study, Johnston et al., (2004) suggested that neutrophils do not participate in RIPI devolvement within the mouse model. Other reports, however, have confirmed the infiltration of neutrophils during early time intervals after irradiation (Österreicher et al., 2004; Abernathy et al., 2015; Farhood et al., 2019). Neutrophils are the innate immune system's effector cells recruited earliest to the site of pathology. Moreover, these polymorphonuclear cells have been shown to store MMP-2 and MMP-9 (pro-enzyme forms) in tertiary granules (Grommes and Soehnlein, 2011). A similar result of neutrophil activation due to induced nanotoxicity to lung tissue was reported by Sydlik et al., (2009) in their study of intratracheally instilled application of carbon nanoparticles. In our study, the increase in neutrophil counts was observed mainly in the group treated with 123.6 nm HANPs during RP and RF phases. Because no study to date has mentioned that application of HA molecule or HANPs induced lung toxicity, we expect that neutrophil recruitment was achieved due to exogenous presence of HANPs in tissue. This property of HA in relation to neutrophils already has been reported (Håkansson and Venge, 1985; McDonald et al., 2008). Furthermore, the crucial determinant of an induced biological effect is nanoparticle size. The results of our study imply moderate variances between groups treated with 86.58 nm HANPs versus 123.6 nm HANPs. Our results show that after irradiation the size of HANPs affected mainly neutrophils and B cells. On the other hand, cytokine levels, as well as the response of alveolar macrophages and T lymphocytes were comparable between the two HANPs groups but differed significantly from that of the irradiated-only group. Thus, understanding the interactions between nanomaterials and immune cells and their tissue distribution and mechanisms is important for the development of safe and effective nanomaterials for biomedical applications.

Overall, our study demonstrated that application of HANPs before irradiation provides substantial attenuation against RIPI. This was particularly significant during signal transduction processes that are relevant for the fibrotic phase. The complex of processes determining how HANPs impact the onset of radiation-induced cellular and molecular signaling patterns needs to be elucidated, and its confirmation remains an aim of our future work. In the end, we anticipate that this study can contribute to constructing a novel and useful vision for the field of radiation oncology that is based on nanomedicine modulation of lung toxicity and strives to develop efficient treatment strategies for patients.

DATA AVAILABILITY STATEMENT

The datasets generated for this study are available on request to the corresponding author.

ETHICS STATEMENT

The animal study was reviewed and approved by Faculty of Military Health Sciences, Hradec Kralove, Czechia.

AUTHOR CONTRIBUTIONS

AL designed the experiments, participated in all the experiments, analyzed the data, wrote the manuscript and produced figures. ZS contributed to the conception and overall design of the study. JaP, KK, and MJ helped with performing of individual *in vivo* experiments and data analysis. JK, JiP, LK, and ZB were responsible for nanoparticle synthesis and characterizations. All authors contributed to the article and approved the submitted version.

FUNDING

These studies were supported by the Ministry of Defence of the Czechia (long-term organization development plan Medical Aspects of Weapons of Mass Destruction of the Faculty of Military Health Sciences, University of Defence) and by the Ministry of Education, Youth and Sport, Czechia (Specific Research Project No: SV/FVZ201805) and by the OP RDE project, Strengthening interdisciplinary cooperation in research of nanomaterials and their effects on living organisms' project no. CZ.02.1.01/0.0/17 048/0007421.

REFERENCES

Abernathy, L. M., Fountain, M. D., Rothstein, S. E., David, J. M., Yunker, C. K., Rakowski, J., et al. (2015). Soy Isoflavones Promote Radioprotection of Normal Lung Tissue by Inhibition of Radiation-Induced Activation of Macrophages and Neutrophils. *J. Thoracic Oncol.* 10 (12), 1703–1712. doi: 10.1097/JTO.0000000000000677

Albeiroti, S., Soroosh, A., and de la Motte, C. A. (2015). Hyaluronan's Role in Fibrosis: A Pathogenic Factor or a Passive Player? *BioMed. Res. Int.* 2015, 790203. doi: 10.1155/2015/790203

Anscher, M. S., Kong, F.-M., Andrews, K., Clough, R., Marks, L. B., Bentel, G., et al. (1998). Plasma transforming growth factor β1 as a predictor of radiation pneumonitis. *Int. J. Radiat. Oncol. Biol. Phys.* 41 (5), 1029–1035. doi: 10.1016/S0360-3016(98)00154-0

Atkinson, J. J., and Senior, R. M. (2003). Matrix metalloproteinase-9 in lung remodeling. *Am. J. Respir. Cell Mol. Biol.* 28 (1), 12–24. doi: 10.1165/rcmb.2002-0166TR

Avenoso, A., Bruschetta G, D., Ascola, A., Scuruchi, M., Mandraffino, G., Saitta, A., et al. (2020). Hyaluronan Fragmentation During Inflammatory Pathologies: A Signal that Empowers Tissue Damage. *Mini Rev. Med. Chem.* 20 (1), 54–65. doi: 10.2174/1389557519666190906115619

Bensadoun, E. S., Burke, A. K., Hogg, J. C., and Roberts, C. R. (1996). Proteoglycan deposition in pulmonary fibrosis. *Am. J. Respir. Crit. Care Med.* 154 (6), 1819–1828. doi: 10.1164/ajrccm.154.6.8970376

Bray, B. A., Sampson, P. M., Osman, M., Giandomenico, A., and Turino, G. M. (1991). Early changes in lung tissue hyaluronan (hyaluronic acid) and hyaluronidase in bleomycin-induced alveolitis in hamsters. *Am. Rev. Respir. Dis.* 143 (2), 284–288. doi: 10.1164/ajrccm/143.2.284

Cantor, J. O. (2007). Potential therapeutic applications of hyaluronan in the lung. *Int. J. Chron. Obstruct. Pulmon. Dis.* 2 (3), 283–288.

Carpenter, M., Epperly, M. W., Agarwal, A., Nie, S., Hricisak, L., Niu, Y., et al. (2005). Inhalation delivery of manganese superoxide dismutase-plasmid/liposomes protects the murine lung from irradiation damage. *Gene Ther.* 12 (8), 685–693. doi: 10.1038/sj.gt.3302468

Chiang, C.-S., Liu, W.-C., Jung, S.-M., Chen, F.-H., Wu, C.-R., McBride, W. H., et al. (2005). Compartmental responses after thoracic irradiation of mice: strain differences. *Int. J. Radiat. Oncol. Biol. Phys.* 62 (3), 862–871. doi: 10.1016/j.ijrobp.2005.02.037

Choi, K. Y., Min, K. H., Na, J. H., Choi, K., Kim, K., Park, J. H., et al. (2009). Self-assembled hyaluronic acid nanoparticles as a potential drug carrier for cancer therapy: synthesis, characterization, and in vivo biodistribution. *J. Mater. Chem.* 19 (24), 4102–4107. doi: 10.1039/b900456d

Choi, K. Y., Chung, H., Min, K. H., Yoon, H. Y., Kim, K., Park, J. H., et al. (2010). Self-assembled hyaluronic acid nanoparticles for active tumor targeting. *Biomaterials.* 31 (1), 106–114. doi: 10.1016/j.biomaterials.2009.09.030

Choi, S.-H., Hong, Z.-Y., Nam, J.-K., Lee, H.-J., Jang, J., Yoo, R. J., et al. (2015). A Hypoxia-Induced Vascular Endothelial-to-Mesenchymal Transition in Development of Radiation-Induced Pulmonary Fibrosis. *Clin. Cancer Res.* 21 (16), 3716–3726. doi: 10.1158/1078-0432.CCR-14-3193

Collum, S. D., Molina, J. G., Hanmandlu, A., Bi, W., Pedroza, M., Mertens, T. C. J., et al. (2019). Adenosine and hyaluronan promote lung fibrosis and pulmonary hypertension in combined pulmonary fibrosis and emphysema. *Dis. Model Mech.* 12 (5), 1–12. doi: 10.1242/dmm.038711

Colon, J., Herrera, L., Smith, J., Patil, S., Komanski, C., Kupelian, P., et al. (2009). Protection from radiation-induced pneumonitis using cerium oxide nanoparticles. *Nanomed.: Nanotechnol. Biol. Med.* 5 (2), 225–231. doi: 10.1016/j.nano.2008.10.003

Cosentino, D., and Piro, F. (2018). Hyaluronic acid for treatment of the radiation therapy side effects: a systematic review. *Eur. Rev. Med. Pharmacol. Sci.* 22 (21), 7562–7572. doi: 10.26355/eurrev_201811_16298

Cyphert, J. M., Trempus, C. S., and Garantziotis, S. (2015). Size Matters: Molecular Weight Specificity of Hyaluronan Effects in Cell Biology. *Int. J. Cell Biol.* 2015, 563818. doi: 10.1155/2015/563818

Dentener, M. A., Vernooy, J. H. J., Hendriks, S., and Wouters, E. F. M. (2005). Enhanced levels of hyaluronan in lungs of patients with COPD: relationship with lung function and local inflammation. *Thorax* 60 (2), 114–119. doi: 10.1136/thx.2003.020842

Dicker, K. T., Gurski, L. A., Pradhan-Bhatt, S., Witt, R. L., Farach-Carson, M. C., and Jia, X. (2014). Hyaluronan: A simple polysaccharide with diverse biological functions. *Acta Biomaterialia.* 10 (4), 1558–1570. doi: 10.1016/j.actbio.2013.12.019

Fallacara, A., Baldini, E., Manfredini, S., and Vertuani, S. (2018). Hyaluronic Acid in the Third Millennium. *Polymers.* 10 (7), 701. doi: 10.3390/polym10070701

Farhood, B., Aliasgharzadeh, A., Amini, P., Rezaeyan, A., Tavassoli, A., Motevaseli, E., et al. (2019). Mitigation of Radiation-Induced Lung Pneumonitis and Fibrosis Using Metformin and Melatonin: A Histopathological Study. *Medicina.* 55 (8), 417. doi: 10.3390/medicina55080417

Finkelstein, J. N., Johnston, C. J., Baggs, R., and Rubin, P. (1994). Early alterations in extracellular matrix and transforming growth factor beta gene expression in mouse lung indicative of late radiation fibrosis. *Int. J. Radiat. Oncol. Biol. Phys.* 28 (3), 621–631. doi: 10.1016/0360-3016(94)90187-2

Gennari, A., de la Rosa, J. M. R., Hohn, E., Pelliccia, M., Lallana, E., Donno, R., et al. (2019). The different ways to chitosan/hyaluronic acid nanoparticles: templated vs direct complexation. Influence of particle preparation on morphology, cell uptake and silencing efficiency. *Beilstein J. Nanotechnol.* 10 (1), 2594–2608. doi: 10.3762/bjnano.10.250

Ghatak, S., Markwald, R. R., Hascall, V. C., Dowling, W., Lottes, R. G., Baatz, J. E., et al. (2017). Transforming growth factor β1 (TGFβ1) regulates CD44V6 expression and activity through extracellular signal-regulated kinase (ERK)-induced EGR1 in pulmonary fibrogenic fibroblasts. *J. Biol. Chem.* 292 (25), 10465–10489. doi: 10.1074/jbc.M116.752451

Giuranno, L., Ient, J., De Ruysscher, D., and Vooijs, M. A. (2019). Radiation-Induced Lung Injury (RILI). *Front. Oncol.* 9, 877. doi: 10.3389/fonc.2019.00877

Grommes, J., and Soehnlein, O. (2011). Contribution of Neutrophils to Acute Lung Injury. *Mol. Med.* 17 (3–4), 293–307. doi: 10.2119/molmed.2010.00138

Haddadi, G. H., Rezaeyan, A., Mosleh-Shirazi, M. A., Hosseinzadeh, M., Fardid, R., Najafi, M., et al. (2017). Hesperidin as Radioprotector against Radiation-induced Lung Damage in Rat: A Histopathological Study. *J. Med. Phys.* 42 (1), 25–32. doi: 10.4103/jmp.JMP_119_16

Haiping, Z., Takayama, K., Uchino, J., Harada, A., Adachi, Y., Kura, S., et al. (2006). Prevention of radiation-induced pneumonitis by recombinant adenovirus-mediated transferring of soluble TGF-beta type II receptor gene. *Cancer Gene Ther.* 13 (9), 864–872. doi: 10.1038/sj.cgt.7700959

Håkansson, L., and Venge, P. (1985). The combined action of hyaluronic acid and fibronectin stimulates neutrophil migration. *J. Immunol.* 135 (4), 2735–2739.

Hanania, A. N., Mainwaring, W., Ghebre, Y. T., Hanania, N. A., and Ludwig, M. (2019). Radiation-Induced Lung Injury: Assessment and Management. *Chest.* 156 (1), 150–162. doi: 10.1016/j.chest.2019.03.033

Huang, G., and Huang, H. (2018). Hyaluronic acid-based biopharmaceutical delivery and tumor-targeted drug delivery system. *J. Controlled Release.* 278, 122–126. doi: 10.1016/j.jconrel.2018.04.015

Hussain, S., Ji, Z., Taylor, A. J., DeGraff, L. M., George, M., Tucker, C. J., et al. (2016). Multiwalled Carbon Nanotube Functionalization with High Molecular Weight Hyaluronan Significantly Reduces Pulmonary Injury. *ACS Nano.* 10 (8), 7675–7688. doi: 10.1021/acsnano.6b03013

Jackson, I. L., Vujaskovic, Z., and Down, J. D. (2010). Revisiting Strain-Related Differences in Radiation Sensitivity of the Mouse Lung: Recognizing and Avoiding the Confounding Effects of Pleural Effusions. *Radiat. Res.* 173 (1), 10–20. doi: 10.1667/RR1911.1

Jang, S. S., Kim, H. G., Lee, J. S., Han, J. M., Park, H. J., Huh, G. J., et al. (2013). Melatonin reduces X-ray radiation-induced lung injury in mice by modulating oxidative stress and cytokine expression. *Int. J. Radiat. Biol.* 89 (2), 97–105. doi: 10.3109/09553002.2013.734943

Jang, S. S., Kim, H. G., Han, J. M., Lee, J. S., Choi, M. K., Huh, G. J., et al. (2015). Modulation of radiation-induced alterations in oxidative stress and cytokine expression in lung tissue by Panax ginseng extract. *Phytother. Res.* 29 (2), 201–209. doi: 10.1002/ptr.5223

Jeannot, V., Gauche, C., Mazzaferro, S., Couvet, M., Vanwonterghem, L., Henry, M., et al. (2018). Anti-tumor efficacy of hyaluronan-based nanoparticles for the co-delivery of drugs in lung cancer. *J. Control Release.* 10275, 117–128. doi: 10.1016/j.jconrel.2018.02.024

Jiang, D., Liang, J., Fan, J., Yu, S., Chen, S., Luo, Y., et al. (2005). Regulation of lung injury and repair by Toll-like receptors and hyaluronan. *Nat. Med.* 11 (11), 1173–1179. doi: 10.1038/nm1315

Jin, H., Yoo, Y., Kim, Y., Kim, Y., Cho, J., and Lee, Y.-S. (2020). Radiation-Induced Lung Fibrosis: Preclinical Animal Models and Therapeutic Strategies. *Cancers* 12 (6), 1561. doi: 10.3390/cancers12061561

Johnson, P., Arif, A. A., Lee-Sayer, S. S. M., and Dong, Y. (2018). Hyaluronan and Its Interactions With Immune Cells in the Healthy and Inflamed Lung. *Front. Immunol.* 9, 2787. doi: 10.3389/fimmu.2018.02787

Johnson, C. G., Stober, V. P., Cyphert-Daly, J. M., Trempus, C. S., Flake, G. P., Cali, V., et al. (2018). High molecular weight hyaluronan ameliorates allergic inflammation and airway hyperresponsiveness in the mouse. *Am. J. Physiology-Lung Cell. Mol. Physiol.* 315 (5), L787–L798. doi: 10.1152/ajplung.00009.2018

Johnston, C. J., Williams, J. P., Elder, A., Hernady, E., and Finkelstein, J. N. (2004). Inflammatory cell recruitment following thoracic irradiation. *Exp. Lung Res.* 30 (5), 369–382. doi: 10.1080/01902140490438915

Khodamoradi, E., Hoseini-Ghahfarokhi, M., Amini, P., Motevaseli, E., Shabeeb, D., AE, M., et al. (2020). Targets for protection and mitigation of radiation injury. *Cell Mol. Life Sci.* 77, 3129–3159. doi: 10.1007/s00018-020-03479-x

Kim, J. K., Srinivasan, P., Kim, J. H., Choi, J., Park, H. J., Byun, M. W., et al. (2008). Structural and antioxidant properties of gamma irradiated hyaluronic acid. *Food Chem.* 109 (4), 763–770. doi: 10.1016/j.foodchem.2008.01.038

Kuehl, C., Zhang, T., Kaminskas, L. M., Porter, C. J. H., Davies, N. M., Forrest, L., et al. (2016). Hyaluronic Acid Molecular Weight Determines Lung Clearance and Biodistribution after Instillation. *Mol. Pharmaceutics* 13 (6), 1904–1914. doi: 10.1021/acs.molpharmaceut.6b00069

Lamas, A., Marshburn, J., Stober, V. P., Donaldson, S. H., and Garantziotis, S. (2016). Effects of inhaled high-molecular weight hyaluronan in inflammatory airway disease. *Respirat. Res.* 17 (1), 123. doi: 10.1186/s12931-016-0442-4

Lauer, M. E., Dweik, R. A., Garantziotis, S., and Aronica, M. A. (2015). The Rise and Fall of Hyaluronan in Respiratory Diseases. *Int. J. Cell Biol.* 2015, e712507. doi: 10.1155/2015/712507

Lee, J. C., Krochak, R., Blouin, A., Kanterakis, S., Chatterjee, S., Arguiri, E., et al. (2009). Dietary flaxseed prevents radiation-induced oxidative lung damage, inflammation and fibrosis in a mouse model of thoracic radiation injury. *Cancer Biol. Ther.* 8 (1), 47–53. doi: 10.4161/cbt.8.1.7092

Li, Y., Rahmanian, M., Widström, C., Lepperdinger, G., Frost, G. I., and Heldin, P. (2000). Irradiation-induced expression of hyaluronan (HA) synthase 2 and hyaluronidase 2 genes in rat lung tissue accompanies active turnover of HA and induction of types I and III collagen gene expression. *Am. J. Respir. Cell Mol. Biol.* 23 (3), 411–418. doi: 10.1165/ajrcmb.23.3.4102

Li, L., Qi, L., Liang, Z., Song, W., Liu, Y., Wang, Y., et al. (2015). Transforming growth factor-β1 induces EMT by the transactivation of epidermal growth factor signaling through HA/CD44 in lung and breast cancer cells. *Int. J. Mol. Med.* 36 (1), 113–122. doi: 10.3892/ijmm.2015.2222

Liang, J., Jiang, D., Griffith, J., Yu, S., Fan, J., Zhao, X., et al. (2007). CD44 is a negative regulator of acute pulmonary inflammation and lipopolysaccharide-TLR signaling in mouse macrophages. *J. Immunol.* 178 (4), 2469–2475. doi: 10.4049/jimmunol.178.4.2469

Liang, J., Jiang, D., Jung, Y., Xie, T., Ingram, J., Church, T., et al. (2011). Role of hyaluronan and hyaluronan-binding proteins in human asthma. *J. Allergy Clin. Immunol.* 128 (2), 403–411.e3. doi: 10.1016/j.jaci.2011.04.006

Lierova, A., Jelicova, M., Nemcova, M., Proksova, M., Pejchal, J., Zarybnicka, L., et al. (2018). Cytokines and radiation-induced pulmonary injuries. *J. Radiat. Res.* 59 (6), 709–753. doi: 10.1093/jrr/rry067

Liguori, V., Guillemin, C., Pesce, G. F., Mirimanoff, R. O., and Bernier, J. (1997). Double-blind, randomized clinical study comparing hyaluronic acid cream to placebo in patients treated with radiotherapy. *Radiother. Oncol.* 42 (2), 155–161. doi: 10.1016/S0167-8140(96)01882-8

Liu, Y.-Y., Lee, C.-H., Dedaj, R., Zhao, H., Mrabat, H., Sheidlin, A., et al. (2008). High-molecular-weight hyaluronan-a possible new treatment for sepsis-induced lung injury: a preclinical study in mechanically ventilated rats. *Crit. Care* 12 (4), R102. doi: 10.1186/cc6982

Mahmood, J., Jelveh, S., Calveley, V., Zaidi, A., Doctrow, S. R., and Hill, R. P. (2011). Mitigation of radiation-induced lung injury by genistein and EUK-207. *Int. J. Radiat. Biol.* 87 (8), 889–901. doi: 10.3109/09553002.2011.583315

Mattheolabakis, G., Milane, L., Singh, A., and Amiji, M. M. (2015). Hyaluronic acid targeting of CD44 for cancer therapy: from receptor biology to nanomedicine. *J. Drug Target* 23 (7–8), 605–618. doi: 10.3109/1061186X.2015.1052072

McDonald, B., McAvoy, E. F., Lam, F., Gill, V., de la Motte, C., Savani, R. C., et al. (2008). Interaction of CD44 and hyaluronan is the dominant mechanism for neutrophil sequestration in inflamed liver sinusoids. *J. Exp. Med.* 205 (4), 915–927. doi: 10.1084/jem.20071765

Meran, S., Luo, D. D., Simpson, R., Martin, J., Wells, A., Steadman, R., et al. (2011). Hyaluronan Facilitates Transforming Growth Factor-β1-dependent Proliferation via CD44 and Epidermal Growth Factor Receptor Interaction. *J. Biol. Chem.* 286 (20), 17618–17630. doi: 10.1074/jbc.M111.226563

Meyer, K., and Palmer, J. W. (1934). The Polysaccharide of the Vitreous Humor. *J. Biol. Chem.* 107 (3), 629–634.

Mun, G.-I., Kim, S., Choi, E., Kim, C. S., and Lee, Y.-S. (2018). Pharmacology of natural radioprotectors. *Arch. Pharm. Res.* 41 (11), 1033–1050. doi: 10.1007/s12272-018-1083-6

Nilsson, K., Bjermer, L., Hellström, S., Henriksson, R., and Hällgren, R. (1990). A Mast Cell Secretogogue, Compound 48/80, Prevents the Accumulation of Hyaluronan in Lung Tissue Injured by Ionizing Irradiation. *Am. J. Respir. Cell Mol. Biol.* 2 (2), 199–205. doi: 10.1165/ajrcmb/2.2.199

Österreicher, J., Pejchal, J., Škopek, J., Mokrý, J., Vilasová, Z., Psutka, J., et al. (2004). Role of type II pneumocytes in pathogenesis of radiation pneumonitis: dose response of radiation-induced lung changes in the transient high vascular permeability period. *Exp. Toxicol. Pathol.* 56 (3), 181–187. doi: 10.1016/j.etp.2004.08.003

Pamujula, S., Kishore, V., Rider, B., Fermin, C. D., Graves, R. A., Agrawal, K. C., et al. (2005). Radioprotection in mice following oral delivery of amifostine nanoparticles. *Int. J. Radiat. Biol.* 81 (3), 251–257. doi: 10.1080/09553000500103470

Park, H.-R., Jo, S.-K., and Jung, U. (2017). Thoracic Irradiation Recruit M2 Macrophage into the Lung, Leading to Pneumonitis and Pulmonary Fibrosis. *J. Radiat. Prot Res.* 42 (4), 177–188. doi: 10.14407/jrpr.2017.42.4.177

Paun, A., Lemay, A.-M., and Haston, C. K. (2010). Gene expression profiling distinguishes radiation-induced fibrosing alveolitis from alveolitis in mice. *Radiat. Res.* 173 (4), 512–521. doi: 10.1667/RR1798.1

Riehl, T. E., Foster, L., and Stenson, W. F. (2012). Hyaluronic acid is radioprotective in the intestine through a TLR4 and COX-2-mediated mechanism. *Am. J. Physiol. Gastrointest. Liver Physiol.* 302 (3), G309–G316. doi: 10.1152/ajpgi.00248.2011

Rube, C. E., Uthe, D., Schmid, K. W., Richter, K. D., Wessel, J., Schuck, A., et al. (2000). Dose-dependent induction of transforming growth factor beta (TGF-beta) in the lung tissue of fibrosis-prone mice after thoracic irradiation. *Int. J. Radiat. Oncol. Biol. Phys.* 47 (4), 1033–1042. doi: 10.1016/S0360-3016(00)00482-X

Schaue, D., Kachikwu, E. L., and McBride, W. H. (2012). Cytokines in Radiobiological Responses: A Review. *Radiat. Res.* 178 (6), 505–523. doi: 10.1667/RR3031.1

Schoenberg, M. D., Brooks, R. E., Hall, J. J., and Schneiderman, H. (1951). Effect of x-irradiation on the hyaluronïdasehyaluronic acid system. *Arch. Biochem.* 30 (2), 333–340.

Singleton, P. A., and Lennon, F. E. (2011). Acute Lung Injury Regulation by Hyaluronan. *J. Allergy Ther.* Suppl 4, 1–9. doi: 10.4172/2155-6121.S4-003

Straub, J. M., New, J., Hamilton, C. D., Lominska, C., Shnayder, Y., and Thomas, S. M. (2015). Radiation-induced fibrosis: mechanisms and implications for therapy. *J. Cancer Res. Clin. Oncol.* 141 (11), 1985–1994. doi: 10.1007/s00432-015-1974-6

Sydlik, U., Gallitz, I., Albrecht, C., Abel, J., Krutmann, J., and Unfried, K. (2009). The Compatible Solute Ectoine Protects against Nanoparticle-induced Neutrophilic Lung Inflammation. *Am. J. Respir. Crit. Care Med.* 180 (1), 29–35. doi: 10.1164/rccm.200812-1911OC

Teder, P., Vandivier, R. W., Jiang, D., Liang, J., Cohn, L., Puré, E., et al. (2002). Resolution of lung inflammation by CD44. *Science.* 296 (5565), 155–158. doi: 10.1126/science.1069659

Venge, P., Pedersen, B., Håkansson, L., Hällgren, R., Lindblad, G., and Dahl, R. (1996). Subcutaneous administration of hyaluronan reduces the number of infectious exacerbations in patients with chronic bronchitis. *Am. J. Respir. Crit. Care Med.* 153 (1), 312–316. doi: 10.1164/ajrccm.153.1.8542136

Webber, J., Meran, S., Steadman, R., and Phillips, A. (2009). Hyaluronan Orchestrates Transforming Growth Factor-β1-dependent Maintenance of Myofibroblast Phenotype. *J. Biol. Chem.* 284 (14), 9083–9092. doi: 10.1074/jbc.M806989200

Wegrowski, J., Lefaix, J. L., and Lafuma, C. (1992). Accumulation of Glycosaminoglycans in Radiation-induced Muscular Fibrosis. *Int. J. Radiat. Biol.* 61 (5), 685–693. doi: 10.1080/09553009214551501

Wirsdörfer, F., and Jendrossek, V. (2016). The Role of Lymphocytes in Radiotherapy-Induced Adverse Late Effects in the Lung. *Front. Immunol.* 7, 591. doi: 10.3389/fimmu.2016.00591

Xu, C., Shi, Q., Zhang, L., and Zhao, H. (2018). High molecular weight hyaluronan attenuates fine particulate matter-induced acute lung injury through inhibition of ROS-ASK1-p38/JNK-mediated epithelial apoptosis. *Environ. Toxicol. Pharmacol.* 59, 190–198. doi: 10.1016/j.etap.2018.03.020

Yoshizaki, A., Iwata, Y., Komura, K., Ogawa, F., Hara, T., Muroi, E., et al. (2008). CD19 Regulates Skin and Lung Fibrosis via Toll-Like Receptor Signaling in a Model of Bleomycin-Induced Scleroderma. *Am. J. Pathol.* 172 (6), 1650–1663. doi: 10.2353/ajpath.2008.071049

Conflict of Interest: The authors declare that the research was conducted in the absence of any commercial or financial relationships that could be construed as a potential conflict of interest.

frontiers in Pharmacology

ORIGINAL RESEARCH
published: 12 November 2020
doi: 10.3389/fphar.2020.587970

Gamma Tocotrienol Protects Mice From Targeted Thoracic Radiation Injury

Vidya P. Kumar, Sasha Stone, Shukla Biswas, Neel Sharma and Sanchita P. Ghosh**

Armed Forces Radiobiology Research Institute, Uniformed Services University of the Health Sciences, Bethesda, MD, United States

Radiation injury will result in multiorgan dysfuntion leading to multiorgan failure. In addition to many factors such as radiation dose, dose rate, the severity of the injury will also depend on organ systems which are exposed. Here, we report the protective property of gamma tocotrienol (GT3) in total as well as partial body irradiation (PBI) model in C3H/HeN male mice. We have carried out PBI by targeting thoracic region (lung-PBI) using Small Animal Radiation Research Platform, an X-ray irradiator with capabilities of an image guided irradiation with a variable collimator with minimized exposure to non-targeted tissues and organs. Precise and accurate irradiation of lungs was carried out at either 14 or 16 Gy at an approximate dose rate of 2.6 Gy/min. Though a low throughput model, it is amenable to change the field size on the spot. No damage to other non-targeted organs was observed in histopathological evaluation. There was no significant change in peripheral blood counts of irradiated mice in comparison to naïve mice. Femoral bone marrow cells had no damage in irradiated mice. As expected, damage to the targeted tissue was observed in the histopathological evaluation and non-targeted tissue was found normal. Regeneration and increase of cellularity and megakaryocytes on GT3 treatment was compared to significant loss of cellularity in saline group. Peak alveolitis was observed on day 14 post-PBI and protection from alveolitis by GT3 was noted. In irradiated lung tissue, thirty proteins were found to be differentially expressed but modulated by GT3 to reverse the effects of irradiation. We propose that possible mode of action of GT3 could be Angiopoietin 2-Tie2 pathway leading to AKT/ERK pathways resulting in disruption in cell survival/angiogenesis.

Keywords: gamma tocotrienol, partial body irradiation, small animal radiation research platform, radiation injury to normal lungs, prophylactic treatment, Thoracic irradiation

OPEN ACCESS

Edited by:
Diane Riccobono, Institut de Recherche Biomédicale des Armées (IRBA), France

Reviewed by:
Sabine François, Institut de Recherche Biomédicale des Armées (IRBA), France
Amit Kunwar, Bhabha Atomic Research Centre (BARC), India

****Correspondence:***
Vidya P. Kumar
vidya.kumar.ctr@usuhs.edu
Sanchita P. Ghosh
sanchita.ghosh@usuhs.edu

Specialty section:
This article was submitted to Translational Pharmacology, a section of the journal Frontiers in Pharmacology

Received: *27 July 2020*
Accepted: *06 October 2020*
Published: *12 November 2020*

Citation:
Kumar VP, Stone S, Biswas S, Sharma N and Ghosh SP (2020) Gamma Tocotrienol Protects Mice From Targeted Thoracic Radiation Injury. Front. Pharmacol. 11:587970. doi: 10.3389/fphar.2020.587970

INTRODUCTION

Gamma tocotrienol (GT3), a naturally occurring isoform of vitamin E (Ghosh et al., 2008; Singh and Hauer-Jensen, 2016), a fat soluble antioxidant has been shown to have radioprotective properties (Ghosh et al., 2009). Further studies showed recovery of hematopoietic stem cells (HSC) and progenitor cells (HPC) in GT3 treated irradiated mice suggesting the prophylactic efficacy of GT3 was through protection of hematopoietic tissue and prevention of persistent DNA damage (Ghosh et al., 2009; Kulkarni et al., 2010). In addition to HSC and HPCs, it has been shown that GT3 mobilizes endothelial progenitor cells (EPCs) as well, by significantly increasing the levels of G-CSF and VEGF, thus ameliorating the damage to the hematopoietic system (Ray et al., 2013). The

protective efficacy of GT3 mediated through G-CSF was demonstrated by abrogating the survival of mice by neutralization of G-CSF using the antibodies (Kulkarni et al., 2013).

In addition to protection of hematopoietic injury, GT3 has been shown to ameliorate gastrointestinal (GI) injury reducing the vascular oxidative stress after TBI (Berbee et al., 2009). In the case of GI injury, plasma citrulline levels were shown to increase in GT3 group on day 7 post-TBI, indicating recovery of intestinal mucosa. This result was confirmed by reduced load of bacterial DNA in the liver in the GT3 pre-treated group when compared to vehicle group. The molecular evidence of the protection of the intestinal crypts has been shown to be due to upregulation of anti-apoptotic and downregulation of pro-apoptotic factors (Suman et al., 2013). Radiation injury to the microvasculature reduces availability of the eNOS cofactor tetrahydrobiopterin (BH4) during early post-radiation phase which in turn results in uncoupling of eNOS increasing the oxidative stress (Landmesser et al., 2003; Cosentino et al., 2008). Pre-treatment with GT3 seems to have protected the tissue by regulating the key proteins in the BH4 pathway (Berbee et al., 2011). Expression levels of several cell signaling proteins in Wnt pathway was attributed to GT3's radioprotective efficacy in mice (Cheema et al., 2018). GT3 seems to have pleiotropic effect that restores or modulates expression of key proteins that regulate various prime processes in the cell such as DNA replication, recombination and repair, development of B-cells and various immunological responses to radiation insult (Cheema et al., 2018).

Previously published studies with GT3 discussed so far were performed using TBI, where mice were exposed to whole body irradiation and lethality was primarily due to either hematopoietic failure or a combination of hematopoietic and gastrointestinal injury. Radiation lethality may occur due to multi-organ failure, depending on total absorbed dose following a radiological event. Historically, there has been a continued interest in studying the efficacy of radiation countermeasures using partial body irradiation (PBI) in order to understand the efficacy from organ specific injuries. Characterization of death due to certain organ specific injury was carried out by exposing animals to PBI such as head, trunk or lower body (pelvis, legs and tail) and dose dependent mortality was studied by probit analysis and compared it to TBI (Sato et al., 1972). The authors concluded that PBI didn't have much influence on the pattern of "daily death" or the period of peak mortality, thus characterizing the death based on syndromes as oral death for head exposure, intestinal death for trunk exposure and bone marrow death for the lower body exposure (Sato et al., 1972). Lung injury often involves degeneration and regeneration of epithelial cells, activation and infiltration of inflammatory cells, disruption of microvasculature, and excessive matrix protein production leading to thickening of the epithelial walls (McDonald et al., 1995; Fan et al., 2001; Mehta, 2005). Radiation-induced lung injury is typically manifested as pneumonitis or fibrosis within months to few years after exposure (McDonald et al., 1995; Fan et al., 2001; Mehta, 2005), however, radiation injury to the thorax may occur in early time points after exposure. Mostly, all previously published studies were performed using CD2F1 mouse model to determine the prophylactic efficacy of GT3 (Ghosh et al., 2009; Kulkarni et al., 2010; Ray et al., 2013; Singh et al., 2016). In this study, we used small animal radiation research platform (SARRP) to evaluate radiation-induced lung injury during 1-30 days post-irradiation in C3H/HeN mice and determined the prophylactic efficacy of GT3 in ameliorating lung injury through pathological and biochemical analysis. We also validated prophylactic efficacy of GT3 against the whole body gamma-radiation. In addition, we have evaluated the role of Ang-2-Tie-2-AKT pathway in the protection of lungs by pre-treatment with GT3.

MATERIALS AND METHODS

Mice

Twelve to fourteen week old C3H/HeN male mice used in these studies were purchased from Envigo Corporation, Indianapolis, IN, USA. The mice were housed in the Armed Forces Radiobiology Research Institute's (AFRRI) vivarium accredited by the Association for Assessment and Accreditation of Laboratory Animal Care-International. The animals received Harlan Teklad Rodent Diet 8604 and acidified water (pH 2.5 – 3.0) ad libitum and were housed under 12 h light/dark cycle and were acclimatized for 2 weeks before the start of each study. All procedures in these studies were performed under an approved protocol by the Department of Defense Institutional Animal Care Use Committee (IACUC) (Ghosh et al., 2009).

GT3 Formulation

Pure GT3 was obtained from Yasoo Health Inc. (Johnson City, TN, United States) (Ghosh et al., 2009) and American River Nutrition (Hadley, MA, United States). GT3 and Tween80® (final concentration 5%) were dissolved separately in small volume of ethanol (to enable uniform mixing) and mixed together and then spin-dried under vacuum. Required volume of saline was added to the tube to achieve a final concentration of either 100 or 200 mg GT3 in 0.1 ml.

Total Body Irradiation (TBI)

In the total body irradiation studies, the experimental animals received a single exposure of Co-60 gamma at an estimated dose rate of 0.6 Gy/min in the AFRRI radiation facility. The mice were placed in ventilated Lucite™ boxes arranged in an array using plastic racks during the exposure. The alanine electron spin resonance (ESR) dosimetry system (ASTM Standard E 1607-94, 1994) was used to measure dose rates to water in cores of acrylic mouse phantoms as described earlier (Ghosh et al., 2009). The radiation field was uniform within ±2%.

Thoracic Radiation (Lung-Partial Body Irradiation)

The experimental animals received an anterior-posterior-posterior-anterior (AP-PA) exposure of X-ray at an estimated

dose rate of 2.6 Gy/min in the AFRRI's SARRP radiation facility (Cho & Kazanzides, 2012). Ionization chambers and alanine dosimeters with traceability to national standards, and mouse phantoms were used to measure radiation doses at 220 kVp and 13 mA. Radiation doses were checked daily using ionization chambers. Determinations of coordinates and isocenter to establish the field of exposure was done using CT scans of the mice. Mice were anesthetized during irradiation using isoflurane. A fluoroscopic X-ray image using portal imaging camera was used to confirm the desired isocenter and field of exposure (**Supplementary Figure S1**). For lung-PBI, C3H/HeN male mice were exposed to 14 or 16 Gy doses of radiation to the lung area (below the neck to diaphragm). Irradiated mice were administered either saline or GT3 (200 mg/kg, SC) 24 h prior to PBI. All the animals were transferred to their respective cages on recovery from anesthesia with free access to food and acidified water, and monitored daily for 30 days (up to three times a day when necessary) for body weight loss, ruffled fur or any behavioral abnormalities. Mice showing signs of moribundity (significant weight loss, ruffled fur, difficulty in breathing and moving) were euthanized immediately by CO_2 inhalation exposure and cervical dislocation according to the AFRRI IACUC protocol guidelines.

Survival Study in Total Body Irradiation Model Using Cobalt-60 Gamma Radiation

C3H/HeN male mice were weighed and randomly distributed into various groups (n = 16/group). There were 16 mice per radiation dose (7.5, 8, 8.5 or 9 Gy at an approximate rate of 0.6 Gy/min) and treatment group (saline, GT3 at either 100 or 200 mg/kg body weight). The mice received SC administration (under the nape of the neck) of either GT3 or saline (the vehicle) 24 h prior to TBI. After irradiation, mice were returned to their original cages with free access to food and acidified water, and monitored daily for 30 days (up to three times a day when necessary) for body weight loss and clinical symptoms of distress and pain. Mice showing signs of moribundity were euthanized immediately by CO_2 inhalation exposure and cervical dislocation according to the AFRRI IACUC protocol guidelines. Surviving animals were euthanized at the completion of the observational period.

Blood and Tissue Collection

Blood and tissues were collected from the experimental animals at various time points post-PBI for analyses. GT3 (200 mg/kg) or saline (n = 12 per group) were administered SC 24 h prior to irradiation. In addition to the irradiated groups of animals, blood and tissues from an age-matched naïve group (n = 12) was collected at each time point. Blood was collected from inferior vena cava under anesthesia on days 1, 14, and 30. Complete blood counts (CBC) and differential analysis was performed using HESKA Element HT (TM) 5 Analyzer system. Sternum, heart, lungs, jejunum and kidney were collected and either processed for histopathological findings or snap frozen in liquid nitrogen. Femurs were collected for isolation of bone marrow cells to carry out Colony Forming Unit (CFU) Assay as described below.

Femoral BM Colony Forming Unit Assay

Clonogenicity of mouse bone marrow cells was quantified in standard semisolid cultures using 1 ml of Methocult GF+ system for mouse cells (Stem Cell Technologies Inc., Vancouver, BC) as reported earlier (Kumar et al., 2018). Briefly, colony forming units (CFU) were assayed on days 1, 14, and 30 from irradiated groups and the age-matched naïve mice. Cells from three femurs from different animals were pooled, washed twice with IMDM and seeded at 1 to 5×10^4 cells per dish in 35-mm^2 cell culture dishes (BD Biosciences). Each sample was plated in duplicate to be scored 14 days after plating. Colonies which included Granulocyte-macrophage colony forming units (CFU-GM), granulocyte-erythrocyte-monocyte-macrophage CFU (CFU-GEMM), colony-forming unit-erythroid (CFU-E) and erythroid burst-forming units (BFU-E) were counted 14 days after plating using a Nikon TS100F microscope. Fifty or more cells were considered one colony. Data are expressed as mean ± standard error of mean (SEM). Statistical significance was determined between irradiated vehicle treated and GT3-treated groups.

Sternal Histopathology

Following blood collection, animals were euthanized, and the sterna were collected. The sterna were fixed in a 20:1 volume of fixative (10% buffered formalin) to tissue for at least 24 h and up to 7 days. Fixed sterna were decalcified for 3 h in 12–18% sodium EDTA (pH 7.4–7.5) and specimens dehydrated using graded ethanol concentrations and embedded in paraffin. Longitudinal 5 μm sections were stained with regular hematoxylin and eosin (H&E) stain. The bone marrow was evaluated *in situ* within sternebrae and graded for megakaryocyte numbers averaged per 10 high power fields at 40× magnification using a BX41 Olympus microscope (Minneapolis, MN) (Kumar et al., 2018).

Histopathology of Lung, Heart and Jejunal Sections

Post-blood collection and euthanasia, collected tissue were fixed in 10% buffered formalin. Tissue sections of heart (longitudinal), lung (standard orientation, embedded on largest area) and jejunum (circular 5 μm sections) were stained with regular hematoxylin and eosin (H&E) stain. A board-certified veterinary pathologist conducted blinded histopathological evaluation of these samples (Sharma et al., 2020).

Proteome Profiler Array

Frozen lung tissue samples were homogenized using the Bullet Blender Tissue Homogenizer (Next Advance, Inc, Troy, NY, United States) in RIPA buffer with protease inhibitors, and total protein content of supernatants was determined by bicinchoninic acid assay. Proteome Profiler Mouse XL Cytokine Arrays (R&D Systems, Minneapolis, MN) were performed per the manufacturer's instructions. For each array,

supernatants from three individual animals were spotted in duplicate, and arrays were performed per condition. Naïve group was used as a control. High resolution images of the blots were analyzed using Western Vision's HLImage++ software (designed to analyze arrays from R&D systems) and GraphPad Prism 7 software (GraphPad Software, 7825 Fay Av., Suite 230, La Jolla, CA 92037, United States) was used to plot the data.

Phosphorylated Proteins From AKT Signaling Pathway

PathScan® AKT Signaling Antibody Array Kit #9700 (Cell Signaling Technology, Inc., Danvers, MA, United States) was used to detect the differential levels of phosphorylated proteins in lung lysates. Frozen lung tissue from naïve and the two irradiated groups (saline and GT3 treated) were homogenized as mentioned earlier for proteome array. The PathScan® kit was used as per the manufacturer's instructions. The data was collected and analyzed using the Odyssey CLx instrument and LiCOR analysis software (LiCor Biosciences).

Immunohistochemistry

Immunohistochemistry involved two preparatory steps – antigen retrieval and staining (Sharma et al., 2020). Unstained sections (4 μM) of formalin-fixed, paraffin-embedded specimens were deparaffinized in xylene, and hydrated in a series of ethanol dilutions (100, 95, and 80% ethanol in water) with final rinse in distilled water. Slides were then incubated for about 40 min in citrate buffer (10 mM Citric Acid, 0.05% Tween 20, pH 6.0) at 95–100°C in a water bath/steamer. At the end of this incubation, the slides were allowed to cool to room temperature, followed by rinsing with PBS-Tween 20 (0.1%). The sections were then processed for immunostaining beginning with blocking (1% BSA, 0.5% TX100 in PBS) for 30 min followed by incubation with primary antibody (Ang-2 (Cell Signaling Technology 2948S), pAKT (Cell Signaling Technology 9271S), pP38 (Cell Signaling Technology 9211S), Tie-2 (Cell Signaling Technology 09D10), pTie-2 (R&D Systems AF3909) at 4°C overnight. After washing the slides with wash buffer (1× PBS, 0.1% triton) five times for 5 min each, the sections were incubated with the secondary antibody for 2 h at room temperature. After secondary antibody incubation again slides were washed five times for 5 min each. Mounting of sections were carried out using Abcam kit (BrightMount- Aqueous Mounting Medium for Fluorescent Staining ab103746). The sections were imaged on Zeiss 700 confocal microscope.

Statistical Analysis

Survival data was plotted as a Kaplan-Meier plot and statistical significance of the survival differences was determined by log-rank test using GraphPad Prism 7 software (GraphPad Software, 7825 Fay Av., Suite 230, La Jolla, CA 92037, United States). For comparison of two different groups, statistical significance was determined using the Holm-Sidak method, with alpha = 0.05. Each pair was analyzed individually, without assuming a consistent standard deviation (SD).

RESULTS

Pre-Treatment of GT3 has Significant Survival Benefit in C3H/HeN Mice Exposed to Total Body Gamma Radiation

To evaluate efficacy of GT3 as a prophylactic countermeasure in C3H/HeN mice, 16 mice/group were administered either saline or GT3 (200 mg/kg) 24 h prior to whole body gamma irradiation. The survival efficacy was evaluated at an 8.5 Gy dose of radiation. When compared with saline group, GT3 group had 94% survival whereas only 6% in saline group, resulting in the Kaplan-Meier curve comparison by Log-rank test p value to be ≤0.0001 (**Figure 1A**). Four doses of radiation were tested to establish dose response on survival. Two doses of GT3 (100 and 200 mg/kg) were tested along with saline group for this study (n = 16 mice/group). As shown in the **Figure 1B**, at the lowest dose of radiation (7.5 Gy) tested, saline group had 50% survival whereas GT3 groups had 100% survival. Interestingly, percent survival in the drug treated group was higher at 200 mg/kg dose compared to the lower dose (100 mg/kg) at all radiation doses (8, 8.5, and 9 Gy). At 8 Gy 75% and 100% survival was observed at 100 and 200 mg/kg, respectively. At 8.5 Gy the difference was wider with 31.25% survival with 100 mg/kg but the higher GT3 dose group had much higher survival (94%). 9 Gy radiation dose was a supra-lethal to the saline group as all animals died before day 30, GT3 at 100 mg/kg also had significant mortality (survival of only 1/16 mice) in comparison to GT3 at 200 mg/kg group with 44% survival.

No Effect on Peripheral Blood Cell Counts After Targeted Irradiation in Lung

Blood was collected from naïve and 14 and 16 Gy lung-irradiated mice at different time points and was analyzed for CBC. There was no significant difference in the cell counts between the naïve and two irradiated groups (saline and GT3 treated) for both radiation doses (**Supplementary Figure S2**).

No Effect on Bone Marrow Progenitor Cell Counts Post-Partial Body Irradiation in Lung

Femoral bone marrow from naïve and 14 and 16 Gy lung-PBI groups were collected on days 1, 14, and 30 post-PBI. Clonogenic assays were carried out to evaluate the extent of damage caused by irradiation, if any. CFU assays measured CFU-GM and CFU-GEMM and BFU-E to evaluate the function of hematopoietic cells. Based on the CFU counts, there was no significant effect of irradiation on the femoral bone marrow (**Supplementary Figure S3**) as this part of the body was spared from irradiation.

Significant Recovery of Sternal Bone Marrow Cellularity Post-Partial Body Irradiation in Lung

Bone marrow architecture and cellularity of mice were evaluated on sternum samples collected on days 1, 14, and

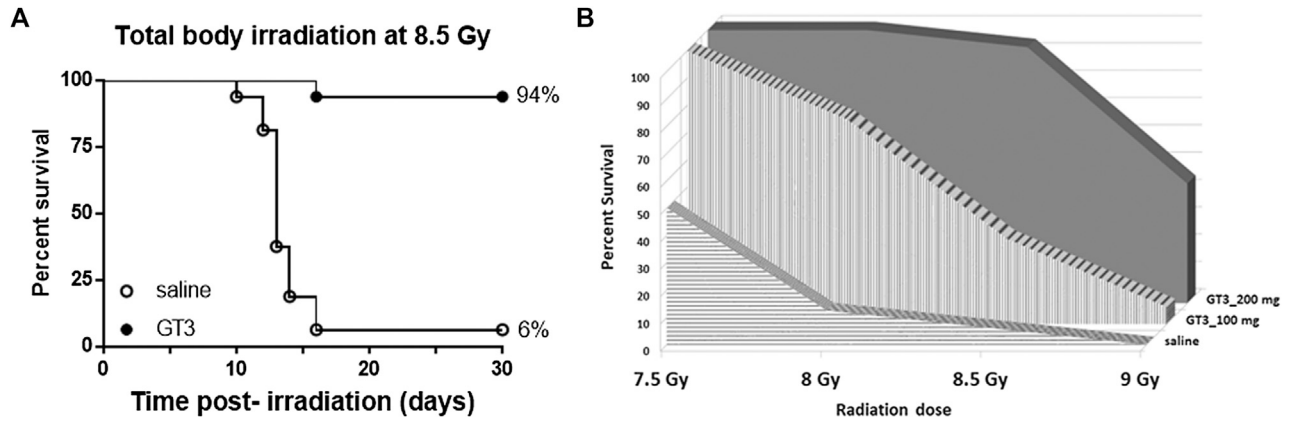

FIGURE 1 | Survival of C3H/HeN male mice following total-body irradiation at an estimated rate of 0.6 Gy/min and SC administration of a single dose of either GT3 or saline as vehicle at 24 h prior to TBI. **(A)** Kaplan-Meier survival curves were plotted using GraphPad software; n = 16 mice per group and trend in survival at 8.5 Gy is compared between vehicle (○) and GT3 (200 mg/kg) group (●) (log-rank test $p < 0.0001$). **(B)** Dose response in terms of radiation doses (7.5, 8, 8.5, and 9 Gy) and doses of GT3 (100 and 200 mg/kg) were evaluated in a 30-days survival study comparing to saline treated group (n = 16/dose of radiation/treatment group).

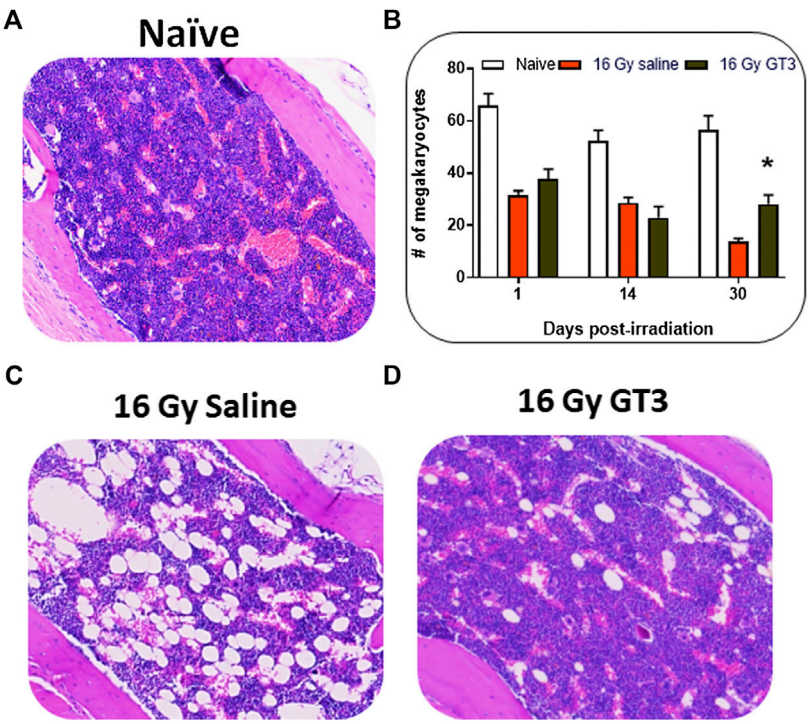

FIGURE 2 | GT3 treatment promoted sternal bone marrow hematopoietic cell recovery after 16 Gy PBI (to thorax) when administered 24 h prior to PBI. Representative sternal bone marrow sections are shown for naïve **(A)**, and from saline **(C)** and GT3 **(D)** treated 16 Gy irradiated mice from day 30 post-PBI. Bone marrow megakaryocyte numbers were quantitated from histological sections from days 1, 14, and 30 post-PBI **(B)**. Significant increase in bone marrow cellularity and megakaryocytes **(B)** were observed on day 30 post-PBI in the GT3 treatment group. Data represented are mean ± standard error of the mean (SEM) for n = 12 mice.

30 post-lung PBI. The extent of recovery from radiation damage was estimated from the H&E stained slides by quantifying the megakaryocytes. Megakaryocytes were evaluated by averaging the number of cells per 10 (40×) high-powered fields (HPFs).

When compared to naive controls, irradiated samples showed significant damage. On day 30 post-PBI, the % cellularity in the GT3 treated PBI group was significantly higher than that of the saline treated group, which was reflected in the number of megakaryocytes as well (**Figure 2**).

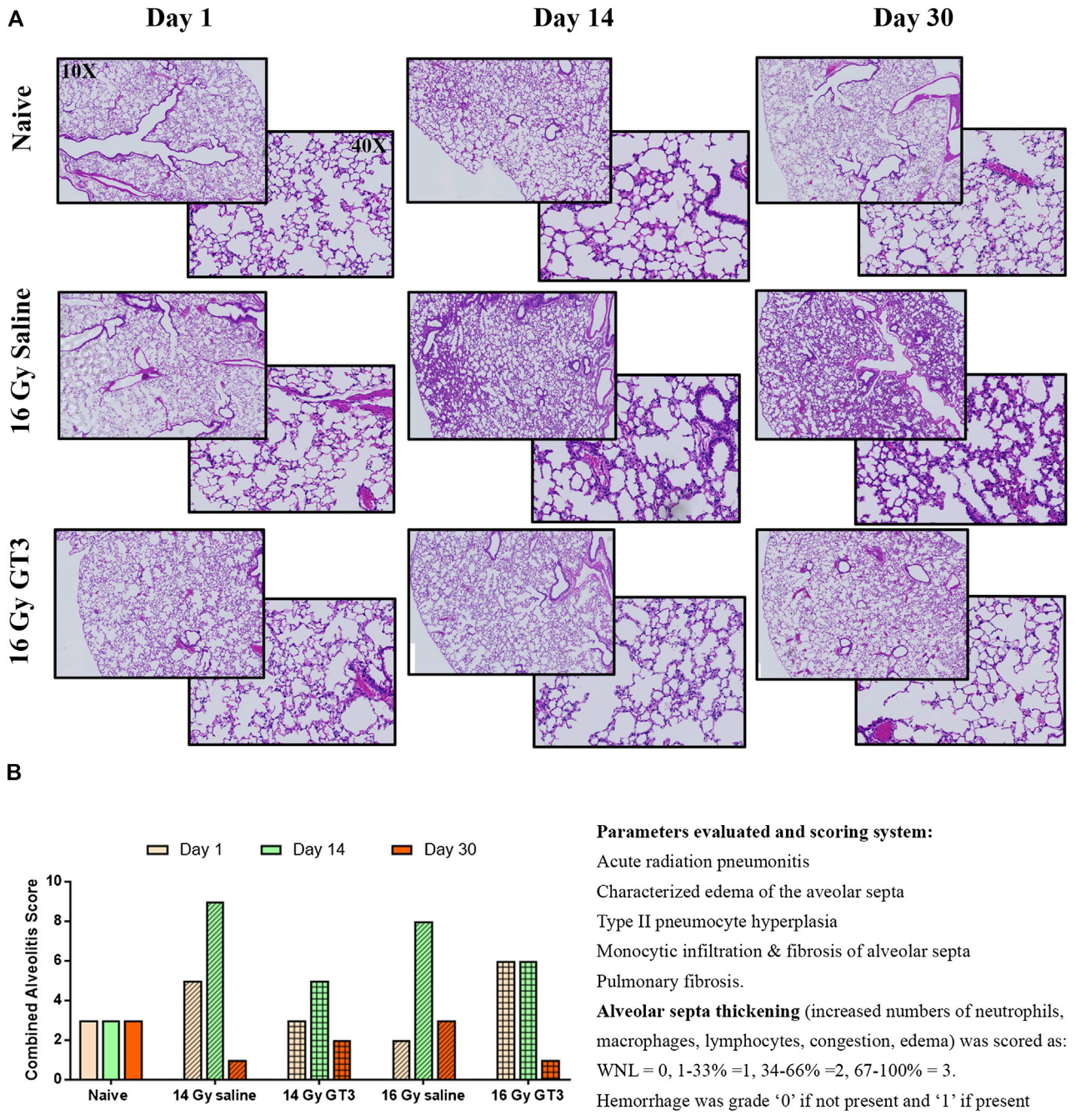

FIGURE 3 | Histopathological evaluation of lungs irradiated at 14 and 16 Gy. Representative H&E stained lung sections from 16 Gy irradiation groups in (shown as 10 and 40 magnification) **(A)** were evaluated for signs of irradiation effects such as characteristic edema of the aveolar septa, type II pneumocyte hyperplasia, monocytic infiltration and fibrosis of alveolar septa, and hyaline membranes that line alveoli; and pulmonary fibrosis. **(B)** Thickening of alveolar septa (increased numbers of neutrophils, macrophages, lymphocytes, congestion, and edema) was scored as: WNL = 0, 1–33% = 1, 34–66% = 2, 67–100% = 3. Hemorrhage was grade "0" if not present and "1" if present regardless of amount.Severe damage to the lung tissue on irradiation was observed on all three days and in both 16 and 14 Gy irradiation doses in saline treated groups. Lung tissue from GT3 treated groups showed less damage and recovery by day 30.

Histopathology of Jejunum

Jejunal tissue samples from naïve and lung-PBI (14 and 16 Gy) groups (saline and GT3 treated) were collected on days 1, 14, and 30 post-PBI and subjected to histopathological evaluation of H&E stained cross sections. There was no difference in the viable crypt count observed between naïve and saline or GT3 treated irradiated (14 and 16 Gy) groups (**Supplementary Figure S4A**).

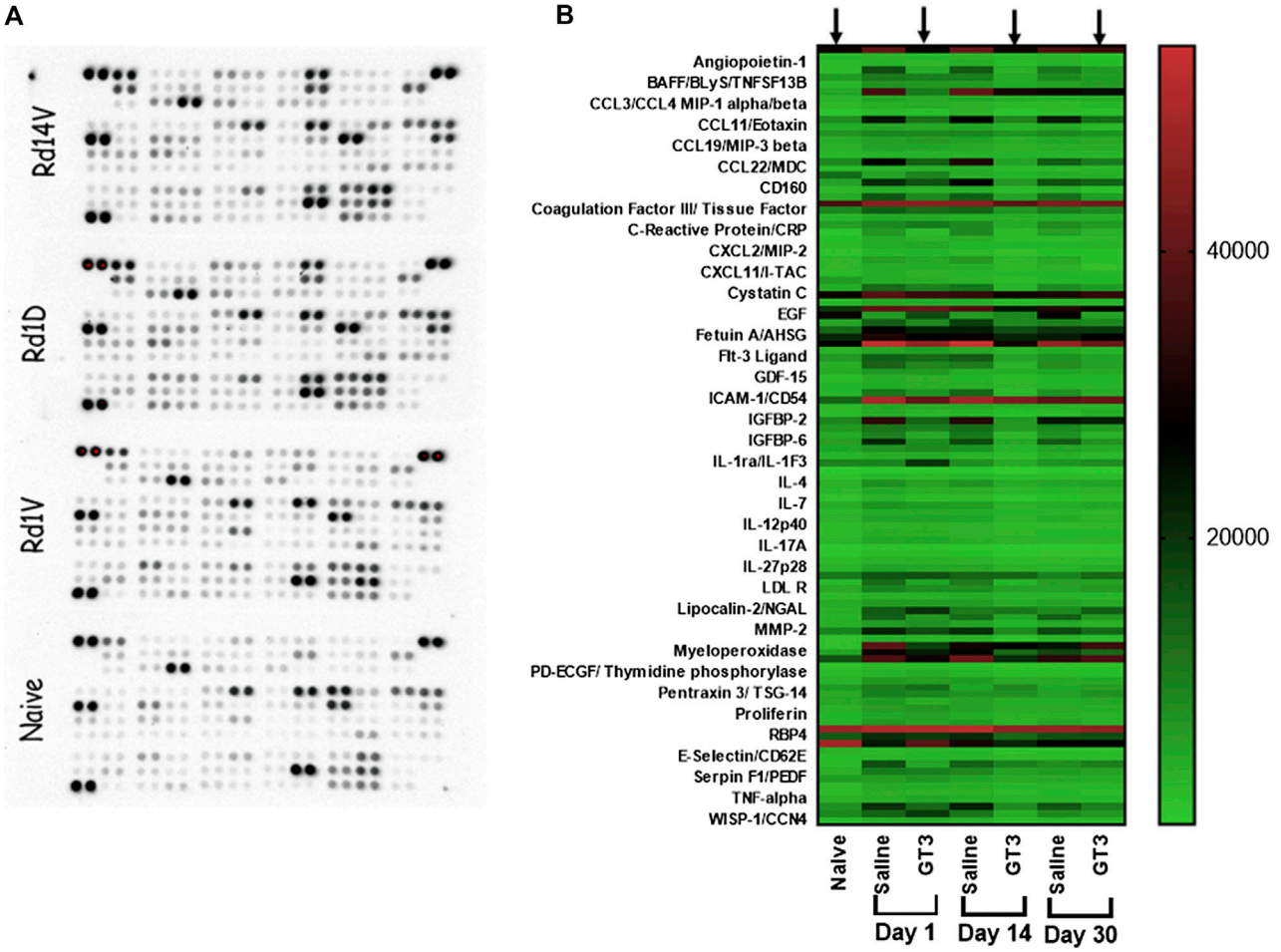

FIGURE 4 | Lung lysates were subjected to a protein Profiler Array of total of 111 cytokines by R&D Systems, a membrane-based sandwich immunoassay. In the kit the capture antibodies were spotted in duplicate on nitrocellulose membranes which bind to specific target proteins in the sample. Captured proteins are detected with biotinylated detection antibodies and visualized using chemiluminescent detection reagents. Signal produced is proportional to the amount of analyte bound. Samples from three groups–naïve, 16 Gy saline and 16 Gy GT3 treated collected on days 1, 14, 30 post-16 Gy lung-PBI were tested. Representative blots are shown in **(A)**. Normalized data from these blots are then represented as a heat-map in **(B)**. Arrows indicate data for GT3 group on different days having similar pattern as the naïve group.

Histopathology of Heart

Heart tissue from naïve and irradiated (14 and 16 Gy lung-PBI) were evaluated by the board certified pathologist for abnormalities and radiation damage. H&E stained sections were evaluated for epicardial thickening and fibrosis, myocardial fibrosis, and coronary artery disease. No effects attributable to irradiation were observed in the mice that received either a 14 or 16 Gy dose when observed at days 1, 14, and 30 post-irradiation (**Supplementary Figure S4B**).

Histopathological Analysis of Lung Sections

H&E stained sections of lung tissue from naïve and irradiated groups (lung-PBI at 14 and 16 Gy) were evaluated by the Board Certified Veterinary Pathologist. The parameters evaluated were for acute radiation pneumonitis, characterized edema of the aveolar septa, Type II pneumocyte hyperplasia, monocytic infiltration and presence of fibrosis (**Figure 3A**). Alveolitis was quantified as a cumulative score of thickening of alveolar septa and extent of hemorrhage (**Figure 3B**). Thickening of alveolar septa as a result of increased numbers of neutrophils, macrophages, lymphocytes causing congestion and edema was scored as: WNL = 0, 1–33% = 1, 34–66% = 2, 67–100% = 3. Hemorrhage was graded as 0 if not present and 1 if present regardless of the amount. Alveolar septa was observed to be multi-focally expanded by neutrophils, macrophage, lymphocytes, congestion, and rarely edema. The peak of this inflammation was seen at day 14 post-PBI. Protection from alveolitis by GT3 was observed on days 14 post-PBI when irradiated at both 14 and 16 Gy. However, by day 30, all irradiated groups showed recovery. In many lung sections on day 14, alveolar septa were multifocally expanded by neutrophils, macrophage, lymphocytes, congestion, and rarely edema. At 30 days post-irradiation, there was much less inflammation, but of interest, large, foamy macrophages were

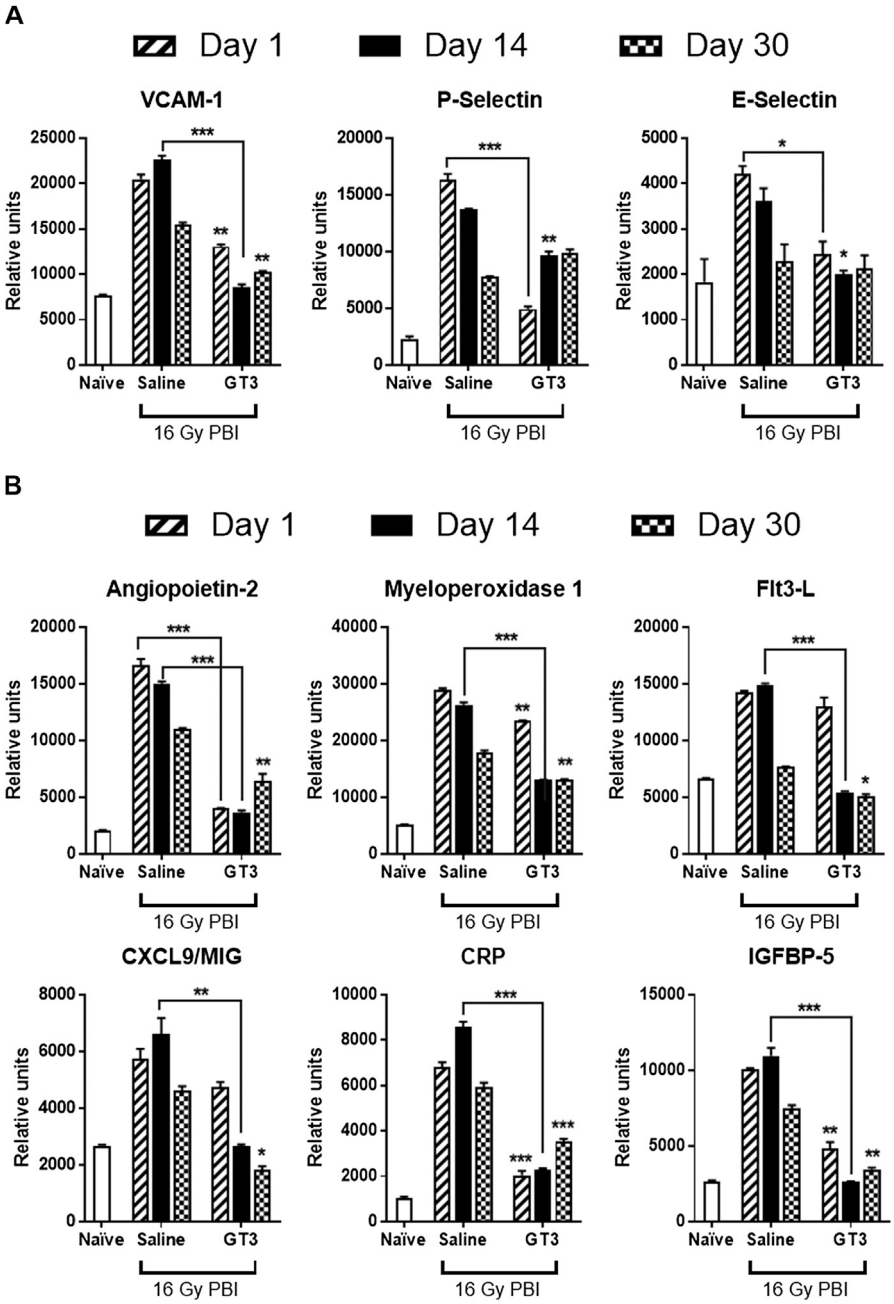

FIGURE 5 | Differential expression of cell adhesion molecules **(A)** and cytokines that were modulation by GT3 **(B)**. **(A)** From the array of 111 cytokines, three cell adhesion molecules (VACM-1, P-selectin and E-selectin) were shortlisted which had shown differential expression in irradiated saline treated group. In the case of VCAM-1 and P-selectin GT3 group showed lower expression closer to the naïve group, whereas saline treated group had much higher protein. **(B)** Six different proteins (Angiopoietin 2, myeloperoxidase 1, Flt3-L, CXCL9, CRP and IGFBP5) were picked based on their higher expression as a result of radiation injury and effective modulation by GT3. Out of the three time-points tested, maximum modulation of hyper-expression was seen on day 14 post-PBI. *p* values: * ≥0.01–0.05, **0.001–0.01, ***≤ 0.01–0.0001.

present in the lungs of irradiated mice which were not as readily apparent in the naïve controls. However, on day 1 post-PBI being too short a time to see structural damage, variations in 14 Gy saline having higher score than 16 Gy saline can be attributed to the animal to animal variation in response to the inflammatory stimuli.

Differential Expression of Inflammatory Cytokines/Chemokines due to Radiation Injury

Lung lysates from all three groups (naïve, 16 Gy PBI saline and GT3) from all three days (days 1, 14, and 30 post-PBI) were

subjected to a proteome profiler cytokine array to estimate the levels of cytokines in these samples (**Figure 4A**). To identify the proteins that were differentially expressed as a result of radiation injury, naïve group was compared to saline treated irradiated group. Effect of pre-PBI treatment by GT3 was evaluated by comparing the expression levels in irradiated saline and GT3 groups. Several cytokines were differentially expressed as a result of radiation injury and inflammation (**Figure 4B**) in saline treated groups on all days (1, 14, and 30 days post-PBI). Even though expression of some proteins were modulated by GT3 on day 1, many of them stayed similar to that in the control (saline) group, thus showing not much protection. By day 14, the expression pattern in GT3 group looked similar to that in naïve group (**Figure 4B** arrows). Vascular cell adhesion molecule-1 (VCAM-1), P-selectin, a cell adhesion molecule and E-selectin, the transmembrane receptor on the surfaces of activated endothelial cells had elevated expression after radiation and stayed high until day 30 (the last data point) (**Figure 5A**) in saline groups. Expression of the cell adhesion molecules is known to rise as response to inflammation (Nakao et al., 1995; Ramsay et al., 1996). VCAM-1 was significantly modulated by GT3 on day 14 (p value 0.0005) compared to saline group. On other days as well, the levels of VCAM-1 were significantly lower (p value 0.004–0.01) in GT3 groups compared to saline groups. On all three days, levels of P-selectin were significantly lower (p values 0.0001–0.01) whereas in the case of E-selectin except for day one (p value 0.05) there was not much difference in the two irradiated groups.

Among several other proteins that were differentially expressed, a few (**Figure 5B**) were short-listed based on the protective effects of GT3. Angiopoietin-2 (Ang-2) levels increase on radiation as seen in the saline treated groups on all three days but GT3 treated animals show significantly lower levels (p values 0.0004–0.008) of this protein in their lung. Similar results (p value $\leq$ 0.0001) were seen in the case of C - reactive protein (CRP), the inflammation response marker. Expression levels of Insulin-like growth factor-binding protein 5 (IGFBP-5) were also observed to be elevated on 16 Gy radiation and with GT3 treatment, the levels were kept significantly lower (p values 0.0005–0.002), close to the basal level. In the case of Myeloperoxidase 1 (MPO) and chemokine (C-X-C motif) ligand 9 (CXCL9), also known as monokine induced by gamma interferon (MIG), though the expression increased on irradiation, the differential effect between saline and GT3 treated groups was observed only on later time-points on days 14 and 30. Most significant effect on FMS-like tyrosine kinase 3 ligand (Flt3L) was seen on day 14 post-irradiation (p value 0.0005).

Elevated Expression of Phosphorylated Proteins From AKT Signaling Pathway, Amelioration by GT3 Pre-treatment

Lung lysates from days 1, 14, and 30 post-PBI prepared as described earlier were subjected to an analysis using an array of phosphorylated proteins from AKT signaling pathway. Expression of these phosphorylated proteins in samples from irradiated groups (saline and GT3) were compared between naïve samples. Sixteen proteins in their phosphorylated forms were assayed for their levels of expression. The changes were not significant on day 1, but on day 14 the saline group looked different from the naïve (**Figure 6A**). The pattern of expression in the GT3 group was similar to that of the naïve group. By day 30, expression of most proteins in their phosphorylated forms seemed to have recovered from the insult. Out of 16 proteins, 8 of them showed significant increase in phosphorylation with irradiation in the saline group when compared to naïve and phosphorylation of AKT (473), S6, GSK-3a and ERK were significantly inhibited in GT3 group when compared to saline group indicating amelioration by GT3 (**Figure 6B**).

Differential Expression or Phosphorylation of Proteins by Immunohistochemistry of Lung Tissue

Increased Ang-2 and pAKT expression post-PBI in lung by Immunofluorescence were inhibited by GT3 pre-treatment (**Figure 7**). In the case of Ang-2 there was barely any immunofluorescence in the naïve samples whereas Ang-2 expression increased in the saline treated group however the group administered with GT3 24 h prior to PBI had much lower immunofluorescence. This result corroborated the findings in the cytokine Protein Profiler. As Ang-2 along with Tie-2 is involved in angiogenesis (Mammoto et al., 2012), levels of Tie-2 (data not shown) and phosphorylated Tie-2 (pTie-2) were tested. There was no difference in levels of Tie-2 (total protein) between the three groups (data not shown). The expression for pTie-2 protein was found to be higher in the naïve group as compared to the irradiated saline treated group however in GT3 treated group pTie-2 florescence was higher than in saline group indicating protection against radiation. The phosphorylation of the downstream protein AKT was also increased on PBI in saline treated group compared to naïve and GT3 treated group. We did not see any difference for the phosphorylated P38 among three different groups.

DISCUSSION

This is a first study that shows the protective role of GT3 against radiation-induced lung injury in mice. Our previous studies have shown that GT3 protected CD2F1 male mice from radiation-induced mortality, improved hematopoietic and gastrointestinal recovery and also induced proliferative cytokines that may play key role in its beneficial effects on the hematopoietic system (Berbee et al., 2009; Ghosh et al., 2009; Kulkarni et al., 2010; Kulkarni et al., 2013). However these studies did not address whether GT3 is also effective in protecting against delayed effects on lungs. The anti-oxidant and anti-inflammatory properties of tocotrienols, specifically GT3 are well documented under various pathological conditions as cancer, heart diseases and diabetes (Aggarwal et al., 2010). Cardioprotective property was proposed to be through cholesterol biosynthesis whereas neuroprotective effects through glutamate-induced activation of c-Src kinase. Attenuation of diabetic conditions have been proposed via

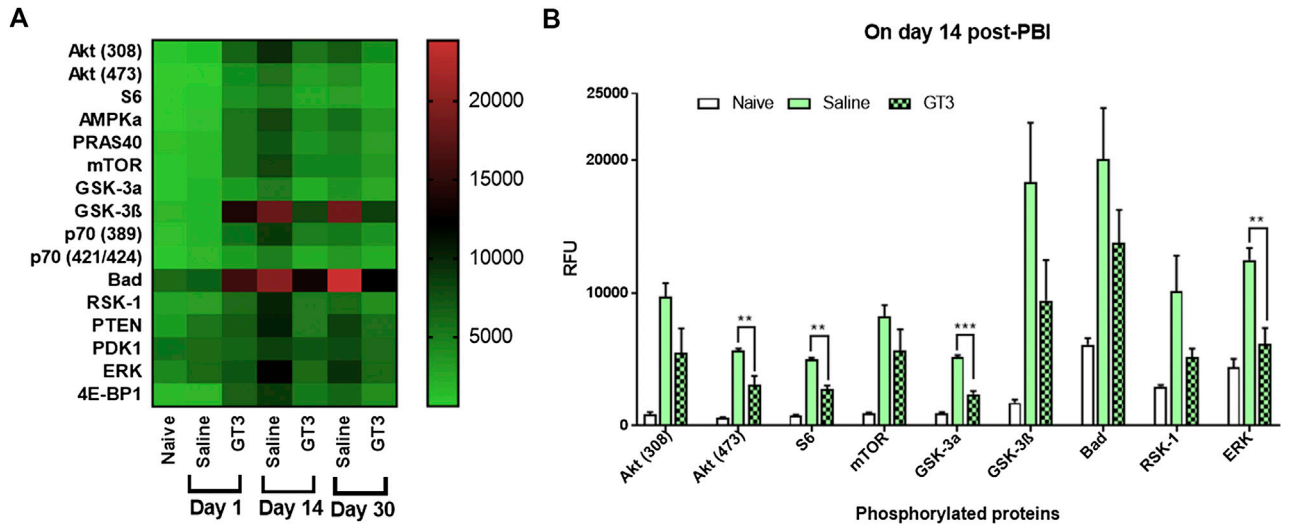

FIGURE 6 | PathScan: Sandwich assay to study differential expression of phosphorylated proteins from AKT pathway. **(A)** A heat map representing the differential expression of different targets screened for naïve and irradiated groups on three time-points. When expression in naïve were compared with the irradiated groups, changes were observed for some of the targets. **(B)** Abrogation of the changes occurring due to radiation injury was seen for some targets in GT3 treated group when compared to saline treated group. Day 14 data is represented as bar graph. **: p = 0.001–0.006, ***: $p < 0.001$.

multiple pathways some of which are modulation of oxidative-nitrosative stress, suppression of the NF-κB signaling pathway and peroxisome proliferator-activated receptor (PPAR) modulation. Because GT3 is more potent antioxidant than vitamin E alpha tocopherol, we hypothesized that GT3 will be effective in protecting against lung injury.

In a scenario of a nuclear explosion either as an accident or a deliberate attack, the most likely type of exposure to occur is partial body irradiation. There might be some shielding due to the building structures or proximity from the site of explosion (DiCarlo et al., 2011). Studying partial body irradiation has many benefits, one could study detrimental effects on a particular organ system by limiting exposure only to the organ of interest, or as stated in the FDA animal rule, just by attenuating effects of H-ARS, one could study the damage on rest of the body system (FDA, 2015). In this study, we demonstrated significant survival efficacy of GT3 pre-treatment in C3H/HeN male mice when exposed to whole body gamma radiation. In addition, we have shown that pre-treatment of GT3 could protect animals from radiation-induced thoracic injury when animals were exposed to targeted lung radiation in SARRP. C3H/HeN male mice were used in this study as they have been reported to develop early inflammation, alveolitis and fibrosis following lung radiation (O'Brien et al., 2005; Ghita et al., 2019). PBI to thorax was considered to specifically study lung damage without having to deal with either hematopoietic or GI syndrome. The choice of doses were based on the literature where lung damage was seen (O'Brien et al., 2005; Pietrofesa et al., 2013; Barshishat-Kupper et al., 2015). GT3 was administered 24 h prior to radiation exposure based on previously shown optimal time of administration (Ghosh et al., 2009). There were no surviving animals post-TBI when GT3 was administered 48, 8, 4, and 2 h prior to radiation.

We showed that radiation exposure to the thorax doesn't affect the peripheral blood parameters as expected. Even femoral bone marrow cells did not seem to have been affected as they were spared from radiation exposure. On the contrary, where the sternum was exposed to radiation, cellularity of the sternal bone marrow was severely depleted in vehicle treated animals. Sixteen Gy is a supralethal dose for C3H/HeN mice with respect to TBI and is expected to be severely damaging the bone marrow cells. But GT3 pre-treatment seems to have assisted accelerated recovery from this damage by day 30 post-PBI. In addition to bone marrow cells, the other rapidly dividing cells would be crypts in the jejunum. As the abdominal area was spared from radiation, jejunal crypts were not damaged in radiated groups when compared to naïve animals. Though heart was exposed to radiation, neither epicardial thickening, myocardial fibrosis, nor coronary artery disease was detected in the histopathological evaluation in the duration of the study (30 days). It is possible that injuries to the heart were not evident in this early time point but would have been observed as a delayed effect. In lungs, infiltration of neutrophils, macrophages, lymphocytes causing congestion after radiation (both 14 and 16 Gy), resulted in the thickening of alveolar septa which in turn lead to edema in radiated vehicle treated animals. With GT3 pre-treatment, in the early time-points, an increase in pro-inflammatory cytokines and hematopoietic growth factors such as G-CSF has been shown in irradiated as well as non-irradiated mice which in turn results in increase in neutrophils (Kulkarni et al., 2012). This could be one of the possible reason for a higher inflammatory score in 16 Gy GT3 group compared to saline group on day 1. The protective properties of GT3 were seen at all three time points days 1, 14, and 30 post-PBI, but the greatest difference was observed on day 14.

Role of Vascular cell adhesion protein 1 (VCAM-1) in inflammation and lung injury is well documented (Epperly

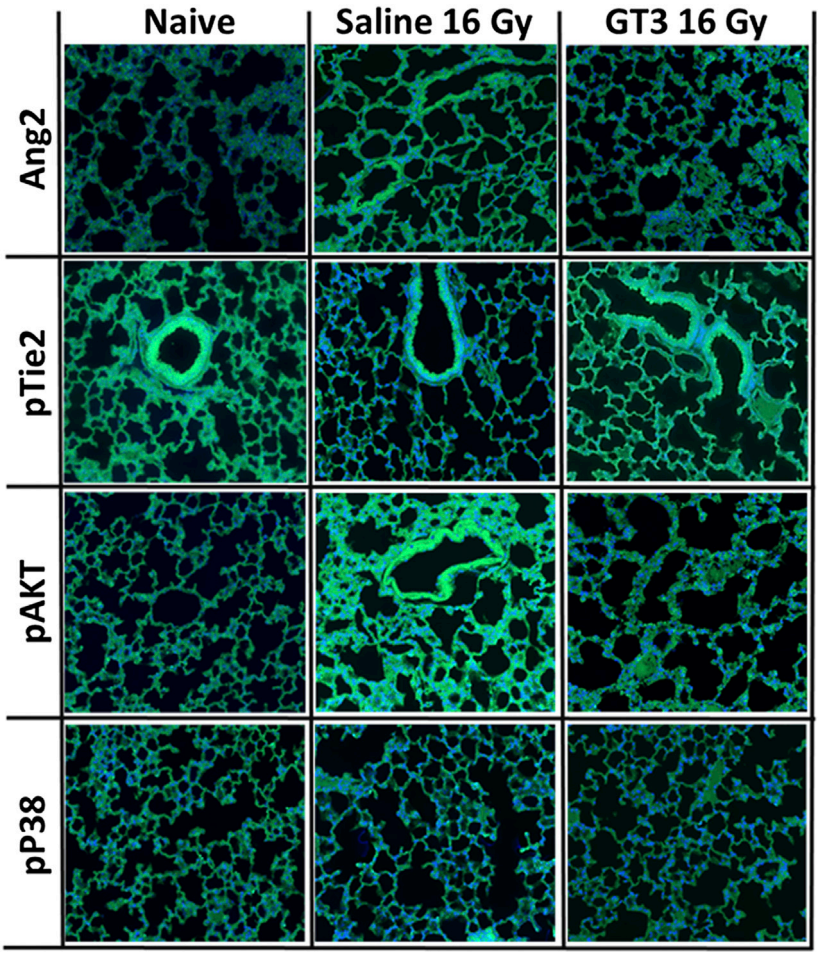

FIGURE 7 | Immunofluorescence (IF) micrographs showing the differential expression of selected proteins. Lung sections from three groups (naïve, day 14 post-PBI 16 Gy irradiated saline and GT3 treated groups) were stained with antibodies against Ang2, pTie2, pAKT and pP38 (green) and DAPI (blue).

et al., 2002; Agassandian et al., 2015). As early as day 1 post-PBI the expression levels of VCAM-1 were seen to be elevated in saline group compared to naïve. Though elevated levels of VCAM-1 have been associated with pulmonary fibrosis (Agassandian et al., 2015) its hyper-expression was seen in the early time points (days 1 and 14 post-PBI). The other two cell adhesion molecules E-selectin and P-selectin which are known to be elevated as a result of inflammation and radiation injury (Nakao et al., 1995; Ramsay et al., 1996), were found to be elevated in the saline group. GT3 could abrogate the levels of P-selectin much more effectively as compared to E-selectin. In all these three biomarkers day 14 seemed to be an important time point as the effectiveness of the countermeasure was seen maximum on this day.

Among the other biomarkers tested, Ang-2 expression was found to be significantly increased in saline group following radiation. Pre-treatment with GT3 was found to ameliorate the effect of radiation injury from early (day 1) to later times (day 30). Several other proteins showed significantly higher expression in lung tissue following radiation. Flt-3 ligand is a known biomarker of hematopoietic injury (Kumar et al., 2018), expression of which was abrogated by GT3. Inflammatory biomarker C-reactive protein (CRP) has also been shown to be an effective indicator of possible radiation pneumonitis in humans (Bai et al., 2019) which was also observed as more than 6 fold increase of the protein in saline treated animals. This increased expression is immediate as of day 1 post-PBI and stayed high even on day 30. On the other hand GT3 kept the levels significantly lower. Upregulation of pro-inflammatory chemokines induced by gamma interferon (MIG/CXCL9) has been shown in various organs as a result of radiation injury (Malik et al., 2010; Lierova et al., 2018). Over expression of Insulin like Growth Factor Binding Protein 5 (IGFBP-5) has been correlated with cellular senescence (Kim et al., 2007) and also identified as profibrotic factor which could be an important target for antifibrotic therapies in the case of Idiopathic Pulmonary Fibrosis (Sureshbabu et al., 2011). Exposure to 16 Gy radiation resulted in increased expression of IGFBP-5 in lung tissue of animals treated with saline. On the other hand, GT3 treated group showed similar levels of the protein as in the naïve, healthy

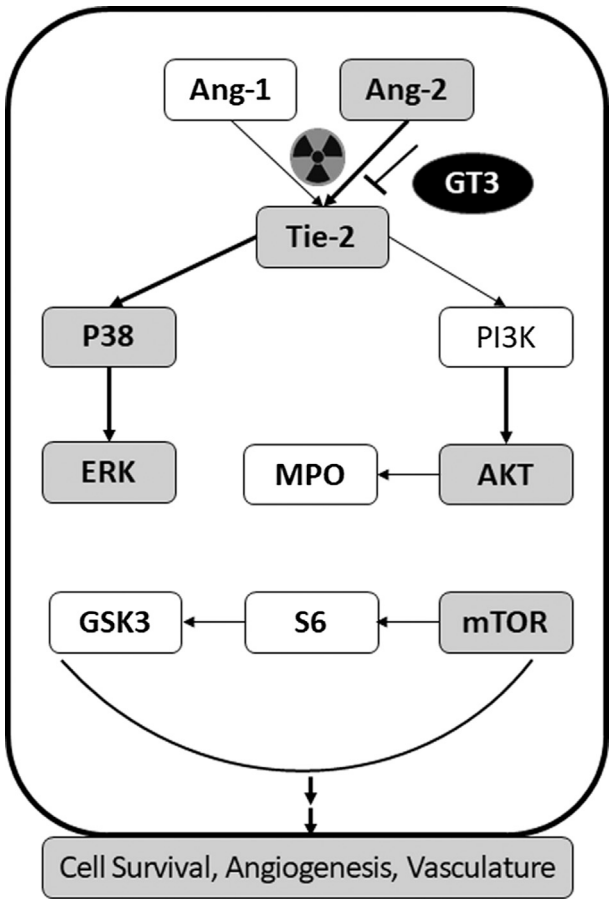

FIGURE 8 | Schematic of the proposed mechanisms of action of GT3. From various assays and methods of detection determining the differential expression of various target proteins from Ang2-Tie2 pathway affecting the downstream pathways AKT and P38 pathways resulting an ultimate effect on cell survival, angiogenesis and vasculature of the lung tissue.

animals. Myeloperoxidase (MPO) has a significant role in inflammatory diseases (Malle et al., 2007; Nussbaum et al., 2013). Radiation insult to the lungs resulted in neutrophil accumulation indicated by the combined alveolitis score, which in turn resulted in significant overexpression of MPO saline treated group. GT3 was able to abrogate the effect on days 14 and 30 post-PBI. Some of the proteins discussed above (Ang-2, MIG, and IGFBP-5) would lead to changes in the AKT inflammatory pathway. Activation of phosphorylation of AKT as a result of radiation exposure has been previously studied in endothelial cells (Edwards et al., 2002; Zingg et al., 2004). Systematic characterization using specific inhibitors led to the role of various growth factors and protein kinases triggering the signal transduction resulting in the increase in the down-stream AKT phosphorylation (Edwards et al., 2002; Zingg et al., 2004). In this study, the phosphorylation of the AKT pathway proteins was studied with respect to differential effects due to radiation injury as well as abrogation of this effect due to GT3 pre-treatment. Delta tocotrienol, another vitamin-E isomer, has been shown to have a radioprotective effect through stimulation of ERK activation-associated mTOR survival pathways (Li et al., 2010).

Authors have shown that proteins that regulate angiogenesis, Ang-1 and Ang-2 have opposing functions in inflammation where Ang-1 mitigates vascular inflammation and leakage, and Ang-2 sensitizes the endothelium to inflammatory cytokines (Makinde and Agrawal, 2011; Gavalas et al., 2013). Downstream of Tie-2 protein is known to regulate inflammation by inhibition of surface adhesion molecule expression ICAM-1 and vascular cell adhesion molecule-1 VCAM-1 (Kim et al., 2001). Increased expression of these cell adhesion molecules was observed in saline treated mice following lung radiation and was inhibited to some extent by GT3 treatment.

Based on these results as described above, we propose the possible mechanism of action of GT3 in protecting lungs from radiation injury to be via Ang-2/Tie-2 signaling pathway (**Figure 8**). This was validated by Ang-2 immunohistochemistry (IHC) of lung tissue from naïve and the two irradiated groups (saline and GT3 treated) where it was clear that the phosphorylation of Tie-2 was inhibited as a result of overexpression of Ang-2 which in turn affected the downstream phosphorylation of AKT as observed both by sandwich immune assay and IHC. On the contrary, there was no effect seen in the phosphorylation of P38 in lung tissue. There was no change in the expression levels of Tie-2 protein on radiation (data not shown).

In conclusion, the pre-treatment of GT3 confers protection to lungs by restoring cellularity and megakaryocytes in sternal bone marrow and lowering the occurrence of alveolitis on day 14 post-PBI. As a result of radiation, there is an increase in the expression of Ang-2 which in turn inhibits phosphorylation of Tie-2. This further increased the phosphorylation of AKT cascading the detrimental effects to downstream processes. Prophylactic administration of GT3 to animals before thoracic radiation, regulated Ang-2/Tie-2/ERK/AKT protein expression. Therefore, we propose a possible mechanism of action of GT3 to be via Ang-2-Tie-2 pathway leading to AKT/ERK pathway affecting the cell survival/angiogenesis.

DATA AVAILABILITY STATEMENT

The raw data supporting the conclusions of this article will be made available by the authors, without undue reservation.

AUTHOR CONTRIBUTIONS

Conceived and designed the experiments: VK and SG Performed the experiments. VK, SS, SB and NS. Analyzed the data: VK, SB, SS. Wrote the paper: VK and SG.

FUNDING

CDMRP (grant#W81XWH-15-2-0054) to SG.

ACKNOWLEDGMENTS

The authors gratefully acknowledge pathologists LTC Culp (USUHS) for histopathological evaluations of slides, the dosimetrists and SARRP operators Sungyop Kim and Dr. David A. Schauer, Kefale Wuddie and Zemenu Aschenake for animal care and manipulations, Dr. Kushal Chakraborty and Betre Legesse for technical assistance, and Anne Trias (American River Nutrition) for providing GT3. The opinions and assertions expressed herein are those of the authors and do not necessarily reflect the official policy or position of the Uniformed Services University or the Department of Defense.

SUPPLEMENTARY MATERIAL

The Supplementary Material for this article can be found online at: https://www.frontiersin.org/articles/10.3389/fphar.2020.587970/full#supplementary-material

REFERENCES

Agassandian, M., Tedrow, J. R., Sembrat, J., Kass, D. J., Zhang, Y., Goncharova, E. A., et al. (2015). VCAM-1 is a TGF-beta1 inducible gene upregulated in idiopathic pulmonary fibrosis. *Cell Signal* 27 (12), 2467–2473. doi:10.1016/j.cellsig.2015.09.003

Aggarwal, B. B., Sundaram, C., Prasad, S., and Kannappan, R. (2010). Tocotrienols, the vitamin E of the 21st century: its potential against cancer and other chronic diseases. *Biochem. Pharmacol.* 80 (11), 1613–1631. doi:10.1016/j.bcp.2010.07.043

ASTM Standard E 1607-94 (1994) Standard practice for use of the alanine-EPR dosimetry system. American Society for Testing and Materials: Philadelphia, PA.

Bai, L., Zhou, B.-S., and Zhao, Y.-X. (2019). Dynamic changes in T-cell subsets and C-reactive protein after radiation therapy in lung cancer patients and correlation with symptomatic radiation pneumonitis treated with steroid therapy. *Canc. Manag. Res.* 11, 7925–7931. doi:10.2147/CMAR.S209286

Barshishat-Kupper, M., McCart, E. A., Freedy, J. G., Tipton, A. J., Nagy, V., Kim, S. Y., et al. (2015). Protein oxidation in the lungs of C57BL/6J mice following X-irradiation. *Proteomes* 3 (3), 249–265. doi:10.3390/proteomes3030249

Berbee, M., Fu, Q., Boerma, M., Pathak, R., Zhou, D., Kumar, K. S., et al. (2011). Reduction of radiation-induced vascular nitrosative stress by the vitamin E analog gamma-tocotrienol: evidence of a role for tetrahydrobiopterin. *Int. J. Radiat. Oncol. Biol. Phys.* 79 (3), 884–891. doi:10.1016/j.ijrobp.2010.08.032

Berbée, M., Fu, Q., Boerma, M., Wang, J., Kumar, K. S., and Hauer-Jensen, M. (2009). gamma-Tocotrienol ameliorates intestinal radiation injury and reduces vascular oxidative stress after total-body irradiation by an HMG-CoA reductase-dependent mechanism. *Radiat. Res.* 171 (5), 596–605. doi:10.1667/RR1632.1

Cheema, A. K., Byrum, S. D., Sharma, N. K., Altadill, T., Kumar, V. P., Biswas, S., et al. (2018). Proteomic changes in mouse spleen after radiation-induced injury and its modulation by gamma-tocotrienol. *Radiat. Res.* 190 (5), 449–463. doi:10.1667/RR15008.1

Cho, N. B., and Kazanzides, P. (2012). A treatment planning system for the small animal radiation research platform (SARRP) based on 3D slicer. *Midas. J.*, 1–8.

Cosentino, F., Hurlimann, D., Delli Gatti, C., Chenevard, R., Blau, N., Alp, N. J., et al. (2008). Chronic treatment with tetrahydrobiopterin reverses endothelial dysfunction and oxidative stress in hypercholesterolaemia. *Heart* 94 (4), 487–492. doi:10.1136/hrt.2007.122184

DiCarlo, A. L., Maher, C., Hick, J. L., Hanfling, D., Dainiak, N., Chao, N., et al. (2011). Radiation injury after a nuclear detonation: medical consequences and the need for scarce resources allocation. *Disaster Med. Public Health Prep.* 5 (Suppl 1), S32–S44. doi:10.1001/dmp.2011.17

Edwards, E, Geng, L, Tan, J, Onishko, H, Donnelly, E, and Hallahan, D. E. (2002). Phosphatidylinositol 3-kinase/Akt signaling in the response of vascular endothelium to ionizing radiation. *Cancer Res.* 62 (16), 4671–4677.

Epperly, M. W., Sikora, C. A., DeFilippi, S. J., Gretton, J. E., Bar-Sagi, D., Archer, H., et al. (2002). Pulmonary irradiation-induced expression of VCAM-I and ICAM-I is decreased by manganese superoxide dismutase-plasmid/liposome (MnSOD-PL) gene therapy. *Biol. Blood Marrow Transplant.* 8 (4), 175–187. doi:10.1053/bbmt.2002.v8.pm12014807

Fan, M., Marks, L. B., Lind, P., Hollis, D., Woel, R. T., Bentel, G. G., et al. (2001). Relating radiation-induced regional lung injury to changes in pulmonary function tests. *Int. J. Radiat. Oncol. Biol. Phys.* 51 (2), 311–317. doi:10.1016/s0360-3016(01)01619-4

FDA (2015). Guidance for industry: product developoment under the animal rule. Available at: http://www.fda.gov/downloads/Drugs/GuidanceComplianceRegulatoryInformation/Guidances/UCM399217.pdf

Gavalas, N., Liontos, M., Trachana, S.-P., Bagratuni, T., Arapinis, C., Liacos, C., et al. (2013). Angiogenesis-related pathways in the pathogenesis of ovarian cancer. *Int. J. Mol. Sci.* 14 (8), 15885–15909. doi:10.3390/ijms140815885

Ghita, M., Dunne, V. L., McMahon, S. J., Osman, S. O., Small, D. M., Weldon, S., et al. (2019). Preclinical evaluation of dose-volume effects and lung toxicity occurring in and out-of-field. *Int. J. Radiat. Oncol. Biol. Phys.* 103 (5), 1231–1240. doi:10.1016/j.ijrobp.2018.12.010

Ghosh, S., Hauer-Jensen, M., and Kumar, K. S. (2008). "Chemistry of tocotrienols," in *Tocotrienols–vitamin E beyond tocopherols*. Editors R. R. Watson and V. R. Preedy (Boca Raton, FL: CRCPress), 379–398.

Ghosh, S. P., Kulkarni, S., Hieber, K., Toles, R., Romanyukha, L., Kao, T. C., et al. (2009). Gamma-tocotrienol, a tocol antioxidant as a potent radioprotector. *Int. J. Radiat. Biol.* 85 (7), 598–606. doi:10.1080/09553000902985128

Kim, I., Moon, S. O., Park, S. K., Chae, S. W., and Koh, G. Y. (2001). Angiopoietin-1 reduces VEGF-stimulated leukocyte adhesion to endothelial cells by reducing ICAM-1, VCAM-1, and E-selectin expression. *Circ. Res.* 89 (6), 477–479. doi:10.1161/hh1801.097034

Kim, K. S., Seu, Y. B., Baek, S. H., Kim, M. J., Kim, K. J., Kim, J. H., et al. (2007). Induction of cellular senescence by insulin-like growth factor binding protein-5 through a p53-dependent mechanism. *Mol. Biol. Cell* 18 (11), 4543–4552. doi:10.1091/mbc.e07-03-0280

Kulkarni, S., Ghosh, S. P., Satyamitra, M., Mog, S., Hieber, K., Romanyukha, L., et al. (2010). Gamma-tocotrienol protects hematopoietic stem and progenitor cells in mice after total-body irradiation. *Radiat. Res.* 173 (6), 738–747. doi:10.1667/RR1824.1

Kulkarni, S., Singh, P. K., Ghosh, S. P., Posarac, A., and Singh, V. K. (2013). Granulocyte colony-stimulating factor antibody abrogates radioprotective efficacy of gamma-tocotrienol, a promising radiation countermeasure. *Cytokine* 62 (2), 278–285. doi:10.1016/j.cyto.2013.03.009

Kulkarni, S. S., Cary, L. H., Gambles, K., Hauer-Jensen, M., Kumar, K. S., and Ghosh, S. P. (2012). Gamma-tocotrienol, a radiation prophylaxis agent, induces high levels of granulocyte colony-stimulating factor. *Int. Immunopharmacol.* 14 (4), 495–503. doi:10.1016/j.intimp.2012.09.001

Kumar, V. P., Biswas, S., Sharma, N. K., Stone, S., Fam, C. M., Cox, G. N., et al. (2018). PEGylated IL-11 (BBT-059): a novel radiation countermeasure for hematopoietic acute radiation syndrome. *Health Phys.* 115 (1), 65–76. doi:10.1097/HP.0000000000000841

Landmesser, U., Dikalov, S., Price, S. R., McCann, L., Fukai, T., Holland, S. M., et al. (2003). Oxidation of tetrahydrobiopterin leads to uncoupling of endothelial cell nitric oxide synthase in hypertension. *J. Clin. Invest.* 111 (8), 1201–1209. doi:10.1172/JCI14172

Li, X. H., Fu, D., Latif, N. H., Mullaney, C. P., Ney, P. H., Mog, S. R., et al. (2010). Delta-tocotrienol protects mouse and human hematopoietic progenitors from gamma-irradiation through extracellular signal-regulated kinase/mammalian target of rapamycin signaling. *Haematologica* 95 (12), 1996–2004. doi:10.3324/haematol.2010.026492

Lierova, A., Jelicova, M., Nemcova, M., Proksova, M., Pejchal, J., Zarybnicka, L., et al. (2018). Cytokines and radiation-induced pulmonary injuries. *J. Radiat. Res.* 59 (6), 709–753. doi:10.1093/jrr/rry067

Makinde, T. O., and Agrawal, D. K. (2011). Increased expression of angiopoietins and Tie2 in the lungs of chronic asthmatic mice. *Am. J. Respir. Cell Mol. Biol.* 44 (3), 384–393. doi:10.1165/rcmb.2009-0330OC

Malik, I. A., Moriconi, F., Sheikh, N., Naz, N., Khan, S., Dudas, J., et al. (2010). Single-dose gamma-irradiation induces up-regulation of chemokine gene expression and recruitment of granulocytes into the portal area but not into other regions of rat hepatic tissue. *Am. J. Pathol.* 176 (4), 1801–1815. doi:10.2353/ajpath.2010.090505

Malle, E., Furtmüller, P. G., Sattler, W., and Obinger, C. (2007). Myeloperoxidase: a target for new drug development? *Br. J. Pharmacol.* 152 (6), 838–854. doi:10.1038/sj.bjp.0707358

Mammoto, T., Chen, J., Jiang, E., Jiang, A., Smith, L. E., Ingber, D. E., et al. (2012). LRP5 regulates development of lung microvessels and alveoli through the angiopoietin-Tie2 pathway. *PLoS One* 7 (7), e41596. doi:10.1371/journal.pone.0041596

McDonald, S., Rubin, P., Phillips, T. L., and Marks, L. B. (1995). Injury to the lung from cancer therapy: clinical syndromes, measurable endpoints, and potential scoring systems. *Int. J. Radiat. Oncol. Biol. Phys.* 31 (5), 1187–1203. doi:10.1016/0360-3016(94)00429-O

Mehta, V. (2005). Radiation pneumonitis and pulmonary fibrosis in non-small-cell lung cancer: pulmonary function, prediction, and prevention. *Int. J. Radiat. Oncol. Biol. Phys.* 63 (1), 5–24. doi:10.1016/j.ijrobp.2005.03.047

Nakao, A., Hasegawa, Y., Tsuchiya, Y., and Shimokata, K. (1995). Expression of cell adhesion molecules in the lungs of patients with idiopathic pulmonary fibrosis. *Chest* 108 (1), 233–239. doi:10.1378/chest.108.1.233

Nussbaum, C., Klinke, A., Adam, M., Baldus, S., and Sperandio, M. (2013). Myeloperoxidase: a leukocyte-derived protagonist of inflammation and cardiovascular disease. *Antioxidants Redox Signal.* 18 (6), 692–713. doi:10.1089/ars.2012.4783

O'Brien, T. J., Létuvé, S., and Haston, C. K. (2005). Radiation-induced strain differences in mouse alveolar inflammatory cell apoptosis. *Can. J. Physiol. Pharmacol.* 83 (1), 117–122. doi:10.1139/y05-005

Pietrofesa, R., Turowski, J., Tyagi, S., Dukes, F., Arguiri, E., Busch, T. M., et al. (2013). Radiation mitigating properties of the lignan component in flaxseed. *BMC Cancer* 13, 179. doi:10.1186/1471-2407-13-179

Ramsay, P. L., Geske, R. S., Montgomery, C. A., and Welty, S. E. (1996). Increased soluble E-Selectin is associated with lung inflammation, and lung injury in hyperoxia-exposed rats. *Toxicol. Lett.* 87 (2–3), 157–165. doi:10.1016/0378-4274(96)03773-3

Ray, S., Kulkarni, S. S., Chakraborty, K., Pessu, R., Hauer-Jensen, M., Kumar, K. S., et al. (2013). Mobilization of progenitor cells into peripheral blood by gamma-tocotrienol: a promising radiation countermeasure. *Int. Immunopharm.* 15 (3), 557–564. doi:10.1016/j.intimp.2012.12.034

Sato, F., Tsuchihashi, S., Nakamura, W., and Eto, H. (1972). LD50(30)s and daily death distributions of whole or partial body irradiated mice. *J. Radiat. Res.* 13 (2), 100–108. doi:10.1269/jrr.13.100

Sharma, N. K., Holmes-Hampton, G. P., Kumar, V. P., Biswas, S., Wuddie, K., Stone, S., et al. (2020). Delayed effects of acute whole body lethal radiation exposure in mice pre-treated with BBT-059. *Sci. Rep.* 10 (1), 6825. doi:10.1038/s41598-020-63818-7

Singh, V. K., and Hauer-Jensen, M. (2016). Gamma-tocotrienol as a promising countermeasure for acute radiation syndrome: current status. *Int. J. Mol. Sci.* 17 (5), 663. doi:10.3390/ijms17050663

Singh, V. K., Kulkarni, S., Fatanmi, O. O., Wise, S. Y., Newman, V. L., Romaine, P. L., et al. (2016). Radioprotective efficacy of gamma-tocotrienol in nonhuman primates. *Radiat. Res.* 185 (3), 285–298. doi:10.1667/RR14127.1

Suman, S., Datta, K., Chakraborty, K., Kulkarni, S. S., Doiron, K., Fornace, A. J., Jr., et al. (2013). Gamma tocotrienol, a potent radioprotector, preferentially upregulates expression of anti-apoptotic genes to promote intestinal cell survival. *Food Chem. Toxicol.* 60, 488–496. doi:10.1016/j.fct.2013.08.011

Sureshbabu, A., Tonner, E., Allan, G. J., and Flint, D. J. (2011). Relative roles of TGF-beta and IGFBP-5 in idiopathic pulmonary fibrosis. *Pulm. Med.* 2011, 517687. doi:10.1155/2011/517687

Zingg, D., Riesterer, O., Fabbro, D., Glanzmann, C., Bodis, S., and Pruschy, M. (2004). Differential activation of the phosphatidylinositol 3'-kinase/Akt survival pathway by ionizing radiation in tumor and primary endothelial cells. *Cancer Res.* 64 (15), 5398–5406. doi:10.1158/0008-5472.CAN-03-3369

Conflict of Interest: The authors declare that the research was conducted in the absence of any commercial or financial relationships that could be construed as a potential conflict of interest.

frontiers in Pharmacology

ORIGINAL RESEARCH
published: 29 January 2021
doi: 10.3389/fphar.2020.607580

Bardoxolone-Methyl (CDDO-Me) Impairs Tumor Growth and Induces Radiosensitization of Oral Squamous Cell Carcinoma Cells

*Cornelius Hermann[1], Simon Lang[2], Tanja Popp[1], Susanne Hafner[3], Dirk Steinritz[2], Alexis Rump[1], Matthias Port[1] and Stefan Eder[1,4]**

[1]Bundeswehr Institute of Radiobiology, Munich, Germany, [2]Bundeswehr Institute of Pharmacology and Toxicology, Munich, Germany, [3]Institute of Pharmacology of Natural Products and Clinical Pharmacology, University of Ulm, Ulm, Germany, [4]Institute and Outpatient Clinic for Occupational, Social and Environmental Medicine, Inner City Clinic, University Hospital of Munich (LMU), Munich, Germany

Radiotherapy represents a common treatment strategy for patients suffering from oral squamous cell carcinoma (OSCC). However, application of radiotherapy is immanently limited by radio-sensitivity of normal tissue surrounding the tumor sites. In this study, we used normal human epithelial keratinocytes (NHEK) and OSCC cells (Cal-27) as models to investigate radio-modulating and anti-tumor effects of the synthetic triterpenoid 2-cyano-3,12-dioxooleana-1,9,-dien-28-oic acid methyl ester (CDDO-Me). Nanomolar CDDO-Me significantly reduced OSCC tumor xenograft-growth *in-ovo* applying the chick chorioallantoic membrane (CAM) assay. In the presence of CDDO-Me reactive oxygen species (ROS) were found to be reduced in NHEK when applying radiation doses of 8 Gy, whereas ROS levels in OSCC cells rose significantly even without radiation. In parallel, CDDO-Me was shown to enhance metabolic activity in malignant cells only as indicated by significant accumulation of reducing equivalents NADPH/NADH. Furthermore, antioxidative heme oxygenase-1 (HO-1) levels were only enhanced in NHEK and not in the OSCC cell line, as shown by immunoblotting. Clonogenic survival was left unchanged by CDDO-Me treatment in NHEK but revealed to be abolished almost completely in OSCC cells. Our results indicate anti-cancer and radio-sensitizing effects of CDDO-Me treatment in OSCC cells, whereas nanomolar CDDO-Me failed to provoke clear detrimental consequences in non-malignant keratinocytes. We conclude, that the observed differential aftermath of CDDO-Me treatment in malignant OSCC and non-malignant skin cells may be utilized to broaden the therapeutic range of clinical radiotherapy.

Keywords: oral squamous cell carcinoma, radiotherapy, reactive oxygen species, heme oxygenase-1, bardoxolone-methyl

OPEN ACCESS

Edited by:
Diane Riccobono, Institut de Recherche Biomédicale des Armées (IRBA), France

Reviewed by:
Benoit Paquette, University of Sherbrooke, Canada
Rabah Iratni, United Arab Emirates University, United Arab Emirates

****Correspondence:***
Stefan Eder
stefanfriedricheder@bundeswehr.org

Specialty section:
This article was submitted to Translational Pharmacology, a section of the journal Frontiers in Pharmacology

Received: *17 September 2020*
Accepted: *09 December 2020*
Published: *29 January 2021*

Citation:
Hermann C, Lang S, Popp T, Hafner S, Steinritz D, Rump A, Port M and Eder S (2021) Bardoxolone-Methyl (CDDO-Me) Impairs Tumor Growth and Induces Radiosensitization of Oral Squamous Cell Carcinoma Cells. Front. Pharmacol. 11:607580. doi: 10.3389/fphar.2020.607580

INTRODUCTION

Malignancies of the oral cavity are among the most common cancers within the European Union. According to estimates of the European Cancer Information System (ECIS) over 45,000 cancer cases of the lip and oral cavity were diagnosed in 2018, representing a crude incidence rate of 8.9 per 100,000 (Likhtarev et al., 2006). Despite advances in modern multidisciplinary treatment modalities

comprising surgery, radio-chemotherapy and targeted pharmacological therapy, the overall outcome of oral squamous cell carcinoma (OSCC) patients still remains dissatisfying (De Felice et al., 2018). Therefore, scientific efforts have previously been made to overcome clinical limitations and side-effects of OSCC treatment regimes. The therapeutic window for radiotherapy is mainly narrowed by local side effects mainly due to damage of surrounding normal tissue when targeting cancer sites. Aside from the recent implementation and constant advancement of intensity-modulated radiotherapy (IMRT), a further strategy to restrict radiation doses for neighboring normal cells lies within the identification of small-molecule drugs allowing for the radio-sensitization of cancer cells and ideally with a radio-protective effect on healthy tissue (Lindemann et al., 2018; Ho et al., 2019; Morra et al., 2019).

The synthetic oleanane triterpenoid 2-cyano-3,12-dioxooleana-1,9,-dien-28-oic acid (CDDO) and its C-28 methyl ester (CDDO-Me, Bardoxolone-methyl) has been shown to exert beneficial therapeutic activities by suppressing inflammation and oxidative stress *in vitro* and *in vivo* at low nanomolar concentrations (Liby and Sporn, 2012). The BEACON-study (ClinicalTrials.gov Identifier: NCT01351675), a randomized, placebo-controlled phase 3 clinical trial, evaluated

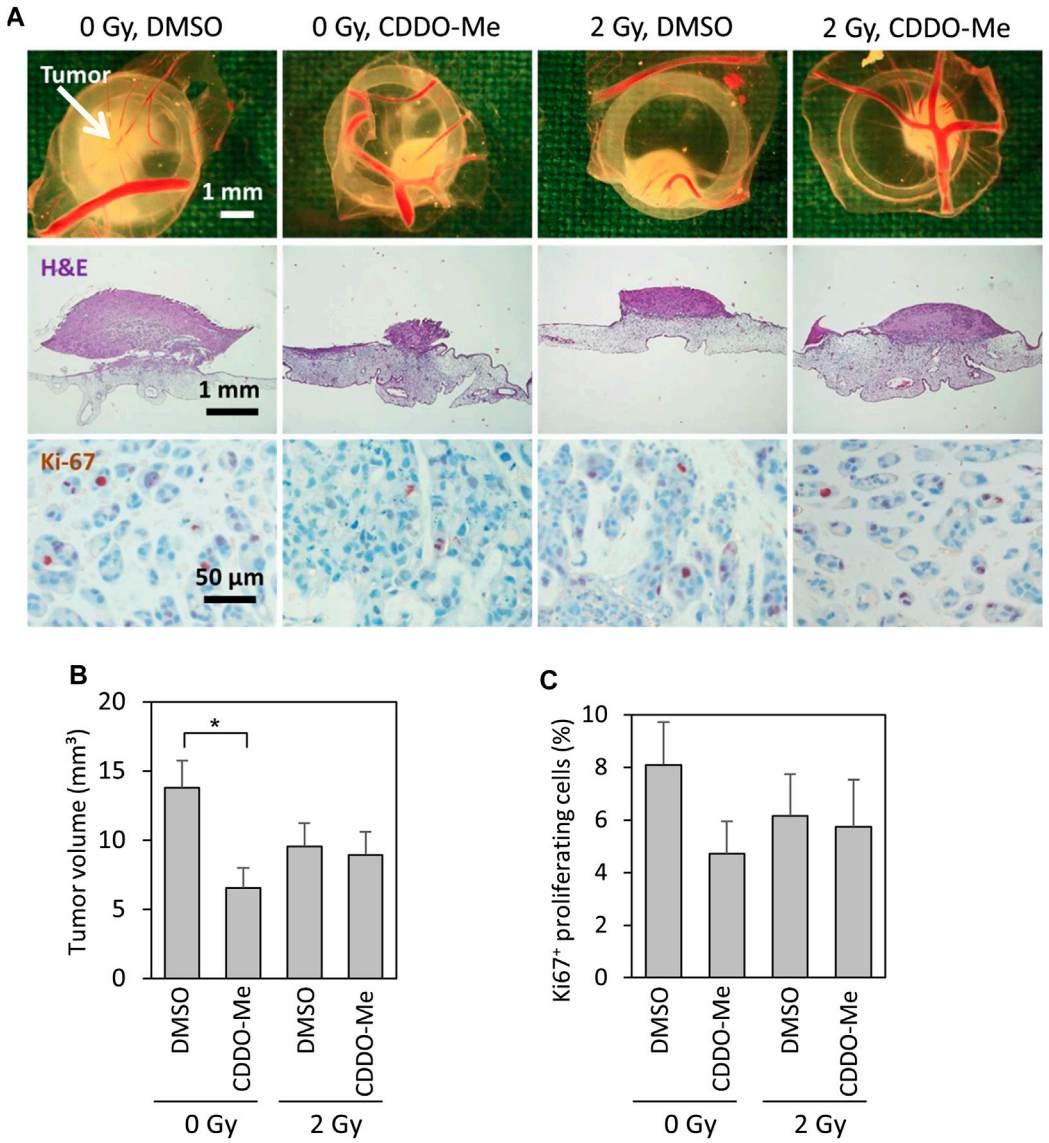

FIGURE 1 | 10 nM CDDO-Me inhibits growth of Cal-27 cell xenografts on the chick egg chorioallantoic membrane *in vivo* **(A)** Representative pictures of tumor xenografts immediately after extraction (first row), overview of tumor and underlying CAM tissue (H and E stained, second row), immunohistochemical staining of Ki-67 + proliferative cells (third row) **(B)** Mean tumor volume of Cal-27 cell cancer xenografts as assessed immediately after extraction. Data are mean ± SEM of 13–15 tumors/group. Statistics: One-way ANOVA, post hoc test: Bonferroni *t*-test; $^{*}p < 0.05$ **(C)** Percentage of proliferating Ki-67 + cells. 226–1,072 cells of each tumor were evaluated. Data are mean ± SEM of 9–13 tumors/group.

CDDO-Me induced effects on the kidney function in 2,185 patients suffering chronic kidney disease and type 2 diabetes. Although the study ultimately had to be terminated due to increased rates of heart failure events, CDDO-Me revealed to increase eGFR and to significantly reduce the hazard for the loss of kidney function (Chin et al., 2018). Besides the inhibition of the nuclear factor κB (NFκB) signaling cascade, activation of the Kelch-like ECH-associated protein 1 (Keap1)/nuclear factor erythroid 2–related factor (Nrf2) pathway is widely regarded as a major mechanism of action for CDDO-Me related cytoprotective effects (Liby and Sporn, 2012; Wang et al., 2014). Stimulation of the Nrf2 pathway mediates the downstream activation of various promoter genes encoding for detoxifying and antioxidative proteins like heme oxygenase 1 (HO-1). The heat-shock protein (HSP)-32 family member HO-1, which has been found in microsomes, mitochondria and nuclei, was demonstrated to catalyze the rate-limiting step of heme catabolism, leading to the formation of biliverdin. The following biliverdin/bilirubin redox cycle system effectively scavenges reactive oxygen species (ROS) and represents a highly conserved cellular control mechanism against oxidative stressors like radiation (Lin et al., 2007; Kim and Park, 2012; Son et al., 2013).

Numerous experimental studies highlighted the efficacy of CDDO-Me for both, prevention and treatment of cancer, albeit predominantly at high nanomolar to micromolar concentrations (Liby and Sporn, 2012; Borella et al., 2019).

However, differential reactions to radiation exposure of normal and cancer cells at equivalent and physiological achievable CDDO-Me concentrations are preferably required when giving consideration to a future usage in radiotherapy. Previously, CDDO-Me has been demonstrated to mitigate radiation-induced damage in normal epithelial cells but not cancer cells of the lung, breast and colon (Kim et al., 2013; El-Ashmawy et al., 2014).

In this study, we analyzed the implications of low nanomolar CDDO-Me in the radiation response and *in ovo* tumor growth of the OSCC cell line Cal-27 and compared the results with findings in normal human epithelial keratinocytes (NHEK) as a model for surrounding healthy skin.

MATERIALS AND METHODS

Cell Culture and Treatment

Cal-27 cells were originally derived from a 56-year old male patient suffering SCC of the tongue and were purchased from Leibniz-Institut DSMZ (Braunschweig, Germany). Cells were cultivated at 37 °C in a 5% CO_2 atmosphere using DMEM GlutaMAX medium (Gibco, Eggenstein, Germany), which was supplemented with 10% FCS (Boehringer, Mannheim, Germany).

Primary normal human epidermal keratinocytes (NHEK) originate from the epidermal stratum basale of an adult single donor and were cultivated at 37 °C and 5% CO_2 in Keratinocyte Growth Medium 2 (both from PromoCell, Heidelberg, Germany).

Unless stated differently, seeded cells were allowed to attach for 24 h, then culture medium was supplemented with 10 nM CDDO-Me or DMSO as solvent control at 0.1 vol% (both from Selleckchem, Houston, United States) and cells were incubated for further 6 h. Subsequently, cells were treated according to the respective protocol.

Radiation Exposure

Cells were exposed to 240 kV X-rays using the YXLON Maxishot (Hamburg, Germany) including a 3 mm beryllium filter at a plateau dose rate of 1 Gy/min at 13 mA. Monitoring of the applied doses was performed by a PTW Unidose dosimeter (PTW Freiburg GmbH, Freiburg, Germany).

Chick Egg Chorioallantoic Membrane as Tumor Xenograft Model

The chick egg chorioallantoic membrane (CAM) tumor model was used as previously described (Zuo et al., 2017; Kuan et al., 2018; Hafner et al., 2019). Briefly, fertilized chicken eggs were incubated at 37 °C and 60% relative air moisture for 7 days before fenestration and placement of a silicone ring (diameter 5 mm) on the vascularized CAM. Cal-27 cells were treated with 10 nM CDDO-Me or DMSO respectively 6 h prior to IR exposure and subsequently harvested. A 1:1 solution of matrigel (BD, Heidelberg, Germany) and medium containing Cal-27 cells (1.5×10^6 cells/egg) was grafted within the ring. The following day, topical treatment with CDDO-Me (10 nM) or vehicle (0.2% DMSO in NaCl 0.9%) was started and continued for two more days. After an incubation period of 4 days at 37 °C, tumors were collected, imaged, fixed in phosphate-buffered 4% formaldehyde solution and embedded in paraffin for immunohistochemical analysis. Slices (5 μm) were stained for H and E and proliferation marker Ki-67 (Dako, Glostrup, Denmark). Mean tumor volume of Cal-27 cells cancer xenografts was assessed immediately after extraction. Tumor volume was calculated according to the formula: $\pi/6$ x length x width^2 (Tomayko and Reynolds, 1989).

Assessment of Cellular Reactive Oxygen Species

In order to show whether CDDO-Me decreases the amount of free reactive oxygen species (ROS) after irradiation within NHEK and Cal-27 cells, we used the DCFDA Cellular ROS Detection Assay Kit according to the manufacturer's instructions (Abcam, Cambridge, United Kingdom). In brief, 2′, 7'–dichlorodihydrofluorescein diacetate (DCFDA) served as a marker which accumulates in living cells and becomes fluorescent upon oxidation. Therefore, 0.5×10^6 cells (Cal-27) or 0.75×10^6 cells (NHEK) were incubated for 24 h in 6 cm diameter Petri dishes. Subsequently, 1 μL/ml medium CDDO-Me stock solution (10 μM in DMSO) was added to the treatment group resulting in 10 nM CDDO-Me, whereas 1 μL/ml medium DMSO was added to the control group and incubated for another 6 h before undergoing X-ray irradiation; 45 min before irradiation, cells were stained with 25 μM DCFDA; 55 mM Tert-Butyl Hydrogen. Peroxide (TBHP) served as positive

control. Immediately after irradiation the cells were detached by trypsinization and measured by flow cytometry using the FACS-Calibur System (BD Biosciences, Franklin Lakes, NJ, United States). Therefore, 10,000 objects per sample were recorded on FL-1 (535 nm) with an excitation wavelength of 488 nm. Single cells were gated via a "forward scatter vs side scatter" scatterplot and the mean intensity of FL-1 was taken as measured value. Experiments were performed in quadruplicate (10,000 cells/experiment). Furthermore, cells were grown on chamber slides for live cell fluorescence imaging. According to the manufacturer's protocol (Abcam) cells were washed, stained with DCFDA and the developing fluorescence was captured by a Zeiss Axioimager 2i fluorescence microscope.

Redox Status

For analysis of the cellular redox homeostasis we used the CellTiter 96® AQueous One Solution Cell Proliferation Assay according to the manufacturer's instructions (Promega, Madison, USA). The assay is based on the bioreduction of MTS [3-(4,5-dimethylthiazol-2-yl)-5-(3-carboxymethoxyphenyl)-2-(4-sulfophenyl)-2H-tetrazolium] to a colored formazan by NADPH or NADH produced in metabolic active cells. Absorbance at 490 nm indicated the amount of formazan formed using the Multiskan™ FC microplate photometer (Thermo Scientific, Westham, United States).

Immunofluorescence Microscopy

We applied immunocytochemistry as described previously (Liebau et al., 2011). Rabbit monoclonal anti-HO-1 (dilution 1:1,000, Cell Signaling, Danvers, United States) served as primary antibody before fluorescence-labeling using Alexa Fluor® 488-conjugate goat polyclonal anti-rabbit (dilution 1:500, Life Technologies, Waltham, United States). Cytoskeleton was stained using TexasRed-conjugated Phalloidin (dilution 1:40, Invitrogen, Mannheim, Germany) and nuclei were counter stained using Fluoroshield Mounting Medium (Abcam, Cambridge, United Kingdom) containing 4,6-diamidino-2-phenylindole (DAPI).

For image acquisition we used a Zeiss Axioimager 2i fluorescence microscope in combination with the ISIS fluorescence imaging system (MetaSystems, Altlussheim, Germany).

Immunoblotting

The XCell Sure Lock™ Mini-Cell Electrophoresis System served as a platform for western blot experiments according to standard protocols. For equalization of protein concentrations, we used the BCA Protein Assay Kit (both from Thermo Scientific, Westham, United States). Amounts of HO-1 were detected using primary rabbit monoclonal anti-HO-1 (dilution 1:1,000, Cell Signaling, Danvers, United States) and secondary HRP-conjugated polyclonal goat anti-rabbit (dilution 1:10,000, Thermo Scientific, Westham, United States). For digital image acquisition we used the myECL™ Imager system (Thermo Scientific, Westham, United States). For calculation of HO-1/GAPDH-ratios greyscale intensity values were determined by ImageJ software, v. 1.51 (NIH, Bethesda, United States).

DNA Double Strand Break Analysis Using Imaging Flow Cytometry

DNA double strand breaks were assessed using phosphohistone γH2AX as a marker. Cells were detached, fixed for 20 min in cold 4% PFA pH 7.0 (Roti-Histofix®, Carl Roth, Karlsruhe, Germany), washed twice, permeabilized for 10 min using 0.1% Triton X (Sigma Aldrich, Darmstadt, Germany) and washed twice again. Staining was performed for 2 h at room temperature using mouse γH2AX antibodies primarily coupled with AlexaFluor® 488 (BioLegend, San Diego, CF, United States). After one additional washing step, cells were resuspended in 100 µl PBS, containing 20 µM DRAQ5 for DNA staining, yielding at least 10^6 cells/ml and measured using the ImageStream® X mkII (Luminex, Austin, TX, United States) imaging flow cytometer (IFC).

Excitation lasers with 488 nm and 642 nm wavelength were used at laser powers adjusted to the sample with the highest expected signal for each data set. The emission wavelengths recorded, were split into different channels on the CCD camera of the IFC. Channel 1 (435–480 nm) was used for the bright field picture and therefore illuminated with a LED of the respective wavelength range; Channel 2 (480–560 nm) recorded the green fluorescent AF488 emission and Channel 5 (642–745 nm) recorded the DRAQ5 signal. The remaining channels were not used; notch filters were activated to block laser scatter from the CCD.

Analysis of γH2AX foci was performed by the spot count feature on custom masks (Range (Peak (M02, Ch02, Bright, 10), 4–100, 0–1)).

Clonogenic Survival Assay

NHEK and Cal-27 cells were cultivated in 6-well plates for 24 h and treated according to the standard protocol. Experiments were stopped after 9 days by fixing cells with 70% ethanol followed by staining with gentian violet. We counted colonies manually by using a Zeiss STEMI SV8 stereomicroscope. Experiments were performed in quadruplicate.

Analysis of Cell Growth and Proliferation

Proliferation was determined by the IncuCyte™ live-cell imaging system (IncuCyte S3, Essen BioScience, United States). Cells (50,000 NHEK cells/12 well; 25,000 Cal-27 cells/12 well) were pre-incubated with CDDO-Me (10 nM) or the solvent control DMSO for 6 h before irradiation. Every 2 h a picture was taken to monitor cell growth for 48 h. The integrated IncuCyte software was used to measure the increase of confluence which was normalized to the initial confluence values.

Statistics

Unless stated elsewhere we tested for significance using one way ANOVA followed by post hoc Bonferroni *t*-test using SigmaPlot software (v. 14.0, Systat Software, Erkrath, Germany). Regarding clonogenic survival assays we calculated plating efficiency (PE) and surviving fraction (SF) as followed: PE = (Colonies counted)/(Cells seeded per well)*100; SF = (Colonies counted)/((cells seeded per well) (PE/100)). The reference basic value (100%) represents the mean SF of untreated control group (DMSO, 0 Gy).

p-values < 0.05 were regarded as statistically significant. Bars indicate mean values ±standard deviation, unless stated elswhere.

RESULTS

CDDO-Me Impaired Tumor Forming Capability of OSCC Cells

Cal-27 cells treated with CDDO-Me 6 h before receiving 2 Gy ionizing radiation (IR) were subsequently implanted on vascularized chick egg chorioallantoic membranes to test the inhibitory capacity of the triterpenoid on tumor growth. After 4 days the volume of CDDO-Me treated tumors was significantly reduced compared to untreated controls (**Figures 1A,B**). The fraction of Ki67-proliferative cells within the tumor tissue revealed to be reduced by trend even though without reaching statistical significance levels (**Figures 1A,C**). Surprisingly, combined treatment of IR and CDDO-Me did not show any additive effect (**Figures 1B,C**).

Treatment With CDDO-Me Affects ROS Levels and Antioxidative Response

The unexpected absence of synergistic effects in the *in ovo* model prompted us to focus on the role of CDDO-Me itself first. Analysis of CDDO-Me cytotoxicity exhibited IC_{50} values of 820 nM in NHEK and 280 nM in Cal-27 cells (data not shown). In order to use CDDO-Me in its low nanomolar effective range in all experiments 10 nM of the substance were used.

Cellular reactive oxygen species (ROS) levels were detected by monitoring the oxidation of the fluorescent probe DCFDA. Cells, which were stained with the probe, irradiated and subsequently examined under the microscope, revealed a dose-dependent increase of fluorescent signal in microscopic analysis (**Figures 2A,B**). Further investigation of ROS activity was based on flow cytometric measurement. While baseline ROS activity was found to be unaltered in the presence of CDDO-Me in non-malignant NHEK (**Figure 2C**), Cal-27 cells responded with significantly increased ROS production during CDDO-Me treatment (**Figure 2D**) which is comparable to the effect of 2 Gy IR. However, no verifiable additional CDDO-Me induced increase of cellular ROS was detectable when Cal-27 cells were irradiated with 2 Gy or 8 Gy respectively. Similarly, a strong generation of NADPH, a potent provider of reducing equivalents, was observed in Cal-27 cells (**Figure 2E**). Additionally, since HO-1 is known for its protective effect against oxidative stress we investigated the expression levels in both cell types. Immunofluorescent staining revealed a ubiquitous production of HO-1 in Cal-27 cells and NHEK (**Figure 3A**). When incubating cells with 10 nM CDDO-Me over 6 h the subcellular localization of HO-1 was left unchanged (data not shown). However, HO-1 levels increased significantly in the whole cell lysate of NHEK in the presence of CDDO-Me as shown by immunoblotting analyzed after 6 and 24 h. In contrast, for Cal-27 cells no significant enhancement of expression level was detected (**Figure 3B**) as further illustrated by the given ratios of HO-1 and housekeeping protein GAPDH in (**Figure 3C**).

CDDO-Me Augmented the Effect of Irradiation in OSCC Cells

Since CDDO-Me is not only described as anti-cancer drug but also as radioprotector of non-cancerous lung cells (El-Ashmawy et al., 2014) we also evaluated the radiomodulatory capacity of CDDO-Me in our epithelial cell model after irradiation. DNA double strand breaks are among the most detrimental effects of irradiation. Therefore, the number of γH2AX foci was counted by an imaging flow cytometer (**Figures 4A,B**). Frequency of double strand breaks increased in a dose-dependent manner in Cal-27 cells, whereas in NHEK increased FOCI only occurred with higher doses (**Figures 4C,D**). Interestingly, CDDO-Me treatment significantly enhanced γH2AX foci frequency following 8 Gy IR in Cal-27 cells only (**Figure 4D**).

In line with these results, irradiation induced ROS dose-dependently in both cell types (**Figures 2C,D**). However, in Cal-27 cells CDDO-Me augmented irradiation-induced ROS production only by trend (**Figure 2D**) whereas in NHEK, irradiated with high doses, CDDO-Me attenuated oxidative stress significantly (**Figure 2C**).

As proposed by the CAM assay CDDO-Me has inhibitory effects on OSCC cell proliferation. To assess the survival and the growth capacity of the cells after CDDO-Me treatment clonogenic assays were performed. Cells were treated with CDDO-Me and further cultivated for 9 days. We observed a significant decline in the number of stained Cal-27 colonies (**Figure 5A**). In accordance, CDDO-Me reduced the surviving fraction in Cal-27 cells by about 70% whereas NHEK surviving fraction remained unaffected (**Figure 5B**).

Finally, the results from our proliferation studies are in line with the above mentioned data. Both cell types were cultivated for 48 h and confluence was monitored over time in a live cell imaging system. Proliferation of NHEK following 8 Gy IR was significantly increased in the presence of CDDO-Me (**Figure 5C**) whereas proliferation of irradiated Cal-27 cells was even further impaired if combined with CDDO-Me treatment (**Figure 5D**).

DISCUSSION

Over the last decades radiotherapy has traditionally played an essential role in the clinical management of oral squamous cell carcinoma (OSCC). Despite the development of various modifications of conventional radiotherapy regimens, there is still a narrow ridge between effective cancer treatment resulting in improved patient's outcome and the prevention of adverse effects by damaging neighboring healthy tissue (Glenny et al., 2010). In this study, the triterpenoid CDDO-Me, when used in nanomolar concentrations, significantly impaired tumor forming capability of OSCC xenografts grown on the CAM of fertilized chicken eggs. CDDO-Me treatment surprisingly did not offer a synergistic or additive effect if combined with IR. A possible reason for the lack of the above mentioned effect might be a cellular preselection of Cal-27 cells upon IR exposure prior to implantation on the chicken CAM. Therefore we wanted to investigate the effect of CDDO-Me in detail on OSCC cells, represented by the *in vitro* Cal-27 cell line. To eludicate the effect on healthy neighboring tissue, we used a non malignant primary keratinocyte cell line

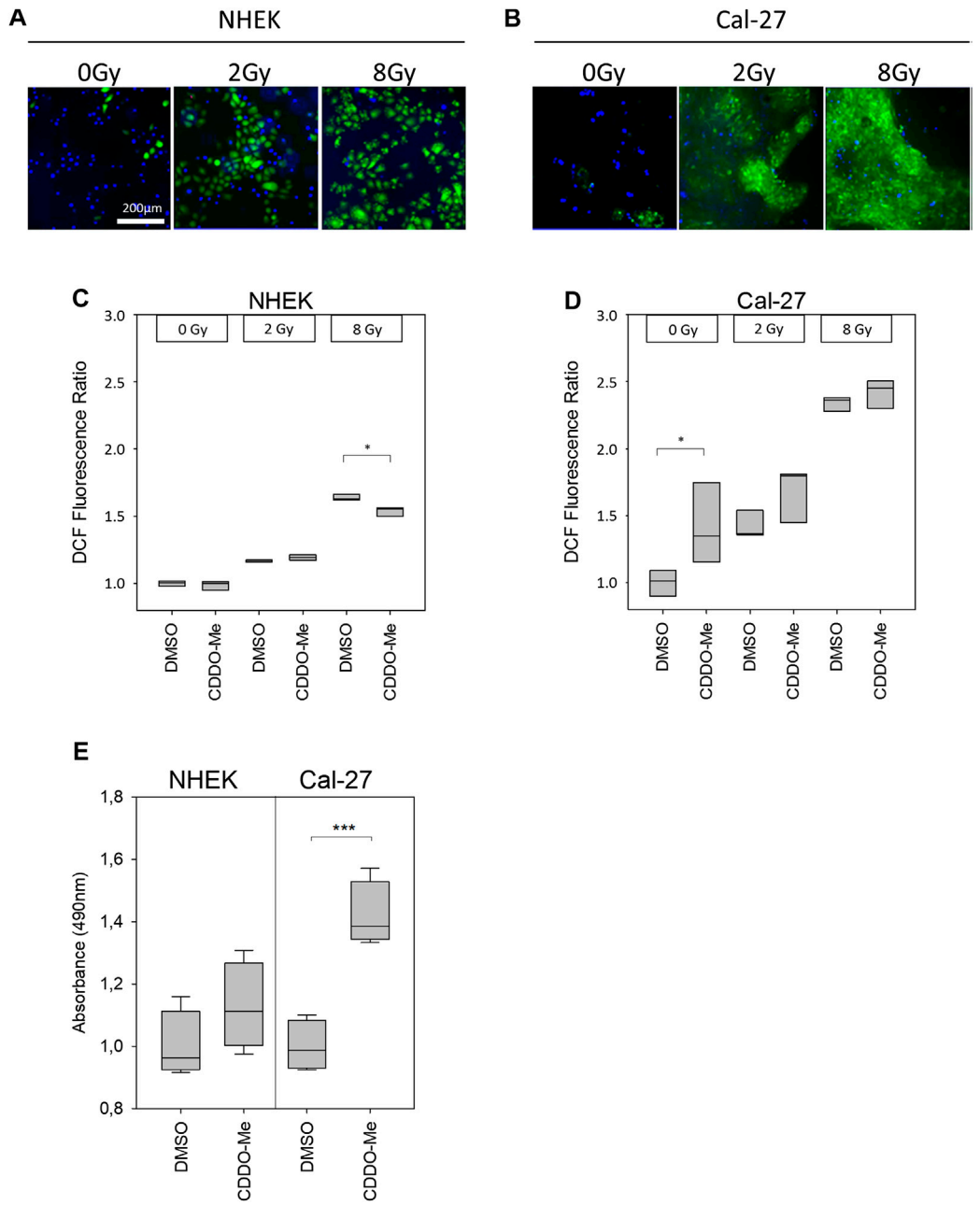

FIGURE 2 | (A and B) Cellular ROS-sensitive DCF levels (green) of NHEK and Cal-27 cells increased in a dose-dependent manner as shown by representative fluorescence microscopy images. Nuclear DAPI staining (blue) was used to indicate the presence of cells **(C and D)** Treatment with 10 nM CDDO-Me was shown to reduce DCF fluorescence intensity within NHEK significantly at high doses (8 Gy). In contrast, solely baseline DCF fluorescence levels of Cal-27 cells appeared to be increased significantly in the presence of 10 nM CDDO-Me. Statistics: Two Way ANOVA, post hoc test: Holm-Sidak method, $*p < 0.05$; $***p < 0.001$ (n = 3) **(E)** Generation of reducing equivalents NADPH or NADH after incubating cells with 10 nM CDDO-Me for 1 h was determined by quantification of MTS formazan product (absorbance at 490 nm). Significance levels were referenced to absorbance at 0 nM CDDO-Me (DMSO). Error bars represent standard deviation. Statistics: One Way ANOVA, post hoc test: Bonferroni *t*-test, $*p < 0.05$; $***p < 0.001$ (n = 4).

(NHEK) alongside with the OSCC cells in our *in vitro* experiments.

We demonstrated that CDDO-Me exerts anti-cancer activity in OSCC cells, while not consistently impairing cell homeostasis of primary keratinocytes even in the presence of ionizing radiation. Our findings are in line with previous studies, which highlighted radio-protective effects of CDDO-Me in normal epithelial cells of the lung, breast and

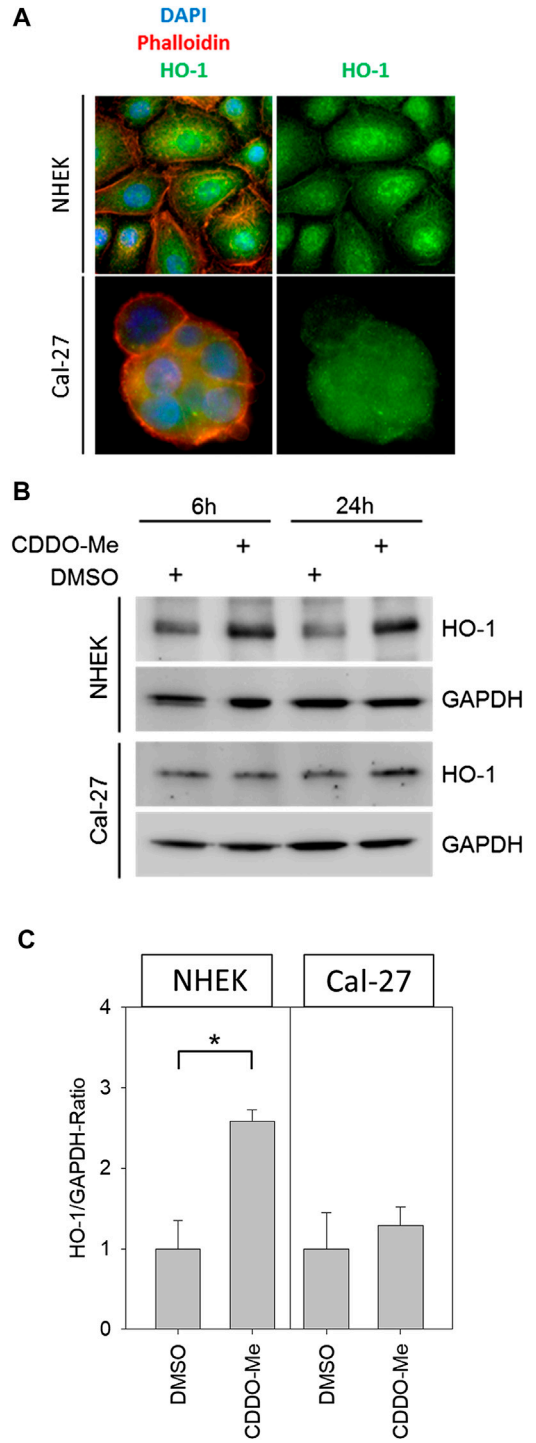

FIGURE 3 | (A) Representative immunofluorescence pictures of NHEK and Cal-27 cells; stained structures are the nucleus (DAPI, blue), actin (Phalloidin-dye conjugate, red) and HO-1 (FITC-Antibodies, green) showing that HO-1 is present ubiquitously in both cell lines **(B)** Western blots of HO-1 and GAPDH from control and treated NHEK and Cal-27 cells **(C)** HO-1/GAPDH ratio determined by western blot; compared groups are control (DMSO) vs. 10 nM CDDO-Me treatment (incubation 6 h and 24 h). HO-1 in NHEK treatment group is significantly increased vs. control, whereas the increase in Cal-27 cells is not significant. Statistics: Welch's *t*-test $^*p < 0.05$; n = 3.

colon but not in cancer cells (Kim et al., 2012; Kim et al., 2013; El-Ashmawy et al., 2014).

Activation of the Nrf2 pathway followed by downstream up-regulation of antioxidant enzymes like HO-1 is widely regarded as a major mechanism of action of CDDO-Me (Liby and Sporn, 2012). In physiological settings the Nrf2/HO-1 cascade represents a key mechanism for normal cells to adapt to oxidative stress conditions, mediating enhanced survival, preserved cellular homeostasis and prevention of carcinogenesis (Nitti et al., 2017). Several studies using rodent models and a case report on a HO-1 deficient patient revealed the radio-protective activity of antioxidant HO-1 in normal tissue, including skin (Yachie et al., 1999; Kapturczak et al., 2004; Zhang et al., 2012).

In our study we found that Cal-27 OSCC cells showed significantly increased ROS activity subsequent to CDDO-Me treatment and since NADPH and NADH proved to be enhanced concomitantly upon CDDO-Me administration we hypothesize that CDDO-Me may selectively trigger ROS accumulation in cancer cells via activation of the mitochondrial metabolism as the major source of intracellular ROS. Additionally, NAPDH serves as the donor of reductive potential to glutathione and therefore finally to restore redox homeostasis (Fernandez-Marcos and Nobrega-Pereira, 2016).

No evidence was found for down-regulated antioxidative defensive mechanisms by CDDO-Me as a potential contributing factor for elevated intracellular ROS levels, since HO-1 concentrations revealed to be even increased by trend in OSCC cells. Contrary to the significantly increased HO-1 in NHEK, this observation failed to reach statistical significance, which may in part be referred to elevated baseline HO-1 expression levels in Cal-27 cells. Constitutive up-regulation of antioxidative adaptive mechanisms is widely regarded to be inherent in malignant cells and was shown to be associated with cancer progression and resistance to therapy (Nogueira and Hay, 2013; Nitti et al., 2017).

Our non malignant primary cell line (NHEK) did not show increased ROS activity due to the treatment with CDDO-Me. On the contrary, when exposed to IR doses as high as 8 Gy, there was even a significant reduction in ROS. This data is supported by significantly enhanced HO-1 levels when treating NHEK with CDDO-Me, indicating radioprotective effects of CDDO-Me possibly mediated via enhanced expression of cellular HO-1. Sole CDDO-Me administration left ROS activity in NHEK unchanged, which argues for direct pharmacological effects finally leading to augmented HO-1 instead of elevated HO-1 levels due to increased oxidative stress.

Surprisingly, the diminished ROS levels found after high dose (8 Gy) irradiation were not potent enough to result in measurable reduction of γH2AX-foci of NHEK whereas it was significantly increased in Cal-27 cells. The missing verification of reduced DNA damage subsequent to reduced ROS in NHEK may in part be explained by the saturation of γH2AX-foci induction commonly observed by administration of high radiation doses (Rothkamm et al., 2015). Furthermore, even radiation with low linear energy transfer, such as X-rays generates DNA double strand breaks to some extent via ROS-independent direct ionization of target DNA molecules, representing a way of action that is not preventable by elevated antioxidative cellular defense mechanisms.

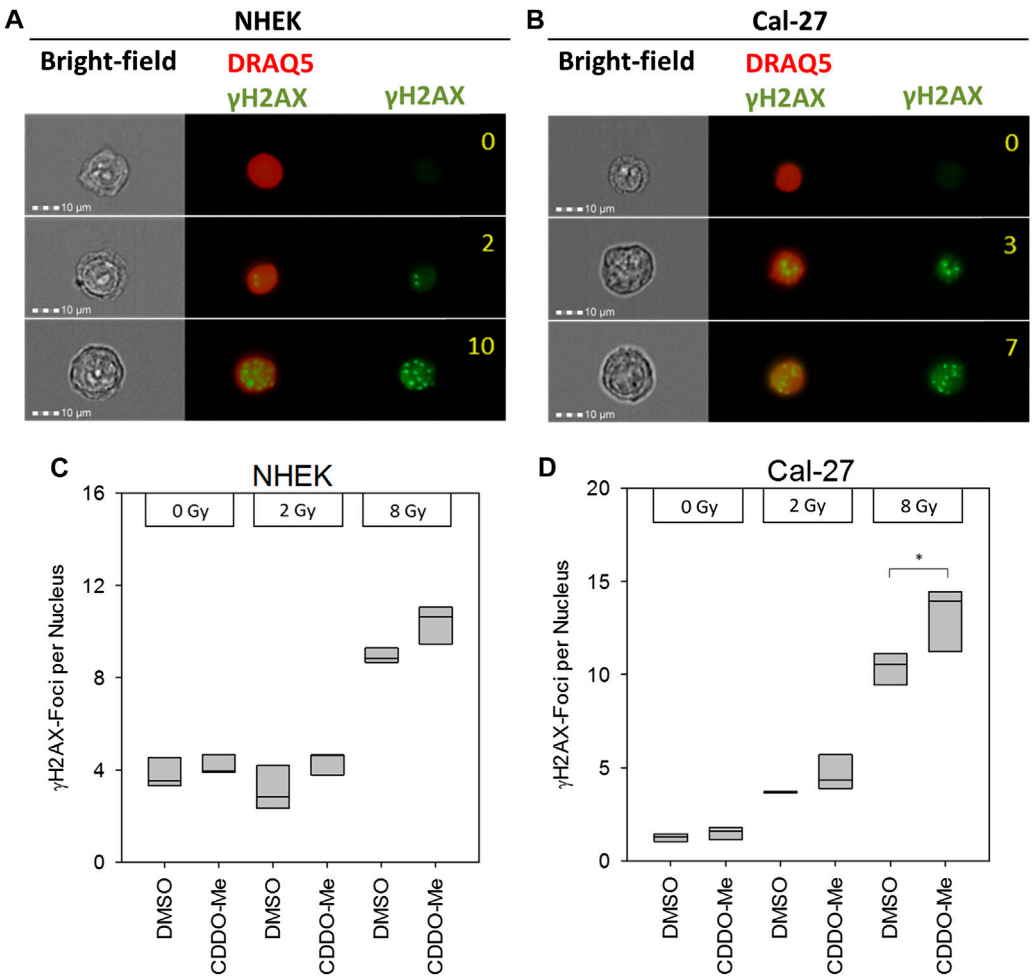

FIGURE 4 | (A and B) Representative pictures of NHEK and Cal-27 cells showing different DNA damage levels as indicated by γH2AX staining using the AMNIS™ image stream flow cytometer. Numbers indicate digitally counted γH2AX-foci frequency **(C and D)** 10 nM CDDO-Me induced significantly elevated γH2AX foci 6 h after irradiation in Cal-27 cells only (8 Gy). Statistics: One Way ANOVA, post hoc test: Bonferroni *t*-test, $^{*}p < 0.05$ (n = 3).

On the other hand, significantly reduced ROS activity in NHEK after 8 Gy points to cytoprotective effects by prevention of oxidative damage to various molecular structures crucial for the maintenance of cell homeostasis, e.g., within cellular membranes or organelles.

By all means, low nanomolar CDDO-Me did neither provoke acute toxic effects (IC_{50} = 820 nM) nor impairment of viability, clonogenicity or radioresistance in NHEK. A recent *in vivo* study even highlighted radioprotective effects for healthy skin when radiation-induced dermatitis was shown to be mitigated when treating mice externally with the CDDO derivative RTA 408 (Nakagami and Masuda, 2016).

OSCC cells showed an increased sensitivity to CDDO-Me when compared to NHEK; IC_{50} values of CDDO-Me were roughly 3-fold lower in Cal-27 cells.

Furthermore, we postulate that the activation of the antioxidative Keap1/Nrf2 pathway, regularly attributed to CDDO-Me, may partially result from elevated ROS levels. Previous studies identified the direct interaction of synthetic triterpenoids with Keap1 to be responsible for the Nrf2 pathway initiation (Dinkova-Kostova et al., 2005). However, activated Nrf2 signaling was shown to be only partially involved in the up-regulation of HO-1 mediated by CDDO-derivatives (Liby et al., 2005). CDDO-Me is well known as a multifunctional drug, which initiates various energy-demanding processes like transcriptional pathways or apoptosis (Liby and Sporn, 2012). The required activation of mitochondrial metabolism for cellular energy supply accompanied by inevitable ROS generation may finally stimulate the up-regulation of antioxidative enzymes like HO-1.

However, further research is needed to illuminate the precise mechanisms and clinical relevance of CDDO-Me induced ROS generation in OSCC cells.

Recent scientific research highlighted the ambivalent role of ROS in cancer (Nogueira and Hay, 2013; Assi 2017). While elevated baseline ROS levels commonly found in highly metabolic active cancer cells are capable to mediate pro-oncogenic characteristics, excessive amounts of intracellular

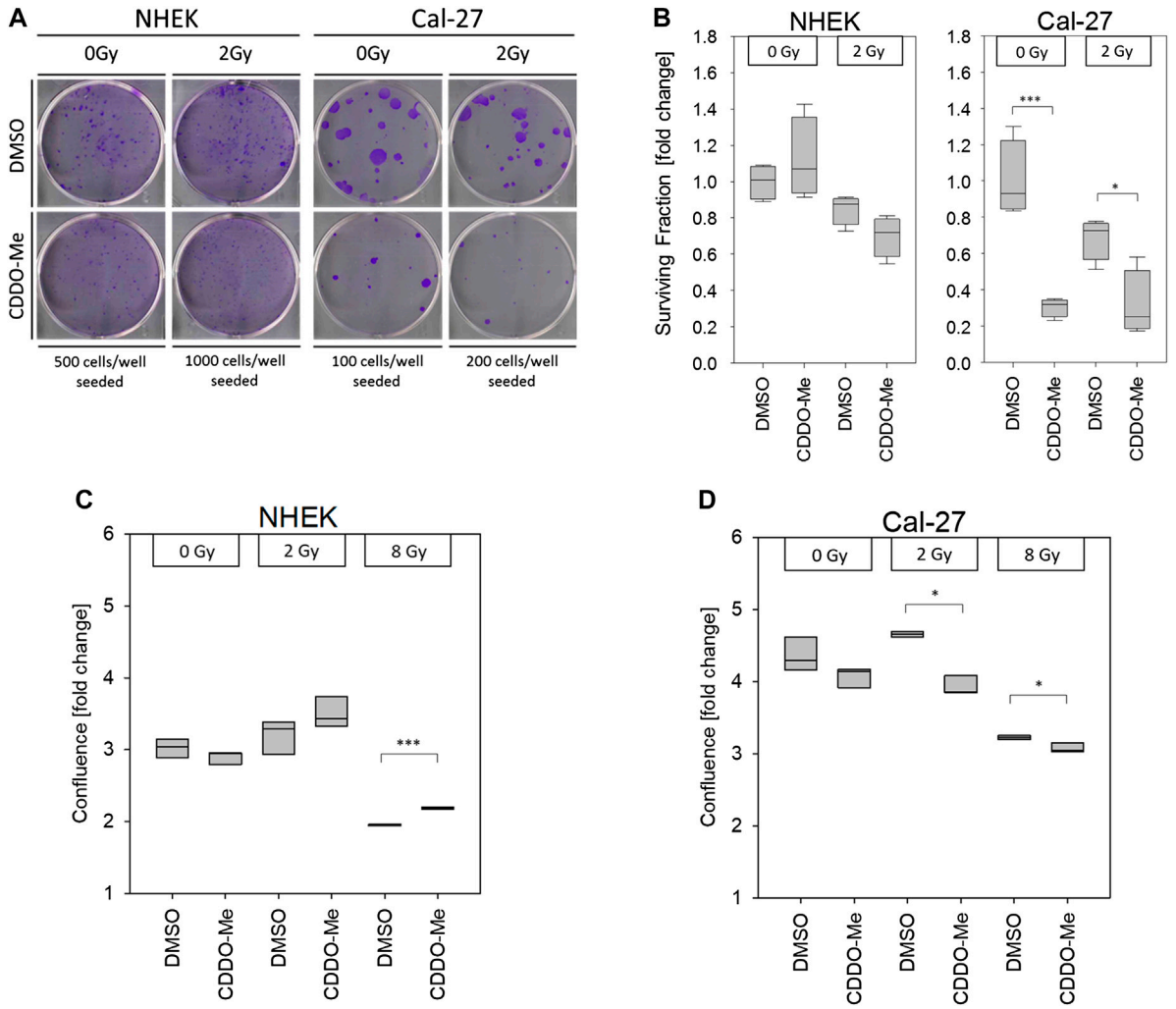

FIGURE 5 | (A) Pictures show representative clonogenic survival assays. All experiments were performed in quadruplicate **(B)** 10 nM CDDO-Me induced no significant changes of cellular survival in NHEK, but significantly impaired Cal-27 cell clonogenicity. Statistics: Two Way ANOVA, post hoc test: Bonferroni *t*-test, $*p < 0.05$; $***p < 0.001$ (n = 3) **(C and D)** Cellular confluency levels after a incubation period of 48 h were analyzed by IncuCyte™ live cell imaging experiments. Treatment with 10 nM CDDO-Me 1 h before irradiation showed significantly increased confluency of NHEK at high doses (8 Gy), whereas decreased confluency of malignant Cal-27 cells indicated sensitization to ionizing radiation (2 Gy and 8 Gy). Confluence is displayed as fold change from start of experiment (t = 0 h). Statistics: Welch's *t*-test, $*p < 0.05$; $***p < 0.001$ (n = 3).

ROS were shown to induce senescence and/or apoptosis. The latter effect is widely exploited by conventional treatment regimens like chemotherapy or radiotherapy (Conklin 2004; Moreb et al., 2017). OSCC colony formation and proliferation was significantly reduced by combined treatment of IR with CDDO-Me pointing to radiosensitizing effects in OSCC cells. As these results were not confirmed or even contrarily in our primary cell line NHEK, we draw the conclusion that CDDO-Me could offer a radiosensitizing effect for certain OSCC cells while not impairing or even protecting the adjectant healty tissue. Finally, this could lead to lower required IR doses during radiotherapy of OSCC patients and thus to less side effects.

DATA AVAILABILITY STATEMENT

The raw data supporting the conclusions of this article will be made available by the authors on request, without undue reservation.

ETHICS STATEMENT

CAM-experiments were performed in compliance with European and German laws for the protection of animals used for scientific purposes.

AUTHOR CONTRIBUTIONS

Following contributions to the present study were made by the respective scientist: HC, LS, and ES: conceptualization and methodology. HS: CAM experiments and statistics. HC, PT, HS, RA, DS, PM, and ES: data analysis; writing, reviewing, and editing of the manuscript. HC and ES: project administration and supervision.

FUNDING

This study was funded by the German Ministry of Defense.

ACKNOWLEDGMENTS

The authors acknowledge excellent technical assistance of M. Peper, R. Ridi, B. Couson, J. Chen and E. Winkler.

REFERENCES

Assi, M. (2017). The differential role of reactive oxygen species in early and late stages of cancer. *Am. J. Physiol. Regul. Integr. Comp. Physiol.* 313 (6), R646–R653. doi:10.1152/ajpregu.00247.2017

Borella, R., Forti, L., Gibellini, L., De Gaetano, A., De Biasi, S., Nasi, M., et al. (2019). Synthesis and anticancer activity of CDDO and CDDO-me, Two derivatives of natural triterpenoids. *Molecules* 24 (22), 4097. doi:10.3390/molecules24224097

Chin, M. P., Bakris, G. L., Block, G. A., Chertow, G. M., Goldsberry, A., Inker, L. A., et al. (2018). Bardoxolone methyl improves kidney function in patients with chronic kidney disease stage 4 and type 2 diabetes: post-hoc analyses from Bardoxolone methyl evaluation in patients with chronic kidney disease and type 2 diabetes study. *Am. J. Nephrol.* 47 (1), 40–47. doi:10.1159/000486398

Conklin, K. A. (2004). Chemotherapy-associated oxidative stress: impact on chemotherapeutic effectiveness. *Integr. Canc. Ther.* 3 (4), 294–300. doi:10.1177/1534735404270335

De Felice, F., Polimeni, A., Valentini, V., Brugnoletti, O., Cassoni, A., Greco, A., et al. (2018). Radiotherapy controversies and prospective in head and neck cancer: a literature-based critical review. *Neoplasia* 20 (3), 227–232. doi:10.1016/j.neo.2018.01.002

Dinkova-Kostova, A. T., Liby, K. T., Stephenson, K. K., Holtzclaw, W. D., Gao, X., Suh, N., et al. (2005). Extremely potent triterpenoid inducers of the phase 2 response: correlations of protection against oxidant and inflammatory stress. *Proc. Natl. Acad. Sci. U.S.A.* 102 (12), 4584–4589. doi:10.1073/pnas.0500815102

El-Ashmawy, M., Delgado, O., Cardentey, A., Wright, W. E., and Shay, J. W. (2014). CDDO-Me protects normal lung and breast epithelial cells but not cancer cells from radiation. *PloS One* 9 (12), e115600. doi:10.1371/journal.pone.0115600

Fernandez-Marcos, P. J., and Nóbrega-Pereira, S. (2016). NADPH: new oxygen for the ROS theory of aging. *Oncotarget* 7 (32), 50814–50815. doi:10.18632/oncotarget.10744

Glenny, A. M., Furness, S., Worthington, H. V., Conway, D. I., Oliver, R., Clarkson, J. E., et al. (2010). Interventions for the treatment of oral cavity and oropharyngeal cancer: radiotherapy. *Cochrane Database Syst. Rev.* 12, CD006387. doi:10.1002/14651858.CD006387.pub2

Hafner, S., Raabe, M., Wu, Y., Wang, T., Zuo, Z., Rasche, V., et al. (2019). High-contrast magnetic resonance imaging and efficient delivery of an albumin nanotheranostic in triple-negative breast cancer xenografts. *Adv. Ther.* 2 (11), 1900084. doi:10.1002/adtp.201900084

Ho, S. Y., Wu, W. S., Lin, L. C., Wu, Y. H., Chiu, H. W., Yeh, Y. L., et al. (2019). Cordycepin enhances radiosensitivity in oral squamous carcinoma cells by inducing autophagy and apoptosis through cell cycle arrest. *Int. J. Mol. Sci.* 20 (21), 5366. doi:10.3390/ijms20215366

Kapturczak, M. H., Wasserfall, C., Brusko, T., Campbell-Thompson, M., Ellis, T. M., Atkinson, M. A., et al. (2004). Heme oxygenase-1 modulates early inflammatory responses: evidence from the heme oxygenase-1-deficient mouse. *Am. J. Pathol.* 165 (3), 1045–1053. doi:10.1016/S0002-9440(10)63365-2

Kim, S. B., Ly, P., Kaisani, A., Zhang, L., Wright, W. E., and Shay, J. W. (2013). Mitigation of radiation-induced damage by targeting EGFR in noncancerous human epithelial cells. *Radiat. Res.* 180 (3), 259–267. doi:10.1667/RR3371.1

Kim, S. B., Pandita, R. K., Eskiocak, U., Ly, P., Kaisani, A., Kumar, R., et al. (2012). Targeting of Nrf2 induces DNA damage signaling and protects colonic epithelial cells from ionizing radiation. *Proc. Natl. Acad. Sci. U.S.A.* 109 (43), E2949–E2955. doi:10.1073/pnas.1207718109

Kim, S. Y., and Park, S. C. (2012). Physiological antioxidative network of the bilirubin system in aging and age-related diseases. *Front. Pharmacol.* 3, 45. doi:10.3389/fphar.2012.00045

Kuan, S. L., Fischer, S., Hafner, S., Wang, T., Syrovets, T., Liu, W., et al. (2018). Boosting antitumor drug efficacy with chemically engineered multidomain proteins. *Adv. Sci.* 5 (8), 1701036. doi:10.1002/advs.201701036

Liby, K., Hock, T., Yore, M. M., Suh, N., Place, A. E., Risingsong, R., et al. (2005). The synthetic triterpenoids, CDDO and CDDO-imidazolide, are potent inducers of heme oxygenase-1 and Nrf2/ARE signaling. *Canc. Res.* 65 (11), 4789–4798. doi:10.1158/0008-5472.CAN-04-4539

Liby, K. T., and Sporn, M. B. (2012). Synthetic oleanane triterpenoids: multifunctional drugs with a broad range of applications for prevention and treatment of chronic disease. *Pharmacol. Rev.* 64 (4), 972–1003. doi:10.1124/pr.111.004846

Liebau, S., Steinestel, J., Linta, L., Kleger, A., Storch, A., Schoen, M., et al. (2011). An SK3 channel/nWASP/Abi-1 complex is involved in early neurogenesis. *PloS One* 6 (3, e18148). doi:10.1371/journal.pone.0018148

Likhtarev, I., Bouville, A., Kovgan, L., Luckyanov, N., Voillequé, P., and Chepurny, M. (2006). Questionnaire- and measurement-based individual thyroid doses in Ukraine resulting from the Chornobyl nuclear reactor accident. *Radiat. Res.* 166 (1 Pt 2), 271–286. doi:10.1667/RR3545.1

Lin, Q., Weis, S., Yang, G., Weng, Y. H., Helston, R., Rish, K., et al. (2007). Heme oxygenase-1 protein localizes to the nucleus and activates transcription factors important in oxidative stress. *J. Biol. Chem.* 282 (28), 20621–20633. doi:10.1074/jbc.M607954200

Lindemann, A., Takahashi, H., Patel, A. A., Osman, A. A., and Myers, J. N. (2018). Targeting the DNA damage response in OSCC with TP53 mutations. *J. Dent. Res.* 97 (6), 635–644. doi:10.1177/0022034518759068

Moreb, J. S., Ucar-Bilyeu, D. A., and Khan, A. (2017). Use of retinoic acid/aldehyde dehydrogenase pathway as potential targeted therapy against cancer stem cells. *Canc. Chemother. Pharmacol.* 79 (2), 295–301. doi:10.1007/s00280-016-3213-5

Morra, F., Merolla, F., Picardi, I., Russo, D., Ilardi, G., Varricchio, S., et al. (2019). CAF-1 subunits levels suggest combined treatments with PARP-inhibitors and ionizing radiation in advanced HNSCC. *Cancers* 11 (10), 1582. doi:10.3390/cancers11101582

Nakagami, Y., and Masuda, K. (2016). A novel Nrf2 activator from microbial transformation inhibits radiation-induced dermatitis in mice. *J. Radiat. Res.* 57 (5), 567–571. doi:10.1093/jrr/rrw039

Nitti, M., Piras, S., Marinari, U. M., Moretta, L., Pronzato, M. A., and Furfaro, A. L. (2017). HO-1 induction in cancer progression: a matter of cell adaptation. *Antioxidants* 6 (2), 29. doi:10.3390/antiox6020029

Nogueira, V., and Hay, N. (2013). Molecular pathways: reactive oxygen species homeostasis in cancer cells and implications for cancer therapy. *Clin. Canc. Res.* 19 (16), 4309–4314. doi:10.1158/1078-0432.CCR-12-1424

Rothkamm, K., Barnard, S., Moquet, J., Ellender, M., Rana, Z., and Burdak-Rothkamm, S. (2015). DNA damage foci: meaning and significance. *Environ. Mol. Mutagen.* 56 (6), 491–504. doi:10.1002/em.21944

Son, Y., Lee, J. H., Chung, H. T., and Pae, H. O. (2013). Therapeutic roles of heme oxygenase-1 in metabolic diseases: curcumin and resveratrol analogues as possible inducers of heme oxygenase-1. *Oxid. Med. Cell Longev.* 2013, 639541. doi:10.1155/2013/639541

Tomayko, M. M., and Reynolds, C. P. (1989). Determination of subcutaneous tumor size in athymic (nude) mice. *Canc. Chemother. Pharmacol.* 24 (3), 148–154. doi:10.1007/BF00300234

Wang, Y. Y., Yang, Y. X., Zhe, H., He, Z. X., and Zhou, S. F. (2014). Bardoxolone methyl (CDDO-Me) as a therapeutic agent: an update on its

pharmacokinetic and pharmacodynamic properties. *Drug Des. Dev. Ther.* 8, 2075–2088. doi:10.2147/DDDT.S68872

Yachie, A., Niida, Y., Wada, T., Igarashi, N., Kaneda, H., Toma, T., et al. (1999). Oxidative stress causes enhanced endothelial cell injury in human heme oxygenase-1 deficiency. *J. Clin. Invest.* 103 (1), 129–135. doi:10.1172/JCI4165

Zhang, S., Song, C., Zhou, J., Xie, L., Meng, X., Liu, P., et al. (2012). Amelioration of radiation-induced skin injury by adenovirus-mediated heme oxygenase-1 (HO-1) overexpression in rats. *Radiat. Oncol.* 7, 4. doi:10.1186/1748-717X-7-4

Zuo, Z., Syrovets, T., Wu, Y., Hafner, S., Vernikouskaya, I., Liu, W., et al. (2017). The CAM cancer xenograft as a model for initial evaluation of MR labelled compounds. *Sci. Rep.* 7, 46690. doi:10.1038/srep46690

Conflict of Interest: The authors declare that the research was conducted in the absence of any commercial or financial relationships that could be construed as a potential conflict of interest.

The handling editor DR declared a past co-authorship with one of the authors MP.

frontiers in Pharmacology

ORIGINAL RESEARCH
published: 02 February 2021
doi: 10.3389/fphar.2021.628018

Co-Therapy of Pegylated G-CSF and Ghrelin for Enhancing Survival After Exposure to Lethal Radiation

Juliann G. Kiang[1,2,3]*, *Min Zhai*[1], *Bin Lin*[1], *Joan T. Smith*[1], *Marsha N. Anderson*[1] and *Suping Jiang*[1]

[1]Radiation Combined Injury Program, Armed Forces Radiobiology Research Institute, Bethesda, MD, United States, [2]Department of Pharmacology and Molecular Therapeutics, Uniformed Services University of the Health Sciences, Bethesda, MD, United States, [3]Department of Medicine, Uniformed Services University of the Health Sciences, Bethesda, MD, United States

Exposure to ionizing radiation (radiation injury, RI) in nuclear-related episode is evident to be life-threatening. RI occurs at levels of organs, tissues, cytosols, or nucleus. Their mechanisms are still not fully understood. FDA approves pegylated granulocyte colony-stimulating factor (Neulasta™, Peg-G-CSF) for acute hematopoietic syndrome and has been shown to save lives after lethal RI. We aimed to test whether Ghrelin enhanced Peg-G-CSF's efficacy to save more lives after lethal RI. B6D2F1/J female mice were used for the study. They received 9.5 Gy (LD50/30 at 0.4 Gy/min) emitted from the ^{60}Co-γ-photon radiation facility. Peg-G-CSF was injected subcutaneously at 1 mg/kg once on days 1, 8, and 15 after irradiation. Ghrelin contains 28 amino acid and is a hunger peptide that has been shown to stimulate food intake, promote intestinal epithelial cell proliferation, elevates immunity, inhibits brain hemorrhage, and increases stress-coping. Ghrelin was injected subcutaneously at 113 μg/kg once on days 1, 2, and 3 after irradiation. Survival, body weight, water consumption, hematology, spleen weight, splenocytes, bone marrow cells, and histology of bone marrow and ileum were performed. We observed that radiation resulted in 30-days survival by 30%. RI decreased their body weights and water consumption volumes. On the 30th day post-RI, platelets and WBCs such as basophils, eosinophils, monocytes, lymphocytes, neutrophils and leukocytes were still significantly decreased in surviving mice. Likewise, their RBC, hemoglobin, hematocrit, and splenocytes remained low; splenomegaly was found in these mice. Bone marrow in surviving RI animals maintained low cellularity with high counts of fat cells and low counts of megakaryocytes. Meanwhile, ileum histology displayed injury. However, mice co-treated with both drugs 24 h after RI resulted in 30-days survival by 45% above the vehicle group. Additionally, the body-weight loss was mitigated, the acute radiation syndrome was reduced. This co-therapy significantly increased neutrophils, eosinophils, leukocytes, and platelets in circulation, inhibited splenomegaly, and increased bone marrow cells. Histopathological analysis showed significant improvement on bone marrow cellularity and ileum morphology. In conclusion, the results provide a proof of concept and suggest that the co-therapy of Peg-G-CSF and Ghrelin is efficacious to ameliorate RI.

Keywords: radiation, survival, G-CSF, ghrelin, enhancement, bone marrow, GI

Edited by:
Ales Tichy,
University of Defence, Czechia

Reviewed by:
Ikuo Kashiwakura,
Hirosaki University, Japan
Hironori Yoshino,
Hirosaki University, Japan

***Correspondence:**
Juliann G. Kiang
juliann.kiang@usuhs.edu

Specialty section:
This article was submitted to Translational Pharmacology, a section of the journal Frontiers in Pharmacology

Received: *10 November 2020*
Accepted: *07 January 2021*
Published: *02 February 2021*

Citation:
Kiang JG, Zhai M, Lin B, Smith JT, Anderson MN and Jiang S (2021) Co-Therapy of Pegylated G-CSF and Ghrelin for Enhancing Survival After Exposure to Lethal Radiation. Front. Pharmacol. 12:628018. doi: 10.3389/fphar.2021.628018

INTRODUCTION

Detonation of nuclear weapons, radiation dispersal devices, or radiation-power plants and equipment will result in ionizing radiation emission so as to cause injuries, namely, radiation injury (RI) or sometimes followed by thermal energy exposure or blast trauma. *In vivo* (Kiang et al., 2012) and *in vitro* (Fukumoto and Kiang, 2011) studies have demonstrated that RI induces pathophysiological responses, including elevation of DNA double-strand breaks, elevation of circulating cytokine/chemokine levels, activation of iNOS and AKT-MAPK pathways, decreases in bone marrow cellularity and small intestinal villi and crypts, and burst of bacterial infection in every organ. As a result, cell death occurs; many organs lose function and then failed (Ledney and Elliott, 2010; Kiang et al., 2012; Fukumoto et al., 2013; Kiang and Ledney, 2013). Consequently, RI results in mortality (Kiang et al., 2010; Ledney and Elliott, 2010; Kiang et al., 2012; Kiang and Ledney, 2013). It is evident that radiation hits nuclus, cytosol, cells, tissues and organs. The detrimental responses are so complicated. This poly-traumatic complexity creates a hardship to identify plausible countermeasures for purpose of prevention or therapy. So, the nation is in need to develop effective drugs or means for taking care of RI, even though FDA has approved G-CSF (Neupogen®), pegylated G-CSF (Neulasta®) (Farese et al., 2013; Hankey et al., 2015), and Leukine for treating acute hemopoietic radiation syndrome (H-ARS).

RI remarkably increases circulating G-CSF (Kiang et al., 2010). It is generally thought that this rise is a possible self-defense mechanism, but its rise is too soon to play a role to repair the damage of radiation-sensitive organs including bone marrow (usually occurs within hours) and GI (usually occurs within days) after RI (Kiang et al., 2012; Kiang et al., 2014b). G-CSF and pegylated G-CSF (Peg-G-CSF) are utilized in hospitals for treating patients injured after radiotherapy or under the radionuclear accidents (Berger et al., 2006). It has been shown that G-CSF or Peg-G-CSF significantly attenuate not only the period of neutropenia and/or aplasia in victims suffered radiation but also strengthen recovery of neutrophil counts post anti-cancer therapy (Berger et al., 2006). They prime and/or stimulate neutrophils in order to enhance their function (Waselenko et al., 2004). The Peg-G-CSF is shown to have a longer and decent biological half-life than G-CSF (Molineux, 2004), therefore, this new formulation permits weekly administrations instead of daily injections; as known that daily injection causes distress and deters irradiated mice. Peg-G-CSF at the dose used in this report did not exhibit toxicity or harmful effects in mice.

Like the natural G-CSF, Peg-G-CSF enable 1) to stimulate the growth and division of myeloid progenitors, 2) to differentiate them into mature granulocytes, and 3) to induce mobilization of hematopoietic stem cell into the bloodstream from the bone marrow. Although our laboratory did not observe acceleration of wound healing (Kiang et al., 2010), Peg-G-CSF helps in wound healing (Badiavas et al., 2003) in addition to recovery of infection (Metcalf, 1990; Metcalf, 2007). When Peg-G-CSF was combined with erythropoietin and stem cell factors, this combinational therapy rescued a hospital technician who was exposed to a 4.5-Gy dose of radiation because this person entered a ^{60}Co-irradiation therapy room by accident (Bertho et al., 2008). Other reports on victims who got exposed to radiation in radiological accidents and received G-CSF treatments have been documented (Singh et al., 2015).

In our B6D2F1/J mouse model (Kiang et al., 2014b; Kiang et al., 2014c), s.c. administrations of G-CSF alone (10 μg/kg, day 1 to day 14 once daily) after RI followed by p.o. administrations of levofloxacin (day 3 to day 21 once daily) and topical applications of gentamicin cream to the wound area (day 1 to day 10 once daily) significantly increased mouse survival by 25% after RI combined with wounding trauma. In a previous experiment, mice were injected with Peg-G-CSF, exhibiting an appreciably longer biological half-life in serum than G-CSF (Molineux, 2004) at 25 μg/mouse, s.c., once +24 h, +8 days, +15 days after 9.5 Gy ($LD_{50/30}$) led to 100% 30-days survival post-RI, while vehicle-treated RI mice exhibited 30-days survival by 70%; significant recovery of monocytes, lymphocytes, and neutrophils in RI mice was observed (Kiang et al., 2014a). In the NHP model, treatment with Peg-G-CSF remarkably recovered neutrophil counts after irradiation at 6 Gy (Farese et al., 2012). Treatment with G-CSF effectively improved platelet and neutrophil counts after irradiation at 2 Gy in canine (MacVttie et al., 1990).

For public health emergency preparedness, there is an need for the most effective medical countermeasures to mitigate/treat RI victims. Because the survival increases in Peg-G-CSF-treated RI mice is around 30% above the vehicle-treated counterpart group (Kiang et al., 2014a), the object of this project was to investigate remedies that could enhance Peg-G-CSF efficacy in treating RI. Ghrelin was selected for this purpose because this co-therapy has been reported to reduce the RI-induced brain hemorrhage (Kiang et al., 2019; Gorbunov and Kiang, 2021) and Ghrelin alone was effective for other organ diseases (Wynne et al., 2005; Vasileious et al., 2013; Pereira et al., 2017; Fritz et al., 2020). Ghrelin is a peptide containing 28 amino acids; it is produced in the stomach during hunger and released into the blood stream to go to the hypothalamus for initiating the desire of food intake (Wynne et al., 2005; Vasileious et al., 2013; Pereira et al., 2017). It binds onto the growth hormone secretagogue receptor (GHS-R) coupling with G protein (Pereira et al., 2017). RI significantly increased interleukin (IL)-18 and enterocyte apoptosis in ileum after RI. The exogenous Ghrelin treatment reduced IL-18, decreased JNK activation and increased enterocytes and tight junction of ileum (Kiang et al., 2020). Moreover, the exogenous Ghrelin treatment significantly recovered lymphocytes, monocytes, and basophils, and enhanced increases in G-CSF in spleen samples after RI (Kiang et al., 2018). Therefore, it was of interest to investigate a hypothesis/concept, whether co-therapy of Peg-G-CSF and Ghrelin could enhance Peg-G-CSF's efficacy to save lives and mitigate ARS after RI.

Herein, the thought that co-therapy with Ghrelin and Peg-G-CSF would demonstrate synergistic therapeutic effects for RI was hypothesized. Therefore, our report proves the hypothesis/concept that this co-therapy indeed enhanced survival probably due to the combined effects of body weight recovery,

platelets recovery, inhibition of splenomegaly and injury of bone marrow and intestine.

METHODS

Experimental Design

B6D2F1/J female mice were divided randomly into eight groups (N = 20–42 per group, conducted in four separated experiments): 1) sham + vehicles, 2) radiation + vehicles, 3) sham + Peg-G-CSF + Ghrelin, 4) radiation + peg- G-CSF + ghrelin, 5) sham + Peg-G-CSF, 6) Radiation + Peg-G-CSF, 7) sham + Ghrelin, and 8) radiation + Ghrelin.

Animals

B6D2F1/J mice were purchased from the Jackson Laboratory, Bar Harbor, ME. Only female mice were used in this study based on the previous studies conducted in this laboratory (Kiang et al., 2010; Ledney and Elliott, 2010). These mice were 14–16 weeks old with an average weight of 24–25 g at the time of irradiation. Male mice were not used here because they are more aggressive to each other when they are housed together resulting in unnecessary injuries as described previously (Ledney and Elliott, 2010). Upon arrival, all mice were acclimated for 7 days. They were housed in plastic microisolator cages on hardwood chip bedding. They were maintained in the vivarium located at the Armed Forces Radiobiology Research Institute accredited by the Association for Assessment and Accreditation of Laboratory Animal Care International (AAALAC International). Acidified tap water as well as commercial rodent chow were made available *ad libitum*. A 12 h 0,600 (light) to 1800 (dark) full-spectrum lighting cycle was used in animal holding rooms, where the temperature was maintained at 21°C. With at least 10 changes/h of 100% conditioned fresh air, the relative humidity was 10%. Commercial rodent chow was Harlan Teklad Rodent Diet 8,604. Acidified water was with pH = 2.5–3.0 in order to inhibition of opportunistic infections.

The Armed Forces Radiobiology Research Institute (AFRRI) Institutional Animal Care and Use Committee (IACUC) approved all animal procedures. The recommendations and guidance of the American Veterinary Medical Association were followed when mice received euthanasia.

Gamma Irradiation

Mice were given 9.5 Gy (Kiang et al., 2014b; Kiang et al., 2019; Kiang et al., 2020) ^{60}Co γ-photon radiation (whole-body bilateral; 0.4 Gy/min; Kiang et al., 2019; Kiang et al., 2020). The exposure time for each irradiation was determined from the mapping data, with application of corrections due to the ^{60}Co decay plus the little variation in the mass energy absorption coefficients for water and soft tissues. The field was uniform within ±2%. With an ionization chamber adjacent to the mouse towers and calibration of dose to the midline soft tissue of mice, the accuracy of the actual dose delivery for each run was verified and recorded.

Preparation and Administration of Pegylated G-CSF and Ghrelin

Pegylated G-CSF [(Peg-G-CSF), aka Neulasta® and pegfilgrastim; NDC: 555-13-019001] is a polyethylene glycol pharmaceutical-formulated-grade drug. It was obtained from the AmerisourceBergen Corporation (Valley Forge, PA). Peg-G-CSF-treated mice were s.c. injected at 1,000 μg/kg in a volume of 0.2 ml 1 day, 8 days, and 15 days after RI (Kiang et al., 2014b; Kiang et al., 2019). This dose was based on the clinical human dose utilized for the purpose of subcutaneous auto-injection by patients. Neulasta® was commercially supplied in 0.6 ml prefilled syringes. Six mg Peg-G-CSF in a sterile, clear, colorless, preservative-free solution containing 30 mg sorbitol, 0.02 mg sodium, 0.02 mg polysorbate 20, and 0.35 mg acetate in water for injection, USP was in each syringe. The vehicle-treated mice received 0.2 ml of vehicle containing 30 mg sorbitol, 0.02 mg sodium, 0.02 mg polysorbate 20, and 0.35 mg acetate in 0.6 ml water (Kiang et al., 2014b; Kiang et al., 2019).

Ghrelin, obtained from Phoenix Pharmaceutical (Burlingame, CA), was subcutaneously (s.c.) administered at three doses of 113 μg/kg in a volume of 0.2 ml 24 h, 48 h, and 72 h after sham or RI. The dose was calculated based on a publication (Shah et al., 2009) and utilized previously (Kiang et al., 2018; Kiang et al., 2020). The vehicle given to control mice was sterile 0.9% sodium chloride solution for injection, USP (Kiang et al., 2020).

Thirty-Day Survival

After irradiation, mice (N = 20–42 per group) were closely monitored for 30 days by the research staff in addition to the regular health checks by vivarium staff. During the 30 days monitoring period, the AFRRI IACUC Policy 020 was followed (Koch et al., 2016).

Body Weight Measurement

Mouse body weights were measured right after irradiation (considered to be day 0). Then their body weights were measured on days 1, 3, 7, 14, 21, and 28.

Measurement of Daily Water Consumption

Mice were housed in four per cage. The drinking bottle was placed on the top of each cage. Mice received drinking water that was contained in a steam-sterilized graduated bottle. A sipping tube with a metal ball inside was connected to the drinking bottle to prevent water leakage. For the first 7 days after irradiation, the volume of water drunk daily was measured. Then, we calculated the average volume of water drunk by each mouse on each day in each cage (Kiang et al., 2014a). Water consumption by each mouse per day was presented as mL/animal/day in the Figure.

Blood Collection, Peripheral Blood Cell Count, Serum Preparation, and Tissue Collection

On day 30 after RI, mice were under deep isoflurane anesthesia via cardiac puncture into a 1 ml-syringe to collect blood samples from each mouse in each group. Then, 300 μL blood was placed

into the EDTA-containing microtube and maintained in a rotator. Blood cell counts were assessed with the ADVIA 2120 Hematology System (Siemens, Deerfield, IL). Differential analysis was carried out with the peroxidase method and the light scattering techniques following the manufacturer's manual

The rest of blood in the 1-ml syringe was put into a microtube with serum separator additive for serum preparation. After at least 30 min coagulation at room temperature, sera were collected after centrifugation at 10,000× g for 10 min, and immediately stored at −80°C for future analysis.

Cervical dislocation was performed after blood draw. Sternums, femurs, ileums, and spleens were collected. The number of animals used for blood samples and tissue samples was up to six per group.

Bone Marrow Cell Count

On day 30 after irradiation, two femurs from each mouse were collected. Bone marrows were flushed out using 3 ml 1x phosphate-buffered saline (PBS) buffer twice. The marrows were then centrifuged at 800× g for 10 min (Sorvall Legend XTR Centrifuge, Thermo Scientific) and the pellets were re-suspended in 10 ml 1x ACK buffer (Invitrogen, Grand Island, NY) and centrifuged at 800× g for 10 min. The resulted pellets were re-suspended in 10 ml 1x PBS buffer. The cell suspensions were then placed in Countess™ cell-counting-chamber slides (Invitrogen) and counted using a Countess™ automated cell counter (Invitrogen) (Kiang et al., 2014b; Kiang et al., 2018). Bone marrow cells were finally centrifuged again at 800x g for 10 min. The cell pellets were stored in −80°C until the future analysis. Bone marrow cells were presented as cells/femur.

Spleen Weight and Splenocyte Count

On day 30 after irradiation, spleens were collected from each surviving mouse (N = 6 mice per group). Spleens were weighed first. Then, each spleen was inserted into a plastic bag containing 10 ml 1× Hank's Balanced Salt Solution (HBSS; Invitrogen, Grand Island, NY), homogenized using Seward Stomacher® 80 (Thermo Scientific), and poured through a 70 mm cell strainer (BD Falcon, Bedford, MA). The bag and strainer were rinsed with 15 ml 1x HBSS again. The fluid with Splenocytes in the tube was then centrifuged at 800× g (Sorvall Legend XTR Centrifuge, Thermo Scientific) for 10 min. The pellets were resuspended in 10 ml 1× ACK lysis buffer (Invitrogen) for 10 min at 37°C to lyse RBCs, mixed by vertexing every 5 min, and then centrifuged at 800× g for 10 min. Splenocyte pellets were collected, resuspended in 10 ml 1× phosphate-buffered saline (PBS). The cell suspension was placed in Countess™ cell-counting-chamber slides (Invitrogen, Eugene, Oregon) and counted with the Countess automated cell counter (Invitrogen). Splenocyte suspension was finally centrifuged again at 800x g for 10 min. The cell pellets were stored in −80°C until the future analysis. The spleen weight was presented in mg and splenocyte counts were presented as cells/spleen.

Histological Examination of Bone Marrow and Intestine

On day 30 after irradiation, sternum and ileum specimens were collected from each mouse in each group (N = 4 mice per group). Sternums and ileum were rinsed in cold saline and then immediately placed in 10% phosphate-buffered formalin. They later were embedded in paraffin. Sternums were sectioned longitudinally and ileums were sectioned transversely. They were stained with Hematoxylin and Eosin. Using Zeiss Axioscan.Z1, the histology slides were scanned and stored. Using Zen two software (Zeiss Company, Thornwood, NY), fat cells and megakaryocytes in each sternum slide at a ×40 magnification were counted in four fields. Villus height, villus width, crypt depth, and crypt numbers in each ileum slide at ×20 magnification were counted. The mucosal injury score represented each slide was given (Kiang et al., 2020) To briefly summarize the standard of scores (Kiang et al., 2020): grade 0 = normal mucosa; grade 1 = development of subepithelial spaces near the tips of the villi with capillary congestion; grade 2 = extension of the subepithelial space with moderate epithelial lifting from the lamina propria; grade 3 = significant epithelial lifting along the length of the villi with a few denuded villus tips; grade 4 = denuded villi with exposed lamina propria, dilated capillaries and reduced crypt depth and counts; and grade 5 = disintegration of the lamina propria, hemorrhage, and ulceration.

Statistical Analysis

We present our data as the mean ± S.E.M. Using a Kaplan-Meier curve and the log rank test for each survival experiment in which 20-42 mice per group were individually tested. One-way ANOVA, two-way ANOVA, studentized-range test, and Student's t-test were used in comparison of groups for hematological analysis (N = 6 per group) and histopathological analysis (N = 4 per group). The statistical significance was considered when p value was less than 5%.

RESULTS

Ghrelin Enhances the Peg-G-CSF Therapy-Induced Survival Improvement After Lethal Irradiation

Radiation is known to decline survival (Kiang et al., 2010). As shown in **Figure 1A**, RI reduced survival down to 30%, therapy of Peg-G-CSF and Ghrelin further increased 30-day mouse survival to 75% ($p < 0.05$ vs. RI + V1+V2). In RI mice treated with either Peg-G-CSF (**Figure 1B**) or Ghrelin (**Figure 1C**) alone, % survival increases above vehicle group was 32% and 0% ($p < 0.05$ vs. RI + p vs. RI + GHR), respectively (**Figure 1D**). The non-irradiated mice treated with either Peg-G-CSF, Ghrelin, or combination of the two survived by 100%, suggesting the doses used were safe, although Ghrelin has been reported to promote fear, anxiety- and depression-like behaviors in rodents (Fritz et al., 2020).

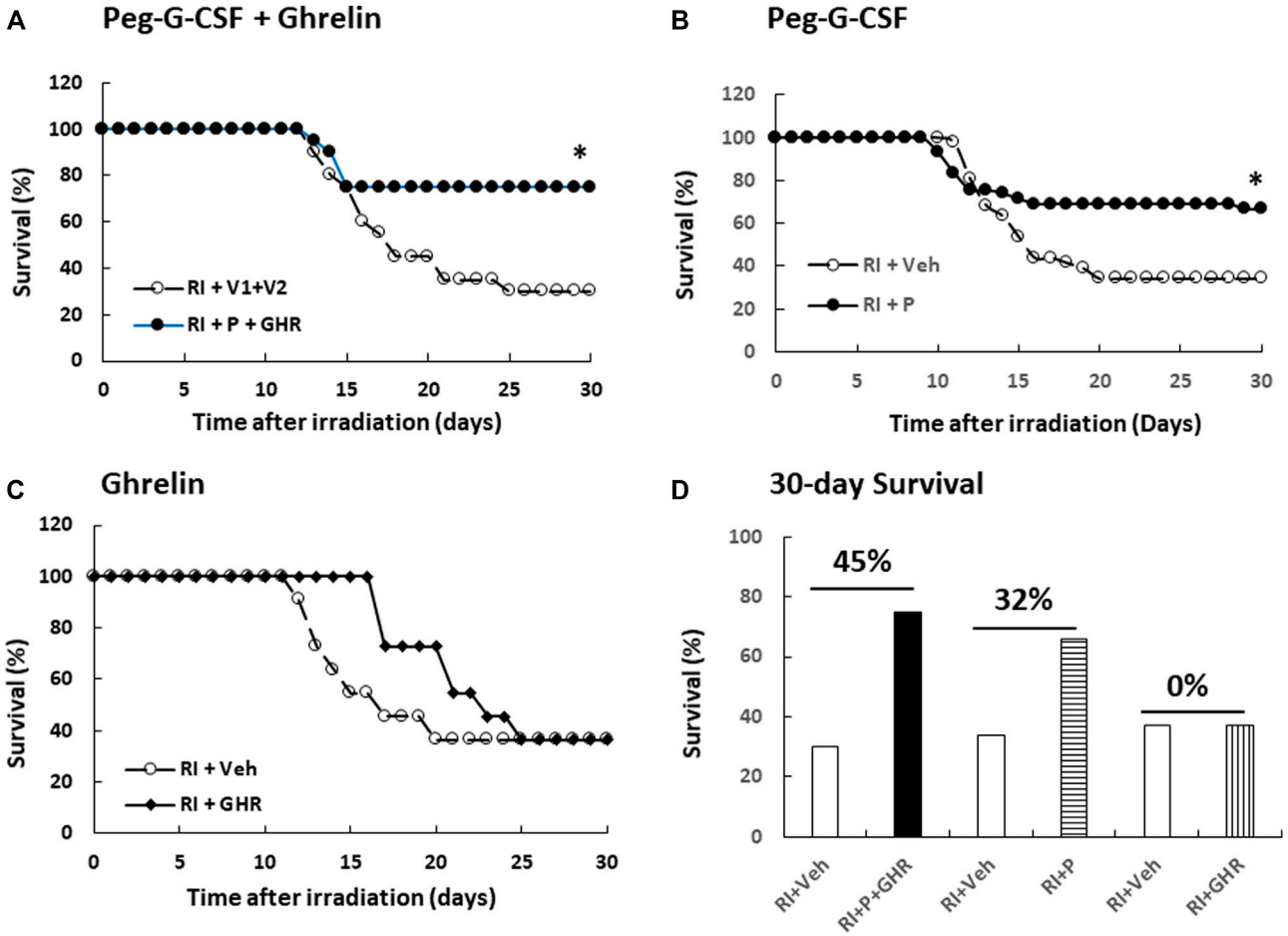

FIGURE 1 | Co-therapy of Peg-G-CSF and Ghrelin reduces mortality after irradiation (RI). *N* = 20–42 per group. Non-irradiated mice treated vehicle, individual drug or combination of the two were survived by 100%. On the **(A)** panel, **p* < 0.05 vs. RI + V1+V2. On the **(B)** panel, **p* < 0.05 vs. RI + Veh, **(C)** Survival curves with Ghrelin treatment. **(D)** Numbers above horizontal lines on the top of two bars represent the percentage of survival differences between the drug-treated group and its respective vehicle group. RI: 9.5 Gy; V1, vehicle for Peg-G-CSF; V2, vehicle for Ghrelin; Veh, vehicle; P, Peg-G-SF; GHR, Ghrelin.

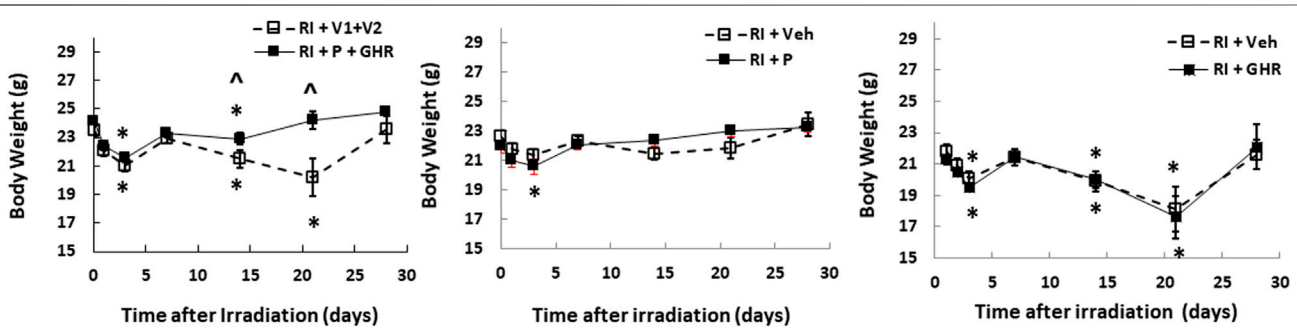

FIGURE 2 | Co-therapy of Peg-G-CSF and Ghrelin mitigates the RI-induced body-weight loss. *N* = 20–22 per group. Data are shown as mean ± sem. **p* < 0.05 vs. day 0; ^*p* < 0.05 vs. RI + *p* + GHR. RI: 9.5 Gy; V1, vehicle for Peg-G-CSF; V2, vehicle for Ghrelin; P, Peg-G-SF; GHR, Ghrelin.

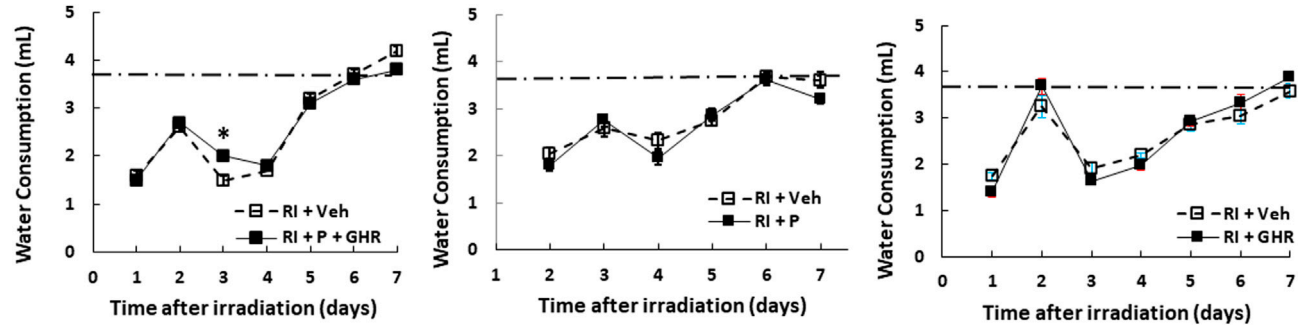

FIGURE 3 | Co-therapy of Peg-G-CSF and GHR increases water consumption after irradiation (RI). *N* = 20–22 per group. The non-irradiated mouse daily water consumption was 3.7 ± 0.1 ml (*N* = 20). Data are shown as mean ± sem. *$p < 0.05$ vs. RI + Veh. RI: 9.5 Gy; Veh, vehicle for Peg-G-CSF and vehicle for Ghrelin; P, Peg-G-SF; GHR, Ghrelin.

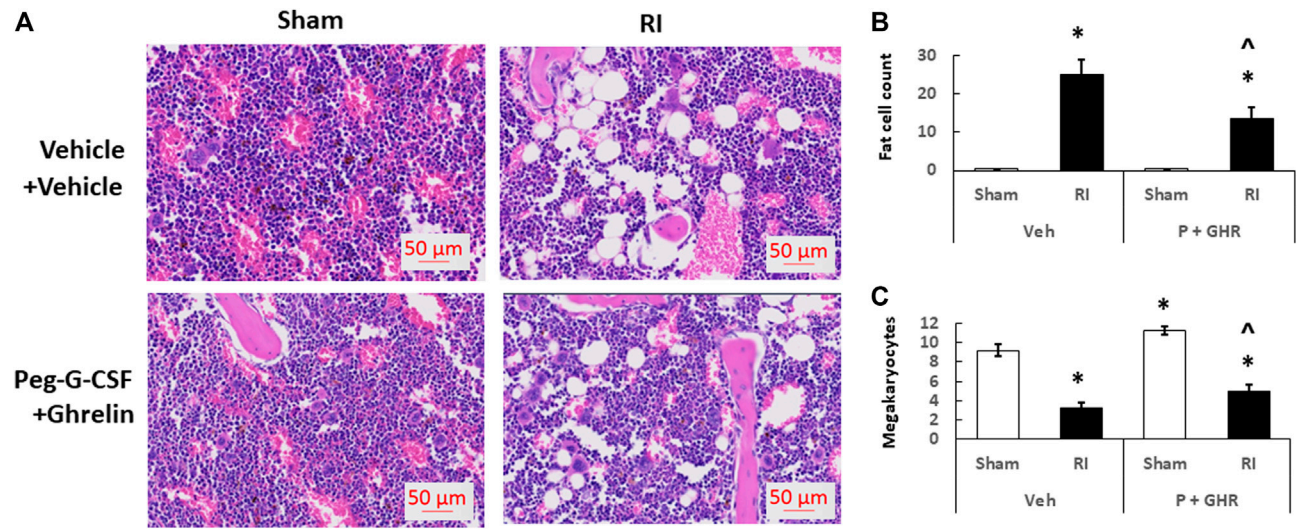

FIGURE 4 | Co-therapy of Peg-G-CSF and GHR recovers bone marrow cellularity after irradiation (RI). Data are shown as mean ± sem. **(B,C)**. Bone marrow histology slides on day 30 post-RI stained with hematoxylin and eosin **(A)**. N = 4 per group. Fat cells **(B)** and megakaryocyte counts **(C)** at four fields with ×20 magnification were measured. *$p < 0.05$ vs. Sham + Veh; ^$p < 0.05$ vs. RI + Veh. RI: 9.5 Gy; Veh,vehicle for Peg-G-CSF and vehicle for Ghrelin; P, Peg-G-SF; GHR, Ghrelin.

Peg-G-CSF and Ghrelin Therapy Mitigates Body Weight Loss After Lethal Irradiation

Radiation lowers the body weight beginning on the 3rd day after lethal radiation exposure (Kiang et al., 2010). Therefore, we measured the body weight after RI. RI significantly decreased the body weight on day 2, bounced back on day 7, then decreased again on day 14, continued to decrease to reach the nadir on day 21, but began to gain the weight back (**Figure 2**). Co-therapy of Peg-G-CSF and GHR attenuated the body-weight loss on days 14 and 21 in the RI mice. Treatment with either Peg-G-CSF or GHR alone had no improvement on the RI-induced body weight loss.

Peg-G-CSF and Ghrelin Therapy Reduces Water Consumption After Radiation Injury

The mouse daily water consumption is 3–4 ml. It is evident that RI significantly reduced water consumption. **Figure 3** shows that in comparison to the sham group (3.7 ± 0.1 ml), RI mice significantly reduced water consumption by 60% on day 1 (1.6 ± 0.1 ml, $p < 0.05$ vs. sham), but went back to baselines on the 7th day. Co-therapy of Peg-G-CSF and Ghrelin increased it in RI mice on day 3, whereas treatment with either Peg-G-CSF or GHR alone had no improvement on the RI-induced water consumption inhibition.

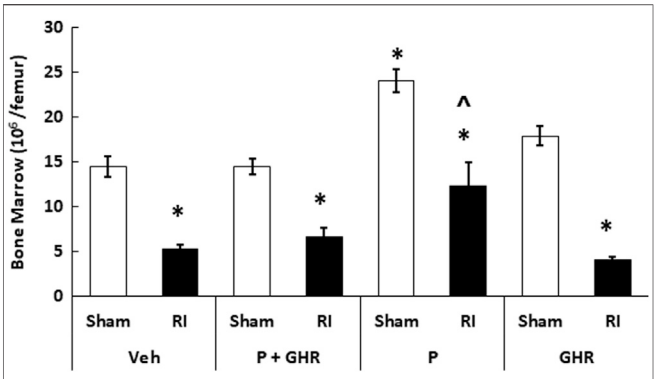

FIGURE 5 | Co-therapy of Peg-G-CSF and Ghrelin increases bone marrow cell counts after irradiation (RI). Bone marrow cells were collected from two femurs of each mouse. *N* = 6 per group. Data are shown as mean ± sem. *$p < 0.05$ vs. Sham + Veh; ^$p < 0.05$ vs. RI + Veh, RI + P + GHR, and RI + GHR. RI: 9.5 Gy; Veh, vehicle for Peg-G-CSF and vehicle for Ghrelin; P, Peg-G-SF; GHR, Ghrelin.

Peg-G-CSF and Ghrelin Therapy Mitigates Bone Marrow Histopathology

Figure 4 depicts that on day 30 after RI, RI significantly reduced the bone marrow cellularity in vehicle-treated mice, supported by increasing counts of adipocyte (**Figure 4B**) and decreasing megakaryocytes counts in bone marrow histology slides (**Figure 4C**). Co-therapy of Peg-G-CSF and Ghrelin immensely mitigated the number of adipocytes (**Figure 4B**) and partially recovered the number of megakaryocytes (**Figure 4C**) in RI mice. It is interestingly noted that the co-therapy significantly elevated megakaryocyte counts in sham mice as well (**Figure 4C**).

Peg-G-CSF and Ghrelin Therapy Mitigates Bone Marrow Cell Counts After Radiation Injury

Figure 5 depicts that on day 30 after RI, the bone marrow cellularity was significantly reduced in mice treated with vehicles. Co-therapy of Peg-G-CSF and Ghrelin induced a significant increase in the cell counts in RI mice. The treatment with Peg-G-CSF alone significantly elevated the cell counts in sham mice and RI mice, while the treatment with Ghrelin alone did not.

Peg-G-CSF and Ghrelin Therapy Mitigates White Blood Cell Loss but Not Red Blood Cell Loss After Radiation Injury in Peripheral Blood

Radiation is known to deplete WBCs (Kiang et al., 2010). As shown in **Figure 6**, in RI mice, combined treatment with Peg-G-CSF and Ghrelin significantly mitigated neutrophils and eosinophils. Treatment with Peg-G-CSF alone increased neutrophils, lymphocytes and eosinophils; treatment with Ghrelin alone significantly elevated lymphocytes and basophils in RI mice.

RI is known to deplete RBCs (Kiang et al., 2010). As shown in **Figure 7**, treatment with Peg-G-CSF and Ghrelin did not mitigate reduction of RBC numbers, hemoglobin levels and hematocrit readings. It is noted that Peg-G-CSF treatment alone significantly mitigated reduction of RI-induced RBC and hemoglobin, whereas treatment with Ghrelin did not improve the RBC counts, hemoglobin levels and hematocrit readings after RI.

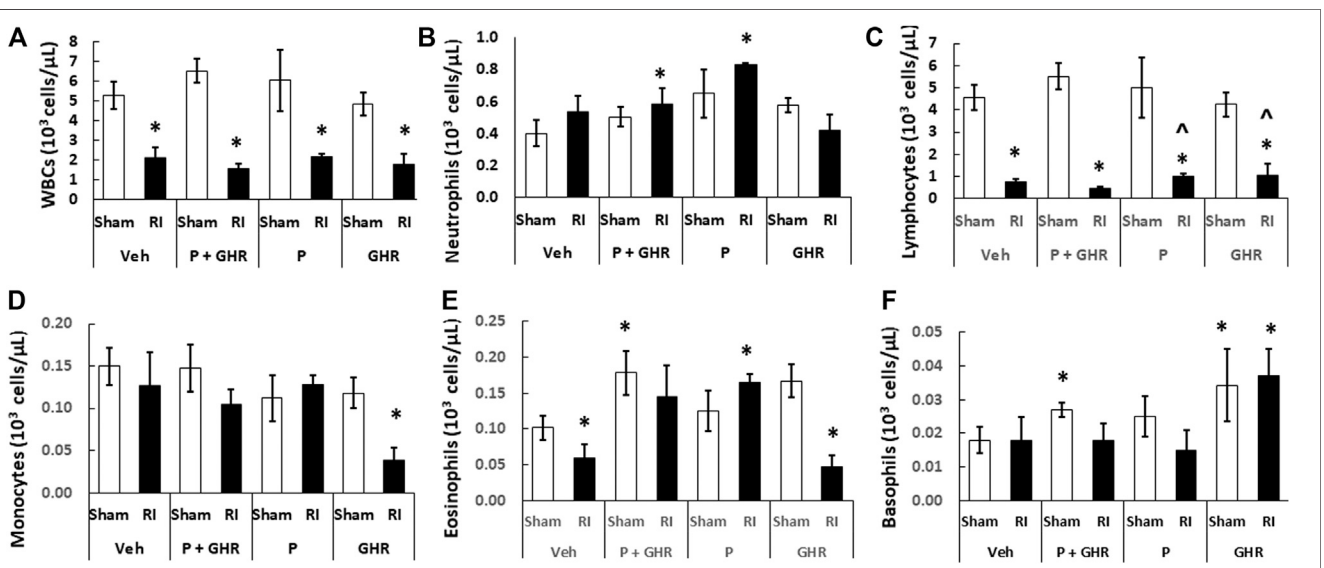

FIGURE 6 | Co-therapy of Peg-G-CSF and Ghrelin significantly increases neutrophils, eosinophils and basophils after irradiation (RI). **(A–F)** WBCs of blood samples collected on day 30 post-RI. *N* = 6 per group. Data are shown as mean ± sem. *$p < 0.05$ vs. Sham + Veh; ^$p < 0.05$ vs. RI + Veh. RI: 9.5 Gy; Veh, vehicle for Peg-G-CSF and vehicle for Ghrelin; P, Peg-G-CSF; GHR, Ghrelin.

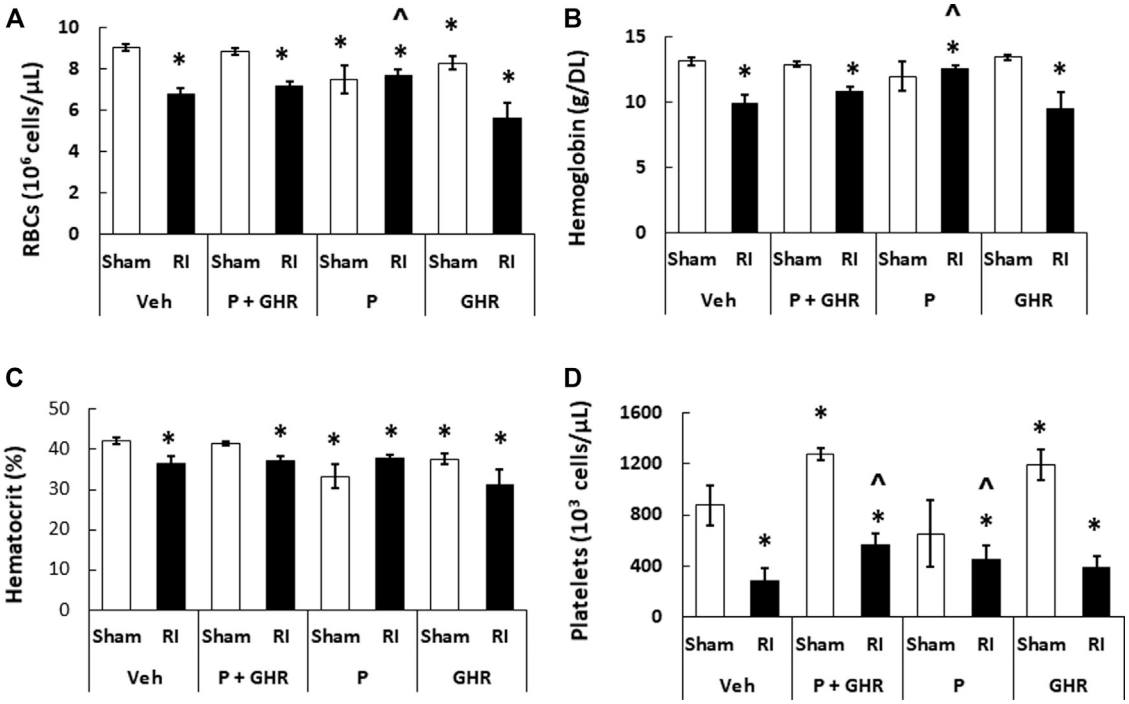

FIGURE 7 | Co-therapy of Peg-G-CSF and Ghrelin significantly mitigate platelet counts but not RBCs, hemoglobin and hematocrit after irradiation (RI). RBCs **(A)**, Hemoglobin **(B)**, Hematocrit, **(C)** and Platelets counts **(D)** in blood samples of sham and RI mice on the 30th day were measured. *N* = 6 per group. Data are shown as mean ± sem. *$p < 0.05$ vs. Sham + Veh; ^$p < 0.05$ vs. RI + Veh. RI: 9.5 Gy; Veh, vehicle for Peg-G-CSF and vehicle for Ghrelin; P, Peg-G-CSF; GHR, Ghrelin.

Peg-G-CSF and Ghrelin Therapy Mitigates the Radiation Injury-Induced Platelet Loss

Figure 4 shows that co-therapy of Peg-G-CSF and Ghrelin induced a significant mitigation of the megakaryocyte loss in surviving RI animals. The number of platelets in peripheral circulation was counted because megakaryocytes are the precursors of circulatory platelets. Peg-G-CSF and Ghrelin combined therapy significantly increased platelets in sham mice and RI mice, which is fully correlated with the increased megakaryocytes in bone marrow samples of sham and RI mice (**Figure 7D**). Treatment with Peg-G-CSF alone mitigated the RI-induced platelet loss while treatment with Ghrelin alone increased platelets in sham mice but not in RI mice.

Peg-G-CSF and Ghrelin Therapy Inhibits the Radiation Injury-Induced Splenomegaly

Spleen is important for survival after lethal RI (Jacobson, 1952). **Figure 8A** shows that RI resulted in splenomegaly. Treatment with Peg-G-CSF and Ghrelin fully inhibited this splenomegaly from occurring. Treatment with Peg-G-CSF alone also inhibited it. In contrast, treatment with Ghrelin did not, which strongly

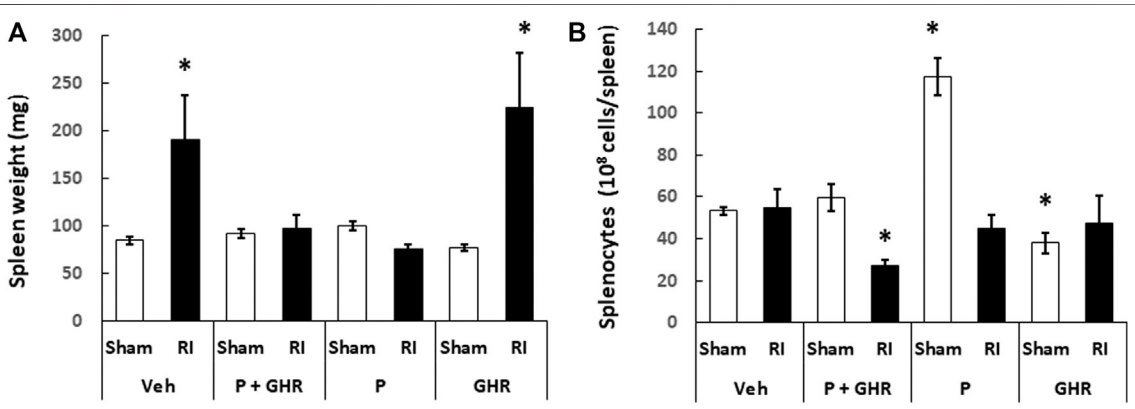

FIGURE 8 | Co-therapy of Peg-G-CSF and Ghrelin inhibits the radiation-induced splenomegaly. Spleen weight **(A)** and splenocytes **(B)** in sham and RI mice on the 30th day were measured. *N* = 6 per group. Data are shown as mean ± sem. *$p < 0.05$ vs. Sham + Veh; RI: 9.5 Gy; Veh, vehicle for Peg-G-CSF and vehicle for Ghrelin; P, Peg-G-SF; GHR, Ghrelin.

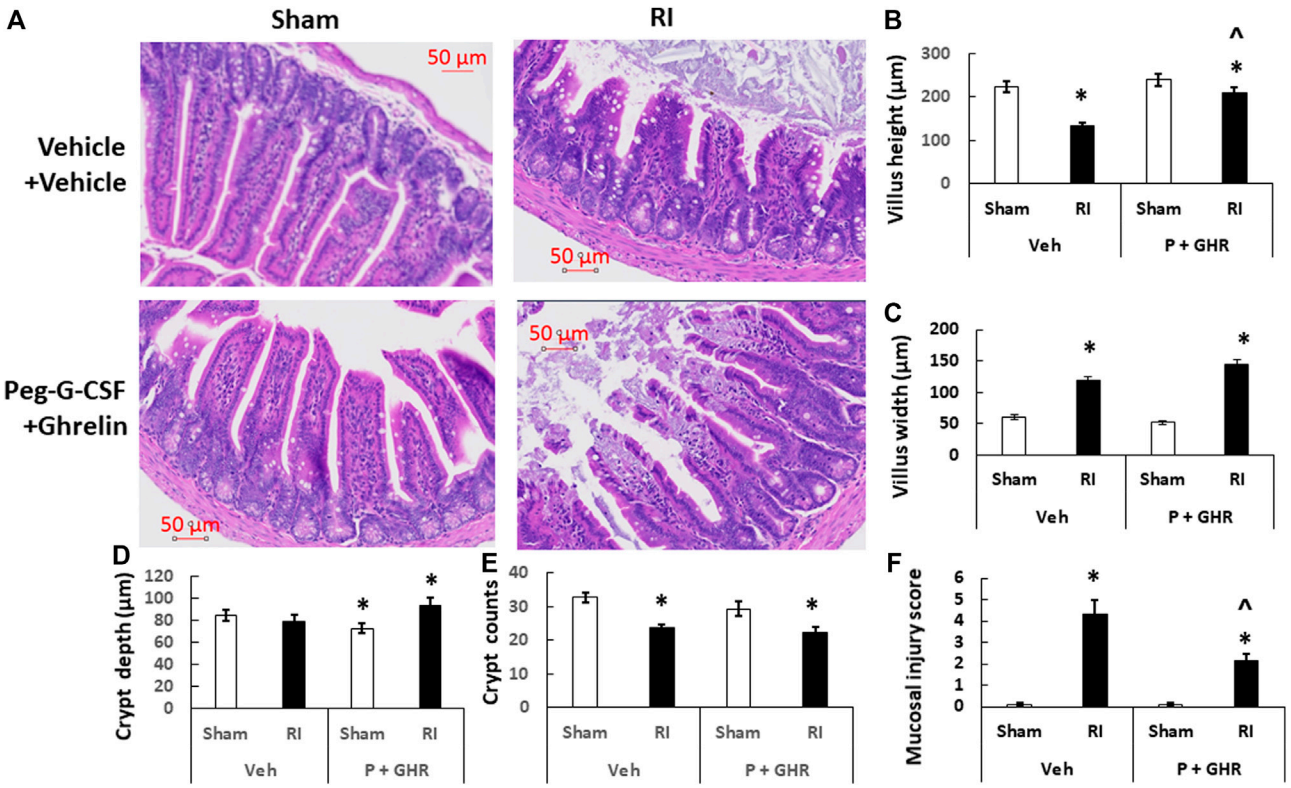

FIGURE 9 | Co-therapy of Peg-G-CSF and Ghrelin mitigates the radiation-induced ileal injury. **(A)** Histology slides stained with H&E of ileums collected on the 30th day post-RI. *N* = 4 per group. **(B–F)** Parameters of ileums including mucosal injury scores, crypt counts and depth, and villus heights and width were assessed. Data are shown as mean ± sem. *$p < 0.05$ vs. Sham + Veh; ^$p < 0.05$ vs. RI + Vehicle. RI: 9.5 Gy; Veh, vehicle for Peg-G-CSF and vehicle for Ghrelin; P, Peg-G-CSF; GHR, Ghrelin.

suggests that Peg-G-CSF is the primary drug to lead to this inhibition.

Although RI induced splenomegaly, **Figure 8B** depicts that splenocyte counts on day 30 after RI had returned to basal levels. Treatment with Peg-g-CSF and Ghrelin reduced the splenocyte counts in RI mice. Treatment with Peg-G-CSF alone dramatically increased the counts in sham mice and recovered the counts in RI mice. On the other hand, treatment with Ghrelin alone lowered splenocytes in sham mice but not in RI mice.

Peg-G-CSF and Ghrelin Therapy Mitigates Intestine Histopathology

RI is known to injure intestine (Kiang et al., 2010). **Figure 9** shows that on day 30 after RI, decreases in villus height, increases in villus width, decreases in crypt counts and increases in mucosal injury score were observed. Treatment with Peg-G-CSF and Ghrelin increased villus height and crypt depth and decreased the mucosal injury score, although the RI-induced increases in villus width and decreases in crypt counts had remained the same.

DISCUSSION

The present paper reports that RI noticeably increased lethality accompanied by body-weight loss and reduced water consumption in mice. These results are in agreement with previous reports in rat (Alpen and Sheline, 1954; Valeriote and Baker, 1964), guinea pig (Korlof, 1956), dog (Brooks, 1952), swine (Baxter et al., 1953), and mice (Ledney et al., 1981; Ledney et al., 1992; Jacob et al., 2010; Ledney and Elliott, 2010; Palmer et al., 2011; Kiang et al., 2012; Kiang and Ledney, 2013; Islam et al., 2015; Kiang and Olabisi, 2019). RI is known to cause massive cellular damage, macro/microcirculation failure, fluid imbalance, immune system inhibition, and acute myelosuppression, thereby, as a result, leading to disruption of vital organ functions. Then, multiple organ dysfunction (MOD) and multiple organ failure (MOF) are manifested and death occurs after irradiation (Brooks et al., 1952; Baxter et al., 1953; Korlof, 1956; Kiang and Olabisi, 2019).

Drugs such as 5-androstenediol (Grace et al., 2012; Whitnall et al., 2002), G-CSF (Farese et al., 2013; Kiang et al., 2014b), Peg-G-CSF (Kiang et al., 2014b; Hankey et al., 2015), and captopril (Islam et al., 2015), were reported to be effective in reducing the lethal RI-induced mortality. Among them, Neupogen (G-CSF) and Neulasta (Peg-G-CSF) are FDA-approved. Even though, the efficacy of either G-CSF or Peg-G-CSF is approximately 30% survival improvement after lethal irradiation exposure. Thus, such a combined therapy of Peg-G-CSF and Ghrelin was attempted and found to result in 75% survival and significantly mitigated body-weight loses after RI, suggesting that keeping up the body weight plays an essential role in this co-therapy.

Peg-G-CSF exhibits an appreciably longer biological half-life in serum than G-CSF (Molineux, 2004). So, daily injections can be avoided as well as eliminating the injection-associated stress. Nonetheless, the Peg-G-CSF's survival efficacy remained similar to G-CSF after irradiation (Kiang et al., 2014b). The Peg-G-CSF survival efficacy data after RI is consistent with that observed in nonhuman primates (Hankey et al., 2015).

RI significantly reduced the bone marrow cell counts as shown by significant decreases in megakaryocyte counts plus significant rises in fat cells (**Figure 4**). The observations are similar to our previous reports (Kiang et al., 2017; Wang et al., 2021). The increase in platelets (**Figure 7D**) is further confirmed with the increases in megakaryocytes in bone marrow. Because the RI-induced hemorrhage occurs, increases in platelets by the co-therapy become critical for healing and subsequent survival (Kiang et al., 2019). Moreover, this increase is primarily contributed by the treatment with Ghrelin but not Peg-G-CSF (**Figure 7D**).

RI significantly reduced WBC counts even on day 30 (Kiang et al., 2010; Kiang et al., 2012). mainly due to very low counts of eosinophils and lymphocytes (**Figure 6**). The data are similar to the finding obtained in nonhuman primates that were irradiated prior to treatment with peg-megakaryocyte growth and development factor in combination with G-CSF therapy (Farese et al., 1996). Peg-G-CSF is known to stimulate myeloid progenitors to proliferate, to differentiate, to become mature granulocytes, to get mobilized into the bloodstream from the bone marrow, and most importantly to make mature neutrophils effective in combating RI-induced infection (Metcalf, 1990; Metcalf, 2007) and wound healing (Badiavas et al., 2003). We think, that the co-therapy increased platelets in sham animals due to Ghrelin, but in RI mice due to both Peg-G-CSF and Ghrelin (**Figure 6**), further reinforced by the recovery of bone marrow cellularity (**Figure 5**).

Reports from our laboratory and other laboratories indicate that Peg-G-CSF treatment alone in mice (Kiang et al., 2014b), G-CSF administration in canines (MacVittie et al., 1990), and an IL-3/G-CSF receptor agonist in nonhuman primates (MacVittie et al., 2000) increased platelet counts after RI. In this study, we found the co-therapy effectively increased platelet counts after RI. These data suggest that recovery of platelets may contribute at least partially to the RI mouse 30-days survival. G-CSF administration to healthy humans is known to trigger endothelial cell activation to lead to an inflammatory process so as to increase platelet counts (Ihara et al., 2008). However, we postulate that Peg-G-CSF administration to healthy mice is incapable of triggering such process resulting in no visible induction of thrombopoiesis in sham mice. On the other hand, Ghrelin enables to increase thrombopoiesis in sham mice.

On day 30 after RI, significantly low hematocrit readings, hemoglobin levels, and RBC counts were remained in surviving mice (**Figure 7**). Despite the RI-induced decreases were fully recovered in Peg-G-CSF treated mice, in Ghrelin-treated mice and co-treated mice no such a recovery was found, suggesting increases in erythropoietin production by Peg-G-CSF may have been antagonized by Ghrelin. It warrants further exploration in this line.

Jacobson (1952) reported that mice with protected spleen survived from the lethal irradiation, suggesting spleen plays a key role for survival. Herein, we observed RI induced a spleen enlargement without altering the splenocyte counts. The co-therapy inhibited this enlargement, which was attributed primarily by Peg-G-CSF's inhibition. Ghrelin treatment alone did not block the RI-induced splenomegaly (**Figure 8**). We also found that the co-therapy reduced splenocytes after RI. In contrast, treatment with either one did not. It is elusive and worth to explore further.

Table 1 summarizes observations of survival, body weight, WBCs, RBCs, platelets, spleen weigh and splenocytes. In the presence of Peg-G-CSF and Ghrelin, mitigation of body weight loss, neutrophil depletion, and platelet reduction are important for survival after RI. Additionally, literature documents that RI at the $LD_{50/30}$ dose damages gastrointestinal system (Kiang and Olabisi, 2019).

Our laboratory has been investigated ileum because the section near caecum is empty and easy for histology examination and analysis. RI reduced the villus height and crypt counts, and increased villus swelling and mucosal injury (**Figure 9**). This co-therapy was effective to combat these detrimental outcomes, very similar to the Ghrelin treatment alone (Kiang et al., 2020) whereas treatment with Peg-G-CSF alone failing to improve the ileum injury has been demonstrated (Wang et al., 2021). These results, taking together with previous observations with either bone marrow hemopoietic stem cells resulting in more than 90% survival (Ledney and Elliott, 2010) or mesenchymal cells failing in survival improvement (Kiang and Gorbunov, 2014), suggest that Ghrelin treatment primarily contributes to the ileum recovery including improvement of tight junctions, enterocytes, sepsis and cell survival by inhibiting IL-18 and bcl-2-like protein 4 (BAX) signals (Kiang et al., 2020), whereas Peg-G-CSF treatment primarily repaires bone marrow by increasing granulocyte, erythrocyte, monocyte, megakaryocyte (GEMM) colonies (Wang et al., 2021). We consider Peg-G-CSF and Ghrelin target bone marrow and intestine, respectively, leading to this enhancement in survival.

To elucidate the underlying molecular mechanisms, tissues from both surviving and moribund animals at early time points

TABLE 1 | Treatment with Peg-G-CSF alone, Ghrelin alone, or the combination of both impacts survival, body weight, WBCs, RBCs, platelets, spleen weight and splenocytes after RI. Survival, body weight, numbers of WBCs, RBCs, and platelets, spleen weight, and splenocytes were reduced after RI and remained low 30 days later. Comparisons are made from data pooled from three separate experiments.

	Increases in survival above RI + Veh (%)	Body weight	WBCs	RBCs	Platelets	Spleen weight	Splenocytes
Peg-G-CSF	32	↓	↓	↑	↓	↓	↑
Ghrelin	0	↓	↓	↓	↑	↑	↑
Peg-G-CSF + ghrelin	45	↑	↓	↓	↑	↓	↓

RI, radiation injury; Veh, vehicles; ↑, increase; ↓, decrease.

are desirable for investigation. Such cytokine profiling for the inflammation status in tissues, cell cycle analysis in bone marrow, DNA damage assay in lymphocytes, stem cell colony forming assay in bone marrow cells, immune cell populations, kidney health, and tight junctions in intestine, bacterial load in heart, liver, and spleen, and apoptosis in bone marrow and intestine are undergoing in our laboratory.

In summary, RI induced mortality, body-weight loss, and dehydration. Co-therapy of Peg-G-CSF and Ghrelin after RI significantly resulted in enhancement of 30-days survival after RI, mitigation of body-weight loss, hematopoietic acute radiation syndrome and GI acute radiation syndrome in RI mice. These results support the hypothesis/concept of the peg-G-CSF and Ghrelin combination as a co-therapy being efficacious for treating RI. Such a co-therapy could provide timely treatments to RI victims so as to save lives after a nuclear accident.

DATA AVAILABILITY STATEMENT

The original contributions presented in the study are included in the article/Supplementary Material, further inquiries can be directed to the corresponding author.

ETHICS STATEMENT

The animal study was reviewed and approved by the Armed Forces Radiobiology Research Institute IACUC committee. The approved IACUC protocols are 2010-12-016 and 2017-01-002 with a biosample sharing approval.

AUTHOR CONTRIBUTION

JK conceived and designed the experiment. MZ, BL, JS, MA, and SJ performed the animal experiment. JK, JS, and MA performed biochemical assays. MZ and MA performed histology examination. JGK completed writing the draft of the manuscript. The final manuscript was read, edited, and approved by all authors.

FUNDING

This project was supported by NIAID-AFRRI IAA AA112044-001-05000 work plan A and AFRRI RAB310934, RAB33529, and RBB34363. The funding agencies have no roles on the experiments.

ACKNOWLEDGMENTS

The authors thank the staff in the Veterinary Sciences Department for caring for animals, staff in the Radiation Dosimetry Department for performing irradiation, and staff in the Big Instrument Center for handling histology slides with hematoxylin and eosin staining.

REFERENCES

Alpen, E. L., and Sheline, G. E. (1954). The combined effects of thermal burns and whole-body x-radiation on survival time and mortality. *Ann. Surg.* 140 (1), 113–118. doi:10.1097/00000658-195407000-00013

Badiavas, E. V., Abedi, M., Butmarc, J., Falanga, V., and Quesnberry, P. (2003). Participation of bone marrow derived cells in cutaneous wound healing. *J. Cell. Physiol.* 196 (2), 245–250. doi:10.1002/jcp.10260

Baxter, H., Drummond, J. A., Stephens-Newsham, L. G., and Randall, R. G. (1953). Studies on acute total body irradiation in animals. I. Effect of streptomycin following exposure to a thermal burn and irradiation. *Plast. Reconstr. Surg.* 12 (6), 439–445. doi:10.1097/00006534-195312000-00007

Berger, M. E., Christensen, D. M., Lowry, P. C., Jones, O. W., and Wiley, A. L. (2006). Medical management of radiation injuries: current approaches. *Occup. Med.* 56 (3), 162–172. doi:10.1093/occmed/kql011

Bertho, J. M., Roy, L., Souidi, M., Benderitter, M., Gueguen, Y., Lataillade, J. J., et al. (2008). New biological indicators to evaluate and monitor radiation-induced damage: an accident case report. *Radiat. Res.* 169 (5), 543–550. doi:10.1667/RR1259.1

Brooks, J. W., Evans, E. I., Ham, W. T., Jr, and Reid, J. D. (1952). The influence of external body radiation on mortality from thermal burns. *Ann. Surg.* 136 (3), 533–545. doi:10.1097/00000658-195209000-00018

Farese, A. M., Hunt, P., Grab, L. B., and MacVittie, T. J. (1996). Combined administration of recombinant human megakaryocyte growth and development factor and granulocyte colony-stimulating factor enhances multilineage hematopoietic reconstitution in nonhuman primates after radiation-induced marrow aplasia. *J. Clin. Invest.* 97 (9), 2145–2151. doi:10.1172/JCI118652

Farese, A. M., Cohen, M. V., Stead, R. B., Jackson, W., 3rd, and Macvittie, T. J. (2012). Pegfilgrastim administered in an abbreviated schedule, significantly improved neutrophil recovery after high-dose radiation-induced myelosuppression in rhesus macaques. *Radiat. Res.* 178 (5), 403–413. doi:10.1667/RR2900.1

Farese, A. M., Cohen, M. V., Katz, B. P., Smith, C. P., Gibbs, A., Cohen, D. M., et al. (2013). Filgrastim improves survival in lethally irradiated nonhuman primates. *Radiat. Res.* 179 (1), 89–100. doi:10.1667/RR3049.1

Fritz, E. M., Singewald, N., and De Bundel, D. (2020). The good, the bad and the unknown aspects of ghrelin in stress coping and stress-related psychiatric disorders. *Front. Synaptic Neurosci.* 12, 594484. doi:10.3389/insyn.2020.594484

Fukumoto, R., Cary, L. H., Gorbunov, N. V., Elliott, T. B., and Kiang, J. G. (2013). Ciprofloxacin modulates cytokine profiles, accelerates bone marrow recovery and mitigates ileum injury after radiation combined with wound trauma. *PLoS One.* 8 (3), e58389. doi:10.1371/journal.pone.0058389

Fukumoto, R., and Kiang, J. G. (2011). Geldanamycin analog 17-DMAG limits apoptosis in human peripheral blood cells by inhibition of p53 activation and its interaction with heat shock protein 90 kDa after ionizing radiation. *Radiat. Res.* 176 (3), 333–345. doi:10.1667/rr2534.1

Gorbunov, V. N., and Kiang, J. G. (2021). Brain damage and patterns of neurovascular disorder following ionizing irradiation complications in radiotherapy and radiation combined injury. *Radiat. Res.*

Grace, M. B., Singh, V. K., Rhee, J. G., Jackson, W. E., 3rd, Kao, T. C., and Whitnall, M. H. (2012). 5-AED enhances survival of irradiated mice in a G-CSF-dependent manner, stimulates innate immune cell function, reduces radiation-induced DNA damage and induces genes that modulate cell cycle progression and apoptosis. *J. Radiat. Res.* 53 (6), 840–853. doi:10.1093/jrr/rrs060

Hankey, K. G., Farese, A. M., Blaauw, E. C., Gibbs, A. M., Smith, C. P., Katz, B. P., et al. (2015). Pegfilgrastim improves survival of lethally irradiated nonhuman primates. *Radiat. Res.* 183 (6), 643–655. doi:10.1667/RR13940.1

Ihara, A., Matsui, K., Minami, R., Uchida, S., Ueda, S., and Nishiura, T. (2008). Granulocyte colony-stimulating factor increases the platelet volume in peripheral stem cell apheresis donors. *Pathophysiol. Haemostasis Thrombosis.* 36 (5), 266–270. doi:10.1159/000252823

Islam, A., Bolduc, D. L., Zhai, M., Kiang, J. G., and Swift, J. M. (2015). Captopril increases survival after whole-body ionizing irradiation but decreases survival

when combined with skin-burn trauma in mice. *Radiat. Res*. 184 (3), 273–279. doi:10.1667/RR14113.1

Jacob, A., Shah, K. G., Wu, R., and Wang, P. (2010). Ghrelin as a novel therapy for radiation combined injury. *Mol. Med*. 16 (3-4), 137–243. doi:10.2119/molmed.2009.00154

Jacobson, L. O. (1952). Evidence for a humoral factor (or factors) concerned in recovery from radiation injury: a review. *Cancer Res*. 12 (5), 315–325.

Kiang, J. G., Jiao, W., Cary, L. H., Mog, S. R., Elliott, T. B., Pellmar, T. C., et al. (2010). Wound trauma increases radiation-induced mortality by increasing iNOS, cytokine concentrations, and bacterial infections. *Radiat. Res*. 173 (3), 319–332. doi:10.1667/RR1892.1

Kiang, J. G., Garrison, B. R., Burns, T. M., Zhai, M., Dews, I. C., Ney, P. H., et al. (2012). Wound trauma alters ionizing radiation dose assessment. *Cell Biosci*. 2, 20. doi:10.1186/2045-3701-2-20

Kiang, J. G., Zhai, M., Liao, P.-J., Bolduc, D. L., Elliott, T. B., and Gorbunov, N. V. (2014a). Pegylated G-CSF inhibits blood cell depletion, increases platelets, blocks splenomegaly, and improves survival after whole-body ionizing irradiation but not after irradiation combined with burn. *Oxid. Med. Cell. Longev*. 2014, 481392. doi:10.1155/2014/481392

Kiang, J. G., Zhai, M., Liao, P.-J., Elliott, T. B., and Gorbunov, N. V. (2014b). Ghrelin therapy improves survival after whole-body ionizing irradiation combined with wound or burn: amelioration of leukocytopenia, thrombopenia, splenomegaly, and bone marrow injury. *Oxid. Med. Cell. Longev*. 2014, 215858. doi:10.1155/2014/215858

Kiang, J. G., Garrison, B. R., Smith, J. T., and Fukumoto, R. (2014c). Ciprofloxacin as a potential radio-sensitizer to tumor cells and a radio-protectant for normal cells: differential effects on γ-H2AX formation, p53 phosphorylation, Bcl-2 production, and cell death. *Mol. Cell. Biochem*. 393 (1-2), 133–143. doi:10.1007/s11010-014-2053-z

Kiang, J. G., Zhai, M., Bolduc, D. L., Smith, J. T., Anderson, M. N., Ho, C., et al. (2017). Combined therapy of pegylated-G-CSF and Alx4100TPO improves survival and mitigate acute radiation syndrome after whole-body ionizing irradiation alone and followed by wound trauma. *Radiat. Res*. 188 (5), 476–490. doi:10.1667/RR14647.1

Kiang, J. G., Anderson, M. N., and Smith, J. T. (2018). Ghrelin therapy sustains granulocyte colony-stimulating factor and keratinocyte factor to mitigate hematopoietic syndrome and spleen after whole-body ionizing irradiation combined with wound. *Cell Biosci*. 8, 27. doi:10.1186/s13578-018-0225-3

Kiang, J. G., Smith, J. T., Anderson, M. N., Umali, M. V., Ho, C., Zhai, M., et al. (2019). A novel therapy, using Ghrelin with pegylated G-CSF, inhibits brain hemorrhage from ionizing radiation or combined radiation injury. *Pharm. Pharmacol. Int. J*. 7 (3), 133–145. doi:10.15406/ppij.2019.07.00243

Kiang, J. G., Smith, J. T., Cannon, G., Anderson, M. N., Ho, C., Zhai, M., et al. (2020). Ghrelin, a novel therapy, corrects cytokine and NF-κB-AKT-MAPK network and mitigates intestinal injury induced by combined radiation and skin-wound trauma. *Cell Biosci*. 10, 63. doi:10.1186/s13578-020-00425-z

Kiang, J. G., and Gorbunov, N. V. (2014). Bone marrow mesenchymal stem cells increases survival after ionizing irradiation combined with wound trauma: characterization and therapy. *J. Cell Sci. Ther*. 5, 190. doi:10.4172/2157-7013.1000190

Kiang, J. G., and Ledney, G. D. (2013). Skin injuries reduce survival and modulate corticosterone, C-reactive protein, complement component 3, IgM, and prostaglandin E2 after whole-body reactor-produced mixed field (n + gamma Photons) Irradiation. *Oxid. Med. Cell. Longev*. 2013, 821541. doi:10.1155/2013/821541

Kiang, J. G., and Olabisi, A. O. (2019). Radiation: a poly-traumatic hit leading to multi-organ death. *Cell Biosci*. 9, 25. doi:10.1186/s13578-019-0286-y

Koch, A., Gulani, J., King, G., Hieber, K., Chappell, M., and Ossetrova, N. (2016). Establishment of early endpoints in mouse total-body irradiation model. *PLoS One*. 11 (8), e0161079. doi:10.1371/journal.pone.0161079

Korlof, B. (1956). Infection of burns, I. A bacteriological and clinical study of 99 cases. II. Animal experiments: burns and total body x-irradiation. *Acta Chiropractic Scandinavian Suppl*. 209, 1–144

Ledney, G. D., and Elliott, T. B. (2010). Combined injury: factors with potential to impact radiation dose assessments. *Health Phys*. 98 (2), 145–152. doi:10.1097/01.HP.0000348466.09978.77

Ledney, G. D., Stewart, D. A., Exum, E. D., and Sheehy, P. A. (1981). Skin wound-enhanced survival and myelocytopoiesis in mice after whole-body irradiation. *Acta Radiol. Oncol*. 20 (1), 29–38. doi:10.3109/02841868109130187

Ledney, G. D., Elliott, T. B., and Moore, M. M. (1992). "Modulations of mortality by tissue trauma and sepsis in mice after radiation injury," in *The biological basis of radiation protection practice*.. Editors K. L. Mossman and W. A. Mills (Baltimore: Williams and Wilkins), 202–217.

MacVittie, T. J., Monroy, R. L., Patchen, M. L., and Souza, L. M. (1990). Therapeutic use of recombinant human G-CSF (rhG-CSF) in a canine model of sublethal and lethal whole-body irradiation. *Int. J. Radiat. Biol*. 57 (4), 723–736. doi:10.1080/09553009014550891

MacVittie, T. J., Farese, A. M., Smith, W. G., Baum, C. M., Burton, E., and McKearn, J. P. (2000). Myelopoietin, an engineered chimeric IL-3 and G-CSF receptor agonist, stimulates multilineage hematopoietic recovery in a nonhuman primate model of radiation-induced myelosuppression. *Blood*. 95 (3), 837–845. doi:10.1182/blood.v95.3.837.003k08_837_845

Metcalf, D. (1990). "The role of the colony-stimulating factors in the treatment of infections frontiers of infectious diseases: new antibacterial strategies," in Proceedings of an international symposium. Brocket Hall, hertfordshire 6-30 to 7-3/1990. Editor H. C. Neu (New York: Churchill Livingstone).

Metcalf, D. (2007). On hematopoietic Stem cell fate. *Immunity*. 26 (6), 669–673. doi:10.1016/j.immuni.2007.05.012

Molineux, G. (2004). The design and development of pegfilgrastim (PEG-metHuG-CSF, Neulasta). *Curr. Pharmacol. Design*. 10 (11), 1235–1244. doi:10.2174/1381612043452613

Palmer, J. L., Deburghgraeve, C. R., Bird, M. D., Hauer-Jensen, M., and Kovacs, E. J. (2011). Development of a combined radiation and burn injury model. *J. Burn Care Res*. 32 (2), 317–323. doi:10.1097/BCR.0b013e31820aafa9

Pereira, J. A. D. S., da Silva, F. C., and de Moraes-Vieira, P. M. M. (2017). The impact of ghrelin in metabolic diseases: an immune perspective. *J. Diabetes Res*. 2017, 4527980. doi:10.1155/2017/4527980

Shah, K. G., Wu, R., Jacob, A., Blau, S. A., Ji, Y., Dong, W., et al. (2009). Human ghrelin ameliorates organ injury and improves survival after radiation injury combined with severe sepsis. *Mol. Med*. 15 (11-12), 407–414. doi:10.2119/molmed.2009.00100

Singh, V. K., Newman, V. L., and Seed, T. M. (2015). Colony-stimulating factors for the treatment of the hematopoietic component of the acute radiation syndrome (H-ARS): a review. *Cytokine*. 71 (1), 22–37. doi:10.1016/j.cyto.2014.08.003

Valeriote, F. A., and Baker, D. G. (1964). The combined effects of thermal trauma and x-irradiation on early mortality. *Radiat. Res*. 22, 693–702

Vasileiou, I., Patsouras, D., Patsouris, E., and Theocharis, S. (2013). Ghrelin and toxicity: recent findings and future challenges. *J. Appl. Toxicol*. 3, 238–245. doi:10.1002/jat.2803

Wang, L., Zhai, M., Lin, B., Cui, W., Hull, L., Li, X., et al. (2021). Peg-G-CSF and L-Citrulline combinational therapy for mitigating skin wound combined radiation injury in a mouse model. *Radiat. Res*.

Waselenko, J. K., MacVittie, T. J., Blakely, W. F., Pesik, N., Wieley, A. L., Dickerson, W. E., et al. (2004). Strategic national stockpile radiation working group. Medical management of the acute radiation syndrome: recommendations of the strategic national stockpile radiation working group. *Ann. Intern. Med*. 140 (12), 1037–1051. doi:10.7326/0003-4819-140-12-200406150-00015

Whitnall, M. H., Elliott, T. B., Landauer, M. R., Wilhelmsen, C. L., McKinney, L., Kumar, K. S., et al. (2002). Protection against gamma-irradiation with 5-androstenediol. *Mil. Med*. 167, 64–65. doi:10.1177/153537020222600707

Wynne, K., Giannitsopoulou, K., Small, C. J., Patterson, M., Frost, G., Ghatei, M. A., et al. (2005). Subcutaneous ghrelin enhances acute food intake in malnourished patients who receive maintenance peritoneal dialysis: a randomized, placebo-controlled trial. *J. Am. Soc. Nephrol*. 16, 2111–2118. doi:10.1681/ASN.2005010039

Conflict of Interest: The authors declare that the research was conducted in the absence of any commercial or financial relationships that could be construed as a potential conflict of interest.

frontiers in Pharmacology

ORIGINAL RESEARCH
published: 26 March 2021
doi: 10.3389/fphar.2021.635792

Comparison of Local and Systemic DTPA Treatment Efficacy According to Actinide Physicochemical Properties Following Lung or Wound Contamination in the Rat

Nina M. Griffiths, Anne Van der Meeren and Olivier Grémy*

Laboratoire de RadioToxicologie, CEA, Université de Paris-Saclay, Bruyères le Châtel, France

OPEN ACCESS

Edited by:
Diane Riccobono, Institut de Recherche Biomédicale des Armées (IRBA), France

Reviewed by:
Sara Dumit, Los Alamos National Laboratory (DOE), Los Alamos, NM, United States
John Klumpp, Los Alamos National Laboratory (DOE), Los Alamos, NM, United States

****Correspondence:***
Nina M. Griffiths
nina.griffiths@cea.fr

Specialty section:
This article was submitted to Translational Pharmacology, a section of the journal Frontiers in Pharmacology

Received: *30 November 2020*
Accepted: *02 February 2021*
Published: *26 March 2021*

Citation:
Griffiths NM, Van der Meeren A and Grémy O (2021) Comparison of Local and Systemic DTPA Treatment Efficacy According to Actinide Physicochemical Properties Following Lung or Wound Contamination in the Rat. Front. Pharmacol. 12:635792. doi: 10.3389/fphar.2021.635792

Purpose: In cases of occupational accidents in nuclear facilities or subsequent to terrorist activities, the most likely routes of internal contamination with alpha-particle emitting actinides, such as plutonium (Pu) and americium (Am), are by inhalation or following wounding. Following contamination, actinide transfer to the circulation and subsequent deposition in skeleton and liver depends primarily on the physicochemical nature of the compound. The treatment remit following internal contamination is to decrease actinide retention and in consequence potential health risks, both at the contamination site and in systemic retention organs as well as to promote elimination. The only approved drug for decorporation of Pu and Am is the metal chelator diethylenetriaminepentaacetic acid (DTPA). However, a limited efficacy of DTPA has been reported following contamination with insoluble actinides, irrespective of the contamination route. The objectives of this work are to evaluate the efficacy of prompt local and/or systemic DTPA treatment regimens following lung or wound contamination by actinides with differing solubility. The conclusions are drawn from retrospective analysis of experimental studies carried out over 10 years.

Materials and Methods: Rat lungs or wounds were contaminated either with poorly soluble Mixed OXide (U, Pu O_2) or more soluble forms of Pu (nitrate or citrate). DTPA treatment was administered promptly after contamination, locally to lungs by insufflation of a powder or inhalation of aerosolized solution or by injection directly into the wound site. Intravenous injections of DTPA were given either once or repeated in combination with the local treatment. Doses ranged from 1 to 30 µmol/kg. Animals were euthanized from day 7–21 and alpha activity levels were measured in urine, lungs, wound, bone and liver for determination of decorporation efficacy.

Results: Different experiments confirmed that whatever the route of contamination, most of the activity is retained at the entry site after insoluble MOX contamination as compared with contamination with more soluble forms which results in very low activities reaching the systemic compartment and subsequent retention in bone and liver. Several DTPA treatment regimens were evaluated that had no significant effect on either lung or

wound levels compared with untreated animals. In contrast, in all cases systemic retention (skeleton and liver) was reduced and urinary excretion were enhanced irrespective of the contamination route or DTPA treatment regimen.

Conclusion: The present study demonstrates that despite limitation of retention in systemic organs, different DTPA protocols were ineffective in removing insoluble actinides deposited in lungs or wound site. For moderately soluble actinides, local or intravenous DTPA treatment reduced activity levels both at contamination and at systemic sites.

Keywords: actinides, contamination, decorporation, DTPA, lung, wound

INTRODUCTION

Internal contamination with high-energy alpha particle emitters such as the actinides plutonium (Pu) or americium (Am), presents a challenge to the design and application of radiation medical countermeasures. In contrast to external gamma radiation exposure, internal contamination following either inhalation or wounding results in deposition of radioactive elements at the primary site of contamination, i.e. lungs or injury site, as well as in systemic target tissues that retain these elements. The primary objective of countermeasures is therefore to reduce these radioactivity levels. Even if stringent radiation protection measures are taken internal contamination with Pu/Am remains a potential hazard for workers involved in various stages of the nuclear fuel cycle such as preparation and reprocessing of used fuel, treatment/conditioning of waste as well as reactor decommissioning. Furthermore, in the event of an attack with a Radiological Dispersal Device or "Dirty Bomb" dissemination of actinides would be a potential health hazard for the general public and first responders resulting in serious radioactive contamination. Contamination by inhalation of aerosols may be associated with exposure of higher numbers of people as compared with contamination after wounding.

Cases of actinide contamination by inhalation have been reported since the initial use of compounds for either military devices or nuclear fuels (Carbaugh and La Bone, 2003; Okladnikova et al., 2005; Grappin et al., 2007). Similarly, accidental entry of actinides following wounding has also been reported (Ilyin, 2001; Falk et al., 2006; James et al., 2007; Sugarman et al., 2018; Klumpp et al., 2020). Indeed, case reports of incidents/accidents, biological assay data and tissues have been collated by registries in several countries (Loffredo et al., 2017; Kathren and Tolmachev, 2019) that provide a valuable source of information.

Inhalation and subsequent deposition of actinides in deep lung compartments results partly in transfer to the bloodstream. The size of this transferable fraction is dependent on a number of variables but in particular, the physicochemical nature of the actinide compounds. In the case of skin contamination, under normal healthy conditions, these compounds do not cross the epidermal skin barrier easily. However, this may be significantly increased after wounding associated with concomitant physical insults that result in loss of skin barrier function. This may be associated with strongly acidic actinide solutions that result in burns as was the case at Rocky Flats in 1965 and Hanford in 1976 (Lagerquist et al., 1967; McMurray, 1983). Such cases of actinide and acid are a dual insult to the skin barrier. Whatever the primary site of contamination (lungs or wound) and subsequent entry into the general circulation, the main sites of secondary long-term retention for Pu and Am are the skeleton and liver (International Commission on Radiological Protection (ICRP), 1986). A small fraction of circulating actinides will be excreted predominantly in urine with minor levels in faeces. More soluble compounds will be transferred more rapidly and in a larger proportion, whether after inhalation or wounding (International Commission on Radiological Protection (ICRP), 1986; National Council on Radiological Protection and Measurements (NCRP), 2006).

The question of the fate of tissue-retained actinides, even initially soluble ones, has been studied particularly with regard to deposition and retention in lungs and eventual effective dose (International Commission on Radiological Protection(ICRP), 1994a). Retention compartments in the lungs can be macrophages, interstitial connective tissue as well as scar tissue (Hahn et al., 2004; Van der Meeren et al., 2012; Van der Meeren et al., 2014; Lamart et al., 2017; Birchall et al., 2019). Regardless of contaminant solubility (from soluble to insoluble forms such as oxides and metals), retained activity may be considered as a "reservoir". Actinides in this "reservoir" may be very slowly dissolved, absorbed into the blood and afterwards transferred to systemic organs so contributing to the systemic long-term effective radiation dose. Countermeasures are also required to address these "reservoir" problems that contribute to the long-term effects of an inhomogeneous chronic irradiation. Following inhalation of actinides pneumonitis, lung fibrosis and tumour development have been observed in a number of species (rat, mouse and dog) (Dudoignon et al., 2003; Muggenburg et al., 2008; Griffiths et al., 2010), as well as in man (Hahn et al., 2004; Newman et al., 2005; Sychugov et al., 2020). The pathological consequences after wounding have been less well-studied. However, a clinical report by Lushbaugh and Langham (1962) observed cutaneous necrosis and fibrosis around the highly active Pu deposit.

As a countermeasure and regardless of the Pu/Am compound and the route of intake, the only approved treatment for decorporation (removal from the body) of Pu/Am in man

remains diethylenetriaminepentaacetic acid (DTPA) as the calcium or zinc salt (Food and Drug Administration, 2003; Grappin and Bérard, 2008). DTPA is a metal chelator that has a high affinity in particular for Pu and Am and first published data on the efficacy of this compound to remove (decorporate) these elements appeared in the 1960s (Norwood, 1960). DTPA is a highly charged acidic compound that has a short plasma half-life, is poorly absorbed and is rapidly eliminated by glomerular filtration. It is considered to circulate mainly in the extracellular fluids where it is able to chelate actinides. In general and as recommended the DTPA solution is administered as soon as possible for the most part by intravenous injection or infusion. Inhalation of the aerosolized DTPA solution is only recommended in cases of contamination by inhalation (Food and Drug Administration, 2003; ANSM, 2011). Experimental DTPA formulations have also been tested in rodents such as liposomes for cell entry enhancement (Grémy et al., 2018) or a dry powder for better delivery into deep lung (Grémy et al., 2010; Grémy et al., 2012).

For local treatment of contaminated wounds, DTPA solution is used for external decontamination as well as for irrigation of the wound site. In addition, intravenous DTPA administration is used concomitantly where excision of contaminated wound is necessary (National Council on Radiological Protection and Measurements. (NCRP), 2009). The beneficial effects of local injection of DTPA to a contaminated wound site have been little studied to date although animal studies have demonstrated this route to be effective (Volf, 1974; Harrison and David, 1979; Stradling et al., 1993; Griffiths et al., 2014).

Many studies have been carried out on the effect of different regimens of DTPA treatment following contamination by inhalation or wounding with single actinides under different chemical forms (oxides, nitrate) but only few studies to date have been carried out following contamination by Mixed U, Pu OXide (MOX) that is used in the nuclear fuel cycle.

This paper presents an overview of *in vivo* data obtained in rat for actinide decorporation by different DTPA regimens of varying physicochemical forms. The principal objective was to compare local and systemic DTPA treatment regimens according to actinide physicochemical properties following lung or wound contamination. As far as possible the same treatment protocols (local, systemic or combined) are compared for each actinide compound in either the lung or wound model of contamination. Efficacy was determined from the key parameters of DTPA-induced increase in urinary actinide excretion together with evidence for reduction in actinide retention at the primary site of contamination, i.e., lung or wound site, and in key secondary retention organs, namely bone and liver.

MATERIALS AND METHODS

Chemicals

Marketed DTPA solution as the calcium trisodium salt [Na_3(Ca-DTPA)] was obtained from the Pharmacie Centrale des Armées (PCA; Orléans, France). DTPA dry powder (75% DTPA) was formulated as previously described in detail elsewhere (Gervelas et al., 2007). This powder has good aerosolization properties due to a median geometric diameter of 4.5 µm and a "crumpled paper" morphology (Gervelas et al., 2007) allowing access to deep alveolar compartments.

Preparation of Actinide Contaminants

Plutonium used for experiments was obtained from two laboratory stock solutions of Pu kept in 2 M HNO_3, acquired from the French Alternative Energies and Atomic Energy Commission (CEA).

Pu Nitrate Solution for Contamination

After evaporation of an aliquot of the first stock Pu solution (86.1% ^{238}Pu, 12.5% ^{239}Pu), Pu was dissolved in distilled water to have a working Pu nitrate solution with low nitrate.

Pu Citrate Solution for Contamination

After Pu purification by anion exchange chromatography of an aliquot of the second stock Pu solution and evaporation (99.5% ^{238}Pu, 0.5% ^{239}Pu), Pu was dissolved in diluted citrate so that final Pu:Na-citrate ratio is 1:10,000.

MOX Suspension for Contamination

Mixed U, Pu OXide (MOX) powder from the rectification step was produced by the MIcronised MASter Blend (MIMAS) procedure at the MELOX installation (Marcoule, France) containing 81% U and 7.1% Pu by mass. At the time of experimentation, the specific activity of the MOX powder was 123.4 kBq/mg and contained ^{241}Am due to aging from ^{241}Pu decay. In terms of mass of each isotope and element (Pu + Am) the composition was 1.7% ^{238}Pu, 88.1% $^{239+240+241}$Pu, and 4.1% ^{241}Am. As a percentage of total Pu plus Am alpha activity ^{238}Pu represented 55%, $^{239+240+241}$Pu 18% and 27% ^{241}Am. For aerosol generation, a suspension of MOX powder in ethanol 100% was diluted using distilled water. For the wound deposit an aliquot of suspension (in ethanol 100%) was used which was diluted in saline (0.9% NaCl) before use. Care was taken to maintain the particles in suspension.

Animals

All the data were obtained from *in vivo* experiments spanning over more than 10 years. In some cases methods have changed, analytical procedures have been upgraded and regulations have been updated. However basic experimental approaches have not changed and are reported as such.

Male Sprague-Dawley rats weighing between 200–450 g were obtained from Charles River, L'Arbresle Cedex France. Animals were maintained at constant temperature (20–24°C), humidity and lighting (12 h light -12 h dark) and fed standard rat chow and water ad libitum. Cages contained tunnels, paper and wood for gnawing to provide enrichment of the environment. General health status and weight was assessed regularly throughout the duration of the experimental period.

For euthanasia animals received buprenorphine (0.02 mg/kg, s.c.; Buprecare, Axience, France), and were injected with a lethal dose sodium pentobarbital (400 mg/kg, i.p. Exagon, Axience,

France) followed by exsanguination from the dorsal aorta or following intra-cardiac puncture.

All experiments were carried out in an accredited facility according to French regulations for animal experimentation under the European directives (2001-246 June 6, 2001 and 2010/63/EU, September 22, 2010). Experiments were approved by the local institutional animal ethics committee and the French Ministry of National Education, Higher Education and Research.

Contamination Procedures

Pulmonary Contamination of Rats by Pu Citrate or Pu Nitrate

Under light gaseous anesthesia (2.5% isoflurane; Aerrane, Baxter, France), rats were contaminated by intra-tracheal instillation of a 200–250 µl volume containing Pu citrate or Pu nitrate solution.

Pulmonary Contamination of Rats by MOX

Conscious rats and restrained in cardboard tubes, were nose-only exposed to a MOX aerosol generated from an aqueous suspension using a compressed air device, as described previously by Andre and colleagues (André et al., 1989). The aerosol had an activity median erodynamic diameter (AMAD) of 4.2 µm and a geometric standard deviation of 2.7.

Wound Contamination of Rats by Pu Nitrate or MOX

For contamination after wounding, animals were anesthetized using sodium pentobarbitone (40 mg/kg, i.p) The left hind leg was clipped and an incision (0.5 cm long, 0.4–0.7 cm deep) using a scalpel (N° 11) was made in the interior aspect of the hind limb. This technique has been previously described in detail (Beitz et al., 2004; Griffiths et al., 2012). Pu nitrate solution (50 µl containing 5–10 kBq) or a suspension of MOX (50 µl containing 20–30 kBq in aqueous solution) was then introduced using a micropipette (Gilson 0–100 µl) and a sterilized cone. The wound was then closed and sutured using resorbable thread and the animals allowed to recover from anesthesia. All animals received anti-inflammatory treatment after contamination using Tolfedine (Vetoquinol, Lure, France; 4 mg/kg, s.c.) or Meloxicam (Metacam, Boehringer Ingelheim, Lyon, France; 1 mg/kg, s.c)

DTPA Treatment Regimens

(a) For pulmonary-contaminated rats:

Two hours following lung contamination with Pu nitrate, animals received either intravenous injection of DTPA solution ("DTPA i.v." group; 30 µmol/kg) or pulmonary insufflation of DTPA powder ("DTPA local" group) using a special device (model DP-4, Penn-Century™). Both insufflation and injection into the lateral tail vein of DTPA were carried out under light gaseous anaesthesia (Isoflurane 2.5%). According to a previous study on this DTPA dry powder, only about 26% may reach deep lung compartments (Gervelas et al., 2007). Thus, insufflation at 20 µmol/kg tested in the present study was estimated to result in a deep lung deposit of approximately 5 µmol/kg of DTPA.

One hour following lung contamination with Pu citrate, animals were either injected with DTPA solution ("DTPA i.v." group; 15 µmol/kg) or nose-only exposed to an aerosol of DTPA solution ("DTPA local" group) diluted in NaCl 0.9% (deep lung deposit of 1.1 µmol/kg), by using an inhalation chamber associated with an Aeroneb® lab micropump nebulizer (technology of a microperforated vibrating membrane; Tem Sega, Pessac, France). The exposure apparatus and DTPA dose determination with ^{111}In have been reported in detail elsewhere (Miccoli et al., 2019).

Two hours following lung contamination with MOX, animals received pulmonary insufflation of DTPA powder ("DTPA local" group; deep lung deposit of about 5 µmol/kg), either alone or starting at day 1 by repeated DTPA intravenous injections (30 µmol/kg) given twice a week from day 1 to day 20 ("DTPA local + i.v". group).

(b) For wound-contaminated rats:

In an accidental situation DTPA treatment of wounds involves washing/flushing for decontamination purposes in addition to systemic DTPA by i.v. injection. In this study the "intra wound-site" was chosen as the way to administer DTPA locally in a controlled manner. This was to simplify the procedure *in vivo* as well as radiation protection issues. Previous studies have shown this to be effective in animals but no data seem to be available for man (Taylor and Sowby, 1962; Volf 1974; Harrison and David, 1979; Stradling et al., 1993; Griffiths et al., 2014).

At 2 h following wound contamination with Pu nitrate, animals received either a single local injection ("DTPA local" group) into the wound site using a Hamilton syringe (0–100 µl; 30G needle; 30 µmol/kg) or a systemic injection of DTPA ("DTPA i.v." group; 30 µmol/kg).

Similarly at 2 h following wound contamination with MOX animals received a single local DTPA injection in the wound site ("DTPA local" group; 30 µmol/kg), either alone or followed one day later by i.v. DTPA administration (30 µmol/kg). Further DTPA i.v. injections were given twice a week up to day 20 ("DTPA local + i.v." group).

In all cases where DTPA was injected at the wound site which may cause local pain, the DTPA solution contained the local anesthetic lidocaine at a final concentration of 0.5% (Xylovet, Ceva Santé Animal, Libourne, France).

Excreta Collection, Tissue Sampling and Activity Measurements

Following contamination animals were housed in metabolism cages for collection of urine and/or faecal samples. At euthanasia at 7 or 21 days depending on studies, the liver, lungs, femurs were removed for radioactivity analyses. In some pulmonary-contaminated rats, a bronchoalveolar lavage was carried out for measurement of macrophage-associated activity as previously described (Van der Meeren et al., 2012).

For measurement of activity, tissue samples were dry-ashed (500–600°C depending on sample) and wet ashed in HNO_3 (2 M) and H_2O_2 (30%) until a clear solution was obtained. Urine

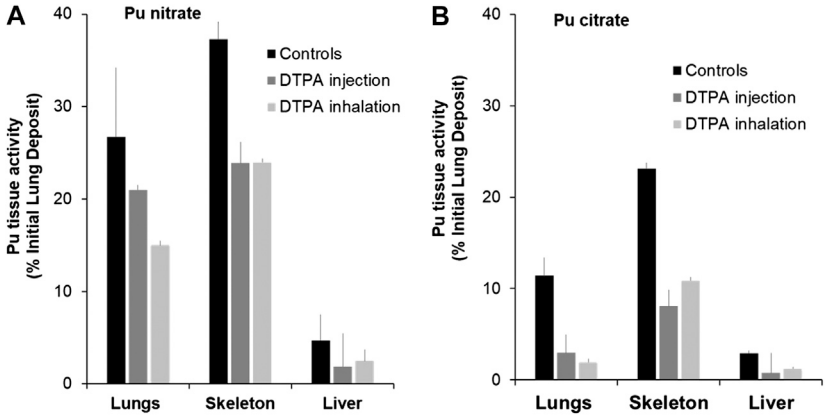

FIGURE 1 | Effect of single systemic or local DTPA administration on tissue activity levels following lung contamination with Pu nitrate **(A)** or Pu citrate **(B)**. Animals were contaminated by intra-tracheal instillation of either Pu nitrate (**A**: 5.5 kBq) or Pu citrate (**B**: 2.8 kBq) and were euthanized at eight or seven days respectively after contamination. After Pu nitrate contamination **(A)**, treatments at 2 h were either intravenous injection of DTPA solution (30 μmol/kg) or insufflation of DTPA powder (approximatively 5 μmol/kg). After Pu citrate contamination **(B)**, treatments at 1 h were either intravenous injection of DTPA solution (15 μmol/kg) or inhalation of nebulized DTPA (1.1 μmol/kg). Data are expressed as a percentage of the initial lung deposit and are the means of three–six animals.

samples were evaporated to dryness and then mineralized as for tissues. The dry residues were taken up into HNO_3 (2–4 ml, 2 M) and an aliquot used for determination of total alpha activity by liquid scintillation counting (Packard Tri-Carb 2500). For tissues containing low levels of radioactivity and for measurement of Pu and Am, samples were analyzed by alpha spectrometry following separation of the two elements by anion exchange (Tru-Spek columns, Eichrom, Rennes, France).

For pulmonary contamination by intratracheal instillation of Pu nitrate/citrate, the Initial Lung Deposit was determined as the activity administered into airways after subtracting it from the activity recovered in in faeces during the first two days after contamination as described previously (Grémy et al., 2012). For pulmonary contamination by MOX inhalation, determination of Initial Lung Deposit was determined by gamma-ray spectrometry of thorax using a NaI detector as MOX contains Am with a gamma signal at 59 keV. This measure occurred only seven days after MOX inhalation so that larger particles initially deposited in the upper airways were eliminated by mucociliary clearance. Initial wound radioactivity (T = 0) was determined by total limb counting using a NaI detector with the anesthetized rat positioned so that the contaminated wound site was within the detector area. Corrections were made for absorption in air and tissue using a tissue-equivalent phantom. The height of the leg and distance from the detector surface was measured in each case. For Pu contaminated wounds using Pu nitrate solution initial activity was determined from the known administered activity minus activity collected on a cleaning swab of the area.

Data Presentation and Analyses

Data are expressed as mean percentage of the Initial Wound Deposit (wounds) or the Initial Lung Deposit (inhalation) in activity ± SD for 3–6 animals.

For comparative purposes reduced tissue activity are expressed as the percentage change as compared with contaminated untreated animals. This referred to as percentage inhibition (tissues). Significant differences between the different exposure groups were compared using the unpaired Student's *t* test.

RESULTS AND DISCUSSION

Single Systemic or Local DTPA Treatment Following Contamination of Lungs or Wound With Pu Nitrate or Pu Citrate

Contamination of Lungs

Figure 1 shows data obtained from studies to investigate early decorporation efficacy of systemic or locally administered DTPA after pulmonary contamination with Pu nitrate (**Figure 1A**) or Pu citrate (**Figure 1B**). Firstly, it should be noted that in both cases a significant amount of activity is retained in the lungs even with the more soluble citrate form. Secondly, as expected in control untreated animals, bone retained higher activities than liver. In order to compare the data concerning the efficacy of the two routes of DTPA administration, i.e., systemic (i.v. of DTPA solution) and pulmonary (insufflation of DTPA dry powder or inhalation of aerosolized DTPA solution), percentage inhibitions of plutonium tissue retention were calculated as compared to untreated animals. Both DTPA administration routes reduce tissue Pu activity. It appears when given rapidly as a single dose within one or 2 h the local pulmonary route is at least as effective as the intravenous route to reduce lung Pu levels (44% inhibition compared with 21% for Pu nitrate (**Table 1**) and 83% compared with 74% for Pu citrate).

In addition it should be noted that inhaled DTPA doses (about 5 μmol/kg for DTPA dry powder insufflation and 1.1 μmol/kg for aerosolized DTPA inhalation) were less than i.v.-administered doses (30 or 15 μmol/kg). Therefore, the bioavailability of DTPA in lungs is better when treatment is local rather than systemic even when the latter is administered at higher doses. Nevertheless, given the reduction in lung activity there is a limited transfer of

TABLE 1 | Reduction of Pu tissue activity levels following single local or systemic DTPA treatment.

Contaminant	DTPA treatment	Wound			Lungs		
		Leg	Skeleton	Liver	Lungs	Skeleton	Liver
Pu nitrate	i.v.	36 ± 15	56 ± 10	80 ± 3	21 ± 7	36 ± 6	60 ± 7
	Local	48 ± 8	49 ± 6	76 ± 3	44 ± 10	36 ± 10	46 ± 25

Animals received Pu nitrate by either intratracheal instillation or following wounding and were euthanized at seven days after contamination. After contamination, treatments at 2 h were either intravenous injection of DTPA solution ("i.v."; 30 µmol/kg) or local administration, either by insufflation of DTPA powder ("Local"; approximately 5 µmol/kg) or injection into the wound site ("Local"; 30 µmol/kg). Data are from five to six animals and are expressed as a percentage reduction as compared with contaminated, untreated animals.

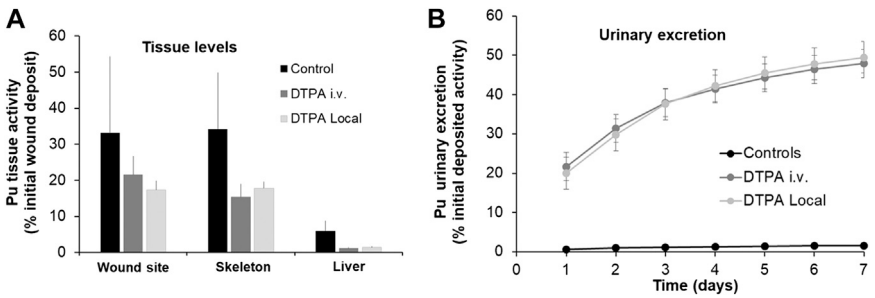

FIGURE 2 | Effect of single systemic or local DTPA administration on tissue **(A)** and urine **(B)** activity levels following wound contamination with Pu nitrate. Animals were contaminated following an incisional wound with Pu nitrate (6 kBq) and were euthanized at seven days after contamination. Urines were collected over seven days. DTPA treatment (30 µmol/kg) by intravenous ("DTPA i.v.") or local injection ("DTPA Local") was given at 2 h. Data are expressed as a percentage of the initial wound deposit and are the means ± S.D. of 5–6 animals.

DTPA given intravenously from blood to lungs that clearly can remove available Pu from lungs.

Pulmonary-administered DTPA reduces Pu burden not only in lungs but also in the liver and bones. This undoubtedly results mainly from chelation of transferable Pu that comprises a large fraction still present in the lungs at early times. The Pu-DTPA complexes formed locally in the lungs will be absorbed into the circulation and then excreted in urine, so preventing systemic tissue deposits. A further explication is that free DTPA can cross the alveolar-capillary barrier to chelate circulating or loosely tissue-bound Pu that will also contribute to a reduction in systemic tissue retention. Indeed it appears that DTPA administered to the lungs, even at a lower dose than the i.v. administration is equally effective. There are no significant differences in bone or liver Pu levels whatever the route of administration (**Figures 1A,B**).

Regardless of the treatment route, it is noteworthy that early chelation efficacy appears lower after pulmonary contamination with Pu nitrate than after Pu citrate as it is a chemical form less soluble, and hence less accessible for chelation.

Contamination of Wounds

A similar approach was used to study the effects of prompt systemic or local DTPA administration following Pu nitrate contamination of wounds. Similar to the data shown above for lungs, both treatment protocols reduced wound site activity, bone and liver retention (**Figure 2A**). In agreement with a significant reduction in actinide retention, urinary excretion was enhanced following a single dose of DTPA either given locally or by intravenous injection at similar dosage (**Figure 2B**). The figure demonstrates a similar efficacy of either systemic or local treatment with regard to reduction in wound and systemic tissue retention (in skeleton: 56 and 49% respectively and in liver: 80 and 76% respectively; **Table 1**) and increase in urinary excretion (**Figures 2A,B**).

Similar to the experiments reported above for Pu lung contamination, DTPA was administered early (2 h) after wound contamination when a substantial part of the transferable fraction of Pu nitrate is still present at the wound site. The decrease in systemic Pu observed after DTPA injection into the wound site probably results mainly from a significant chelation of accessible Pu prior to transfer to the circulation. Free DTPA could also be transferred to chelate circulating Pu. This would contribute additionally to the reduction of bone and liver retention.

With regard to DTPA i.v. injection chelation will take place mainly in the systemic compartment. However, it is possible that circulating DTPA gains access to the wound site, given the type of incisional wound and will chelate accessible transferable Pu. Nevertheless, there are no differences in tissue reduction whatever the route of DTPA administration (**Figure 2A**; **Table 1**).

The data obtained with moderately soluble Pu nitrate indicate that a single local lung or wound administration of DTPA is effective in reducing the levels of activity at the primary site of contamination (lung or wound). **Table 1** shows the data obtained for these two comparative studies. In order to compare the efficacy of the treatment routes the data are shown as the percentage reduction as compared to the untreated animals.

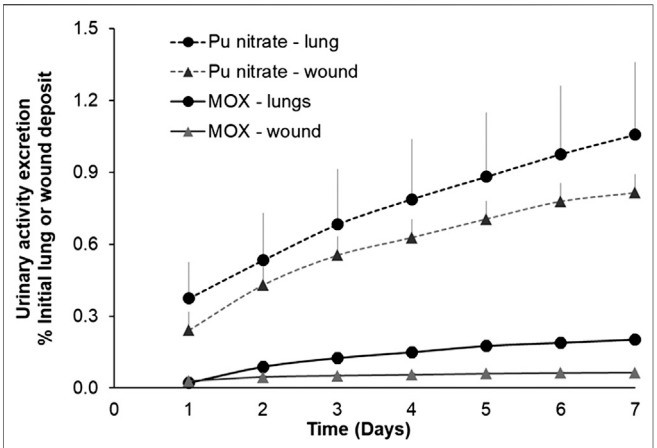

FIGURE 3 | Urinary excretion profiles following lung or wound contamination with MOX or Pu nitrate. Animals were contaminated with MOX by nose-only inhalation (12 kBq) or by a deposit into an incisional wound (13 kBq) as already described. For Pu nitrate pulmonary contamination was by intratracheal instillation (5.5 kBq) or a wound deposit (6 kBq). Data are expressed as a percentage of the initial lung or wound deposit and are the means ± S.D. for three to six animals.

Therefore for Pu nitrate a single dose either intravenous or to the primary site of contamination will reduce tissue retention and consequently committed effective radiation dose.

Different Actinide Forms and Urinary Excretion Profiles

Incidents of contaminated personnel however may not just involved well-characterized nitrate or citrate forms of a single pure actinide. Given the different stages of the nuclear fuel cycle and treatment of used fuel the probability of exposure to far less soluble compounds, such as oxide forms, is greater. This study was carried out using the poorly soluble nuclear mixed oxide compound MOX, and the results compared to that of Pu nitrate contamination.

As an example of differing biokinetic profiles of these actinide forms **Figure 3** shows cumulative urinary actinide excretion following either lung or wound contamination with MOX or Pu nitrate. The data clearly show differences in urinary excretion between the two physicochemical forms.

Following contamination by inhalation or wounding, the cumulative excretion of Pu nitrate over the seven-day period represented some 1 and 0.7% respectively of the total initial deposit. In contrast, following contamination with MOX cumulative 7-days urinary excretion was some five to ten-fold less than following Pu nitrate (0.2% lung, 0.06% wound). This low excretion is in accordance with the less soluble nature of MOX considered as a type "S" form of inhaled compound (International Commission on Radiological Protection (ICRP), 1994b). Similarly given the particulate nature of MOX it may be considered in the moderate to strong retention category in the NCRP model (2006). This is also in agreement with data obtained for insoluble oxides of Pu after either inhalation (Stather et al., 1982; Grémy et al., 2012) or wounding (Bistline et al., 1974).

For contamination of lungs (12 kBq) or wounds (13 kBq) with the same MOX compound, it seems there is a greater transfer from lungs to the systemic compartment under these experimental conditions as indicated by the higher cumulative urinary excretion (**Figure 3**). Two factors may contribute to this higher transfer from lungs 1) a significantly greater surface area (around 0.3 m^2 for rat lung; Fröhlich et al., 2016) for transfer in lungs compared with a very small area in the wound (roughly 0.05 cm^2) 2) higher blood perfusion leading to higher absorption into the circulation. Nevertheless, this fraction of activity solubilized, absorbed into the blood, then partially excreted is a very small fraction of the total activity administered (<0.2%) since MOX is very predominantly comprised of insoluble particles which are likely to remain at the primary site (lungs, wound) of contamination.

Prompt Local DTPA Treatment Alone or in Combination With Repeated Systemic DTPA Treatments Following Contamination of Lungs or Wound With MOX

A further study was dedicated to using a local approach followed or not by repeated systemic DTPA injections in order to test the efficacy following contamination of lungs or wound with the poorly soluble MOX.

Urinary Activity Excretion

A single local DTPA treatment administered at 2 h either to lungs (**Figure 4A**) or to the wound site (**Figure 4B**) significantly increased the cumulative 7-days urinary excretion of total alpha activity by some 5 and 3 fold respectively. These data are in agreement with other reports following inhalation of Pu oxide or Pu nitrate or simulated wound contamination both in experimental animal studies (Bistline et al., 1974; Guilmette and Muggenburg, 1993; Grémy et al., 2012; Griffiths et al., 2014) and in man (McInroy et al., 1995; Grappin et al., 2007). It can also be observed that cumulative urinary excretion of activity increased exponentially for the first three days and then levels off. This is presumably related in part to MOX low solubility as well as quick elimination of DTPA from the primary site of contamination.

In order to target the slowly dissolving fraction of MOX from the contamination site, repeated i.v. DTPA administration was started at one day after the initial local treatment. However, no further increases were observed in excretion with the combined treatment as compared to the single local treatment as indicated by similar values for cumulative excretion (approximatively 5 fold in inhalation study; approximatively 3 fold in wound study) (**Figures 4A,B**). These data clearly show the importance and benefit of prompt administration of a single local dose of DTPA. These findings are in agreement with a previous study following inhalation of PuO_2 followed by local lung DTPA treatment (Grémy et al., 2012). The present work along with this previous study indicates a good bioavailability of DTPA at the primary site of contamination both in the case of early DTPA powder insufflation (in lungs) or early DTPA solution local

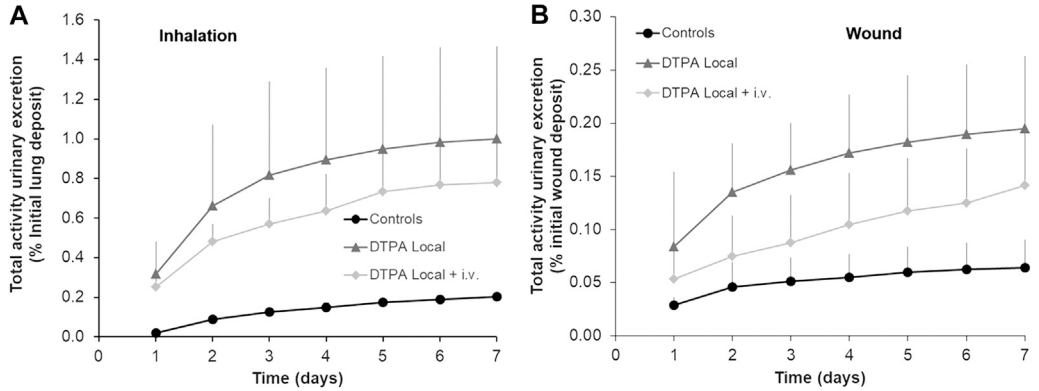

FIGURE 4 | Effect of local DTPA or local DTPA followed by DTPA systemic administrations on cumulative urinary activity excretion following lung **(A)** or wound contamination **(B)** with MOX. Animals were contaminated with MOX either by inhalation (12 kBq) or deposited in a wound (13 kBq) as described. Local administration to lungs (DTPA powder about 5 μmol/kg) or wound (DTPA solution 30 μmol/kg) was started at 2 h ("DTPA Local"). For combined local and systemic DTPA treatment ("DTPA Local + i.v."), animals received the local dose at 2 h then two intravenous DTPA per week from day one to day 20 (30 μmol/kg). Data are expressed as a percentage of the initial lung or wound deposit and are the means ± S.D. of 3–6 animals.

injection (at the wound site), and hence an expected significant chelation of the transferable fraction of actinides.

In the MOX powder at the time of contamination, Am represents around 27% of total Pu plus Am alpha activity as compared with 13.3% at the time of acquisition (2002). This is due to aging of the supplied powder as a result of the decay of ^{241}Pu initially present in the compound. One day after MOX inhalation an enrichment of Am was observed following local DTPA (44 ± 5%) and combined local and i.v. DTPA administration (45 ± 3%). This is in agreement with a previous study where urinary Am levels were increased following inhalation of aged PuO_2 containing Am (Grémy et al., 2010). Similarly, after contamination by wounding urinary Am was enriched to 67 ± 18% (local DTPA) and 63 ± 8% (local + i.v. DTPA) in the treated groups. There were no differences between the treatment groups.

In lungs or at wound sites locally administered DTPA may compete with same endogenous ligands to form Pu or Am complexes such as citrate or transferrin. Transferrin is accepted to be the main protein ligand for circulating Pu but has less affinity for Am (Ansoborlo et al., 2007). Transferrin is found in lungs to be greater than plasma levels (Bell et al., 1981) due to plasma leakage and local secretion by alveolar type-1 cells (Chen et al., 2006). Transferrin is also an acute phase protein that would be expected to be present rapidly in significant quantities at the incisional wound site (Helson et al., 1983). Consequently, the increased proportion of urinary Am following DTPA treatment may be explained by better chelation availability for Am than for Pu at the primary sites of contamination as well as in the systemic compartment, given the difference between the stability constants of transferrin for the solubilized form of Pu/Am (Ansoborlo et al., 2007).

These observations demonstrate the efficacy of DTPA treatment and are in agreement with other findings both in man and in animals (Newton et al., 1983; Grappin et al., 2007; Sérandour et al., 2007; Grémy et al., 2010). The increased urinary

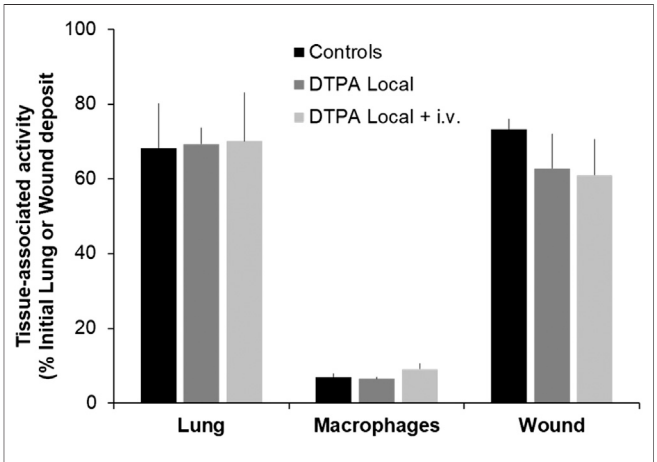

FIGURE 5 | Effect of local DTPA or local DTPA followed by DTPA systemic administrations on activity levels at the primary site of contamination. Animals were contaminated by MOX inhalation (12 kBq) or deposition in a wound (13 kBq) as described, and were euthanized 21 days later. Local administration to lungs (DTPA powder about 5 μmol/kg) or wound (DTPA solution 30 μmol/kg) was started at 2 h ("DTPA Local"). For combined local and systemic DTPA treatment ("DTPA Local + i.v.") animals received the local dose at 2 h then two intravenous DTPA per week from day one to day 20 (30 μmol/kg). Alveolar macrophages were prepared as described and for data normalization for comparative purposes of DTPA efficacy are expressed as activity per 10^6 macrophages and as a function of the initial lung deposit. Data are the means ± S.D. of 3–6 animals.

excretion of activity may be explained by chelation of actinides in systemic compartments and/or directly at the primary site of contamination (lungs, wound) followed by transfer to the circulation of the actinide-DTPA complexes and subsequent urinary excretion. At these early times, solubilized Pu/Am available for chelation is still largely within the extracellular space, at the primary site of contamination (lung–epithelial lining fluids- or wound–blood, extracellular matrix) and/or in the circulation within blood/interstitial fluids and/or loosely

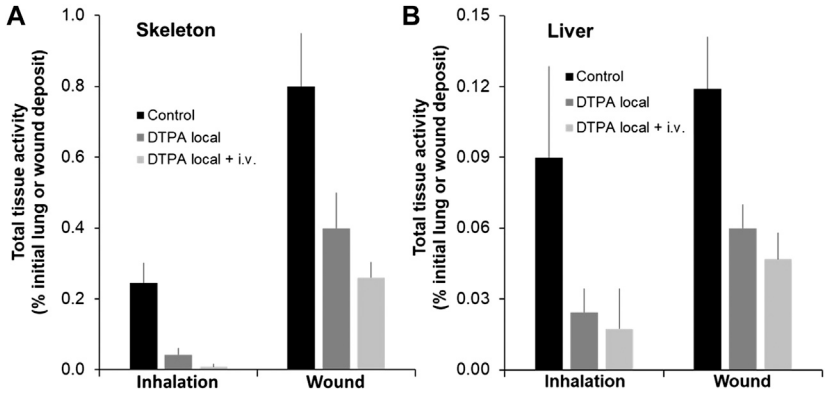

FIGURE 6 | Effect of local DTPA or local DTPA followed by DTPA systemic administrations on skeletal **(A)** and liver **(B)** total activity levels following lung or wound contamination with MOX. Animals were contaminated by MOX inhalation (12 kBq) or deposition in a wound (13 kBq) as described. Local administration to lungs (DTPA powder about 5 μmol/kg) or wound (DTPA solution 30 μmol/kg) was started at 2 h ("Local"). For combined local and systemic DTPA treatment ("Local + i.v.") animals received the local dose at 2 h then two intravenous DTPA injections per week from day one to day 20 (30 μmol/kg). Rats were euthanized 21 days following contamination. Data are expressed as a percentage of the initial total alpha activity deposit. Data are the means ± S.D. of 4–6 animals.

TABLE 2 | Reduction of tissue activity levels by local or combined local and systemic DTPA treatment following MOX contamination.

Contaminant	DTPA treatment	Wound			Lungs		
		Leg	Skeleton	Liver	Lungs	Skeleton	Liver
MOX	Local	12 ± 15	67 ± 10	73 ± 3	6 ± 2	82 ± 6	73 ± 11
	Local + i.v.	14 ± 8	84 ± 6	81 ± 3	12 ± 3	97 ± 3	80 ± 24

Animals were contaminated by MOX inhalation or deposition in a wound and received DTPA treatment as described. Local administration ("Local") to lungs (DTPA powder insufflation; about 5 μmol/kg) or wound (DTPA solution injection into the wound site; 30 μmol/kg) was started at 2 h. For combined local and systemic DTPA treatment ("Local + i.v.") animals received the local dose at 2 h then two intravenous DTPA per week from day one to day 20 (30 μmol/kg). Animals were euthanized 21 days after contamination and skeletal and liver activity levels measured. Data are expressed as a percentage reduction as compared with untreated animals with four to six animals/group.

bound to systemic tissue surfaces. Intracellular chelation would be a possibility but at these early times this would be expected to be negligible as compared to extracellular chelation.

Tissue Activity Levels

At the end of the 21-days study period, animals were euthanized and tissue levels of total alpha activity measured. It is interesting to note that for a similar activity local deposit (12 kBq lungs and 13 kBq wound) a similar amount of activity remains at 21 days in either case (around 70%) in untreated animals. No significant differences between controls and DTPA-treated animals were seen at the primary site of contamination (lungs or wound) in terms of activity as measured by external counting (**Figure 5**). Activity levels were also measured in macrophages obtained from bronchoalveolar lavage but as for whole lung, no reduction in macrophage-associated activity was observed whatever the treatment schedule. The absence of a measurable effect on lung or wound activity after treatment is undoubtedly due to the inability of DTPA to dissolve, and hence mobilize, oxides (Grémy et al., 2010) such as MOX that is composed primarily of insoluble oxide particles. As previously shown following inhalation of aged PuO_2, early insufflation of DTPA powder significantly removed the dissolved fraction within the epithelial lining fluid leading to reduced retention of Pu and Am in bone and liver (Grémy et al., 2010). However this represents an extremely small fraction of the total lung burden (0.1%). Even though local DTPA treatment reduced activity in this fraction changes were undetected by measurement of total lung activity.

Following inhalation of MOX, a single local treatment to the lungs with the powder formulation of DTPA leads to an 82% reduction in the skeleton and a 73% reduction in the liver of total alpha activity (**Figures 6A,B**; **Table 2**). In the group that received the combined treatment (early local then delayed repeated systemic treatments) a further reduction in skeleton (97%; $p < 0.05$) was observed (**Figure 6A**; **Table 2**). Similarly following wound contamination and local DTPA treatment total activity levels were reduced by some 67 and 73% in skeleton and liver respectively (**Figures 6A,B**; **Table 2**). As observed after lung contamination the combined treatment further reduced these levels particularly in skeleton (84% $p < 0.01$). There was also a further inhibition in liver (81% $p < 0.05$) (**Figures 6A,B**; **Table 2**). It is interesting to note that after inhalation, the reduction of Pu in systemic tissues after local DTPA treatment appears greater in rats contaminated with MOX than in rats contaminated with the more soluble Pu nitrate. However, the levels of solubilized Pu/Am, and hence available for chelation, are much lower for MOX

TABLE 3 | Comparative efficacy of two different DTPA treatment protocols on tissue Pu and Am levels.

	Bone				Liver			
	% Initial activity	Inhibition (%)	% Initial activity	% Inhibition	% Initial activity	% Inhibition	% Initial activity	% Inhibition
Treatment	**Pu**		**Am**		**Pu**		**Am**	
(A): Inhalation								
None	0.182 ± 0.043		0.063 ± 0.016		0.041 ± 0.022		0.049 ± 0.018	
Local	0.037 ± 0.017	80	0.008 ± 0.02	87	0.016 ± 0.007	61	0.011 ± 0.004	78
Local + i.v.	0.009 ± 0.006*	95	0.002 ± 0.001*	97	0.008 ± 0.004	81	0.004 ± 0.001*	92
Difference local vs local + i.v.	*$p < 0.05$		* $p < 0.05$		NS		*$p < 0.05$	
(B): Wound								
None	0.523 ± 0.080		0.264 ± 0.075		0.052 ± 0.009		0.067 ± 0.015	
Local	0.188 ± 0.041	64	0.072 ± 0.007	73	0.024 ± 0.008	54	0.023 ± 0.009	66
Local + i.v.	0.089 ± 0.048**	83	0.039 ± 0.015***	85	0.013 ± 0.012	75	0.004 ± 0.002**	95
Difference local vs local + i.v.	**$p < 0.01$		*** $p < 0.005$		NS		** $p < 0.01$	

Animals were contaminated by MOX inhalation or deposition in a wound and received DTPA treatment as described. Data are expressed as a percentage of the initial total activity and as % inhibition (reduction in tissue activity as compared with untreated animals with 4–6 animals/group). Data were compared between the two treatment groups using a two-tailed unpaired t test. p *values are also given.*

than for Pu nitrate and DTPA will be in a far higher molar excess which may explain the higher efficacy.

Tissue samples were also analyzed for both Pu and Am. Following MOX inhalation local DTPA treatment reduced bone Pu and Am by some 80 and 87% respectively (**Table 3**). The combined treatment reduced Pu and Am levels by 95 and 97% respectively (**Table 3**). With regard to the liver, local DTPA treatment after MOX inhalation resulted in a 61 and 78% reduction in Pu and Am (**Table 3**). As observed for bone, the combined treatment further reduced Pu and Am levels in the liver (81% and 92% inhibition respectively).

Following MOX wound contamination local DTPA inhibited bone Pu and Am retention by 64 and 73% (**Table 3**) and observed after MOX inhalation the combined treatment further reduced bone retention of both elements (Pu 83% and Am 85% inhibition). For the liver, local DTPA injection led to a 54 and 66% reduction in Pu and Am (**Table 3**). The combined treatment further reduced Pu and Am levels in the liver (75 and 95% inhibition respectively).

Regardless of the contamination mode, the treatment regimen, and the organ, activity decreases in tissues were somewhat higher for Am than for Pu, presumably associated with a better chelation of Am than Pu at the primary sites of contamination as well as in the systemic compartments.

The percentages of Pu and Am in tissue samples are also compared to that of the administered MOX (27%). Similar percentages of Am were found in lungs, wound or bone whatever the route of contamination or DTPA treatment. On the contrary, an enrichment of Am in liver samples was observed similar to already shown for Urine. In this case there was a two-fold increase in untreated animals (inhalation 55 ± 5% Am; wound 56 ± 3% Am) and these values were unchanged by DTPA treatment. This was observed in other soft tissues such as kidney and testicles (data not shown). Thus in addition to the urinary excretion data, these observations are in agreement with the higher solubility of Am as compared to Pu, both from MOX or aged Pu oxides containing Am and so a higher transfer from lungs or wounds to systemic sites (Paquet et al., 2003; Ramounet-Le Gall et al., 2003; Bertelli et al., 2010; Van der Meeren and Grémy, 2010).

It is clear that either treatment regimen can reduce systemic tissue retention yet neither treatment regimen results in mobilization of measurable MOX total alpha activity from the primary site of contamination i.e., lungs or wound site (**Figure 5**). In the case of MOX contamination by inhalation, local DTPA will chelate the rapidly soluble transferable fraction of Pu/Am (f_r) that represents a very small fraction of the deposited activity. The only other approach to eliminate high activity MOX particles would be to use bronchopulmonary lavage. The use of this technique as a countermeasure for lung contamination with insoluble actinides has been addressed over the years in experimental models (see Muggenburg et al., 1977; Nolibé et al., 1989; National Council on Radiological Protection and Measurements. (NCRP), 2009). A more recent paper concluded that bronchopulmonary lavage should be considered a viable treatment option for PuO_2 intakes in order to prevent deterministic effects at lung doses over 6 Gy (Morgan et al., 2010).

With regard to wound contamination, excision of the wound site is often practiced and has indeed been employed in several cases of accidental contamination in man (Bailey et al., 2003; Laroche et al., 2010; Schadilov et al., 2010; Sugarman et al., 2018; Klumpp et al., 2020). In general surgical removal of the contaminated site is combined with both local (washing of the wound) and intravenous DTPA. The latter will prevent further retention in systemic sites resulting from contaminant blood absorption from the wound site during surgery.

An early treatment with DTPA irrespective of the actinide in all cases reduced Pu/Am levels in systemic tissues. As DTPA was given either one or 2 h after contamination, it is likely that chelation occurs in the extracellular fluid, probably at primary site of contamination and in the systemic compartment. For the more soluble actinide forms, reduction at the primary contamination site is achieved which suggests that the actinide

TABLE 4 | Comparative efficacy of two different DTPA treatment protocols on tissue levels and urinary excretion of activity.

Contaminant	DTPA treatment	Wound			Inhalation		
		Wound site	Systemic	Urine	Lungs	Systemic	Urine
Pu nitrate	i.v.	↘	↘	↗	↘	↘	↗[1]
	Local	↘	↘	↗	↘	↘	↗[1]
MOX	Local	0	↘	↗	0	↘	↗
	Local + i.v.	0	↘↘	↗	0	↘↘	↗

"Systemic" represents skeleton plus liver the main retention organs for Pu/Am after transfer to the circulation. The arrows represent the change in percentage reduction either decrease or increase. For insoluble actinides (MOX), two arrows mean greater inhibition than one arrow (combined treatment "Local + i.v." vs. local treatment "Local")

[1]*Includes published data from Grémy et al., 2012.*

is accessible to chelation by DTPA. In addition, DTPA was given only once reinforcing the importance of contaminant and chelator in the same biological compartments at the same time. Similar results were observed with Am nitrate in the wound model (data not shown) and indeed DTPA treatment at 30 min after contamination with either Pu or Am nitrate showed the same efficacy (data not shown). In accordance with decreased tissue levels, urinary excretion of activity was also enhanced by the different DTPA treatments. These data are in agreement with other studies either following lung or wound contamination. For MOX it appears that an additional systemic DTPA treatment further reduces tissue levels. However, tissue levels in this case are less than one percent of the administered dose as compared with 20–30% following contamination with Pu nitrate.

CONCLUSION

The objective of this work was to compare different DTPA administration regimens following either pulmonary or wound contamination with different actinide forms. Firstly, the studies confirmed the differential behavior of the different forms following either pulmonary or wound contamination. The more soluble forms are absorbed to a greater extent resulting in higher urinary excretion together with greater skeleton and liver retention. Secondly, the early chelation single treatments tested show that it is possible to reduce tissue alpha-emitting actinide levels that will in consequence decrease the committed effective dose (**Table 4**). This is important. As a first line treatment after Pu nitrate or citrate contamination, a single, local and prompt delivery of DTPA to the primary site of contamination appears as a good alternative to intravenous administration. In addition, local treatment also reduces retention in the secondary target organs, liver and bone. Rapid administration of DTPA is thus crucial to success in order to chelate the free, transferable fraction of activity present at the primary site of contamination. Moreover, locally administered DTPA would be expected to decrease systemic retention by chelation of already transferred activity.

In the case of MOX contamination, local lung or wound activity was unaffected by local or combined local and intravenous DTPA administration. Most of the activity remained at the contamination site. However, a single local DTPA administration did reduce retention in bone and liver. When combined with systemic DTPA tissue activity was further reduced. This indicates that follow-up chelation is advantageous. For the poorly soluble MOX it is clear whatever the regime used that although DTPA administration reduces systemic tissue levels it has little influence on activity levels at the primary site of contamination. In this case, radiation dose would be much greater in lungs or wound site rather than systemic organs. This leaves the question of adequate treatment for activity remaining at these primary sites of contamination, "the reservoir" unsolved. This still needs to be addressed in order to limit pathological consequences. In terms of clinical approaches and for radiation countermeasures it is therefore important to ascertain what actinide form is involved in order to administer the appropriate DTPA treatment regimen.

DATA AVAILABILITY STATEMENT

The original contributions presented in the study are included in the article/Supplementary Material, further inquiries can be directed to the corresponding author.

ETHICS STATEMENT

The animal study was reviewed and approved by Ethics Committee of the Life Science Division of the CEA (CETEA-CEA DSV IdF) N° 44.

AUTHOR CONTRIBUTIONS

All authors (NG, OG, and AVDM) contributed and participated in the design of and the carrying out of the experimental procedures. NG wrote the manuscript and all authors contributed to and approved the submitted version.

FUNDING

This work was cofunded by AREVA NC/Orano Cycle and CEA as part of a collaborative framework.

ACKNOWLEDGMENTS

The authors wish to thank J. C. Wilk, D. Renault, P. Pochard, and K. Devilliers for animal care and experimental *in vivo* expertise.

The authors are also grateful to M-C. Abram, S. Coudert, and Q. Chau for radiochemical analyses, alpha and gamma spectrometry and to J. Piechowski for many fruitful discussions. The authors wish to acknowledge L. Doublet, F. Huet, M. Convers and C. Boucq for help and advice concerning radiation protection measures.

REFERENCES

André, S., Charuau, J., Rateau, G., Vavasseur, C., and Métivier, H. (1989). Design of a new inhalation device for rodents and primates. *J. Aerosol. Sci.* 20 (6), 647–651. doi:10.1016/0021-8502(89)90053-0

ANSM (2011). Piratome sheet #4: Ca-DTPA. Available at https://www.ansm.sante.fr/var/ansm_site/storage/original/application/95fa0049adfd7ec1ba6dc888da7c9a9d (Accessed August 1, 2018).

Ansoborlo, É., Amekraz, B., Moulin, C., Moulin, V., Taran, F., Bailly, T., et al. (2007). Review of actinide decorporation with chelating agents. *C. R. Chim.* 10, 1010–1019. doi:10.1016/j.crci.2007.01.015

Bailey, B. R., Eckerman, K. F., and Townsend, L. W. (2003). An analysis of a puncture wound case with medical intervention. *Radiat. Prot. Dosim.* 105 (1–4), 509–512. doi:10.1093/oxfordjournals.rpd.a006293

Beitz, A. J., Newman, A., Shepard, M., Ruggles, T., and Eikmeier, L. (2004). A new rodent model of hind limb penetrating wound injury characterized by continuous primary and secondary hyperalgesia. *J. Pain* 5 (1), 26–37. doi:10.1016/j.jpain.2003.09.004

Bell, D. Y., Haseman, J. A., Spock, A., McLennan, G., and Hook, G. E. (1981). Plasma proteins of the bronchoalveolar surface of the lungs of smokers and nonsmokers. *Am. Rev. Respir. Dis.* 124 (1), 72–79. doi:10.1164/arrd.1981.124.1.72

Bertelli, L., Waters, T. L., Miller, G., Gadd, M. S., Eaton, M. C., and Guilmette, R. A. (2010). Three plutonium chelation cases at Los Alamos National Laboratory. *Health Phys.* 99 (4), 532–538. doi:10.1097/HP.0b013e3181d18c61

Birchall, A., Puncher, M., Hodgson, A., and Tolmachev, S. Y. (2019). The importance and quantification of plutonium binding in human lungs. *Health Phys.* 117 (2), 133–142. doi:10.1097/HP.0000000000000827

Bistline, R. W., Lebel, J. L., and Dagle, G. E. (1974). "Translocation dynamics of plutonium (NO3)4 and plutoniumO2 from plutonium puncture wounds to lymph nodes and major organs of beagles," in Radiation and the lymphatic system Editor. J. E. Ballou (Virginia, United States: Springfield) US AEC Report Conf-740930.

Carbaugh, E. H., and La Bone, T. R. (2003). Two case studies of highly insoluble plutonium inhalation with implications for bioassay. *Radiat. Prot. Dosim.* 105, 133–138. doi:10.1093/oxfordjournals.rpd.a006208

Chen, J., Chen, Z., Chintagari, N. R., Bhaskaran, M., Jin, N., Narasaraju, T., et al. (2006). Alveolar type I cells protect rat lung epithelium from oxidative injury. *J. Physiol.* 572572 (Pt 3), 625–638. doi:10.1113/jphysiol.2005.103465

Dudoignon, N., Guillet, K., and Fritsch, P. (2003). Evaluation of risk factors for lung tumour induction in rats exposed to either NpO(2) or PuO(2) aerosols. *Int. J. Radiat. Biol.* 79, 169–174. doi:10.1080/0955300031000086299

Falk, R. B., Daugherty, N. M., Aldrich, J. M., Furman, F. J., and Hilmas, D. E. (2006). Application of multi-compartment wound models to plutonium-contaminated wounds incurred by former workers at rocky flats. *Health Phys.* 91, 128–143. doi:10.1097/01.HP.0000203314.17612.63

Food and Drug Administration (2003). Guidance for industry on pentetate calcium trisodium and pentetate zinc trisodium for treatment of internal contamination with plutonium, americium or curium; availability. *Fed. Regist.* 68 (178), 53984–53988.

Fröhlich, E., Mercuri, A., Wu, S., and Salar-Behzadi, S. (2016). Measurements of disposition, lung surface area and lung fluid for simulation of inhaled compounds. *Front. Pharmacol.* 24 (7), 181. doi:10.3389/fphar.2016.00181

Gervelas, C., Sérandour, A. L., Geiger, S., Grillon, G., Fritsch, P., Taulelle, C., et al. (2007). Direct lung delivery of a dry powder formulation of DTPA with improved aerosolization properties: effect on lung and systemic decorporation of plutonium. *J. Cont. Release* 118, 78–86. doi:10.1016/j.jconrel.2006.11.027

Grappin, L., and Bérard, P. (2008). Autorisation de mise sur le marché du Ca-DTPA. *Radioprotection* 43, 465–456. doi:10.1051/radiopro:2008047

Grappin, L., Berard, P., Menetrier, F., Carbone, L., Courtay, C., Castagnet, X., et al. (2007). Treatment of actinide exposures: a review of Ca-DTPA injections inside CEA-COGEMA plants. *Radiat. Prot. Dosim.* 127, 435–439. doi:10.1093/rpd/ncm296

Grémy, O., Miccoli, L., Lelan, F., Bohand, S., Cherel, M., and Mougin-Degraef, M. (2018). Delivery of DTPA through liposomes as a good strategy for enhancing plutonium decorporation regardless of treatment regimen. *Radiat. Res.* 189 (5), 477–489. doi:10.1667/RR14968.1

Grémy, O., Tsapis, N., Bruel, S., Renault, D., and Van der Meeren, A. (2012). Decorporation approach following rat lung contamination with a moderately soluble compound of plutonium using local and systemic Ca-DTPA combined chelation. *Radiat. Res.* 178 (3), 217–223. doi:10.1667/rr2866.1

Grémy, O., Tsapis, N., Chau, Q., Renault, D., Abram, M. C., and Van der Meeren, A. (2010). Preferential decorporation of americium by pulmonary administration of DTPA dry powder after inhalation of aged PuO(2) containing americium in rats. *Radiat. Res.* 174 (5), 637–644. doi:10.1667/RR2203.1

Griffiths, N. M., Coudert, S., Renault, D., Wilk, J. C., and Van der Meeren, A. (2014). Actinide handling after wound entry with local or systemic decorporation therapy in the rat. *Int. J. Radiat. Biol.* 90 (11), 989–995. doi:10.3109/09553002.2014.886797

Griffiths, N. M., Van der Meeren, A., Fritsch, P., Abram, M. C., Bernaudin, J. F., and Poncy, J. L. (2010). Late-occurring pulmonary pathologies following inhalation of mixed oxide (uranium + plutonium oxide) aerosol in the rat. *Health Phys.* 99 (3), 347–356. doi:10.1097/HP.0b013e3181c75750

Griffiths, N. M., Wilk, J. C., Abram, M. C., Renault, D., Chau, Q., Helfer, N., et al. (2012). Internal contamination by actinides after wounding: a robust rodent model for assessment of local and distant actinide retention. *Health Phys.* 103 (2), 187–194. doi:10.1097/HP.0b013e31825aa202

Guilmette, R. A., and Muggenburg, B. A. (1993). Decorporation therapy for inhaled plutonium nitrate using repeatedly and continuously administered DTPA. *Int. J. Radiat. Biol.* 63 (3), 395–403. doi:10.1080/09553009314550521

Hahn, F. F., Romanov, S. A., Guilmette, R. A., Nifatov, A. P., Diel, J. H., and Zaytseva, Y. (2004). Plutonium microdistribution in the lungs of Mayak workers. *Radiat. Res.* 161 (5), 568–581. doi:10.1667/rr3175

Harrison, J. D., and David, A. J. (1979). Experimental studies of the use of DTPA and other agents to limit the systemic burden of plutonium after wound contamination. *Radiat. Res.* 77 (3), 534–546. doi:10.2307/3575164

Helson, L., Rosenspire, K., Kapellaris, A., Bigler, R. E., Richards, P., Srivastava, S. C., et al. (1983). Uptake of ruthenium-labeled transferrin in healing wounds. *Int. J. Nucl. Med. Biol.* 10 (4), 237–239. doi:10.1016/0047-0740(83)90086-4

Ilyin, L. (2001). "Skin wounds and burns contaminated by radioactive substances (metabolism, decontamination, tactics, and techniques of medical care)," in *Management of radiation accidents*. 2nd Edn (Boca Raton, FL: CRC Press), 363–419.

International Commission on Radiological Protection (ICRP) (1986). *The metabolism of plutonium and related elements. International Commission on Radiation Protection Publication 48*. (Oxford: Pergamon Press).

International Commission on Radiological Protection (ICRP) (1994a). *Human respiratory tract model for radiological protection. International Commission on Radiation Protection Publication 66*. (Oxford: Pergamon Press).

International Commission on Radiological Protection (ICRP) (1994b). *Dose coefficients for intakes of radionuclides by workers. International Commission on Radiation Protection Publication 68*. (Oxford: Pergamon Press).

James, A. C., Sasser, L. B., Stuit, D. B., Glover, S. E., and Carbaugh, E. H. (2007). USTUR whole body case 0269: demonstrating effectiveness of i.v. CA-DTPA for Pu. *Radiat. Prot. Dosim.* 127 (1–4), 449–455. doi:10.1093/rpd/ncm473

Kathren, R. L., and Tolmachev, S. Y. (2019). The US transuranium and uranium registries (USTUR): a five-decade follow-up of plutonium and uranium workers. *Health Phys.* 117 (2), 118–132. doi:10.1097/HP.0000000000000963

Klumpp, J., Bertelli, L., Dumit, S., Gadd, M., Poudel, D., and Waters, T. L. (2020). Response to a skin puncture contaminated with ^{238}Pu at Los Alamos national laboratory. *Health Phys.* 119 (6), 704–714. doi:10.1097/HP.0000000000001250

Lagerquist, C. R., Allen, I. B., and Holman, K. L. (1967). Plutonium excretion following contaminated acid burns and prompt DTPA treatments. *Health Phys.* 13, 1–4. doi:10.1097/00004032-196701000-00001

Lamart, S., Miller, B. W., Van der Meeren, A., Tazrart, A., Angulo, J. F., and Griffiths, N. M. (2017). Actinide bioimaging in tissues: comparison of emulsion and solid track autoradiography techniques with the iQID camera. *PLoS One* 12 (10), e0186370, doi:10.1371/journal.pone.0186370

Laroche, P., Cazoulet, A., Bohand, S., Schoen, V., Bey, E., Roche, H., et al. (2010). "The French armed forces health service and the surgical management of a plutonium-contaminated patient at Percy Military Hospital, France," in *The medical basis for radiation-accident preparedness. Medical management*. Editors D. M. Christensen, S. L. Sugarman, and F. M. O'Hara (Oak Ridge, TN: ORAU).

Loffredo, C., Goerlitz, D., Sokolova, S., Leondaridis, L., Zakharova, M., Revina, V., et al. (2017). The Russian human radiobiological tissue repository: a unique resource for studies of plutonium-exposed workers. *Radiat. Prot. Dosim.* 173, 10–15. doi:10.1093/rpd/ncw303

Lushbaugh, C. C., and Langham, J. (1962). A dermal lesion from implanted plutonium. *Arch. Dermatol.* 86, 461–464. doi:10.1001/archderm.1962.01590100075016

McInroy, J. F., Kathren, R. L., Toohey, R. E., Swint, M. J., and Breitenstein, B. D. (1995). Postmortem tissue contents of ^{241}Am in a person with a massive acute exposure. *Health Phys.* 69, 318–323. doi:10.1097/00004032-199509000-00002

McMurray, B. J. (1983). 1976 Hanford americium exposure incident: accident description. *Health Phys.* 45 (4), 847–853. doi:10.1097/00004032-198310000-00002

Miccoli, L., Ménétrier, F., Laroche, P., and Grémy, O. (2019). Chelation treatment by early inhalation of liquid aerosol DTPA for removing plutonium after rat lung contamination. *Radiat. Res.* 192, 630–639. doi:10.1667/RR15451.1

Morgan, C., Bingham, D., Holt, D. C., Jones, D. M., and Lewis, N. J. (2010). Therapeutic whole lung lavage for inhaled plutonium oxide revisited. *J. Radiol. Prot.* 30, 735–746. doi:10.1088/0952-4746/30/4/007

Muggenburg, B. A., Felicetti, S. A., and Silbaugh, S. A. (1977). Removal of inhaled radioactive particles by lung lavage–a review. *Health Phys.* 33, 213–220. doi:10.1097/00004032-197709000-00006

Muggenburg, B. A., Guilmette, R. A., Hahn, F. F., Diel, J. H., Mauderly, J. L., Seilkop, S. K., et al. (2008). Radiotoxicity of Inhaled $^{239}PuO_2$ in dogs. *Radiat. Res.* 170, 736–757. doi:10.1667/RR1409.1

National Council on Radiological Protection and Measurements (NCRP) (2006). "Development of a biokinetic model for radionuclide-contaminated wounds and procedures for their assessment, dosimetry, and treatment," in Recommendations of the national council on radiation protection and measurements NCRP report no. 156. Bethesda, MD. Available at: https://ncrponline.org/publications/reports/ncrp-report-156/.

National Council on Radiological Protection and Measurements. (NCRP) (2009). "Management of persons contaminated with radionuclides," in NCRP report no. 161 I national Council on radiation protection and measurements. Bethesda, MD. Available at: https://ncrponline.org/publications/reports/ncrp-report-161/.

Newman, L. S., Mroz, M. M., and Ruttenber, A. J. (2005). Lung fibrosis in plutonium workers. *Radiat. Res.* 164 (2), 123–131. doi:10.1667/rr3407

Newton, D., Taylor, B. T., and Eakins, J. D. (1983). Differential clearance of plutonium and americium oxides from human lung. *Health Phys.* 44, 431–439. doi:10.1097/00004032-198306001-00041

Nolibé, D., Métivier, H., Masse, R., and Chrétien, J. (1989). Benefits and risks of bronchopulmonary lavage: a review. *Radiat. Prot. Dosim.* 26, 337–343. doi:10.1093/oxfordjournals.rpd.a080427

Norwood, W. D. (1960). DTPA-effectiveness in removing internally-deposited plutonium from humans. *J. Occup. Med.* 2, 371–376. doi:10.1097/00043764-196008000-00002

Okladnikova, N. D., Scott, B. R., Tokarskaya, Z. B., Zhuntova, G. V., Khokhryakov, V. F., Syrchikov, V. A., et al. (2005). Chromosomal aberrations in lymphocytes of peripheral blood among Mayak facility workers who inhaled insoluble forms of ^{239}Pu. *Radiat. Prot. Dosim.* 113, 3–13. doi:10.1093/rpd/nch417

Paquet, F., Chazel, V., Houpert, P., Guilmette, R., and Muggenburg, B. (2003). Efficacy of 3,4,3-LI(1,2-HOPO) for decorporation of Pu, Am and U from rats injected intramuscularly with high-fired particles of MOX. *Radiat. Prot. Dosimetry* 105, 521–525. doi:10.1093/oxfordjournals.rpd.a006296

Ramounet-Le Gall, B., Rateau, G., Abram, M.-C., Grillon, G., Ansoborlo, E., Berard, P., et al. (2003). *In vivo* measurement of Pu dissolution parameters of MOX aerosols and related uncertainties in the values of the dose per unit intake. *Radiat. Prot. Dosim.* 105, 153–156. doi:10.1093/oxfordjournals.rpd.a006212

Schadilov, A. E., Belosokhov, M. V., and Levina, E. S. (2010). A case of wound intake of plutonium isotopes and ^{241}Am in a human: application and improvement of the NCRP wound model. *Health Phys.* 99 (4), 560–567. doi:10.1097/HP.0b013e3181c34989

Sérandour, A. L., Tsapis, N., Gervelas, C., Grillon, G., Fréchou, M., Deverre, J. R., et al. (2007). Decorporation of plutonium by pulmonary administration of Ca-DTPA dry powder: a study in rat after lung contamination with different plutonium forms. *Radiat. Prot. Dosim.* 127, 472–476. doi:10.1093/rpd/ncm300

Stather, J. W., Stradling, G. N., Smith, H., Payne, S., James, A. C., Strong, J. C., et al. (1982). Decorporation of $^{238}PuO_2$ from the hamster by inhalation of chelating agents. *Health Phys.* 42, 520–525.

Stradling, G. N., Gray, S. A., Moody, J. C., Pearce, M. J., Wilson, I., Burgada, R., et al. (1993). Comparative efficacies of 3,4,3-LIHOPO and DTPA for enhancing the excretion of plutonium and americium from the rat after simulated wound contamination as nitrates. *Int. J. Radiat. Biol.* 64 (1), 133–140. doi:10.1080/09553009314551191

Sugarman, S. L., Findley, W. M., Toohey, R. E., and Dainiak, N. (2018). Rapid response, dose assessment, and clinical management of a plutonium-contaminated puncture wound. *Health Phys.* 115, 57–64. doi:10.1097/HP.0000000000000821

Sychugov, G., Azizova, T., Osovets, S., Kazachkov, E., Revina, V., and Grigoryeva, E. (2020). Morphological features of pulmonary fibrosis in workers occupationally exposed to alpha radiation. *Int. J. Radiat. Biol.* 96 (4), 448–460. doi:10.1080/09553002.2020.1721601

Taylor, D. M., and Sowby, F. D. (1962). The removal of americium and plutonium from the rat by chelating agents. *Phys. Med. Biol.* 7, 83–91. doi:10.1088/0031-9155/7/1/306

Van der Meeren, A., and Grémy, O. (2010). Isotopic and elemental composition of plutonium/americium oxides influence pulmonary and extra-pulmonary distribution after inhalation in rats. *Health Phys.* 99, 380–387. doi:10.1097/HP.0b013e3181c61fba

Van der Meeren, A., Gremy, O., Renault, D., Miroux, A., Bruel, S., Griffiths, N., et al. (2012). Plutonium behavior after pulmonary administration according to solubility properties, and consequences on alveolar macrophage activation. *J. Radiat. Res.* 53 (2), 184–194. doi:10.1269/jrr.11112.PMID:22510590

Van der Meeren, A., Moureau, A., and Griffiths, N. M. (2014). Macrophages as key elements of mixed-oxide [U-Pu(O_2)] distribution and pulmonary damage after inhalation? *Int. J. Radiat. Biol.* 90 (11), 1095–1103. doi:10.3109/09553002.2014.943848

Volf, V. (1974). Experimental background for prompt treatment with DTPA of ^{239}Pu-contaminated wounds. *Health Phys.* 27, 273–277. doi:10.1097/00004032-197409000-000051

Conflict of Interest: The authors declare that the research was conducted in the absence of any commercial or financial relationships that could be construed as a potential conflict of interest.

frontiers in Pharmacology

ORIGINAL RESEARCH
published: 22 April 2021
doi: 10.3389/fphar.2021.676396

RRx-001 Radioprotection: Enhancement of Survival and Hematopoietic Recovery in Gamma-Irradiated Mice

*Kimberly J. Jurgensen[1,2], William K. J. Skinner[3], Bryan Oronsky[4], Nacer D. Abrouk[4], Andrew E. Graff[3], Reid D. Landes[5], William E. Culp[6], Thomas A. Summers Jr[7] and Lynnette H. Cary[2]**

[1]Henry M. Jackson Foundation for the Advancement of Military Medicine, Bethesda, MD, United States, [2]Scientific Research Department, Armed Forces Radiobiology Research Institute, Uniformed Services University, Bethesda, MD, United States, [3]Department of Radiation Oncology, Walter Reed National Military Medical Center, Bethesda, MD, United States, [4]EpicentRx, Inc., San Diego, CA, United States, [5]Department of Biostatistics, University of Arkansas for Medical Sciences, Little Rock, AR, United States, [6]Director, Biomedical Instrumentation Center, Uniformed Services University of the Health Sciences, Bethesda, MD, United States, [7]Department of Pathology, Uniformed Services University, Bethesda, MD, United States

OPEN ACCESS

Edited by:
Roberto Paganelli,
University of Studies G. d'Annunzio Chieti and Pescara, Italy

Reviewed by:
Andrea Delli Pizzi,
University of Studies G. d'Annunzio Chieti and Pescara, Italy
Joel S Greenberger,
University of Pittsburgh Medical Center, United States

***Correspondence:**
Lynnette H. Cary
lynnette.cary@usuhs.edu

Specialty section:
This article was submitted to Translational Pharmacology, a section of the journal Frontiers in Pharmacology

Received: 05 March 2021
Accepted: 06 April 2021
Published: 22 April 2021

Citation:
Jurgensen KJ, Skinner WKJ, Oronsky B, Abrouk ND, Graff AE, Landes RD, Culp WE, Summers TA and Cary LH (2021) RRx-001 Radioprotection: Enhancement of Survival and Hematopoietic Recovery in Gamma-Irradiated Mice. Front. Pharmacol. 12:676396. doi: 10.3389/fphar.2021.676396

The present studies evaluate the *in vivo* prophylactic radioprotective effects of 1-bromoacetyl-3, 3-dinitroazetidine (RRx-001), a phase III anticancer agent that inhibits c-myc and downregulates CD-47, after total body irradiation (TBI), in lethally and sublethally irradiated CD2F1 male mice. A single dose of RRx-001 was administered by intraperitoneal (IP) injection 24 h prior to a lethal or sublethal radiation dose. When irradiated with 9.35 Gy, the dose lethal to 70% of untreated mice at 30 days ($LD_{70/30}$), only 33% of mice receiving RRx-001 (10 mg/kg) 24 h prior to total body irradiation (TBI) died by day 30, compared to 67% in vehicle-treated mice. The same pretreatment dose of RRx-001 resulted in a significant dose reduction factor of 1.07. In sublethally TBI mice, bone marrow cellularity was increased at day 14 in the RRx-001-treated mice compared to irradiated vehicle-treated animals. In addition, significantly higher numbers of lymphocytes, platelets, percent hematocrit and percent reticulocytes were observed on days 7 and/or 14 in RRx-001-treated mice. These experiments provide proof of principle that systemic administration of RRx-001 prior to TBI significantly improves overall survival and bone marrow regeneration.

Keywords: hematopoietic acute radiation syndrome (H-ARS), radiation, countermeasures, RRx-001, total body irradiation (TBI)

INTRODUCTION

Ionizing radiation causes damage to normal tissues, ranging from genetic mutations to cell death (Hall and Giaccia, 2012). The harmful effects of ionizing radiation on normal tissues are a major concern for military and emergency responders to nuclear accidents and terrorist events due to the risk of acute and delayed radiation injuries (CDC, 2010). Additionally, radioprotection is a critical issue in cancer treatment. Despite significant technological improvements in radiation delivery in recent years, normal tissue toxicity remains a major dose-limiting factor in therapeutic radiology (Johnke et al., 2014; Nakamura et al., 2014).

Extensive efforts over the past several decades have resulted in two Food and Drug Administration (FDA) approved drugs available for prophylactic radioprotection of non-hematopoietic tissue, amifostine (Ethyol) and palifermin (Kepivance) (Wasserman and Brizel, 2001). However, neither amifostine nor palifermin have been FDA approved for accidental or emergency radiation exposures.

Only three drugs have been FDA approved for the treatment of hematopoietic acute radiation syndrome (H-ARS): 1) Granulocyte colony-stimulating factor (G-CSF, Filgrastim, or Neupogen), 2) Pegfilgrastim (PegG-CSF, Neulasta), and 3) Granulocyte macrophage colony-stimulating factor (GM-CSF, Sargramostim, or Leukine). All work by promoting granulocytes that make up the majority of circulating white blood cells (WBCs) (Mehta et al., 2015). These drugs are radiomitigators and although they have been shown to be effective in multiple animal models of H-ARS, studies have also shown that with prolonged use they may exacerbate radiation induced long-term bone marrow injury, as well as, the long-term recovery from hematopoietic syndrome by promoting hematopoietic stem cell (HSC) proliferation and differentiation leading to HSC exhaustion, in part by promoting HSC senescence (Li et al., 2015).

These limitations require a search for a radioprotective or radiomitigating agent that is deemed sufficiently safe and effective both to shield patients from normal tissue side effects during radiotherapy without simultaneously protecting tumor cells, and to increase survival for the military and first responders in the event of nuclear and radiological emergencies, as well as astronauts exposed to cosmic radiation that would otherwise have been blocked or absorbed by the Earth's atmosphere.

One minimally toxic option currently under investigation as an anticancer agent in Phase III clinical trials is RRx-001, a small cyclic nitro compound with the IUPAC nomenclature, 1-bromoacetyl-3,3-dinitroazetidine (Ning et al., 2012). Preclinical and clinical research demonstrated that RRx-001 is a vascular normalizer that repolarizes tumor associated macrophages (TAM) from an M2 to M1 phenotype and through c-myc inhibition downregulates expression of the CD47 checkpoint on cancer cells (Cabrales, 2019). These changes effectively mobilize TAMs to seek out and destroy tumor cells, which, in the process, along with improved tumor blood flow, increases susceptibility to chemotherapy and radiation (Ning et al., 2012). RRx-001 is tested clinically to be used as a single agent, and in combination with chemotherapy and/or radiation as a chemo- and radiosensitizer.

Early human phase I and II data have demonstrated broad-spectrum anticancer activity in the absence of typical chemotherapy-related toxicities (Reid et al., 2015). Paradoxically, in non-transformed cells, RRx-001 treatment protects normal tissue from radiation and chemotherapy damage (Ning et al., 2012). *In vivo* studies showed that administration of RRx-001 prior to cisplatin treatment is prophylactic against the development of renal toxicity and chromosomal aberrations (Oronsky et al., 2017). In preclinical testing, RRx-001 (10 mg/kg) given 30 min prior to total body irradiation (10–15 Gy) protected the intestines of C3H mice as shown by an increased number of viable crypt cells (Ning et al., 2012).

The aim of this study was to determine if prophylactic systemic administration of RRx-001 24 h prior to TBI significantly improves overall survival in CD2F1 mice compared to the vehicle control. A 30-day TBI lethality experiment ($LD_{70/30}$ of 9.35 Gy) demonstrated that 24-h prophylactic intraperitoneal (IP) administration of RRx-001 increased overall survival and median survival time in CD2F1 mice. A follow-up experiment to identify the dose reduction factor (DRF) showed that RRx-001 provided a statistically significant DRF of 1.07 compared to the vehicle control. In sublethally TBI mice, prophylactic IP administration of RRx-001 was found to significantly reduce severe reticulocytopenia and leukopenia in addition to improving cellular recovery in bone marrow.

MATERIALS AND METHODS

RRx-001 Drug Preparation

RRx-001 as a powder was obtained from EpicentRx Inc (Mountain View, CA) and formulated according to the manufacturer's instructions. Briefly, 100% dimethyl sulfoxide (DMSO) (Amresco, Solon, OH) was added to RRx-001, vortexed for 30–60 s and incubated at room temperature for 15 min. Sterile water (Teknova, Hollister, CA) was added to bring the final concentration of DMSO to 5% and the solution vortexed for 2 min. The 2.0 mg/ml RRx-001 stock solution was made up fresh before each experiment. The vehicle control, 5% DMSO in sterile water, was made up following the same procedure. 10 mg/kg RRx-001 or vehicle was injected intraperitoneal (IP) or intravenous (IV) 24 h prior to irradiation or sham-irradiation.

Mice

Eight-to ten-week-old CD2F1/Hsd male mice were purchased from Envigo (Dublin, VA) and maintained at the Armed Forces Radiobiology Research Institute (AFRRI, Bethesda, MD) vivarium. Mice were allowed to acclimate for at least 7 days prior to initiation of the study. Mice were randomized (3–4/cage) and conventionally housed in sterile polycarbonate boxes with filtered lids (Microisolator, Lab Products Inc., Seaford, DE) and autoclaved hardwood chip bedding. Mice had ad libitum access to Harlan Teklad Rodent diet 8604 (Purina Mills, St. Louis, MO) and acidified water (pH 2.5–3.0). All mice were housed in a controlled environment with a 12-h light-dark cycle, a temperature of 23 ± 2°C, 50 ± 20% relative humidity and 10–15 cycles per hour of fresh air. According to vendor health reports, mice were free of viral, fungal, bacterial, and parasitic adventitial pathogens. All animal procedures were performed in accordance with institutional guidelines, the principles outlined in the National Research Council's Guide for the Care and Use of Laboratory Animals and approved by AFRRI's Institutional Animal Care and Use Committee.

Irradiation

Unanesthetized mice were placed in well-ventilated Plexiglas restrainers and irradiated bilaterally at AFRRI's Cobalt-60 (Co-60) gamma irradiation facility. Sham-irradiated mice were also placed in identical Plexiglas restrainers and kept in a room shielded from irradiation at the same time. In each experiment, the dose to the abdominal cores of the animals was delivered at a dose rate of approximately 0.6 Gy/min. Dosimetry was performed prior to the irradiation of the animals using the highly accurate alanine/electron spin resonance (ESR) dosimetry system (American Society for Testing and Materials, Standard E 1607) to measure dose rates (to water) in the cores of acrylic mouse phantoms, which were located in the compartments of the exposure rack. A calibration curve based on standard alanine calibration dosimeters provided by the National Institute of Standards and Technology (NIST, Gaithersburg, MD) was used to measure the doses. The accuracy of AFRRI's dose rate calibrations has been verified several times using the services of the National Physics Laboratory (United Kingdom National Standards Laboratory, London, United Kingdom) and the M.D. Anderson Cancer Center (Houston, TX). The corrections applied to the measured dose rates in the phantoms were for a small difference in the Co-60 energy between the mass energy-absorption coefficients for soft tissue and water, as well as source decay. The radiation field was uniform within ±1.2%.

Radioprotection Survival Study

For the survival study, mice underwent TBI at 9.35 Gy [the LD70/30 (Kumar et al., 2018)] at a dose rate of 0.6 Gy/min using gamma photons. Twenty-four hours prior to irradiation, 12 mice received 10 mg/kg RRx-001; the remaining 12 mice received the vehicle control (5% DMSO in sterile H2O) by IP or IV injection. Mice were monitored at least twice a day for 30 days post-irradiation. During the critical period (days 10–20), mice were monitored at least three times a day with no more than 10 h between observations. Mice displaying any signs of discomfort received food in their cage as a wet mash. Mice displaying overt dyspnea, weight loss, lethargy, or other markers of moribundity and appearing to be in distress were humanely euthanized in a separate room using carbon dioxide gas followed by cervical dislocation after breathing stopped as a confirmatory method of euthanasia. The IV survival study had 24 mice total. The IP survival study was repeated with an additional 24 mice; thus, for final analysis, each of the two treatment groups had 24 mice (48 mice in total).

Prophylactic Dose Reduction Factor (DRF) Study

We sought to estimate the DRF of RRx-001 prophylactically administered 24 h prior to TBI. Half of the allotted animals were randomized to receive 10 mg/kg of RRx-001, and the other half to receive 5% DMSO in sterile H_20 by IP injection. Within each treatment group, we further equally randomized mice among six radiation doses: 7.5, 8, 8.5, 9, 9.5, and 10 Gy for vehicle-treated mice, and 8.5, 9, 9.5, 10, 10.5, and 11 Gy for drug-treated mice. In order to detect a DRF of 1.10 with 0.90 power on a one-sided 0.05 significance level test, we calculated 84 mice (split equally among all 12 treatment-radiation groups) were needed. This calculation assumed an LD50/30 for vehicle mice of 8.9 Gy, the aforementioned radiation doses, and a lethality slope of 25 on log10 radiation dose in a probit regression (Kodell et al., 2010). However, as part of an ongoing feasibility study, we used 16 mice per treatment-radiation group (192 in total), which would allow detection of a DRF = 1.06 with 0.90 power. Mice were monitored at least twice a day post-irradiation, and at least 3 times a day during the critical period (days 7–20) with no more than 10 h between observations. Mice displaying any signs of discomfort received food in their cage as a wet mash. Mice displaying markers of moribundity and appearing to be in distress were humanely euthanized as described previously. Survival to 45 days after irradiation was recorded and survival to 30 days was analyzed.

Hematopoietic Study

To determine the pathophysiological effects of RRx-001 on hematopoietic protection in mice, a sublethal dose of TBI (7 Gy at 0.6 Gy/min using Co-60) was used (Ghosh et al., 2009). Sixty (60) CD2F1 male mice were randomized into four experimental groups: 1) irradiation + vehicle, 2) irradiation + RRx-001, 3) sham-irradiation + vehicle, and 4) sham-irradiation + RRx-001. Either 10 mg/kg RRx-001 or the vehicle control were IP injected 24 h prior to either irradiation or sham-irradiation (day 0). The 15 mice within each group were then randomized (3 mice/group/timepoint) to be humanely euthanized on days 2, 7, 14, 21, and 28 post-irradiation (day 0). Blood was removed by cardiocentesis using a 1 ml syringe with a 23 g needle in mice anesthetized with 3–5% isoflurane (Baxter, Deerfield, IL). This was performed as a terminal procedure, and followed by cervical dislocation as a confirmatory method of euthanasia. A portion of the sample was immediately transferred into EDTA tubes (Sarstedt Inc., Newton, NC) and gently rotated until the time of analysis. The tubes were analyzed for a complete blood count with differential and reticulocytes using the ADVIA 2120 (Siemens Medical Solutions Diagnostics, Dublin, Ireland), and Microsoft software version 5.9 (Microsoft Corp., Redmond, WA) to generate the data. Serum was separated from the rest of the blood sample for an enzyme-linked immunosorbent assay (ELISA), and bone marrow and sternebrae were then collected. These procedures were repeated with an additional 60 mice; thus, providing $n = 6$ mice/group/time point (120 mice in total) for analysis.

Sternum Marrow Histopathology

Sternebrae collected during the hematopoietic study were fixed in 10% zinc-buffered formalin for at least 24 h and up to 7 days. Fixed sternebrae were decalcified for 3 h in 12–18% sodium EDTA (pH 7.4–7.5) and specimens dehydrated using graded ethanol concentrations and embedded in paraffin. Longitudinal 4 μm sections were stained with regular hematoxylin and eosin. Two board-certified pathologists conducted histopathological evaluation of the samples. One of the pathologists scored all the samples blindly. Bone marrow was evaluated *in situ* within

sternebrae and graded (grade 1: ≤10%; grade 2: 11–30%; grade 3: 31–60%; grade 4: 61–89%; grade 5: ≥90%) for total cellularity. Megakaryocytes were also quantified based on the average per 10 high power fields (HPF) at 400× magnification using a BX43 or BX53 microscope (Olympus, Minneapolis, MN). Images were captured with an Olympus DP22 camera and imported into Olympus cellSens Standard software for review.

Colony Forming Unit Assay

Bone marrow was collected from both femurs of CD2F1 mice during the hematopoietic study as described previously (Kumar et al., 2018) and were pooled so that $n = 3$ mice/group/day. The pooled bone marrow cells were suspended in semisolid cultures using 1 ml of MethoCult™ GF+ system for mouse cells per 35-mm cell culture dish and plated in triplicate (Stem Cell Technologies, Vancouver, BC, Canada) according to the manufacturer's instructions. Sham-irradiated groups were plated at 1×10^4 cells. Irradiated (7 Gy) groups were plated at 4×10^4 cells. All colonies were counted 12 days after incubation and 50+ cells constituted one colony. Data is represented as the mean ± SEM of $n = 3$ mice/group/time point for a total of 57 animals.

Circulating Levels of G-CSF

Serum collected from the hematopoietic study was used to detect circulating levels of G-CSF using the mouse G-CSF Quantikine ELISA kit (R&D Systems, Minneapolis, MN) and following manufacturer's instructions. The cytokine detection limit was 5 pg/ml and the G-CSF positive control was between 97.9–163.2 pg/ml. Data is represented as the mean ± SEM of $n = 2$–3 mice/group/time point for a total of 50 animals.

Statistical Analyses

For the survival study, estimated survival curves were produced with Kaplan-Meier's method, and compared with a two-sided log-rank test. For the DRF study, we estimated the DRF and its 95% confidence interval with probit regression of mouse mortality on treatment and log10-transformed radiation dose as described elsewhere (Landes et al., 2013). For the pathophysiology study, blood and bone marrow parameters were estimated and compared between treatment groups using analysis of variance (ANOVA), with treatment and euthanasia day as factors. In the ANOVA of bone marrow parameters, pathology was included as a factor. Finally, to determine whether ANOVA results depended on normal assumptions, we also compared treatment groups using nonparametric analogues of the ANOVAs, such as Wilcoxon–Mann–Whitney tests and Kruskal–Wallis analyses as sensitivity analyses.

For all analyses, $p < 0.05$ was considered significant; we also present 95% confidence intervals. Given the nature of the experiments, sample size determination based on the power to detect group differences was not an a-priori consideration, the multiplicity of comparisons impact on significance is deemed unimportant since most p values were highly significant. We used R software (Version 3.4.3, 2016) and SAS/STAT software, version 9.4, SAS System for Windows (SAS Institute, Cary, NC, United States) for analyses, and R software and GraphPad Prism version 7.03 (GraphPad Software, La Jolla, CA) for figures. Data and software code for producing the results in this work are available upon request.

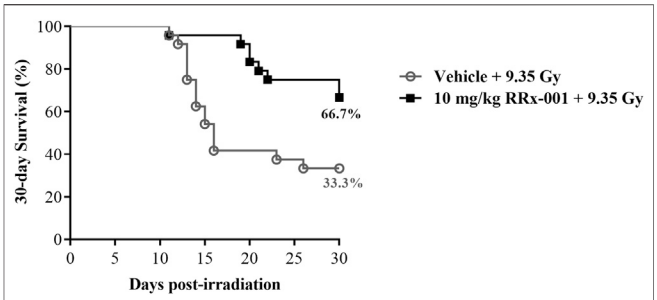

FIGURE 1 | Kaplan–Meier 30-day survival curves illustrating the increased and prolonged survival of CD2F1 mice prophylactically treated by IP injection with 10 mg/kg RRx-001 compared to the vehicle control, 24 h prior to 9.35 Gy whole body irradiation; log-rank $\chi^2_{(1)} = 7.65$, $p = 0.006$. $N = 12$ mice/group (24 mice total) per experiment. The experiment was performed in duplicate (48 mice total).

RESULTS

Pretreatment With RRx-001 Increases Survival After Lethal Total Body Irradiation

Survival improvement in favor of IP pretreatment with one dose of 10 mg/kg RRx-001 over vehicle control in mice 24 h prior to a lethal TBI of 9.35 Gy was highly significant: 67% of RRx-001 treated animals survived to 30 days compared to 33% of vehicle treated animals (log-rank $\chi^2_{(1)} = 7.65$, $p = 0.006$; **Figure 1**). The results also demonstrated that 24-h prophylactic IP administration of RRx-001 increased median survival time by at least 14 days over that for vehicle treated animals. When mice were administered 10 mg/kg RRx-001 or vehicle by IV injection 24 h prior to a lethal TBI of 9.35 Gy, survival was significantly higher after 30 days in the RRx-001 treated mice: 50% survival in RRx-001 treated mice vs. 8% survival in vehicle treated mice (log-rank $\chi^2_{(1)} = 5.62$, $p = 0.018$; **Supplementary Figure S1**).

Determination of DRF Showed RRx-001 Increases Resistance to Radiation Lethality

Before estimating the DRF, we first checked the assumption of a common slope on radiation dose for the vehicle- and RRx-001-treated groups from the initial survival study results, each having a slope of 37.6 and 41.5, respectively. This difference of 3.8 in slopes is negligible based on the 95% confidence intervals (CI: −15.9, 23.5). Fitting the common-slope model, the $LD_{50/30}$ for mice treated prophylactically with RRx-001 was 9.85 Gy, and for vehicle-treated mice was 9.18; thus, the DRF was 1.07 (CI: 1.04, 1.10) (**Figure 2**). In the IP survival study, 2 RRx-001-treated mice died on day 30; therefore, mice were monitored for survival out to day 45. On day 34, one

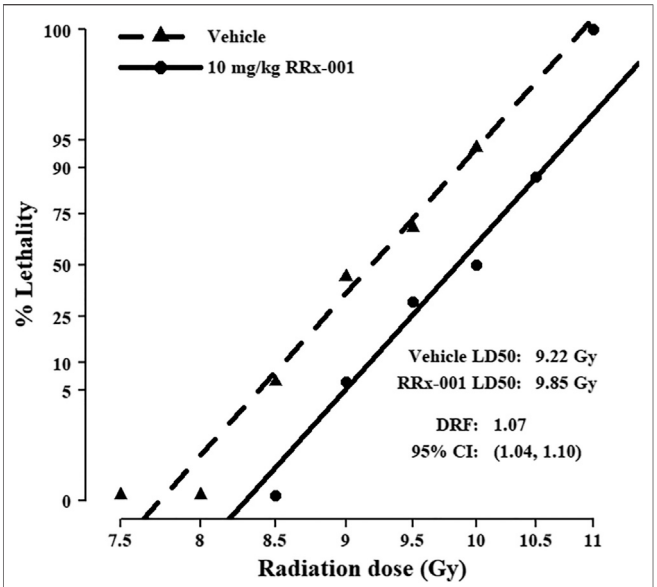

FIGURE 2 | Probit mortality curves for 192 mice equally randomized to prophylactic treatment with 10 mg/kg RRx-001 or vehicle control; mice were further equally randomized among the six indicated TBI doses to determine the DRF (n = 16 mice/group). $LD_{50/30}$ and DRF were estimated with probit regression of mortality on $\log_{10}$ dose of radiation. The $LD_{50/30}$ for vehicle pre-treated mice was 9.22 (95% CI: 9.03, 9.41), and for RRx-001 pre-treated mice was 9.85 (95% CI: 9.66, 10.05); thus, the DRF was 1.07 (95% CI: 1.04, 1.10). The common slope was 39.6 (95% CI: 29.8, 49.4).

vehicle-treated mouse in the 10 Gy group was the only casualty between day's 31–45.

RRx-001 Reduced Pancytopenia After Sublethal Irradiation

In both pretreatment groups of mice, an acute irradiation at a sublethal dose induced severe reticulocytopenia and leukopenia (**Table 1**). Reticulocyte levels reached a nadir around day 7, increased to levels notably above baseline at day 21, then returned to near-baseline levels by day 28. Throughout the fluctuation over the first 21 days, RRx-001 pretreated mice were estimated to be closer to baseline levels than those pretreated with vehicle. White blood cells and lymphocytes also reached their nadir around day 7, and though levels started to increase, they did not reach baseline levels by day 28. However, white blood cells and lymphocyte levels in irradiated mice pretreated with RRx-001 tended to increase faster than that of their vehicle-pretreated peers. After irradiation, levels of neutrophils and platelets reached their nadir by day 7, and remained at low cellular levels through day 14. From days 7–14, levels in the RRx-001 pretreated mice did not drop as low as that in the vehicle-pretreated mice. After day 14, neutrophil and platelet levels in both groups improved over the next two weeks. Percent hematocrit reached its lowest point 14 days after irradiation, with the level in RRx-001 pretreated mice remaining slightly higher than that in vehicle-pretreated mice. Hematocrit levels were back to baseline levels by day 21 in both pretreatment groups.

RRx-001 Increases Bone Marrow Recovery After Irradiation

To determine the effect of RRx-001 on bone marrow, a histopathological analysis of bone marrow sternebrae was performed and the cellularity, as reported by grade (grade 1: ≤10%; grade 2: 11–30%; grade 3: 31–60%; grade 4: 61–89%; grade 5: ≥90% cellularity), and megakaryocyte numbers (averaged per 10 high-powered fields; HPF) were ascertained by two pathologists, one of which scored all the samples blindly (TAS, WEC). In determining significance for grade of cellularity and average number of megakaryocytes per 10 HPF, the differences between pathologists and the interaction between treatment and pathologist were not significantly different.

The overall cellularity of the bone marrow in both the sham-irradiated RRx-001- and vehicle-pretreated groups never

TABLE 1 | Prophylactic treatment with RRx-001 Reduced Pancytopenia after Sublethal Irradiation.

Time after radiation	Treatment group	WBC ($\times10^3$ cells/μL)	ALC ($\times10^3$ cells/μL)	ANC ($\times10^3$ cells/μL)	Platelets ($\times10^3$ cells/μL)	% Hematocrit	% Reticulocytes
Average days 2, 7, 14, 21, 28	Vehicle + sham	5.01 ± 0.31	3.75 ± 0.26	0.91 ± 0.06	913.66 ± 52.55	41.59 ± 0.44	2.54 ± 0.07
	RRx-001 + Sham	4.73 ± 0.27	3.38 ± 0.21	0.97 ± 0.06	**1,067.73 ± 32.26	41.66 ± 0.45	2.62 ± 0.07
Day 2	Vehicle +7 Gy	0.82 ± 0.14	0.07 ± 0.01	0.67 ± 0.13	863.00 ± 88.08	39.27 ± 0.85	ND
	RRx-001 + 7 Gy	1.38 ± 0.20	0.07 ± 0.01	1.13 ± 0.20	979.00 ± 40.35	41.07 ± 0.82	ND
Day 7	Vehicle +7 Gy	0.18 ± 0.05	0.08 ± 0.03	0.07 ± 0.01	93.33 ± 16.29	30.08 ± 0.99	0.03 ± 0.01
	RRx-001 + 7 Gy	0.21 ± 0.03	0.04 ± 0.00	*0.11 ± 0.02	*133.40 ± 16.74	31.36 ± 1.00	0.05 ± 0.01
Day 14	Vehicle +7 Gy	0.25 ± 0.03	0.18 ± 0.02	0.06 ± 0.01	78.33 ± 9.97	25.27 ± 0.62	1.62 ± 0.28
	RRx-001 + 7 Gy	*0.70 ± 0.20	*0.49 ± 0.14	*0.14 ± 0.03	*143.25 ± 36.54	*28.38 ± 0.55	*4.05 ± 1.08
Day 21	Vehicle +7 Gy	1.19 ± 0.13	0.51 ± 0.08	0.52 ± 0.04	371.60 ± 66.29	40.40 ± 0.36	7.08 ± 1.59
	RRx-001 + 7 Gy	1.11 ± 0.11	0.46 ± 0.03	0.50 ± 0.07	448.33 ± 40.37	39.38 ± 1.58	6.06 ± 1.03
Day 28	Vehicle +7 Gy	2.20 ± 0.34	0.77 ± 0.19	1.17 ± 0.20	595.50 ± 135.15	35.83 ± 2.18	2.62 ± 0.09
	RRx-001 + 7 Gy	2.69 ± 0.33	1.18 ± 0.32	1.09 ± 0.11	497.60 ± 116.12	39.02 ± 1.57	*3.66 ± 0.40

*Values are the mean ± SEM (n = 2–3 mice/group/time point); ND, not determined. *p < 0.05 comparing the irradiated groups/time point. Significance was determined using a parametric test consisting of a general linear model ANOVA and the Kruskal–Wallis nonparametric test. **p < 0.01 comparing the nonirradiated groups combining days 2, 7, 14, 21 and 28. Significance was determined using the longitudinal mixed model repeated measures analysis. This experiment was performed in duplicate.*

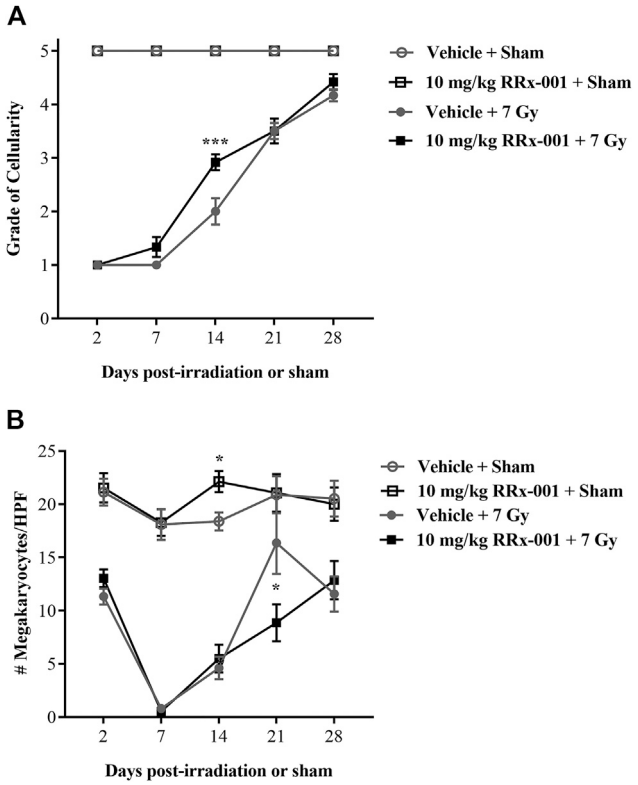

FIGURE 3 | RRx-001 significantly increased the grade of bone marrow cellularity but not megakaryocytes after sublethal total body irradiation **(A)** Pretreatment with 10 mg/kg RRx-001 significantly increased the grade of bone marrow cellularity (grade 1: ≤10%; grade 2: 11–30%; grade 3: 31–60%; grade 4: 61–89%; grade 5: ≥90%) on day 14 after irradiation compared to the vehicle control; ***$p < 0.0001$ **(B)** In the sham-treated groups, RRx-001 had a significant increase in average megakaryocyte number per 10 HPF compared to the vehicle control on day 14; *$p = 0.041$. However, in the irradiated groups on day 21 there was a significant spike in megakaryocyte numbers in the vehicle-treated group compared to the RRx-001-treated group; *$p = 0.029$. Error bars show mean ± SEM. Significance was determined using a parametric test consisting of a general linear model ANOVA and the Kruskal–Wallis nonparametric test. $N = 3$ mice/group/time point (60 mice total) per experiment. The experiment was performed in duplicate (120 mice total).

dropped below 90% during the duration of the study and therefore maintained a grade of 5 (**Figure 3A**). As expected after irradiation, both the RRx-001- and vehicle-pretreated groups had a massive loss in bone marrow cellularity, with all mice having grade 1 cellularity by day 2 after radiation. At day 7, a slight increase in cellularity was observed by the pathologists in the irradiated, RRx-001-pretreated mice compared to the irradiated, vehicle-pretreated mice. Irradiated mice pretreated with RRx-001, significantly accelerated hematopoietic recovery as determined by the grade of bone marrow cellularity compared with vehicle-pretreated, irradiated mice on day 14. By day 21, both vehicle- and RRx-001-treated irradiated mice displayed equivalent bone marrow cellularity, and improvement continued in both pretreatment groups through day 28; however, neither irradiated group reached cellularity grade 5.

Counts of megakaryocytes in sham-irradiated mice were similar over 28 days for the two pretreatment groups, except at day 14 when RRx-001 pretreated mice had more than vehicle-pretreated mice (**Figure 3B**). Irradiation-induced decreases in megakaryocyte counts were evident at day 2 in the two pretreatment groups, and continued to drop to near 0 by day 7. However, after day 7, both pretreatment groups of irradiated mice started recovering toward baseline levels of megakaryocytes through day 28, but failed to fully recover to the levels of sham-irradiated mice. Interestingly, the vehicle-pretreated mice had more megakaryocytes than RRx-001 pretreated mice at day 21, but these two groups were similar again by day 28.

Figure 4 depicts representative bone marrow histopathology from each experimental group at day 14, where 4A and 4B denote normal bone marrow morphology and cellularity in sham-irradiated mice, treated with either vehicle or RRx-001, respectively. The irradiated vehicle-treated group (4C) showed a significant loss of bone marrow cellularity with an increase in infiltration by adipocytes compared to the irradiated RRx-001-treated group (4D) on day 14 where significant recovery of bone marrow cellularity was observed.

DISCUSSION

This is the first study to report that RRx-001 administered IP 24 h prior to an $LD_{70/30}$ dose of TBI significantly decreased and delayed lethality in CD2F1 mice. In this study, 33% of mice receiving vehicle before undergoing irradiation with the $LD_{70/30}$ dose survived to 30 days, compared to 67% of the mice pretreated

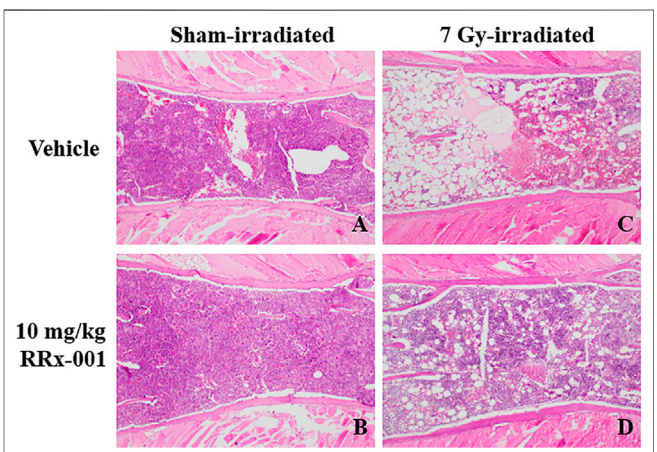

FIGURE 4 | Photomicrographs of H&E stained thin sections of bone marrow sterna showing representative bone marrow cellularity in all groups on day 14. Panels **(A)** and **(B)**: Bone marrow sterna pretreated with either vehicle or 10 mg/kg RRx-001 on day 14 after sham-irradiation. Panel **(C)**: Vehicle-treated sternal bone marrow 14 days after sublethal irradiation illustrated severe hypocellularity as evident by marrow space demonstrating only residual stromal fat (visualized as increased marrow white space). Panel **(D)**: RRx-001-treated sternal bone marrow 14 days after sublethal irradiation showed significantly increased cellularity as seen by the increased amounts of cells stained purple and decrease in the visualized stromal adipose tissue (white space) (×100 magnification).

with RRx-001 (**Figure 1**). RRx-001 extended the median survival time by at least 14 days over the median survival time for vehicle-treated mice. We chose to use the IP method of drug administration to maintain consistency with the previous findings, however similar results were seen when mice were administered RRx-001 by IV injection 24 h prior to radiation (**Supplementary Figure S1**). This demonstrates that RRx-001 efficacy is not dependent on route of administration. Moreover, in the sublethally irradiated CD2F1 mice, RRx-001 reduced radiation augmented cellular recovery in bone marrow.

The hallmark of the acute radiation syndrome and hematopoietic subsyndrome is pancytopenia and bone marrow failure. A sharp decrease, or complete depletion of bone marrow cells is likely to cause death due to severe immunosuppression (Hall and Giaccia, 2012). To determine the underlying RRx-001-mediated mechanism of protection against H-ARS, mice were sublethally irradiated and humanely sacrificed at various time points to collect blood and bone marrow. In both the vehicle- and RRx-001-treated irradiated groups, myelosuppression was observed, along with severe reticulocytopenia and leukopenia up until day 14. However, significantly higher levels of leukocytes, reticulocytes and platelets on day 14 were seen in the irradiated RRx-001-treated group as compared to the irradiated vehicle control. In addition, the level of neutrophils in RRx-001 treated mice were significantly higher on both days 7 and 14 compared to the vehicle control (**Table 1**). Increased bone marrow cellularity was observed on day 14 post-irradiation in the RRx-001 treatment group compared to the vehicle control (**Figures 3**, **4**). In addition, improvement in bone marrow hematopoietic progenitor cell recovery was observed in RRx-001 treated irradiated mice, compared to vehicle treated irradiated mice by day 21 (**Supplementary Figure S2**). Collectively, these results suggest that the cellular protection mechanism of RRx-001 involves accelerated hematopoietic regeneration or mobilization of leukocytes, reticulocytes and platelets, which prevented or delayed mortality from infection and sepsis. Alternatively, and/or in addition to accelerated myeloreconstitution, RRx-001 may have protected hematopoietic stem and progenitor cells.

In previous studies, RRx-001 has shown the ability to increase reactive oxygen and nitrogen species (RONS) (Ning et al., 2012) and activate compensatory responses that enable the cells and tissues to better withstand the deleterious effects of subsequent exposure to higher levels of RONS (Cabrales et al., 2017). The major difference between RRx-001 and other potential redox-active radioprotectors is that RRx-001 has demonstrated minimal toxicity and systemic deliverability (Reid et al., 2015) as well as evidence of anti-cancer activity and potential radiochemoprotection in multiple tumor types such as small-cell lung carcinoma and melanoma brain metastases (Carter et al., 2016) (Kim et al., 2016). Pretreatment paradigms with low-level oxidative stressors have been previously and extensively described in cell-survival studies from yeast, mammalian and human cells *in vitro*, as well as in animal models *in vivo* (Wolff et al., 1988). RRx-001 appears to increase DNA repair activity through activation of the nuclear factor erythroid 2-related factor (Nrf2) transcription factor, which regulates antioxidant response element (ARE) genes (Ning et al., 2015). RRx-001 may also modulate the activation of p53 (Das et al., 2016), thereby altering the response of cells to DNA damage and potentially reducing apoptosis and/or senescence. The increase in ARE via Nrf2 activation (Ning et al., 2015) provides an intriguing mechanism of action for radioprotection. In support of this, preliminary *in vitro* studies from our lab provided evidence RRx-001 treatment increased heme oxygenase-1 (HO-1), an Nrf2 activated antioxidant response element, protein expression in mesenchymal stem cells, monocytes, and macrophages (data not shown). Work by Hedblom et al., confirmed that HO-1 functions to prevent DNA damage, reduce senescence, improve proliferation, and modulate cytokine expression in macrophages (Hedblom et al., 2019). Additional reports, including one from an HO-1 deficient patient, highlight the role of HO-1 in cellular protection against inflammation and oxidative stress (Yachie et al., 1999).

Recombinant G-CSF is utilized in the clinic to attenuate chemotherapeutic-induced toxicity, and is one of three FDA approved medical countermeasures for ARS. However, in contrast to regulated administration of G-CSF, low level endogenous G-CSF expression is typical in healthy individuals and mice, and G-CSF elevation in serum is correlated with inflammation, infection, and tissue damage, and accompanies additional inflammatory stimuli such as interleukin (IL)–1β, and tumor necrosis factor-alpha. G-CSF levels subsequently decline with recovery [reviewed in (Theron et al., 2020)]. Increased circulating G-CSF in response to radiation exposure was previously demonstrated and was not dose rate dependent (Kiang et al., 2018), or radiation quality dependent (Ossetrova et al., 2018). We saw modulation of serum G-CSF in irradiated RRx-001 treated mice (**Supplementary Figure S3**). Based on our data, RRx-001 may reduce inflammation and tissue damage. Further studies testing the circulating levels of IL-1β, IL-6 or other pro-inflammatory cytokines would support our finding. Taken together, it appears that RRx-001 treatment reduced inflammation, accelerated bone marrow recovery, and aided in immune health recovery after radiation. Most of the effects thought to promote survival occurred at or beyond day 14. Further kinetic studies would be important to optimize dosing of RRx-001 for radioprotection. Careful scientific design might allow the investigation of the relevance of RRx-001 mediated upregulation of HO-1 expression in radioprotection in our model.

Amifostine was initially developed by the United States Army as part of their nuclear warfare program (Wasserman and Brizel, 2001; Koukourakis, 2002). Animal experiments demonstrated radioprotective effects to the skin, mucosa, hair follicles, intestinal wall, and salivary glands (Koukourakis, 2002) and subsequently lead to its use in randomized control trials. Several trials demonstrated that amifostine reduced acute and chronic xerostomia in head and neck cancer patients treated with chemoradiation (Brizel et al., 2000; Veerasarn et al., 2006; Gu et al., 2014). However, due to amifostine's unacceptable adverse effect profile at therapeutic doses, it is not often used clinically. The second drug, palifermin, is a modified version of keratinocyte growth factor (KGF) (Wasserman and Brizel, 2001; Johnke et al.,

2014) that is approved to reduce oral mucositis. In 2015, G-CSF was the first FDA approved countermeasure for the management of H-ARS under the FDA Animal Rule. This rule is intended to facilitate the development of new drugs and biologic products as medical countermeasures for chemical, biological, radiological, and nuclear threats when human efficacy studies cannot be ethically conducted (Food and Drug Administration, 2002; Farese and MacVittie, 2015). G-CSF increased production, effector differentiation, and early release of neutrophils, thereby reducing the duration of severe neutropenia, and minimizing the risk of bacteremia and sepsis (Mehta et al., 2015). G-CSF has been shown to increase survival in non-human primates who were exposed to lethal (myelosuppressive) doses of radiation within the H-ARS model (Farese et al., 2013; Farese et al., 2014). PegG-CSF is a modified, pegylated form of G-CSF with an increased plasma half-life, allowing for less frequent dosing than G-CSF. PegG-CSF has also been shown to improve survival in non-human primates after exposure to lethal doses of radiation (Hankey et al., 2015). The most recent FDA approved countermeasure for H-ARS is GM-CSF (Singh and Seed, 2018).

Even though there has been an overwhelming amount of data available to substantiate the efficacy of these FDA approved radioprotectors and radiomitigators, each has their own limitations and scope of use. The major limitation of amifostine is its serious adverse side effect profile, which results in high rates of discontinuation when given in conjunction with head and neck radiotherapy (Rades et al., 2004). In contrast, palifermin, has been shown to have a well-tolerated toxicity profile; however, its major limitation is its narrow scope of use, which is restricted to the improvement of oral mucositis as demonstrated by a randomized control trial in patients who received total body irradiation as part of a conditioning regimen prior to stem cell transplant (Spielberger et al., 2004). In addition, palifermin is also administered intravenously for three consecutive days making it an unlikely candidate for emergency use. Although G-CSF, pegG-CSF and GM-CSF have been shown to be effective in multiple animal models of H-ARS, they are radiomitigators and would therefore not provide protection for military and first responders in the event of nuclear and radiological emergencies, as well as astronauts before incoming bursts of increased cosmic radiation. In addition, studies have shown that prolonged use can affect long-term recovery from hematopoietic syndrome by promoting hematopoietic stem cell (HSC) proliferation and differentiation leading to HSC exhaustion, partly from promoting HSC senescence and may also may exacerbate radiation induced long-term bone marrow injury (Li et al., 2015).

In conclusion, the increasing potential of terrorists with dirty bombs, nuclear power plant accidents, rogue states with nuclear weapons and long-range delivery systems, as well as the exciting possibility of deep space travel, all continue to present a significant risk of dangerous radiation exposure. Therefore, effective radioprotection is a clear unmet need that RRx-001, as a possible dual-purpose agent with applications in clinical oncology, radiation accidents, nuclear weapons incidents, terrorism, space travel, and radiation site cleanup, has the potential to address. As this study is a proof-of-concept, it is limited by the selection of one 10 mg/kg dose of RRx-001, one time point of 24 h prior to TBI, and IP injection, which would not be the intended human route of administration. Dose, time and route of administration optimization studies in the small animal model, as well as future studies in additional animal models, combined with mechanistic studies in appropriate *in vitro* models are required to support RRx-001 as a medical countermeasure candidate.

DATA AVAILABLITY STATEMENT

The raw data supporting the conclusion of this article will be made available by the authors, without undue reservation.

ETHICS STATEMENT

The animal study was reviewed and approved by the Armed Forces Radiobiology Research Institute's Institutional Animal Care and Use Committee.

AUTHOR CONTRIBUTIONS

KJ, WS, and LC carried out the experiments. KJ, WS, LC, and RL contributed to experimental design. KJ, LC, RL, NA, WC, and TS contributed to data analysis. NA and RL performed the statistical analyses. WC and TS performed the histopathology and contributed to writing that section of the manuscript. KJ, BO, and AG wrote the first draft of the manuscript. All authors contributed to manuscript revision, read, and approved the submitted version.

FUNDING

This project was supported by the Armed Forces Radiobiology Research Institute Intramural Fund (Grant RBB934361). RL received support from grant R21 CA184756 awarded by NIH/NCI and grant 1P20GM109005-01A1 awarded by NIGMS/NIH.

ACKNOWLEDGMENTS

The authors would like to thank Melissa Alvarez, Dylan Dunn and HMI Thong Nguyen for their assistance and support. The authors would also like to thank Dr Sanchita Ghosh for her guidance in the DRF study design and Dr Gregory Holmes-Hampton for his guidance on survival studies.

SUPPLEMENTARY MATERIAL

The Supplementary Material for this article can be found online at: https://www.frontiersin.org/articles/10.3389/fphar.2021.676396/full#supplementary-material.

REFERENCES

Brizel, D. M., Wasserman, T. H., Henke, M., Strnad, V., Rudat, V., Monnier, A., et al. (2000). Phase III Randomized Trial of Amifostine as a Radioprotector in Head and Neck Cancer. *J. Clin. Oncol.* 18, 3339–3345. doi:10.1200/jco.2000.18.19.3339

Cabrales, P., Caroen, S., Oronsky, A., Carter, C., Trepel, J., Summers, T., et al. (2017). The Macrophage Stimulating Anti-cancer Agent, RRx-001, Protects against Ischemia-Reperfusion Injury. *Expert Rev. Hematol.* 10, 575–582. doi:10.1080/17474086.2017.1324779

Cabrales, P. (2019). RRx-001 Acts as a Dual Small Molecule Checkpoint Inhibitor by Downregulating CD47 on *Cancer* Cells and SIRP-α on Monocytes/Macrophages. *Transl. Oncol.* 12, 626–632. doi:10.1016/j.tranon.2018.12.001

Carter, C. A., Oronsky, B. T., Caroen, S. Z., Scicinski, J. J., Degesys, A., Kim, M. M., et al. (2016). RRx-001 in Refractory Small-Cell Lung Carcinoma: A Case Report of a Partial Response after a Third Reintroduction of Platinum Doublets. *Case Rep. Oncol.* 9, 171–176. doi:10.1159/000444631

CDC (2010). CDC Grand Rounds: Radiological and Nuclear Preparedness. *MMWR Morb. Mortal Wkly. Rep.* 59, 1178–1181.

Das, D. S., Ray, A., Das, A., Song, Y., Tian, Z., Oronsky, B., et al. (2016). A Novel Hypoxia-Selective Epigenetic Agent RRx-001 Triggers Apoptosis and Overcomes Drug Resistance in Multiple Myeloma Cells. *Leukemia* 30, 2187–2197. doi:10.1038/leu.2016.96

Farese, A. M., Brown, C. R., Smith, C. P., Gibbs, A. M., Katz, B. P., Johnson, C. S., et al. (2014). The Ability of Filgrastim to Mitigate Mortality Following LD50/60 Total-Body Irradiation Is Administration Time-dependent. *Health Phys.* 106, 39–47. doi:10.1097/hp.0b013e3182a4dd2c

Farese, A. M., Cohen, M. V., Katz, B. P., Smith, C. P., Gibbs, A., Cohen, D. M., et al. (2013). Filgrastim Improves Survival in Lethally Irradiated Nonhuman Primates. *Radiat. Res.* 179, 89–100. doi:10.1667/rr3049.1

Farese, A. M., and Macvittie, T. J. (2015). Filgrastim for the Treatment of Hematopoietic Acute Radiation Syndrome. *Drugs Today* 51, 537–548. doi:10.1358/dot.2015.51.9.2386730

Food and Drug Administration (2002). New Drug and Biological Drug Products; Evidence Needed to Demonstrate Effectiveness of New Drugs when Human Efficacy Studies Are Not Ethical or Feasible. Final Rule. *Fed. Regist.* 67, 37988–37998.

Ghosh, S. P., Kulkarni, S., Hieber, K., Toles, R., Romanyukha, L., Kao, T.-C., et al. (2009). Gamma-tocotrienol, a Tocol Antioxidant as a Potent Radioprotector. *Int. J. Radiat. Biol.* 85, 598–606. doi:10.1080/09553000902985128

Gu, J., Zhu, S., Li, X., Wu, H., Li, Y., and Hua, F. (2014). Effect of Amifostine in Head and Neck Cancer Patients Treated with Radiotherapy: a Systematic Review and Meta-Analysis Based on Randomized Controlled Trials. *PLoS One* 9, e95968. doi:10.1371/journal.pone.0095968

Hall, E. J., and Giaccia, A. J. (2012). *Radiobiology for the Radiologist*. Philadelphia: Lippincott Williams & Wilkins.

Hankey, K. G., Farese, A. M., Blaauw, E. C., Gibbs, A. M., Smith, C. P., Katz, B. P., et al. (2015). Pegfilgrastim Improves Survival of Lethally Irradiated Nonhuman Primates. *Radiat. Res.* 183, 643–655. doi:10.1667/rr13940.1

Hedblom, A., Hejazi, S. M., Canesin, G., Choudhury, R., Hanafy, K. A., Csizmadia, E., et al. (2019). Heme Detoxification by Heme Oxygenase-1 Reinstates Proliferative and Immune Balances upon Genotoxic Tissue Injury. *Cell Death Dis.* 10, 72. doi:10.1038/s41419-019-1342-6

Johnke, R. M., Sattler, J. A., and Allison, R. R. (2014). Radioprotective Agents for Radiation Therapy: Future Trends. *Future Oncol.* 10, 2345–2357. doi:10.2217/fon.14.175

Kiang, J. G., Smith, J. T., Hegge, S. R., and Ossetrova, N. I. (2018). Circulating Cytokine/Chemokine Concentrations Respond to Ionizing Radiation Doses but Not Radiation Dose Rates: Granulocyte-Colony Stimulating Factor and Interleukin-18. *Radiat. Res.* 189, 634–643. doi:10.1667/rr14966.1

Kim, M. M., Parmar, H., Cao, Y., Knox, S. J., Oronsky, B., Scicinski, J., et al. (2016). Concurrent Whole Brain Radiotherapy and RRx-001 for Melanoma Brain Metastases. *Neuro Oncol.* 18, 455–456. doi:10.1093/neuonc/nov317

Kodell, R. L., Lensing, S. Y., Landes, R. D., Kumar, K. S., and Hauer-Jensen, M. (2010). Determination of Sample Sizes for Demonstrating Efficacy of Radiation Countermeasures. *Biometrics* 66, 239–248. doi:10.1111/j.1541-0420.2009.01236.x

Koukourakis, M. (2002). Amifostine in Clinical Oncology: Current Use and Future Applications. *Anti Cancer Drugs* 13, 181–209. doi:10.1097/00001813-200203000-00001

Kumar, V. P., Biswas, S., Sharma, N. K., Stone, S., Fam, C. M., Cox, G. N., et al. (2018). PEGylated IL-11 (BBT-059): A Novel Radiation Countermeasure for Hematopoietic Acute Radiation Syndrome. *Health Phys.* 115, 65–76. doi:10.1097/hp.0000000000000841

Landes, R. D., Lensing, S. Y., Kodell, R. L., and Hauer-Jensen, M. (2013). Practical Advice on Calculating Confidence Intervals for Radioprotection Effects and Reducing Animal Numbers in Radiation Countermeasure Experiments. *Radiat. Res.* 180, 567–574. doi:10.1667/rr13429.1

Li, C., Lu, L., Zhang, J., Huang, S., Xing, Y., Zhao, M., et al. (2015). Granulocyte Colony-Stimulating Factor Exacerbates Hematopoietic Stem Cell Injury after Irradiation. *Cell Biosci* 5, 65. doi:10.1186/s13578-015-0057-3

Mehta, H. M., Malandra, M., and Corey, S. J. (2015). G-CSF and GM-CSF in Neutropenia. *J.I.* 195, 1341–1349. doi:10.4049/jimmunol.1500861

Nakamura, K., Sasaki, T., Ohga, S., Yoshitake, T., Terashima, K., Asai, K., et al. (2014). Recent Advances in Radiation Oncology: Intensity-Modulated Radiotherapy, a Clinical Perspective. *Int. J. Clin. Oncol.* 19, 564–569. doi:10.1007/s10147-014-0718-y

Ning, S., Bednarski, M., Oronsky, B., Scicinski, J., Saul, G., and Knox, S. J. (2012). Dinitroazetidines Are a Novel Class of Anticancer Agents and Hypoxia-Activated Radiation Sensitizers Developed from Highly Energetic Materials. *Cancer Res.* 72, 2600–2608. doi:10.1158/0008-5472.can-11-2303

Ning, S., Sekar, T. V., Scicinski, J., Oronsky, B., Peehl, D. M., Knox, S. J., et al. (2015). Nrf2 Activity as a Potential Biomarker for the Pan-Epigenetic Anticancer Agent, RRx-001. *Oncotarget* 6, 21547–21556. doi:10.18632/oncotarget.4249

Ossetrova, N. I., Stanton, P., Krasnopolsky, K., Ismail, M., Doreswamy, A., and Hieber, K. P. (2018). Biomarkers for Radiation Biodosimetry and Injury Assessment after Mixed-Field (Neutron and Gamma) Radiation in the Mouse Total-Body Irradiation Model. *Health Phys.* 115, 727–742. doi:10.1097/hp.0000000000000938

Rades, D., Fehlauer, F., Bajrovic, A., Mahlmann, B., Richter, E., and Alberti, W. (2004). Serious Adverse Effects of Amifostine during Radiotherapy in Head and Neck Cancer Patients. *Radiother. Oncol.* 70, 261–264. doi:10.1016/j.radonc.2003.10.005

Reid, T., Oronsky, B., Scicinski, J., Scribner, C. L., Knox, S. J., Ning, S., et al. (2015). Safety and Activity of RRx-001 in Patients with Advanced Cancer: a First-In-Human, Open-Label, Dose-Escalation Phase 1 Study. *Lancet Oncol.* 16, 1133–1142. doi:10.1016/s1470-2045(15)00089-3

Singh, V. K., and Seed, T. M. (2018). An Update on Sargramostim for Treatment of Acute Radiation Syndrome. *Drugs Today* 54, 679–693. doi:10.1358/dot.2018.54.11.2899370

Spielberger, R., Stiff, P., Bensinger, W., Gentile, T., Weisdorf, D., Kewalramani, T., et al. (2004). Palifermin for Oral Mucositis after Intensive Therapy for Hematologic Cancers. *N. Engl. J. Med.* 351, 2590–2598. doi:10.1056/nejmoa040125

Theron, A. J., Steel, H. C., Rapoport, B. L., and Anderson, R. (2020). Contrasting Immunopathogenic and Therapeutic Roles of Granulocyte Colony-Stimulating Factor in Cancer, *Pharmaceuticals* 13(11):406. doi:10.3390/ph13110406

Veerasarn, V., Phromratanapongse, P., Suntornpong, N., Lorvidhaya, V., Sukthomya, V., Chitapanarux, I., et al. (2006). Effect of Amifostine to Prevent Radiotherapy-Induced Acute and Late Toxicity in Head and Neck Cancer Patients Who Had Normal or Mild Impaired Salivary Gland Function. *J. Med. Assoc. Thai* 89, 2056–2067.

Wasserman, T. H., and Brizel, D. M. (2001). The Role of Amifostine as a Radioprotector. *Oncology* 15, 1349–1360.

Wolff, S., Afzal, V., Wiencke, J. K., Olivieri, G., and Michaeli, A. (1988). Human Lymphocytes Exposed to Low Doses of Ionizing Radiations Become Refractory to High Doses of Radiation as Well as to Chemical Mutagens that Induce Double-Strand Breaks in DNA. *Int. J. Radiat. Biol.* 53, 39–48. doi:10.1080/09553008814550401

Yachie, A., Niida, Y., Wada, T., Igarashi, N., Kaneda, H., Toma, T., et al. (1999). Oxidative Stress Causes Enhanced Endothelial Cell Injury in Human Heme Oxygenase-1 Deficiency. *J. Clin. Invest.* 103, 129–135. doi:10.1172/jci4165

Oronsky, B., Reid, T. R., Larson, C., Carter, C. A., Brzezniak, C. E., Oronsky, A., and Cabrales, P. (2017). RRx-001 protects against cisplatin-induced toxicities. *J. Cancer Res. Clin. Oncol.* 143(9), 1671. doi:10.1007/s00432-017-2416-4

Conflict of Interest: BO and NA are employed by the company of EpicentRx.

The remaining authors declare that the research was conducted in the absence of any commercial or financial relationships that could be construed as a potential conflict of interest.

frontiers in Pharmacology

ORIGINAL RESEARCH
published: 26 April 2021
doi: 10.3389/fphar.2021.633131

Novel Murine Biomarkers of Radiation Exposure Using An Aptamer-Based Proteomic Technology

*Mary Sproull, Uma Shankavaram and Kevin Camphausen**

Radiation Oncology Branch, National Cancer Institute, Bethesda, MD, United States

Purpose: There is a need to identify new biomarkers of radiation exposure both for use in the development of biodosimetry blood diagnostics for radiation exposure and for clinical use as markers of radiation injury. In the current study, a novel high-throughput proteomics screening approach was used to identify proteomic markers of radiation exposure in the plasma of total body irradiated mice. A subset panel of significantly altered proteins was selected to build predictive models of radiation exposure and received radiation dose useful for population screening in a future radiological or nuclear event.

Methods: Female C57BL6 Mice of 8–14 weeks of age received a single total body irradiation (TBI) dose of 2, 3.5, 8 Gy or sham radiation and plasma was collected by cardiac puncture at days 1, 3, and 7 post-exposure. Plasma was then screened using the aptamer-based SOMAscan proteomic assay technology, for changes in expression of 1,310 protein analytes. A subset panel of protein biomarkers which demonstrated significant changes ($p < 0.05$) in expression following radiation exposure were used to build predictive models of radiation exposure and radiation dose.

Results: Detectable values were obtained for all 1,310 proteins included in the SOMAscan assay. For the Control vs. Radiation model, the top predictive proteins were immunoglobulin heavy constant mu (IGHM), mitogen-activated protein kinase 14 (MAPK14), ectodysplasin A2 receptor (EDA2R) and solute carrier family 25 member 18 (SLC25A18). For the Control vs. Dose model, the top predictive proteins were cyclin dependent kinase 2/cyclin A2 (CDK2. CCNA2), E-selectin (SELE), BCL2 associated agonist of cell death (BAD) and SLC25A18. Following model validation with a training set of samples, both models tested with a new sample cohort had overall predictive accuracies of 85% and 73% for the Control vs. Radiation and Control vs. Dose models respectively.

Conclusion: The SOMAscan proteomics platform is a useful screening tool to evaluate changes in biomarker expression. In our study we were able to identify a novel panel of radiation responsive proteins useful for predicting whether an animal had received a radiation exposure and to what dose they had received. Such diagnostic tools are needed for future medical management of radiation exposures.

Keywords: biomarker, somascan, biodosimetry, radiation, medical countermeasure

OPEN ACCESS

Edited by:
Lynnette H. Cary, Uniformed Services University of the Health Sciences, United States

Reviewed by:
Lakshman Singh, The University of Melbourne, Australia
Antonella Bertucci, Loma Linda University, United States

****Correspondence:***
Kevin Camphausen
camphauk@mail.nih.gov

Specialty section:
This article was submitted to Translational Pharmacology, a section of the journal Frontiers in Pharmacology

Received: *24 November 2020*
Accepted: *12 April 2021*
Published: *26 April 2021*

Citation:
Sproull M, Shankavaram U and Camphausen K (2021) Novel Murine Biomarkers of Radiation Exposure Using An Aptamer-Based Proteomic Technology. Front. Pharmacol. 12:633131. doi: 10.3389/fphar.2021.633131

INTRODUCTION

Mass casualty medical management of potential radiological or nuclear events primarily require diagnostics to effectively identify individuals who have received a radiation exposure. Many promising approaches are currently under development including point-of-care and high-throughput off-site approaches (Garty et al., 2016; Balog et al., 2020; Jacobs et al., 2020). These diagnostics are based on physiological biomarkers of radiation injury found primarily in the blood and include a wide array of molecules at the genomic, proteomic, metabolomic, and transcriptomic level. In addition, some methodologies for characterizing radiation exposure utilize cytogenetic markers, lymphocyte depletion kinetics and electron paramagnetic resonance (EPR). Cumulatively, this variety of biomarker classes represent the complex physiologic interaction of biological mechanisms involved in ionizing radiation injury (Sproull and Camphausen, 2016). At the proteomic level several key biomarkers of radiation exposure have been established in mammalian models of radiation exposure and include Flt3 ligand (FL), a marker of hematopoietic stem cell recovery, acute phase response proteins c-reactive protein (CRP) and serum amyloid A (SAA) and other markers such as salivary alpha amylase (AMY1) and monocyte chemotactic protein 1 (MCP1) (Ossetrova et al., 2011; Sproull et al., 2017; Balog et al., 2019).

Characterization of proteomic biomarkers of radiation exposure and novel proteomic biomarkers of other disease states have previously been done using singleplex ELISA assay or using multiplex immunoassay approaches including reverse phase protein arrays (RPPAs), bead-based assays or electrochemiluminescent-antibody based technologies (Sproull et al., 2013; Boellner and Becker, 2015; Sproull et al., 2015; Himburg et al., 2016; Blakely et al., 2018; Kuang et al., 2018). Multiplex approaches have clear benefits in exploratory studies for biomarker discovery in terms of cost and efficiency as they maximize target screening using less sample volume. To date, the best of these various multiplex platforms could offer was target screening at the level of a few hundred proteomic targets. In the current study, we sought to take advantage of emerging high-throughput technologies which examine changes in the mammalian proteome through high level multiplex approaches. With access to a larger array of protein targets, changes in the mammalian proteome due to radiation injury can be better characterized. Using the innovative aptamer-based SOMA-scan proteomic assay technology, plasma from C57BL6 mice was screened for changes in expression of 1,310 protein analytes following a total body radiation exposure of 2, 3.5 or 8 Gy. A subset panel of proteins which demonstrated significant changes in expression following radiation exposure was selected to build predictive models of radiation exposure. In mass casualty medical management of events involving radiation exposure, screening to identify those individuals who have received a radiation exposure is a key element (Sullivan et al., 2013). Yet, different predictive diagnostics of radiation exposure may be needed at different levels of triage. To address this need, we created two predictive models of radiation exposure. Firstly, a "Control vs. Radiation" model was developed to predict whether an individual had received a radiation exposure and needed further triage or had not received a radiation exposure and could be sent home. We also developed a "Control vs. Dose" model to predict how great a radiation dose an individual had received which is useful for guiding subsequent medical management decisions.

For this study, model building and validation were completed with two separate sample sets to independently test the strength of the respective models. This study identifies both novel proteomic biomarkers of radiation exposure and two useful predictive models of radiation exposure using the Somalogic SOMAscan platform.

METHODS

Animal Model

For the murine model used in this study, 8–14 week old female C57BL6 mice received a single total body irradiation (TBI) dose of 2, 3.5, 8 Gy or sham radiation. All mice receiving TBI were confined using a standard pie jig preventing movement. All animal studies were conducted in accordance with the principles and procedures outlined in the NIH Guide for the Care and Use of Animals and procedures were approved by the NIH Lab Animal Safety Program under an approved protocol. Plasma was collected by cardiac puncture using a heparinized syringe at days 1, 3, and 7 post-irradiation in Lithium Heparin blood collection tubes (BD Biosciences). Mice received 2.5–5.5% Isoflurane anesthesia during cardiac puncture for blood collection. Plasma was spun at 10,000 RCF for 10 min at 4°C and all samples were stored at −80°C.

Dosimetry

For the murine *in vivo* model utilized in this study, a Pantak X-ray source was used at a dose rate of 2.28 Gy/min. Dose rate was calibrated based upon the procedures described in American Association of Physicist in Medicine (AAPM) Task Group Report 61 (TG-61) with regard to the following conditions: X-ray tube potential was 300 kV, half value layer (HVL) is 0.8 mm Copper (Cu), source to surface distance (SSD) was 50 cm. Dose rate was measured at 2 cm depth in solid water phantom using a PTW model: N23342 ion chamber and Inovision, model 35040 electrometer.

SomaLogic SOMAscan Assay

Approximately 150 ul of plasma per sample was used for the Somalogic SOMAscan Assay which uses a novel protein-capture aptamer-based technology (Rohloff et al., 2014). For this study the SOMAscan HTS Assay 1.3 K was used and processed through the Center for Human Immunology at the National Institutes of Health. The assay included measurement of 1,310 protein analytes.

Statistical Analysis

In brief, data was received in the form of Relative Fluorescent Units (RFU) for each of the 1,310 proteins in the SOMAscan

assay after normalizing for intraplate and interplate variation. These RFU scores for each protein were log2 and z-score transformed. Statistical data analysis was performed using R (Team, 2015). In this study, we investigated the effect of feature selection and prediction algorithm on the performance of prediction method thoroughly. We considered the following feature selection and prediction methods implemented sequentially: differential expression analysis, random forest, regularized regression analysis, and linear discriminant analysis (**Supplementary Figure S1**). For these methods, we studied the effects of feature selection and the number of features on prediction.

Differential expression analysis: To remove invariant data from the analysis, we first performed *t*-test or ANOVA analysis depending on whether there two groups (Control vs. RT) or multiple groups (Control vs. Dose) respectively. Significance test with ($p \leq 0.05$) were selected for further analysis.

Feature selection: Random Forest (RF) is a classification algorithm using sets of random decision trees which are generated by a bootstrap sampling for decision and voting (Breiman, 2001; Banfield et al., 2007). We implemented Boruta algorithm which is a wrapper built around random forest. Boruta is a feature selection algorithm and feature ranking based on the RF algorithm. Boruta's benefits are to decide the significance of a variable and to assist the statistical selection of important variables. Besides, we can manage the strictness of the algorithm by adjusting the *p*-value that defaults to 0.01. This method allowed us to capture all the important and interesting features with respect to the outcome variable (either RT model or Dose model).

Elastic-Net Analysis

It is evident that good classification and prediction requires good predictors. Elastic-net regularization uses ridge and LASSO penalties simultaneously to take advantages of both regularization methods (Zou and Hastie, 2005). Elastic-net provides shrinkage and automatic variable selection. Since Elastic-net feature selection is the result of random permutations, we tend to get slightly different set of features with each iteration. Since our main goal is to find stable set of features for wider application, we implemented 20 iterations of elastic-net computations resulting in 20 independent models. We then ranked the features by how often each feature is present in maximum number of models and selected top ranked four features.

Linear Discriminant Analysis

Linear discriminant analysis (LDA) is used to find linear combinations of features which characterize or discriminate two or more classes. LDA is simple and fast. LDA was used for the purpose of final feature selection and classification. A permutation test evaluated whether the specific classification of the individuals between groups is significantly better than random classification in any two arbitrary groups (Bylesjö et al., 2006). Finally, we performed model performance evaluation with the new data for prediction accuracy. The significance of each model and importance of each feature in the model is further tested by multivariate and univariate anova tests for both training and testing models. The results were shown as heatmap and PCA plots.

RESULTS

Multivariate Model Generation

In the current study, we sought to take advantage of an emerging technology, the Somalogic SOMAscan assay, to identify novel biomarkers of radiation exposure using a multiplex-analysis approach and use these findings to build radiation exposure and dose prediction models. The radiation exposure model (Control vs. RT) was designed to differentiate only between exposed and unexposed animals with the exposed animals receiving a TBI dose between 2 and 8 Gy. The dose prediction model (Control vs. Dose) was designed to both differentiate between exposed and unexposed and between the exposed by dose (2, 3.5, and 8 Gy). To this end, values for all 1,310 SOMAmer targets were obtained for each control and radiation treated sample. SOMAmer targets which demonstrated significant changes in expression following radiation exposure were selected using an ANOVA test ($p < 0.05$) and then filtered by rank using a Random Forest analysis. From this subset of proteins, the top four ranked proteins were selected for each model. For the Control vs. Radiation (RT) model, the top predictive proteins were immunoglobulin heavy constant mu (IGHM), mitogen-activated protein kinase 14 (MAPK14), ectodysplasin A2 receptor (EDA2R) and solute carrier family 25 member 18 (SLC25A18). For the Control vs. Dose model, the top predictive proteins were cyclin dependent kinase 2/cyclin A2 (CDK2. CCNA2), E-selectin (SELE), BCL2 associated agonist of cell death (BAD) and SLC25A18. For each model, a training set of samples was used to generate the model and determine its predictive accuracy and a subsequent set of test samples was later collected and used to validate each model.

Multivariate Control vs. RT Prediction Model

The Control vs. RT prediction model was structured using SOMAmer data for IGHM, MAPK14, EDA2R, and SLC25A18. Samples included un-irradiated controls and samples from TBI C57BL6 mice receiving either 2, 3.5, or 8 Gy collected at days 1, 3 or 7 post-exposure. Samples were pooled into control and irradiated (RT) groups. Heatmap clustering of the training set of samples showed good congruency for the Control vs. RT samples (**Figure 1A**). Principle component analysis (PCA) of the sample grouping also showed good separation of the Control vs. RT samples for the training model (**Figure 1B**). Analysis of the new test set of samples used to validate the model showed less precise clustering of the Control vs. RT samples as compared to the training set. As shown in **Figure 2A** heatmap clustering of Control vs. RT samples was less congruent with some overlap between control and irradiated samples. Similarly, in **Figure 2B**, sample clustering using PCA showed less separation between the control and irradiated groups as compared to the training sample set. Illustration of the individual expression patterns for

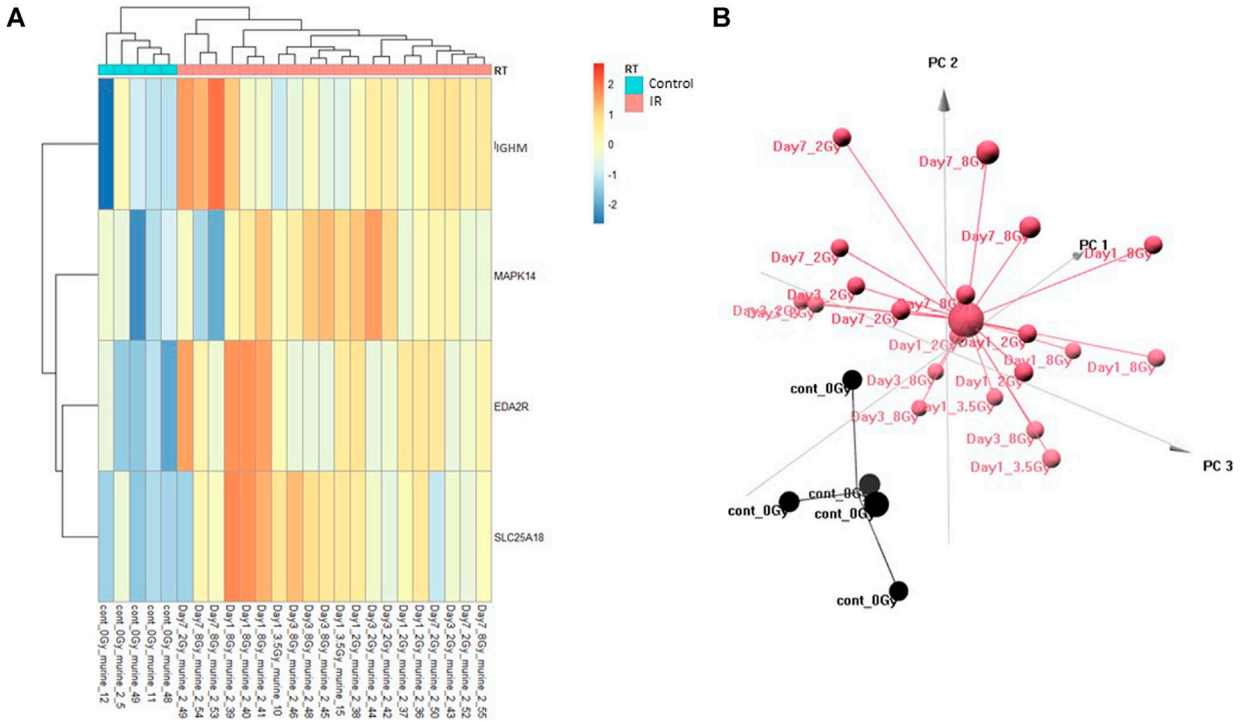

FIGURE 1 | Control vs. RT Training Model. Analysis of proteomic expression within the sample cohort used for model building of the Control vs. RT Training model using top selected proteins IGHM, MAPK14, EDA2R and SL25A18. Findings are represented by **(A)** heatmap and **(B)** PCA.

each of the proteins used in the model are shown for both the training model samples and test model samples in **Figure 3**. Significant changes in the expression patterns for IGHM, EDA2R, MAPK14, and SLC25A18 was seen in the training model samples as measured by Students t-test ($p < 0.01$), but only for EDA2R, MAPK14, and SLC25A18 in the test model samples ($p < 0.05$) as shown in **Figures 3A,B** respectively. Other than the difference in IGHM expression between the training and test model samples, all the proteins for this model showed similar trends in expression between the two sample sets.

Multivariate Control vs. Dose Prediction Model

The Control vs. Dose prediction model was structured using SOMAmer data for CDK2/CCNA2, SELE, BAD and SLC25A18. Samples included un-irradiated controls and samples from TBI C57BL6 mice receiving either 2, 3.5 or 8 Gy collected at days 1, 3 or seven post-exposure. Sample groups were determined by each dose. Heatmap clustering of the training set of samples was generally consistent yet there was some overlap between the samples as shown in **Figure 4A**. Similarly, PCA showed reasonable clustering within groups but some overlap between exposure groups (**Figure 4B**). Analysis of the new test set of samples used to validate the model showed a similar level of overlap between groups with the tightest clustering for the 8 Gy Day 1 samples (**Figure 5A**). PCA additionally showed some overlap between sample groups (**Figure 5B**). Illustration of the individual expression patterns for each of the proteins used in the model are shown for both the training model samples and test model samples in **Figure 6**. Significant changes in the expression patterns for SELE, SLC25A18, CDK2/CCNA2, and BAD was seen in the training model samples by Students t-test ($p < 0.05$), but only for SELE, SLC25A18 and CDK2/CCNA2 in the test model samples as shown in **Figures 6A,B** respectively. Comparison of respective expression trends in the Control vs. Dose model showed more variation between the training and test model sample sets than was seen in the Control vs. RT model. This is to be expected as these samples, when separated by individual dose, result in a much smaller N for each group.

Model Variance and Predictive Accuracy

Following analysis of the expression patterns of the respective proteins within the sample cohorts used to construct and test each model, we wished to test the overall strength of each model. For both the Control vs. RT and Control vs. Dose prediction models, algorithm development using a linear discriminant analysis approach was completed with consideration for dose groups but irrespective of collection time post-exposure. To test the significance of the validation data, both a multivariate (MANOVA) and univariate approach (ANOVA) were used to test whether there were significant differences between the sample groups (**Table 1**). Though the multivariate test demonstrated overall significance between the test groups (control vs. RT or control vs. Dose) it does not tell us for which individual protein comparisons there is a significant observed mean differences.

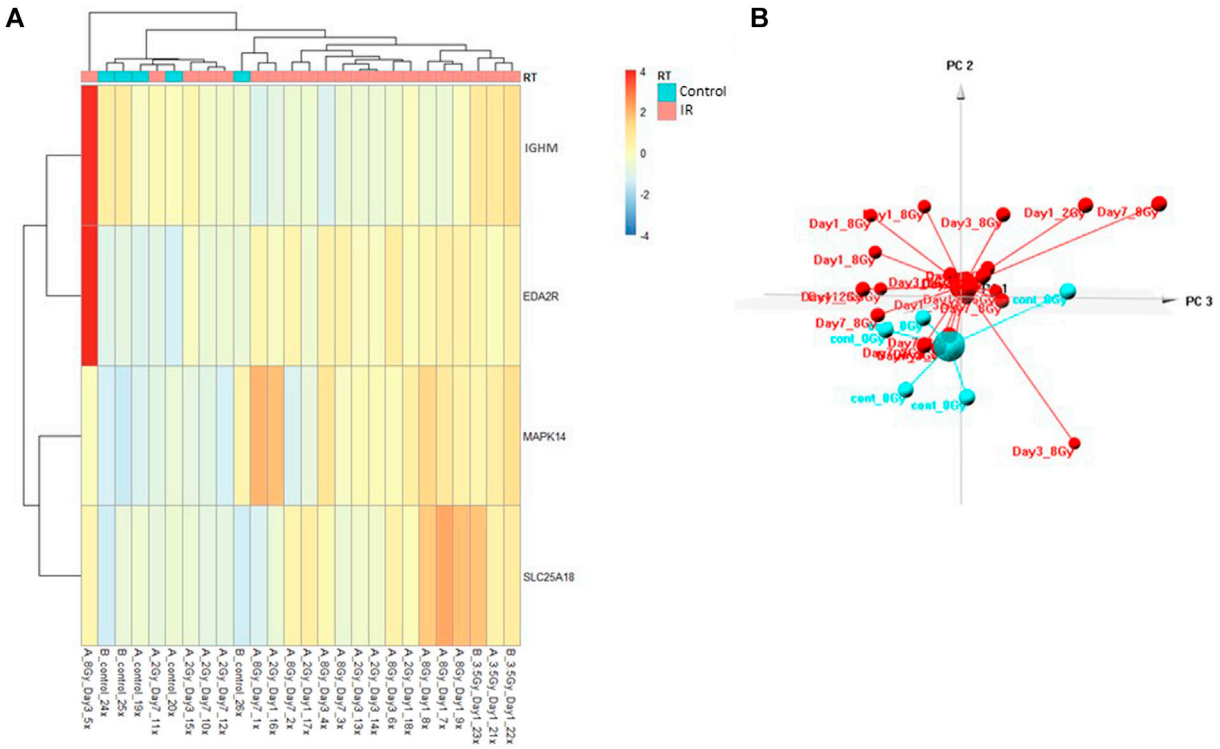

FIGURE 2 | Control vs. RT Test Model. Analysis of proteomic expression within the sample cohort used for testing of the Control vs. RT Test model using top selected proteins IGHM, MAPK14, EDA2R, and SKC25A18. Findings are represented by **(A)** heatmap and **(B)** PCA.

Therefore, a series of univariate ANOVAs were performed to determine the significance of these differences.

As shown in **Table 1**, for the Control vs. RT training model, significance was seen at both the multivariate ($p < 0.001$) and univariate level for all proteins ($p < 0.01$–0.001). The Control vs. RT test model was similarly significant at the multivariate level ($p < 0.01$) and at the univariate level for all the individual proteins ($p < 0.05$) excepting IGHM. For the Control vs. Dose training model, significant differences were seen between test groups both at the multivariate level ($p < 0.001$) and at the univariate level for all proteins ($p < 0.05$–0.001). The Control vs. Dose test model was similarly significant at the multivariate level ($p < 0.001$) and at the univariate level for all the individual proteins ($p < 0.05$) excepting BAD.

Predictive accuracy was determined for each respective model (**Table 2**). The Control vs. RT model had a 100% overall predictive accuracy for the training model but only 85% for the test model. The Control vs. Dose model had a 96% overall predictive accuracy for the training model and 73% for the test model. In both models the predictive accuracy decreased when the training model was tested with fresh samples. Predictive accuracies for each individual sample set demonstrate the dose groups where the model was less successful at dose prediction with only 50% predictive accuracy for the 2 Gy group in the Control vs. Dose training model and 33% predictive accuracy for the control group in the Control vs. Dose test model. These results demonstrate the relative strength of the respective models to identify which animals have received a radiation exposure and which radiation dose they have received.

DISCUSSION

This study presents two novel predictive models of radiation exposure using the high throughput proteomic screening Somalogic SOMAscan platform. Using a relatively small amount (150 ul) of plasma 1,310 proteins were screened for expression changes following a total body irradiation exposure. Using this approach, two predictive models of radiation exposure were built and validated with separate test samples. Both the Control vs. RT and Control vs. Dose models had good overall predictive accuracies of 85% and 73% respectively. Though the predictive accuracies for the tested models were lower than the training models, the additional step of testing each model with independent samples further validates the strength of the respective predictive algorithms. It also demonstrates model stability relative to internal technical variables intrinsic to the Somalogic SOMAscan assay and biological variables inherent to individual animals, as the samples used for the training model and the samples used to subsequently test the model were collected more than a year apart. As we have demonstrated previously, factors which affect successful application of a multivariate dose prediction algorithm include variation in technical and biological variables (Sproull et al., 2019). The

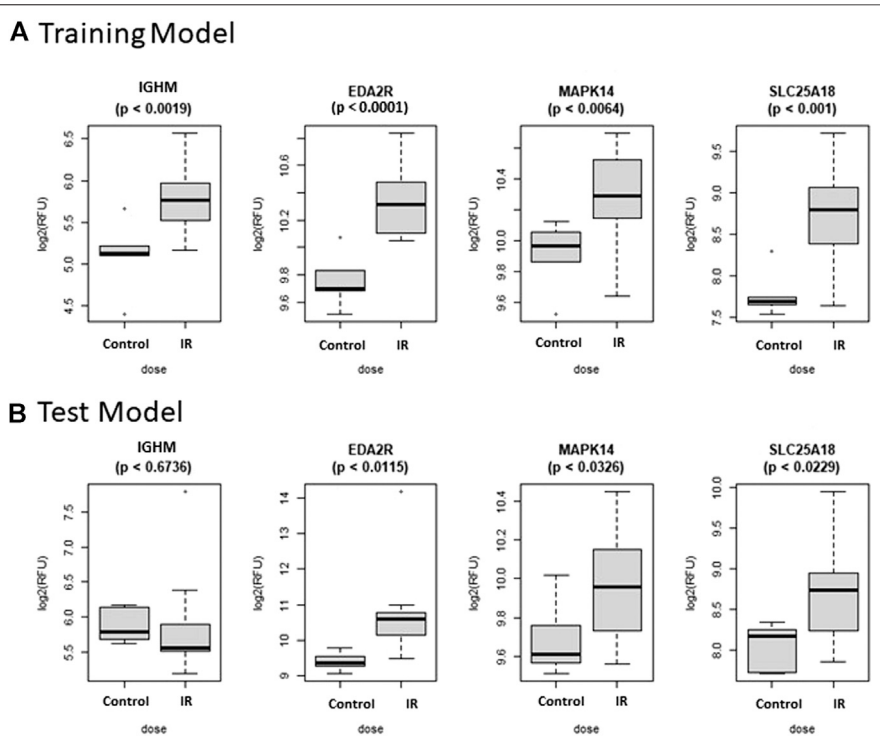

FIGURE 3 | Comparison of Selected Proteins in Control vs. RT Model. Individual biomarker expression profiles for each Control vs. RT Model protein are shown for the sample sets used for both the **(A)** Training and **(B)** Test models.

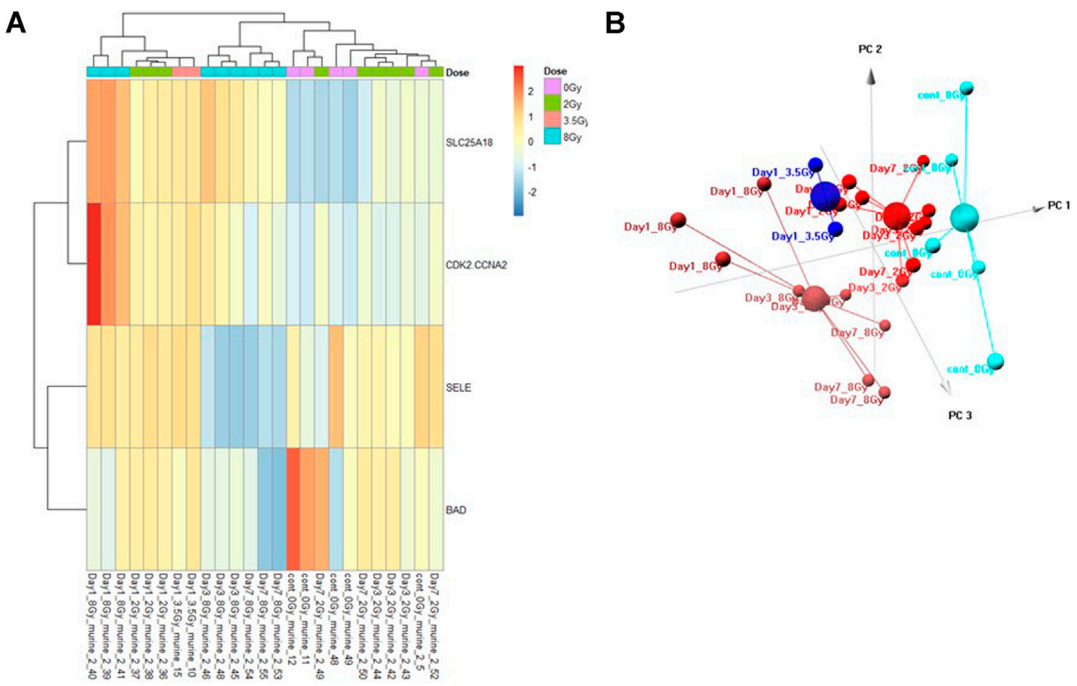

FIGURE 4 | Control vs. Dose Training Model. Analysis of proteomic expression within the sample cohort used for model building of the Control vs. Dose Training model using top selected proteins SL25A18, CDK2/CCNA2, SELE, and BAD. Findings are represented by **(A)** heatmap and **(B)** PCA.

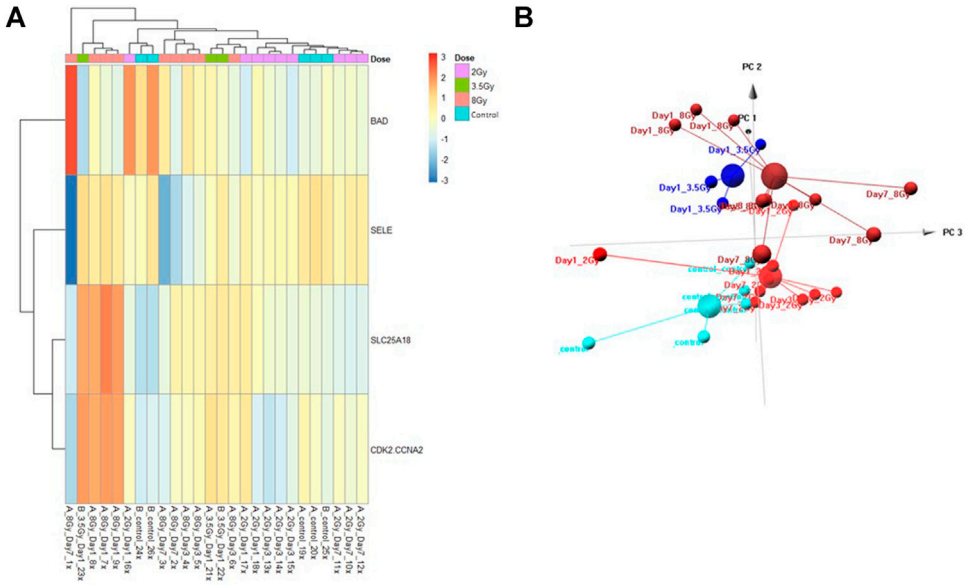

FIGURE 5 | Control vs. Dose Test Model. Analysis of proteomic expression within the sample cohort used for testing of the Control vs. Dose Test model using top selected proteins SL25A18, CDK2/CCNA2, SELE, and BAD. Findings are represented by **(A)** heatmap and **(B)** PCA.

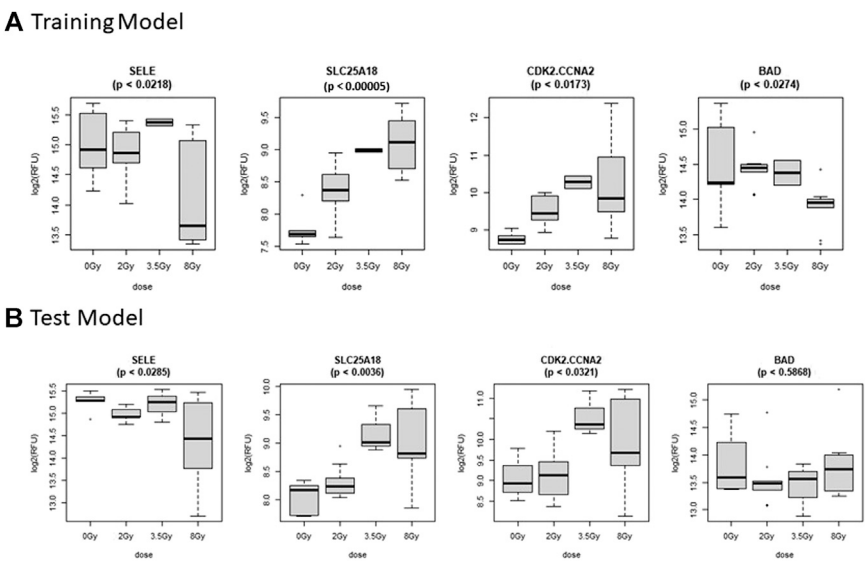

FIGURE 6 | Comparison of Selected Proteins in Control vs. Dose Model. Individual biomarker expression profiles for each Control vs. Dose Model protein are shown for the sample sets used for both the **(A)** Training and **(B)** Test models.

relatively high overall prediction values of the current models demonstrate the strength of the algorithm and stability of the SOMAscan assay.

Although key proteomic biomarkers of radiation injury have been established, much remains unknown regarding the complex interaction of injury related pathways following radiation exposure (DiCarlo et al., 2011). The key proteins chosen for model building in this study were selected based on their relative significance within the data set. Yet, most of the selected biomarkers including EDA2R, IGHM, MAPK14, SLC25A18, BAD, CDK2/CCNA2 are not well established biomarkers of radiation exposure. Though changes at the protein expression level of BAD, and at the gene expression level for EDA2R and IGHM following radiation exposure have been reported, these markers are not well characterized as radiation responsive proteins (Chorna et al., 2005; Himburg et al., 2016; Karim

TABLE 1 | Model Validation Analysis of Variance. Models were validated using both multivariate analysis of variance (MANOVA) and univariate analysis of variance (ANOVA) for both the Control vs. RT and Control vs. Dose training and test models. *p*-values represent the Pr (>F), the *p*-value of the given effect and F statistic.

Analysis of variance model validation					
Control vs. RT training model		*p* value	Control vs. Dose training model		*p* value
Multivariate analysis		3.47*E* – 06	Multivariate analysis		5.30*E* – 08
Univariate analysis			Univariate analysis		
	IGHM	0.002		SELE	0.022
	EDA2R	1.479*E* – 04		SLC25A18	4.81*E* – 05
	MAPK14	0.006		CDK.CCNA2	0.017
	SLC25A18	0.001		BAD	0.027
Control vs. RT test model			Control vs. Dose test model		
Multivariate analysis		0.008	Multivariate analysis		8.76*E* – 07
Univariate analysis			Univariate analysis		
	IGHM	0.674		SELE	0.028
	EDA2R	0.011		SLC25A18	3.60*E* – 03
	MAPK14	0.033		CDK.CCNA2	0.032
	SLC25A18	0.023		BAD	0.587

TABLE 2 | Model Predictive Accuracy. Summary of the predictive accuracy scores for each model using a linear discriminant analysis approach. Both overall predictive accuracy scores and predictive accuracy scores by test group were generated for both Control Vs. RT and Control vs. Dose training and test models.

Predictive accuracy across models					
Control vs. RT training model			Control vs. Dose training model		
Overall predictive accuracy		100%	Overall predictive accuracy		96%
Accuracy by test group			Accuracy by test group		
	Control	100%		0 Gy	100%
	RT	100%		2 Gy	50%
				3.5 Gy	100%
				8 Gy	100%
Control vs. RT test model			Control vs. Dose test model		
Overall predictive accuracy		85%	Overall predictive accuracy		73%
Accuracy by test group			Accuracy by test group		
	Control	81%		0 Gy	33%
	RT	100%		2 Gy	89%
				3.5 Gy	89%
				8 Gy	40%

et al., 2016). CDK2/CCNA2, SLC25A18, and MAPK14 have not been reported to demonstrate changes in expression directly linked to radiation exposure, though these proteins are indirectly related to radiation induced injury as SLC25A18 is involved in energy metabolism and MAPK14 and CDK2/CCNA1 are involved in DNA damage repair (Liang et al., 2013; Maier et al., 2016; Yoo et al., 2020). E-selectin however, has been reported in multiple studies to demonstrate changes in expression following radiation exposure (Hallahan and Virudachalam, 1997; Liu et al., 2012).

Surprisingly we did not find that established protein biomarkers of radiation exposure such as AMY1, FL, and MCP1, or acute phase reactant proteins such as CRP or SAA were among the top significantly changed proteins within the SOMAscan assay (Ossetrova et al., 2011; Sproull et al., 2017; Balog et al., 2020). One confounder in comparing proteomic expression trends across different technologies is the lack of universal homology in capture or binding molecules. While this confounder has the potential to restrict testing and validation within the same technology, it also provides novel opportunities to discover new radiation responsive biomarkers within specific platforms. Advantages to the SOMAscan platform include its automated high-throughput capacity and its large multiplex approach (>1,300 targets) to proteomic analysis using a small sample volume. This multiplex capacity has also recently been increased to 4,500 targets using the same sample volume which will allow for greater characterization of changes within the mammalian proteome. These current data also establish a data cohort of proteomic expression changes relative to total body radiation exposures in C57BL6 mice within the Somalogic SOMAscan platform. This total body irradiation data can be used as a baseline comparison for future screening of other types of radiation exposures including partial body exposures and organ specific exposures which have more practical value for medical management of radiological or nuclear event exposures. This study presents a novel cohort of protein biomarkers with potential predictive value for radiation exposure.

DATA AVAILABILITY STATEMENT

The raw data supporting the conclusions of this article will be made available by the authors, without undue reservation, to any qualified researcher.

ETHICS STATEMENT

The animal study was reviewed and approved by the NIH Lab Animal Safety Program

AUTHOR CONTRIBUTIONS

For this study, MS and KC conceived of the experimental design. MS conducted all animal work and experiments. US conducted all bioinformatic and statistical analyses. All authors contributed to assessment of findings and editing the manuscript.

ACKNOWLEDGMENTS

This research was supported in part by funding from the Radiation and Nuclear Countermeasures Program, #Y2-OD-0332–01 NIAID, by the Intramural Research Program of the National Institutes of Health, National Cancer Institute, #ZIA SC 010373. The authors would also like to thank the Center for Human Immunology at the Clinical Center at the National Institutes of Health and Brian Sellers for their invaluable scientific and technical assistance with the Somalogic SOMAscan platform.

SUPPLEMENTARY MATERIAL

The Supplementary Material for this article can be found online at: https://www.frontiersin.org/articles/10.3389/fphar.2021.633131/full#supplementary-material.

REFERENCES

Balog, R. P., Bacher, R., Chang, P., Greenstein, M., Jammalamadaka, S., Javitz, H., et al. (2019). Development of a Biodosimeter for Radiation Triage Using Novel Blood Protein Biomarker Panels in Humans and Non-human Primates. *Int. J. Radiat. Biol.* 96, 1–13.

Balog, R. P., Bacher, R., Chang, P., Greenstein, M., Jammalamadaka, S., Javitz, H., et al. (2020). Development of a Biodosimeter for Radiation Triage Using Novel Blood Protein Biomarker Panels in Humans and Non-human Primates. *Int. J. Radiat. Biol.* 96 (1), 22–34. doi:10.1080/09553002.2018.1532611

Banfield, R. E., Hall, L. O., Bowyer, K. W., and Kegelmeyer, W. P. (2007). A Comparison of Decision Tree Ensemble Creation Techniques. *IEEE Trans. Pattern Anal. Mach. Intell.* 29 (1), 173–180. doi:10.1109/tpami.2007.250609

Blakely, W. F., Bolduc, D. L., Debad, J., Sigal, G., Port, M., Abend, M., et al. (2018). Use of Proteomic and Hematology Biomarkers for Prediction of Hematopoietic Acute Radiation Syndrome Severity in Baboon Radiation Models. *Health Phys.* 115 (1). doi:10.1097/hp.0000000000000819

Boellner, S., and Becker, K.-F. (2015). Reverse Phase Protein Arrays-Quantitative Assessment of Multiple Biomarkers in Biopsies for Clinical Use. *Microarrays* 4 (2), 98–114. doi:10.3390/microarrays4020098

Breiman, L. (2001). Random Forests. *Machine Learn.* 45 (1), 5–32. doi:10.1023/a:1010933404324

Bylesjö, M., Rantalainen, M., Cloarec, O., Nicholson, J. K., Holmes, E., and Trygg, J. (2006). OPLS Discriminant Analysis: Combining the Strengths of PLS-DA and SIMCA Classification. *J. Chemometrics* 20 (8–10), 341–351. doi:10.1002/cem.1006

Chorna, I. V., Datsyuk, L. O., and Stoika, R. S. (2005). Expression of Bax, Bad and Bcl-2 Proteins under X-Radiation Effect towards Human Breast Carcinoma MCF-7 Cells and Their Doxorubicin-Resistant Derivatives. *Exp. Oncol.* 27 (3), 196–201.

DiCarlo, A. L., Maher, C., Hick, J. L., Hanfling, D., Dainiak, N., Chao, N., et al. (2011). Radiation Injury after a Nuclear Detonation: Medical Consequences and the Need for Scarce Resources Allocation. *Disaster Med. Public Health Prep.* 5 (0 1), S32–S44. doi:10.1001/dmp.2011.17

Garty, G., Turner, H. C., Salerno, A., Bertucci, A., Zhang, J., Chen, Y., et al. (2016). THE DECADE OF THE RABiT (2005-15). *Radiat. Prot. Dosimetry* 172 (1-3), 201–206. doi:10.1093/rpd/ncw172

Hallahan, D. E., and Virudachalam, S. (1997). Ionizing Radiation Mediates Expression of Cell Adhesion Molecules in Distinct Histological Patterns within the Lung. *Cancer Res.* 57 (11), 2096–2099.

Himburg, H. A., Sasine, J., Yan, X., Kan, J., Dressman, H., and Chute, J. P. (2016). A Molecular Profile of the Endothelial Cell Response to Ionizing Radiation. *Radiat. Res.* 186 (2), 141–152. doi:10.1667/rr14444.1

Jacobs, A. R., Guyon, T., Headley, V., Nair, M., Ricketts, W., Gray, G., et al. (2020). Role of a High Throughput Biodosimetry Test in Treatment Prioritization after a Nuclear Incident. *Int. J. Radiat. Biol.* 96 (1), 57–66. doi:10.1080/09553002.2018.1532615

Karim, S., Mirza, Z., Chaudhary, A., Abuzenadah, A., Gari, M., and Al-Qahtani, M. (2016). Assessment of Radiation Induced Therapeutic Effect and Cytotoxicity in *Cancer* Patients Based on Transcriptomic Profiling. *Int. J. Mol. Sci.* 17 (2), 250. doi:10.3390/ijms17020250

Kuang, Z., Huang, R., Yang, Z., Lv, Z., Chen, X., Xu, F., et al. (2018). Quantitative Screening of Serum Protein Biomarkers by Reverse Phase Protein Arrays. *Oncotarget* 9 (66), 32624–32641. doi:10.18632/oncotarget.25976

Liang, N., Jia, L., Liu, Y., Liang, B., Kong, D., Yan, M., et al. (2013). ATM Pathway Is Essential for Ionizing Radiation-Induced Autophagy. *Cell Signal.* 25 (12), 2530–2539. doi:10.1016/j.cellsig.2013.08.010

Liu, S., Sammons, V., Fairhall, J., Reddy, R., Tu, J., Hong Duong, T. T., et al. (2012). Molecular Responses of Brain Endothelial Cells to Radiation in a Mouse Model. *J. Clin. Neurosci.* 19 (8), 1154–1158. doi:10.1016/j.jocn.2011.12.004

Maier, P., Hartmann, L., Wenz, F., and Herskind, C. (2016). Cellular Pathways in Response to Ionizing Radiation and Their Targetability for Tumor Radiosensitization. *Int. J. Mol. Sci.* 17 (1), 102. doi:10.3390/ijms17010102

Ossetrova, N. I., Sandgren, D. J., and Blakely, W. F. (2011). C-Reactive Protein and Serum Amyloid A as Early-phase and Prognostic Indicators of Acute Radiation Exposure in Nonhuman Primate Total-Body Irradiation Model. *Radiat. Measurements* 46 (9), 1019–1024. doi:10.1016/j.radmeas.2011.05.021

Rohloff, J. C., Gelinas, A. D., Jarvis, T. C., Ochsner, U. A., Schneider, D. J., Gold, L., et al. (2014). Nucleic Acid Ligands with Protein-like Side Chains: Modified Aptamers and Their Use as Diagnostic and Therapeutic Agents. *Mol. Ther. - Nucleic Acids* 3 (10), e201–e. doi:10.1038/mtna.2014.49

Sproull, M., Avondoglio, D., Kramp, T., Shankavaram, U., and Camphausen, K. (2013). Correlation of Plasma FL Expression with Bone Marrow Irradiation Dose. *PLoS One* 8 (3), e58558. doi:10.1371/journal.pone.0058558

Sproull, M., Kramp, T., Tandle, A., Shankavaram, U., and Camphausen, K. (2017). Multivariate Analysis of Radiation Responsive Proteins to Predict Radiation Exposure in Total-Body Irradiation and Partial-Body Irradiation Models. *Radiat. Res.* 187, 251. doi:10.1667/RR14558.1

Sproull, M., and Camphausen, K. (2016). State-of-the-Art Advances in Radiation Biodosimetry for Mass Casualty Events Involving Radiation Exposure. *Radiat. Res.* 186 (5), 423–435. doi:10.1667/rr14452.1

Sproull, M., Kramp, T., Tandle, A., Shankavaram, U., and Camphausen, K. (2015). Serum Amyloid A as a Biomarker for Radiation Exposure. *Radiat. Res.* 184 (1), 14–23. doi:10.1667/rr13927.1

Sproull, M., Shankavaram, U., and Camphausen, K. (2019). Comparison of Proteomic Biodosimetry Biomarkers across Five Different Murine Strains. *Radiat. Res.* 192 (6), 640–648. doi:10.1667/rr15442.1

Sullivan, J. M., Prasanna, P. G. S., Grace, M. B., Wathen, L. K., Wallace, R. L., Koerner, J. F., et al. (2013). Assessment of Biodosimetry Methods for a Mass-Casualty Radiological Incident. *Health Phys.* 105 (6), 540–554. doi:10.1097/hp.0b013e31829cf221

Team, R. C. R. (2015). *A Language and Environment for Statistical Computing*. Vienna, Austria: RFoundation for Statistical Computing.

Yoo, H. C., Yu, Y. C., Sung, Y., and Han, J. M. (2020). Glutamine Reliance in Cell Metabolism. *Exp. Mol. Med.* 52 (9), 1496–1516. doi:10.1038/s12276-020-00504-8

Zou, H., and Hastie, T. (2005). Regularization and Variable Selection via the Elastic Net. *J. R. Stat. Soc B* 67 (2), 301–320. doi:10.1111/j.1467-9868.2005.00503.x

Conflict of Interest: The authors declare that the research was conducted in the absence of any commercial or financial relationships that could be construed as a potential conflict of interest.

frontiers in Pharmacology

ORIGINAL RESEARCH
published: 27 April 2021
doi: 10.3389/fphar.2021.646076

Radiation Increases Bioavailability of Lisinopril, a Mitigator of Radiation-Induced Toxicities

Meetha Medhora[1,2,3,4,5], Preeya Phadnis[6], Jayashree Narayanan[1], Tracy Gasperetti[1], Jacek Zielonka[7,8], John E. Moulder[1], Brian L. Fish[1] and Aniko Szabo[9]*

[1]Department of Radiation Oncology, Medical College of WI, Milwaukee, WI, United States, [2]Department of Medicine, Medical College of WI, Milwaukee, WI, United States, [3]Department of Physiology, Medical College of WI, Milwaukee, WI, United States, [4]Cardiovascular Center, Medical College of WI, Milwaukee, WI, United States, [5]Research Service, Department of Veterans Affairs, Zablocki VAMC, Milwaukee, WI, United States, [6]GlobalReach BI, San Francisco, CA, United States, [7]Department of Biophysics, Medical College of WI, Milwaukee, WI, United States, [8]Cancer Center Redox and Bioenergetics Shared Resource, Medical College of WI, Milwaukee, WI, United States, [9]Institute for Health and Equity, Division of Biostatistics, Medical College of WI, Milwaukee, WI, United States

OPEN ACCESS

Edited by:
Lynnette H. Cary, Uniformed Services University of the Health Sciences, United States

Reviewed by:
Regina M Day, Uniformed Services, University of the Health Sciences, Bethesda, Maryland, United States
Lakshman Singh, The University of Melbourne, Australia

***Correspondence:**
Meetha Medhora
medhoram@mcw.edu

Specialty section:
This article was submitted to Translational Pharmacology, a section of the journal Frontiers in Pharmacology

Received: *24 December 2020*
Accepted: *24 March 2021*
Published: *27 April 2021*

Citation:
Medhora M, Phadnis P, Narayanan J, Gasperetti T, Zielonka J, Moulder JE, Fish BL and Szabo A (2021) Radiation Increases Bioavailability of Lisinopril, a Mitigator of Radiation-Induced Toxicities. Front. Pharmacol. 12:646076. doi: 10.3389/fphar.2021.646076

There are no FDA-approved drugs to mitigate the delayed effects of radiation exposure that may occur after a radiological attack or nuclear accident. To date, angiotensin-converting enzyme inhibitors are one of the most successful candidates for mitigation of hematopoietic, lung, kidney, and brain injuries in rodent models and may mitigate delayed radiation injuries after radiotherapy. Rat models of partial body irradiation sparing part of one hind leg (leg-out PBI) have been developed to simultaneously expose multiple organs to high doses of ionizing radiation and avoid lethal hematological toxicity to study the late effects of radiation. Exposures between 9 and 14 Gy damage the gut and bone marrow (acute radiation syndrome), followed by delayed injuries to the lung, heart, and kidney. The goal of the current study is to compare the pharmacokinetics (PK) of a lead angiotensin converting enzyme (ACE) inhibitor, lisinopril, in irradiated vs. nonirradiated rats, as a step toward licensure by the FDA.

Methods: Female WAG/RijCmcr rats were irradiated with 12.5–13 Gy leg-out PBI. At day 35 after irradiation, during a latent period for injury, irradiated and nonirradiated siblings received a single gavage (0.3 mg, 0.6 mg) or intravenous injection (0.06 mg) of lisinopril. Plasma, urine, lung, liver and kidney levels of lisinopril were measured at different times. PK modeling (R package) was performed to track distribution of lisinopril in different compartments.

Results: A two-compartment (central plasma and periphery) PK model best fit lisinopril measurements, with two additional components, the gavage and urine. The absorption and renal clearance rates were similar between nonirradiated and irradiated animals (respectively: ratios 0.883, $p = 0.527$; 0.943, $p = 0.605$). Inter-compartmental clearance (from plasma to periphery) for the irradiated rats was lower than for the nonirradiated rats (ratio 0.615, $p = 0.003$), while the bioavailability of the drug was 33% higher (ratio = 1.326, $p < 0.001$).

Interpretation: Since receptors for lisinopril are present in endothelial cells lining blood vessels, and radiation induces vascular regression, it is possible that less lisinopril remains bound in irradiated rats, increasing circulating levels of the drug. However, this study cannot rule out changes in total amount of lisinopril absorbed or excreted long-term, after irradiation in rats.

Keywords: pharmacokinetics, renin-angiotensin system, delayed effects of radiation, pulmonary vasculature, mitigation

INTRODUCTION

There are no FDA-approved drugs to mitigate the delayed effects of radiation exposure that may occur after a radiological attack or nuclear accident (Singh et al., 2015b; Dicarlo et al., 2018). To date, angiotensin-converting enzyme inhibitors, a popular class of drugs commonly used to treat hypertension and heart disease (Riegger, 1989; Inagami 1999; Bicket 2002), are one of the most successful candidates for mitigation of radiation-induced injuries. They suppress the renin-angiotensin system (Bicket 2002) which regulates multiple physiological pathways (Inagami 1999; Rodgers and diZeraga, 2013). In preclinical models, radiation-induced injuries to the lung (Molteni et al., 2000; Kma et al., 2012; Medhora et al., 2012), kidney (Moulder et al., 2011; Fish et al., 2016), brain (Robbins et al., 2010) and hematopoietic tissues (Day et al., 2013; McCart et al., 2019, CM Orschell and GN Cox, personal communication) have been described to be mitigated by angiotensin converting enzyme inhibitors. There is also evidence that this class of drugs may mitigate delayed radiation injuries in humans treated with radiotherapy for cancer (Sun et al., 2018; Kharofa et al., 2012; Jenkins and Watts, 2011 and; Jenkins and Welsh, 2011).

Angiotensin-converting enzyme catalyzes the synthesis of a peptide, angiotensin II, which constricts blood vessels to increase blood pressure (Bicket 2002). Inhibition of the enzyme therefore blocks the constriction of blood vessels and lowers blood pressure. The enzyme is present on endothelial cells that line blood vessels (Heeneman et al., 2007). The lung, which is responsible for gas exchange between the air and the blood is rich in blood vessels and endothelial cells. Tissue distribution of lisinopril has been previously studied by planar anterior imaging in Sprague Dawley rats (Femia et al., 2008). A series of chelates were conjugated to lisinopril and their binding evaluated *in vitro* against purified rabbit lung angiotensin-converting enzyme. A lead conjugate was then labeled with technetium-99 m (^{99m}Tc) and injected in rats to study uptake. In this study it was found that the drug bound significantly to the internal tissues, with over 18% of the signal recovered primarily in the lungs after 10 min, as compared to only 0.15% in the blood. Since radiation decreases vascular density in the lung and other organs, angiotensin converting enzyme and its activity is reduced in irradiated lungs (Ghosh et al., 2009). Similarly, well perfused organs such as the heart, gut, liver and kidney also have abundant endothelial cells which may decrease after irradiation (Baker et al., 2009; Stewart et al., 2010). It is not known how distribution of angiotensin-converting enzymes may be altered after radiation to these organs.

In order to test countermeasures for radiation-induced injuries to multiple organs after a radiological attack, total and partial body exposures are used in preclinical models (Singh et al., 2015a; MacVittie et al., 2019; Parker et al., 2019; Thrall et al., 2019). In rats, models of partial body irradiation sparing part of one hind leg (leg-out PBI) have been developed to simultaneously expose multiple organs to high doses of ionizing radiation without inducing hematological toxicity (Fish et al., 2016; Medhora et al., 2019). In this unique model, exposures between 9 and 14 Gy acutely damage the gut and bone marrow (acute radiation syndrome), followed by delayed injuries to the lung, heart, and kidney (Fish et al., 2016; Medhora et al., 2019). The acute radiation syndrome covers gastrointestinal injury between days 3–7, and hematopoietic cell depletion from days 8–30. Beyond day 30, rats experience delayed effects, with damage to the lungs, kidneys and other organs. Lung injury can be fatal at 13 Gy or higher to the thorax and typically occurs between days 40–90, while fatal renal injury manifests after >120-days (Fish et al., 2016).

To advance development of angiotensin-converting enzyme inhibitors as countermeasures for radiation damage, the FDA requires that their pharmacokinetics (PK) and pharmacodynamics (PD) be determined in irradiated subjects to understand how levels of the drug change with time after radiation (US FDA 2015). It is not known if such parameters are altered after leg-out PBI. Therefore, the current study evaluates PK of a lead angiotensin-converting enzyme inhibitor, lisinopril, as a step toward licensure for mitigation of radiation injury. The effect of radiation on PK of lisinopril was conducted at 35 days after radiation, since this time is within a latent window of injury in the model used. It does not coincide with lethal effects of the acute radiation syndrome or delayed effects of radiation that may only transiently interfere with oral drug delivery, absorption and metabolism. In addition, an angiotensin converting enzyme in the same family as lisinopril, enalapril, had efficacy to mitigate radiation pneumonitis when delivered as late as 35 days after radiation (Gao et al., 2013).

MATERIALS AND METHODS

Animal Care

All animal protocols were approved by Institutional Animal Care and Use Committees (IACUC) at the Medical College of Wisconsin (MCW). Based upon direction from the IACUC, rats were designated as morbid and euthanized if they met specified veterinarian's criteria as described previously

TABLE 1 | Sample sizes.

Group	Route	Administered lisinopril (mg/kg)	Plasma measurements	Urine measurements	Sample size
No radiation	Gavage	0	1	0	4
No radiation	Gavage	300	0	1	4
No radiation	Gavage	300	1	0	55
No radiation	Gavage	300	2	0	2
No radiation	Gavage	600	0	1	6
No radiation	Gavage	600	1	1	3
No radiation	Gavage	600	2	0	9
No radiation	Gavage	600	4	0	9
No radiation	IV	60	0	1	6
No radiation	IV	60	1	0	11
No radiation	IV	60	1	1	3
No radiation	IV	60	2	0	3
Radiation	Gavage	300	0	1	5
Radiation	Gavage	300	1	0	58
Radiation	Gavage	300	2	0	2
Radiation	Gavage	600	0	1	6
Radiation	Gavage	600	2	0	8
Radiation	Gavage	600	4	0	8
Radiation	IV	60	0	1	6
Radiation	IV	60	1	0	11

(Medhora et al., 2015). WAG/RijCmcr rats bred at MCW were weaned to Teklad 8604 (Envigo, Madison WI) rodent diet along with hyper-chlorinated water. The rats were housed in a 14 h/10 h light/dark cycle, at 22°C with humidity maintained between 30 and 70%.

Materials

Reagents were purchased from Sigma-Aldrich, St. Louis, MO. Solvents for liquid chromatography-mass spectrometry (LC-MS) analyses were of HPLC LC-MS grade. Enalaprilat (sc-205669) and (S)-Lisinopril-d5 (sc-220030) were purchased from Santacruz Biotechnology, Dallas, TX, United States.

Experimental Procedures

Sample sizes are listed in **Table 1**.

Leg–Out PBI in Rats

WAG/RijCmcr female rats were irradiated without the use of anesthetics at 11–12 weeks of age weighing ~155 g. All irradiations were done between 8–11 am. For leg-out PBI, non-anesthetized rats were immobilized in a plastic jig and irradiated using a XRAD-320 orthovoltage x-ray system (Precision X-Ray, North Branford, Connecticut). The x-ray system was operated at 320 kVp and 13 mA, with a half value layer of 1.4 mm Cu and a dose-rate of 1.75 Gy min^{-1} for total doses of 12.5 or 13 Gy. During the irradiation, each rat was confined in a chamber which allows irradiation of two rats simultaneously. One hind limb of each rat was carefully externalized from the chamber and shielded with a 0.25-inch lead block. The dose to this leg was 2 Gy. The dual-chambered jig was placed on a plane perpendicular to the beam direction, with distance from source to the midline of rats set at 61 cm. Collimator jaws and dosimetry were used as previously described (Medhora et al., 2014). The irradiation field at midline was large enough to cover both chambers with adequate (at least 2 cm) margins. Supportive care was provided to rats receiving 13 Gy. Supportive care consisted of delivery of the antibiotic Enrofloxacin (10 mg/kg/day) from days 1–14 in the drinking water, and hydration by daily subcutaneous injection of saline (40 ml/kg/day) from days 3–7, post-irradiation.

Administration of Lisinopril: Gavage and Intravenous Injection

At 35 days post-irradiation, irradiated rats or age-matched controls were administered a single dose of lisinopril (21CEC PX Pharm Ltd. United Kingdom; dissolved in filtered reverse-osmosis water). Depending on treatment group, lisinopril was administered either by oral gavage or an intravenous (IV) injection via the tail vein. For oral gavage, the rats were manually restrained, and a gavage needle attached to a syringe was inserted into the esophagus and 0.4 ml of either 0.3 mg/rat or 0.6 mg/rat lisinopril was delivered. A different group of rats received lisinopril at a diluted (1:10) dose of 0.06 mg/rat injected IV via the tail vein. The rats were manually restrained, and facilitation of tail vein dilation was achieved with dipping the tails in warm water. Once the veins were dilated, a 25-gauge needle attached to a syringe was inserted into the tail vein and 0.4 ml of lisinopril administered.

Blood Collection

Blood was collected via the jugular vein in order to measure lisinopril levels in the plasma at various timepoints. Rats were anesthetized with 3–5% isoflurane, the forelimbs restrained in the caudo-dorsal direction and a 23-gauge needle inserted into the center of the jugular fossa by a trained technician. The needle and syringe were coated with EDTA and ~0.5 ml blood was collected at each timepoint. Platelet free plasma was obtained by first centrifuging the blood at 1,000 x g for

15 min and re-centrifuging the supernatant at 10,000 x g for 10 min. All centrifugations were carried out at 4°C.

Urine Collection

Urine was collected in a Nalgene rat metabolic cage. A rat was placed in the metabolic cage with access to food and water for 24 h. After 24 h urine volume was recorded, and an aliquot was frozen and stored at −80°C for LC-MS analyses.

Measurements of Lisinopril

At day 35 after irradiation, all rats received a single gavage or intravenous dose of lisinopril (0.3 or 0.06 mg). Plasma was measured 1–4 times in each animal, at 0, 0.5, 1, 1.5, 2, 2.5, 3, 4, 5, 6, 8, 24 or 48 h after oral gavage, and 5 min, 1.5 and 24 h after intravenous injection. The renal clearance (amount excreted in urine) was measured 24 h after either gavage or injection. Terminal measurements of lisinopril in the kidney, liver and lung were made at 5 min and 1.5 h after IV injection of lisinopril. Measurements of lisinopril in the lungs and kidneys were performed after 24- and 48-h following gavage administration.

Determination of Lisinopril Levels in Rat Plasma or Urine by LC-MS/MS

Aliquots (0.1 ml) of rat plasma or urine were extracted with ~3 volumes of cold acidified methanol spiked with enalaprilat as an internal standard (0.3 ml of methanol, 20 μL of 0.1 M HCl and 3 μL of 0.1 mM enalaprilat), mixed well and allowed to stand for 5 min before centrifugation at 14,000 rpm for 5 min at 4°C. The supernatant was passed through a Phree phospholipid removal plate (Phenomenex) and the eluate dried completely under a flux of air and reconstituted with 120 μL of LC-MS mobile phase (5% acetonitrile, 95% water, 0.1% formic acid), spiked with 1 μM of lisinopril-d_5 used as a second internal standard. The sample was vortexed thoroughly for 15 min at 4°C and centrifuged for 30 min at 20,000 g. 80 μL of the supernatant was transferred to HPLC autosampler vials and processed for lisinopril analyses by LC-MS/MS. The analyses were performed using a Shimadzu Nexera-2 UHPLC system coupled to Shimadzu LCMS-8030 triple quadrupole mass detector. Samples were injected into C_{18} reversed phase column (Waters Cortecs UPLC C_{18} 2.1 mm × 50 mm, 1.6 μm) thermostated at 40°C and equilibrated with 0.1% formic acid in water:acetonitrile (95:5). Compounds were eluted by increasing the concentration of acetonitrile in the mobile phase from 5 to 40% over 2.5 min at the flow rate of 0.5 ml/min. Detection was carried out using electrospray ionization (ESI) source in the multiple reaction monitoring (MRM) mode, using the following transitions: 406.1 > 84.1 (lisinopril), 411.1 > 84.1 (lisinopril-d_5), and 349.0 > 206.1 (enalaprilat).

Determination of Lisinopril Levels in Rat Lung, Liver, and Kidney Tissues

The lungs, liver and kidneys were harvested, weighed, and powdered in liquid nitrogen. A total of one lung (left), one lobe of liver (middle) and one kidney (right)/rat was used for extraction. To the pulverized tissue, 1 ml of cold DPBS was added, vortexed well and extracted with 3.23 ml of acidified methanol containing enalaprilat as internal standard (3 ml of methanol, 200 μL of 0.1 M HCl, 10 μL of 0.1 mM enalaprilat, and 20 μL of water). The sample was incubated overnight on a shaker at 4°C. The extract was then centrifuged at 14,000 rpm for 5 min at 4°C. The supernatant was passed through a Phree phospholipid removal plate and the eluate dried under a flux of air. The dried residue was reconstituted and analyzed by LC-MS/MS as described above for plasma/urine samples.

Determination of Efficiency of Extraction of Lisinopril

The efficiency of extraction of lisinopril from blood, plasma, urine, lungs, liver and kidney samples was estimated using spike-in experiments. Age-matched naïve rats (n = 3–5) that were not irradiated, were used for this study. A known volume of lisinopril from a stock of 1 mg/ml was added to a known volume of harvested blood, plasma or urine *in vitro*. Similarly, a known volume of stock lisinopril was added to a measured aliquot of suspension containing pulverized lung, liver or kidney in DPBS as described above. The samples were then analyzed by LC-MS/MS as already described for plasma and tissues, after again adding enalaprilat as an internal standard. The estimated amount of lisinopril in each sample was compared with the actual amount used to spike the same sample. The ratios were used to determine the efficiency of extraction. For modeling, the measured lisinopril concentrations/amounts were divided by the corresponding extraction efficiencies.

Measurement of Kidney Function

Previous published work has shown that rising blood urea nitrogen (BUN) levels are superior to histopathology for assessing kidney injury (Moulder et al., 2011) To measure BUN, rats were anesthetized with 3–5% isoflurane for blood draws conducted by an experienced technician. The BUN was assayed from serum as described previously (Cohen et al., 1994; Medhora et al., 2014) using a urease-nitroprusside colorimetric assay. BUN values were expressed as mg/dL of serum and means with 95% confidence intervals were used for statistical analysis. Urine protein (UP) and creatinine (UC) were also measured as described (Moulder et al., 2011). The UP/UC ratio is used as a sensitive indicator of kidney function to measure urine-concentrating defects that occur upon renal radiation injury and to normalize for animal size differences.

Statistical Methods

Non-compartmental Estimates

Non-compartmental estimates based on gavage-administered plasma concentrations were computed using the R package PK version 1.3.5. The concentrations were normalized to 300 μg of drug administered, and time was measured in hours. The AUC 0-tlast was calculated using the linear trapezoidal rule on the arithmetic means at the different time points. Bootstrap t confidence intervals are reported.

Two-Compartment Pharmacokinetics Model

Pharmacokinetic (PK) modeling was performed on the data to measure distribution of the drug in different tissues (compartments). The two compartments fitted with observed data were the central compartment (plasma) and the peripheral

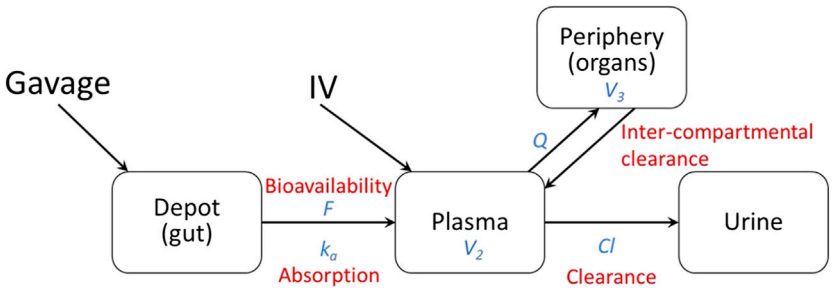

FIGURE 1 | Diagram of two-compartment fitted model.

compartment (internal tissues such as lungs, liver, kidneys, etc.). Administration by gavage was modeled using the gut as a depot to include bioavailability (F) and absorption (k_a) from the gut (**Figure 1**). The diffusion of lisinopril between the plasma and peripheral compartments was modeled by Q, the inter-compartmental clearance rate, where larger numbers reflect more diffusion between the two compartments. Clearance out of the system was modeled by Cl, the renal clearance rate via urine (**Figure 1**). The model was fitted using the open-source R package Nonlinear Mixed-Effects Model Development and Simulation (nlmixr) along with related R packages.

More specifically, the following differential equation system was fitted:

$$\frac{\mathrm{d}}{\mathrm{d}t}\left(Y_{\mathrm{depot}}\right) = -k_a * Y_{\mathrm{depot}},$$

$$\frac{\mathrm{d}}{\mathrm{d}t}\left(Y_{\mathrm{plasma}}\right) = +F * k_a * Y_{\mathrm{depot}} - Cl * C_{\mathrm{plasma}} - Q * C_{\mathrm{plasma}} + Q * \frac{Y_{\mathrm{peri}}}{V_3},$$

$$\frac{\mathrm{d}}{\mathrm{d}t}\left(Y_{\mathrm{peri}}\right) = +Q * C_{\mathrm{plasma}} - Q * \frac{Y_{\mathrm{peri}}}{V_3},$$

$$\frac{\mathrm{d}}{\mathrm{d}t}\left(Y_{\mathrm{urine}}\right) = +Cl * C_{\mathrm{plasma}}.$$

where Y_{depot}, Y_{plasma}, Y_{peri}, and Y_{urine} are the amount of lisinopril in the gut (depot), plasma (central), peripheral, and urine compartments, respectively, in μmoles; V_2 and V_3 are the apparent volumes of the plasma and the peripheral compartments in liters (L); and $C_{\mathrm{plasma}} = Y_{\mathrm{plasma}}/V_2$ is the concentration of lisinopril within the plasma compartment in μmoles/L.

An additive error with compartment-specific variance was assumed for the plasma, peripheral, and urine compartments. Multiple measurements from the same animal were linked via a log-normally distributed multiplicative random effect on the compartment volumes V_2 and V_3.

The observed measurements are the concentration in plasma, C_{plasma} and the (cumulative) amount in the urine, Y_{urine}. The administered lisinopril amount (in g) was converted to moles via dividing by its mass (405.5 g/mol).

The model was fitted to the plasma and urine data, the accumulation in the peripheral compartment was inferred from the model.

RESULTS

Non-compartmental (AUC) estimates showed significantly higher lisinopril circulating in irradiated animals over the first 24 h (radiation/no radiation ratio 1.42, $p < 0.0001$). When the same model was plotted on a log scale, the lisinopril in both irradiated and non-irradiated animals did not reach zero, indicating the existence of at least one other internal compartment in the PK model.

Based on visual predictive checks and a formal likelihood ratio test ($p < 0.001$), a two internal-compartments PK model including plasma and peripheral compartments, with two additional external compartments to model gavage and urine, best fit the plasma and urine concentrations (see **Figures 2**, **3**). The goodness-of-fit was quantified as $R^2 = 90.1\%$. The dashed lines in **Figures 2**, **3** show the best-fit one-compartment model. Compared to this, the two-compartment model shown by solid lines better fit the data measured in the urine (**Figure 2**) and plasma (**Figure 3**) especially at later time points.

The model returned two kinds of parameters, the base rates in non-irradiated animals (**Table 2**) and the ratio of rates for irradiated animals (**Table 3**). The model parameters for irradiated animals can be calculated using the base rate estimate from **Table 2** multiplied by the corresponding ratio from **Table 3**.

This model yielded estimates for the ratios of absorption, clearance, inter-compartment clearance, and bioavailability (proportion of the dose that reaches the systemic circulation) of lisinopril between non-irradiated and irradiated rats. p-values were calculated based on whether the ratio differed significantly from 1. The absorption and renal clearance rates were similar between non-irradiated and irradiated animals (respectively: ratio 0.883, $p = 0.527$; ratio 0.943, $p = 0.605$). The inter-compartmental clearance for the irradiated rats was significantly lower than for the non-irradiated rats (ratio 0.615, $p = 0.003$), while the bioavailability of the drug was 33% higher (ratio = 1.326, $p < 0.001$) (see **Table 3**).

The model parameters were used to plot inferred amounts of lisinopril in plasma, the peripheral compartment, and urine over time. **Figure 2** shows the model-inferred curves fitted to the measured data values. Although the urine sample was collected only once in a subset of animals, this data was crucial for the ability of the model to separate bioavailability from absorption

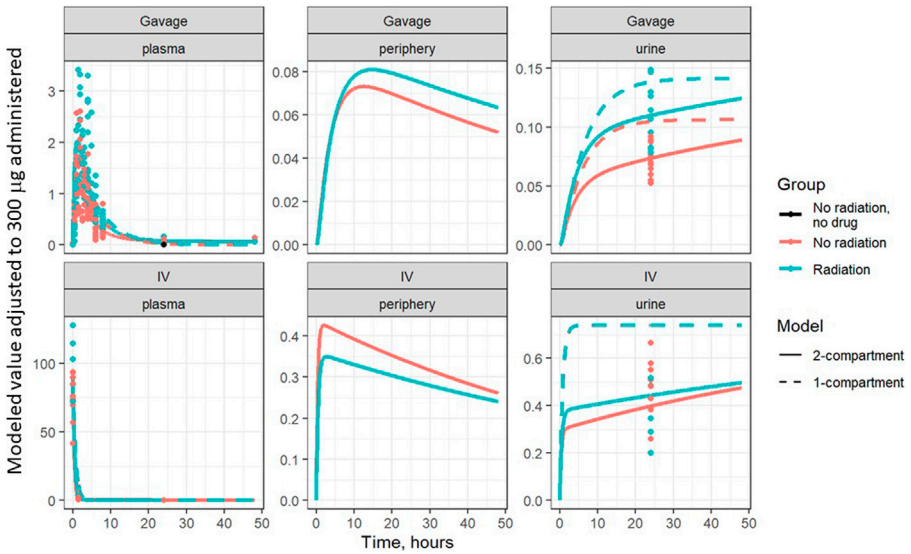

FIGURE 2 | Lisinopril over time in plasma, periphery, and urine, broken out by delivery technique, plotted on a linear scale. Points are measured data values. Solid curves are fitted values from the two-compartment model, not adjusted for bioavailability. Dashed lines represent the best-fit one-compartment model.

rate (the urine measurements broken out by delivery technique and group are shown in **Table 4**). Note that the models in **Figure 2** have not been adjusted for bioavailability, leading to the appearance that the lisinopril retained in irradiated tissue differs by delivery technique. **Figure 4** shows the model-inferred curves adjusted for equivalent bioavailability, by dividing the model output by the relevant bioavailability estimate (0.192 for non-irradiated rats and 0.254 for irradiated rats) (see **Tables 2**, **3**). This demonstrates that the delivery technique does not affect the amount of lisinopril retained in irradiated tissue.

Figure 5 shows the plasma concentration of gavage-administered lisinopril over 48 and 8 h, on both log and linear scales. The difference in peak concentration shows the higher bioavailability of lisinopril in irradiated vs non-irradiated rats. The log-scale plots make clear that the plasma concentration never reaches zero.

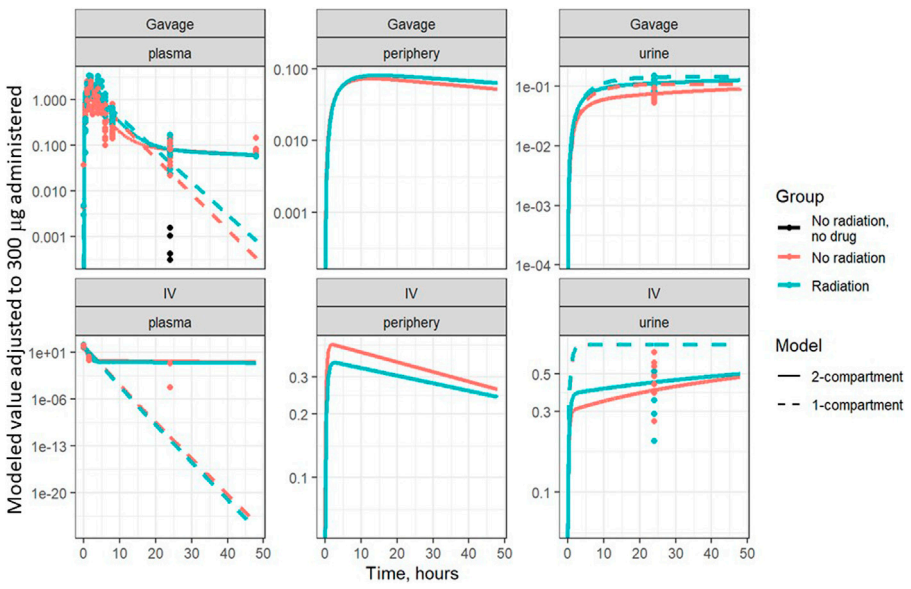

FIGURE 3 | Same data as **Figure 2**, plotted on a log scale. Points are measured data values. Solid curves are fitted values from the two-compartment model, not adjusted for bioavailability. Dashed lines represent the best-fit one-compartment model.

TABLE 2 | Two-compartment model base parameter estimates for control group, including 95% confidence interval bounds; fitted to plasma + urine data. L represents liters in the units column.

Parameter	Estimate	Lower 95% CI	Upper 95% CI	Units
Absorption rate	0.279	0.197	0.395	1/hr
Renal clearance rate	0.009	0.008	0.011	L/hr
Central volume	0.008	0.007	0.010	L
Inter-compartmental clearance rate	0.014	0.011	0.017	L/hr
Peripheral volume (lung)	0.513	0.360	0.730	L
Bioavailability	0.192	0.167	0.221	Scalar

TABLE 3 | Two-compartment model parameter ratio estimates for radiation group, including 95% confidence interval bounds and *p*-values; fitted to plasma + urine data.

Parameter	Estimate	Lower 95% CI	Upper 95% CI	*p*-value
Absorption rate ratio	0.883	0.599	1.300	0.527
Renal clearance rate ratio	0.943	0.756	1.177	0.605
Inter-compartmental clearance rate ratio	0.615	0.445	0.850	0.003
Bioavailability ratio	1.326	1.142	1.538	<0.001

TABLE 4 | Measured lisinopril excreted in urine per 300 μg administered (μmoles).

Route	Group	Sample size	Geometric mean (μmoles)	Standard deviation (μmoles)
Gavage	No radiation	13	0.072	0.013
Gavage	Radiation	11	0.11	0.026
IV	No radiation	9	0.46	0.13
IV	Radiation	6	0.37	0.14

Figure 6 shows the plasma concentration of IV-administered lisinopril over 24 and 2 h, on both log and linear scales. The difference in plasma concentrations seen after 5 h reflects the reduced inter-compartmental clearance rate, i.e., there is less lisinopril in the plasma because less is being cleared to the plasma from the peripheral compartment. This difference is less apparent in the gavage data due to the increased bioavailability of gavage-administered lisinopril in irradiated rats.

Finally, BUN values (see Materials and Methods) were used to infer renal function at the same timepoint at which the PK studies were conducted. The results are plotted in **Figure 7**. There was no difference in BUN between irradiated and non-irradiated rats indicating renal function was not changed at 35 days after irradiation. Another sensitive measure of renal function, the urine protein to urine creatinine ratio (UP/UC), did not differ between irradiated rats at 35 days after irradiation (0.20 (0.22–0.31)) compared to non-irradiated control rats (0.24 (0.19–0.28)).

DISCUSSION

The non-significance of the difference in absorption rates paired with the significant increase in bioavailability suggests that radiation increases the bioavailability of lisinopril independently of its absorption from the gut. Further studies specifically designed to measure absorption are needed to confirm this result, since irradiation is known to breach the integrity of the intestinal barrier (Booth et al., 2012). However, gastrointestinal injury peaks within 7 days after irradiation in the rat (Fish et al., 2016; Fish et al., 2020), so it is possible that the injury is repaired (at least partially) by 35 days when the current study was conducted.

The reduction in inter-compartmental clearance suggests that circulating lisinopril is cleared more slowly from the central plasma compartment in irradiated animals. However, from the results presented here we cannot determine if radiation interferes with lisinopril leakage/diffusion into the periphery or reduced lisinopril is bound to the vasculature, especially in the peripheral compartments such as the lung, liver and kidney, which are known to be well perfused with blood. Since lisinopril has been shown to bind substantially to the peripheral compartment in the absence of radiation (Femia et al., 2008), the latter explanation is consistent with the binding of lisinopril to angiotensin converting enzyme (its receptor) found on vascular endothelial cells lining the blood vessels. Since radiation induces vascular regression in organs and tissues (Baker et al., 2009; Ghosh et al., 2009; Stewart et al., 2010), irradiated rats may have fewer receptors leaving more unbound lisinopril to circulate in the blood.

Lisinopril is not known to be metabolized *in vivo*, but instead removed primarily by excretion via the kidney (Beermann 1988). Since the renal clearance rates were similar between nonirradiated and irradiated animals we

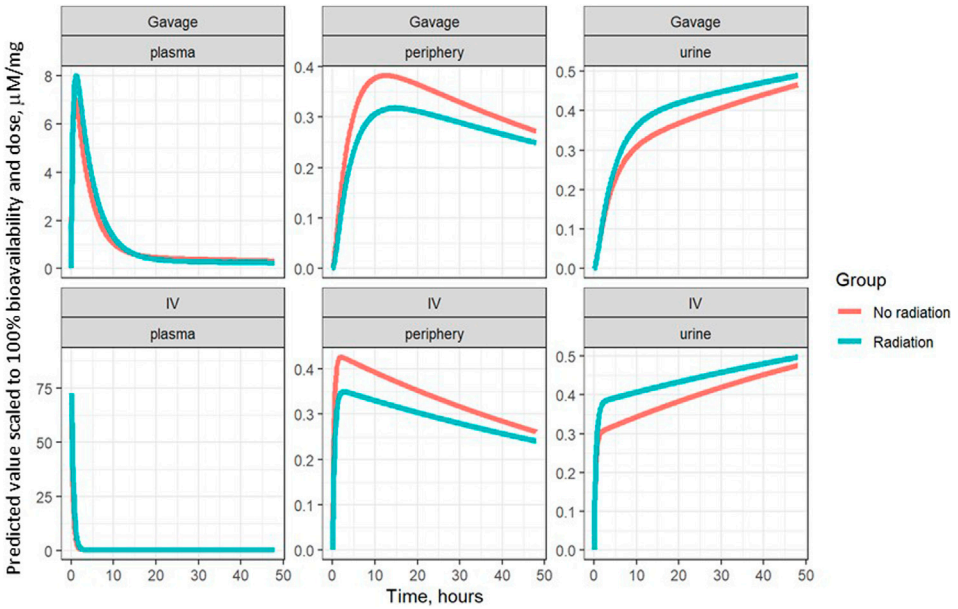

FIGURE 4 | Model-inferred estimates for lisinopril over time in plasma, lungs, and urine, adjusted for bioavailability, broken out by delivery technique.

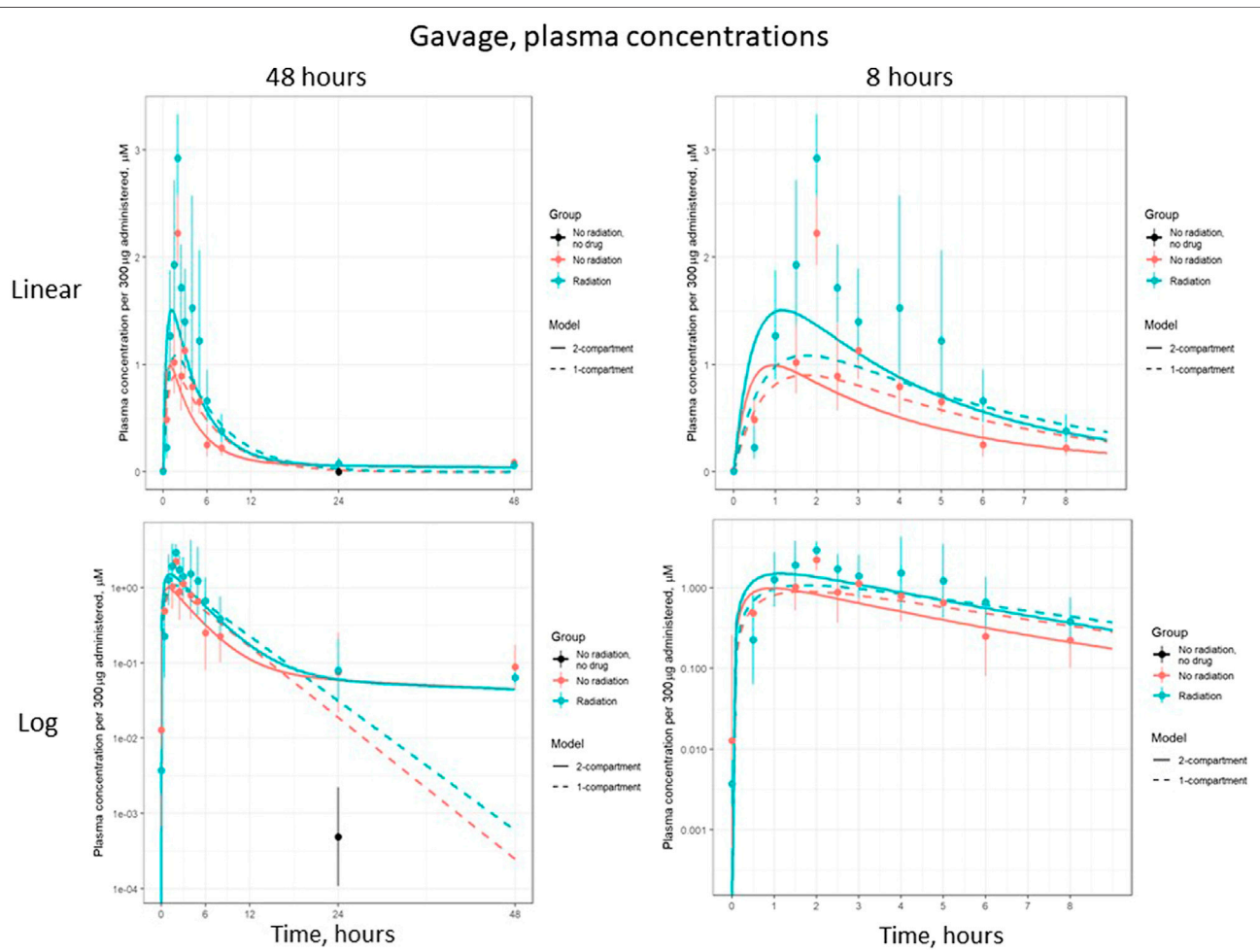

FIGURE 5 | Plasma concentration of lisinopril (geometric mean ± SD) when administered by gavage, broken out by time and scale.

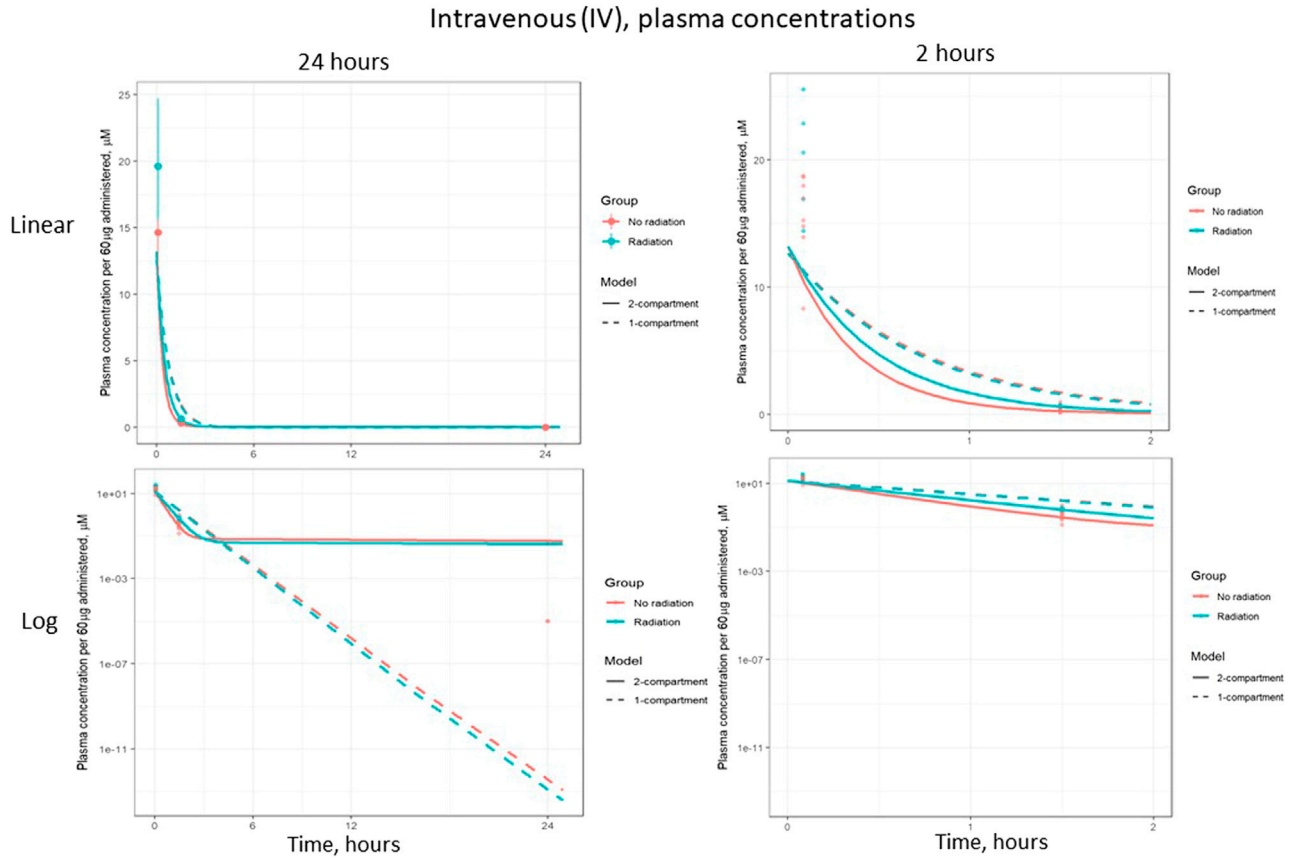

FIGURE 6 | Plasma concentration of lisinopril (geometric mean ± SD) when administered by intravenous (IV) injection, broken out by time and scale.

checked the kidney function in these rats to confirm renal function had not changed. Levels of BUN and UP/UC are commonly used as a biomarker to follow renal function and are actually superior to histopathology for assessing radiation nephropathy in irradiated WAG/Rij rats (Moulder et al., 2011). As with renal clearance, the BUN and UP/UC were not different at 35 days after irradiation (**Figure 7**). It should be noted that BUN levels and UP/UC ratio do ultimately rise after radiation (by 90 days) in the same rat model (Fish et al., 2016).

The PK of lisinopril has been described in humans and are somewhat comparable to the results described in this paper. The peak serum levels in humans are 6–8 h (Beermann 1988), compared to 2–3 h in rats in the current study. Though bioavailability was increased by radiation, the model-based circulating half-life of the drug remained similar in irradiated (2.5 h) and non-irradiated (2.8 h) rats. The inter-individual variation was 4-6-fold in humans (Beermann 1988) and 3-4-fold in nonirradiated rats injected with lisinopril (result not shown). Variation in irradiated rats at 90 min was 1.8-fold after IV injection. After oral administration by gavage, variation was 1.6-fold and 2.7-fold in non-irradiated and irradiated rats respectively at 90 min (data not shown). Similar to the multiple phasic plots observed in **Figures 2–6**, a polyphasic decrease in circulating lisinopril over time occurred in humans. Both species demonstrated an initial linear drop followed by a slower terminal phase (Beermann 1988, **Figure 5**). The prolonged terminal phase in humans (half-life of 46.7 h) was postulated to be due to binding of lisinopril to angiotensin-converting enzyme (Beermann 1988). The model-based estimate of the terminal half-life is 65 h in nonirradiated rats and 83 h in irradiated rats in this study, and also could be postulated to be due to the tight binding of lisinopril to its receptor, angiotensin converting enzyme.

In summary, irradiation of multiple organs increases circulating levels of lisinopril when administered at 35 days after exposure. Statistical modeling suggests that this is caused by a decreased amount of lisinopril distributed in the periphery of irradiated rats. Since lisinopril is known to bind with high affinity to angiotensin converting enzyme, which is present on cells lining the blood vessels, the vascular compartment of the periphery is the most likely site to hold this bound lisinopril. Though the current study suggests the rates of absorption and clearance of lisinopril are not altered at 35 days after radiation, further studies specifically targeting such measurements must be conducted for confirmation. Absorption over a longer time (but at the same rate) in irradiated rats given gavage, could result in increased bioavailability, and cannot be ruled out since

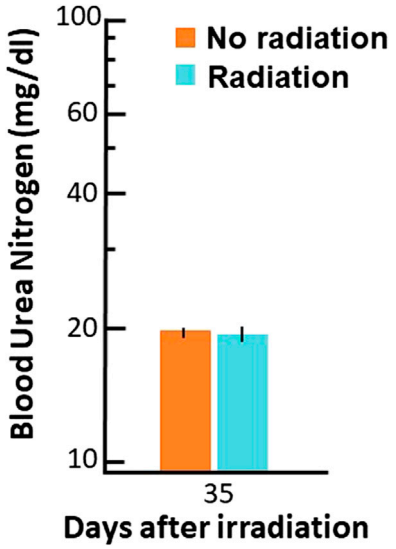

FIGURE 7 | Blood urea nitrogen (BUN, mg/dl (log scale on *Y*-axis)) values at 35 days after radiation. Data are shown as means and 95% confidence intervals.

excretion from the gut into the feces was not measured in this study. Also, the model-based terminal renal excretion was prolonged (83 vs. 65 h) in irradiated rats, indicating that clearance may be altered. In addition, since the gut is injured between 6 and 10 days (Booth et al., 2012; Fish et al., 2016; Fish et al., 2020) and the kidney after 90 days (Fish et al., 2016; Fish et al., 2020) post-irradiation, it is also possible that the PK of lisinopril will be different around these time points.

Lisinopril is widely used to regulate blood pressure or treat cardiovascular disease. Angiotensin-converting enzyme expression is increased in cardiac fibrosis and disease (Harada et al., 1999; Dilsizian et al., 2007). The results from radiation injury in the current study indicate the possibility that bioavailability may be altered by other pathological conditions as well. The unique result of increased bioavailability in this study after radiation is consistent with a reduction in blood vessel density, which has been previously described (Baker et al., 2009; Ghosh et al., 2009; Stewart et al., 2010).

DATA AVAILABILITY STATEMENT

The raw data supporting the conclusions of this article will be made available by the authors, without undue reservation.

ETHICS STATEMENT

The animal study was reviewed and approved by Institutional Animal Care and Use Committee (IACUC) at the Medical College of Wisconsin.

AUTHOR CONTRIBUTIONS

Conceptualization, MM, BF; Methodology, MM, BF, JN, TG, JZ; Formal Analysis, MM, PP, BF, AS; Original Draft Preparation and Writing, MM, PP, JN, JZ, JEM, AS, BLF; Review & Editing, MM, PP, JN, TG, JZ, JM, AS, BF.

FUNDING

NIAID AI107305 (supported establishment of PK of lisinopril after radiation), NIAID AI133594 (supported refinement of animal model and related techniques) Department of Radiation Oncology, Medical College of Wisconsin (supported preparation of manuscript and miscellaneous experiments to complete the study).

ACKNOWLEDGMENTS

The LC-MS analyses were performed in Medical College of Wisconsin Cancer Center Redox and Bioenergetics Shared Resource. The authors wish to thank Dana Scholler for excellent animal care and technical assistance.

REFERENCES

Baker, J. E., Fish, B. L., Su, J., Haworth, S. T., Strande, J. L., Komorowski, R. A., et al. (2009). 10 Gy total body irradiation increases risk of coronary sclerosis, degeneration of heart structure and function in a rat model. *Int. J. Radiat. Biol.* 85 (12), 1089–1100. doi:10.3109/09553000903264473

Beermann, B. (1988). Pharmacokinetics of lisinopril. *Am. J. Med.* 85 (3B), 25–30. doi:10.1016/0002-9343(88)90346-4

Bicket, D. P. (2002). Using ACE inhibitors appropriately. *Am. Fam. Physician* 66 (3), 461–468.

Booth, C., Tudor, G., Tudor, J., Katz, B. P., and MacVittie, T. J. (2012). Acute gastrointestinal syndrome in high-dose irradiated mice. *Health Phys.* 103 (4), 383–399. doi:10.1097/hp.0b013e318266ee13

Cohen, E. P., Moulder, J. E., Fish, B. L., and Hill, P. (1994). Prophylaxis of experimental bone marrow transplant nephropathy. *J. Lab. Clin. Med.* 124 (3), 371–380.

Day, R. M., Davis, T. A., Barshishat-Kupper, M., McCart, E. A., Tipton, A. J., and Landauer, M. R. (2013). Enhanced hematopoietic protection from radiation by the combination of genistein and captopril. *Int. Immunopharmacology* 15 (2), 348–356. doi:10.1016/j.intimp.2012.12.029

DiCarlo, A. L., Cassatt, D. R., Dowling, W. E., Esker, J. L., Hewitt, J. A., Selivanova, O., et al. (2018). Challenges and benefits of repurposing products for use during a radiation public Health emergency: lessons learned from biological threats and other disease treatments. *Radiat. Res.* 190 (6), 659–676. doi:10.1667/RR15137.1

Dilsizian, V., Eckelman, W. C., Loredo, M. L., Jagoda, E. M., and Shirani, J. (2007). Evidence for tissue angiotensin-converting enzyme in explanted hearts of ischemic cardiomyopathy using targeted radiotracer technique. *J. Nucl. Med.* 48 (2), 182–187.

Femia, F. J., Maresca, K. P., Hillier, S. M., Zimmerman, C. N., Joyal, J. L., Barrett, J. A., et al. (2008). Synthesis and evaluation of a series of 99mTc(CO)3+ lisinopril complexes for *in vivo* imaging of angiotensin-converting enzyme expression. *J. Nucl. Med.* 49 (6), 970–977. doi:10.2967/jnumed.107.049064

Fish, B. L., Gao, F., Narayanan, J., Bergom, C., Jacobs, E. R., Cohen, E. P., et al. (2016). Combined hydration and antibiotics with lisinopril to mitigate acute and delayed high-dose radiation injuries to multiple organs. *Health Phys.* 111 (5), 410–419. doi:10.1097/HP.0000000000000554

Fish, B. L., MacVittie, T. J., Szabo, A., Moulder, J. E., and Medhora, M. (2020). WAG/RijCmcr rat models for injuries to multiple organs by single high dose ionizing radiation: similarities to nonhuman primates (NHP). *Int. J. Radiat. Biol.* 96 (1), 81–92. doi:10.1080/09553002.2018.1554921

Gao, F., Fish, B. L., Moulder, J. E., Jacobs, E. R., and Medhora, M. (2013). Enalapril mitigates radiation-induced pneumonitis and pulmonary fibrosis if started 35 days after whole-thorax irradiation. *Radiat. Res.* 180 (5), 546–552. doi:10.1667/RR13350.1

Ghosh, S. N., Wu, Q., Mäder, M., Fish, B. L., Moulder, J. E., Jacobs, E. R., et al. (2009). Vascular injury after whole thoracic x-ray irradiation in the rat. *Int. J. Radiat. Oncol. Biol. Phys.* 74 (1), 192–199. doi:10.1016/j.ijrobp.2009.01.006

Harada, K., Sugaya, T., Murakami, K., Yazaki, Y., and Komuro, I. (1999). Angiotensin II type 1A receptor knockout mice display less left ventricular remodeling and improved survival after myocardial infarction. *Circulation* 100 (20), 2093–2099. doi:10.1161/01.cir.100.20.2093

Heeneman, S., Sluimer, J. C., and Daemen, M. J. A. P. (2007). Angiotensin-converting enzyme and vascular remodeling. *Circ. Res.* 101 (5), 441–454. doi:10.1161/CIRCRESAHA.107.148338

Inagami, T. (1999). Molecular biology and signaling of angiotensin receptors: an overview. *J. Am. Soc. Nephrol.* 10 (Suppl. 11), S2–S7.

Jenkins, P., and Watts, J. (2011). An improved model for predicting radiation pneumonitis incorporating clinical and dosimetric variables. *Int. J. Radiat. Oncol. Biol. Phys.* 80 (4), 1023–1029. doi:10.1016/j.ijrobp.2010.03.058

Jenkins, P., and Welsh, A. (2011). Computed tomography appearance of early radiation injury to the lung: correlation with clinical and dosimetric factors. *Int. J. Radiat. Oncol. Biol. Phys.* 81 (1), 97–103. doi:10.1016/j.ijrobp.2010.05.017

Kharofa, J., Cohen, E. P., Tomic, R., Xiang, Q., and Gore, E. (2012). Decreased risk of radiation pneumonitis with incidental concurrent use of angiotensin-converting enzyme inhibitors and thoracic radiation therapy. *Int. J. Radiat. Oncology*Biology*Physics* 84 (1), 238–243. doi:10.1016/j.ijrobp.2011.11.013

Kma, L., Gao, F., Fish, B. L., Moulder, J. E., Jacobs, E. R., and Medhora, M. (2012). Angiotensin converting enzyme inhibitors mitigate collagen synthesis induced by a single dose of radiation to the whole thorax. *Jrr* 53 (1), 10–17. doi:10.1269/jrr.11035

MacVittie, T. J., Farese, A. M., Parker, G. A., Jackson, W., 3rd., Booth, C., Tudor, G. L., et al. (2019). The gastrointestinal subsyndrome of the acute radiation syndrome in rhesus macaques: a systematic Review of the lethal dose-response relationship with and without medical management. *Health Phys.* 116 (3), 305–338. doi:10.1097/HP.0000000000000903

McCart, E. A., Lee, Y. H., Jha, J., Mungunsukh, O., Rittase, W. B., Summers, T. A., Jr., et al. (2019). Delayed captopril administration mitigates hematopoietic injury in a murine model of total body irradiation. *Sci. Rep.* 9 (1), 2198. doi:10.1038/s41598-019-38651-2

Medhora, M., Gao, F., Fish, B. L., Jacobs, E. R., Moulder, J. E., and Szabo, A. (2012). Dose-modifying factor for captopril for mitigation of radiation injury to normal lung. *J. Radiat. Res.* 53 (4), 633–640. doi:10.1093/jrr/rrs004

Medhora, M., Gao, F., Gasperetti, T., Narayanan, J., Khan, A. H., Jacobs, E. R., et al. (2019). Delayed effects of acute radiation exposure (deare) in juvenile and old rats: mitigation by lisinopril. *Health Phys.* 116 (4), 529–545. doi:10.1097/HP.0000000000000920

Medhora, M., Gao, F., Glisch, C., Narayanan, J., Sharma, A., Harmann, L. M., et al. (2015). Whole-thorax irradiation induces hypoxic respiratory failure, pleural effusions and cardiac remodeling. *J. Radiat. Res.* 56 (2), 248–260. doi:10.1093/jrr/rru095

Medhora, M., Gao, F., Wu, Q., Molthen, R. C., Jacobs, E. R., Moulder, J. E., et al. (2014). Model development and use of ACE inhibitors for preclinical mitigation of radiation-induced injury to multiple organs. *Radiat. Res.* 182 (5), 545–555. doi:10.1667/RR13425.1

Molteni, A., Moulder, J. E., Cohen, E. F., Ward, W. F., Fish, B. L., Taylor, J. M., et al. (2000). Control of radiation-induced pneumopathy and lung fibrosis by angiotensin-converting enzyme inhibitors and an angiotensin II type 1 receptor blocker. *Int. J. Radiat. Biol.* 76 (4), 523–532. doi:10.1080/095530000138538

Moulder, J. E., Cohen, E. P., and Fish, B. L. (2011). Captopril and losartan for mitigation of renal injury caused by single-dose total-body irradiation. *Radiat. Res.* 175 (1), 29–36. doi:10.1667/RR2400.1

Parker, G. A., Li, N., Takayama, K., Farese, A. M., and MacVittie, T. J. (2019). Lung and heart injury in a nonhuman primate model of partial-body irradiation with minimal bone marrow sparing: histopathological evidence of lung and heart injury. *Health Phys.* 116 (3), 383–400. doi:10.1097/HP.0000000000000936

Riegger, A. J. G. (1989). ACE inhibitors in congestive heart failure. *Cardiology* 76 (Suppl. 2), 42–49. doi:10.1159/000174558

Robbins, M. E., Zhao, W., Garcia-Espinosa, M. A., and Diz, D. I. (2010). Renin-angiotensin system blockers and modulation of radiation-induced brain injury. *Curr. Drug Targets* 11 (11), 1413–1422. doi:10.2174/1389450111009011413

Rodgers, K. E., and diZerega, G. S. (2013). Contribution of the local RAS to hematopoietic function: a novel therapeutic target. *Front. Endocrinol.* 4, 157. doi:10.3389/fendo.2013.00157

Singh, V. K., Newman, V. L., Berg, A. N., and MacVittie, T. J. (2015a). Animal models for acute radiation syndrome drug discovery. *Expert Opin. Drug Discov.* 10 (5), 497–517. doi:10.1517/17460441.2015.1023290

Singh, V. K., Romaine, P. L. P., and Seed, T. M. (2015b). Medical countermeasures for radiation exposure and related injuries. *Health Phys.* 108 (6), 607–630. doi:10.1097/HP.0000000000000279

Stewart, F. A., Hoving, S., and Russell, N. S. (2010). Vascular damage as an underlying mechanism of cardiac and cerebral toxicity in irradiated cancer patients. *Radiat. Res.* 174 (6), 865–869. doi:10.1667/RR1862.1

Sun, F., Sun, H., Zheng, X., Yang, G., Gong, N., Zhou, H., et al. (2018). Angiotensin-converting enzyme inhibitors decrease the incidence of radiation-induced pneumonitis among lung cancer patients: a systematic Review and meta-analysis. *J. Cancer* 9 (12), 2123–2131. doi:10.7150/jca.24665

Thrall, K. D., Mahendra, S., Jackson, M. K., Jackson, W., 3rd., Farese, A. M., and MacVittie, T. J. (2019). A comparative dose-response relationship between sexes for mortality and morbidity of radiation-induced lung injury in the rhesus macaque. *Health Phys.* 116 (3), 354–365. doi:10.1097/HP.0000000000000925

U.S. Food and Drug Administration (2015). Guidance for industry: product development under the animal rule Available at: https://www.fda.gov/regulatory-information/search-fda-guidance-documents/product-development-under-animal-rule ((Accessed October 12th, 2020).

Conflict of Interest: The remaining authors declare that the research was conducted in the absence of any commercial or financial relationships that could be construed as a potential conflict of interest.

frontiers in Pharmacology

REVIEW
published: 10 May 2021
doi: 10.3389/fphar.2021.624844

Repurposing Pharmaceuticals Previously Approved by Regulatory Agencies to Medically Counter Injuries Arising Either Early or Late Following Radiation Exposure

Vijay K. Singh[1,2]* *and Thomas M Seed*[3]

[1]Division of Radioprotectants, Department of Pharmacology and Molecular Therapeutics, F. Edward Hébert School of Medicine, Uniformed Services University of the Health Sciences, Bethesda, MD, United States, [2]Armed Forces Radiobiology Research Institute, Uniformed Services University of the Health Sciences, Bethesda, MD, United States, [3]Tech Micro Services, Bethesda, MD, United States

OPEN ACCESS

Edited by:
Ales Tichy,
University of Defence, Czechia

Reviewed by:
Uhee Jung,
Korea Atomic Energy Research Institute (KAERI), South Korea
Thomas MacVittie,
Radiation Biology, United States
Badri Pandey,
Bhabha Atomic Research Centre (BARC), India

***Correspondence:**
Vijay K. Singh
vijay.singh@usuhs.edu

Specialty section:
This article was submitted to Translational Pharmacology, a section of the journal Frontiers in Pharmacology

Received: 01 November 2020
Accepted: 26 April 2021
Published: 10 May 2021

Citation:
Singh VK and Seed TM (2021) Repurposing Pharmaceuticals Previously Approved by Regulatory Agencies to Medically Counter Injuries Arising Either Early or Late Following Radiation Exposure. Front. Pharmacol. 12:624844. doi: 10.3389/fphar.2021.624844

The increasing risks of radiological or nuclear attacks or associated accidents have served to renew interest in developing radiation medical countermeasures. The development of prospective countermeasures and the subsequent gain of Food and Drug Administration (FDA) approval are invariably time consuming and expensive processes, especially in terms of generating essential human data. Due to the limited resources for drug development and the need for expedited drug approval, drug developers have turned, in part, to the strategy of repurposing agents for which safety and clinical data are already available. Approval of drugs that are already in clinical use for one indication and are being repurposed for another indication is inherently faster and more cost effective than for new agents that lack regulatory approval of any sort. There are four known growth factors which have been repurposed in the recent past as radiomitigators following the FDA Animal Rule: Neupogen, Neulasta, Leukine, and Nplate. These four drugs were in clinic for several decades for other indications and were repurposed. A large number of additional agents approved by various regulatory authorities for given indications are currently under investigation for dual use for acute radiation syndrome or for delayed pathological effects of acute radiation exposure. The process of drug repurposing, however, is not without its own set of challenges and limitations.

Keywords: acute radiation syndrome, delayed effects of acute radiation exposure, radiation countermeasures, regulatory agencies, repurposing

INTRODUCTION

Exposure to intense ionizing radiation will evoke invariably significant damage to selective tissues of vital organ systems of the body; most notably, the vascular, blood-forming, gastrointestinal, and reproductive systems. Following such intense irradiation, acute lymphohematopoietic tissue damage rapidly manifests as evidenced by rapid changes in clinically relevant blood parameters, namely by fast, time-dependent decreases in blood cell concentrations (specifically lymphocytes, granulocytes, and thrombocytes/platelets) (Gale et al., 2019).

The degree and frequency to which these major ionizing radiation-induced pathophysiological responses are expressed are clearly dependent on a multitude of factors that encompass not only the

nature of the radiation exposure, but also the extent and location of bodily exposure. These response variables are superimposed on the all-important biological makeup of the exposed individual (age, gender, overall health status, as well as basic physiologic and genetic constitutions of the exposed individual). Lest we forget that 'time' is key in order to bring the physics of radiation together with biological elements in order for these irradiation pathologies to fully develop and be expressed.

At acute radiation doses of >10 Gy with high dose rates, exposed individuals will die very quickly (i.e., hours to a few days) from largely untreatable neurovascular effects. At doses of >2 to <10 Gy, injury to hematopoietic tissue (bone marrow) and the gastrointestinal (GI) tract is obvious (Hall and Giaccia, 2012). Survivors of such radiation exposures will also fall subject to the delayed effects (known as delayed effects of acute radiation exposure, DEARE), which may include involvement of other organs such as the lungs, kidneys, and heart (Singh and Seed, 2020b). These sub-syndromes, their animal models, mechanism of injury, and medical countermeasures have been discussed in several reviews (Williams et al., 2010a; Williams et al., 2010b; Williams and McBride, 2011; Williams et al., 2012; Williams J. P. et al., 2016). Despite substantial efforts over the last several decades to advance effective and safe radiation medical countermeasures for acute radiation syndrome (ARS) and for DEARE, a limited number of countermeasures have been fully approved by the Food and Drug Administration (FDA) for clinical use for humans (Singh et al., 2017a; Singh et al., 2017b; Singh and Seed, 2017; Singh and Seed, 2020b). Thus, there is a serious need for government agencies, academicians, and corporate entities to make a joint effort to get multiple agents that can be used either before or after irradiation approved for each indication in the shortest possible time. There are several promising radiation countermeasures under investigation for regulatory approval for ARS and DEARE (Singh et al., 2017a; Singh et al., 2017b; Singh and Seed, 2017; Singh and Seed, 2020a).

Under any mass casualty event due to a nuclear/radiological scenario, the number of individuals requiring medical care will be enormous, but the real number of people critically injured by high doses of radiation will be limited (Singh and Seed, 2020b). The radiation-injuries may be grouped based on 'time' to manifest radiation injury and etiology of the injuries. Based on the 'time,' injuries may be grouped in terms of early/acute, delayed, or late occurrence. Further, they can be characterized as being of either 'deterministic' or 'stochastic' origins, with the 'early arizing' pathologies dominated by 'deterministic' responses, while the 'late-arizing' responses divided more evenly by the prevalence of long-developing pathologies of a 'stochastic' nature. It should be noted that the 'deterministic' responses/pathologies often share common features regardless of whether they arise relatively early following acute exposures or if they arise relatively late following various exposure modalities (e.g., acute, chronic, fractionated exposures). By contrast, a sizable fraction of the late-arizing pathologies have a stochastic, probabilistic nature, with 'cancer' being the group's arch type (Seed et al., 1984; Seed et al., 1985; Upton, 1985; Singh and Seed, 2020b).

Cancer that develops long after radiation exposure is often associated both temporally and causally with initial mutagenic processes. A commonly held concept, with ample experimental support, is that cancer risks following radiation exposures (or exposures of other types of toxic physiochemical agents) can be substantially mitigated pharmacologically by blocking exposure-related mutagenesis (Grdina et al., 1985; Grdina et al., 2000; Grdina et al., 2002; Singh and Seed, 2019). In this regard, there are numerous categories of anti-cancer drugs that are currently in use with some having anti-mutagenic activity as well. These drugs include alkylating agents, anti-metabolites, natural products, and hormones (Ali et al., 2012). The more prominent of these agents specifically designed to limit toxicant-induced mutagenesis include phosphorothioates (amifostine/WR1065) and nitroxides (Tempol) (Johnstone et al., 1995; Grdina et al., 2000; Grdina et al., 2002; Seed et al., 2002). Clearly, there is a significant opportunity for drug developers and the pharmaceutical industry to repurpose previously FDA-approved drugs for the treatment of various types of cancers, particularly to confer radiation-enhancing effects. Some promising agents include aspirin, statins, and metformin which have the ability to enhance outcomes in cancer patients by decreasing the radiation dose, and also reduce the treatment expense (Khan et al., 2019). The reader should note, however, that we have limited the scope of this article to only acute and delayed effects of irradiation and not to 'cancer,' per se.

The targeting specificity of drugs in clinical use for given indications appears to decrease over time as new information accumulates (Papapetropoulos and Szabo, 2018). Identification of additional molecular targets for a drug may be an issue for the therapeutic agent already under clinical use from a specificity perspective. At the same time, such additional information regarding new targets and associated activities for a given drug may offer further therapeutic potential, leading to the repurposing of the same drug for another indication. Drug repurposing (also known as dual use) is another way of utilizing known drugs for other indications. The specific drug might be in the clinic for a specific indication, or may be withdrawn from development as a result of issues related to efficacy, side effects, or commercial considerations. Drug rescuing is a similar phenomenon; it is the process(es) that refers to circumstances where the failed agent for one indication is investigated later with the objective of introducing it for another indication (Sharlow, 2016). Such repurposing efforts in the drug development arena are vital to having enough drugs for various indications with limited resources.

A current, prime example of the latter 'repurposing process' involves the antiviral agent, remdesivir (Gilead Sciences, Inc., Foster City, CA) and its use in treating severely ill COVID-19 infected patients (Gilead Sciences Inc., 2020). This agent was originally part of a bank of antivirals set aside by Gilead that was deemed in initial clinical testing to be ineffective in managing SARS (severe acute respiratory syndrome)-like infections, but was later rescued, clinically retested, and subsequently brought through the FDA's regulatory approval process in record time in order to pursue it as an effective remedy for the current raging COVID-19 (Coronavirus disease 2019) pandemic (US Food and Drug Administration, 2020b).

Conventional drug development has a roughly 90% attrition rate; this is to say that 90% of the candidate drugs studied in

TABLE 1 | US FDA-approved growth factors for other indications repurposed for H-ARS as radiomitigators.

FDA-approved drugs	Indications of earlier approval	Repurposed indication	Date of repurpose	Comments	References*
Neupogen/ filgrastim/G-CSF	Five different indications of neutropenia and for mobilization of autologous hematopoietic progenitors	Adult patients of H-ARS	March 2015	Requires full supportive care: blood products and individualized antibiotics; can be delayed up until 24 h after irradiation	Farese and MacVittie (2015); U.S. Food and Drug Administration (2015); Amgen Inc. (2015)
Neulasta/PEGylated filgrastim/PEGylated G-CSF	Decreases infections as displayed by febrile neutropenia	Adult and pediatric patients of H-ARS	November 2015	Needs full supportive care: blood products and personalized antibiotics; can be delayed until one day after irradiation	National Institute of Allergic and Infectious Diseases (2015); Amgen Inc. (2015)
Leukine/ sargramostim/ GM-CSF	Five different indications for shortening time to neutrophil recovery, mobilization of hematopoietic progenitors, acceleration of myeloid reconstitution, and treatment of delayed neutrophil recovery	Adult and pediatric patients of H-ARS	March 2018	Requires minimal supportive care: antibiotics and fluid; can be delayed until 48 h after irradiation	U.S. Food and drug Administration (2018); Singh and Seed (2018); Sanofi-Aventis U.S. LLC (2018); Gale and Armitage (2021); Zhong et al. (2020)
Nplate/romiplostim/ synthetic TPO	Adult and pediatric patients of immune thrombocytopenia	Adult and pediatric patients of H-ARS	January 2021	Requires minimal supportive care: antibiotics and fluid; should be administered as soon as possible after suspected or confirmed exposure to radiation	Amgen Inc. (2021); Wong et al. (2020); Wong et al. (2020)

The NHP studies were performed at different research sites under the control of respective IACUC rules that may well have dictated that studies of lethal effects must include blood transfusions. The specific medical countermeasures was tested with and without blood transfusions as required based on a trigger-to-treat.

preclinical models that lack toxicity in small as well as large animals and that are well accepted by human studies, ultimately never receive regulatory approval for clinical use (Mullard, 2016). Second attempts to redevelop drugs already in clinical evaluation saves time and money. The time saved has been estimated to be in the range of 12–14 years, and the overall cost saved for FDA approval is in the range of $40–80 million. The latter compares to the >$2 billion to develop an agent from the initial *in vitro* work and associated 'hit selection'. The number of new drugs approved by regulatory agencies per billion USD spent for development has been reduced to one half every 9 years since 1950, underscoring the declining efficiency of drug development (Kakkar et al., 2018).

There is also a distinct possibility of failure in this repurposing route as well; a possibility that also increases the overall cost for successful repurposing (Ishida et al., 2016; Cha et al., 2018; Gelosa et al., 2020). There is another fact which needs to be taken into consideration in favor of repurposing. A significant proportion of funding for such repurposing goes to the large Phase III trials that are mandatory in order to validate the efficacy for the repurposed drug. The high cost associated with such Phase III trials is due to the large numbers of patients that are generally needed for regulatory approval. Furthermore, the repurposed medicinals may not require an approval for use in patients. If the repurposed drug demonstrates robust efficacy for a second indication, medical professionals may prescribe such drugs off-label, specifically for diseases which have limited treatment options.

Drug development programs for medical countermeasures designed for radiation-induced ARS and related radiation-injuries are restricted in a regulatory sense, as they are being developed using the FDA Animal Rule and cannot be evaluated for efficacy in a clinical setting due to ethical reasons (Allio, 2016; U.S. Food and Drug Administration, 2015a).

FDA Approved Agents Repurposed for ARS

Four growth factors/cytokines approved by the US FDA for several indications were in clinic for several decades. These agents were repurposed as radiomitigators for ARS, or more specifically for H-ARS (a hematopoietic sub-syndrome of ARS), following the Animal Rule during the last six years (U.S. Food and Drug Administration, 2015a). These agents are Neupogen (filgrastim), Neulasta (PEGylated filgrastim), Leukine (sargramostim), and Nplate (romiplostim) (**Table 1**) (Amgen Inc., 2015a; Amgen Inc., 2015b; Farese and MacVittie, 2015; National Institute of Allergic and Infectious Diseases, 2015; U.S. Food and Drug Administration, 2015b; U.S. Food and drug Administration, 2018b; Sanofi-Aventis U.S. LLC, 2018; Singh and Seed, 2018; Clayton et al., 2020; Wong et al., 2020a; Wong et al., 2020b; Singh and Seed, 2020b; Zhong et al., 2020; Amgen Inc., 2021; Gale and Armitage, 2021). The data for these growth factors in context of their human use as radiation countermeasures have been recently reviewed (Farese and MacVittie, 2015; Singh and Seed, 2018; Singh and Seed, 2020b; Wong et al., 2020a; Wong et al., 2020b; Zhong et al., 2020; Gale and Armitage, 2021). These articles also discuss various types of medical management used for testing these agents in large animal model.

Filgrastim, PEGylated filgrastim, and sargramostim have some basic structural differences. Sargramostim is a glycosylated product prepared in an expression system using *Saccharomyces cerevisiae,* while filgrastim is a product of the *Escherichia coli* expression system and is not glycosylated. Furthermore, the comparison of efficacy and treatment outcomes of these two countermeasures is not relevant since these two proteins bind to different receptors (Gale and Armitage, 2021). Receptors for filgrastim/G-CSF (granulocyte colony-stimulating factor) and

TABLE 2 | US FDA-approved drugs for other indications currently being investigated for repurposing for acute and delayed effects of radiation exposure.

FDA-approved drugs	Indication(s) for FDA approval	Indication for repurposing	Comments	Relevant references*
Amifostine/Ethyol	Reduces renal toxicity as a result of cisplatin treatment for ovarian cancer, reduces irradiation-induced xerostomia in head and neck cancer patients	H-ARS	Promising agent but dose required for protection from ARS has severe side effects/toxicity	Singh and Seed (2019); Cumberland Pharmaceuticals Inc. (2017)
Promacta/Doptelet	Thrombocytopenia/idiopathic thrombocytopenic purpura (ITP)	H-ARS	These agents stimulate platelet/thrombocyte production and hematopoietic recovery	Parameswaran et al. (2014); Jacobson et al. (2017); Erickson-Miller et al. (2009); U.S. Food and Drug Administration (2018); Dova Pharmaceuticals (2019); Shirley (2018)
Capoten/Vasotec/ Prinivil/Ramipril	Angiotensin-converting enzyme inhibitors, indicated for hypertension	Radiation injury of lung and kidney/ DEARE	Helpful for early and late-arizing radiation injuries as a prophylaxis and mitigator	Singh et al. (2017); U.S. Food and Drug Adsministration (2015); Rosen et al. (2015)
Palifermin	Indicated for oral mucositis in individuals with hematopoietic stem cell transplantation for malignancies	ARS	Truncated N-terminal recombinant keratinocyte growth factor	Vadhan-Raj et al. (2013); Lauritano et al. (2014); Johnke et al. (2014); Rosen et al. (2015)
Erythropoietin	Indicated for anemia linked to renal dysfunction	ARS	Used during the accidents of Tokai-mura, Japan and Henan Province, China	Gianoncelli et al. (2015); Agarwal and McBride (2016); Covic and Abraham (2015); Nagayama et al. (2002); Liu et al. (2008)
IL-3	Not fully approved by the FDA for ARS	ARS	Used during the accident of Nyasvizh, Belarus and Soreq, Israel	Nabholtz et al. (2002); International Atomic Energy Agency (1993); International Atomic Energy Agency (1996)
IL-11/Oprelvekin	Indicated for thrombocytopenia after myelosuppressive chemotherapy in individuals with non-myeloid malignancies	ARS	Radiomitigator and radioprotector	No author listed (1998); Potten 1995; Potten (1996); Burnett et al. (2013); Hauer-Jensen (2014)
Statin	Indicated for atherosclerosis and hypercholesterolemia	ARS	Anti-inflammatory due to inhibition of 3-hydroxy-3-methylglutaryl coenzyme A reductase	Gotto (2003); Grobbee and Bots (2003); Diomede et al. (2001); Sizar et al. (2020); Williams et al. (2004); Wang et al. (2007)
Pentoxifylline	Indicated for claudication and pain in case of occlusive peripheral arterial disease	H-ARS	Methyl xanthine derivative with immunomodulating, anti-inflammatory, antioxidant, and vascular effects	McCarty et al. (2016); Boerma et al. (2008); Berbée et al. (2011); Kulkarni et al. (2013)
Xigris	Indicated for high risk sepsis linked with acute organ dysfunction	ARS	Recombinant human activated protein C	Aneja and Fink (2007); Bernard et al. (2001); Griffin et al. (2006); Geiger et al. (2012)
CpG-ODN	Approved as adjuvants for vaccines	ARS	Stimulates innate as well as adaptive immune responses	Fehér (2019); Zhang et al. (2013); Zhang et al. (2011); Zhang et al. (2011)
Auranofin/Ridaura	Indicated for rheumatoid arthritis	ARS	It is an anti-inflammatory, anti-cancer, neuroprotective, and cardioprotective agent	Nag et al. (2019); Nardon et al. (2016)
Diclofenac sodium	Indicated in osteoarthritis, rheumatoid arthritis, and ankylosing spondylitis	ARS	Benzene-acetic acid derivative	US Food and Drug Administration (2020); Novartis (2005); Alok et al. (2013)
Metformin	Indicated for type 2 diabetes	ARS	Used for FDA-approved as well as for off-label indications	Corcoran and Jacobs (2020); Miller et al. (2014); Xu et al. (2015)
Surfaxin	Indicated for the prevention of respiratory distress syndrome in infants	Lung injury/ DEARE	Helpful for mitigation of lung injury after targeted thoracic irradiation	Piehl and Fernandez-Bustamante (2012); Christofidou-Solomidou et al. (2017)
Diethylcarbamazine citrate	An anti-filarial drug used to treat filariasis	Lung injury/ DEARE	Known for anti-fibrotic, anti-oxidative, anti-inflammatory, and anti-carcinogenic properties	Hawking (1979); Queto et al. (2010); Farzipour et al. (2020)
Mozobil	Indicated for autologous transplantation in cases of non-Hodgkin's lymphoma and multiple myeloma	H-ARS	With G-CSF and agents inducing G-CSF increases peripheral blood $CD34^+$ cells, increases neutrophils	De Clercq (2019); De Clercq (2009); De Clercq (2010); Singh et al. (2014); Singh et al. (2014); Singh et al. (2010); Singh et al. (2012); Singh et al. (2013); Dykstra (2017)
Silverlon	Indicated for blister injuries caused by sulfur mustard, wound and burn contact dressing	Cutaneous radiation injuries	Received FDA approval for multiple indications since 2003	DiCarlo et al. (2018); Argentum Medical (2019); Aurora et al. (2018); Pozza et al. (2014)
Ciprofloxacin	Indicated for severe infections caused by Gram-negative bacteria	ARS and combined injury	Effective in murine model of irradiation and wound	Imrie et al. (1995); Fukumoto et al. (2014); Fukumoto et al. (2013); Sahakitrungruang et al. (2011)

sargramostim/GM-CSF (granulocyte-macrophage colony-stimulating factor) belong to the well-known cytokine receptor family. Differences in the expression of receptors are responsible for the functional disparities between filgrastim and sargramostim (Gale and Armitage, 2021). Biological activity may also depend on how sargramostim is processed. Such distinctions result in differences in the efficacy and safety profiles of these two agents in clinical settings (Stull et al., 2005). Filgrastim use is significantly greater than sargramostim in most hematology and oncology settings.

Data gathered from preclinical testing using non-human primates (NHPs) suggest differences in optimal time of drug administration after radiation exposure and the intensity of supportive care required for the above four agents. The results of these NHP studies have been reviewed thoroughly relative to the various testing conditions employed with these four countermeasures (Wong et al., 2020a; Wong et al., 2020b; Gale and Armitage, 2021). The optimal time for filgrastim and PEGylated filgrastim treatment initiation is 24 h post-irradiation, as opposed to 48 h post-irradiation for sargramostim. Filgrastim/PEGylated filgrastim is effective with full supportive care including blood products and individualized antibiotics. Filgrastim was not effective with minimal or no supportive care (Gluzman-Poltorak et al., 2014; Farese and MacVittie, 2015). Sargramostim and romiplostim were found to be effective with moderate supportive care without blood products. It has not been investigated with intensive supportive care/blood products or without any supportive care (Wong et al., 2020a; Wong et al., 2020b; Gale and Armitage, 2021). Sargramostim is available in lyophilized form, which may offer benefits under situations of limited infrastructure. PEGylated filgrastim has an advantage over the other two when availability of medical personnel is limited, as only two doses are needed. It is important to note that direct comparisons of these four agents in respect of time of administration and supportive care in NHP models are lacking and need additional investigations. Additional drawbacks of these growth factors is their cost and storage conditions (specifically for Neupogen and Neulasta). Furthermore, these agents lack radioprotective efficacy when administered prior to irradiation and have limited potential for long-term storage.

There is significant knowledge for the use of these agents after radiological or nuclear (Rad/Nuc) accidents in humans that, in general, support the concept that they serve to accelerate bone marrow recovery and improve survival-based outcomes (Singh et al., 2015). Unfortunately, due to the observational nature of such studies, 'essential control' subjects are missing and claims of efficacy and safety in humans exposed to Rad/Nuc accidents remain, accordingly, untested. Nevertheless, these agents were approved following the Animal Rule of the FDA and three agents are available in the US Strategic National Stockpile/ Vendor Managed Inventory.

Regulatory Agency Approved Drugs for Repurposing for the Treatment of Radiation Injury

There are several agents approved for human use for a large number of indications by regulatory agencies which are being investigated in various laboratories to repurpose for ARS, DEARE, and other types of late-arizing injuries that arise from either non-acute external exposures or from internally deposited radionuclides.

Agents Being Investigated for Repurposing for ARS

In addition to the four FDA-approved radiomitigators mentioned above, several previously FDA-approved agents are being evaluated for possible expanded indications for preventing, mitigating, or treating accidental or unwanted radiation injuries (**Table 2**). A selected number of these prospectively useful agents are listed below and are briefly described. We have focused on agents which have FDA approval for one or more indications and are being investigated as radiation countermeasures either alone or in combination with another agent.

Amifostine

As mentioned above, only limited drugs have been approved by the US FDA to counter radiation injury, although several additional agents are currently under investigation. The thiol group in amifostine {WR-2721, 2-[(3-aminopropyl)amino] ethanethiol dihydrogen phosphate, Ethyol (trihydrate form of amifostine)} acts as a free radical scavenger, and this group of compounds represents one of the most effective classes of radioprotectors (Grdina et al., 2000; Kouvaris et al., 2007). However, they are generally not well tolerated due to a number of side effects that serve to limit the optimal dosing required for radioprotection of ARS (Singh and Seed, 2019). Preclinical studies using animal models suggested that amifostine protects normal tissues from injuries caused by irradiation (Rasey et al., 1988; Singh and Seed, 2019). Common side effects of such agents include vomiting, diarrhea, and hypotension. These effects result in adverse behavioral responses and decreased performance (Bogo et al., 1985). The FDA has approved amifostine for limited clinical use (Singh and Seed, 2019). In brief, amifostine, however promising as a radioprotector, has not been considered suitable for use in the general civilian population, high-risk individuals, or special operation military forces.

Amifostine is fully approved by the US FDA for these two clinical indications: 1) to diminish renal toxicity associated with the use of chemotherapy of cisplatin in patients with ovarian cancer, and 2) to decrease xerostomia in individuals undergoing post-operative radiotherapy for head and neck cancers (Brizel et al., 2000; Cumberland Pharmaceuticals Inc., 2017). The enhanced absorption of amifostine by the kidney and salivary glands may be a significant contributor for the noted protection of these relevant organs and tissues.

Significant attempts have been made by scientists, academicians, and government agencies to render amifostine more useful by reducing its side effects and toxicity by developing a large number of novel analogs, new formulations, and also new drug delivery approaches. The objective of such efforts is to preserve or improve the efficacy and also prolong the therapeutic window. Specifically, amifostine is being extensively investigated in various laboratories to make it more user-friendly

(Seed, 2005; Seed et al., 2014). Such efforts include: 1) the synthesis of better tolerated analogs with minimal side effects (Davidson et al., 1980; Brown et al., 1988), 2) the identification of additional molecular targets using omics approaches (Cheema et al., 2019; Seed et al., 2019; Singh and Seed, 2019; Cheema et al., 2020), 3) the development of synergy to combine lower doses of amifostine and other effective pharmacologicals with limited or no side effects (Srinivasan et al., 1992; Singh et al., 2016), 4) the use of another agent to reduce its emetic effects (Seed, 2005), and 5) the optimization of the efforts for 'slow-release' delivery (Fatome et al., 1987; Srinivasan et al., 2002; Pamujula et al., 2010). These approaches proved useful to a limited extent in reducing its side effects and toxicity, but have not been successful in eliminating its toxicity completely. Recently, these approaches to make amifostine more useful have been reviewed (Singh and Seed, 2019). We believe that amifostine, with its several positive characteristics, deserves more investigation in order to pursue and eventually receive full regulatory approval for generalized use outside clinical settings for radiation exposure emergencies.

The poly-pharmacy approach appears to be very encouraging, where low doses of amifostine are being combined with other radiation countermeasures under development with the objective to increase the efficacy of amifostine and avoid its side effects. There are several agents that have been tested in combination with amifostine, and results of some of these studies are encouraging (Singh et al., 2016; Singh and Seed, 2019). Specifically, amifostine has been tested in combination with growth factors/cytokines (G-CSF), metformin, antioxidative agents (other thiols), vitamin E components (tocopherol and tocotrienol), prostaglandin E2, β-glucan, Broncho-Vaxom, and a polysaccharide from *Sipunculus nudus*, etc [recently reviewed (Singh and Seed, 2019)].

Mozobil

Mozobil (AMD3100 or plerixafor) was initially identified as an anti-HIV agent (De Clercq, 2019). It specifically blocks the CXCR4 receptor, the co-receptor of T-lymphotropic HIV strains. Mozobil mobilizes the $CD34^+$ hematopoietic progenitors to blood by blocking the chemokine receptor (CXCR4) and disturbing CXCR12 and CXCR4 interaction, which is responsible for tethering stem cells to bone marrow cells (Broxmeyer et al., 2005). Such $CD34^+$ cell mobilization occurs when mozobil is used either alone or with G-CSF. Mozobil received US FDA approval for transplantation in individuals with multiple myeloma or patients with Non-Hodgkin's Lymphoma (NHL) in 2008 (De Clercq, 2019). It can also be used in other malignancies and hereditary disorders (e.g., hepatopulmonary syndrome and WHIM, a congenital immune deficiency). New antagonists of CXCR4, KRH 1636, and CX0714 have also been reported that are not structurally similar to mozobil but may behave in a similar fashion (De Clercq, 2009; De Clercq, 2010).

There are several reports where mozobil has been used in combination with radiation countermeasures inducing G-CSF (e.g. γ-tocotrienol, tocopherol succinate) in animal models to mobilize progenitors, and such mobilized progenitors have been successfully used to protect mice exposed to supralethal doses of radiation which lead to GI-ARS and H-ARS (Singh et al., 2010; Singh et al., 2012; Singh et al., 2013; Singh et al., 2014a; Singh et al., 2014b). These mobilized progenitors have been administered to mice several days after radiation exposure and still retain significant survival benefits. It has been discussed that mozobil along with G-CSF increases blood $CD34^+$ cells that may result in improved neutrophils. Such combination also increases other blood cells leading to better outcomes in patients receiving irradiation (Dykstra, 2017).

Cytokines, Pro-Inflammatory Cytokine Inhibitors and Related Chimeric Recombinants

Several cytokines mitigate radiation injury in tissues and also accelerate tissue recovery. As noted earlier, four growth factors/cytokines have already been repurposed as radiomitigators for ARS, specifically H-ARS. Other type-specific or general classes of cytokines/growth factors need to be reevaluated as potentially useful countermeasures for acute radiation exposures. For example, recombinants that selectively inhibit cytokines (pro-inflammatory) also reduce fibrosis and late tissue injury linked to irradiation, or chimeric growth factors such as myelopoietin. An efficacious (as shown in preclinical animal models) chimeric recombinant, does the same in terms of mitigating acute hematopoietic injury. Some cytokines have been approved by the FDA for other indications, and efforts are being made to develop these agents as radiation countermeasures.

Palifermin

This is the truncated N-terminal keratinocyte growth factor, and this agent is also called as fibroblast growth factor-7. It stimulates epithelial cell proliferation and acts in a paracrine manner. It has its effects on various tissues such as the hepatocytes of the liver, intestine, type II pneumocytes of the lung, keratinocytes in squamous epithelia, hair follicular cells, and transitional urothelial cells (Danilenko, 1999; Farrell et al., 1999). Palifermin received FDA approval to prevent oral mucositis in individuals undergoing stem cell transplant for hematological cancers (Vadhan-Raj et al., 2013; Johnke et al., 2014; Lauritano et al., 2014). This agent is useful for repair and protection of epithelial cells through fibroblast growth factor receptor-2b (FGFR-2b). Its efficacy is a result of stimulation of cell proliferation and being anti-apoptotic (Finch et al., 2013). Palifermin treatment has been shown to prevent radiation-induced gastrointestinal injury in mice (Cai et al., 2013). Palifermin has also been shown to ameliorate radiotherapy and chemotherapy-induced mucosal toxicity (Finch et al., 2013).

Erythropoietin

There are several bioengineered analogs of EPO such as Aransep, Epoetin, Epogen, Darbepoetin, and Procrit. These agents are approved by the FDA for various hematologic indications. Their primary indication is for the treatment of severe anemia via stimulation of erythropoiesis (associated with chronic renal dysfunction) as a result of intense chemotherapy or radiotherapy (Covic and Abraham, 2015; Gianoncelli et al., 2015; Agarwal and

McBride, 2016). These recombinant agents are not approved by the U.S. FDA as a radiation medical countermeasure for use in radiation casualty scenarios. Regardless of this current regulatory status, it is commonly believed that these agents would be used by attending physicians if clinical conditions of radiation exposed patients called for their use. In this regard, it is important to note that EPO was indeed used during the radiological accidents of Tokai-mura in Japan and Henan Province in China for the treatment of exposed victims (Nagayama et al., 2002; Liu et al., 2008).

Interleukin-3

Although recombinant IL-3 stimulates myelopoiesis, this agent has not been pursued actively as a medical countermeasure for ARS or for chemotherapy-induced myelosuppression (Hammond et al., 1990; Lord et al., 1991). Furthermore, leridistim (myelopoietin, a chimeric dual G-CSF and IL-3 receptor agonist) is not being developed as a countermeasure, despite promising initial results showing its efficacy in ameliorating severe, radiation-induced neutropenia within large, experimental animals (MacVittie et al., 2000). A phase III trial with leridistim and G-CSF demonstrated G-CSF to be better than leridistim in preventing chemotherapy-induced neutropenia (Nabholtz et al., 2002). Although IL-3 is not approved by the U.S. FDA as a radiation medical countermeasure, it has been used for treating radiation-exposed victims of Israel–Soreq and Belarus–Nyasvizh with positive treatment outcomes (International Atomic Energy Agency, 1993; International Atomic Energy Agency, 1996) and accordingly, there is a basis for further investigating this agent as a radiation medical countermeasure.

Interleukin-11 (IL-11, Oprelvekin)

Oprelvekin is recombinant IL-11 and is produced in *E. coli*. It has a molecular weight of 19 kDa and is non-glycosylated due to being a product of *E. coli*. This polypeptide is 177 AA compared with 178 AA in the natural IL-11. Oprelvekin binds to the IL-11R leading to a signal transduction cascade. In preclinical models, Oprelvekin (Neumega) demonstrated potent thrombopoietic activity during compromised hematopoiesis. It is an FDA approved drug and is indicated for thrombocytopenia in individuals with non-myeloid malignancies following myelosuppressive chemotherapy (No author listed, 1998). It is also used for the therapy of inflammatory bowel disease. IL-11 has been used for acute and chronic radiation injuries as part of cytokine treatment (Seed et al., 2001). In a murine model of radiation injury, IL-11 has been shown to improve crypt counts and reduce mucosal injury (Potten, 1995; Potten, 1996). This agent has been used before as well as after irradiation, suggesting that it is both a radioprotector and a radiomitigator (Potten, 1995; Burnett et al., 2013), but its route of administration needs investigation to avoid significant toxicity (Hauer-Jensen, 2014).

Thrombopoietin

Treatment for thrombocytopenia as a result of high dose radiation exposure is an important area of radiation countermeasure development, as severe thrombocytopenia can be life-threatening and is a good indicator of mortality risk (Stickney et al., 2007). The thrombocytopenia was a better predictor of mortality of acutely irradiated rhesus NHPs when compared to comparatively measured parameters of neutropenia. There is significant discussion about the possibility that TPO or a related growth and development factor can exert significant survival benefit as demonstrated in preclinical irradiated animal models. Specifically, TPO increases survival benefits in irradiated mice. It has also been shown to increase hematopoietic recovery in the C57BL/6J strain of mice at a dose of 0.3 μg/mouse when administered either 2 h before or 2 h post-irradiation (Mouthon et al., 1999; Mouthon et al., 2002). Finally, in acutely radiation exposed victims of the Tokai-mura criticality accident, TPO has been reported to be beneficial (Nagayama et al., 2002).

Several molecules targeting TPO receptor binding sites have been developed. Nplate (also known as romiplostim) and Promacta of Amgen and Glaxo SmithKline, respectively, have been approved by the FDA to treat idiopathic thrombocytopenic purpura (Kuter, 2007). Romiplostim is a synthetic TPO agonist and is FDA-approved for the treatment of low platelet counts in individuals with immune thrombocytopenia. It binds to TPO c-Mpl receptor, preferentially stimulates platelet generation in the bone marrow (Parameswaran et al., 2014; Jacobson et al., 2017), and also possesses a peptide domain recognized by the TPO receptor linked to an Fc carrier domain that increases its plasma half-life. The pharmacodynamics of romiplostim and its effect on platelet production in rodents and NHPs (rhesus and cynomolgus) have been investigated with both intravenous (*iv*) bolus and subcutaneous (*sc*) administrations (Krzyzanski et al., 2013).

Romiplostim has been shown to protect γ-irradiated C57BL/6J mice when administered intraperitoneally (*ip*) 2 h post-irradiation and continued for 3 or 5 days as a daily administration at a dose of 50 μg/kg (Yamaguchi et al., 2018). At 30 days post-irradiation, complete blood cell counts of irradiated and romiplostim-treated mice were comparable to unirradiated mice. It was not effective, however, if treatment was started 24 h or 48 h post-irradiation (9 Gy), or if higher doses of radiation (>9 Gy) were used (Mouthon et al., 2002). In another study, this agent was found to increase mouse survival, support hematopoiesis, reduce injury to tissues, increase mesenchymal stem cells in the spleen, and suppress several miRNA linked to radiation-induced leukemogenesis (Yamaguchi et al., 2019). Furthermore, ~40% survival enhancement was observed after administration of this agent as a single dose of 30 μg/kg. Its combination with PEGylated filgrastim or more frequent dosing did not show any additional benefit (Bunin et al., 2020). In a recent study, several proteins (out of 269 proteins) were found to be increased in the serum of C57BL/6J mice (keratin, type II cytoskeletal 1, fructose-1, 6-bisphosphatase, cytosolic 10-formyltetrahydrofolate dehydrogenase, peptidyl-prolyl *cis*-trans isomerase A, glycine N-methyltransferase, glutathione S-transferase Mu 1, regucalcin, fructose-bisphosphate aldolase B and betain–homocysteine S-methyltransferase 1) exposed to a lethal dose of ^{137}Cs γ-rays whole-body radiation. Treatment with romiplostim administered *ip* daily at a dose of 50 μg/kg for 3 days

starting 2 h post-irradiation decreased these proteins. These proteins were suggested to be indicators of the high-dose radiation injury (Nishida et al., 2020).

Romiplostim and PEGfilgrastim administration, either alone or in combination, provided improvements in hematology compared with control NHPs without any treatment (Wong et al., 2020b). The combination of both drugs demonstrated the most significant hematological (particularly neutrophils and platelets) benefits. The above results supported the development of romiplostim as radiation medical countermeasures for use in humans. This agent has been used off-label in a phase II clinical study for efficacy and safety for thrombocytopenia in chemotherapy patients (Wang et al., 2012). There were a few treatment-associated adverse events resulting from romiplostim use, including cerebrovascular accidents and increases in bone marrow blasts.

In another study, different combinations of erythropoietin (EPO), G-CSF, romiplostim, and nandrolone decanoate were administered to female C57BL/6J Jcl mice 2 h post-irradiation with 7 Gy (100% lethal). The administration of romiplostim in combination with EPO and G-CSF for 5 days starting soon after radiation exposure provided 100% protection in mice when there was 100% mortality in untreated control animals. The CBC analyses demonstrated complete hematologic recovery in irradiated and drug-treated surviving animals (Hirouchi et al., 2015).

Recently, romiplostim was evaluated in male and females NHPs without blood products. Administration of romiplostim following irradiation of NHPs resulted in improved survival and hematological profiles (Wong et al., 2020a; Wong et al., 2020b). In the latest study, there were 20 males and 20 females in each treatment and vehicle group (Wong et al., 2020a). Further improvements were noted when romiplostim was used in combination with PEGfilgrastim. Survival was better in males compared with females. In January 2021, romiplostim received FDA approval for the treatment of radiation exposed adult and pediatrics patients (Amgen Inc., 2021). The recommended dose of Nplate is 10 μg/kg once as a *sc* injection as soon as possible after exposure to more than 2 Gy.

Eltrombopag (also known as Promacta) is another FDA-approved agonist of TPO receptor indicated for immune thrombocytopenia, chronic hepatitis C patient thrombocytopenia, and patients of aplastic anemia. This agent has a long half-life and is reported to be orally effective. It boosts megakaryocytes and promotes a rise in platelet counts. It has demonstrated a significant increase in platelet counts in chimpanzees when administered at 10 mg/kg/day for 5 days (Erickson-Miller et al., 2009). The development path for this agent is difficult since it is found to be effective only in chimpanzees and humans. It is not effective in other animal models. Due to the lack of access of the full array of animal models that might be applied in preclinical evaluations of the drug as a potential radiation countermeasure, its development has limitations. The species specificity of eltrombopag is due to the presence of a histidine (499 of human TpoR), which is required for binding (Erickson-Miller et al., 2009; DiCarlo et al., 2011a). There is a lysine residue in place of histidine in all other animals investigated (DiCarlo et al., 2011b). It is not easy to use chimpanzees for the development of radiation medical countermeasures or for the development of any drug due to its endangered status. Romiplostim and eltrombopag are also investigated as a treatment for thrombocytopenia of other etiologies (DiCarlo et al., 2011a; DiCarlo et al., 2011b; Liesveld et al., 2013).

Avatrombopag (Doptelet; Dova Pharmaceuticals) is used for the treatment of thrombocytopenia. This is a second-generation small molecule thrombopoietin receptor agonist that is orally bioavailable. It activates thrombopoietin receptors and increases megakaryocyte proliferation/differentiation and platelet production (DiCarlo et al., 2018; Shirley, 2018; U.S. Food and Drug Administration, 2018b; Dova Pharmaceuticals, 2019). Avatrombopag has received its FDA approval for the treatment of periprocedural thrombocytopenia with chronic liver disease. Thrombocytopenia potentially affects the management of chronic liver disease due to the increased risk of bleeding during surgery or liver biopsy. It is also recommended for immune thrombocytopenia and as an alternative to platelet transfusions (Cheloff and Al-Samkari, 2019; Dlugosz-Danecka et al., 2019; Xu and Cai, 2019; Poordad et al., 2020). Lusutrombopag (Mulpleta) is another FDA-approved thrombopoietin receptor agonist which is orally effective for thrombocytopenia in patients with chronic liver disease (Abdela, 2019; Clemons Bankston and Al-Horani, 2019). There are obvious reasons to attempt to develop these agents as pharmacologic countermeasures to acute radiation injuries (DiCarlo et al., 2018; Shirley, 2018; U.S. Food and Drug Administration, 2018a; Dova Pharmaceuticals, 2019).

ALXN4100TPO is another TPO receptor agonist that has the very useful clinical attribute of reducing the potential for the generation of endogenous TPO antibodies. It was shown to increase megakaryopoiesis and prevent radiation-induced death by annulling thrombocytopenia as well as bone marrow atrophy in the murine model (Satyamitra et al., 2011). Relative to its effect on survival of acutely irradiated mice, the drug has been shown to have a dose reduction factor of 1.32 when administered prophylactically and 1.11 when given following irradiation (Satyamitra et al., 2013). Although this agent has demonstrated efficacy as a radiation countermeasure when tested against acute gamma ray exposures (^{60}Co γ-rays), it failed to protect mice against mixed field (γ and neutron) exposures (Cary et al., 2012).

Other Agents

Metformin

Metformin is a biguanide drug used in the management of type II diabetes (Corcoran and Jacobs, 2020). It controls free radical generation and cellular metabolism, and these effects may be due to the activation of adenosine monophosphate-activated protein kinase. This agent has been demonstrated to have radiomitigative efficacy for acute radiation syndrome (Miller et al., 2014; Xu et al., 2015). Metformin stimulated hematopoietic functions and spleen colony formation when administered *ip* to C3H mice at a dose of 250 mg/kg 24 h post-total body irradiation with 7 Gy (Miller et al., 2014). Spleen colony formation was also shown when this

agent was used in combination with other antioxidant agents such as amifostine, captopril, MESNA, or N-acetyl-cysteine (NAC). Metformin administration in combination with these agents significantly increased survival. Metformin was administered 24 h post-irradiation with captopril (200 mg/kg), NAC (400 mg/kg), and MESNA (300 mg/kg). Each of these agents are FDA-approved and have well-characterized safety profiles as well. Metformin alone or in combination with other sulfhydryl agents listed above demonstrated protective efficacy when administered 24 h post-irradiation compared with efficacy for prophylactic amifostine. Metformin at a dose of 250 mg/kg/day orally one day prior to irradiation and 7 days post-irradiation with 4.0 Gy reduced DNA damage and free radical generation in mice. Such changes were linked to an increase in hematopoietic stem cells in bone marrow and stem cell function (Xu et al., 2015).

Statins

Statins are structural analogs of inhibitors of 3-hydroxy-3-methylglutarylcoenzyme A, which is a rate-limiting enzyme for the synthesis of cholesterol, and serves to upregulate low-density lipoprotein (LDL). Therefore, these very effective drugs are most commonly used clinically for reducing LDL (Diomede et al., 2001; Gotto, 2003; Grobbee and Bots, 2003) and, consequently, to treat atherosclerosis and hypercholesterolemia (Sizar et al., 2020). In addition, statins are well known to reduce the expression of chemokines. Recruitment of inflammatory cells has also been shown to be reduced by statins in various tissues. Lovastatin treatments of irradiated mice (15 Gy whole-lung irradiation) starting immediately after irradiation or 8 weeks post-irradiation (three times a week) demonstrated a reduction in lung tissue lymphocytes and macrophages. This treatment also improved rates of survival, decreased collagen content, and decreased chemoattractant protein-1 compared to the control group (Williams et al., 2004). Further, the statin treatments appeared to dampen the radiation-induced increases in chemoattractant protein-1 levels.

Simvastatin treatments have been shown to mitigate, to a limited extent, radiation-induced enteric injury, as evidenced by improved structural integrity of the mucosa, reduced neutrophil infiltration (myeloperoxidase-positive cells), decreased thickening of the intestinal wall as well as subserosa, and reduced accumulation of collagen I (Wang et al., 2007). The effect of simvastatin was pronounced for delayed injury as compared to injury that manifests early. Simvastatin treatments ameliorate intestinal damage in thrombomodulin mutant mice. This suggests that the protective effect of this drug is independent of protein C activation. Accordingly, statins, in general, are being considered for clinical evaluation to reduce the side effects of targeted irradiation of the intestine and on other normal tissues as well.

Pentoxifylline

Pentoxifylline is a derivative of methyl xanthin and is shown to possess anti-inflammatory, immunomodulating, and antioxidant properties (Ozturk et al., 2004; Hepgül et al., 2010). It is also known to have phosphodiesterase inhibiting activity. It has FDA approval for claudication and associated arterial disease of the limbs (McCarty et al., 2016). It also reduces the risk of radiation injury in lungs of both experimental animals and radiotherapy patients when administered orally (Koh et al., 1995; Rube et al., 2002; Ozturk et al., 2004). When administered thrice a day at a dose of 400 mg/kg to radiotherapy patients, pentoxifylline is helpful in acute and chronic radiation injuries (Ozturk et al., 2004). In preclinical experimental models, pentoxifylline treatment at a dose of 100 mg/kg/day reduced tumor necrosis factor-α protein and mRNA. In a murine model, it raised glutathione levels and inhibited lipid peroxidation after radiation exposure. Lipid peroxidation may be helpful for the radioprotective efficacy of pentoxifylline (Rube et al., 2002; Hepgül et al., 2010).

It has been shown that treatment with pentoxifylline and α-tocopherol has advantageous effects on myocardial fibrosis induced by irradiation (radiation-induced heart disease) as well as beneficial effects on ventricular function in a preclinical, small animal (rat) model (Boerma et al., 2008).

The combination of γ-tocotrienol and pentoxifylline increased bone marrow G-CSF, IL-1α, IL-9, and IL-6 in the murine model. This combination appeared to be effective in modifying the extent of intestinal injury as well as modulating vascular peroxynitrite production following acute irradiation (Berbée et al., 2011). However, survival studies of mutant mice deficient in endothelial nitric oxide synthase demonstrated that endothelial nitric oxide synthase was not needed for protection of these two agents to lethal irradiation. Combined treatments with both agents increased survival over a single treatment of γ-tocotrienol. However, combined treatments appeared not to have reduced GI injury or vascular oxidative stress beyond what was provided by γ-tocotrienol alone. In terms of the radioprotective efficacy of the combined treatment on the hematopoietic system, the treatment course was tested in the murine model of whole-body γ-radiation (Kulkarni et al., 2013). The combination of these two agents was effective when pentoxifylline was administered 15 min prior to irradiation and γ-tocotrienol 24 h before irradiation. The dose of pentoxifylline was 200 mg/kg and the γ-tocotrienol dose was also 200 mg/kg. The dose reduction factor of this combination was 1.5. Hematopoietic recovery was better in the combined treatment group compared to the single treatment (Kulkarni et al., 2013). Mevalonate was used to abrogate the inhibitory effect of γ-tocotrienol on 3-hydroxy-3-methyl-glutaryl-CoA reductase, and calmodulin was used to reverse the inhibitory effects of phosphodiesterase by pentoxifylline. Mevalonate had no effect on the radioprotection of the γ-tocotrienol and pentoxifylline combination. Since calmodulin abrogated the beneficial effects of these two drug combinations, it was suggested that the mechanism of radioprotection by these drugs involves inhibition of phosphodiesterase.

Xigris

Xigris (Drotrecogin Alfa - active ingredient in Xigris, a recombinant form of human activated protein C) has FDA approval for the indication of sepsis and acute organ dysfunction with higher risk of mortality (Aneja and Fink, 2007). It is not indicated for sepsis in patients with a lower possibility of mortality (Bernard et al., 2001; Griffin et al., 2006).

Findings of a study using the murine model suggest that pharmacologic augmentation of the protein C pathway by recombinant thrombomodulin and activated protein C may offer an approach for the mitigation of radiation-induced tissue injury and lethality (Geiger et al., 2012).

Diclofenac Sodium

Diclofenac sodium {2-[(2,6-dichlorophenyl)amino] benzeneacetic acid, monosodium salt} is a derivative of benzeneacetic acid. It is a non-steroidal anti-inflammatory agent and has FDA approval for osteoarthritis, rheumatoid arthritis, and ankylosing spondylitis (US Food and Drug Administration, 2020a). Recently, the FDA approved this drug (diclofenac sodium topical gel, 1%) for non-prescription (OTC, over-the-counter) use for the treatment of arthritic pain. This process is known as switch of prescription (Rx)-to-OTC (Novartis, 2005). Such a prescription drug switch to non-prescription status can be done only after demonstrating that the medication is safe as well effective, and can be used as self-medication based on the description in the drug label.

This agent has demonstrated significant radioprotective efficacy against whole-body 9 Gy irradiation in C57BL/6 mice (Alok et al., 2013). Recently, it has also been shown to reduce formation of dicentric chromosome, γ-H2AX foci, and micronuclei in response to gamma-radiation exposure in peripheral blood lymphocytes of humans. Both pre and post-irradiation treatments demonstrated efficacy, suggesting that it may work to limit radiation-induced clastogenesis when administered either prophylactically, prior to irradiation, or mitigatively, shortly following exposure (Alok and Agrawala, 2020).

CpG-ODN

Bacterial DNA is one of the principal pathogen associated molecular patterns (PAMPs). The recognition of PAMPs is mediated through various Toll-like receptor (TLR) members (Underhill and Ozinsky, 2002; Vasselon and Detmers, 2002). The unmethylated CpG motifs occurrence is higher in the genomes of prokaryotes. This is due to the differences in the methylation as well as the use of dinucleotides. (Cardon et al., 1994). The innate immune system detects such unmethylated CpG motifs through TLRs (Hemmi et al., 2000; Takeshita et al., 2001). During an infection, the release of unmethylated CpG-DNA is known as a danger signal. Such a danger signal to the innate immune system generates a defensive immune response for the host (Wagner, 1999). CpG motifs in synthetic oligodeoxynucleotides (ODN) stimulate a response similar to bacterial DNA, and have ODNs have various therapeutic uses (Krieg et al., 1995; Klinman et al., 1996). Such CpG ODNs have US FDA approval as adjuvants for vaccines (Fehér, 2019). The studies with CpG ODN demonstrate that they stimulate innate as well as adaptive immune responses (Klinman, 2004). CpG ODNs interact with TLR-9 and are rapidly internalized by the cells, and they also interact with TLR-9 on the surface of endocytic vesicles (Hemmi et al., 2000; Ishii et al., 2002). Three different classes of CpG ODNs have been characterized: 'K,' 'D,' and 'C' (Klinman, 2004). These agents have been investigated as radiation countermeasures and were found to ameliorate hematopoietic and intestinal injuries induced by radiation exposure in the murine model (Zhang et al., 2011a; Zhang et al., 2011b; Zhang et al., 2013).

Auranofin (Ridaura)

Auranofin is an anti-inflammatory, anti-cancer, neuro-protective, and cardioprotective agent (Han et al., 2008; Madeira et al., 2013; Liu et al., 2014; Hu et al., 2018). It inhibits DNA damage-induced apoptosis in the gut by inhibiting acetylation of p53; it also has an anti-inflammatory effect in colitis (Debnath et al., 2012; Nag et al., 2019). It induces mRNA expression of the heme oxygenase-1 enzyme to promote anti-inflammatory action and reduce H_2O_2 production to reduce oxidative stress (Madeira et al., 2013). Ridaura is approved for the treatment of rheumatoid arthritis (Nardon et al., 2016). Auranofin has demonstrated radioprotective activity within gut tissue against a low LET (linear energy transfer) clinically relevant dose of radiation in the murine model (Nag et al., 2019).

Regulatory Agency Approved Drugs Under Redevelopment for Additional Clinical Indications or Currently Being Investigated for Repurposing for DEARE

Exposure to a high dose of irradiation can cause ARS, a serious clinical syndrome carrying elevated mortality risk. Individuals that are fortunate enough to survive ARS often fall subject to a number of secondary, evolving post-exposure disease states, as documented in various mammalian species, and that are characterized by specific, manifest morbidities and their associated increased mortality risks. Therefore, surviving ARS carries additional risks that often rise with time and with often dire consequences. Such long-term, 'late-effects' of radiation exposures have been studied extensively over many decades starting from the dawn of the nuclear age, but this complex of diseases has renewed interest (and has been in part relabeled/recharacterized as 'delayed acute radiation effects' or DEARE) of late due to the advent of potential preventive treatments (Medhora et al., 2012; Singh and Seed, 2020b). This disease complex, this syndrome, DEARE, expresses as chronic illnesses involving several important organ systems including, but not limited to the lung, kidney, heart, and GI tract (MacVittie, 2015; MacVittie et al., 2019; Unthank et al., 2019). Expression of delayed effects takes several months to years, and ultimately results in multi-organ failure and mortality. The lung from animals with DEARE demonstrates pneumonitis and fibrosis, and the development of countermeasures for such an indication is very important. There are a several drugs under development for DEARE and its subclinical entities.

Angiotensin-Converting Enzyme Inhibitor (ACEi) - Captopril

ACEi has been shown to mitigate late-arizing radiation associated injuries in various organs/organ systems prone to manifest such delayed/late effects, e.g., kidney and lung (Moulder et al., 1993a; Geraci et al., 1995; Molteni et al., 2000; Moulder et al., 2007). Captopril is an ACEi containing a sulfhydryl-analog of proline,

and it is known to reduce blood pressure. This agent has FDA approval for the indication of hypertension (U.S. Food and Drug Adsministration, 2015). Usually, ACEi has been evaluated for possible radioprotective/radiomitigative properties. Captopril increases kidney function in animal models of radiation injury (Robbins and Hopewell, 1986; Cohen et al., 1992; Moulder et al., 1993b; Robbins and Diz, 2006; Rosen et al., 2015). The agent has been extensively investigated in various animal models of different organ injuries as a result of radiation exposure in several laboratories (Moulder and Cohen, 2007; Ghosh et al., 2009; Davis et al., 2010; Moulder et al., 2011; Kma et al., 2012; Medhora et al., 2012a; Medhora et al., 2014; van der Veen et al., 2015). Captopril has also demonstrated the mitigation of various parameters of radiation-induced lung injury in several animal models (Ward et al., 1988; Ward et al., 1990). It has also been shown to reduce renal failure in patients undergoing radiation therapy (Cohen et al., 2008). Captopril administered with drinking water (140–180 mg/m^2/day, comparable with clinical dose) has a dose modifying factor of 1.07–1.17 for survival at 80 days. Its dose modifying factor for tachypnea at 42 days after a single dose of X-ray exposure is 1.21–1.35 (Medhora et al., 2012b).

Captopril and perindopril, another ACEi, have been shown to control radiation-induced injury through the recovery of various blood cell components (Charrier et al., 2004; Davis et al., 2010). Such recovery was linked to the improved survival of progenitors. Its action may be partly due to reduction in inflammation (Zakheim et al., 1975) or the transient quiescence of some types of cells (Chisi et al., 2000; Davis et al., 2010). The effects of ACEi drugs on radiation-induced DNA damage have not been demonstrated (Day et al., 2013). Incoming data suggests that administration of low doses of captopril as late as 48 h post-irradiation for 2 weeks improves survival in mice, and such increased survival is also linked with hematopoietic recovery as well as reduction in inflammation (McCart et al., 2019). Captopril, lisinopril (Prinivil), enalapril (Vasotec), and ramipril (Altace) all appear to mitigate radiation-induced nephropathy in rats. Captopril has been shown to be a better mitigator than lisinopril, enalapril, or ramipril. Fosinopril is not an effective radiomitigator for irradiation associated pneumonitis, and it does not mitigate radiation-induced nephropathy (Moulder et al., 2014). These results from a large number of studies demonstrate that captopril is a drug to mitigate radiation injury in humans. In another radiation study of delayed effects, captopril, enalapril, and fosinopril have been shown to increase relative rates of survival against lethal irradiation (Medhora et al., 2014). The use of enalapril in rats at a clinically relevant dose after partial-body irradiation has shown promise for protecting the lungs and kidneys (Cohen et al., 2016).

Captopril has also been evaluated as a countermeasure in a murine model of irradiation plus skin burn (Islam et al., 2015). Results of this study demonstrated that captopril may act in a different way in two types of injuries; namely, irradiation alone and radiation plus a skin burn injury (combined injury). This study also demonstrated that captopril along with an antibiotic may be inappropriate for treating combined injury (Islam et al., 2015).

Recently, a study was performed with ramipril, another ACEi approved by the FDA, investigating the drug's potential mitigative actions on irradiation associated myelopathy of the cervical spinal cord model using female Sprague Dawley rats (Saager et al., 2020). Contrary to other ACEi, ramipril (more specifically, its active form ramiprilat) crosses the blood brain barrier (BBB) (Nordström et al., 1993). Administration of ramipril reduced the frequency of paralysis at higher photon doses (LINAC - linear accelerator) and also for exposures with high-LET carbon ions, suggesting that ramipril's effect is independent of the radiation quality (Saager et al., 2020).

Surfaxin

Respiratory distress syndrome (RDS) is an important cause of mortality in neonates. Surfaxin (lucinactant) is a synthetic, peptide-containing surfactant approved by the FDA in 2012, and it is used clinically for the prevention of infantile RDS (Piehl and Fernandez-Bustamante, 2012). Because acute radiation-induced lung injury commonly manifests as acute pneumonitis and pulmonary fibrosis, and because surfactant is a well-recognized natural physiologic protectant of lung tissue that is often depleted during various pulmonary pathophysiologic conditions, investigators explored the possibility that therapeutic doses of surfactant (Surfaxin/lucinactant) might well mitigate subsequent evolving lung disease. This concept (mitigative potential of lucinactant) has been tested in a murine model for its mitigative actions on lung injuries. Intranasal administration of KL4 surfactant (lucinactant, 120 mg/kg, twice daily) to C57BL/6 mice after irradiation preserved lung function and reduced lung inflammation and oxidative stress, along with corresponding decreases in total white cell counts, absolute neutrophil counts, and in bronchoalveolar lavage fluids. This agent appeared to be a countermeasure for the mitigation of radiation-induced lung injury (Christofidou-Solomidou et al., 2017).

Diethylcarbamazine Citrate

Diethylcarbamazine citrate (DEC) is an antifilarial drug used to treat filariasis (Hawking, 1979). Since the prevalence of lymphatic filariasis is rare in the US, DEC is no longer approved by the FDA, but physicians can obtain this drug from the Center for Disease Control once the patient is confirmed to have the disease based on positive laboratory diagnostic results. In addition, it has anti-fibrotic, antioxidative, anti-inflammatory, and anti-carcinogenic properties (Queto et al., 2010). It mitigates inflammation in the lung because it reduces lipoxygenase, cyclooxygenase enzymes, and nitric oxide in tissue (Queto et al., 2010). DEC effectively reduces the oxidative stress and inflammation in radiation-induced lung injury at a dose of 10 mg/kg in mice. DEC did not show any side effects. However, at a dose of 50 mg/kg or 100 mg/kg, adverse effects were noted (Farzipour et al., 2020). DEC was administered to test animals once a day for 8 days and the treated mice were then irradiated (total-body irradiation, X-rays, 5 Gy) on day 9. The efficacy of DEC was investigated by evaluating oxidative stress by histopathological

examination one week after irradiation using lung tissue. Biochemical data revealed increased production of nitric oxide, malonyldialdehyde, and protein carbonyl levels in irradiated animal lungs. In untreated control animals, histopathology examinations revealed acute lung injury along with increased numbers of tissue infiltrating inflammatory cells. DEC treatments prior to radiation exposure appeared to have mitigated the oxidative stress and histological injury within the irradiated animals. Surprisingly, the optimal radioprotective efficacy was seen at 10 mg/kg compared with higher doses. The highest dose of 100 mg/kg did not show protective or anti-inflammatory effects in mice, while the intermediate dose, 50 mg/kg, proved to be somewhat less effective than the lowest tested dose of 10 mg/kg. This study provides suggestive observations indicating that DEC has antioxidant and anti-inflammatory properties at a dose of 10 mg/kg, and that it might be considered for the treatment of radiation-induced lung injury.

Regulatory Agency Approved Drugs Under Redevelopment for New Indications Related to Cutaneous Injuries or Being Evaluated for Possible Repurposing

Radiation exposures of skin with significantly higher doses of radiation (>15–20 Gy) result in a discrete clinical manifestation characterized by initial erythema, followed by blistering and necrosis. Usually, such necrosis appears 10–30 days after exposure and depends on the extent and quality of irradiation, but in extreme situations, necrosis can appear within 48 h (Peter and Gottlöber, 2002). Peter and Gottlober described the guiding diagnostic and therapeutic principles for individuals with cutaneous radiation injuries (Peter and Gottlöber, 2002). A current strategy, however, employs just two basic steps: first, the initial surgical removal excision of the necrotic tissue in order to prevent recurrence and second, a more recent therapeutic modality that employs treatments with autologous keratinocytes plus allogeneic stem cell administration (Lataillade et al., 2007; Bey et al., 2010). Swine are appropriate for studying radiation-induced cutaneous injury, and the data from NHPs for cutaneous effects are limited. There are several radiation medical countermeasures demonstrating efficacy for the cutaneous injury (Singh and Seed, 2017).

Silverlon

Argentum Medical has received FDA approval for multiple indications for Silverlon over a period of more than 20 years. In 2019, it was repurposed for blister injuries caused by sulfur mustard (Argentum Medical, 2019). It is extensively used to manage acute skin wounds and first and second-degree thermal burns. There is interest to repurpose Silverlon burn and wound dressings for large scale scenarios as a result of chemical, thermal, and radiological exposure events (DiCarlo et al., 2018). Silverlon burn dressings are elastic bandages of nylon with incorporated metallic silver. Silverlon burn dressings and Silverlon burn gloves have been extensively used by the US military (Pozza et al., 2014; Aurora et al., 2018).

Regulatory Agency Approved Drugs Under Redevelopment for New 'Late Effects' Indications or Being Evaluated for Possible Repurposing

Exposures to chronic irradiation are either continuous or intermittent and can cause a wide variety of serious injuries, especially those at moderate or low dose rates, that often remain latent for prolonged periods, but evolve with time into potentially fatal diseases. Due to the basic nature of these injuries, often involving radiation-induced changes within genomes of targeted cells within key organ systems of the body, the diseases that eventually manifest are distinct from those disease entities that arise relatively early following acute, intense radiation exposures. We are referring to, of course, a prominent category of radiation-induced late-effects, namely cancer (Rowley, 1985; Seed et al., 1985; Upton, 1985; Baskar et al., 2012; Jargin, 2014; Ozasa et al., 2019; Jargin, 2020). In terms of radiation induction, these late-arizing cancers are often described as being stochastic in nature, with the risk of developing the disease (cancer) following exposure but rather probabilistic relative to the size of the exposed population. This contrasts to the early arising, deterministic-type diseases in which disease risk is directly proportional to the level and intensity of the exposure to the individual. Both acute or chronic exposures to relatively low doses of radiation does not generally cause immediate health problems, but such radiation exposure is a contributing factor for cancer risk to individuals (National Research Council, Biological Effects of Ionizing Radiation, 1990; Khan et al., 2019). It is important to note that a risk that is low for an individual can still result in large numbers of additional cancers in a large population (vs. risk for the population) over an extended period of time.

It is known that combining radiotherapy with chemotherapeutic drugs (e.g., cisplatin) generally improves efficacy for various cancer treatments. However, such a combined treatment strategy comes at a cost due to increased toxicity. Nevertheless, there are opportunities to investigate drug combinations that may increase the benefit of radiotherapy without increasing toxicity inordinately (Khan et al., 2019). Several classes of anti-carcinogenic/anti-mutagenic drugs are being investigated, and a large number of such agents are in preclinical stages of evaluation. The important agents among such drugs are phosphorothioates (amifostine/WR1065) (Grdina et al., 1985; Diamond et al., 1996; Kataoka et al., 1996; Grdina et al., 2000; Grdina et al., 2002). The phosphorothioates are potent radioprotectors when used prior to radiation exposure. As mentioned earlier, such agents have substantial side-effects and toxicity, specifically performance decrement, when administered at doses needed for survival benefits. Investigations from several laboratories over a long period of time have suggested that these drugs can be used post-irradiation and can still preserve a degree of their anti-carcinogenic/anti-mutagenic efficacy, with such effects achieved with much lower and less toxic doses (Grdina et al., 2002; Singh and Seed, 2019). Other agents under development for repurposing include aspirin, vascular endothelial growth factor inhibitors, tumor hypoxia modifiers, immune-checkpoint inhibitors, and DNA double

strand break repair modifiers (Khan et al., 2019). Such strategies offer the potential to enhance treatment outcomes for patients with malignancies, principally by decreasing the extent of fractional irradiation, thus reducing radiation-induced side effects. Another benefit would be the decrease in overall cost of treatment. In brief, the success of repurposing such drugs represents "low hanging fruit" in the area of drug development.

Regulatory Agency Approved Drugs Under Redevelopment or Being Repurposed for New Clinical Indications Related to Radiation Combined Injury

Radiation combined injury is a condition where radiation injury is combined with another insult such as burns, blunt trauma, skin wounds, infection, or hemorrhage. Combined injury is usually more lethal compared with lethality as a result of irradiation alone, or another insult inflicted without irradiation (Anno and Bloom, 2002; Knudson et al., 2002a; Knudson et al., 2002b; DiCarlo et al., 2010). Combined injury accelerates fluid imbalance, cellular injury, circulation failure, myelosuppression, and disorder of organ function leading to multi-organ failure. Regardless of the advancement of knowledge of the radiological injury, there is limited knowledge for therapeutics for combined injury. We do not have an FDA-approved countermeasure for such injuries. Efforts are continuing to develop countermeasures for combined injuries either by developing new countermeasures or repurposing FDA-approved drugs for other indications.

Ciprofloxacin

Ciprofloxacin (Cipro) is an FDA-approved fluoroquinolone for the treatment of Gram-negative bacterial infection. It has immunomodulatory and anti-inflammatory potential rather than just being an antibacterial agent (Lahat et al., 2007), and it is also known to enhance neutrophil recovery after bone marrow transplants, suggesting its probable repurposing as a CBRN (chemical, biological, radiological, and nuclear) countermeasure (Imrie et al., 1995). It has been tested in a murine model of radiation combined injury (irradiation and wound). Cipro-treated mice demonstrated enhanced survival when treatment was started 2 h after insult, and such treatment was continued for three weeks (Fukumoto et al., 2014). Its treatment enhanced mouse survival to 80% compared to 35% survival in the control group.

Cipro induced erythropoietin in the kidney and bone morphogenetic protein-4 in macrophages of spleen. Also, its treatment increased $CD71^{+}$ colony-forming erythrocytic progenitors (colony forming unit-erythroid; CFUe) in the spleens of treated mice (Fukumoto et al., 2014). Cipro ameliorated combined injury-induced progressive anemia by day 10 post-irradiation. In another study, Cipro treatment (90 mg/kg, q. d., *po*, after combined injury) reduced pro-inflammatory cytokines and chemokines including IL-6 and KC (keratinocyte-derived chemokine, called IL-8 in humans), and enhanced IL-3 production in B6D2F1/J mice (Fukumoto et al., 2013). Animals treated with Cipro demonstrated a higher repopulation of bone marrow cells, low apoptosis, and autophagy in ileal villi. Systemic bacterial infections were mitigated, along with the mitigation of the IgA production. Cipro treatment protected 100% of mice compared to 80% protection in vehicle-treated mice. This report suggested that Cipro may prove to be a useful therapeutic for combined injury. Cipro has also been reported to enhance recovery from hemorrhagic radiation proctitis in radiotherapy patients (Sahakitrungruang et al., 2011). The study suggests that this rather simple antibiotic treatment is both effective and safe for proctitis induced by radiation-exposure. There was improvement in the extent of rectal bleeding, bowel frequency and urgency, as well as diarrhea. Additionally, Cipro has been investigated in the NHP model at the Armed Forces Radiobiology Research Institute using irradiated animals, but results are not yet published.

In addition to the drugs discussed above, there are several dietary supplements (such as melatonin, available without a prescription as an OTC drug) and agents under the GRAS (generally recognized as safe) category that can be developed much faster compared to other conventional prescription drugs (Williams G. M. et al., 2016).

Regulatory Agency Approved Drugs Under Redevelopment or Repurposing for Treatments of Patients Subjected to Internally Deposited Radionuclides

Internal contamination with radionuclides remains a threat to civilians and the military alike, as such agents may be internalized through inhalation, ingestion, and exposure to wounds. Internalized radionuclides resulting from either radiological accidents or from a deliberate radiological/nuclear attack would require immediate medical treatment. Current treatment options vary and some carry treatment risks. However, the benefits of these treatments generally outweigh the risks. There are only four FDA-approved agents to either prevent radionuclide uptake or to treat individuals with internalized radionuclides: Prussian Blue (ferric hexacyanoferrate), potassium iodide (KI; ThyroShield), trisodium zinc diethylenetriaminepentaacetate (Zn-DTPA), and trisodium calcium diethylenetriaminepentaacetate (Ca-DTPA) (Centers for Disease Control and Prevention, 2016). These drugs are helpful to block the uptake, dilute, bind, or chelate internalized radionuclides. Apart from the use of KI, there is still scant evidence that the above listed agents provide substantial preventive/therapeutic benefits to victims with internalized radionuclides.

Although a limited number of agents have been FDA-approved, several pharmacologic countermeasures are under development for heavy metal toxicities and perhaps internalized radionuclides as well (Singh et al., 2017a; Singh et al., 2017b; Singh and Seed, 2017). Desferal, deferoxamine mesylate (N-[5-[3-[(5 aminopentyl)hydroxycarbamoyl] propionamido]pentyl]-3-[[5-(Nhydroxyacetamido)pentyl] carbamoyl]propionohydroxamic acid monomethanesul-fonate

(salt)) is an FDA-approved iron-chelating agent (Novartis, 2011). Cuprimine (Penicillamine - 3-mercapto-D-valine) is an FDA-approved agent for the indication of Wilson's disease (for removal of excess copper by binding), to reduce cystine excretion, and to treat rheumatoid arthritis (MERCK and Co, 2004). This agent is also being evaluated for the treatment of internalized radionuclides.

DISCUSSION

Though we are in the age of personalized medicine that attempts to tailor therapies for individuals and specific clinical indications, therapeutic agents that target a large number of diseases regardless of differences in individual patient backgrounds would remain vital for the treatment of a large number of common disorders. Repurposing drugs is defined as 'finding another novel therapeutic indication for a drug that has been already approved for another indication by a regulatory authority' (Oprea and Mestres, 2012). This is a novel strategy for finding new therapeutic uses for existing agents that can capitalize on prior investments. This approach is of interest to the drug industry due to the associated monetary benefits to the corporate 'bottom-line'. Certain clinical applications may be more appropriate for repurposing than others due to the differences in side effects and safety of the drugs involved. These activities are beyond the identification of new targets for existing drugs of another indication. As stated above, despite approximately 90% of drugs failing after progressing to advanced clinical trials and prior to subsequent regulatory approval, it remains encouraging to note that there are still a large number of experimental therapeutic molecules appropriate for human use currently under investigation. There are more than 10,000 approved experimental drugs that can potentially be repurposed. Repurposing is an especially important drug development strategy for rare diseases that require therapeutic options, but have limited resources (Sharlow, 2016).

Radiation induced diseases, especially those that originate from accidental or unwanted exposures, would certainly fall into this category of 'rare diseases'. Nevertheless, the term 'rare' is clearly a relative term in the context of such unwanted radiation exposures; for example, going from a few individuals exposed accidentally during an industrial accident to potentially thousands of individuals exposed as a consequence of a large scale radiological/nuclear attack by terrorists on an urban center. Regardless, there is a real and urgent need to have additional safe and effective pharmaceuticals in storage within the National Strategic Stockpile. It would seem that at present, we (the United States of America) are woefully understocked and ill-prepared for a major radiological/nuclear exposure event. It is our opinion that additional resources need to be allocated by the federal government along with appropriate leadership, and cooperative alliances between the responsible federal agencies and the pharmaceutical industry must be established in order to correct this glaring medical deficit that most certainly impacts national security.

The development of new pharmacologic entities *de novo* for rare diseases is not generally very appealing to large pharmaceutical companies due to the minimal profitability of such endeavors and the associated impact on their financial 'bottom-lines'. Accordingly, drug repurposing represents an attractive strategy to accelerate the progress of a drug from the laboratory to the clinic, as this pathway bypasses many of the steps of conventional drug development, leading to reduced time and significant cost saving for drug regulatory approval. The examples of repurposing Neupogen, Neulasta, and Leukine as radiomitigators for H-ARS following the FDA Animal Rule demonstrate the advantages of repurposing any widely used drugs that have enormous preclinical and clinical data available, as well as the experience of using the agents in millions of patients over several decades. This should serve as a success story for the drug development of radiation medical countermeasures following the repurposing route (Farese and MacVittie, 2015; National Institute of Allergic and Infectious Diseases, 2015; Singh and Seed, 2018; Gale and Armitage, 2021).

Drug repurposing has been facilitated by the availability of FDA-approved drug libraries, and there are several commercial libraries available for these repurposing efforts (Collins, 2011). However, there are major challenges including regulatory hurdles that need to be tackled (Williams G. M. et al., 2016). There are numerous reasons for failures in the repurposing field which include patent considerations, regulatory considerations, and organizational hurdles in addition to the legal and intellectual property barriers.

With respect to the attempts to repurpose drugs as potential medicinals that might impact public health and overall national security (e.g., CBRN medical countermeasures), strong input from the federal government in active collaboration with the pharmaceutical industry is absolutely essential in order to achieve success in bringing such critically needed medicinals through advanced testing, regulatory approval, and to the shelves of the National Pharmaceutical Stockpiles; and, of course, to the commercial marketplace itself.

Sometimes the repurposing of a drug becomes complicated due to a variety of commercial concerns (and not necessarily 'public health or national security concerns'); for example, a concern of the developing/sponsoring pharmaceutical organization is that new indications may undermine existing markets of the drug. The sponsoring corporation of a blockbuster pharmaceutical is usually not interested in another indication, especially for rare diseases. Drug sponsoring corporations become wary that during the investigation for repurposing, some information may come to light which can adversely affect the existing market of the drug. Anticipated lower drug prices for the repurposed drug, short patent duration, and overall low return on investment are some of the many reasons that the drug industry tends to be uninterested in repurposing endeavors. Another important aspect is the intellectual property rights (IPR) (Nosengo, 2016). Though some aspects of IPR may no longer be binding or cannot be used, several other patenting/IPR aspects for

different dosing, different administration routes, poly-pharmacy approach, and combined usage are available to protect the interest of repurposing. Drug development professionals agree that the perfect candidate for a repurposing program would be a safe and off-patent pharmaceutical agent for which a novel target is known. The efficacious dose of such a drug for a new indication should be within the dose range for an already-approved indication (Oprea and Mestres, 2012).

AUTHOR CONTRIBUTIONS

VS and TS drafted the manuscript and reviewed. Both authors have read and approved the final version of the manuscript.

FUNDING

The authors acknowledge the intramural research support from the Uniformed Services University of the Health Sciences/Armed Forces Radiobiology Research Institute (AFR-B2-9173) to VS.

ACKNOWLEDGMENTS

The opinions or assertions contained herein are the private views of the authors and are not necessarily those of the Uniformed Services University of the Health Sciences or the Department of Defense. We are thankful to Jatinder Singh for literature searches and to Alana Carpenter for editing the manuscript.

REFERENCES

Abdela, J. (2019). Current Advance in Thrombopoietin Receptor Agonists in the Management of Thrombocytopenia Associated with Chronic Liver Disease: Focus on Avatrombopag. *Clin. Med. Insights Blood Disord.* 12, 1179545X1987510. doi:10.1177/1179545X19875105

Agarwal, A. B., and McBride, A. (2016). Understanding the Biosimilar Approval and Extrapolation Process-A Case Study of an Epoetin Biosimilar. *Crit. Rev. oncology/hematology* 104, 98–107. doi:10.1016/j.critrevonc.2016.04.016

Ali, R., Mirza, Z., Ashraf, G. M., Kamal, M. A., Ansari, S. A., Damanhouri, G. A., et al. (2012). New Anticancer Agents: Recent Developments in Tumor Therapy. *Anticancer Res.* 32, 2999–3005.

Allio, T. (2016). Product Development under FDA's Animal Rule: Understanding FDA's Expectations and Potential Implications for Traditional Development Programs. *Ther. Innov. Regul. Sci.* 50, 660–670. doi:10.1177/2168479016641717

Alok, A., and Agrawala, P. K. (2020). Repurposing Sodium Diclofenac as a Radiation Countermeasure Agent: a Cytogenetic Study in Human Peripheral Blood Lymphocytes. *Mutat. Res.* 856-857, 503220. doi:10.1016/j.mrgentox.2020.503220

Alok, A., Adhikari, J. S., and Chaudhury, N. K. (2013). Radioprotective Role of Clinical Drug Diclofenac Sodium. *Mutat. Research/Genetic Toxicol. Environ. Mutagenesis* 755, 156–162. doi:10.1016/j.mrgentox.2013.06.015

Amgen Inc. (2015a). Neulasta (Pegfilgrastim) Injection for Subcutaneous Use. Available at: http://pi.amgen.com/united_states/neulasta/neulasta_pi_hcp_english.pdf (Accessed November 19, 2015).

Amgen Inc. (2015b). Neupogen (Filgrastim) Injection for Subcutaneous or Intravenous Use. Available at: http://pi.amgen.com/united_states/neupogen/neupogen_pi_hcp_english.pdf (Accessed April 02, 2015).

Amgen Inc. (2021). NPLATE® (Romiplostim) for Injection, for Subcutaneous Use. Available at: https://www.accessdata.fda.gov/drugsatfda_docs/label/2021/125268s167lbl.pdf (Accessed January 29, 2021).

Aneja, R., and Fink, M. P. (2007). Promising Therapeutic Agents for Sepsis. *Trends Microbiol.* 15, 31–37. doi:10.1016/j.tim.2006.11.005

Anno, G. H., and Bloom, R. M. (2002). Combined Effects Modeling of Ionizing Radiation and Biological Agent Exposures. *Mil. Med.* 167 (2 Suppl. l), 107–109. doi:10.1093/milmed/167.suppl_1.107

Argentum Medical (2019). Argentum Medical Announces 510(k) Clearance of Silverlon Burn and Wound Care Products for Vapor Sulfur Mustard Indication. Available at: https://www.silverlon.com/newsroom/argentum-medical-announces-510k-clearance-of-silverlon-burn-and-wound-care-products-for-vapor-sulfur-mustard-indication (Accessed June 23, 2020).

Aurora, A., Beasy, A., Rizzo, J. A., and Chung, K. K. (2018). The Use of a Silver-Nylon Dressing during Evacuation of Military Burn Casualties. *J. Burn Care Res.* 39, 593–597. doi:10.1093/jbcr/irx026

Baskar, R., Lee, K. A., Yeo, R., and Yeoh, K.-W. (2012). *Cancer* and Radiation Therapy: Current Advances and Future Directions. *Int. J. Med. Sci.* 9, 193–199. doi:10.7150/ijms.3635

Berbée, M., Fu, Q., Garg, S., Kulkarni, S., Kumar, K. S., and Hauer-Jensen, M. (2011). Pentoxifylline Enhances the Radioprotective Properties of γ-Tocotrienol: Differential Effects on the Hematopoietic, Gastrointestinal and Vascular Systems. *Radiat. Res.* 175, 297–306. doi:10.1667/RR2399.1

Bernard, G. R., Vincent, J.-L., Laterre, P.-F., LaRosa, S. P., Dhainaut, J.-F., Lopez-Rodriguez, A., et al. (2001). Efficacy and Safety of Recombinant Human Activated Protein C for Severe Sepsis. *N. Engl. J. Med.* 344, 699–709. doi:10.1056/NEJM200103083441001

Bey, E., Prat, M., Duhamel, P., Benderitter, M., Brachet, M., Trompier, F. o., et al. (2010). Emerging Therapy for Improving Wound Repair of Severe Radiation Burns Using Local Bone Marrow-Derived Stem Cell Administrations. *Wound Repair Regen.* 18, 50–58. doi:10.1111/j.1524-475X.2009.00562.x

Boerma, M., Roberto, K. A., and Hauer-Jensen, M. (2008). Prevention and Treatment of Functional and Structural Radiation Injury in the Rat Heart by Pentoxifylline and Alpha-Tocopherol. *Int. J. Radiat. Oncol. Biol. Phys.* 72, 170–177. doi:10.1016/j.ijrobp.2008.04.042

Bogo, V., Jacobs, A. J., and Weiss, J. F. (1985). Behavioral Toxicity and Efficacy of WR-2721 as a Radioprotectant. *Radiat. Res.* 104 (2 Pt 1), 182–190. doi:10.2307/3576614

Brizel, D. M., Wasserman, T. H., Henke, M., Strnad, V., Rudat, V., Monnier, A., et al. (2000). Phase III Randomized Trial of Amifostine as a Radioprotector in Head and Neck Cancer. *J. Clin. Oncol.* 18, 3339–3345. doi:10.1200/JCO.2000.18.19.3339

Brown, D. Q., Graham, W. J., 3rd, MacKenzie, L. J., Pittock, J. W., 3rd, and Shaw, L. M. (1988). Can WR-2721 Be Improved upon? *Pharmacol. Ther.* 39 (1-3), 157–168. doi:10.1016/0163-7258(88)90057-5

Broxmeyer, H. E., Orschell, C. M., Clapp, D. W., Hangoc, G., Cooper, S., Plett, P. A., et al. (2005). Rapid Mobilization of Murine and Human Hematopoietic Stem and Progenitor Cells with AMD3100, a CXCR4 Antagonist. *J. Exp. Med.* 201, 1307–1318. doi:10.1084/jem.20041385

Bunin, D. I., Bakke, J., Green, C. E., Javitz, H. S., Fielden, M., and Chang, P. Y. (2020). Romiplostim (Nplate) as an Effective Radiation Countermeasure to Improve Survival and Platelet Recovery in Mice. *Int. J. Radiat. Biol.* 96, 145–154. doi:10.1080/09553002.2019.1605465

Burnett, A. F., Biju, P. G., Lui, H., and Hauer-Jensen, M. (2013). Oral Interleukin 11 as a Countermeasure to Lethal Total-Body Irradiation in a Murine Model. *Radiat. Res.* 180, 595–602. doi:10.1667/RR13330.1

Cai, Y., Wang, W., Liang, H., Sun, L., Teitelbaum, D. H., and Yang, H. (2013). Keratinocyte Growth Factor Pretreatment Prevents Radiation-Induced Intestinal Damage in a Mouse Model. *Scand. J. Gastroenterol.* 48, 419–426. doi:10.3109/00365521.2013.772227

Cardon, L. R., Burge, C., Clayton, D. A., and Karlin, S. (1994). Pervasive CpG Suppression in Animal Mitochondrial Genomes. *Proc. Natl. Acad. Sci.* 91 (9), 3799–3803. doi:10.1073/pnas.91.9.3799

Cary, L. H., Ngudiankama, B. F., Salber, R. E., Ledney, G. D., and Whitnall, M. H. (2012). Efficacy of Radiation Countermeasures Depends on Radiation Quality. *Radiat. Res.* 177 (5), 663–675. doi:10.1667/rr2783.1

Centers for Disease Control and Prevention (2016). Emergency Preparedness and Response. Available at: http://emergency.cdc.gov/radiation/countermeasures.asp (Accessed September 1, 2016).

Cha, Y., Erez, T., Reynolds, I. J., Kumar, D., Ross, J., Koytiger, G., et al. (2018). Drug Repurposing from the Perspective of Pharmaceutical Companies. *Br. J. Pharmacol.* 175, 168–180. doi:10.1111/bph.13798

Charrier, S., Michaud, A., Badaoui, S., Giroux, S., Ezan, E., Sainteny, F., et al. (2004). Inhibition of Angiotensin I-Converting Enzyme Induces Radioprotection by Preserving Murine Hematopoietic Short-Term Reconstituting Cells. *Blood* 104, 978–985. doi:10.1182/blood-2003-11-3828

Cheema, A. K., Li, Y., Girgis, M., Jayatilake, M., Simas, M., Wise, S. Y., et al. (2019). Metabolomic Studies in Tissues of Mice Treated with Amifostine and Exposed to Gamma-Radiation. *Sci. Rep.* 9, 15701. doi:10.1038/s41598-019-52120-w

Cheema, A. K., Li, Y., Girgis, M., Jayatilake, M., Fatanmi, O. O., Wise, S. Y., et al. (2020). Alterations in Tissue Metabolite Profiles with Amifostine-Prophylaxed Mice Exposed to Gamma Radiation. *Metabolites* 10, 211. doi:10.3390/metabo10050211

Cheloff, A. Z., and Al-Samkari, H. (2019). Avatrombopag for the Treatment of Immune Thrombocytopenia and Thrombocytopenia of Chronic Liver Disease. *J. Blood Med.* 10, 313–321. doi:10.2147/JBM.S191790

Chisi, J. E., Briscoe, C. V., Ezan, E., Genet, R., Riches, A. C., and Wdzieczak-Bakala, J. (2000). Captopril Inhibits In Vitro and In Vivo the Proliferation of Primitive Haematopoietic Cells Induced into Cell Cycle by Cytotoxic Drug Administration or Irradiation but Has No Effect on Myeloid Leukaemia Cell Proliferation. *Br. J. Haematol.* 109 (3), 563–570. doi:10.1046/j.1365-2141.2000.02073.x

Christofidou-Solomidou, M., Pietrofesa, R. A., Arguiri, E., Koumenis, C., and Segal, R. (2017). Radiation Mitigating Properties of Intranasally Administered KL4Surfactant in a Murine Model of Radiation-Induced Lung Damage. *Radiat. Res.* 188, 571–584. doi:10.1667/RR14686.1

Clayton, N. P., Khan-Malek, R. C., Dangler, C. A., Zhang, D., Ascah, A., Gains, M., et al. (2020). Sargramostim (Rhu GM-CSF) Improves Survival of Non-human Primates with Severe Bone Marrow Suppression after Acute, High-Dose, Whole-Body Irradiation. *Radiat. Res.* 195, 191–199. doi:10.1667/RADE-20-00131.1

Clemons Bankston, P., and Al-Horani, R. A. (2019). New Small Molecule Drugs for Thrombocytopenia: Chemical, Pharmacological, and Therapeutic Use Considerations. *Int. J. Mol. Sci.* 20, 3013. doi:10.3390/ijms20123013

Cohen, E. P., Fish, B. L., and Moulder, J. E. (1992). Treatment of Radiation Nephropathy with Captopril. *Radiat. Res.* 132 (3), 346–350. doi:10.2307/3578243

Cohen, E. P., Irving, A. A., Drobyski, W. R., Klein, J. P., Passweg, J., Talano, J.-A. M., et al. (2008). Captopril to Mitigate Chronic Renal Failure after Hematopoietic Stem Cell Transplantation: a Randomized Controlled Trial. *Int. J. Radiat. Oncology*Biology*Physics* 70, 1546–1551. doi:10.1016/j.ijrobp.2007.08.041

Cohen, E. P., Fish, B. L., and Moulder, J. E. (2016). Clinically Relevant Doses of Enalapril Mitigate Multiple Organ Radiation Injury. *Radiat. Res.* 185, 313–318. doi:10.1667/RR4243.S1

Collins, F. S. (2011). Mining for Therapeutic Gold. *Nat. Rev. Drug Discov.* 10, 397. doi:10.1038/nrd3461

Corcoran, C., and Jacobs, T. F. (2020). "Metformin," in *StatPearls* (FL: Treasure Island).

Covic, A., and Abraham, I. (2015). State-of-the-art Biosimilar Erythropoietins in the Management of Renal Anemia: Lessons Learned from Europe and Implications for US Nephrologists. *Int. Urol. Nephrol.* 47, 1529–1539. doi:10.1007/s11255-015-1042-9

Cumberland Pharmaceuticals Inc. (2017). ETHYOL- Amifostine Injection, Powder, Lyophilized, for Solution. Available at: https://www.accessdata.fda.gov/drugsatfda_docs/label/2017/020221s033lbl.pdf (Accessed February 12, 2020).

Danilenko, D. M. (1999). Preclinical and Early Clinical Development of Keratinocyte Growth Factor, an Epithelial-specific Tissue Growth Factor. *Toxicol. Pathol.* 27 (1), 64–71. doi:10.1177/019262339902700113

Davidson, D. E., Grenan, M. M., and Sweeney, T. R. (1980). "Biological Characteristics of Some Improved Radioprotectors," in *Radiation Sensitizers, Their Use in the Clinical Management of* Cancer. Editor L. W. Brady (New York, Masson: Masson Publishing), 309–320.

Davis, T. A., Landauer, M. R., Mog, S. R., Barshishat-Kupper, M., Zins, S. R., Amare, M. F., et al. (2010). Timing of Captopril Administration Determines Radiation Protection or Radiation Sensitization in a Murine Model of Total Body Irradiation. *Exp. Hematol.* 38 (4), 270–281. doi:10.1016/j.exphem.2010.01.004

Day, R. M., Davis, T. A., Barshishat-Kupper, M., McCart, E. A., Tipton, A. J., and Landauer, M. R. (2013). Enhanced Hematopoietic Protection from Radiation by the Combination of Genistein and Captopril. *Int. Immunopharmacology* 15, 348–356. doi:10.1016/j.intimp.2012.12.029

De Clercq, E. (2009). The AMD3100 Story: the Path to the Discovery of a Stem Cell Mobilizer (Mozobil). *Biochem. Pharmacol.* 77, 1655–1664. doi:10.1016/j.bcp.2008.12.014

De Clercq, E. (2010). Recent Advances on the Use of the CXCR4 Antagonist Plerixafor (AMD3100, Mozobil) and Potential of Other CXCR4 Antagonists as Stem Cell Mobilizers. *Pharmacol. Ther.* 128, 509–518. doi:10.1016/j.pharmthera.2010.08.009

De Clercq, E. (2019). Mozobil (Plerixafor, AMD3100), 10 Years after its Approval by the US Food and Drug Administration. *Antivir. Chem. Chemother.* 27, 204020661982938. doi:10.1177/2040206619829382

Debnath, A., Parsonage, D., Andrade, R. M., He, C., Cobo, E. R., Hirata, K., et al. (2012). A High-Throughput Drug Screen for *Entamoeba Histolytica* Identifies a New Lead and Target. *Nat. Med.* 18, 956–960. doi:10.1038/nm.2758

Diamond, A. M., Dale, P., Murray, J. L., and Grdina, D. J. (1996). The Inhibition of Radiation-Induced Mutagenesis by the Combined Effects of Selenium and the Aminothiol WR-1065. *Mutat. Res.* 356 (2), 147–154. doi:10.1016/0027-5107(96)00016-4

DiCarlo, A. L., Ramakrishnan, N., and Hatchett, R. J. (2010). Radiation Combined Injury: Overview of NIAID Research. *Health Phys.* 98, 863–867. doi:10.1097/HP.0b013e3181a6ee32

DiCarlo, A. L., Poncz, M., Cassatt, D. R., Shah, J. R., Czarniecki, C. W., and Maidment, B. W. (2011a). Medical Countermeasures for Platelet Regeneration after Radiation Exposure. Report of a Workshop and Guided Discussion Sponsored by the National Institute of Allergy and Infectious Diseases, Bethesda, MD, March 22-23, 2010. *Radiat. Res.* 176 (1), e0001–0015. doi:10.1667/RROL01.1

DiCarlo, A. L., Poncz, M., Cassatt, D. R., Shah, J. R., Czarniecki, C. W., and Maidment, B. W. (2011b). Development and Licensure of Medical Countermeasures for Platelet Regeneration after Radiation Exposure. *Radiat. Res.* 176, 134–137. doi:10.1667/RR2610.1

DiCarlo, A. L., Cassatt, D. R., Dowling, W. E., Esker, J. L., Hewitt, J. A., Selivanova, O., et al. (2018). Challenges and Benefits of Repurposing Products for Use during a Radiation Public Health Emergency: Lessons Learned from Biological Threats and Other Disease Treatments. *Radiat. Res.* 190, 659–676. doi:10.1667/RR15137.1

Diomede, L., Albani, D., Sottocorno, M., Donati, M. B., Bianchi, M., Fruscella, P., et al. (2001). *In vivo* anti-inflammatory Effect of Statins Is Mediated by Nonsterol Mevalonate Products. *Arterioscler Thromb. Vasc. Biol.* 21, 1327–1332. doi:10.1161/hq0801.094222

Dlugosz-Danecka, M., Zdziarska, J., and Jurczak, W. (2019). Avatrombopag for the Treatment of Immune Thrombocytopenia. *Expert Rev. Clin. Immunol.* 15 (4), 327–339. doi:10.1080/1744666X.2019.1587294

Dova Pharmaceuticals (2019). Dova Pharmaceuticals Announces FDA Approval of Supplemental New Drug Application for DOPTELET® (Avatrombopag) for Treatment of Chronic Immune Thrombocytopenia (ITP). Available at: https://dova.com/wp-content/uploads/2019/06/doptelet-itp-approval-press-release-6-26-19.pdf (Accessed June 22, 2020).

Dykstra, J. C. (2017). Development of BIO 300 as a Medical Countermeasure for H-ARS and DEARE-lung. *Regulatory/Scientific Challenges and Benefits of Repurposing Licensed Products for a Radiation Indication*. Rockville, MD, USA.

Erickson-Miller, C. L., Delorme, E., Tian, S.-S., Hopson, C. B., Landis, A. J., Valoret, E. I., et al. (2009). Preclinical Activity of Eltrombopag (SB-497115), an Oral, Nonpeptide Thrombopoietin Receptor Agonist. *Stem Cells* 27, 424–430. doi:10.1634/stemcells.2008-0366

Farese, A. M., and MacVittie, T. J. (2015). Filgrastim for the Treatment of Hematopoietic Acute Radiation Syndrome. *Drugs Today (Barc)* 51, 537–548. doi:10.1358/dot.2015.51.9.2386730

Farrell, C. L., Rex, K. L., Kaufman, S. A., Dipalma, C. R., Chen, J. N., Scully, S., et al. (1999). Effects of Keratinocyte Growth Factor in the Squamous Epithelium of the Upper Aerodigestive Tract of Normal and Irradiated Mice. *Int. J. Radiat. Biol.* 75 (5), 609–620. doi:10.1080/095530099140258

Farzipour, S., Amiri, F. T., Mihandoust, E., Shaki, F., Noaparast, Z., Ghasemi, A., et al. (2020). Radioprotective Effect of Diethylcarbamazine on Radiation-

Induced Acute Lung Injury and Oxidative Stress in Mice. *J. Bioenerg. Biomembr* 52, 39–46. doi:10.1007/s10863-019-09820-9

Fatome, M., Courteille, F., Laval, J. D., and Roman, V. (1987). Radioprotective Activity of Ethylcellulose Microspheres Containing WR 2721, after Oral Administration. *Int. J. Radiat. Biol. Relat. Stud. Phys. Chem. Med.* 52 (1), 21–29. doi:10.1080/09553008714551441

Fehér, K. (2019). Single Stranded DNA Immune Modulators with Unmethylated CpG Motifs: Structure and Molecular Recognition by Toll-like Receptor 9. *Curr. Protein Pept. Sci.* 20, 1060–1068. doi:10.2174/1389203720666190830162149

Finch, P. W., Mark Cross, L. J., McAuley, D. F., and Farrell, C. L. (2013). Palifermin for the Protection and Regeneration of Epithelial Tissues Following Injury: New Findings in Basic Research and Pre-clinical Models. *J. Cel. Mol. Med.* 17, 1065–1087. doi:10.1111/jcmm.12091

Fukumoto, R., Cary, L. H., Gorbunov, N. V., Lombardini, E. D., Elliott, T. B., and Kiang, J. G. (2013). Ciprofloxacin Modulates Cytokine/chemokine Profile in Serum, Improves Bone Marrow Repopulation, and Limits Apoptosis and Autophagy in Ileum after Whole Body Ionizing Irradiation Combined with Skin-Wound Trauma. *PloS one* 8, e58389. doi:10.1371/journal.pone.0058389

Fukumoto, R., Burns, T. M., and Kiang, J. G. (2014). Ciprofloxacin Enhances Stress Erythropoiesis in Spleen and Increases Survival after Whole-Body Irradiation Combined with Skin-Wound Trauma. *PloS one* 9, e90448. doi:10.1371/journal.pone.0090448

Gale, R. P., and Armitage, J. O. (2021). Use of Molecularly-Cloned Haematopoietic Growth Factors in Persons Exposed to Acute High-Dose, High-Dose Rate Whole-Body Ionizing Radiations. *Blood Rev.* 45, 100690. doi:10.1016/j.blre.2020.100690

Gale, R. P., Armitage, J. O., and Hashmi, S. K. (2019). Emergency Response to Radiological and Nuclear Accidents and Incidents. *Br. J. Haematol.* 192, 968–972. doi:10.1111/bjh.16138

Geiger, H., Pawar, S. A., Kerschen, E. J., Nattamai, K. J., Hernandez, I., Liang, H. P. H., et al. (2012). Pharmacological Targeting of the Thrombomodulin-Activated Protein C Pathway Mitigates Radiation Toxicity. *Nat. Med.* 18, 1123–1129. doi:10.1038/nm.2813

Gelosa, P., Castiglioni, L., Camera, M., and Sironi, L. (2020). Repurposing of Drugs Approved for Cardiovascular Diseases: Opportunity or Mirage? *Biochem. Pharmacol.* 177, 113895. doi:10.1016/j.bcp.2020.113895

Geraci, J. P., Sun, M. C., and Mariano, M. S. (1995). Amelioration of Radiation Nephropathy in Rats by Postirradiation Treatment with Dexamethasone And/or Captopril. *Radiat. Res.* 143 (1), 58–68. doi:10.2307/3578926

Ghosh, S. N., Zhang, R., Fish, B. L., Semenenko, V. A., Li, X. A., Moulder, J. E., et al. (2009). Renin-Angiotensin System Suppression Mitigates Experimental Radiation Pneumonitis. *Int. J. Radiat. Oncol. Biol. Phys.* 75 (5), 1528–1536. doi:10.1016/j.ijrobp.2009.07.1743

Gianoncelli, A., Bonini, S. A., Bertuzzi, M., Guarienti, M., Vezzoli, S., Kumar, R., et al. (2015). An Integrated Approach for a Structural and Functional Evaluation of Biosimilars: Implications for Erythropoietin. *BioDrugs* 29, 285–300. doi:10.1007/s40259-015-0136-3

Gilead Sciences Inc. (2020). Pipeline - Remdesivir. Available at: https://www.gilead.com/science-and-medicine/pipeline (Accessed July 18, 2020).

Gluzman-Poltorak, Z., Vainstein, V., and Basile, L. A. (2014). Recombinant Interleukin-12, but Not Granulocyte-Colony Stimulating Factor, Improves Survival in Lethally Irradiated Nonhuman Primates in the Absence of Supportive Care: Evidence for the Development of a Frontline Radiation Medical Countermeasure. *Am. J. Hematol.* 89, 868–873. doi:10.1002/ajh.23770

Gotto, A. M., Jr. (2003). Treating Hypercholesterolemia: Looking Forward. *Clin. Cardiol.* 26 (1 Suppl. 1), 21–28. doi:10.1002/clc.4960261307

Grdina, D. J., Nagy, B., Hill, C. K., Wells, R. L., and Peraino, C. (1985). The Radioprotector WR1065 Reduces Radiation-Induced Mutations at the Hypoxanthine-Guanine Phosphoribosyl Transferase Locus in V79 Cells. *Carcinogenesis* 6, 929–931. doi:10.1093/carcin/6.6.929

Grdina, D. J., Kataoka, Y., and Murley, J. S. (2000). Amifostine: Mechanisms of Action Underlying Cytoprotection and Chemoprevention. *Drug Metabol Drug Interact* 16 (4), 237–279. doi:10.1515/dmdi.2000.16.4.237

Grdina, D. J., Murley, J. S., Kataoka, Y., and Epperly, W. (2002). Relationships between Cytoprotection and Mutation Prevention by WR-1065. *Mil. Med.* 167 (2 Suppl. l), 51–53. doi:10.1093/milmed/167.suppl_1.51

Griffin, J. H., Fernández, J. A., Mosnier, L. O., Liu, D., Cheng, T., Guo, H., et al. (2006). The Promise of Protein C. *Blood Cell Mol. Dis.* 36, 211–216. doi:10.1016/j.bcmd.2005.12.023

Grobbee, D. E., and Bots, M. L. (2003). Statin Treatment and Progression of Atherosclerotic Plaque Burden. *Drugs* 63, 893–911. doi:10.2165/00003495-200363090-00004

Hall, E. J., and Giaccia, A. J. (2012). *Radiobiology for the Radiobiologist*. Philadelphia, PA: Lippincott Williams and Wilkins.

Hammond, W. P., Boone, T. C., Donahue, R. E., Souza, L. M., and Dale, D. C. (1990). A Comparison of Treatment of Canine Cyclic Hematopoiesis with Recombinant Human Granulocyte-Macrophage Colony-Stimulating Factor (GM-CSF), G-CSF, Interleukin-3, and Canine G-CSF. *Blood* 76 (3), 523–532. doi:10.1182/blood.v76.3.523.523

Han, S., Kim, K., Kim, H., Kwon, J., Lee, Y.-H., Lee, C.-K., et al. (2008). Auranofin Inhibits Overproduction of Pro-inflammatory Cytokines, Cyclooxygenase Expression and PGE2 Production in Macrophages. *Arch. Pharm. Res.* 31, 67–74. doi:10.1007/s12272-008-1122-9

Hauer-Jensen, M. (2014). Toward Development of Interleukin-11 as a Medical Countermeasure for Use in Radiological/nuclear Emergencies. *Dig. Dis. Sci.* 59, 1349–1351. doi:10.1007/s10620-014-3074-x

Hawking, F. (1979). Diethylcarbamazine and New Compounds for the Treatment of Filariasis. *Adv. Pharmacol. Chemother.* 16, 129–194. doi:10.1016/s1054-3589(08)60244-6

Hemmi, H., Takeuchi, O., Kawai, T., Kaisho, T., Sato, S., Sanjo, H., et al. (2000). A Toll-like Receptor Recognizes Bacterial DNA. *Nature* 408, 740–745. doi:10.1038/35047123

Hepgül, G., Tanrıkulu, S., Ünalp, H. R., Akguner, T., Erbil, Y., Olgaç, V., et al. (2010). Preventive Effect of Pentoxifylline on Acute Radiation Damage via Antioxidant and Anti-inflammatory Pathways. *Dig. Dis. Sci.* 55, 617–625. doi:10.1007/s10620-009-0780-x

Hirouchi, T., Ito, K., Nakano, M., Monzen, S., Yoshino, H., Chiba, M., et al. (2015). Mitigative Effects of a Combination of Multiple Pharmaceutical Drugs on the Survival of Mice Exposed to Lethal Ionizing Radiation. *Curr. Pharm. Biotechnol.* 17 (2), 190–199. doi:10.2174/1389201016666150826125331

Hu, M., Zhang, Z., Liu, B., Zhang, S., Chai, R., Chen, X., et al. (2018). Deubiquitinase Inhibitor Auranofin Attenuated Cardiac Hypertrophy by Blocking NF-Kb Activation. *Cell Physiol Biochem* 45, 2421–2430. doi:10.1159/000488230

Imrie, K. R., Prince, H. M., Couture, F., Brandwein, J. M., and Keating, A. (1995). Effect of Antimicrobial Prophylaxis on Hematopoietic Recovery Following Autologous Bone Marrow Transplantation: Ciprofloxacin versus Co-trimoxazole. *Bone Marrow Transpl.* 15 (2), 267–270.

International Atomic Energy Agency (1993). The Radiological Accident in Soreq, IAEA. Available at: http://www-pub.iaea.org/books/IAEABooks/3798/The-Radiological-Accident-in-Soreq (Accessed February 20, 2014).

International Atomic Energy Agency (1996). The Radiological Accident at the Irradiation Facility in Nesvizh. Available at: http://www-pub.iaea.org/books/IAEABooks/4712/The-Radiological-Accident-at-the-Irradiation-Facility-in-Nesvizh (Accessed February 10, 2014).

Ishida, J., Konishi, M., Ebner, N., and Springer, J. (2016). Repurposing of Approved Cardiovascular Drugs. *J. Transl Med.* 14, 269. doi:10.1186/s12967-016-1031-5

Ishii, K. J., Takeshita, F., Gursel, I., Gursel, M., Conover, J., Nussenzweig, A., et al. (2002). Potential Role of Phosphatidylinositol 3 Kinase, rather Than DNA-dependent Protein Kinase, in CpG DNA-Induced Immune Activation. *J. Exp. Med.* 196 (2), 269–274. doi:10.1084/jem.20020773

Islam, A., Bolduc, D. L., Zhai, M., Kiang, J. G., and Swift, J. M. (2015). Captopril Increases Survival after Whole-Body Ionizing Irradiation but Decreases Survival when Combined with Skin-Burn Trauma in Mice. *Radiat. Res.* 184, 273–279. doi:10.1667/RR14113.1

Jacobson, A. E., Shah, N., and Setty, B. A. (2017). Romiplostim for Therapy-Related Thrombocytopenia in Pediatric Malignancies. *Pediatr. Blood Cancer* 64, e26473. doi:10.1002/pbc.26473

Jargin, S. V. (2014). Chernobyl-related Cancer and Precancerous Lesions: Incidence Increase vs. Late Diagnostics. *Dose Response* 12 (3), 404–414. doi:10.2203/dose-response.13-039.jargin

Jargin, S. (2020). Thyroid Cancer after Chernobyl: Re-evaluation Needed. *Tjpath.* 37 (1), 1-6. doi:10.5146/tjpath.2020.01489

Johnke, R. M., Sattler, J. A., and Allison, R. R. (2014). Radioprotective Agents for Radiation Therapy: Future Trends. *Future Oncol.* 10, 2345–2357. doi:10.2217/fon.14.175

Johnstone, P. A., DeGraff, W. G., and Mitchell, J. B. (1995). Protection from Radiation-Induced Chromosomal Aberrations by the Nitroxide Tempol. *Cancer* 75 (9), 2323–2327. doi:10.1002/1097-0142(19950501)75:9<2323::aid-cncr2820750922>3.0.co;2-2

Kakkar, A. K., Singh, H., and Medhi, B. (2018). Old Wines in New Bottles: Repurposing Opportunities for Parkinson's Disease. *Eur. J. Pharmacol.* 830, 115–127. doi:10.1016/j.ejphar.2018.04.023

Kataoka, Y., Perrin, J., Hunter, N., Milas, L., and Grdina, D. J. (1996). Antimutagenic Effects of Amifostine: Clinical Implications. *Semin. Oncol.* 23 (4 Suppl. 8), 53–57.

Khan, M. K., Nasti, T. H., Buchwald, Z. S., Weichselbaum, R. R., and Kron, S. J. (2019). Repurposing Drugs for *Cancer* Radiotherapy. *Cancer J.* 25, 106–115. doi:10.1097/PPO.0000000000000369

Klinman, D. M., Yi, A. K., Beaucage, S. L., Conover, J., and Krieg, A. M. (1996). CpG Motifs Present in Bacteria DNA Rapidly Induce Lymphocytes to Secrete Interleukin 6, Interleukin 12, and Interferon Gamma. *Proc. Natl. Acad. Sci.* 93 (7), 2879–2883. doi:10.1073/pnas.93.7.2879

Klinman, D. M. (2004). Immunotherapeutic Uses of CpG Oligodeoxynucleotides. *Nat. Rev.* 4, 249–258. doi:10.1038/nri1329

Kma, L., Gao, F., Fish, B. L., Moulder, J. E., Jacobs, E. R., and Medhora, M. (2012). Angiotensin Converting Enzyme Inhibitors Mitigate Collagen Synthesis Induced by a Single Dose of Radiation to the Whole Thorax. *J. Radiat. Res.* 53 (1), 10–17. doi:10.1269/jrr.11035

Knudson, G. B., Ainsworth, E. J., Eng, R. R., Fry, R. J., Kearsley, E., Multon, E. T., et al. (2002a). Nuclear/biological/chemical Combined Injury Effects: Expert Panel Consensus. *Mil. Med.* 167 (2 Suppl. l), 113–115. doi:10.1093/milmed/167.suppl_1.113

Knudson, G. B., Elliott, T. B., Brook, I., Shoemaker, M. O., Pastel, R. H., Lowy, R. J., et al. (2002b). Nuclear, Biological, and Chemical Combined Injuries and Countermeasures on the Battlefield. *Mil. Med.* 167 (2 Suppl. l), 95–97. doi:10.1093/milmed/167.suppl_1.95

Koh, W. J., Stelzer, K. J., Peterson, L. M., Staker, B. L., Ward, W. F., Russell, K. J., et al. (1995). Effect of Pentoxifylline on Radiation-Induced Lung and Skin Toxicity in Rats. *Int. J. Radiat. Oncol. Biol. Phys.* 31 (1), 71–77. doi:10.1016/0360-3016(94)E0307-6

Kouvaris, J. R., Kouloulias, V. E., and Vlahos, L. J. (2007). Amifostine: The First Selective-Target and Broad-Spectrum Radioprotector. *Oncol.* 12, 738–747. doi:10.1634/theoncologist.12-6-738

Krieg, A. M., Yi, A. K., Matson, S., Waldschmidt, T. J., Bishop, G. A., Teasdale, R., et al. (1995). CpG Motifs in Bacterial DNA Trigger Direct B-Cell Activation. *Nature* 374 (6522), 546–549. doi:10.1038/374546a0

Krzyzanski, W., Sutjandra, L., Perez-Ruixo, J. J., Sloey, B., Chow, A. T., and Wang, Y.-M. (2013). Pharmacokinetic and Pharmacodynamic Modeling of Romiplostim in Animals. *Pharm. Res.* 30, 655–669. doi:10.1007/s11095-012-0894-2

Kulkarni, S., Chakraborty, K., Kumar, K. S., Kao, T.-C., Hauer-Jensen, M., and Ghosh, S. P. (2013). Synergistic Radioprotection by Gamma-Tocotrienol and Pentoxifylline: Role of cAMP Signaling. *ISRN Radiol.* 2013 (1), 11. doi:10.5402/2013/390379

Kuter, D. J. (2007). New Thrombopoietic Growth Factors. *Blood* 109, 4607–4616. doi:10.1182/blood-2006-10-019315

Lahat, G., Halperin, D., Barazovsky, E., Shalit, I., Rabau, M., Klausner, J., et al. (2007). Immunomodulatory Effects of Ciprofloxacin in TNBS-Induced Colitis in Mice. *Inflamm. Bowel Dis.* 13, 557–565. doi:10.1002/ibd.20077

Lataillade, J., Doucet, C., Bey, E., Carsin, H., Huet, C., Clairand, I., et al. (2007). New Approach to Radiation Burn Treatment by Dosimetry-Guided Surgery Combined with Autologous Mesenchymal Stem Cell Therapy. *Regenerative Med.* 2, 785–794. doi:10.2217/17460751.2.5.785

Lauritano, D., Petruzzi, M., Di Stasio, D., and Lucchese, A. (2014). Clinical Effectiveness of Palifermin in Prevention and Treatment of Oral Mucositis in Children with Acute Lymphoblastic Leukaemia: a Case-Control Study. *Int. J. Oral Sci.* 6, 27–30. doi:10.1038/ijos.2013.93

Liesveld, J. L., Phillips, G. L., 2nd, Becker, M., Constine, L. S., Friedberg, J., Andolina, J. R., et al. (2013). A Phase 1 Trial of Eltrombopag in Patients Undergoing Stem Cell Transplantation after Total Body Irradiation. *Biol. Blood Marrow Transplant.* 19, 1745–1752. doi:10.1016/j.bbmt.2013.10.002

Liu, Q., Jiang, B., Jiang, L. P., Wu, Y., Wang, X. G., Zhao, F. L., et al. (2008). Clinical Report of Three Cases of Acute Radiation Sickness from a (60)Co Radiation Accident in Henan Province in China. *J. Radiat. Res.* 49 (1), 63–69. doi:10.1269/jrr.07071

Liu, N., Li, X., Huang, H., Zhao, C., Liao, S., Yang, C., et al. (2014). Clinically Used Antirheumatic Agent Auranofin Is a Proteasomal Deubiquitinase Inhibitor and Inhibits Tumor Growth. *Oncotarget* 5, 5453–5471. doi:10.18632/oncotarget.2113

Lord, B. I., Molineux, G., Pojda, Z., Souza, L. M., Mermod, J. J., and Dexter, T. M. (1991). Myeloid Cell Kinetics in Mice Treated with Recombinant Interleukin-3, Granulocyte Colony-Stimulating Factor (CSF), or Granulocyte-Macrophage CSF In Vivo. *Blood* 77 (10), 2154–2159. doi:10.1182/blood.v77.10.2154.bloodjournal77102154

MacVittie, T. J., Farese, A. M., Smith, W. G., Baum, C. M., Burton, E., and McKearn, J. P. (2000). Myelopoietin, an Engineered Chimeric IL-3 and G-CSF Receptor Agonist, Stimulates Multilineage Hematopoietic Recovery in a Nonhuman Primate Model of Radiation-Induced Myelosuppression. *Blood* 95 (3), 837–845. doi:10.1182/blood.v95.3.837.003k08_837_845

MacVittie, T. J., Farese, A. M., and Kane, M. A. (2019). ARS, DEARE, and Multiple-Organ Injury: A Strategic and Tactical Approach to Link Radiation Effects, Animal Models, Medical Countermeasures, and Biomarker Development to Predict Clinical Outcome. *Health Phys.* 116, 453. doi:10.1097/HP.0000000000001050

MacVittie, T. J. (2015). The MCART Consortium Animal Model Series. *Health Phys.* 109, 335–341. doi:10.1097/HP.0000000000000318

Madeira, J. M., Renschler, C. J., Mueller, B., Hashioka, S., Gibson, D. L., and Klegeris, A. (2013). Novel Protective Properties of Auranofin: Inhibition of Human Astrocyte Cytotoxic Secretions and Direct Neuroprotection. *Life Sci.* 92, 1072–1080. doi:10.1016/j.lfs.2013.04.005

McCart, E. A., Lee, Y. H., Jha, J., Mungunsukh, O., Rittase, W. B., Summers, T. A., Jr., et al. (2019). Delayed Captopril Administration Mitigates Hematopoietic Injury in a Murine Model of Total Body Irradiation. *Sci. Rep.* 9 (1), 2198. doi:10.1038/s41598-019-38651-2

McCarty, M. F., O'Keefe, J. H., and DiNicolantonio, J. J. (2016). Pentoxifylline for Vascular Health: a Brief Review of the Literature. *Open heart* 3, e000365. doi:10.1136/openhrt-2015-000365

Medhora, M., Gao, F., Fish, B. L., Jacobs, E. R., Moulder, J. E., and Szabo, A. (2012a). Dose-modifying Factor for Captopril for Mitigation of Radiation Injury to Normal Lung. *J. Radiat. Res.* 53, 633–640. doi:10.1093/jrr/rrs004

Medhora, M., Gao, F., Jacobs, E. R., and Moulder, J. E. (2012b). Radiation Damage to the Lung: Mitigation by Angiotensin-Converting Enzyme (ACE) Inhibitors. *Respirology (Carlton, Vic* 17 (1), 66–71. doi:10.1111/j.1440-1843.2011.02092.x

Medhora, M., Gao, F., Wu, Q., Molthen, R. C., Jacobs, E. R., Moulder, J. E., et al. (2014). Model Development and Use of ACE Inhibitors for Preclinical Mitigation of Radiation-Induced Injury to Multiple Organs. *Radiat. Res.* 182, 545–555. doi:10.1667/RR13425.1

MERCK & Co. (2004). CUPRIMINE®. Available at: https://www.accessdata.fda.gov/drugsatfda_docs/label/2004/19853s012,014lbl.pdf (Accessed July 25, 2020).

Miller, R. C., Murley, J. S., and Grdina, D. J. (2014). Metformin Exhibits Radiation Countermeasures Efficacy when Used Alone or in Combination with Sulfhydryl Containing Drugs. *Radiat. Res.* 181, 464–470. doi:10.1667/RR13672.1

Molteni, A., Moulder, J. E., Cohen, E. F., Ward, W. F., Fish, B. L., Taylor, J. M., et al. (2000). Control of Radiation-Induced Pneumopathy and Lung Fibrosis by Angiotensin-Converting Enzyme Inhibitors and an Angiotensin II Type 1 Receptor Blocker. *Int. J. Radiat. Biol.* 76, 523–532. doi:10.1080/095530000138538

Moulder, J. E., and Cohen, E. P. (2007). Future Strategies for Mitigation and Treatment of Chronic Radiation-Induced Normal Tissue Injury. *Semin. Radiat. Oncol.* 17, 141–148. doi:10.1016/j.semradonc.2006.11.010

Moulder, J. E., Cohen, E. P., Fish, B. L., and Hill, P. (1993a). Prophylaxis of Bone Marrow Transplant Nephropathy with Captopril, an Inhibitor of Angiotensin-Converting Enzyme. *Radiat. Res.* 136 (3), 404–407. doi:10.2307/3578554

Moulder, J. E., Fish, B. L., and Cohen, E. P. (1993b). Treatment of Radiation Nephropathy with ACE Inhibitors. *Int. J. Radiat. Oncol. Biol. Phys.* 27 (1), 93–99. doi:10.1016/0360-3016(93)90425-u

Moulder, J. E., Fish, B. L., and Cohen, E. P. (2007). Treatment of Radiation Nephropathy with ACE Inhibitors and AII Type-1 and Type-2 Receptor Antagonists. *Curr. Pharm. Des.* 13 (13), 1317–1325. doi:10.2174/138161207780618821

Moulder, J. E., Cohen, E. P., and Fish, B. L. (2011). Captopril and Losartan for Mitigation of Renal Injury Caused by Single-Dose Total-Body Irradiation. *Radiat. Res.* 175 (1), 29–36. doi:10.1667/rr2400.1

Moulder, J. E., Cohen, E. P., and Fish, B. L. (2014). Mitigation of Experimental Radiation Nephropathy by Renin-Equivalent Doses of Angiotensin Converting Enzyme Inhibitors. *Int. J. Radiat. Biol.* 90, 762–768. doi:10.3109/09553002.2014.938375

Mouthon, M.-A., Van der Meeren, A., Gaugler, M.-H., Visser, T. P., Squiban, C., Gourmelon, P., et al. (1999). Thrombopoietin Promotes Hematopoietic Recovery and Survival after High-Dose Whole Body Irradiation. *Int. J. Radiat. Oncol. Biol. Phys.* 43 (4), 867–875. doi:10.1016/s0360-3016(98)00477-5

Mouthon, M. A., Van der Meeren, A., Vandamme, M., Squiban, C., and Gaugler, M. H. (2002). Thrombopoietin Protects Mice from Mortality and Myelosuppression Following High-Dose Irradiation: Importance of Time Scheduling. *Can. J. Physiol. Pharmacol.* 80 (7), 717–721. doi:10.1139/y02-090

Mullard, A. (2016). Parsing Clinical Success Rates. *Nat. Rev. Drug Discov.* 15, 447. doi:10.1038/nrd.2016.136

Nabholtz, J.-M., Cantin, J., Chang, J., Guevin, R., Patel, R., Tkaczuk, K., et al. (2002). Phase III Trial Comparing Granulocyte Colony-Stimulating Factor to Leridistim in the Prevention of Neutropenic Complications in Breast Cancer Patients Treated with Docetaxel/doxorubicin/cyclophosphamide: Results of the BCIRG 004 Trial. *Clin. Breast Cancer* 3, 268–275. doi:10.3816/CBC.2002.n.030

Nag, D., Bhanja, P., Riha, R., Sanchez-Guerrero, G., Kimler, B. F., Tsue, T. T., et al. (2019). Auranofin Protects Intestine against Radiation Injury by Modulating P53/p21 Pathway and Radiosensitizes Human Colon Tumor. *Clin. Cancer Res.* 25, 4791–4807. doi:10.1158/1078-0432.CCR-18-2751

Nagayama, H., Misawa, K., Tanaka, H., Ooi, J., Iseki, T., Tojo, A., et al. (2002). Transient Hematopoietic Stem Cell Rescue Using Umbilical Cord Blood for a Lethally Irradiated Nuclear Accident Victim. *Bone Marrow Transpl.* 29, 197–204. doi:10.1038/sj.bmt.1703356

Nardon, C., Pettenuzzo, N., and Fregona, D. (2016). Gold Complexes for Therapeutic Purposes: an Updated Patent Review (2010-2015). *Curr. Med. Chem.* 23, 3374–3403. doi:10.2174/0929867323666160504103843

National Institute of Allergic and Infectious Diseases (2015). Pegfilgrastim Approved for Treating Acute Radiation Syndrome. Available at: https://www.niaid.nih.gov/topics/radnuc/Pages/pegfilgrastim.aspx (Accessed August 18, 2016).

National Research Council, Biological Effects of Ionizing Radiation (1990). *Health Effects of Exposure to Low Levels of Ionizing Radiation*. Washington, DC: The National Academies Press.

Nishida, T., Yamaguchi, M., Tatara, Y., and Kashiwakura, I. (2020). Proteomic Changes by Radio-Mitigative Thrombopoietin Receptor Agonist Romiplostim in the Blood of Mice Exposed to Lethal Total-Body Irradiation. *Int. J. Radiat. Biol.* 96, 1125–1134. doi:10.1080/09553002.2020.1787546

No author listed (1998). Recombinant IL-11 Approved as Platelet Booster. *Nat. Biotechnol.* 16, 7. doi:10.1038/nbt0198-7

Nordström, M., Abrahamsson, T., Ervik, M., Forshult, E., and Regårdh, C. G. (1993). Central Nervous and Systemic Kinetics of Ramipril and Ramiprilat in the Conscious Dog. *J. Pharmacol. Exp. Ther.* 266, 147–152.

Nosengo, N. (2016). Can You Teach Old Drugs New Tricks? *Nature* 534, 314–316. doi:10.1038/534314a

Novartis (2005). Voltaren (Diclofenac Sodium Enteric-Coated Tablets) - Prescribing Information. Available at: https://www.accessdata.fda.gov/drugsatfda_docs/label/2006/019201s035lbl.pdf (Accessed June 09, 2020).

Novartis (2011). Desferal® Deferoxamine Mesylate for Injection USP. Available at: https://www.accessdata.fda.gov/drugsatfda_docs/label/2011/016267s050lbl.pdf (Accessed July 25, 2020).

Oprea, T. I., and Mestres, J. (2012). Drug Repurposing: Far beyond New Targets for Old Drugs. *Aaps J.* 14, 759–763. doi:10.1208/s12248-012-9390-1

Ozasa, K., Cullings, H. M., Ohishi, W., Hida, A., and Grant, E. J. (2019). Epidemiological Studies of Atomic Bomb Radiation at the Radiation Effects Research Foundation. *Int. J. Radiat. Biol.* 95, 879–891. doi:10.1080/09553002.2019.1569778

Ozturk, B., Egehan, I., Atavci, S., and Kitapci, M. (2004). Pentoxifylline in Prevention of Radiation-Induced Lung Toxicity in Patients with Breast and Lung Cancer: a Double-Blind Randomized Trial. *Int. J. Radiat. Oncol. Biol. Phys.* 58 (1), 213–219. doi:10.1016/s0360-3016(03)01444-5

Pamujula, S., Graves, R. A., Freeman, T., Srinivasan, V., Bostanian, L. A., Kishore, V., et al. (2010). Oral Delivery of Spray Dried PLGA/amifostine Nanoparticles. *J. Pharm. Pharmacol.* 56, 1119–1125. doi:10.1211/0022357044210

Papapetropoulos, A., and Szabo, C. (2018). Inventing New Therapies without Reinventing the Wheel: the Power of Drug Repurposing. *Br. J. Pharmacol.* 175, 165–167. doi:10.1111/bph.14081

Parameswaran, R., Lunning, M., Mantha, S., Devlin, S., Hamilton, A., Schwartz, G., et al. (2014). Romiplostim for Management of Chemotherapy-Induced Thrombocytopenia. *Support Care Cancer* 22, 1217–1222. doi:10.1007/s00520-013-2074-2

Peter, R. U., and Gottlöber, P. (2002). Management of Cutaneous Radiation Injuries: Diagnostic and Therapeutic Principles of the Cutaneous Radiation Syndrome. *Mil. Med.* 167 (2 Suppl. l), 110–112.

Piehl, E., and Fernandez-Bustamante, A. (2012). Lucinactant for the Treatment of Respiratory Distress Syndrome in Neonates. *Drugs Today (Barc)* 48, 587–593. doi:10.1358/dot.2012.48.9.1835160

Poordad, F., Terrault, N. A., Alkhouri, N., Tian, W., Allen, L. F., and Rabinovitz, M. (2020). Avatrombopag, an Alternate Treatment Option to Reduce Platelet Transfusions in Patients with Thrombocytopenia and Chronic Liver Disease-Integrated Analyses of 2 Phase 3 Studies. *Int. J. Hepatol.* 2020 (1), 11. doi:10.1155/2020/5421632

Potten, C. S. (1995). Interleukin-11 Protects the Clonogenic Stem Cells in Murine Small-Intestinal Crypts from Impairment of Their Reproductive Capacity by Radiation. *Int. J. Cancer* 62 (3), 356–361. doi:10.1002/ijc.2910620321

Potten, C. S. (1996). Protection of the Small Intestinal Clonogenic Stem Cells from Radiation-Induced Damage by Pretreatment with Interleukin 11 Also Increases Murine Survival Time. *Stem Cells* 14, 452–459. doi:10.1002/stem.140452

Pozza, M., Matthew, P., and Lunardi, F. (2014). Experience in Treating Combat Burns in Afghanistan by Using Silver-Nylon Dressing. *J. Spec. Oper. Med.* 14, 1–5.

Queto, T., Xavier-Elsas, P., Gardel, M. A., de Luca, B., Barradas, M., Masid, D., et al. (2010). Inducible Nitric Oxide synthase/CD95L-dependent Suppression of Pulmonary and Bone Marrow Eosinophilia by Diethylcarbamazine. *Am. J. Respir. Crit. Care Med.* 181, 429–437. doi:10.1164/rccm.200905-0800OC

Rasey, J. S., Spence, A. M., Badger, C. C., Krohn, K. A., Vera, D. M., and Livesey, J. C. (1988). Specific Protection of Different Normal Tissues. *Pharmacol. Ther.* 39 (1-3), 33–43. doi:10.1016/0163-7258(88)90037-x

Robbins, M. E., and Diz, D. I. (2006). Pathogenic Role of the Renin-Angiotensin System in Modulating Radiation-Induced Late Effects. *Int. J. Radiat. Oncol. Biol. Phys.* 64, 6–12. doi:10.1016/j.ijrobp.2005.08.033

Robbins, M. E., and Hopewell, J. W. (1986). Physiological Factors Effecting Renal Radiation Tolerance: a Guide to the Treatment of Late Effects. *Br. J. Cancer Suppl.* 7, 265–267.

Rosen, E. M., Day, R., and Singh, V. K. (2015). New Approaches to Radiation Protection. *Front. Oncol.* 4, 381. doi:10.3389/fonc.2014.00381

Rowley, J. D. (1985). Chromosome Abnormalities in Human Leukemia as Indicators of Mutagenic Exposure. *Carcinog Compr. Surv.* 10, 409–418.

Rube, C. E., Wilfert, F., Uthe, D., Schmid, K. W., Knoop, R., Willich, N., et al. (2002). Modulation of Radiation-Induced Tumour Necrosis Factor Alpha (TNF-Alpha) Expression in the Lung Tissue by Pentoxifylline. *Radiother. Oncol.* 64 (2), 177–187. doi:10.1016/s0167-8140(02)00077-4

Saager, M., Hahn, E. W., Peschke, P., Brons, S., Huber, P. E., Debus, J., et al. (2020). Ramipril Reduces Incidence and Prolongates Latency Time of Radiation-Induced Rat Myelopathy after Photon and Carbon Ion Irradiation. *J. Radiat. Res.* 61, 791–798. doi:10.1093/jrr/rraa042

Sahakitrungruang, C., Thum-Umnuaysuk, S., Patiwongpaisarn, A., Atittharnsakul, P., and Rojanasakul, A. (2011). A Novel Treatment for Haemorrhagic Radiation Proctitis Using Colonic Irrigation and Oral Antibiotic Administration. *Colorectal Dis.* 13, e79–e82. doi:10.1111/j.1463-1318.2010.02527.x

Sanofi-Aventis U.S. LLC (2018). LEUKINE® (Sargramostim) for Injection, for Subcutaneous or Intravenous Use. Available at: https://www.accessdata.fda.gov/drugsatfda_docs/label/2018/103362s5240lbl.pdf?utm_campaign=20180329%20MCMiandutm_medium=emailandutm_source=Eloqua (Accessed April 01, 2018).

Satyamitra, M., Lombardini, E., Graves, J., 3rd, Mullaney, C., Ney, P., Hunter, J., et al. (2011). A TPO Receptor Agonist, ALXN4100TPO, Mitigates Radiation-

Induced Lethality and Stimulates Hematopoiesis in CD2F1 Mice. *Radiat. Res.* 175, 746–758. doi:10.1667/RR2462.1

Satyamitra, M., Lombardini, E., Peng, T., Devore, D., Graves, J., 3rd, Mullaney, C., et al. (2013). Preliminary Nonclinical Toxicity, Pharmacokinetics, and Pharmacodynamics of ALXN4100TPO, a Thrombopoietin Receptor Agonist, in CD2F1 Mice. *Int. J. Toxicol.* 32, 100–112. doi:10.1177/1091581813482336

Seed, T. M., Fritz, T. E., Tolle, D. V., Poole, C. M., Lombard, L. S., Doyle, D. E., et al. (1984). "Survival Patterns and Hemopathological Responses of Dogs under Continuous Gamma Irradiation," in *Response of Different Species to Total Body Irradiation*. Editors J. J. Broerse and T. J. MacVittie (Dordrecht, Netherlands: Martinus Niijhoff), 137–159. doi:10.1007/978-94-009-6048-0_9

Seed, T. M., Kaspar, L. V., Fritz, T. E., and Tolle, D. V. (1985). "Cellular Responses in Chronic Radiation Leukemogenesis," in *Carcinogenesis*. Editors E. Huberman and S. H. Barr (New York: Raven Press), 363–379.

Seed, T. M., Inal, C. E., and Deen, J. E. (2001). "Assessment of a Combined G-CSF Plus IL-11 Cytokine Treatment for Radiation-Induced Hematopoietic Injury," 48th Annual Meeting of the Radiation Research Society. San Juan, Puerto Rico

Seed, T. M., Tolle, D. V., and Fritz, T. E. (2002). "Haematological Responses to Chronic Irradiation: The Past Argonne Experience and Future AFRRI Initiatives," in *Chronic Irradiation: Tolerance and Failure in Complex Biological Systems. Advanced Research Workshop on Protracted, Intermittent or Chronic Irradiation : Biological Effects and Mechanisms of Tolerence (2001 : Ulm, Germany)*. Editors T. M. Fliedner, L. E. Feinendegen, and J. W. Hopewell (London: British Institute of Radiology), 94–102.

Seed, T. M., Inal, C. E., and Singh, V. K. (2014). Radioprotection of Hematopoietic Progenitors by Low Dose Amifostine Prophylaxis. *Int. J. Radiat. Biol.* 90, 594–604. doi:10.3109/09553002.2014.899450

Seed, T., Singh, V. K., and Hanlon, B. K. (2019). Early and Late Changes in Radiation-Induced Gene Expression Arrays Following Radioprotection with Amifostine. *J. Radiat. Cancer Res.* 10, 44–57. doi:10.4103/jrcr.jrcr_5_19

Seed, T. M. (2005). Radiation Protectants: Current Status and Future Prospects. *Health Phys.* 89 (5), 531–545. doi:10.1097/01.hp.0000175153.19745.25

Sharlow, E. R. (2016). Revisiting Repurposing. *ASSAY Drug Develop. Tech.* 14, 554–556. doi:10.1089/adt.2016.766

Shirley, M. (2018). Avatrombopag: First Global Approval. *Drugs* 78, 1163–1168. doi:10.1007/s40265-018-0949-8

Singh, V. K., and Seed, T. M. (2017). A Review of Radiation Countermeasures Focusing on Injury-specific Medicinals and Regulatory Approval Status: Part I. Radiation Sub-syndromes, Animal Models and FDA-Approved Countermeasures. *Int. J. Radiat. Biol.* 93, 851–869. doi:10.1080/09553002.2017.1332438

Singh, V. K., and Seed, T. M. (2018). An Update on Sargramostim for Treatment of Acute Radiation Syndrome. *Drugs Today* 54, 679–693. doi:10.1358/dot.2018.54.11.2899370

Singh, V. K., and Seed, T. M. (2019). The Efficacy and Safety of Amifostine for the Acute Radiation Syndrome. *Expert Opin. Drug Saf.* 18, 1077–1090. doi:10.1080/14740338.2019.1666104

Singh, V. K., and Seed, T. M. (2020a). BIO 300: a Promising Radiation Countermeasure under Advanced Development for Acute Radiation Syndrome and the Delayed Effects of Acute Radiation Exposure. *Expert Opin. Investig. Drugs* 29, 429–441. doi:10.1080/13543784.2020.1757648

Singh, V. K., and Seed, T. M. (2020b). Pharmacological Management of Ionizing Radiation Injuries: Current and Prospective Agents and Targeted Organ Systems. *Expert Opin. Pharmacother.* 21, 317–337. doi:10.1080/14656566.2019.1702968

Singh, V. K., Brown, D. S., Kao, T.-C., and Seed, T. M. (2010). Preclinical Development of a Bridging Therapy for Radiation Casualties. *Exp. Hematol.* 38, 61–70. doi:10.1016/j.exphem.2009.10.008

Singh, V. K., Wise, S. Y., Singh, P. K., Ducey, E. J., Fatanmi, O. O., and Seed, T. M. (2012). α-Tocopherol Succinate- and AMD3100-Mobilized Progenitors Mitigate Radiation-Induced Gastrointestinal Injury in Mice. *Exp. Hematol.* 40, 407–417. doi:10.1016/j.exphem.2012.01.005

Singh, V. K., Wise, S. Y., Singh, P. K., Posarac, A., Fatanmi, O. O., Ducey, E. J., et al. (2013). Alpha-tocopherol Succinate-Mobilized Progenitors Improve Intestinal Integrity after Whole Body Irradiation. *Int. J. Radiat. Biol.* 89, 334–345. doi:10.3109/09553002.2013.762137

Singh, V. K., Wise, S. Y., Fatanmi, O. O., Beattie, L. A., and Seed, T. M. (2014a). Preclinical Development of a Bridging Therapy for Radiation Casualties. *Health Phys.* 106, 689–698. doi:10.1097/HP.0000000000000089

Singh, V. K., Wise, S. Y., Fatanmi, O. O., Scott, J., Romaine, P. L. P., Newman, V. L., et al. (2014b). Progenitors Mobilized by Gamma-Tocotrienol as an Effective Radiation Countermeasure. *PloS one* 9, e114078. doi:10.1371/journal.pone.0114078

Singh, V. K., Newman, V. L., and Seed, T. M. (2015). Colony-stimulating Factors for the Treatment of the Hematopoietic Component of the Acute Radiation Syndrome (H-ARS): A Review. *Cytokine* 71, 22–37. doi:10.1016/j.cyto.2014.08.003

Singh, V. K., Fatanmi, O. O., Wise, S. Y., Newman, V. L., Romaine, P. L. P., and Seed, T. M. (2016). The Potentiation of the Radioprotective Efficacy of Two Medical Countermeasures, Gamma-Tocotrienol and Amifostine, by a Combination Prophylactic Modality. *Radiat. Prot. Dosimetry* 172, 302–310. doi:10.1093/rpd/ncw223

Singh, V. K., Garcia, M., and Seed, T. M. (2017a). A Review of Radiation Countermeasures Focusing on Injury-specific Medicinals and Regulatory Approval Status: Part II. Countermeasures for Limited Indications, Internalized Radionuclides, Emesis, Late Effects, and Agents Demonstrating Efficacy in Large Animals with or without FDA IND Status. *Int. J. Radiat. Biol.* 93, 870–884. doi:10.1080/09553002.2017.1338782

Singh, V. K., Hanlon, B. K., Santiago, P. T., and Seed, T. M. (2017b). A Review of Radiation Countermeasures Focusing on Injury-specific Medicinals and Regulatory Approval Status: Part III. Countermeasures under Early Stages of Development along with 'standard of Care' Medicinal and Procedures Not Requiring Regulatory Approval for Use. *Int. J. Radiat. Biol.* 93, 885–906. doi:10.1080/09553002.2017.1332440

Sizar, O., Khare, S., Jamil, R. T., and Talati, R. (2020). "Statin Medications," in *StatPearls* (FL: Treasure Island).

Srinivasan, V., Weiss, J. F., and Kumar, K. S. (1992). "Radioprotection by Combination of WR-151327, Vitamin E and Selenomethionine.," 40th Annual Meeting of the Radiation Research Society. Salt Lake City, UT.

Srinivasan, V., Pendergrass, J. A., Jr., Kumar, K. S., and Landauer, M. R. (2002). Seed TM. Radioprotection, Pharmacokinetic and Behavioural Studies in Mouse Implanted with Biodegradable Drug (Amifostine) Pellets. *Int. J. Radiat. Biol.* 78 (6), 535–543. doi:10.1080/095530002317577358

Stickney, D. R., Dowding, C., Authier, S., Garsd, A., Onizuka-Handa, N., Reading, C., et al. (2007). 5-androstenediol Improves Survival in Clinically Unsupported Rhesus Monkeys with Radiation-Induced Myelosuppression. *Int. Immunopharmacol* 7 (4), 500–505. doi:10.1016/j.intimp.2006.12.005

Stull, D. M., Bilmes, R., Kim, H., and Fichtl, R. (2005). Comparison of Sargramostim and Filgrastim in the Treatment of Chemotherapy-Induced Neutropenia. *Am. J. Health Syst. Pharm.* 62, 83–87. doi:10.1093/ajhp/62.1.83

Takeshita, F., Leifer, C. A., Gursel, I., Ishii, K. J., Takeshita, S., Gursel, M., et al. (2001). Cutting Edge: Role of Toll-like Receptor 9 in CpG DNA-Induced Activation of Human Cells. *J. Immunol.* 167 (7), 3555–3558. doi:10.4049/jimmunol.167.7.3555

Underhill, D. M., and Ozinsky, A. (2002). Toll-like Receptors: Key Mediators of Microbe Detection. *Curr. Opin. Immunol.* 14 (1), 103–110. doi:10.1016/s0952-7915(01)00304-1

Unthank, J. L., Ortiz, M., Trivedi, H., Pelus, L. M., Sampson, C. H., Sellamuthu, R., et al. (2019). Cardiac and Renal Delayed Effects of Acute Radiation Exposure: Organ Differences in Vasculopathy, Inflammation, Senescence and Oxidative Balance. *Radiat. Res.* 191, 383–397. doi:10.1667/RR15130.1

Upton, A. C. (1985). "Biological Basis for Assessing Carcinogenic Risks of Low-Level Radiation," in *The Role of Chemicals. and Radiation in the Etiology of Cancer, Carcinogenesis- A Comprehensive Survey*. Editors E. Huberman and S. H. Barr (New York: Raven Press), 381–401.

U.S. Food and Drug Administration (2015a). FDA Approves Neupogen for Treatment of Patients with Radiation-Induced Myelosuppression Following a Radiological/nuclear Incident. Silver Spring, MD, USA: U.S. Food and Drug Administration. Available at: http://www.fda.gov/EmergencyPreparedness/Counterterrorism/MedicalCountermeasures/AboutMCMi/ucm443245.htm (Accessed July 6, 2016).

U.S. Food and Drug Administration (2015b). Guidance Document: Product Development under the Animal Rule. Available at: http://www.fda.gov/downloads/drugs/guidancecomplianceregulatoryinformation/guidances/ucm399217.pdf (Accessed March 15, 2020).

U.S. Food and drug Administration (2018a). FDA Approves Leukine for Acute Radiation Syndrome. Available at: https://www.fda.gov/downloads/EmergencyPreparedness/Counterterrorism/MedicalCountermeasures/AboutMCMi/UCM603226.pdf (Accessed April 01, 2018).

U.S. Food and Drug Administration (2018b). FDA Approves New Drug for Patients with Chronic Liver Disease Who Have Low Blood Platelets and Are Undergoing a Medical Procedure. Available at: https://www.fda.gov/news-events/press-announcements/fda-approves-new-drug-patients-chronic-liver-disease-who-have-low-blood-platelets-and-are-undergoing (Accessed June 22, 2020).

U.S. Food and Drug Adsministration (2015). Angiotensin-converting Enzyme Inhibitor (ACE Inhibitor) Drugs. Available at: https://www.fda.gov/drugs/postmarket-drug-safety-information-patients-and-providers/angiotensin-converting-enzyme-inhibitor-ace-inhibitor-drugs (Accessed June 20, 2020).

US Food and Drug Administration (2020a). Coronavirus (COVID-19) Update: FDA Issues Emergency Use Authorization for Potential COVID-19 Treatment. Available at: https://www.fda.gov/news-events/press-announcements/coronavirus-covid-19-update-fda-issues-emergency-use-authorization-potential-covid-19-treatment (Accessed July18, 2020).

US Food and Drug Administration (2020b). FDA Approves Three Drugs for Nonprescription Use through Rx-To-OTC Switch Process. Available at: https://www.fda.gov/news-events/press-announcements/fda-approves-three-drugs-nonprescription-use-through-rx-otc-switch-process (Accessed 09 July, 2020).

Vadhan-Raj, S., Goldberg, J. D., Perales, M. A., Berger, D. P., and van den Brink, M. R. (2013). Clinical Applications of Palifermin: Amelioration of Oral Mucositis and Other Potential Indications. *J. Cel Mol Med* 17, 1371–1384. doi:10.1111/jcmm.12169

van der Veen, S. J., Ghobadi, G., de Boer, R. A., Faber, H., Cannon, M. V., Nagle, P. W., et al. (2015). ACE Inhibition Attenuates Radiation-Induced Cardiopulmonary Damage. *Radiother. Oncol.* 114, 96–103. doi:10.1016/j.radonc.2014.11.017

Vasselon, T., and Detmers, P. A. (2002). Toll Receptors: a Central Element in Innate Immune Responses. *Infect. Immun.* 70 (3), 1033–1041. doi:10.1128/iai.70.3.1033-1041.2002

Wagner, H. (1999). Bacterial CpG DNA Activates Immune Cells to Signal Infectious Danger. *Adv. Immunol.* 73, 329–368. doi:10.1016/s0065-2776(08)60790-7

Wang, J., Boerma, M., Fu, Q., Kulkarni, A., Fink, L. M., and Hauer-Jensen, M. (2007). Simvastatin Ameliorates Radiation Enteropathy Development after Localized, Fractionated Irradiation by a Protein C-independent Mechanism. *Int. J. Radiat. Oncol. Biol. Phys.* 68 (5), 1483–1490. doi:10.1016/j.ijrobp.2007.03.036

Wang, E. S., Lyons, R. M., Larson, R. A., Gandhi, S., Liu, D., Matei, C., et al. (2012). A Randomized, Double-Blind, Placebo-Controlled Phase 2 Study Evaluating the Efficacy and Safety of Romiplostim Treatment of Patients with Low or Intermediate-1 Risk Myelodysplastic Syndrome Receiving Lenalidomide. *J. Hematol. Oncol.* 5, 71. doi:10.1186/1756-8722-5-71

Ward, W. F., Kim, Y. T., Molteni, A., and Solliday, N. H. (1988). Radiation-induced Pulmonary Endothelial Dysfunction in Rats: Modification by an Inhibitor of Angiotensin Converting Enzyme. *Int. J. Radiat. Oncol. Biol. Phys.* 15 (1), 135–140. doi:10.1016/0360-3016(88)90357-4

Ward, W. F., Molteni, A., Ts'ao, C., and Hinz, J. M. (1990). The Effect of Captopril on Benign and Malignant Reactions in Irradiated Rat Skin. *Br. J. Radiol.* 63, 749–354. doi:10.1259/0007-1285-63-749-349

Williams, J. P., and McBride, W. H. (2011). After the Bomb Drops: a New Look at Radiation-Induced Multiple Organ Dysfunction Syndrome (MODS). *Int. J. Radiat. Biol.* 87, 851–868. doi:10.3109/09553002.2011.560996

Williams, J. P., Hernady, E., Johnston, C. J., Reed, C. M., Fenton, B., Okunieff, P., et al. (2004). Effect of Administration of Lovastatin on the Development of Late Pulmonary Effects after Whole-Lung Irradiation in a Murine Model. *Radiat. Res.* 161 (5), 560–567. doi:10.1667/rr3168

Williams, J. P., Brown, S. L., Georges, G. E., Hauer-Jensen, M., Hill, R. P., Huser, A. K., et al. (2010a). Animal Models for Medical Countermeasures to Radiation Exposure. *Radiat. Res.* 173, 557–578. doi:10.1667/RR1880.1

Williams, J. P., Johnston, C. J., and Finkelstein, J. N. (2010b). Treatment for Radiation-Induced Pulmonary Late Effects: Spoiled for Choice or Looking in the Wrong Direction? *Curr. Drug Targets* 11, 1386–1394. doi:10.2174/1389450111009011386

Williams, J. P., Jackson, I. L., Shah, J. R., Czarniecki, C. W., Maidment, B. W., and DiCarlo, A. L. (2012). Animal Models and Medical Countermeasures Development for Radiation-Induced Lung Damage: Report from an NIAID Workshop. *Radiat. Res.* 177 (5), e0025–0039. doi:10.1667/rrol04.1

Williams, G. M., Kobets, T., Iatropoulos, M. J., Duan, J.-D., and Brunnemann, K. D. (2016). GRAS Determination Scientific Procedures and Possible Alternatives. *Regul. Toxicol. Pharmacol.* 79 (Suppl. 2), S105–S111. doi:10.1016/j.yrtph.2016.06.015

Williams, J. P., Calvi, L., Chakkalakal, J. V., Finkelstein, J. N., O'Banion, M. K., and Puzas, E. (2016). Addressing the Symptoms or Fixing the Problem? Developing Countermeasures against Normal Tissue Radiation Injury. *Radiat. Res.* 186, 1–16. doi:10.1667/RR14473.1

Wong, K., Bunin, D. I., Bujold, K., Javitz, H. S., Bakke, J., Gahagen, J., et al. (2020a). Annual cnference of Radiation Research Society, Virtual.

Wong, K., Chang, P. Y., Fielden, M., Downey, A. M., Bunin, D., Bakke, J., et al. (2020b). Pharmacodynamics of Romiplostim Alone and in Combination with Pegfilgrastim on Acute Radiation-Induced Thrombocytopenia and Neutropenia in Non-human Primates. *Int. J. Radiat. Biol.* 96, 155–166. doi:10.1080/09553002.2019.1625488

Xu, H., and Cai, R. (2019). Avatrombopag for the Treatment of Thrombocytopenia in Patients with Chronic Liver Disease. *Expert Rev. Clin. Pharmacol.* 12, 859–865. doi:10.1080/17512433.2019.1649137

Xu, G., Wu, H., Zhang, J., Li, D., Wang, Y., Wang, Y., et al. (2015). Metformin Ameliorates Ionizing Irradiation-Induced Long-Term Hematopoietic Stem Cell Injury in Mice. *Free Radic. Biol. Med.* 87, 15–25. doi:10.1016/j.freeradbiomed.2015.05.045

Yamaguchi, M., Hirouchi, T., Yokoyama, K., Nishiyama, A., Murakami, S., and Kashiwakura, I. (2018). The Thrombopoietin Mimetic Romiplostim Leads to the Complete Rescue of Mice Exposed to Lethal Ionizing Radiation. *Sci. Rep.* 8 (1), 10659. doi:10.1038/s41598-018-29013-5

Yamaguchi, M., Hirouchi, T., Yoshioka, H., Watanabe, J., and Kashiwakura, I. (2019). Diverse Functions of the Thrombopoietin Receptor Agonist Romiplostim Rescue Individuals Exposed to Lethal Radiation. *Free Radic. Biol. Med.* 136, 60–75. doi:10.1016/j.freeradbiomed.2019.03.023

Zakheim, R. M., Mattioli, L., Molteni, A., Mullis, K. B., and Bartley, J. (1975). Prevention of Pulmonary Vascular Changes of Chronic Alveolar Hypoxia by Inhibition of Angiotensin I-Converting Enzyme in the Rat. *Lab. Invest.* 33, 57–61.

Zhang, C., Lin, J., Cui, J., Li, B., Liu, C., Wang, J., et al. (2011a). Radioprotection of Bone Marrow Hematopoiesis by CpG-Oligodeoxynucleotides Administered to Mice after Total-Body Irradiation. *J. Radiat. Res.* 52, 828–833. doi:10.1269/jrr.10098

Zhang, C., Ni, J., Gao, F., Sun, D., Zhou, C., Cheng, Y., et al. (2011b). The Mechanism for the Ameliorative Effect of CpG-Oligodeoxynucleotides on Bone Marrow Hemopoiesis Radiation Injury. *Basic Clin. Pharmacol. Toxicol.* 109, 11–16. doi:10.1111/j.1742-7843.2011.00695.x

Zhang, C., Ni, J., Li, B.-L., Gao, F., Liu, H., Liu, W., et al. (2013). CpG-Oligodeoxynucleotide Treatment Protects against Ionizing Radiation-Induced Intestine Injury. *PloS one* 8, e66586. doi:10.1371/journal.pone.0066586

Zhong, Y., Pouliot, M., Downey, A.-M., Mockbee, C., Roychowdhury, D., Wierzbicki, W., et al. (2020). Efficacy of Delayed Administration of Sargramostim up to 120 hours Post Exposure in a Nonhuman Primate Total Body Radiation Model. *Int. J. Radiat. Biol.* 1, 17. doi:10.1080/09553002.2019.1673499

Conflict of Interest: Author TS is chief consultant of Tech Micro Services and declares no conflict of interest.

The remaining author declares that the research was conducted in the absence of any commercial or financial relationships that could be construed as a potential conflict of interest.

frontiers in Pharmacology

ORIGINAL RESEARCH
published: 17 May 2021
doi: 10.3389/fphar.2021.634477

Polypharmacy to Mitigate Acute and Delayed Radiation Syndromes

Tracy Gasperetti[1†], Tessa Miller[1†], Feng Gao[1], Jayashree Narayanan[1], Elizabeth R. Jacobs[2,3,4,5], Aniko Szabo[6], George N. Cox[7], Christie M. Orschell[8], Brian L. Fish[1] and Meetha Medhora[1,2,3,4,5]*

[1]Department of Radiation Oncology, Medical College of Wisconsin, Milwaukee, WI, United States, [2]Department of Medicine, Medical College of Wisconsin, Milwaukee, WI, United States, [3]Department of Physiology, Medical College of Wisconsin, Milwaukee, WI, United States, [4]Cardiovascular Center, Medical College of Wisconsin, Milwaukee, WI, United States, [5]Department of Veterans Affairs, Research Service, Zablocki VAMC, Milwaukee, WI, United States, [6]Institute for Health and Equity, Division of Biostatistics, Medical College of Wisconsin, Milwaukee, WI, United States, [7]Bolder BioTechnology Inc., Boulder, CO, United States, [8]Department of Medicine, Indiana University School of Medicine, Indianapolis, IN, United States

There is a need for countermeasures to mitigate lethal acute radiation syndrome (ARS) and delayed effects of acute radiation exposure (DEARE). In WAG/RijCmcr rats, ARS occurs by 30-days following total body irradiation (TBI), and manifests as potentially lethal gastrointestinal (GI) and hematopoietic (H-ARS) toxicities after >12.5 and >7 Gy, respectively. DEARE, which includes potentially lethal lung and kidney injuries, is observed after partial body irradiation >12.5 Gy, with one hind limb shielded (leg-out PBI). The goal of this study is to enhance survival from ARS and DEARE by polypharmacy, since no monotherapy has demonstrated efficacy to mitigate both sets of injuries. For mitigation of ARS following 7.5 Gy TBI, a combination of three hematopoietic growth factors (polyethylene glycol (PEG) human granulocyte colony-stimulating factor (hG-CSF), PEG murine granulocyte-macrophage-CSF (mGM-CSF), and PEG human Interleukin (hIL)-11), which have shown survival efficacy in murine models of H-ARS were tested. This triple combination (TC) enhanced survival by 30-days from ~25% to >60%. The TC was then combined with proven medical countermeasures for GI-ARS and DEARE, namely enrofloxacin, saline and the angiotensin converting enzyme inhibitor, lisinopril. This combination of ARS and DEARE mitigators improved survival from GI-ARS, H-ARS, and DEARE after 7.5 Gy TBI or 13 Gy PBI. Circulating blood cell recovery as well as lung and kidney function were also improved by TC + lisinopril. Taken together these results demonstrate an efficacious polypharmacy to mitigate radiation-induced ARS and DEARE in rats.

Keywords: polypharmacy, acute radiation syndrome, delayed effects of acute radiation exposure, mitigation, hematopoietic growth factor, lisinopril, supportive care, radiation pneumonitis

OPEN ACCESS

Edited by:
Lynnette H. Cary, Uniformed Services University of the Health Sciences, United States

Reviewed by:
Nazareno Paolocci, Johns Hopkins University, United States
Ann Farese, University of Maryland, Baltimore, United States

****Correspondence:***
Tracy Gasperetti
tgasperetti@mcw.edu

[†]These authors have contributed equally to this work and share first authorship

Specialty section:
This article was submitted to Translational Pharmacology, a section of the journal Frontiers in Pharmacology

Received: *27 November 2020*
Accepted: *19 April 2021*
Published: *17 May 2021*

Citation:
Gasperetti T, Miller T, Gao F, Narayanan J, Jacobs ER, Szabo A, Cox GN, Orschell CM, Fish BL and Medhora M (2021) Polypharmacy to Mitigate Acute and Delayed Radiation Syndromes. Front. Pharmacol. 12:634477. doi: 10.3389/fphar.2021.634477

INTRODUCTION

Heightened global tensions have resulted in a worldwide threat of accidental or belligerent radiation exposure. The United States has initiated extensive research for adequate preparedness in case of such events. The National Institute of Allergy and Infectious Diseases (NIAID) developed a program to study the mechanisms of radiation-induced injuries as well as specific countermeasures to mitigate these injuries (DiCarlo et al., 2008; DiCarlo et al., 2011). Ionizing radiation alone can result in a broad

spectrum of biological tissue damage and lethality in mammals. Sequential injuries to multiple organs occur after exposure of whole animals to radiation, which patterns radiation-damage observed in humans (Fish et al., 2020). The acute radiation syndrome (ARS) occurs first, with gastrointestinal (GI) injury starting within a week after exposure followed by bone marrow toxicity in rodents, nonhuman primates (NHP) and humans (Fliedner et al., 2005; Unthank et al., 2015; Fish et al., 2020). Survivors of ARS proceed to develop the delayed effects of acute radiation exposure (DEARE) which manifest as multiple, spatial sequelae including lung injury (radiation pneumonitis after ~42-days) and kidney injury (radiation nephropathy after ~120-days), depending on the initial radiation dose. In rodents, other organs such as the brain, heart, etc. also manifest DEARE but these injuries are lethal at PBI doses higher than those that cause lethality by bone marrow or lung toxicities (Moulder, 2014; Boerma et al., 2016). Approval of drugs to mitigate such radiation injuries requires pivotal efficacy screening through the Food and Drug Administration (FDA) Animal Rule, using animal models that manifest responses similar to humans (USFDA, 2015b). Therefore, in order to identify mitigators for radiation injuries we have developed rat models to simulate the damage from exposure to near total body volumes. Following single high exposures to radiation to the total body in WAG/RijCmcr rats (equivalent to 5–12 Gy in humans), ARS occurs within the first 30-days. This syndrome covers gastrointestinal injury (days 3–7) and hematopoietic cell depletion (days 8–30). Partial bone marrow shielding (5–8%), and supportive care are needed for rats to survive ARS past 30-days, at doses >12.5 Gy, after which they will experience DEARE, with damage to the lungs, kidneys, and other organs. Lung injury can be fatal at 13 Gy or higher and occurs between days 40–90 while lethal renal injury manifests after doses as low as 8–9 Gy (Moulder et al., 2011), but after more than 120-days (Fish et al., 2016).

Currently, several agents have demonstrated efficacy to mitigate ARS (Ng et al., 2020; REMM, 2020). However, only granulocyte colony-stimulating factor (G-CSF, Neupogen), granulocyte macrophage colony-stimulating factor (GM-CSF, Leukine) and PEGylated G-CSF (Neulasta) are approved by the U.S. Food and Drug Administration (FDA) to be used after exposure to myelosuppressive doses of radiation (USFDA, 2015a; USFDA, 2021; Amgen, 2015a; Amgen, 2015b; Sanofi-Aventis, 2018). Recently, Nplate (romiplostim) has also been approved by the FDA to be used after similar doses of radiation for the treatment of thrombocytopenia (Amgen, 2021; USFDA, 2021). These cytokines are kept in the Strategic National Stockpile which is managed by the U.S. Department of Health and Human Services and the Office of the Assistant Secretary for Preparedness and Response (REMM, 2020).

Another promising hematopoietic growth factor (HGF) is Interleukin (IL)-11, a member of the IL-6-type cytokine family (Lee et al., 2012). It is approved to treat chemotherapy-induced thrombocytopenia. IL-11 also protects against renal injury in mice, human proximal tube injury in culture, and attenuates the inflammatory responses in a murine model of lipopolysaccharide-induced sepsis.

In addition, PEGylated GM-CSF and PEG-IL11 have been shown in rodents to possess longer half-lives and induce longer-lasting increases in hematopoietic cells through neutrophil recovery and their ability to increase immune function in rodents (Plett et al., 2014; Kumar et al., 2018; Cox et al., 2020). We used a combination of these PEG-HGF mitigators (PEG-GM-CSF, PEG-G-CSF, and PEG-IL-11, Bolder Biotechnology Inc., 2425 55th St., Suite 210, Boulder, CO 80301 United States) for the current study, and will refer to them as a triple combination (TC). The TC included a PEGylated murine (m) derivative of GM-CSF (PEG mGM-CSF), to closely match species specificity observed for GM-proteins. However, PEGylated human (h) derivatives of G-CSF (PEG hG-CSF) and IL-11 (PEG hIL-11) were included in the TC, since they are known to be bioactive in rodents.

ACE inhibitors are one of few mitigators for DEARE in rats. The use of an ACE inhibitor significantly decreased morbidity caused by pneumonitis (Kma et al., 2012) even if started 35-days after irradiation (Gao et al., 2013). The ACE inhibitor lisinopril decreased renal injury in rats given 13 Gy leg-out partial body irradiation (leg-out PBI) (Fish et al., 2016). Leg-out PBI exposes the whole body to irradiation, except for part of one hind leg that is shielded. This allows for bone marrow repopulation to allow DEARE to manifest in the lung and kidneys without bone marrow transplantation. In addition, ACE inhibitors including lisinopril, reduced the prevalence of radiation-induced pneumonitis in cancer patients treated with radiotherapy (Jenkins and Watts, 2011; Jenkins and Welsh, 2011; Kharofa et al., 2012), indicating efficacy in humans. However, ACE inhibitors have not shown efficacy to mitigate ARS in rats (Fish et al., 2016) but are efficacious in mice (Davis et al., 2010; Barshishat-Kupper et al., 2011; McCart et al., 2019), which necessitates the evaluation of combining ACE inhibitors with other promising mitigators.

Our ultimate goal is to treat both ARS and DEARE. Since no single agent has been identified, we are developing a compatible, multi-agent approach. We are combining promising mitigators to demonstrate efficacy for at least four sequelae that occur after irradiation. Female WAG/RijCmcr rats given leg-out PBI provide some of the best characterized models available for such studies. These models were used in this initial proof of concept study. Future studies with adult, geriatric and pediatric models using male and female rats will help confirm the efficacy of this approach for FDA approval.

METHODS

Animal Care

All animal use was approved by the Institutional Animal Care and Use Committees (IACUC) at the Medical College of Wisconsin and care for the rats was provided as previously described (Fish et al., 2016). All rats were fed Teklad 8904 diet and provided reverse osmosis (RO) hyper-chlorinated water ad libitum. In order to study the efficacy of a combination of drugs for ARS and DEARE, two sets of experiments using different injury models were used.

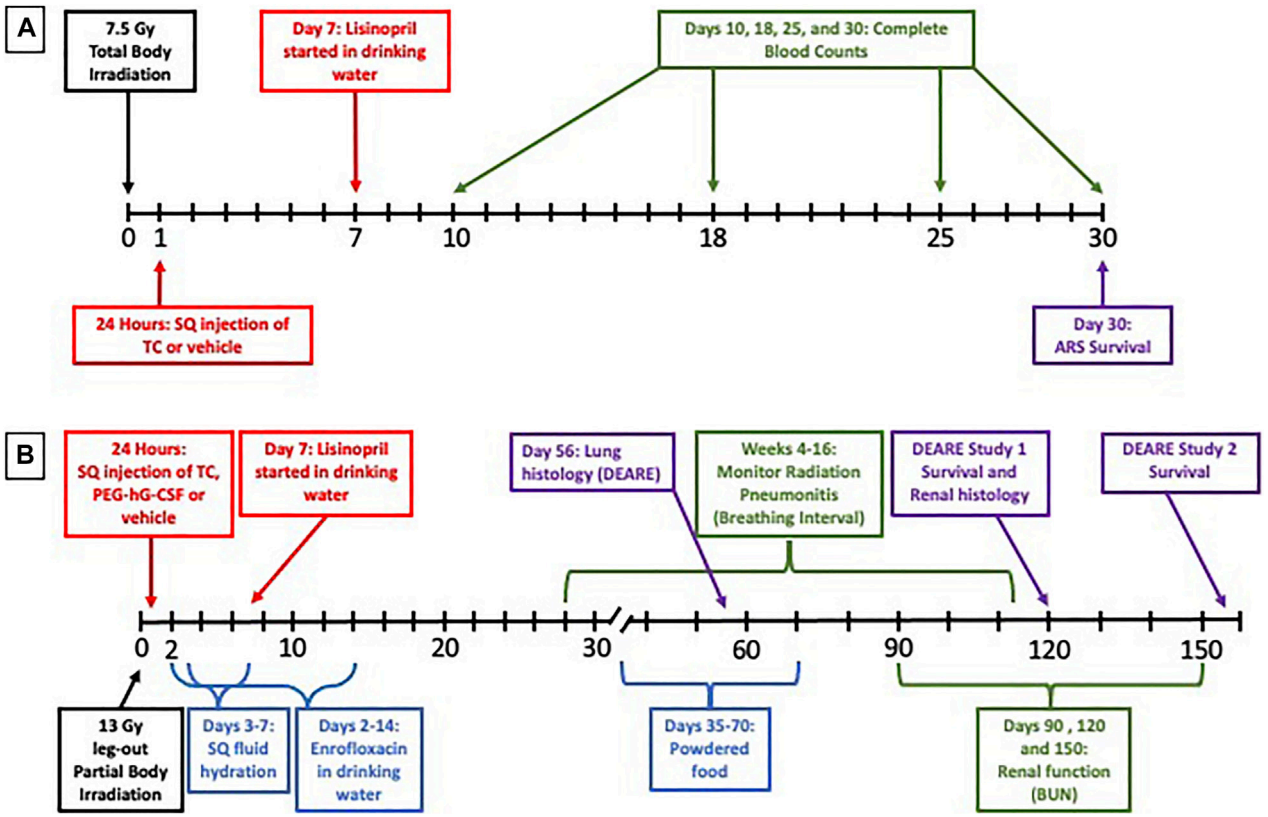

FIGURE 1 | Experimental design. To study the Acute Radiation Syndrome (ARS) **(A)**, female WAG/RijCmcr rats (11–12 weeks of age) were irradiated with 7.5 Gy total body irradiation (TBI). At 24-h post-irradiation, all rats received a subcutaneous (SQ) injection of either the triple combination (TC, consisting of PEG-hG-CSF, PEG mGM-CSF and PEG hIL-11) or vehicle and the ACE inhibitor lisinopril was started in the drinking water (24 mg m^{-2} d^{-1}) in two groups at 7 days post-irradiation. A subset of each treatment group was bled at days 10, 18, 25, and 30-days and complete blood counts were analyzed. The ARS experiment was terminated at 30-days.To study the Delayed Effects of Acute Radiation Syndrome (DEARE) **(B)**, female WAG/RijCmcr rats (11–12 weeks of age) were irradiated with 13 Gy leg-out partial body irradiation (leg-out PBI). At 24-h post-irradiation, all rats received a subcutaneous (SQ) injection of either the triple combination (TC, consisting of PEG-hG-CSF, PEG mGM-CSF and PEG hIL-11), PEG-hG-CSF or vehicle and the ACE inhibitor lisinopril was started in the drinking water (24 mg m^{-2} d^{-1}) in two groups at 7 days post-irradiation. Supportive care consisting of antibiotics (enrofloxacin, 10 mg kg^{-1} d^{-1}, days 2–14) in the drinking water, SQ fluid hydration (saline, 40 ml kg^{-1} d^{-1}, days 3–7) and supplemental powdered diet (days 35–70) were provided to all rats in the DEARE study. Radiation pneumonitis was monitored weekly by recording breathing rates (weeks 4–16) and while radiation nephropathy was monitored by measuring the blood urea nitrogen (BUN, days 90, 120, and 150). Lungs and kidneys were harvested at 56 and 120 days respectively to observe lung and renal radiation injury. The DEARE studies were terminated at 120 or 160-days.

Acute Radiation Syndrome Study

Total Body Irradiation in Rats

Female WAG/RijCmcr rats (11–12 weeks of age) were given total body irradiation (TBI) without the use of anesthetics. All rats were placed in a plastic jig and were irradiated using a XRAD 320 KV orthovoltage x-ray system (Precision X-Ray, North Branford, Connecticut) as previously described (Medhora et al., 2019). The X-ray system was operated at 320 kVp and 13 mAs with a half value layer of 1.4 mm Cu and a dose-rate of 1.75 Gy min^{-1} for a total dose of 7.5 Gy.

Dosimetry for Irradiation (Medhora et al., 2014)

A Soft X-Ray ionization Chamber (PTW, Germany) was used to collect depth dose information. Absolute calibration measurements were made using a Farmer-type ionization chamber and a Kiethley electrometer. This system was calibrated for the orthovoltage energy range at the Accredited Dosimetry Calibration Laboratory located at University of Wisconsin, Madison, WI. Measurements performed in this laboratory are directly traceable to the National Institute of Standards and Technology. The ionization was measured in air and then converted to absolute dose in water following the American Association of Physicists in Medicine Task Group-61 protocol (Ma et al., 2001). The dose rate for TBI was defined at the midline of the rat and was calculated as described for TBI and leg-out PBI using measured output of the machine and the depth dose data. Then the irradiation time, including appropriate timer error of the X-ray machine, was calculated to deliver the required dose in one fraction using a posterior-to-anterior beam. Gafcromic film EBT2 (ISP, United States) sandwiched between slabs of solid water phantom was used to obtain profile distributions. The dose at the centers of the two rat chambers varied by 2%, and rats were randomly assigned to chambers to avoid any resulting bias. The irradiation field at midline was large enough to cover both chambers with adequate (at least 2 cm) margins.

Interventions

The experimental design of the ARS study can be visualized in **Figure 1A**. After irradiation, rats were randomly assigned to one of five study arms: 1) 7.5 Gy TBI ($n = 27$); 2) 7.5 Gy TBI + vehicle ($n = 41$); 3) 7.5 Gy TBI + TC ($n = 39$); 4) 7.5 Gy TBI + vehicle + lisinopril ($n = 27$); or 5) 7.5 Gy TBI + TC + lisinopril ($n = 36$). A group of age-matched non-irradiated controls ($n = 12$) were also included in this study. A single dose of either TC (2.75 ml kg^{-1}, 10 mM Sodium Phosphate, 4% Mannitol, 1% Sucrose; PEG hG-CSF 0.55 mg kg^{-1}; PEG mGM-CSF 0.55 mg kg^{-1}; PEG hIL-11 0.165 mg kg^{-1}) (Bolder BioTechnology, Boulder, CO) or the matched vehicle (2.75 ml kg^{-1}, 10 mM Sodium Phosphate, 4% Mannitol, 1% Sucrose) was subcutaneously injected into assigned groups 24-h post-irradiation. At 7-days post-irradiation, when recovery from GI toxicity is usually observed, lisinopril (21CEC PX Pharm Ltd. United Kingdom; 24 mg m^{-2} d^{-1}) was started in the drinking water and continued until termination (groups 4 and 5). Secondary endpoints for GI-ARS were not included in the protocol because the dose of radiation in the TBI model (7.5 Gy) was well below the threshold to observe non-invasive symptoms of GI injury such as diarrhea (doses >11 Gy in WAG/RijCmcr rats, Fish et al., 2020). The TC were not expected to alter GI-ARS based on other studies with the components of the TC (Chua et al., 2014; Cox et al., 2020). Whole blood was collected via the jugular vein at days 10-, 18-, 25-, and 30-post-irradiation. The experiment was terminated at 30-days and the rats were euthanized.

Blood Cell Counts

A subset of rats from each study arm including: 1) 7.5 Gy TBI control ($n = 12$), 2) 7.5 Gy TBI + vehicle ($n = 11$), 3) 7.5 Gy TBI + TC ($n = 11$), 4) 7.5 Gy TBI + vehicle + lisinopril ($n = 11$), or 5) 7.5 Gy TBI + TC + lisinopril ($n = 11$), were anesthetized with 3–5% isoflurane and bled via jugular vein by a trained technician (Medhora et al., 2019). EDTA was used to prevent blood clotting. Whole blood was sent to Marshfield Laboratories (Marshfield, WI) for complete blood counts (CBC). Hematocrit, neutrophils, platelets, red blood cells, percent reticulocytes, and absolute reticulocytes were analyzed to monitor hematopoietic injury.

Statistical Analyses

Analysis for 30-day morbidity was shown by Kaplan-Meier plots and tested for differences between groups by Cox regression. Neutrophil counts were analyzed using linear mixed effects models with a random animal intercept to account for repeated measures. Based on a Box-Cox analysis, the counts were log-transformed for analysis because this step improved the linearity of the effects and the normality and homoskedasticity of the residuals. The results were summarized by pairwise comparison of treatments within each day and were adjusted for multiple testing within each time-point using Tukey's method. Analyses were performed using R 3.5.0 (R Foundation for Statistical Computing, Vienna, Austria).

Delayed Effects of Acute Radiation Exposure Study

Leg-Out Partial Body Irradiation in Rats

Female WAG/RijCmcr rats (11–12 weeks of age) were given leg-out PBI without the use of anesthetics as previously described (Medhora et al., 2019). This model of irradiation exposes the entire body of the rat to ionizing radiation except for one hind limb which is out of the field. Therefore, it is referred to as leg-out PBI rather than TBI since the entire rat is not exposed to radiation. Briefly, rats were immobilized in a plastic jig and irradiated in the same manner as described for TBI, to a total dose of 13 Gy. To allow for bone marrow recovery, one hind limb of each rat was carefully externalized from the jig and shielded from radiation with a 0.25-inch lead block. The dose to this leg was ~2 Gy (5–8% bone marrow shielding). Dosimetry was conducted as previously described for the Acute Radiation Syndrome study (Medhora et al., 2014; Medhora et al., 2015).

Interventions

The experimental design of the DEARE experiments can be visualized in **Figure 1B**. All rats were given supportive care of enrofloxacin (10 mg kg^{-1} d^{-1}) from days 2–14 post-irradiation and subcutaneous fluid hydration (saline, 40 ml kg^{-1} d^{-1}) from days 3 to 7 post-irradiation, as described previously (Fish et al., 2016). To study DEARE to 120-days, female rats were randomly assigned to one of five study arms: 1) Non-irradiated + vehicle (for TC, $n = 10$); 2) 13 Gy leg-out PBI + vehicle ($n = 28$); 3) 13 Gy leg-out PBI + TC ($n = 21$); 4) 13 Gy leg-out PBI + PEG-hG-CSF ($n = 21$); or 5) 13 Gy leg-out PBI + TC + lisinopril ($n = 16$). To study DEARE to 160-days, female rats were randomly assigned to one of the following four study arms: 1) 13 Gy leg-out PBI + vehicle (for TC) ($n = 12$); 2) 13 Gy leg-out PBI + TC ($n = 12$); 3) 13 Gy leg-out PBI + vehicle + lisinopril ($n = 12$); or 4) 13 Gy leg-out PBI + TC + lisinopril ($n = 12$). Since lisinopril is soluble in water, no vehicle specific for lisinopril was required. A single dose of either TC, vehicle for TC (see ARS study) or PEG-hG-CSF (BBT-015 0.55 mg kg^{-1}, Bolder BioTechnology, Boulder, CO) was subcutaneously injected into assigned groups 24 h post-irradiation. At 7-days post-irradiation, lisinopril (21CEC PX Pharm Ltd. United Kingdom; 24 mg m^{-2} d^{-1}) was started in the drinking water and continued until termination in one group. All rats provided powdered diet in addition to pelleted diet days 35–70 post-irradiation due to tooth loss following leg-out PBI. Tooth loss is observed when the head of rats is not shielded during exposure, but the teeth grow back by day 70. The supplemental powdered food eliminates weight loss due to the inability to eat pelleted food.

Since lethal GI injury occurs at doses >11 Gy leg-out PBI (Fish et al., 2020) without supportive care and above 13 Gy with supportive care, secondary endpoints for GI toxicity were not included. For the 120-days DEARE study, breathing rates (BR) were recorded every other week starting at week 4 post-irradiation and continuing through week 16 to evaluate lung function. Blood was collected via jugular vein at 90- and 120-days post-irradiation to monitor blood urea nitrogen (BUN) levels. BUN is a measure of renal function. For the 120-days study, at day 56 (during radiation pneumonitis), random sets of rats from each study arm were euthanized for lung histology (peak of pneumonitis). At termination (day 120), rats were euthanized, and the kidneys harvested for histology.

The second DEARE study was terminated at 160-days, with survival serving as the primary end point. BUNs were measured at 90-, 120- and 150-days post-irradiation.

Blood was harvested, followed by necropsy for all rats that were identified as moribund to confirm morbidity due to lethal radiation pneumonitis or nephropathy as the cause of death.

Measurement of Breathing Interval

To monitor radiation pneumonitis, breathing rates and body weights were measured every other week from weeks 4 to 16, as previously described (Medhora et al., 2014; Medhora et al., 2015). Rats were placed in a plastic restrainer for 5 min for two consecutive training days to allow the rats to become acclimated to the apparatus. On the third day, the restrainer was placed in a transparent EMKA plethysmograph (Scireq Scientific Respiratory Equipment Inc., Montreal, QC, Canada) which measured the frequency of pressure changes. Each rat was recorded for a maximum of 10 min and the mean breathing rate was calculated from four steady 15 s recordings. The inverse of the breathing rates was calculated to derive the breathing interval or time/breath in minutes. Higher breathing rates and lower breathing intervals are associated with more lung damage. The breathing interval was set to 0 for all animals that were moribund during pneumonitis to account for attrition (Medhora et al., 2012; Gao et al., 2014; Medhora et al., 2020).

Measurement of Blood Urea Nitrogen

A sensitive method to assess radiation-induced nephropathy is to measure the serum BUN levels which correlate well with renal histopathology as previously published (Moulder et al., 2011). Rats were anesthetized with isoflurane (3–5%) and blood was drawn via the jugular vein by a trained technician at days 90 and 120 post-irradiation (Medhora et al., 2019). The BUN was assayed from serum as described previously (Cohen et al., 1994; Medhora et al., 2014; Fish et al., 2016) using a urease-nitroprusside colorimetric assay. BUN values were expressed as mg dL^{-1} of serum and medians with 20–80% ranges were used for statistical analysis. Irradiated rats with BUN > 120 mg dl^{-1} had lethal radiation nephropathy and were euthanized and given a value of 120 mg dl^{-1} to account for attrition, since such rats were previously confirmed to have severe and irreversible renal damage (Moulder et al., 1993; Fish et al., 2016; Medhora et al., 2020).

Lung Histology

A subset of irradiated rats from the 120-days DEARE study was assigned for lung histology at 56-days after 13 Gy leg-out PBI as described previously (Medhora et al., 2014; Medhora et al., 2015). Briefly, the lungs were harvested, inflated, and fixed by gravity using 10% buffered formalin (Fisher Scientific, Pittsburg, PA) and the left lung was embedded in paraffin. Whole mount left lung sections (4 µm thick) were stained with H&E. Five (20×) fields from each rat were randomly selected and scored by operators blinded to the treatment groups. Vessel wall thickness, alveolar wall thickness, and foamy macrophages were scored as described previously (Medhora et al., 2014; Medhora et al., 2015). Higher scores indicated more severe lung injury.

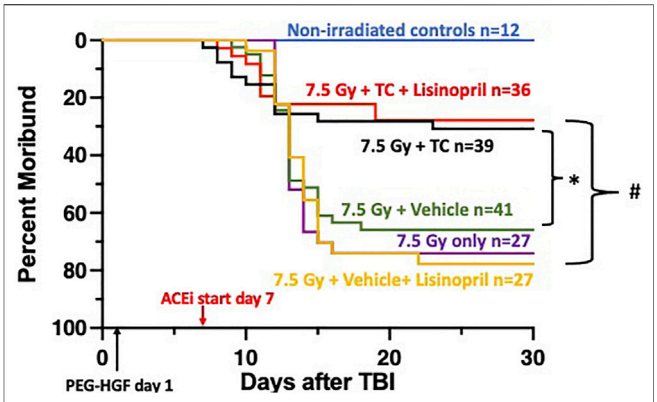

FIGURE 2 | Mitigation of hematopoietic-acute radiation syndrome (H-ARS) by triple combination with and without lisinopril. Kaplan-Meier plots show morbidity through 30-days after 7.5 Gy total body irradiation (TBI). The triple combination (TC, consisting of PEG-hG-CSF, PEG mGM-CSF and PEG hIL-11) or vehicle were given subcutaneously 24-h after TBI (designated by PEG-HGF) and the ACE inhibitor, lisinopril, was started in the drinking water 7 days after irradiation. The number of rats in each group is designated by the "*n*." Non-irradiated controls are represented with the blue line. Morbidity was not different in the three irradiated groups given 7.5 Gy only, with vehicle or lisinopril, but survival was enhanced in the group which received the TC (p = 0.05, denoted by * compared to 7.5 Gy + vehicle group). Survival was increased in the irradiated group receiving TC and lisinopril compared to the irradiated rats receiving the vehicle for TC and lisinopril ($p < 0.05$, denoted by #).

Kidney Histology

At the termination of the study (120-days post 13 Gy leg-out PBI), the kidneys were harvested, cut into halves and immediately fixed in 10% buffered formalin and processed for paraffin embedding. Kidney sections were stained with H&E, and the kidney injury blinded and assessed in coded samples as described earlier (Moulder et al., 1993). Kidneys were scored as follows: absence of renal cyst (0); presence of microscopic (1+); and macroscopic (2+) cysts. Glomerular sclerosis was assessed by studying 20 random glomeruli per slide as follows: 1–2 sclerosed glomeruli (1+); 3–4 sclerosed glomeruli (2+); or 5 or more sclerosed glomeruli (3+). Interstitial fibrosis was assessed on an increasing scale as none (0); scattered (1+); or diffuse (2+). Glomerular mesangiolysis was assessed as absent (0); variably present (1+); present in most glomeruli (2+); and present in all glomeruli (3+). These scores were then aggregated to get a composite histologic score. Higher scores indicated more severe renal injury.

Statistical Analyses

Analysis for morbidity after 30-days is shown by Kaplan-Meier plots and the three growth-factor treated groups were analyzed using Cox regression, with pairwise comparisons using a multivariate normal distribution-based single-step adjustment for multiple comparison control. Breathing intervals are shown as means with 95% CIs. BUN values are shown as medians and 20–80% ranges. Statistical differences of breathing intervals and BUN values were calculated by the ANOVA on Ranks with multiple comparisons by the Dunnett's method and both accounted for attrition. For analyses of histological results, a

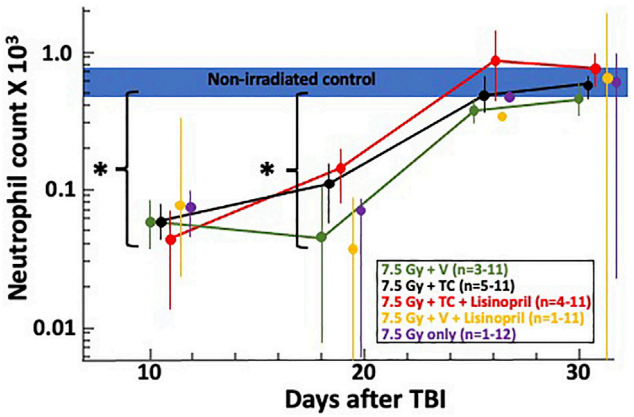

FIGURE 3 | Neutrophil recovery through 30-days post 7.5 Gy total body irradiation (TBI) is shown on a log-scale for the neutrophil count ($\times 10^3$). The horizontal blue bar represents the neutrophil counts for non-irradiated controls. Asterisks (*) represent $p < 0.02$ as compared to non-irradiated controls. At 18 days, the two irradiated groups given the triple combination (TC, consisting of PEG-hG-CSF, PEG mGM-CSF and PEG hIL-11) with (red) and without lisinopril (black), had higher neutrophil counts ($p \leq 0.005$) than the irradiated groups given the vehicle and lisinopril (yellow). Neutrophil counts returned to levels resembling non-irradiated controls by 25-days post-irradiation. The "*n*" values represent the number of rats alive in each group between 10 and 30 days after irradiation which decreased over time due to rats becoming moribund. Error bars represent 95% CIs for the mean.

one-way ANOVA was used to determine significance. All pairwise multiple comparisons were conducted with the Holm-Sidak method as post-hoc analysis. In case data failed either normality or equal variance tests, ANOVA on ranks with all pairwise multiple comparisons by Dunn's method were used.

RESULTS

Mitigation of Acute Radiation Syndrome

Enhanced Survival After 7.5 Gy TBI With PEG-HGFs

Rats were irradiated with 7.5 Gy TBI at 11–12 weeks of age and randomly assigned to one of five treatment groups to assess morbidity due to hematopoietic injury (see *Methods*). At 24-h post-irradiation, rats were injected subcutaneously with TC or vehicle. The ACE inhibitor, lisinopril, was started in the drinking water 7-days post-irradiation in two irradiated groups, one that received TC and one that received the vehicle for TC. **Figure 2** shows a Kaplan-Meier survival plot to 30-days post-irradiation, through hematopoietic acute radiation syndrome (H-ARS) for the five treatment groups and age-matched, non-irradiated controls. At 30-days post-irradiation, 69% of the rats that received 7.5 Gy TBI, but no TC, were moribund. The addition of the TC improved survival ($p = 0.05$) compared to irradiated animals receiving the vehicle only. The rats that received 7.5 Gy TBI with TC and lisinopril also had enhanced survival as compared to the vehicle and lisinopril group, with only 28% morbidity ($p < 0.05$). Therefore, TC improves survival, even in the presence of lisinopril. None of the non-irradiated control rats were moribund in this study.

Effects of PEG-HGFs and Lisinopril on Recovery of blood BCell Counts After Radiation

Complete blood cell counts at 10-, 18-, 25- and 30-days post-irradiation were measured as a secondary endpoint to examine the bone marrow injury after TBI. Blood collection began at 10-days post-irradiation since this is typically when hematopoietic injury is observed in this model. **Figure 3** shows at 10-days the neutrophil count had dropped for all irradiated groups compared to the control (non-irradiated) group (denoted by a blue bar). At day 18, neutrophils in all irradiated groups were still lower than in the control group. Neutrophils in the irradiated groups given the TC, with or without lisinopril, were significantly higher than irradiated rats given the vehicle and lisinopril ($p \leq 0.005$). All irradiated groups were not different from control values by day 25. Platelet counts were not reported due to inconsistent reporting in a number of samples.

Mitigation of Delayed Effects of Acute Radiation Exposure to 120 days

Survival After 13 Gy Leg-Out PBI With Lisinopril

Rats were irradiated with 13 Gy leg-out PBI at 11–12 weeks of age and randomly assigned to one of four treatment groups (see *Methods* and **Figure 4**) to assess survival through DEARE to 120-days. Since PEG-G-CSF (Neulasta, Amgen) is an approved medical countermeasure for ARS, we tested Bolder BioTechnology's PEG-hG-CSF (BBT-015, one of the components of the TC) alone to determine if it altered

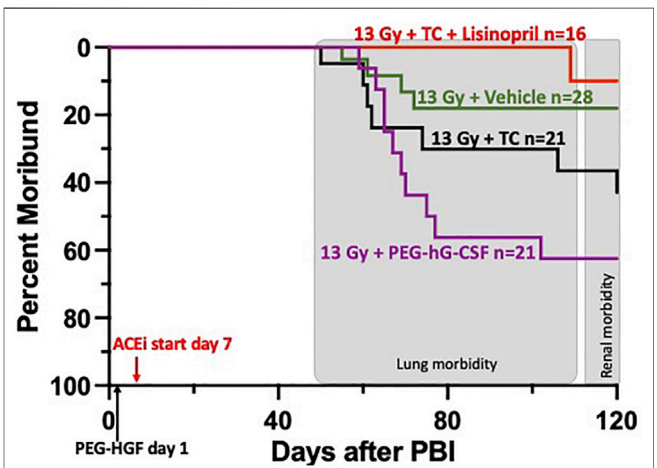

FIGURE 4 | Kaplan-Meier plot representing morbidity from DEARE up to 120 days post 13 Gy partial body irradiation with one hind limb shielded (leg-out PBI). The triple combination (TC, consisting of PEG-hG-CSF, PEG mGM-CSF and PEG hIL-11), vehicle or PEG-hG-CSF (BBT-015) were given subcutaneously 24 h post leg-out PBI (designated by PEG-HGF) and the ACE inhibitor, lisinopril, was started in the drinking water 7 days post irradiation (24 mg m^{-2} d^{-1}). All irradiated rats were given supportive care with subcutaneous hydration (40 ml kg^{-1} d^{-1}) and enrofloxacin (10 mg kg^{-1} d^{-1}) from days 3–7 to 2–14, respectively,. There was trend in lower morbidity in irradiated rats that received TC + lisinopril compared to irradiated rats that received PEG-hG-CSF, but this was not significant ($p = 0.07$). Shaded (gray) areas represent the timing for the lung and renal injuries.

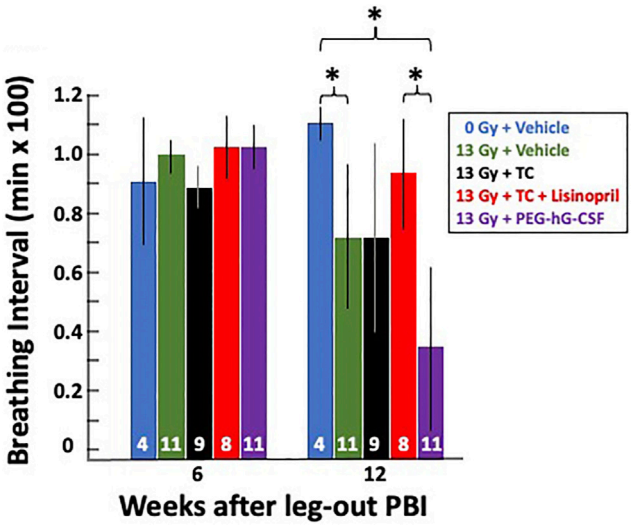

FIGURE 5 | Radiation pneumonitis is mitigated by lisinopril after 13 Gy leg-out PBI. Graphical representation of breathing intervals as a secondary and functional endpoint for lung injury were obtained from all 13 Gy leg-out PBI irradiated treatment groups and non-irradiated controls. Breathing rates were recorded biweekly from weeks 4 to 16 post-irradiation and converted to breathing intervals (see *Methods*). The bars represent means with 95% CIs. Rats moribund with lung injury confirmed at necropsy (13 Gy + vehicle n = 2, 13 Gy + PEG-hG-CSF n = 6, 13 Gy + TC n = 2) were given a breathing interval of 0 at 12 weeks to account for attrition. Numbers in the bars represent N in each group. Asterisks represent $p < 0.05$ between treatment groups at 12 weeks, in brackets: 0 Gy + vehicle vs. 13 Gy + PEG-hG-CSF, 0 Gy vehicle vs. 13 Gy + vehicle, 13 Gy + TC + lisinopril vs. 13 Gy + PEG-hG-CSF.

morbidity during DEARE. The study was terminated at 120-days and **Figure 4** shows a Kaplan-Meier survival plot for these four treatment groups. By 120-days, 63% of the irradiated rats given PEG-hG-CSF only were moribund, with the majority occurring between 60 and 80 days coinciding with pneumonitis (Fish et al., 2016). There was morbidity in all groups starting at 50-days post-irradiation except in the irradiated rats that received TC + lisinopril (6% morbidity). Though the addition of lisinopril trended to increase survival to 120-days in the irradiation rats given TC, this did not reach significance from the 13 Gy + PEG-hG-CSF only group (p = 0.07).

Mitigation of Radiation Pneumonitis With Lisinopril

Breathing Interval Measurements to Monitor Lung Injury During Pneumonitis

As a secondary endpoint and to monitor the progression of pneumonitis, breathing rates were recorded biweekly starting at week 4 until week 16 (see *Methods*). The breathing rates were then converted to breathing intervals (1/breathing rates in min/breath) to account for attrition from lethal pneumonitis (see *Methods*). **Figure 5** shows the mean breathing intervals of each group at 6-and 12-weeks post-irradiation with 95% CIs. There was no difference in breathing intervals at the 6-weeks time point prior to the onset of pneumonitis. All irradiated groups had lower breathing intervals compared to non-irradiated rats at 12-weeks which correlates to the peak of radiation induced lung injury (radiation pneumonitis). The treatment group receiving the vehicle and also the group given PEG-hG-CSF had significantly decreased ($p < 0.05$) breathing intervals when compared to the non-irradiated controls at 12-weeks. This was not observed in the irradiated group given the TC. The irradiated group given PEG-hG-CSF also had significantly decreased ($p < 0.05$) breathing intervals when compared to the treatment group given TC and lisinopril. The addition of lisinopril to TC but not TC alone, mitigated the radiation-induced lung injury that was observed with PEG-hG-CSF alone at 12-weeks.

Histological Changes at 56-days to Determine Lung Injury During Pneumonitis

Histological changes in the lungs during pneumonitis were monitored in a subset of rats at 56-days post-irradiation after lung inflation and staining with H&E (see *Methods*). **Figure 6A** shows representative lungs from each group that were scored on three characteristic histological changes in irradiated lungs: vessel wall thickness (black arrow), alveolar wall thickness (green arrow) and foamy macrophages (red arrow). Non-irradiated lungs had a lacy architecture with open alveolar spaces, thin walls, patent blood vessels and few macrophages. The irradiated lungs had more congestion and many more infiltrating cells with tissue damage as compared to the non-irradiated lungs, except for the rats that received the TC + lisinopril (red bars, **Figure 6B**). These lungs were more comparable to control lungs with morphometric measurements indicating lower histological scores (**Figures 6B–D**). Vessel walls (**Figure 6B**) were significantly thicker in 13 Gy vehicle and 13 Gy PEG-hG-CSF groups compared to non-irradiated lungs and 13 Gy TC + lisinopril groups ($p < 0.05$). Alveolar wall thickness (**Figure 6C**) increased in all irradiated groups, but was significantly different in the vehicle, TC and PEG-hG-CSF groups but not the TC + lisinopril groups compared to the lungs from non-irradiated rats. Foamy macrophages (**Figure 6D**) were abundant in all irradiated groups, except for the TC + lisinopril group, which was not different from the non-irradiated group lungs. These results show histological injuries in irradiated lungs which were mitigated with TC + lisinopril.

Mitigation of Radiation Nephropathy With Lisinopril

Blood Urea Nitrogen Measurements to Monitor Renal Injury

Blood urea nitrogen (BUN) measurements were used to determine renal injury during radiation nephropathy. Rats in all groups were bled via jugular vein at 90- and 120-days post-irradiation and their median BUNs with 20–80% ranges are plotted in **Figure 7**. BUNs for the non-irradiated controls are represented by a shaded, horizontal blue bar. All irradiated rats had an increase in BUN values at 90-days which continued to increase by 120-days. The 13 Gy TC + lisinopril group had significantly lower BUNs as compared to the other irradiated rats ($p < 0.05$).

Histological Chages at 120-Days to Determine Renal Injury

Renal histology at 120-days was also used to quantify kidney injury during radiation nephropathy. When the study was

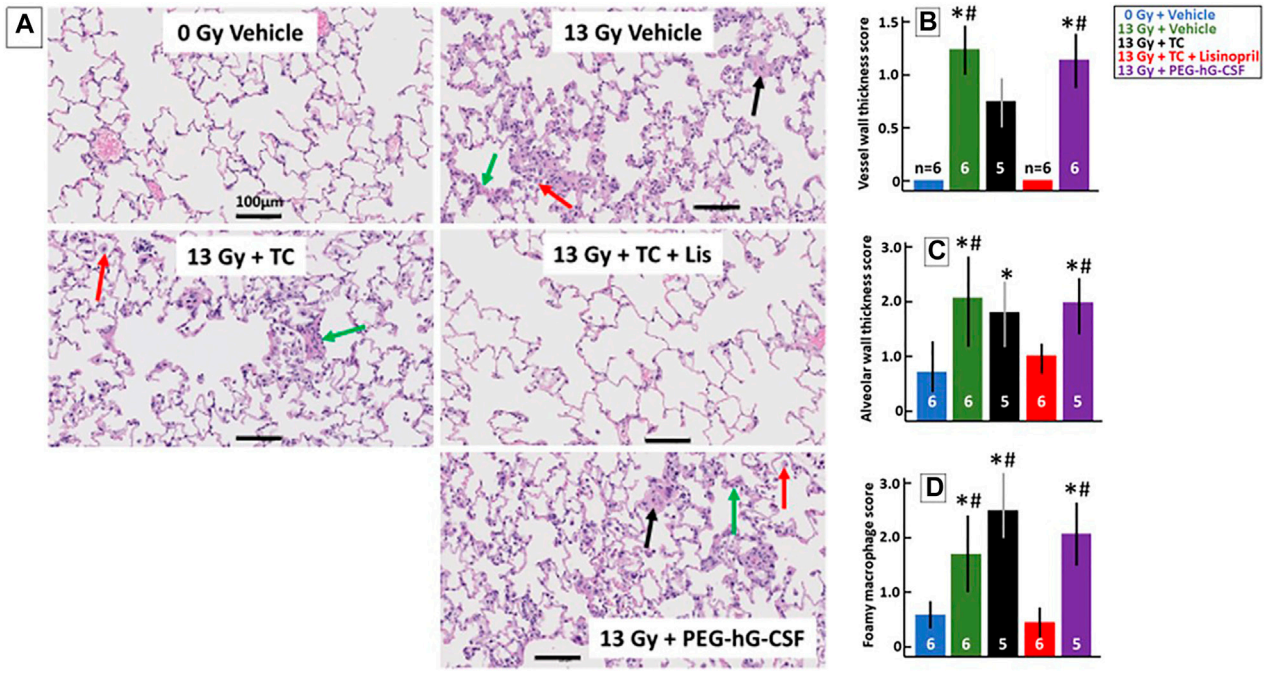

FIGURE 6 | Lisinopril mitigates histological lung injury after 13 Gy leg-out PBI. Representative histological sections of lung tissue harvested at 56-days after 13 Gy leg-out PBI were stained with H&E for each treatment group **(A)**. Irradiated rats given the vehicle or PEG-hG-CSF showed increased alveolar wall thickness cellularity (green arrow), increased vessel wall thickness (black arrow) and foamy macrophages (red arrow). Black bars represent 100 μm. Graphical representations of the H&E-stained lung sections are shown for vessel wall thickness **(B)**, alveolar wall thickness **(C)** and foamy macrophages **(D)**. Vessel wall thickness **(B)** were increased in irradiated rats given the vehicle or PEG-hG-CSF, whereas TC + lisinopril mitigated lung injury ($p < 0.05$, denoted by * compared to controls and # compared to TC + lisinopril). Irradiation increased alveolar wall thickness **(C)** in all irradiated groups compared to control ($p < 0.05$, denoted by *) except for the TC + lisinopril group. Alveolar wall thickness was also increased compared to the TC + lisinopril group in the irradiated vehicle and PEG-hG-CSF groups ($p < 0.05$, denoted by #). Foamy macrophages **(D)** were significantly increased in irradiated rats given the vehicle, TC or PEG-hG-CSF ($p < 0.05$, denoted by * compared to controls and # compared to TC + lisinopril). Numbers in the bars represent N in each group and bars are means with standard deviations.

terminated at 120-days, kidney sections were stained with H&E and blinded for scoring histological changes (see *Methods*). **Figure 8A** shows examples of representative histology of all treatment groups. Tissue sections were also given a composite score by the presence of protein casts (green arrow), glomerular sclerosis (black arrow) and glomerular mesangiolysis (red arrow). All irradiated groups showed histological evidence of injury as shown in the graph in **Figure 8B** by increased composite scores. Irradiated rats that received the TC had a higher composite histology score in comparison to the non-irradiated rats and the irradiated rats that received TC + lisinopril. The irradiated rats that received TC + lisinopril showed mitigation of structural damage in the kidney as compared to the other irradiated groups.

Mitigation of Delayed Effects of Acute Radiation Exposure to 160 Days

Survival After 13 Gy Leg-Out PBI With Lisinopril

Since renal failure (BUN > 120 mg/dl) occurs beyond 120 days, a separate group of rats were tested for 160-days. Rats were irradiated with 13 Gy leg-out PBI at 11–12 weeks of age and randomly assigned to one of four treatment groups (see *Methods* and **Figure 9**) to assess survival (primary end point) through 160-days. **Figure 9** shows a Kaplan-Meier survival plot for these four treatment groups. By 160-days, all of the irradiated rats given vehicle or TC were moribund. One rat in the vehicle and lisinopril group (**Figure 9**) was moribund at 11 days, possibly from H-ARS since internal hemorrhaging was observed without obvious GI injury at necropsy. GI lethality usually occurs by 7 days in this model (Fish et al., 2020). The first (lung) sequelae occurred between 60 and 80 days coinciding with pneumonitis (Fish et al., 2016) followed by a second (renal) phase after 140 days (representing radiation nephropathy). Only 1/12 rats in the 13 Gy + vehicle + lisinopril was moribund during pneumonitis while no rats in this group developed severe nephropathy up to 150 days (**Figure 9**). The experiment was terminated at 160 days at which time survival for all rats given TC + lisinopril was 100% ($p = 0.0001$, 13 Gy + TC + lisinopril vs. 13 Gy + TC).

Mitigation of Radiation Nephropathy With Lisinopril

Surviving rats in all groups were bled via jugular vein at 90-, 120- and 150-days post-irradiation and their median BUNs with 20–80% ranges are plotted in **Figure 10**. BUNs for the non-irradiated controls are represented by a shaded, horizontal blue bar. All irradiated rats had an increase in BUN values at 90-days. The BUN of irradiated rats given vehicle or TC continued to increase at 120- and again at 150-days. However, rats given 13 Gy + lisinopril with vehicle or TC had significantly lower BUNs as

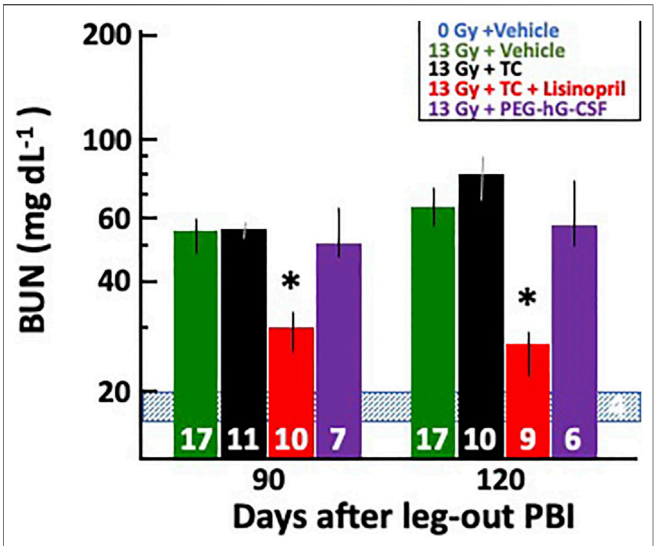

FIGURE 7 | Mitigation of radiation nephropathy after 13 Gy leg-out PBI by lisinopril. The graph shows medians and 20–80% ranges for blood urea nitrogen (BUN in mg dL^{-1}) in rats at 90- and 120-days post irradiation. Asterisks (*) represent $p < 0.05$ as compared to irradiation only, irradiation with triple combination (TC) and irradiation with PEG-hG-CSF groups at the corresponding times show increased BUN levels. The normal BUN for non-irradiated rats ranges between 18 and 21 mg dl^{-1} and is represented by the shaded, horizontal blue bar. Numbers in the bars represent N in each group. The decrease in N's between 90- and 120-days post-irradiation were not due to radiation nephropathy; therefore, they were not given a value of 120 mg dl^{-1}.

compared to irradiated rats given TC ($p < 0.05$) indicating non-lethal radiation-induced renal injury.

DISCUSSION

The goal of these studies was to assess a promising polypharmacy approach of combining a triple combination of growth factors with the ACE inhibitor lisinopril to mitigate ARS and DEARE in two rat models of irradiation (7.5 Gy TBI and 13 Gy leg-out PBI).

Mitigation of ARS by the Triple Combination in the Presence of Lisinopril

The TC consisting of PEG-hG-CSF, PEG mGM-CSF and PEG hIL-11 mitigated morbidity of the hematopoietic injury of ARS after TBI (**Figures 2**, **3**). The addition of lisinopril to the TC also resulted in increased survival. Survival in TC + lisinopril treated rats was not different from that of TC alone. Thus, even though lisinopril on its own did not mitigate morbidity, it did not alter efficacy of the TC. The advantage of TC to enhance survival during ARS as compared to FDA-approved mitigators such as G-CSF (Neupogen) or GM-CSF (Leukine), is that TC was only injected once vs. multiple injections required for a single non-pegylated growth factor (USFDA, 2015a). Interestingly, recent studies in four mouse strains have found enhanced survival with an abbreviated schedule of G-CSF (Neupogen, 0.17 mg kg^{-1}) given for 3 days after irradiation compared to a 16-days schedule (Satyamitra et al., 2017). PEGylated growth factors that possess longer biological half-lives, increased survival to 30-days post-irradiation in irradiated mice after only one treatment (0.1 mg kg^{-1}) (Chua et al., 2014). A shortened schedule is an important consideration in the context of a mass casualty event such as a nuclear accident or radiological attack, where single injections would be more convenient than multiple daily injections. Future studies investigating efficacy of a single dose of TC in a second species such as irradiated NHP will be required for approval of TC as a mitigator of H-ARS, via the FDA Animal Rule.

In clinical settings, G-CSF is used by neutropenic patients until neutrophil recovery is achieved (USFDA, 2015a). Similarly, G-CSF, when injected in irradiated mice until day 16, helps to increase neutrophil counts (Plett et al., 2012), likely causing the 35% increase in survival observed in mice. In the current study, complete blood counts taken between 10 and 30-days post-irradiation showed that TC with or without lisinopril enhanced neutrophil counts by 18 but not 10-days as compared to lisinopril alone. Thus, the TC appeared to accelerate recovery of neutrophils after 10-days, suggesting a similarity to the mechanism reported in mice. GM-CSF accelerated neutrophil recovery as a single agent but different injury model in rats (Cox et al., 2020; Singh and Seed, 2020), justifying its use in the TC. Though mGM-CSF has a very fast half-life in rats (terminal half-life was 1.1 h (Cox et al., 2020), the half-life of PEG mGM-CSF is much longer (terminal half-life of 17.2 h (Cox et al., 2020). The dose used in the current study (0.55 mg kg^{-1}) is higher than effective doses given to NHP and that used in the clinic (7 μg kg^{-1} day^{-1}), though only a single dose was given to rats as compared to multiple doses to NHP (unpublished results) and humans as per dosing recommendations for LEUKINE®).

Evidence in mice also suggests hematopoietic growth hormones may protect hematopoietic stem cells by promoting quiescence, thereby maintaining stem cell production (Davis et al., 2008). PEG-GM-CSF and PEG-IL-11 have been shown to cause acceleration of red blood cells and platelet recovery in mice (Plett et al., 2014). PEG-IL-11 increased the induction period of the hematopoietic stem cells compared to IL-11 (Lee et al., 2012; Kumar et al., 2018) and been shown to increase bone marrow cellularity, megakaryocytes, and hematopoietic recovery in mice (Kumar et al., 2018). These mechanisms observed in mice need to be tested in rats, in future studies to confirm the mechanisms of action of TC.

Other studies have shown that the ACE inhibitor captopril increased survival in irradiated mice to day 30 (Davis et al., 2010; Day et al., 2013), though this was not the case for rats (Moulder et al., 1993). The ACE inhibitor captopril has been shown to improve reticulocyte, leukocytes, erythrocytes, and platelet counts in irradiated mice (Davis et al., 2010; Barshishat-Kupper et al., 2011). There were no significant differences in these metrics in this study with lisinopril (results not shown).

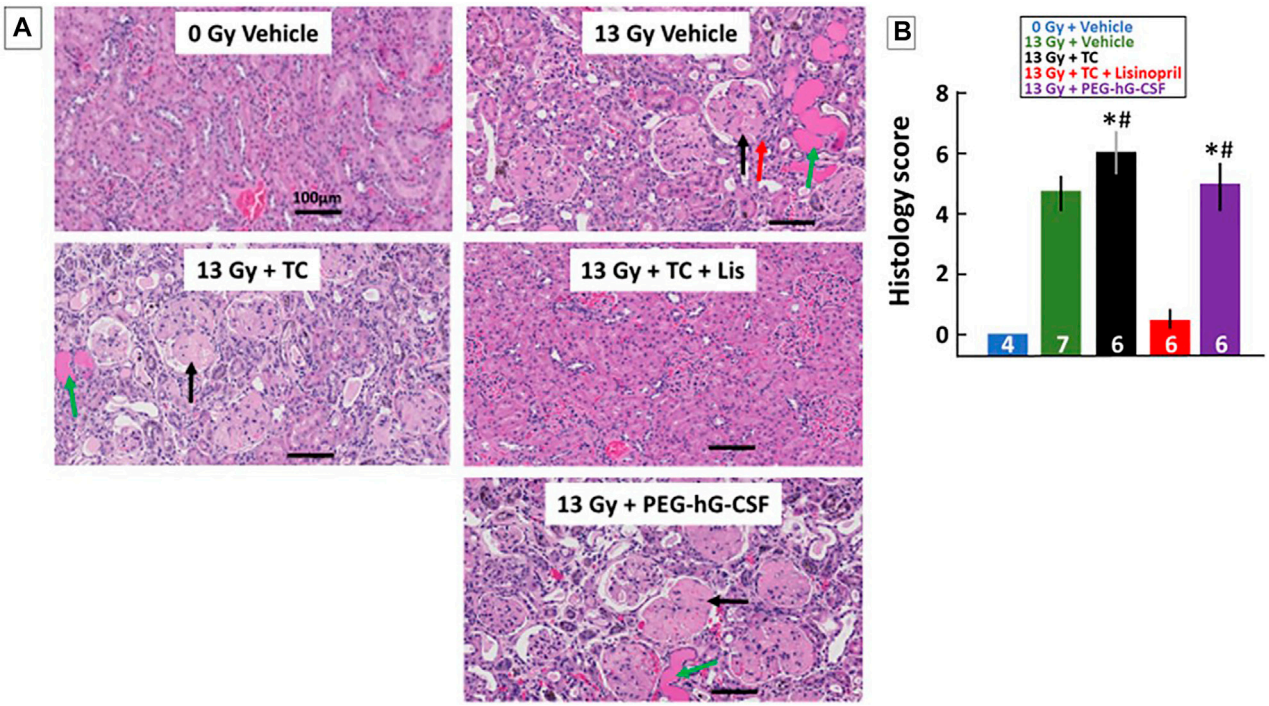

FIGURE 8 | Kidney injury mitigated by lisinopril after 13 Gy leg-out PBI. Representative histological sections of kidneys for each treatment group **(A)** were harvested at the termination of the study (120-days) after 13 Gy leg-out PBI, fixed and stained with H&E. Irradiated rats given the vehicle or PEG-hG-CSF showed increased protein casts (green arrow), glomerular sclerosis (black arrow) and glomerular mesangiolysis (red arrow) compared to non-irradiated rats. The irradiated and triple combination (TC) group showed increased protein casts and glomerular sclerosis while the addition of lisinopril mitigated these histological changes. Graphical representations of the H&E-stained kidney sections are shown in **(B)** as a composite histological score. Renal injury was increased with irradiation, the asterisks (*) represents $p < 0.05$ as compared to non-irradiated controls while the pound symbol (#) represents $p < 0.05$ as compared to the irradiated + TC + lisinopril. Numbers in the bars represent N in each group and bars are means with standard deviation.

Secondary endpoints for GI toxicity were not evaluated because the dose of radiation after 7.5 Gy was well below the threshold to observe external GI injury (seen above 12.5 Gy in WAG/RijCmcr rats, Fish et al., 2020).

Mitigation of DEARE by Lisinopril in the Presence of TC

Lisinopril has been used to mitigate lung-DEARE in rats after 12.5–13 Gy leg-out PBI (Fish et al., 2016) which was confirmed with secondary endpoints of breathing interval and lung histology. Our current data show that the TC + lisinopril also enhances survival and mitigates the progression of pneumonitis and nephropathy in irradiated rats. Though the mechanism of mitigation of radiation injury is not confirmed, ACE inhibitors are known to benefit cardiovascular function (Goodfriend et al., 1996; Inagami, 1999). This action may play an important role in mitigating radiation-induced injury to well vascularized organs such as the heart, lungs and kidneys. TC alone, which benefits the immune system, but not endovascular injury was not able to mitigate radiation pneumonitis or nephropathy. IL-11 has proven to be an effective mitigator against radiation induced renal injury in mice (Lee et al., 2012). However, we did not find this to be the case with TC which contains IL-11, unless the TC was combined with lisinopril, as indicated by renal histology and BUN levels. It is possible that the benefits of IL-11 were neutralized by the other two growth factors in TC, indicating further experimentation is needed in the future. Lisinopril alone has previously shown to be an effective mitigator against renal injury in the same model as used in this study (Fish et al., 2016). It continued to mitigate nephropathy in rats in the current study in the presence of growth factors that may be used to mitigate ARS; therefore, TC does not interfere with the mitigating effects of lisinopril for DEARE in rats.

Secondary endpoints for GI toxicity were not evaluated to minimize handling of rats in the first 7-days after 13 Gy and because the leg-out PBI dose used (13 Gy) has been described in previous studies to largely spare lethal GI-toxicity (Medhora et al., 2019).

Interestingly, compared to irradiated rats given PEG-hG-CSF (BBT-015) alone, the breathing intervals in irradiated rats given TC + lisinopril were significantly improved in the current study. This is consistent with previous data, which using a different injury model in rats, showed that lung injury is exacerbated by G-CSF (Adachi et al., 2003). Since G-CSF is a component of TC, the results indicate that lisinopril may have efficacy to mitigate pneumonitis in irradiated rats that have been given G-CSF. The TC + lisinopril group also demonstrated lung and renal histology

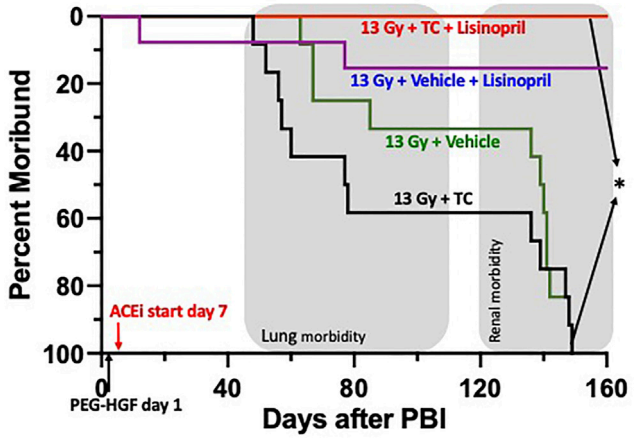

FIGURE 9 | Kaplan-Meier plot representing morbidity from DEARE up to 160 days post 13 Gy partial body irradiation with one hind limb shielded (leg-out PBI). The triple combination (TC, consisting of PEG-hG-CSF, PEG mGM-CSF and PEG hIL-11), or vehicle were given subcutaneously 24 h post PBI and the ACE inhibitor, lisinopril, was started in the drinking water 7-days post-irradiation. All irradiated rats were given supportive care. All irradiated rats that received TC + lisinopril survived to 160 days as compared to 100% morbidity for irradiated rats that received TC alone ($p < 0.0001$). Survival of irradiated rats given vehicle + lisinopril was over 90%, while irradiated rats given only the vehicle were moribund before 160 days. Shaded (gray) areas represent the timing for the lung and renal injuries.

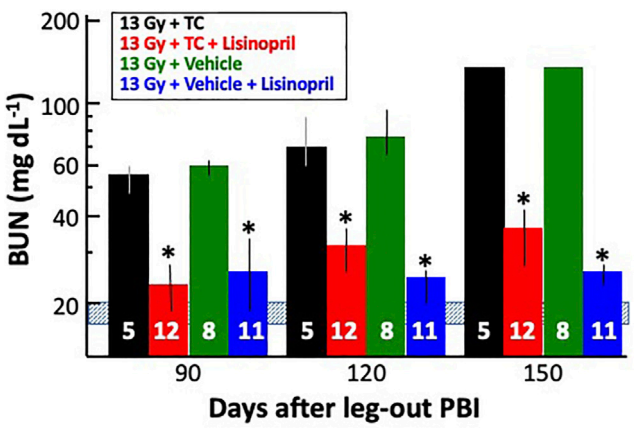

FIGURE 10 | Mitigation of radiation nephropathy after 13 Gy leg-out PBI by lisinopril (~24 mg m^{-2} d^{-1}). The graph shows medians and 20–80% ranges for blood urea nitrogen (BUN in mg dL^{-1}) in rats at 90-, 120- and 150-days post-irradiation. Asterisks (*) represent $p < 0.05$ as compared to 13 Gy + TC (triple combination, black bar) at the corresponding times. The normal BUN for non-irradiated rats ranges between 18–21 mg dl^{-1} and is represented by the shaded, horizontal blue bar. All rats with 13 Gy + TC and 13 Gy + vehicle were moribund after 120 days with a BUN ≥ 120 mg dl^{-1} and were given a BUN ≥ 120 mg dl^{-1} at 150 days. Numbers in the bars represent *N* in each group.

that was not different from non-irradiated rats. TC alone did not improve these metrics as seen by increased vessel wall thickness, alveolar wall thickness and foamy macrophages in the lung, or protein casts and glomerular sclerosis in the kidney (**Figures 6**, **8**). In summary, in a rat model, lisinopril mitigated lung and kidney DEARE in the presence of TC, administered early after radiation, so that the combination was effective for mitigation of both ARS and DEARE.

ACE inhibitors were evaluated in the clinic and reported to improve outcomes for radiation-induced pneumonitis in cancer patients (Jenkins and Welsh, 2011; Kharofa et al., 2012). Other similar clinical studies did not detect clear benefits of these drugs against radiation pneumonitis (Bracci et al., 2016; Small et al., 2018; Sun et al., 2018; Sio et al., 2019). One limitation of these trials was difficulty in accrual which resulted in underpowered analyses. In addition, it is not clear if the consistent high (though approved) doses of ACE inhibitors used in preclinical studies were given to all patients.

Limitations

There are several limitations of the current study. First, we have not tested each hematopoietic growth factor (PEG-GM-CSF or PEG-IL-11) separately in rats to determine if either of these alone could mitigate ARS or if they were additive. In fact, any one of these factors could even be deleterious by itself, partially neutralizing the beneficial effects of the others. Though mitigation of G-CSF was controversial (Neta, 1988; Neta et al., 1988) each growth factor was tested in mice and enhanced survival as well as hematopoietic cell recovery during ARS (Plett et al., 2014). Second, there was no correction for attrition in the blood count studies. It is uncertain if the results from moribund animals, when included with those from survivors, could further alter blood cell counts and the results presented in **Figure 3**. Also, as results are different in rats than what has been reported in mice, we do not know how these mitigators will impact humans. Further research must be done in order to determine the efficacy of this polypharmacy approach in other species. Lastly, not understanding the basis for mitigation of each agent is an important limitation. Knowledge of the mechanisms of radiation-induced bone marrow injury in rats will permit better comparison to mice and humans. Mechanistic studies are not in the scope of the current study, the goal of which is to demonstrate for the first time a polypharmacy approach toward mitigating four sequelae arising from irradiation of multiple organs. The individual and combined mechanisms of action for each agent (hydration, antibiotic, each growth factor, and lisinopril) on each sequela must be pursued in future work.

CONCLUSION

A triple combination of hematopoietic growth factors (TC) given with the ACE inhibitor lisinopril, successfully mitigated ARS and DEARE in two rat irradiation models used in the current study. The TC + lisinopril group showed decreased morbidity, faster neutrophil recovery and less lung and renal injury, which in some instances was comparable to the non-irradiated control rats. Using PEGylated drugs meant only one administration of

hematopoietic growth factors was needed compared to other studies using non-pegylated growth factors requiring multiple injections. Thus, PEGylation is advantageous for a mass casualty accident or attack, as emergency personnel and health care staff would not be needed to deliver repeated dosing. The combination of growth factors and lisinopril was safe and compatible in the rat models and may be an effective medical countermeasure for humans by mitigating acute and delayed injuries in the event of a nuclear disaster or accident.

DATA AVAILABILITY STATEMENT

The raw data supporting the conclusions of this article will be made available by the authors, without undue reservation.

ETHICS STATEMENT

The animal study was reviewed and approved by Institutional Animal Care and Use Committee at the Medical of Wisconsin.

AUTHOR CONTRIBUTIONS

Conceptualization, MM, BF, CO, and GC; Methodology, BF, TG, FG, JN, and TM; Formal Analysis, BF, AS, FG, TM, TG, and MM; Original Draft Preparation and Writing, TM, TG, and MM; Review and Editing, MM, TG, TM, BF, FG, JN, EJ, AS, GC, and CO.

FUNDING

This study was supported by NIH/NIAID U01AI133594, U01AI107305, VHA BX003833, Department of Radiation Oncology, MCW and NIH/NIAID Grant no: U01AI107340 to Bolder BioTechnology. Inc. and Indiana University School of Medicine.

ACKNOWLEDGMENTS

The authors wish to thank Dana Scholler for excellent animal care and technical assistance and Eric P. Cohen for his assistance in scoring kidney slides. We also thank Christine M. Fam for preparing the TC, TC vehicle and PEG-hG-CSF (BBT-015) solutions. Tissues were paraffin embedded, sectioned and stained by the Children's Research Institute Histology Core, Milwaukee, Wisconsin. The studies in this manuscript were also part of TM's master's thesis entitled "Polypharmacy with pegylated-hematopoietic growth factors (PEG-HGFs) and lisinopril mitigates acute radiation syndrome and its delayed effects" which was accepted in 2020 from the Medical College of Wisconsin.

REFERENCES

Adachi, K., Suzuki, M., Sugimoto, T., Yorozu, K., Takai, H., Uetsuka, K., et al. (2003). Effects of Granulocyte Colony-Stimulating Factor (G-CSF) on Bleomycin-Induced Lung Injury of Varying Severity. *Toxicologic Path.* 31, 665–673. doi:10.1080/01926230390244924410.1080/714044700

Amgen (2015b). *Inc. "Neulasta Prescribing Information."*. Thousand Oaks, CA. Available at: http://pi.amgen.com/united_states/neulasta/neulasta_pi_hcp_english.pdf (Accessed March 28th, 2021).

Amgen (2015a). *Inc. "Neupogen Prescribing Information."*. Thousand Oaks, CA. Available at: http://pi.amgen.com/united_states/neupogen/neupogen_pi_hcp_english.pdf (Accessed March 28th, 2021).

Amgen (2021). *Inc. "Nplate Prescribing Information."*. Thousand Oaks, CA. Available at: https://www.pi.amgen.com/~/media/amgen/repositorysites/pi-amgen-com/nplate/nplate_pi_hcp_english.pdf (Accessed March 28th, 2021).

Barshishat-Kupper, M., Mungunsukh, O., Tipton, A. J., McCart, E. A., Panganiban, R. A. M., Davis, T. A., et al. (2011). Captopril Modulates Hypoxia-Inducible Factors and Erythropoietin Responses in a Murine Model of Total Body Irradiation. *Exp. Hematol.* 39 (3), 293–304. doi:10.1016/j.exphem.2010.12.002

Boerma, M., Sridharan, V., Mao, X.-W., Nelson, G. A., Cheema, A. K., Koturbash, I., et al. (2016). Effects of Ionizing Radiation on the Heart. *Mutat. Research/Reviews Mutat. Res.* 770 (Pt B), 319–327. doi:10.1016/j.mrrev.2016.07.003

Bracci, S., Valeriani, M., Agolli, L., De Sanctis, V., Maurizi Enrici, R., and Osti, M. F. (2016). Renin-Angiotensin System Inhibitors Might Help to Reduce the Development of Symptomatic Radiation Pneumonitis after Stereotactic Body Radiotherapy for Lung *Cancer*. *Clin. Lung Cancer* 17 (3), 189–197. doi:10.1016/j.cllc.2015.08.007

Chua, H. L., Plett, P. A., Sampson, C. H., Katz, B. P., Carnathan, G. W., MacVittie, T. J., et al. (2014). Survival Efficacy of the PEGylated G-CSFs Maxy-G34 and Neulasta in a Mouse Model of Lethal H-ARS, and Residual Bone Marrow Damage in Treated Survivors. *Health Phys.* 106 (1), 21–38. doi:10.1097/HP.0b013e3182a4df10

Cohen, E. P., Moulder, J. E., Fish, B. L., and Hill, P. (1994). Prophylaxis of Experimental Bone Marrow Transplant Nephropathy. *J. Lab. Clin. Med.* 124 (3), 371–380.

Cox, G. N., Lee, J. I., Rosendahl, M. S., Chlipala, E. A., and Doherty, D. H. (2020). Characterization of a Long-Acting Site-specific PEGylated Murine GM-CSF Analog and Analysis of its Hematopoietic Properties in Normal and Cyclophosphamide-Treated Neutropenic Rats. *Protein J.* 39 (2), 160–173. doi:10.1007/s10930-020-09894-0

Davis, T. A., Landauer, M. R., Mog, S. R., Barshishat-Kupper, M., Zins, S. R., Amare, M. F., et al. (2010). Timing of Captopril Administration Determines Radiation Protection or Radiation Sensitization in a Murine Model of Total Body Irradiation. *Exp. Hematol.* 38 (4), 270–281. doi:10.1016/j.exphem.2010.01.004

Davis, T. A., Mungunsukh, O., Zins, S., Day, R. M., and Landauer, M. R. (2008). Genistein Induces Radioprotection by Hematopoietic Stem Cell Quiescence. *Int. J. Radiat. Biol.* 84 (9), 713–726. doi:10.1080/09553000802317778

Day, R. M., Davis, T. A., Barshishat-Kupper, M., McCart, E. A., Tipton, A. J., and Landauer, M. R. (2013). Enhanced Hematopoietic Protection from Radiation by the Combination of Genistein and Captopril. *Int. Immunopharmacology* 15 (2), 348–356. doi:10.1016/j.intimp.2012.12.029

DiCarlo, A. L., Hatchett, R. J., Kaminski, J. M., Ledney, G. D., Pellmar, T. C., Okunieff, P., et al. (2008). Medical Countermeasures for Radiation Combined Injury: Radiation with Burn, Blast, Trauma And/or Sepsis. Report of an NIAID Workshop, March 26-27, 2007. *Radiat. Res.* 169, 712–721. doi:10.1667/RR1295.1

DiCarlo, A. L., Maher, C., Hick, J. L., Hanfling, D., Dainiak, N., Chao, N., et al. (2011). Radiation Injury after a Nuclear Detonation: Medical Consequences and the Need for Scarce Resources Allocation. *Disaster Med. Public Health Prep.* 5, S32–S44. doi:10.1001/dmp.2011.17

Fish, B. L., Gao, F., Narayanan, J., Bergom, C., Jacobs, E. R., Cohen, E. P., et al. (2016). Combined Hydration and Antibiotics with Lisinopril to Mitigate Acute and Delayed High-Dose Radiation Injuries to Multiple Organs. *Health Phys.* 111 (5), 410–419. doi:10.1097/HP.0000000000000554

Fish, B. L., MacVittie, T. J., Szabo, A., Moulder, J. E., and Medhora, M. (2020). WAG/RijCmcr Rat Models for Injuries to Multiple Organs by Single High Dose Ionizing Radiation: Similarities to Nonhuman Primates (NHP). *Int. J. Radiat. Biol.* 96 (1), 81–92. doi:10.1080/09553002.2018.1554921

Fliedner, T. M., Dörr, H. D., and Meineke, V. (2005). Multi-organ Involvement as a Pathogenetic Principle of the Radiation Syndromes: a Study Involving 110 Case Histories Documented in SEARCH and Classified as the Bases of Haematopoietic Indicators of Effect. *Bjr* Supplement_27, 1–8. doi:10.1259/bjr/77700378

Gao, F., Fish, B. L., Moulder, J. E., Jacobs, E. R., and Medhora, M. (2013). Enalapril Mitigates Radiation-Induced Pneumonitis and Pulmonary Fibrosis if Started 35 Days after Whole-Thorax Irradiation. *Radiat. Res.* 180 (5), 546–552. doi:10.1667/RR13350.1

Gao, F., Fish, B. L., Szabo, A., Schock, A., Narayanan, J., Jacobs, E. R., et al. (2014). Enhanced Survival from Radiation Pneumonitis by Combined Irradiation to the Skin. *Int. J. Radiat. Biol.* 90 (9), 753–761. doi:10.3109/09553002.2014.922722

Goodfriend, T. L., Elliott, M. E., and Catt, K. J. (1996). Angiotensin Receptors and Their Antagonists. *N. Engl. J. Med.* 334 (25), 1649–1655. doi:10.1056/NEJM199606203342507

Inagami, T. (1999). Molecular Biology and Signaling of Angiotensin Receptors: an Overview. *J. Am. Soc. Nephrol.* 10 Suppl 11 (Suppl. 11), S2–S7.

Jenkins, P., and Watts, J. (2011). An Improved Model for Predicting Radiation Pneumonitis Incorporating Clinical and Dosimetric Variables. *Int. J. Radiat. Oncology*Biology*Physics* 80 (4), 1023–1029. doi:10.1016/j.ijrobp.2010.03.05880

Jenkins, P., and Welsh, A. (2011). Computed Tomography Appearance of Early Radiation Injury to the Lung: Correlation with Clinical and Dosimetric Factors. *Int. J. Radiat. Oncology*Biology*Physics* 81 (1), 97–103. doi:10.1016/j.ijrobp.2010.05.017

Kharofa, J., Cohen, E. P., Tomic, R., Xiang, Q., and Gore, E. (2012). Decreased Risk of Radiation Pneumonitis with Incidental Concurrent Use of Angiotensin-Converting Enzyme Inhibitors and Thoracic Radiation Therapy. *Int. J. Radiat. Oncology*Biology*Physics* 84 (1), 238–243. doi:10.1016/j.ijrobp.2011.11.013

Kma, L., Gao, F., Fish, B. L., Moulder, J. E., Jacobs, E. R., and Medhora, M. (2012). Angiotensin Converting Enzyme Inhibitors Mitigate Collagen Synthesis Induced by a Single Dose of Radiation to the Whole Thorax. *Jrr* 53 (1), 10–17. doi:10.1269/jrr.11035

Kumar, V. P., Biswas, S., Sharma, N. K., Stone, S., Fam, C. M., Cox, G. N., et al. (2018). PEGylated IL-11 (BBT-059): A Novel Radiation Countermeasure for Hematopoietic Acute Radiation Syndrome. *Health Phys.* 115 (1), 65–76. doi:10.1097/HP.0000000000000841

Lee, H. T., Park, S. W., Kim, M., Ham, A., Anderson, L. J., Brown, K. M., et al. (2012). Interleukin-11 Protects against Renal Ischemia and Reperfusion Injury. *Am. J. Physiology-Renal Physiol.* 303 (8), F1216–F1224. doi:10.1152/ajprenal.00220.2012

Ma, C.-M., Coffey, C. W., DeWerd, L. A., Liu, C., Nath, R., Seltzer, S. M., et al. (2001). AAPM Protocol for 40-300 kV X-Ray Beam Dosimetry in Radiotherapy and Radiobiology. *Med. Phys.* 28 (6), 868–893. doi:10.1118/1.1374247

McCart, E. A., Lee, Y. H., Jha, J., Mungunsukh, O., Rittase, W. B., Summers, T. A., Jr, et al. (2019). Delayed Captopril Administration Mitigates Hematopoietic Injury in a Murine Model of Total Body Irradiation. *Sci. Rep.* 9 (1), 2198. doi:10.1038/s41598-019-38651-2

Medhora, M., Gao, F., Fish, B. L., Jacobs, E. R., Moulder, J. E., and Szabo, A. (2012). Dose-modifying Factor for Captopril for Mitigation of Radiation Injury to Normal Lung. *J. Radiat. Res.* 53 (4), 633–640. doi:10.1093/jrr/rrs004

Medhora, M., Gao, F., Gasperetti, T., Narayanan, J., Khan, A. H., Jacobs, E. R., et al. (2019). Delayed Effects of Acute Radiation Exposure (DEARE) in Juvenile and Old Rats: Mitigation by Lisinopril. *Health Phys.* 116 (4), 529–545. doi:10.1097/HP.0000000000000920

Medhora, M., Gao, F., Glisch, C., Narayanan, J., Sharma, A., Harmann, L. M., et al. (2015). Whole-thorax Irradiation Induces Hypoxic Respiratory Failure, Pleural Effusions and Cardiac Remodeling. *J. Radiat. Res.* 56 (2), 248–260. doi:10.1093/jrr/rru095

Medhora, M., Gao, F., Wu, Q., Molthen, R. C., Jacobs, E. R., Moulder, J. E., et al. (2014). Model Development and Use of ACE Inhibitors for Preclinical Mitigation of Radiation-Induced Injury to Multiple Organs. *Radiat. Res.* 182 (5), 545–555. doi:10.1667/RR13425.1

Medhora, M., Gasperetti, T., Schamerhorn, A., Gao, F., Narayanan, J., Lazarova, Z., et al. (2020). Wound Trauma Exacerbates Acute, but Not Delayed, Effects of Radiation in Rats: Mitigation by Lisinopril. *Ijms* 21 (11), 3908. doi:10.3390/ijms21113908

Moulder, J. E. (2014). 2013 Dade W. Moeller Lecture. *Health Phys.* 107 (2), 164–171. doi:10.1097/HP.0000000000000082

Moulder, J. E., Cohen, E. P., and Fish, B. L. (2011). Captopril and Losartan for Mitigation of Renal Injury Caused by Single-Dose Total-Body Irradiation. *Radiat. Res.* 175 (1), 29–36. doi:10.1667/RR2400.1

Moulder, J. E., Fish, B. L., and Cohen, E. P. (1993). Treatment of Radiation Nephropathy with ACE Inhibitors. *Int. J. Radiat. Oncology*Biology*Physics* 27 (1), 93–99. doi:10.1016/0360-3016(93)90425-u

Neta, R., Oppenheim, J. J., and Douches, S. D. (1988). Interdependence of the Radioprotective Effects of Human Recombinant Interleukin 1 Alpha, Tumor Necrosis Factor Alpha, Granulocyte Colony-Stimulating Factor, and Murine Recombinant Granulocyte-Macrophage Colony-Stimulating Factor. *J. Immunol.* 140 (1), 108–111.

Neta, R. (1989). Cytokines in Radioprotection and Therapy of Radiation Injury. *Biotherapy* 1 (1), 41–45. doi:10.1007/BF02170134

Ng, J., Guo, F., Marneth, A. E., Ghanta, S., Kwon, M.-Y., Keegan, J., et al. (2020). Augmenting Emergency Granulopoiesis with CpG Conditioned Mesenchymal Stromal Cells in Murine Neutropenic Sepsis. *Blood Adv.* 4 (19), 4965–4979. doi:10.1182/bloodadvances.2020002556

Plett, P. A., Chua, H. L., Sampson, C. H., Katz, B. P., Fam, C. M., Anderson, L. J., et al. (2014). PEGylated G-CSF (BBT-015), GM-CSF (BBT-007), and IL-11 (BBT-059) Analogs Enhance Survival and Hematopoietic Cell Recovery in a Mouse Model of the Hematopoietic Syndrome of the Acute Radiation Syndrome. *Health Phys.* 106 (1), 7–20. doi:10.1097/HP.0b013e3182a4dd4e

Plett, P. A., Sampson, C. H., Chua, H. L., Joshi, M., Booth, C., Gough, A., et al. (2012). Establishing a Murine Model of the Hematopoietic Syndrome of the Acute Radiation Syndrome. *Health Phys.* 103 (4), 343–355. doi:10.1097/HP.0b013e3182667309

Radiation Emergency Medical Management (2020). Myeloid Cytokines for Treatment of Acute Exposure to Myelosuppressive Doses of Radiation: Hematopoietic Subsyndromeof Acute Radiation Syndrome (H-ARS). Available at: https://www.remm.nlm.gov/cytokines.htm (Accessed November 14th, 2020).[

Sanofi-Aventis Llc, S.-A. U. (2018). *Leukine Prescribing Information*. NJ: Bridgewater. . Available at: https://www.accessdata.fda.gov/drugsatfda_docs/label/2018/103362s5240lbl.pdf?utm_campaign=20180329% (Accessed March 28th, 2021).

Satyamitra, M., Kumar, V. P., Biswas, S., Cary, L., Dickson, L., Venkataraman, S., et al. (2017). Impact of Abbreviated Filgrastim Schedule on Survival and Hematopoietic Recovery after Irradiation in Four Mouse Strains with Different Radiosensitivity. *Radiat. Res.* 187 (6), 659–671. doi:10.1667/RR14555.1

Singh, V. K., and Seed, T. M. (2020). Pharmacological Management of Ionizing Radiation Injuries: Current and Prospective Agents and Targeted Organ Systems. *Expert Opin. Pharmacother.* 21 (3), 317–337. doi:10.1080/14656566.2019.1702968

Sio, T. T., Atherton, P. J., Pederson, L. D., Zhen, W. K., Mutter, R. W., Garces, Y. I., et al. (2019). Daily Lisinopril vs Placebo for Prevention of Chemoradiation-Induced Pulmonary Distress in Patients with Lung *Cancer* (Alliance MC1221): A Pilot Double-Blind Randomized Trial. *Int. J. Radiat. Oncology*Biology*Physics* 103 (3), 686–696. doi:10.1016/j.ijrobp.2018.10.035

Small, W., Jr, James, J. L., Moore, T. D., Fintel, D. J., Lutz, S. T., Movsas, B., et al. (2018). Utility of the ACE Inhibitor Captopril in Mitigating Radiation-Associated Pulmonary Toxicity in Lung *Cancer*. *Am. J. Clin. Oncol.* 41 (4), 396–401. doi:10.1097/COC.0000000000000289

Sun, F., Sun, H., Zheng, X., Yang, G., Gong, N., Zhou, H., et al. (2018). Angiotensin-converting Enzyme Inhibitors Decrease the Incidence of Radiation-Induced Pneumonitis Among Lung *Cancer* Patients: A Systematic Review and Meta-Analysis. *J. Cancer* 9 (12), 2123–2131. doi:10.7150/jca.24665

Unthank, J. L., Miller, S. J., Quickery, A. K., Ferguson, E. L., Wang, M., Sampson, C. H., et al. (2015). Delayed Effects of Acute Radiation Exposure in a Murine Model of the H-ARS. *Health Phys.* 109 (5), 511–521. doi:10.1097/HP.0000000000000357

U.S. Food and Drug Administration (2015a). *FDA Approves Radiation Medical Countermeasure*. Available at: https://www.fda.gov/emergency-preparedness-and-response/about-mcmi/fda-approves-radiation-medical-countermeasure (Accessed September 30th, 2020).

U.S. Food and Drug Administration (2015b). Guidance for Industry: Product Development under the Animal Rule. Available at: https://www.fda.gov/regulatory-information/search-fda-guidance-documents/product-development-under-animal-rule (Accessed October 12th, 2020).

U.S. Food and Drug Administration (2021). *Radiological and Nuclear Emergency Preparedness Information from FDA*. Available at: https://www.fda.gov/emergency-preparedness-and-response/mcm-issues/radiological-and-nuclear-emergency-preparedness-information-fda#fastfacts (Accessed March 25th, 2021).

Conflict of Interest: GC is an employee of Bolder BioTechnology, Inc. and has a financial interest in the company. GC and CO are inventors on patents related to use of PEG-HGFs to treat ARS. GC, CO, BF, and MM are inventors on a pending patent application related to the use of combinations of HGF and ACE inhibitors to treat ARS.

The remaining authors declare that the research was conducted in the absence of any commercial or financial relationships that could be construed as a potential conflict of interest.

frontiers in Pharmacology

REVIEW
published: 18 May 2021
doi: 10.3389/fphar.2021.662437

Extracellular Vesicles for the Treatment of Radiation Injuries

Lalitha Sarad Yamini Nanduri[1], *Phaneendra K. Duddempudi*[2], *Weng-Lang Yang*[1], *Radia Tamarat*[3] *and Chandan Guha*[1,4,5,6]*

[1]Department of Radiation Oncology, Albert Einstein College of Medicine, Montefiore Medical Center, New York, NY, United States, [2]Department of Biochemistry, Albert Einstein College of Medicine, Montefiore Medical Center, New York, NY, United States, [3]Institut de Radioprotection et de Sûreté Nucléaire (IRSN), Fontenay-aux-Roses, France, [4]Department of Pathology, Albert Einstein College of Medicine, Montefiore Medical Center, New York, NY, United States, [5]Department of Urology, Albert Einstein College of Medicine, Montefiore Medical Center, New York, NY, United States, [6]Institute for Onco-Physics, Albert Einstein College of Medicine, Montefiore Medical Center, New York, NY, United States

Normal tissue injury from accidental or therapeutic exposure to high-dose radiation can cause severe acute and delayed toxicities, which result in mortality and chronic morbidity. Exposure to single high-dose radiation leads to a multi-organ failure, known as acute radiation syndrome, which is caused by radiation-induced oxidative stress and DNA damage to tissue stem cells. The radiation exposure results in acute cell loss, cell cycle arrest, senescence, and early damage to bone marrow and intestine with high mortality from sepsis. There is an urgent need for developing medical countermeasures against radiation injury for normal tissue toxicity. In this review, we discuss the potential of applying secretory extracellular vesicles derived from mesenchymal stromal/stem cells, endothelial cells, and macrophages for promoting repair and regeneration of organs after radiation injury.

Keywords: acute radiation syndrome, radio mitigation, medical countermeasures against radiation, mesenchymal stromal/stem cells, endothelial cells, macrophages, extracellular vesicles, radiation injuries

OPEN ACCESS

Edited by:
Diane Riccobono, Institut de Recherche Biomédicale des Armées (IRBA), France

Reviewed by:
Shiang Y. Lim, University of Melbourne, Australia
Nicola Alessio, Università della Campania Luigi Vanvitelli, Italy
Ramon Lopez Perez, German Cancer Research Center (DKFZ), Germany
Umberto Galderisi, University of Campania Luigi Vanvitelli, Italy

***Correspondence:**
Chandan Guha
cguhamd@gmail.com

Specialty section:
This article was submitted to Translational Pharmacology, a section of the journal Frontiers in Pharmacology

Received: *01 February 2021*
Accepted: *04 May 2021*
Published: *18 May 2021*

Citation:
Nanduri LSY, Duddempudi PK, Yang W-L, Tamarat R and Guha C (2021) Extracellular Vesicles for the Treatment of Radiation Injuries. Front. Pharmacol. 12:662437. doi: 10.3389/fphar.2021.662437

INTRODUCTION

The first report of detrimental effects of ionizing radiation on healthy normal tissues came to light after the atomic bomb explosions in 1945. This unprecedented event introduced to the world the lethal radiation poisoning or sickness, also known as acute radiation syndrome (ARS), where a relatively large number of people can be affected by sudden exposure to high amounts of irradiation over a short period of time due to nuclear power plant accidents or atomic war. The extent of damage to an organism depends on the duration and the dosage of radiation with very high mortality after a threshold dose. ARS is a multi-organ failure syndrome caused by a combination of radiation dose-dependent direct cytocidal effects of irradiation on tissue stem and progenitor cells and the supporting sinusoidal endothelial and mesenchymal cells of the stem cell niche, with subsequent neutropenia, anemia, and thrombocytopenia due to bone marrow failure. With higher doses, manifestations of gastro-intestinal (GI)-ARS with loss of the intestinal mucosal barrier, bacteremia, septic shock, and systemic inflammatory response syndrome ensues. In addition to such accidental exposures, normal tissues succumb to radiation during radiotherapy in cancer patients, which is often unavoidable (Singh et al., 2018). For instance, in head and neck cancer patients, salivary glands are often present in the field of radiation (Coppes and Stokman, 2011), resulting in loss of stem cells, irreversible loss of saliva production over the years, leading to Xerostomia. Therefore, therapeutic strategies to ameliorate radiation-induced normal tissue toxicity are of great importance for tissues such as bone marrow, intestine, liver, and lung.

At the cellular level, radiation exposure inflicts direct damage by ionizing biological macromolecules such as DNA, RNA, lipids, and proteins. Indirect damage to cells occurs *via* radiation-induced generation of reactive oxygen species (ROS), such as superoxide and hydroxide radicals from the radiolysis of intracellular water, which results in the oxidation of biological macromolecules. Radiation-induced single-strand (SSBs) and double-strand DNA breaks (DSBs) are considered the major events leading to cell death, cell cycle arrest, and senescence (Panganiban et al., 2012).

Radiation medical countermeasures (MCMs) are agents administered either as preventive or as mitigators post-exposure to radiation. The mitigators improve radiation-induced physiological damage such as cellular toxicity, apoptosis, and loss of stem cells. The radiation protectants prevent radiation-induced toxicity, for instance, by scavenging the free-radicals and reducing oxidative damage to cells. Several candidate MCMs were being identified and investigated (Singh and Seed, 2020). The cytokines Neupogen® (G-CSF), Neulasta® (pegylated G-CSF), Leukine® (GM-CSF), and Nplate® (thrombopoietin receptor agonist) are radiation MCMs that received approval from the Food and Drug Administration (FDA) in the US for treating patients exposed to acute high doses of radiation that suppresses the functions of bone marrow and immune system.

Organ Damage Induced by Radiation

Mitotically active cells such as tissue-resident stem cells are more sensitive to radiation. Radiation-induced loss of stem cells is reported in multiple organs such as the bone marrow (Green and Rubin, 2014), intestine (Kulkarni et al., 2016), liver (Guha et al., 1999), lung (Giuranno et al., 2019), salivary gland (Coppes and Stokman, 2011; Rocchi and Emmerson, 2020), and brain (Leavitt et al., 2019). In the bone marrow, hematopoietic stem cells (HSCs) produce all the blood cell lineages (Bouchareychas et al., 2020). The HSC self-renewal capacity and differentiation potential are partly regulated by a complex multicellular network in the bone marrow microenvironment referred to as a niche. This bone marrow niche is composed of many different cell types such as mesenchymal stromal/stem cells (MSCs), adipocytes, osteocytes, and glial cells. Exposure to high-dose radiation during radiotherapy for leukemia and other bone malignancies results in the apoptosis of HSCs, decreasing their number and potential to self-renew and differentiate (Mendelson and Frenette, 2014). However, both *in vitro* and *in vivo* studies have shown that MSCs from bone marrow are relatively resistant to ionizing radiation and maintain their differentiation potential even exposure to high dose radiation (Singh et al., 2012; Nicolay et al., 2015; Ruhle et al., 2018). In addition to bone marrow cell loss, radiation also causes an increased endothelial cell (EC) permeability, imbalance in osteogenesis, damage to the bone microenvironment, and therefore infection susceptibility. The intestine is also a mitotically active tissue with actively proliferating crypt base cells identified as intestinal stem cells (ISCs), which are surrounded by MSCs, ECs, macrophages (Mϕs), and lymphocytes. In addition to accidental exposure, radiotherapy for abdominal and kidney cancer patients causes damage to the intestine, resulting in loss of intestinal crypts, loss of mucosal barrier, and leading to microbial infection and inflammation (Kulkarni et al., 2016). Lung tissue is often exposed to radiation in patients undergoing radiotherapy for lung and esophageal cancers (Giuranno et al., 2019). This results in cell loss, edema of the alveolar walls, increased vascular permeability, and inflammation. Radiation-induced damage to the healthy liver occurs during radiotherapy for hepatocellular carcinoma resulting in occlusion of central vein lumina, EC toxicity, and hepatocellular atrophy (Guha et al., 1999; Benderitter et al., 2014). In addition to these acute effects, delayed toxicities were reported in most tissues leading to multi-organ failure. A schema on summary of the timeline and pathophysiologic changes following radiation exposure in different organs is represented in **Figure 1**.

Cell Therapy and Limitations

Stem cell therapy have been used to develop as radiation MCM (Rios et al., 2017). Stem cell transplantation led to the recovery of radiation-induced normal tissue toxicity in the bone (Becker et al., 1963), skin (Riccobono et al., 2012; Horton et al., 2013), salivary gland (Kojima et al., 2011; Lim et al., 2013; Nanduri et al., 2014; Maimets et al., 2016), brain (Acharya et al., 2015; Liao et al., 2017; Leavitt et al., 2019; Soria et al., 2019; Chu et al., 2020), and intestine (Saha et al., 2011; Gong et al., 2016; Zheng et al., 2016). Different types of stem cells were investigated in these studies for their potential to engraft, differentiate, repair, and regenerate radiation-damaged tissues. Allogenic bone marrow transplants are promising cell therapeutic strategies to recover radiation-induced bone marrow damage. However, challenges remain with the expansion and maintenance of HSCs *in vitro* (Walasek et al., 2012) and the ability of transplanted HSCs to engraft, self-renew and differentiate (Mendelson and Frenette, 2014). The number of resident stem cells in adult tissues is minimal and needs to be expanded *in vitro* to generate sufficient cells for the clinical translation. Moreover, stem cells' purification and selection strategies, such as flow-cytometry-based sorting, are not always suitable for clinical translation. Embryonic stem cells and genetically reprogrammed induced pluripotent stem cells (iPSC) or iPSC-derived differentiated cells such as hepatocytes, ECs are being investigated for regenerative application (Lee et al., 2019). Also, using the viral transduction methods to genetically engineer and modify the characteristics of the cells such as iPSCs poses a safety concern for clinical use. The transplantation of stem cells or MSCs may not have an immediate effect on attenuating organ injury. These transplanted cells need to be first engrafted in the body, and under some conditions, they need to further differentiate to other cell types to execute the needed biological activities. The long process of developing therapeutic effect by cell transplantation is not suitable for accidental radiation exposure where immediate repair and regenerative measures are required.

Studies have suggested that the secretome of various stem cells contains the critical growth factors and signaling molecules for the stem cell-driven regeneration *via* paracrine signaling route, mainly by extracellular vesicles (EVs) (Berger et al., 2017; Taheri

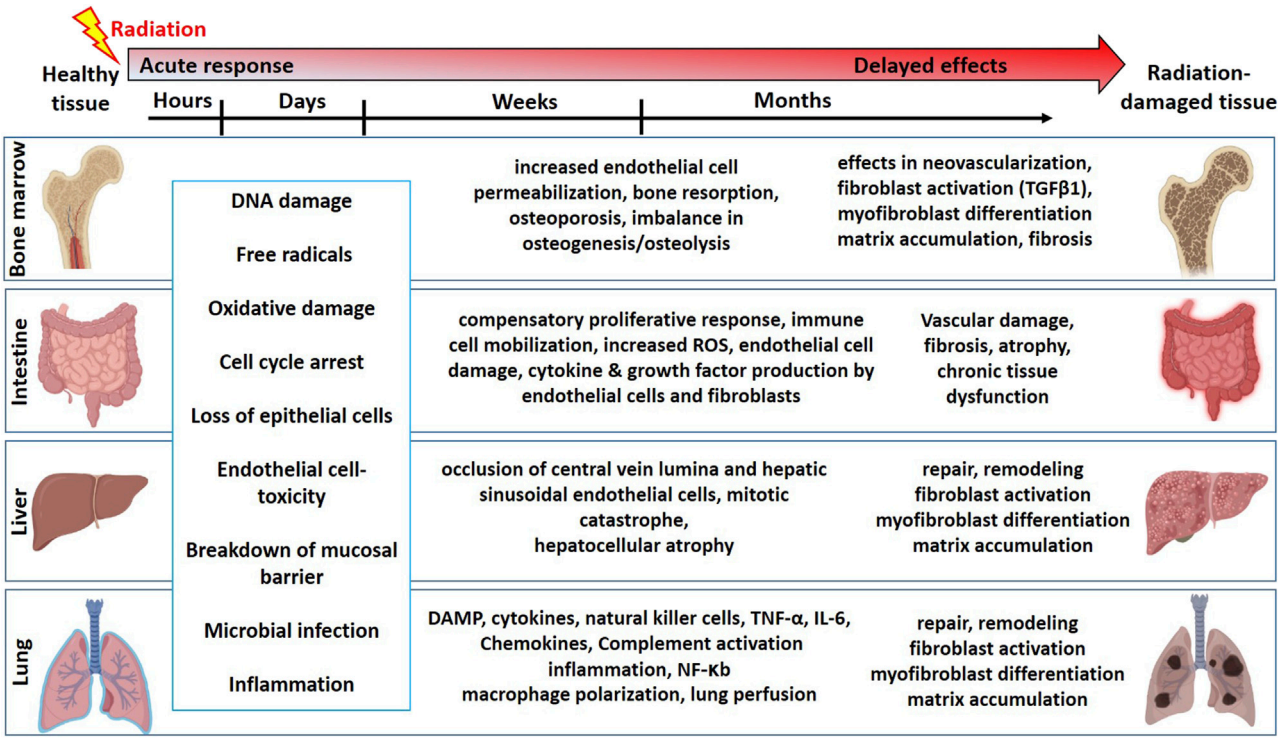

FIGURE 1 | The timeline and pathophysiologic changes in the bone marrow, intestine, liver, and lung for the development of normal tissue toxicity after high dose radiation exposure (Graphics adapted from BioRender.com).

et al., 2019). Therefore, EVs released from various cell types can be an alternative to cell therapeutics.

Extracellular Vesicles Derived From Cells as Therapeutics

EVs are the body's own nanoparticles that constitute a significant cell-to-cell communication system in multicellular organisms. According to the recent nomenclature stated by the International Society of Extracellular Vesicles (ISEV), EVs are broadly classified into plasma membrane-derived large microvesicles of 500–1,300 nm or endoplasmic reticulum-endosome derived small EVs of 30–200 nm (Thery et al., 2018). EV membranes contain various integrins, lipids, and proteins, each with a specific role; for instance, tetraspanins contribute to target cell selection (Rana et al., 2012). Molecules, such as CD9, CD63, CD81, tumor susceptibility gene 101 (TSG101), are used as signature biomarkers in the characterization of EVs; however, their expression levels vary, depending on the source of cell types. The content of EV and methodologies for characterizing EVs are summarized in **Figure 2**. Their unique nano-size, short life span makes EVs ideal messengers to travel between complex cellular fluid and selective membraned cellular structures. Depending on the cellular state of origin, EVs package either protein, small regulatory RNA, or lipids in addition to fragments of DNA (Witwer et al., 2019). However, the fate decisions that regulate this packaging are still under investigation.

Radiation stem cells and adversely affects the microenvironment. In the intestine, the stem cell niche supports ISC growth and crypt regeneration and is composed of MSCs, ECs, Mϕs, and lymphocytes which are affected due to radiation. Transplantation of mouse bone marrow adherent stromal cell (BMASC) culture system enriched for MSCs ($CD90^+/CD105^+/CD29^+$), myeloid cells ($CD45+/CD11b^+$), and ECs ($CD34^+/CD31^+$) improved the survival mice exposed to whole-body irradiation (WBI) (Saha et al., 2011). However, transplantation with the BMASC culture system depleted of myeloid cells or MSCs lost the beneficial effect. This study suggests that a combination of ECs, Mϕs, and MSCs is necessary for the complete regeneration of the damaged intestine. In this review we have focused on the bone marrow derived MSC-, EC- and Mϕ-derived EVs for radiation injuries.

MESENCHYMAL STROMAL/STEM CELL-EVs

Multipotent MSCs from multiple sources such as bone marrow, umbilical cord, and adipose tissue are the most widely tested stem cells. The regenerative potential of these cells is attributed to their multi-lineage differentiation potential, secretory, immune-modulatory, and homing capabilities (Viswanathan et al., 2019; Nolta et al., 2020). From 2008 to date, several clinical trials are in progress worldwide with MSCs for neurologic,

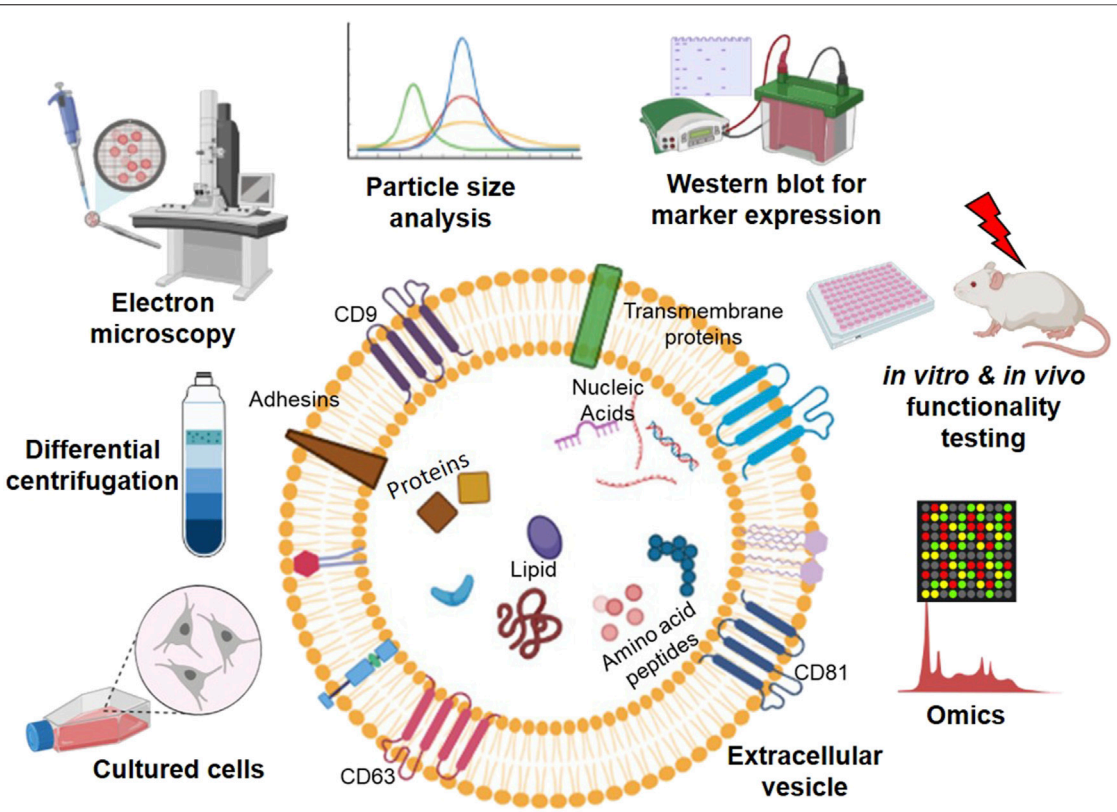

FIGURE 2 | An overview of workflow in studying extracellular vesicles (EVs). EVs contain a lipid bilayer membrane that encapsulates various molecules, including proteins, nucleic acids, amino acids/peptides, and lipids, for cell-to-cell communication. EVs are secreted from the cultured cells from various sources and isolated from the cell culture medium using ultracentrifugation. The isolated EVs can be characterized by (left to right on the top of EV) electron microscopy, particle size analysis, Western blotting, *in vitro* and *in vivo* functional testing, and high throughput-omics analysis (Graphics adapted from BioRender.com).

cardiovascular, pulmonary, liver, bone, skin, intestinal, and muscle abnormalities, including the most recent COVID-19 (Moll et al., 2019). The most common route of administration of MSCs is intravenous; however, intraperitoneal, subcutaneous routes are also being tested clinically (Kabat et al., 2020). In pre-clinical models, MSCs were shown to be distributed to lung, heart, and kidney after systemic transplantation. Recent reports have attributed this regenerative potential of MSCs to their paracrine signaling mechanism *via* EVs (Caplan and Dennis, 2006). In general, MSC-EVs package heterogeneous cargo such as nucleic acids, protein, and lipids. Studies have shown that >150 different miRNA are present in MSC-EVs to regulate a wide range of signaling pathways (Ferguson et al., 2018). The potential of MSC-EVs to repair tissue injury was reported in the heart (Phinney and Pittenger, 2017), kidney (Zhang et al., 2016), lung (Wang et al., 2020), liver (Tan et al., 2014), intestine (Accarie et al., 2020), and cartilage (Wong et al., 2020). MSC-EVs were shown to be anti-inflammatory, anti-oxidative, pro-angiogenic (Komaki et al., 2017), anti-fibrotic (Grange et al., 2019), promote epithelial cell growth (Gatti et al., 2011; Alcayaga-Miranda et al., 2016; Tsiapalis and O'Driscoll, 2020), improve myocardial infarction (Xu R. et al., 2019), promote Mϕ M2 polarization and wound healing.

Biological Activities of Bone Marrow MSC-EVs

Bone marrow-derived mesenchymal stromal/stem cells (BMMSCs) were first reported by Friedenstein et al. (1968). According to the International Society for Cell and Gene Therapy (ISCT), MSCs are defined as adherent cells possessing tri-lineage differentiation potential into osteocytes, chondrocytes, adipocytes, and express markers CD73, CD90, and CD105 (Dominici et al., 2006). The published materials from the last decade referred to in this review have analyzed one or a few of these properties to define the BMMSC population used to obtain EVs. Minimal information for studies of extracellular vesicles (MISEV) 2018 has given guidelines for the preparation of EVs from various BMMSCs (Thery et al., 2018; Witwer et al., 2019). Based on these guidelines, human MSCs need to be characterized as positive for CD105, CD73, CD90 expression and negative for CD45, CD34, CD14, CD11b, CD79α or CD19. In addition, the differentiation potential of human BMMSCs into osteocytes, adipocytes, and chondrocytes needs to be confirmed.

EVs isolated from mice, rats, and human BMMSCs have been studied for their regenerative potential in different organ injury models (**Table 1**). Mouse BMMSC-EVs were reported to promote

TABLE 1 | The biological effect of BMMSC-EVs on organ and cell repair in various non-radiation injury models.

EV source	EV Characterization	Model	Effect	Signaling	References
Mouse BM MSCs	<200 nm	Traumatic brain injury	Cognitive recovery, neuroblast proliferation, reduced neural inflammation	-	Zhang et al. (2015)
	NTA	Necrotic entero colitis	Reduced intestinal toxicity	-	Rager et al. (2016)
Rat BMMSCs	<300 nm, EM, flow cytometry for CD81, CD63	*In vitro* model of Alzheimer's disease	Neuroprotective	Catalase, reduced oxidative stress	de Godoy et al. (2018)
	<200 nm EM, WB for HSP70, TSG101, CD63, CD81	Myocardial injury	Reduce inflammation, promote M2 macrophage polarization	NF-κB	Xu et al. (2019a)
	<200 nm, EM, WB for CD63, CD81, Alix	Myocardial infarction	Inhibition of myocardial infarction	ATG13, mTOR, autophagy	Zou et al. (2019)
	<200 nm, EM, WB for CD63, CD81, CD9	Bone fracture	Endothelial cell proliferation, osteoblast proliferation	HIF-1α-VEGF, BMP-2/Smad1/RUNX2	Zhang et al. (2020a)
Human BMMSCs	EM, immunolabeling CD9, CD63	Acute kidney injury	Proliferate proximal tubular epithelial cells	IGF-1	Tomasoni et al. (2013)
	<200 nm, EM, WB for CD9, Flotillin1	Angiogenesis assays	Endothelial cell proliferation	EMMPRIN	Vrijsen et al. (2016)
	EM, CD63 ELISA	Optical nerve crush	Retinal ganglion cell protection	-	Mead and Tomarev (2017)
	<200 nm, EM, WB for CD9, CD63, CD81, TSG101, Alix	Carbon tetrachloride-induced liver fibrosis	Improved liver function reduced inflammation and fibrosis	Wnt/β-catenin	Rong et al. (2019)
	<200 nm, EM, WB for CD9, CD63, CD81	Rat calvaria bone defect	Bone regeneration, angiogenesis	VEGF, ANG1, ANG2	Takeuchi et al. (2019)

angiogenesis *via* extracellular matrix metalloproteinase inducer (Vrijsen et al., 2016), stabilize endothelial-barrier function *via* hepatocyte growth factor (Wang et al., 2017). Rat BMMSC-EVs were reported to reduce oxidative stress *via* catalase (de Godoy et al., 2018), improve cognitive recovery, and reduce neural inflammation in the traumatic brain injury model (Zhang et al., 2015).

BMMSC-EVs for Radiation-Induced Bone Marrow Injury

Mitotically active bone marrow is highly susceptible to radiation. Exposure to radiation results in increased vascular permeability, loss of hematopoietic stem-progenitor cells, osteopenia, arrest of bone growth, and bone marrow stromal cell apoptosis, eventually leading to fibrosis (Pacheco and Stock, 2013).

Murine BMMSC ($CD44^+/CD24^+/CD105^+/Sca\text{-}1^+$and $CD31^-/CD11b^-/CD45^-/CD34^-/CD86^-$) derived EVs could rescue bone marrow hematopoietic cells from radiation damage *in vitro* and *in vivo* (Wen et al., 2016). In this study, when treated with murine BMMSC-EVs, the irradiated mouse hematopoietic cell line (Factor Dependent Continuous-Paterson 1) showed increased proliferation and reduced apoptosis. The authors further studied the potential of mouse and human BMMSC-EVs to rescue murine hematopoietic radiation damage *in vivo*. Seven days post 1 Gy WBI of B6. SJL mice, bone marrow-lineage negative cells were isolated and cultured with 2×10^9 murine MSC-EV particles/ml or vehicle for 48 h. These cells were intravenously injected into 2 Gy WBI C57BL/6 mice. Mice that received BMMSC-EV treated irradiated bone marrow hematopoietic cells showed a significant increase in engraftment at 36 weeks compared to those transplanted with vehicle-treated cells. Whole bone marrow cells that were harvested at 36-weeks post-transplant were able to recover the bone marrow after secondary transplantation into lethally irradiated mice. Similarly, intravenous injection of 4×10^9 human MSC-EV particles/ml into 5 Gy WBI mice showed improved granulocytes and white blood cells at three and five weeks post-radiation.

Another report from the same group investigated the biodistribution of DiD-labelled MSC-EVs in irradiated bone marrow using different doses, injection schedules, and timing post-radiation (Wen et al., 2019). They showed that 5 Gy WBI mice treated with BMMSC-EVs had a significant increase in the uptake of EVs by $CD11b^+$ and $F4/80^+$ cells in the spleen compared to that of femur bone marrow at 6 and 24 h post-radiation. Besides, an increase in uptake of EVs was observed in a radiation dose-dependent manner when injected 6 h post-radiation into mice at 1, 3, or 6 Gy radiation. This study also reported a dose-dependent increase in EV uptake in bone marrow, spleen, and liver when injected with 2×10^8, 2×10^9, and 2×10^{10} particles of BMMSC-EVs, 24 h post-5 Gy WBI. Similarly, after three intravenous injections of 2×10^9 EV particles to 5 Gy WBI mice, a significant increase in EV load was observed in the liver and spleen compared to a single injection.

Zuo et al. (2019) reported that Sprague-Dawley rat BMMSC-EVs alleviate radiation-induced bone loss in rats that received 16 Gy Cesium radiation to the knee joint of the left hind limb (Zuo et al., 2019). In their study, BMMSC-EVs were isolated *via* ultracentrifugation and were <100 nm in size, expressed CD63, CD81, TSG101, and negative for Calnexin. The amount of EVs at 1.6 mg/kg or 1×10^6 BMMSCs were injected into the tail vein of 16 Gy irradiated rats. Bone volume fraction (BV/TV) is the parameter to determine the volume of mineralized bone per unit volume of the sample. The BV/TV of the non-irradiated

mice was 67.6%, while it was decreased to 30.9% in the irradiated mice 28 days post-radiation. However, the BV/TV of the irradiated mice transplanted with BMMSCs and BMMSC-EVs was increased by 53 and 13%, respectively, compared to the irradiated mice without transplantation. Furthermore, incubation of BMMSC-EVs with 6 Gy irradiated BMMSCs *in vitro* showed a decrease in DSB as determined by γ-H2AX staining at 2, 4, and 12 h post-radiation; an increase in antioxidant effect *via* increasing the expression of superoxide dismutase (SOD) 1 and 2 at 12 h and 24 h post-radiation and activation of Wnt/β-catenin signaling in BMMSCs, which could be the mechanisms of improving bone loss observed in irradiated rats with BMMSC-EV treatment. This study also showed that BMMSC-EVs treatment restored the radiation-induced loss of BMMSCs differentiation potential as indicated by an increase in calcium deposition, Runx2 expression (osteogenic), and oil red O staining (adipogenic) compared to irradiated cells without treatment (Zhou et al., 2018).

BMMSC-EVs for Radiation-Induced Intestinal Injury

Stem cell-driven regeneration in the intestine is mediated by cycling leucine-rich repeat-containing G-protein coupled receptor 5 ($Lgr5^+$) stem cells at the crypt base *via* a Wnt signaling pathway (Barker et al., 2007). These crypts are in close contact with stromal cells such as mesenchymal cells, ECs, Mϕs, and lymphocytes that provide the signaling factors for intestinal regeneration. Radiation damage to the intestine leads to the loss of these rapidly cycling $Lgr5^+$ stem cells to the impairment of epithelial regeneration, showing an irreversible loss of crypt-villi, EC apoptosis, and loss of mucosal barrier. Collectively these contribute to septic shock and systemic inflammatory response as a radiation-induced gastrointestinal syndrome.

Accarie et al. (2020) has shown that EVs that are <250 nm and $CD81^+$ derived from human BMMSCs mitigate intestinal toxicity in a mouse model of ARS (Accarie et al., 2020). This study compared the effect of intravenous injection of 600 µg of BMMSC-EVs after 10 Gy WBI. A 3.5-days delay in death was observed in nude mice that received three injections of BMMSC-EVs at 6, 24, and 48 h post-10 Gy WBI in comparison to untreated, irradiated control mice. Also, the expression of tight junction protein claudin-3 was more preserved at the membrane of small intestine epithelium in BMMSC-EV treated mice than in irradiated, non-treated controls. At 3 days post-WBI, a dose-dependent decrease in apoptotic cells, an increase in $Ki67^+$ cells in the crypts, and less alteration of crypt-villus architecture was observed in BMMSC-EV-treated mice in comparison to the irradiated mice without treatment.

The direct effect of human BMMSC-EVs on the ISCs after radiation has not been studied yet. Reserve ISCs like radio-resistant cells expressing Keratin19 (Krt19) (Asfaha et al., 2015) and Polycomb complex protein (Bmi1) (Yan et al., 2012) were shown to be generating $Lgr5^+$ cells for recovering the functional cell loss after radiation. However, other growth factors and EVs from multiple cell sources that can stimulate these stem cells need to be further investigated.

BMMSC-EVs for Radiation-Induced Liver Injury

During radiotherapy for hepatocellular carcinoma, normal liver tissue is often exposed to radiation. This results in liver sinusoidal endothelial cell toxicity, atrophy of hepatocytes, and occlusion of veins, gradually leading to loss of liver function and progressing toward radiation-induced liver disease (RILD) or radiation hepatitis (Benderitter et al., 2014). An increase in inflammatory cytokines such as tumor necrosis factor-alpha (TNF-α), interleukin (IL)-1β, and IL-6 was observed in the early phase of RILD. Currently, there is no effective treatment for RILD.

Congenic hepatocyte transplantation *via* intra-splenic injection is shown to repair acute and late effects of RILD (Guha et al., 1999). Intra-splenic transplantation of liver sinusoidal endothelial cells combined with hepatocyte growth factor into partial hepatic irradiation rodent model was shown to ameliorate radiation-induced sinusoidal obstructive syndrome and repopulate the irradiated sinusoidal endothelium by eight weeks after transplantation (Kabarriti et al., 2010). Challenges with orthotropic liver transplantation and the minimal availability of donor hepatocytes for safe transplant limit the use of hepatocyte transplantation to treat liver diseases.

EVs derived from MSCs from the human umbilical cord (Li et al., 2013), bone marrow (Rong et al., 2019), and embryonic stem cells (Tan et al., 2014) have been reported to alleviate liver injury in drug-induced hepatic injury models (Lou et al., 2017; Phinney and Pittenger, 2017). Herrera et al. (2010) have shown that microvesicles derived from human liver stem cells ($CD29^+$/$CD44^+$/$CD73^+$/$CD90^+$) accelerated liver regeneration in 70% hepatectomized rats (Herrera et al., 2010). Rong et al. (2019) showed that human BMMSC-EVs (<200 nm) effectively alleviated liver fibrosis by inhibiting Wnt/β-catenin signaling in the carbon tetrachloride -induced liver damage model (Rong et al., 2019). Even though MSC-EVs were shown to alleviate various drug-induced or physical hepatic injury models, their potential to recover radiation-induced liver injury is not well studied.

BMMSC-EVs for Radiation-Induced Lung Injury

Radiation-induced pneumonitis and radiation-induced pulmonary fibrosis are the major early and delayed lung toxicities in cancer patients undergoing thoracic radiotherapy. Radiation-induced DNA damage and free radicals result in epithelial cell death leading to lung mucositis. This is followed by an increase in inflammatory cytokines (TNF-α and IL-6), natural killer (NK) cells, Mϕ polarization, edema, and lung perfusion, eventually activating fibroblasts and myofibroblast differentiation to fibrosis in the irradiated lung (Kabarriti et al., 2020). MSCs derived from the umbilical cord (Wei et al., 2020), bone marrow (Lee et al., 2012), and adipose tissue (Dong et al., 2015) were reported to be attenuating various models of lung injury.

Human umbilical cord-MSCs could repair radiation-induced lung injury (RILI) by inhibiting myofibroblastic differentiation of

human lung fibroblasts (Xu S. et al., 2019; Zhang et al., 2019). Human adipose-MSCs were shown to downregulate TNF-α signaling in the 15 Gy-irradiated lungs and prevent the epithelial-mesenchymal transition of irradiated type II alveolar epithelial cells (Dong et al., 2015). Klein 2017 showed that conditioned media from aorta-MSCs restored SOD1 expression and protected EC loss in the lung of RILI mice (Klein et al., 2017). These studies have demonstrated the effectiveness of using different sources of MSCs, which warrants further investigation on MSC-EVs for treating RILI.

ENDOTHELIAL CELL-EVs

The heart pumps the blood carrying nutrients and oxygen to all the cells in our body *via* arteries to capillaries and collects the blood *via* veins for waste removal and purification. The collective action of the blood vascular system and lymphatics maintains the fluid level in the body. All these vessels are lined by ECs that play an important role in vascular homeostasis. In addition, ECs mediate immune responses, involve in inflammation, coagulation, and angiogenesis (Orfanos et al., 2004). ECs differ based on their location; for instance, micro versus macrovascular ECs have a distinct response to physiologic and inflammatory stimuli (Stevens et al., 2008).

Radiation induces EC dysfunction, such as increased permeability, apoptosis, and detachment from the basement membrane of the vessels (Flamant and Tamarat, 2016). This often leads to inflammation, fibrosis, and damage to tissue microvasculature depending upon the radiation dose. Radiation-induced EC toxicity is reported in various tissues such as the intestine (Paris et al., 2001; Wang et al., 2007), lungs (Ghobadi et al., 2012; Ziegler et al., 2017), central nervous system (Peña et al., 2000), and parotid glands (Xu et al., 2010). Ionizing radiation-induced long-term senescence was reported in ECs (Lafargue et al., 2017). Prevention or inhibition of EC toxicity was reported to protect the intestine (Rotolo et al., 2012), central nervous system (Peña et al., 2000), and lungs (Klein et al., 2017) against radiation-induced damage. EC transplantation has been shown to be beneficial in mouse models of hemophilia (Follenzi et al., 2008), hepatectomy (Melgar-Lesmes et al., 2017), and lethal irradiation in mice (Chute et al., 2007).

Biological Activities of EC-EVs

Like many mammalian cells, ECs respond to stimuli and produce heterogeneous cargo containing EVs. A distinct proteomic cargo was reported in human umbilical vein endothelial cells (HUVECs) when stimulated with TNF-α (Letsiou and Bauer, 2018). Similar changes were reported in the proteome cargo of EVs from human pulmonary artery endothelial cells treated with mechanical cyclic stretch or lipopolysaccharides (Letsiou et al., 2015). Van Balkom 2015 analyzed the miRNA profile of human microvascular endothelial cells (HMEC-1) and thus-derived EVs. The study showed that EC-EVs contain miRNA's related to the regulation of angiogenesis, proliferation, and differentiation (van Balkom et al., 2015). Endothelial progenitor cell-EVs were shown to improve atherosclerotic endothelial dysfunction in a mouse model of atherosclerotic diabetes (Bai et al., 2020). EC-EVs were shown to enhance EC proliferation (Wang et al., 2019) and act against apoptosis and inflammation (Andrews and Rizzo, 2016). EC-EVs from various sources were shown to be neuroprotective (Xiao et al., 2017), improve sepsis (Zhou et al., 2018), and improve high D-glucose-induced endothelial dysfunction (Saez et al., 2018).

HUVEC-EVs were shown to protect human neuroblastoma SH-SY5Y cells from ischemia-reperfusion injury *in vitro* (Xiao et al., 2017). Endothelial colony-forming cells (ECFC)-EVs inhibited apoptosis and reduced ischemic kidney injury in mice (Vinas et al., 2018). Brain EC-EVs promoted motor function and Synapsin I expression in the cerebral artery occlusion model of rats (Gao et al., 2020). EVs from HUVECs cultured in high glucose media restored wound healing of basal glucose cultured HUVECs compared to EVs from HUVECs cultured in basal media (Saez et al., 2018). EVs isolated from HUVECs cultured under high glucose increase intercellular adhesion molecule 1 (ICAM1) expression in Mono-Mac-6 cells, a monocytic cell line (Saez et al., 2019). HUVEC-EVs showed a decrease in cardiomyocyte death, protected against hypoxia *via* extracellular signal-regulated protein kinase (ERK1/2) and mitogen-activated protein kinase (MAPK) signaling (Davidson et al., 2018). The cardioprotective effect was not observed when treated with EV depleted conditioned media. Increased axonal growth and upregulation of miRNA related to the regulation of Sema6A, Phosphatase and Tensin Homolog (PTEN), and RhoA was observed with rat cerebral EC-EVs *in vitro* (Zhang Y. et al., 2020). Vascular smooth muscle cells showed an increased vascular cell adhesion molecule 1 (VCAM1) expression and leukocyte adhesion when cultured with rat cerebral EC- EVs (Boyer et al., 2020). The summary of utilizing various biological activities of EC-EVs in treating different non-radiation injury models discussed in this review are listed in **Table 2**.

EC-EVs for Radiation-Induced Bone Marrow Injury

The bone marrow microenvironment regulates HSC fate in homeostasis and after injury (Mendelson and Frenette, 2014). In addition to osteoblasts and stromal cells, ECs occupy a significant role in niche signals for HSCs, and EC toxicity is one of the major consequences of multi-organ failure in ARS. Piryani et al. (2019) studied whether EC-EVs could regulate HSC regeneration after ionizing radiation (Piryani et al., 2019). EVs were isolated from bone marrow ECs of C57BL/6 mice *via* differential centrifugation to obtain <200 nm in size and expressed CD31, vascular endothelial (VE)-cadherin. At 24 h after either 5 Gy (hematopoietic assays) or 8 Gy (for survival) WBI, 1.9×10^9 particles of EV were intravenously injected daily for four days. Irradiated mice with EC-EV treatment showed improved bone marrow cellularity, hematopoietic stem and progenitor cell content, preserved EC architecture, and showed a 50% survival advantage. Among the 48 cytokines tested, EC-EVs increased the expression level of tissue inhibitor of

TABLE 2 | The biological effect of endothelial cell-EVs on organ and cell repair in various non-radiation injury models.

EV source	EV Characterization	Model	Effect	Signaling	References
HUVECs	<200 nm, EM, WB for CD9, HSP70, TSG101	Cerebral ischemia-reperfusion injury	SH-SY5Y nerve cell protection	-	Xiao et al. (2017)
ECFCs	<200 nm, WB for CD81, TSG101	Kidney ischemic injury	Inhibition of apoptosis, reduced ischemic injury	miR-486–5p, PTEN	Vinas et al. (2018)
Senescent HUVECs	EM, WB for CD63, CD9; Calnexin, β-actin negative	HUVECs *in vitro*	Decreases in VE-cadherin, β-catenin, decreased cell growth and impaired migration potential	β-catenin	Wong et al. (2019)
HUVECs	<200 nm, EM, flow cytometry for CD63	Adult rat cardiomyocytes co-culture *in vitro*	Decreased cell death of cardiomyocytes, protection against hypoxia	ERK1/2, MAPK	Davidson et al. (2018)
HUVECs conditioned with basal and high glucose	<300 nm, EM, WB for CD63, CD81	HUVECs growth, wound healing *in vitro*	Induced endothelial dysfunction in HUVECs	ICAM-1	Saez et al. (2018)
HUVECs and monocytes	<300 nm, EM, WB for CD63	Monocytes (MM6) and HUVECs under high glucose *in vitro*	Increase ICAM-1 expression in MM6 cells	ICAM-1	Saez et al. (2019)
Brain ECs (bEnd.3)	EM	Rat cerebral artery occlusion model	Promoted motor function, synapsing in dendrites	miR-126–3p	Gao et al. (2020)
Rat cerebral ECs (CECs) and ischemic-CECs	<200 nm, EM, WB for CD63, CD31, Alix; calnexin, zo-1 negative	Axon culture *in vitro*	Increased axonal growth, upregulation of miRNA	Sema6A, PTEN, and RhoA	Zhang et al. (2020b)
Rat aortic endothelial and vascular smooth muscle cells	<200 nm, EM, WB forTSG101, Flotillin; VDAC negative	Vascular smooth muscle cells *in vitro*	Increased VCAM1 expression and leukocyte adhesion to vascular smooth muscle cells	HMGB1	Boyer et al. (2020)

metalloproteinase 1, which is essential in vascular remodeling post-ischemia (Mandel et al., 2017). The above study suggests that EC-EVs have the potential to protect post-radiation damaged ECs.

A thorough investigation needs to be performed to examine EC-EVs as radiation MCM to mitigate injury in other organs such as the intestine, liver, and lung. Specific types of ECs have distinct potential and actions (Rafii et al., 2016). The characteristics of EVs from various cell types such as the aorta, endothelial progenitor cells, and organs such as lung and liver need to be studied to facilitate tissue-specific regeneration after radiation injury.

MACROPHAGE-EVs

Macrophages are the phagocytic immune cells that originate from monocytes and circulate in the blood. They differentiate in various tissues as tissue-resident Mϕs such as alveolar Mϕs in the lung, Kupffer cells in the liver, microglia in the brain, and splenic Mϕs in the spleen. They are distinguished by their morphology, the pathogens they interact with, the levels and type of cytokines they produce. They present antigens to T-cells and initiate inflammation, release cytokines that activate other immune cells. Inflammatory monocytes and tissue-resident Mϕs play a crucial role in tissue repair, regeneration, and fibrosis. Insults to healthy tissues result in increased release of damage-associated molecular patterns (DAMPs). This initiates an inflammatory cascade involving recruitment, proliferation, and activation of various hematopoietic and non-hematopoietic mediators (neutrophils, Mϕs, innate lymphoid cells (ILCs), NK cells, B cells, T cells, fibroblasts, epithelial cells, ECs, and stem cells) which collectively work for tissue repair (Wynn et al., 2013). Mϕs are a great source of Wnt ligands that activate epithelial regeneration potential in injury models of the liver (Boulter et al., 2013) and kidney (Lin et al., 2010). However, Mϕs undergo reprogramming in response to the damage signals and can be pro-inflammatory M1 or anti-inflammatory M2 phenotype. M1 and M2 Mϕs possess distinct chemokine profiles and differ in the metabolism of iron, folate, and glucose (Mantovani et al., 2013). Mϕs are studied widely for their role in tissue repair and their potential for tissue regeneration.

Biological Activities of Mϕ-EVs

Mϕ-EVs are gaining a lot of interest as therapeutics. Tissue repair potential of Mϕ-EVs was reported in models of atherosclerosis (Bouchareychas et al., 2020), cardiac injury (Dai et al., 2020), wound healing (Li et al., 2019), hair loss (Rajendran et al., 2020), dextran sulfate sodium induced-colitis (Schubart et al., 2019; Yang et al., 2019), vascular repair in intravascular stunt-implant (Wallis et al., 2020) and skin diseases (Kim et al., 2019). Mϕ-EVs from various sources were shown to be angiogenic (Yan et al., 2020), influence neural action potential (Vakili et al., 2020), anti-inflammatory, and could convert M1 to M2 polarization (Kim et al., 2019). M2 Mϕ-EVs were shown to be anti-inflammatory in the atherosclerosis model by reducing nuclear factor kappa-light-chain-enhancer of activated B cells (NF-κB) and TNF-α signaling (Bouchareychas et al., 2020). Mϕ-EVs were shown to promote Wnt-signaling for hair growth (Rajendran et al., 2020) and intestinal regeneration (Saha et al., 2016). The summary of various biological activities of Mϕ-EVs in treating different non-radiation organ injury models as discussed in this review is listed in **Table 3**.

TABLE 3 | The biological effect of macrophage-EVs on organ repair in various non-radiation injury models.

EV source	EV Characterization	Model	Effect	Signaling	References
Murine bone marrow-derived macrophages (BMDM) and BMDM-treated with IL-4	<200 nm, EM, WB for CD9, Alix, Flotillin	Atherosclerosis	Reduced excessive hematopoiesis in bone marrow, number of macrophages; reduction in necrotic lesions	miRNA regulation of NF-kB, TNF-a	Bouchareychas et al. (2020)
Murine RAW 264.7 cells	<200 nm, EM, WB for CD63, Alix	Diabetic rat	Inhibited secretion of pro-inflammatory cytokines, induced endothelial cell proliferation, migration and re-epithelialization of the wound	TNF-α, IL-6 inhibition, P-AKT activation	Li et al. (2019)
Murine bone marrow-derived M2b macrophages	<200 nm, EM, WB for CD9, CD63, CD81	DSS-colitis	Increase in Treg cells, IL-4 in the spleen, suppression of IL-1β, IL-6, IL-17A	CCL1/CCR8	Yang et al. (2019)
Murine bone marrow-derived M2 macrophages	<200 nm, EM, WB for CD63, Alix	Cutaneous wound mice model	Increased M2 at the wound site, increased angiogenesis, re-epithelialization and collagen deposition	Activation of arginase, inhibition of iNOS	Kim et al. (2019)

Mϕ-EVs for Radiation-Induced Intestine Injury

Saha et al. (2011) have developed an enrichment culture system from mouse BMASCs containing MSCs ($CD90^+/CD105^+/CD29^+$), myeloid cells ($CD45+/CD11b^+$), and ECs ($CD34^+/CD31^+$) (Saha et al., 2011). After transplanting into mice subjected to 18 Gy abdominal radiation, BMASCs have promoted ISC regeneration and improved their survival, whereas either depletion of myeloid cells or MSCs failed to regenerate the irradiated intestine, suggesting that myeloid cells and MSC mediated regeneration. Mϕs support crypt regeneration, coordinate signals from gut microbes, injured epithelium, and help ISC regeneration (Pull et al., 2005). Mϕs activated by toll-like receptor 9 was shown to ameliorate intestinal injury post-radiation (Saha et al., 2011). Wnt signaling has an important role in ISC proliferation and regeneration in the intestine. Earlier reports from our group by Saha et al. (2016) have studied Mϕ-EVs for intestinal regeneration. To understand the specific role of Wnt signing from Mϕs for intestinal repair, this study generated mice with macrophage-restricted ablation of Porcupine ($Porcn^{fl/fl}$), a gene essential for Wnt synthesis. These *Porcn*-depleted (null) mice have normal intestine but are hypersensitive to radiation injury compared to wild-type mice. The intestine in these mice showed loss of Lgr5+ cells, reduced crypt depth and number, and decreased survival after WBI (Saha et al., 2016). These mice were rescued from radiation lethality when treated with conditioned medium from wild-type bone marrow macrophages (BMM) but not with medium from Porcn-null mice BMM.

Furthermore, they have isolated EVs from the BMM-conditioned media using ultracentrifugation. These EVs were positive for TSG101, CD9, and Alix. When tested using T-cell factor/lymphoid enhancer factor (TCF/LEF)-luciferase reporter cell line, BMM-EVs showed activation of Wnt signaling. BMM-conditioned media improved the survival of mice post-18.5 Gy abdominal radiation. In contrast, the EV depleted media could not rescue, indicating that BMM-EVs carrying Wnt ligands that improve intestinal regeneration after radiation injury.

EVs FOR RADIATION MCM

The potent anti-inflammatory, anti-fibrotic characteristics of BMMSC-EVs, angiogenic and anti-inflammatory properties of EC- and Mϕ-EVs make them promising candidates for regenerative application. The summary of EVs derived from these three cell types that have been discussed in this review on interacting with various signaling molecules is depicted in **Figure 3**. With such diverse potential, EVs from these cells have been extensively studied for radiation-induced injury. In **Table 4**, we summarized the potential of BMMSC-, EC- and Mϕ-EVs in repairing bone marrow, intestine, and lung as discussed in this review.

The success of radiation MCM depends mainly on the efficacy, timing, and dosage of treatment into radiation-damaged tissues. The bio-distribution of EVs *in vivo* is the crucial driver in the success of MCM and is influenced by the damage model, cell source of EVs, and route of administration. The route of administration of EVs affects biodistribution to various organs (Wiklander et al., 2015). Studies have shown that modification of EVs will influence their biodistribution *in vivo* (Royo et al., 2020). Therefore, strategies to modify EVs for targeted organ-specific delivery are of great interest for radiation injuries. For example, tissue-specific ECs were known to have specific functions (Rafii et al., 2016). This can be further investigated in terms of EVs from tissue-specific ECs. For instance, lung EC- EVs preferentially distribute to the lung over other tissues providing a lung-targeted therapy.

Alternately, cutting-edge gene-editing technology can be applied to improve or modify the characteristics of EVs. For example, EVs derived from engineered cells overexpressing key growth factors such as Wnt ligands, epidermal growth factor, and fibroblast growth factor could be tested in radiation injury models. Though the overall effect of EVs in radiation-injury models was published, the detailed molecular mechanism of EVs for radiation repair is still not well understood.

EVs for ARS

Whole-body exposure to high doses of radiation in a short duration leads to the development of ARS, often characterized by damage to hematopoietic, gastrointestinal, and neurovascular systems. It is implacable to conduct a human clinical trial to test radiation MCMs. Instead, FDA has provided "Animal Rule" as guidance for radiation MCM approval. Animal models of the whole body, partial body, or abdominal radiation are often used to develop radiation MCMs for ARS. For treating the acute

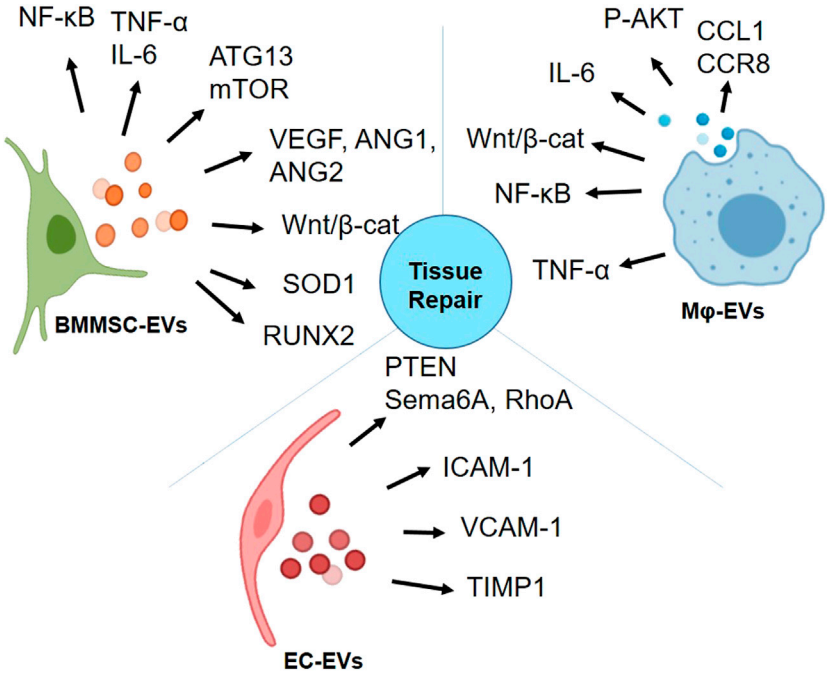

FIGURE 3 | Activation of proteins involved in various signaling pathways by bone marrow mesenchymal stromal/stem cell (BMMSC)-extracellular vesicles (EVs), endothelial cell (EC)-EVs, and macrophage (Mϕ)-EVs for tissue repair (Graphics adapted from BioRender.com).

effects of radiation during the accidental event, the therapeutic agents may not be accessible immediately. Therefore, evaluating the efficacy of the radiation MCM candidates is set to be administered at least 24 h after radiation exposure for the first dose. EVs are suitable to develop as radiation MCMs due to their targeted action in a very short duration. However, multiple doses of EVs might be necessary to enhance their efficacy. On the other hand, radiation damage like ARS involves multi-organ failure, and single cell-source derived EVs with specific signaling might not yield a successful recovery. Therefore, a combination of the stem, immune, differentiated, or reprogrammed cell-derived EVs might be necessary for a broader range of efficacy.

EVs for Delayed Effects of Acute Radiation Exposure

In addition to the acute effects, delayed effects of acute radiation exposure (DEARE) are reported in ARS survivors. Irradiation injury causes DNA damage through free radicals, SSBs, and DSBs. Even though the DNA damage is repaired, the process is not always efficient. The defects in the DNA damage response pathway result in the development of either cell cycle arrest (mitotic catastrophe, senescence) (Li et al., 2018) or cell death (apoptosis, necrosis, and autophagy). Cells in the senescence stage undergo mitotic arrest while being metabolically active. Senescent cells can cause chronic inflammation and disruption of surrounding tissue structure and function *via* the production of ROS, inflammatory mediators (IL-6, IL-18, and TGF-β), growth factors, and extracellular proteases. This process collectively refers to as senescence-associate secretory phenotype (SASP) (Li et al., 2018). The molecules secreted from SASP can also be packed in EV format (Misawa et al., 2020). This persistent insult from SASP leads to the delayed effect of irradiation-induced senescence, such as fibrosis in the lung (Citrin et al., 2013; He et al., 2019), oral mucositis (Iglesias-Bartolome et al., 2012), cardiovascular disease (Stewart et al., 2013), hypo-salivation (Peng et al., 2020), hematopoietic cell senescence (Wang et al., 2011). It has also been shown that low radiation can affect the autophagic flux, and activation of autophagy may decrease the senescence induced by radiation and prevent deterioration (Alessio et al., 2015).

Further SASP can lead to radiation-induced bystander effect (RIBE) (Uribe-Etxebarria et al., 2017). RIBE is a condition in which the radiated cells cause a stress response in the neighboring cells resulting in DNA damage, apoptosis, genomic instability, and cell death. Previously cell-to-cell communication of various components of SASP such as IL-6, IL-8, and TGF-β were considered as inducers of senescence in neighboring cells. However, the newly emerging focus is that EVs secreted from irradiated cells also played an essential role in modulating senescence in non-irradiated surrounding cells. For example, non-irradiated cells became senescent when treated with EVs isolated from irradiated cells. This observation was made in primary human fibroblasts isolated from neonatal foreskin (Elbakrawy et al., 2020), breast epithelial cancer cells (Al-Mayah et al., 2015), salivary gland stem/progenitor cells (Peng et al., 2020).

In an *in vivo* study, the damaged DNA foci were significantly higher in non-irradiated mouse fibroblast cells when treated with

TABLE 4 | Application of BMMSC-, EC- and macrophage-EVs for organ repair in radiation injury models.

Stromal Cell Source	Characterization	EV Isolation method	EV Characterization	Target tissue	Model tested	Route of administration	Dose of EV	Storage	References
Human MSC (Lonza, MD, USA #PT-3001)	NA	NA	Average of 231.3 ± 124.6 nm, EM, WB for CD9, CD63, CD81, TSG101, HSP70	Bone marrow	5 Gy WBI in C57BL/6 mice	Intravenous	2×10^8, 2×10^9 and 2×10^{10} particles/ mouse	PBS with 1% DMSO, at -80°C	Wen et al. (2019)
Rat bone marrow	Negative for CD34, CD45; Positive for CD29, CD44 and CD90	Differential centrifugation	EM, WB CD63, CD81; Negative for Calnexin	Bone marrow	16 Gy Knee joint irradiated Sprague-Dawley Rats	Intravenous	1.6 mg/kg	PBS, at -80°C	Zuo et al. (2019)
Murine and human bone marrow	Negative for CD31, CD45, CD11b, CD34 and CD86; Positive for CD44, CD29, CD105, Sca-1	Differential centrifugation	NanosightNS500, EM, WB for CD9, CD63, CD81	Bone marrow	2, 5 and 9.5 Gy Cesium WBI	Intravenous	4×10^9 particles/ mouse	10% DMSO, at -80°C for 6 months	Wen et al. (2016)
Immortalized E1-MYC 16.3 human embryonic stem cells	Negative for CD45; Positive for CD73, CD105	Tangential flow filtration	<200 nm, EM	Intestine	WBI in nude mice	Intra-venous	600 µg of EV, 6h, 24h, and 48h post-WBI	Paracrine Therapeutics's-Proprietary technique, stored at -20°C	Accarie et al. (2020)
Mouse bone marrow endothelial cells	NA	Differential centrifugation	<200 nm; WB for CD31, VE-cadherin; EM	Bone marrow	5 and 8 Gy Cesium WBI	four days i.v., starting 24 h post-WBI	1.9×10^9 particles of EV per injection	NA	Piryani et al. (2019)
Mouse bone marrow macrophages	Positive for CD11b	Differential centrifugation	WB for CD9, TSG101, Alix	Intestine	18.5 Gy Abdominal Irradiation	Intra-venous	500 µl of EV and conditioned media	NA	Saha et al. (2016)

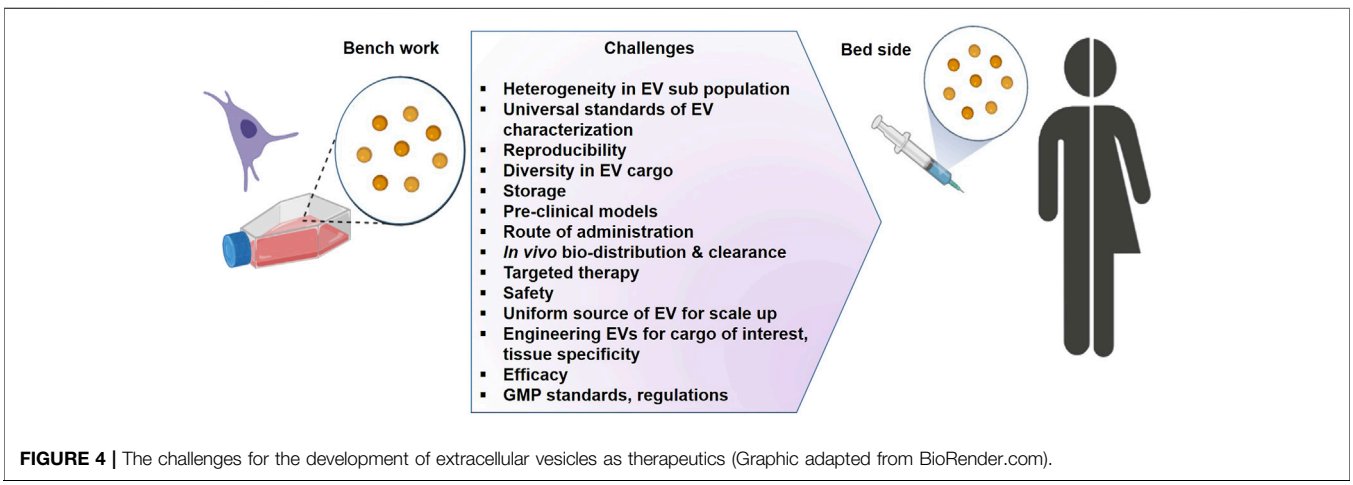

FIGURE 4 | The challenges for the development of extracellular vesicles as therapeutics (Graphic adapted from BioRender.com).

the irradiated mouse's serum-EVs than non-irradiated mouse serum-EVs (Ariyoshi et al., 2019). In another study, downregulation of antioxidant enzyme genes and cellular redox system (iNOS2) genes was observed in non-irradiated mice as a bystander effect when injected with bone marrow-EVs from irradiated mice (Hargitai et al., 2021). In the same token, recent evidence suggests that EVs as SASP, secreted from senescent cells might contribute to tumorigenesis and age-associated pathologies (Misawa et al., 2020). It can be a potential mechanism to explain a high incidence of cancer developed in the survivors after radiation exposure.

Senescent cells can be targeted for therapeutic purposes, i.e., *via* senolytic drugs. These drugs are usually small

molecules that can selectively remove senescent cells. In comparison, senolytics can be used as MCMs for DEARE such as fibrosis.

The research for developing MSCs or MSC-EVs as senolytics is limited. MSC therapy alleviates irradiation-induced bronchial–alveolar epithelial cellular senescence and inhibits the secretion of SASP factors such as the chemokine (C-C motif) ligand 2 (CCL2) and urokinase-type plasminogen activator (Plau/uPA). In this study, aortic MSC and BMMSCs were administered at 0.5 million cells 24 h after irradiation (Klein et al., 2016). Similarly, EVs from the human placenta MSC reduced the senescence in the ECs after whole thoracic radiation. The miRNA-214-3p from EVs inhibited the Ataxia telangiectasia mutated signaling pathway of senescence in ECs and further downregulated the expression of SASP factors, resulting in attenuation of fibrosis (Lei et al., 2020). Therefore, MSC-EVs have the potential to act as senolytics, further reducing the DEARE injury in normal cells.

CHALLENGES IN DEVELOPING EVs FOR CLINICAL USE

Characterization and Production

EVs are classified based on immunolabeling of EV surface proteins such as tetraspanins, integrins, cell adhesion molecules, and growth factor receptors (Lotvall et al., 2014; Buzas et al., 2018). The heterogeneity in size and content of the EV populations makes it challenging to purify a single EV population (Kowal et al., 2016). Therefore, the basic understanding of the size, either with dynamic light scattering-based techniques or electron microscopy; immunolabeling with markers such as CD63 and CD9 are necessary for the characterization of the EV population of interest. EVs produced by even a single cell type have subpopulations within; therefore, more numbers of surface markers need to be analyzed. An antibody array such as Exo-CheckTM (System Biosciences) measures up to 8 surface markers expressed on EVs in a single sample is advantageous. Using immortalized stable cell lines as a source of EVs can be a way to obtain pure, sub-population-specific EVs. Alternately, methods that can design and control the cargo in EVs, such as genetically engineered cell lines, will promote EVs as drug delivery systems with a targeted action (Luan et al., 2017).

Studies that report specific cell-derived EVs should include the passage number of cells, seeding density, and culture conditions, which are essential parameters affecting the production and characteristics of EVs. Also, the dose of EVs used in pre-clinical models is often represented as micrograms of protein or particle number in some studies. Though particle concentration seems to be an ideal reference, such state-of-the-art facilities measuring particle number and concentration of EVs are not always available in every research laboratory. The number of EVs obtained from 1 million mouse BMMSCs under specific culture conditions might differ among each laboratory. Therefore, additional information as mentioned in **Tables 1–4** will help researchers compare their results. Also, it will expand our knowledge on the average EV production potential of different cell types under specific culture conditions.

EVs derived from specific cell types interact with distinct signaling molecules, as described in **Figure 3**. Therefore, knowledge of various signaling pathways that specific cell-EVs can modulate is a prerequisite for developing targeted therapies. Luciferase reporter constructs containing specific promoter response elements are used to generate stable cell lines to monitor the activity of the transcription factors. Upon addition of specific ligands or test compounds with predicted activation, reporter activity can be measured by adding a light-emitting-substrate for the quantification. For example, HEK293 cells having TCF/LEF luciferase reporter construct have been used to monitor the Wnt activation by mouse BMM-EVs (McBride et al., 2017). Similarly, NF-κB reporter cells have been treated with MSC-EVs, and their increase in luminescence has been detected for NF-κB activation (Goloviznina et al., 2016). Similar luciferase-reporter cell lines for the notch, hedgehog, and Wnt signaling are commercially available (Accegen) to test whether specific cell-derived EVs can stimulate these singling pathways. Further, various platforms such as nCounter®-Stem Cell Characterization Panel (NanoString Technologies), that contain a panel of around 770 genes is available to evaluate stem cell viability and functionality. Such platforms need to be developed for screening the potential of biomolecules present in EVs. Alternately, conventional proteomics and miRNA sequencing are also available for detailed cargo profiling in the EVs of interest.

The small size and short life span of EVs make it more challenging to track them *in vivo*; however, *ex vivo* membrane labeling of EVs or labeled EVs (CD63-GFP) from reporter-cell lines or mice (Luo et al., 2020) are an alternate. Tracking EVs with these strategies will reveal their bio-distribution *in vivo* and help design better dosing strategies to target radiation-induced injury.

In situations such as accidental exposure to radiation (DiCarlo et al., 2017), the EVs need to be administered within 24–48 h to rescue bone marrow. In such a scenario, scaled-up and cryopreserved EVs should to be available to the patients in a short period of time. Therefore, EV-biobanks operated with clinical good manufacturing practice (cGMP) standards under FDA regulations are necessary to support the development of EV-therapeutics.

Biogenesis of EVs is a cellular response to physiological stimuli; therefore, *in vitro* culture conditions and treatments such as growth factors can influence the quantitative and qualitative production of EVs. For instance, serum-free culture or usage of exosome-free serum is often used to culture cells for EV production, which might alter the natural EV production threshold. On the other hand, parameters such as pH, temperature, and cryopreservation conditions can alter the EV uptake by cells (Cheng et al., 2019). Therefore, optimization of these parameters is needed to improve the purity and yield of EVs and their efficacy.

Standardization

Heterogeneity in the EV sub-populations poses them as challenging for developing as therapeutics. Simultaneously,

their diversity in containing various protein, nucleic acid, and lipid in the cargo makes them attractive for targeted delivery with multi-functional activity. Thorough characterization of EVs according to MISEV guidelines and reproducibility in the generation of EVs of interest is essential. GMP grade methodologies for EV preparation need to be developed for clinical translation. To further develop EVs as radiation MCM, the quality of cell source, cell culture, and method of EV preparation need to be standardized and reproducible across respective fields, followed by the *in vitro* and *in vivo* functionality assessment.

With the growing interest in the EVs for research and for clinical use, it is extremely important for universally acceptable methods and standards. ISEV community and its tools such as EV-TRACK and EV-METRIC are supporting EV-based research laboratories with centralized knowledge of EVs (Van Deun et al., 2017) (Royo et al., 2020). Researchers can submit their experimental data related to the method of isolation, characterization, and analysis from their projects to obtain constructive input and validation from EV-TRACK. In addition, workshops, conferences, and interactive scientific discussions organized by ISEV are enhancing the collaborative network of the EV research community, share, expand the knowledge between research laboratories around the globe, and collectively troubleshoot the challenges in EV research.

Expansion

Large-scale production of EVs is dependent on the type of cell source and method of isolation. Scaling up from T-flasks to bioreactors can increase the production of EVs. However, these changes in the culturing environment might influence cells and thereby change the characteristics of EVs. Therefore, these parameters need to be standardized in the scale-up process. The quality of EVs and their bioactivity need to be confirmed after the scale-up. Methods of EV isolation include but are not limited to differential/density-gradient ultracentrifugation, tangential flow filtration, bind/elute chromatography, size-specific separation, and immunolabeling-based EV selection. There is a unique principle and advantage for each of these methods. Ultracentrifugation is the most popularly used (Royo et al., 2020) and considered the gold standard; however, it might not be suitable for the purification of EVs on a large scale. Therefore, a combination of techniques might be an alternate strategy to obtain pure EVs.

Storage

Another major challenge in EV research is their storage. Literature suggests storing EVs at +4°C for a few weeks. EVs can be stored long-term at −80°C either in PBS or with cryo-protectants such as DMSO, Trehalose (Bosch et al., 2016), and glycerol (Jeyaram and Jay, 2017). For cryopreservation of various cell types, commercial reagents such as CryoStor, and NutriFreez are available. More GMP suitable cryopreservation reagents need to be developed for EV preservation. On other hand freeze-dried EVs can be a greater source for long-term storage and therapeutic applications (El Baradie et al., 2020).

Safety and Side Effects

In cell transplant studies, the *in vivo* microenvironment signals might influence viability, proliferation, and functionality of the transplanted cells. This might not be an issue in EV therapeutics since they do not replicate or differentiate and are short-lived. However, EVs that are naturally produced by a cell type are not necessarily specific to one tissue. Also, the multi-factorial bioactivity of EVs might cause side effects, a safety concern for targeted therapy. Another function of EVs secreted from the cells is a self-defense mechanism to maintain cellular homeostasis by removing the toxic molecules from the cells (Wallis et al., 2020).

To enhance a more targeted approach and minimize side effects, EVs can be locally administered to a specific tissue, such as intra-glandular injections at the site of injury. Alternately, engineered cells that produce tissue-specific EVs could be used.

EVs obtained from genetically engineered and immortalized cell lines might differ from naturally occurring EVs. Therefore, they need to be verified for purity, characterization, mechanism of action, *in vivo* biodistribution, and bioactivity. Genetically engineered cell-derived EVs might carry oncogenic remnants; therefore, they need to be verified for immunogenic and tumorigenic side effects.

There is a growing interest in using EVs as natural drug-delivery vehicles. Physical and chemical methods are used for drug-loading into the EVs. Hence, any immunogenic effect arising from these methodologies in the processing of EVs needs to be verified.

Overall, EVs are no exception with respect to having safety regulations for therapeutic application. Aspects such as production methods, purification, dosing, storage, and administration are important to check points for safe EV therapeutics.

CONCLUSION

An overview of the literature clearly indicates that research on EVs suffers from limitations. A number of technical points remain to be urgently clarified as summarized in **Figure 4**. However, the complexity of EVs heterogeneity and functions has to be taken into account. One of the most urgent challenges is to set up methods to characterize separately each kind of EVs in order to precisely define their individual cargoes and functions. The first challenge is how to define and measure EVs in a reproducible manner, their large scale production and purification for their use in case of mass casualties. In addition, understanding the molecular mechanisms governing EV formation, release, and clearance, as well as those involved in cell–cell communication, will enable us to envision new therapeutic strategies for favoring tissue repair. As described in this review several biological features provide EVs as an attractive tool for regenerative medicine. The advancement of translational research directed toward treating battlefield injury will have multiple cross over opportunities for their applications within the population. They will surely be a part of innovative therapeutic interventions as soon as few technical barriers are solved.

The adaptability of BMMSC-, EC- and Mϕ-derived EVs exhibit a remarkable capacity to adapt to the requirements of the damaged tissue in which the vesicles integrate and provide a promising option to address for the medical field after radiation exposure and complication of radiotherapy in order to support a personalized treatment. MSC therapy has established an extensive safety profile in the clinical setting and compared to the other cell types such as the endothelial progenitor cells, they present important advantage related to their isolation, culture and high scale production. Thus, in case of a radiological or nuclear event, the use of MSC-EV approach will provide a promising option to address the unmet needs that are critically important in the medical management of mass casualties.

AUTHOR CONTRIBUTIONS

LN, W-LY, RT, and CG conceptualized the content of the manuscript. LN initiated the draft, and PD contributed several sections. LN, PD, and W-LY edited and revised the manuscript. RT and CG revised and supervised the completion of the manuscript.

FUNDING

This work is supported by the US National Institute of Health (NIH) grants U01AI38324, U01AI133608, and U01DK103155 (to CG), and U01AI133655 (to W-LY).

REFERENCES

Accarie, A., l'Homme, B., Benadjaoud, M. A., Lim, S. K., Guha, C., Benderitter, M., et al. (2020). Extracellular Vesicles Derived from Mesenchymal Stromal Cells Mitigate Intestinal Toxicity in a Mouse Model of Acute Radiation Syndrome. *Stem Cel Res Ther*. 11 (1), 371. doi:10.1186/s13287-020-01887-1

Acharya, M. M., Rosi, S., Jopson, T., and Limoli, C. L. (2015). Human Neural Stem Cell Transplantation Provides Long-Term Restoration of Neuronal Plasticity in the Irradiated hippocampus. *Cel Transpl.* 24 (4), 691–702. doi:10.3727/096368914X684600

Al-Mayah, A., Bright, S., Chapman, K., Irons, S., Luo, P., Carter, D., et al. (2015). The Non-targeted Effects of Radiation Are Perpetuated by Exosomes. *Mutat. Research/Fundamental Mol. Mech. Mutagenesis* 772, 38–45. doi:10.1016/j.mrfmmm.2014.12.007

Alcayaga-Miranda, F., Varas-Godoy, M., and Khoury, M. (2016). Harnessing the Angiogenic Potential of Stem Cell-Derived Exosomes for Vascular Regeneration. *Stem Cell Int.* 2016, 1–11. doi:10.1155/2016/3409169

Alessio, N., Del Gaudio, S., Capasso, S., Di Bernardo, G., Cappabianca, S., Cipollaro, M., et al. (2015). Low Dose Radiation Induced Senescence of Human Mesenchymal Stromal Cells and Impaired the Autophagy Process. *Oncotarget* 6 (10), 8155–8166. doi:10.18632/oncotarget.2692

Andrews, A. M., and Rizzo, V. (2016). Microparticle-Induced Activation of the Vascular Endothelium Requires Caveolin-1/Caveolae. *PLoS One* 11 (2), e0149272. doi:10.1371/journal.pone.0149272

Ariyoshi, K., Miura, T., Kasai, K., Fujishima, Y., Nakata, A., and Yoshida, M. (2019). Radiation-Induced Bystander Effect Is Mediated by Mitochondrial DNA in Exosome-like Vesicles. *Sci. Rep.* 9 (1), 9103. doi:10.1038/s41598-019-45669-z

Asfaha, S., Hayakawa, Y., Muley, A., Stokes, S., Graham, T. A., Ericksen, R. E., et al. (2015). Krt19+/Lgr5− Cells Are Radioresistant Cancer-Initiating Stem Cells in the Colon and Intestine. *Cell Stem Cell* 16 (6), 627–638. doi:10.1016/j.stem.2015.04.013

Bai, S., Yin, Q., Dong, T., Dai, F., Qin, Y., Ye, L., et al. (2020). Endothelial Progenitor Cell-Derived Exosomes Ameliorate Endothelial Dysfunction in a Mouse Model of Diabetes. *Biomed. Pharmacother.* 131, 110756. doi:10.1016/j.biopha.2020.110756

Barker, N., van Es, J. H., Kuipers, J., Kujala, P., van den Born, M., Cozijnsen, M., et al. (2007). Identification of Stem Cells in Small Intestine and Colon by Marker Gene Lgr5. *Nature* 449 (7165), 1003–1007. doi:10.1038/nature06196

Becker, A. J., McCULLOCH, E. A., and Till, J. E. (1963). Cytological Demonstration of the Clonal Nature of Spleen Colonies Derived from Transplanted Mouse Marrow Cells. *Nature* 197, 452–454. doi:10.1038/197452a0

Benderitter, M., Caviggioli, F., Chapel, A., Coppes, R. P., Guha, C., Klinger, M., et al. (2014). Stem Cell Therapies for the Treatment of Radiation-Induced Normal Tissue Side Effects. *Antioxid. Redox Signaling* 21 (2), 338–355. doi:10.1089/ars.2013.5652

Berger, C. N., Crepin, V. F., Roumeliotis, T. I., Wright, J. C., Carson, D., Pevsner-Fischer, M., et al. (2017). Citrobacter Rodentium Subverts ATP Flux and Cholesterol Homeostasis in Intestinal Epithelial Cells *In Vivo*. *Cel Metab.* 26 (5), 738–752. doi:10.1016/j.cmet.2017.09.003

Bosch, S., de Beaurepaire, L., Allard, M., Mosser, M., Heichette, C., Chrétien, D., et al. (2016). Trehalose Prevents Aggregation of Exosomes and Cryodamage. *Sci. Rep.* 6, 36162. doi:10.1038/srep36162

Bouchareychas, L., Duong, P., Covarrubias, S., Alsop, E., Phu, T. A., Chung, A., et al. (2020). Macrophage Exosomes Resolve Atherosclerosis by Regulating Hematopoiesis and Inflammation via MicroRNA Cargo. *Cel Rep.* 32 (2), 107881. doi:10.1016/j.celrep.2020.107881

Boulter, L., Lu, W.-Y., and Forbes, S. J. (2013). Differentiation of Progenitors in the Liver: a Matter of Local Choice. *J. Clin. Invest.* 123 (5), 1867–1873. doi:10.1172/JCI66026

Boyer, M. J., Kimura, Y., Akiyama, T., Baggett, A. Y., Preston, K. J., Scalia, R., et al. (2020). Endothelial Cell-derived Extracellular Vesicles Alter Vascular Smooth Muscle Cell Phenotype through High-mobility Group Box Proteins. *J. Extracellular Vesicles* 9 (1), 1781427. doi:10.1080/20013078.2020.1781427

Buzás, E. I., Tóth, E. Á., Sódar, B. W., and Szabó-Taylor, K. É. (2018). Molecular Interactions at the Surface of Extracellular Vesicles. *Semin. Immunopathol* 40 (5), 453–464. doi:10.1007/s00281-018-0682-0

Caplan, A. I., and Dennis, J. E. (2006). Mesenchymal Stem Cells as Trophic Mediators. *J. Cel. Biochem.* 98 (5), 1076–1084. doi:10.1002/jcb.20886

Cheng, Y., Zeng, Q., Han, Q., and Xia, W. (2019). Effect of pH, Temperature and Freezing-Thawing on Quantity Changes and Cellular Uptake of Exosomes. *Protein Cell* 10 (4), 295–299. doi:10.1007/s13238-018-0529-4

Chu, C., Gao, Y., Lan, X., Lin, J., Thomas, A. M., and Li, S. (2020). Stem-Cell Therapy as a Potential Strategy for Radiation-Induced Brain Injury. *Stem Cel Rev Rep.* 16 (4), 639–649. doi:10.1007/s12015-020-09984-7

Chute, J. P., Muramoto, G. G., Salter, A. B., Meadows, S. K., Rickman, D. W., Chen, B., et al. (2007). Transplantation of Vascular Endothelial Cells Mediates the Hematopoietic Recovery and Survival of Lethally Irradiated Mice. *Blood* 109 (6), 2365–2372. doi:10.1182/blood-2006-05-022640

Citrin, D. E., Shankavaram, U., Horton, J. A., Shield, W., 3rd, Zhao, S., Asano, H., et al. (2013). Role of Type II Pneumocyte Senescence in Radiation-Induced Lung Fibrosis. *J. Natl. Cancer Inst.* 105 (19), 1474–1484. doi:10.1093/jnci/djt212

Coppes, R., and Stokman, M. (2011). Stem Cells and the Repair of Radiation-Induced Salivary Gland Damage. *Oral Dis.* 17 (2), 143–153. doi:10.1111/j.1601-0825.2010.01723.x

Dai, Y., Wang, S., Chang, S., Ren, D., Shali, S., Li, C., et al. (2020). M2 Macrophage-Derived Exosomes Carry microRNA-148a to Alleviate Myocardial Ischemia/reperfusion Injury via Inhibiting TXNIP and the TLR4/NF-Kb/nlrp3 Inflammasome Signaling Pathway. *J. Mol. Cell Cardiol.* 142, 65–79. doi:10.1016/j.yjmcc.2020.02.007

Davidson, S. M., Riquelme, J. A., Zheng, Y., Vicencio, J. M., Lavandero, S., and Yellon, D. M. (2018). Endothelial Cells Release Cardioprotective Exosomes that May Contribute to Ischaemic Preconditioning. *Sci. Rep.* 8 (1), 15885. doi:10.1038/s41598-018-34357-z

de Godoy, M. A., Saraiva, L. M., de Carvalho, L. R. P., Vasconcelos-Dos-Santos, A., Beiral, H. J. V., Ramos, A. B., et al. (2018). Mesenchymal Stem Cells and Cell-Derived Extracellular Vesicles Protect Hippocampal Neurons from Oxidative Stress and Synapse Damage Induced by Amyloid-β Oligomers. *J. Biol. Chem.* 293 (6), 1957–1975. doi:10.1074/jbc.M117.807180

DiCarlo, A. L., Tamarat, R., Rios, C. I., Benderitter, M., Czarniecki, C. W., Allio, T. C., et al. (2017). Cellular Therapies for Treatment of Radiation Injury: Report from a NIH/NIAID and IRSN Workshop. *Radiat. Res.* 188 (2), e54–e75. doi:10.1667/RR14810.1

Dominici, M., Le Blanc, K., Mueller, I., Slaper-Cortenbach, I., Marini, F. C., Krause, D. S., et al. (2006). Minimal Criteria for Defining Multipotent Mesenchymal Stromal Cells. The International Society for Cellular Therapy Position Statement. *Cytotherapy* 8 (4), 315–317. doi:10.1080/14653240600855905

Dong, L.-H., Jiang, Y.-Y., Liu, Y.-J., Cui, S., Xia, C.-C., Qu, C., et al. (2015). The Anti-fibrotic Effects of Mesenchymal Stem Cells on Irradiated Lungs via Stimulating Endogenous Secretion of HGF and PGE2. *Sci. Rep.* 5, 8713. doi:10.1038/srep08713

El Baradie, K. B. Y., Nouh, M., O'Brien III, F., Iii, Liu, Y., Fulzele, S., Eroglu, A., et al. (2020). Freeze-Dried Extracellular Vesicles from Adipose-Derived Stem Cells Prevent Hypoxia-Induced Muscle Cell Injury. *Front. Cel Dev. Biol.* 8, 181. doi:10.3389/fcell.2020.00181

Elbakrawy, E., Kaur Bains, S., Bright, S., Al-Abedi, R., Mayah, A., Goodwin, E., et al. (2020). Radiation-Induced Senescence Bystander Effect: The Role of Exosomes. *Biology* 9 (8), 191. doi:10.3390/biology9080191

Ferguson, S. W., Wang, J., Lee, C. J., Liu, M., Neelamegham, S., Canty, J. M., et al. (2018). The microRNA Regulatory Landscape of MSC-Derived Exosomes: a Systems View. *Sci. Rep.* 8 (1), 1419. doi:10.1038/s41598-018-19581-x

Flamant, S., and Tamarat, R. (2016). Extracellular Vesicles and Vascular Injury: New Insights for Radiation Exposure. *Radiat. Res.* 186 (2), 203–218. doi:10.1667/RR14482.1

Follenzi, A., Benten, D., Novikoff, P., Faulkner, L., Raut, S., and Gupta, S. (2008). Transplanted Endothelial Cells Repopulate the Liver Endothelium and Correct the Phenotype of Hemophilia A Mice. *J. Clin. Invest.* 118 (3), 935–945. doi:10.1172/JCI32748

Friedenstein, A. J., Petrakova, K. V., Kurolesova, A. I., and Frolova, G. P. (1968). Heterotopic Transplants of Bone Marrow. *Transplantation* 6 (2), 230–247. doi:10.1097/00007890-196803000-00009

Gao, B., Zhou, S., Sun, C., Cheng, D., Zhang, Y., Li, X., et al. (2020). Brain Endothelial Cell-Derived Exosomes Induce Neuroplasticity in Rats with Ischemia/Reperfusion Injury. *ACS Chem. Neurosci.* 11 (15), 2201–2213. doi:10.1021/acschemneuro.0c00089

Gatti, S., Bruno, S., Deregibus, M. C., Sordi, A., Cantaluppi, V., Tetta, C., et al. (2011). Microvesicles Derived from Human Adult Mesenchymal Stem Cells Protect against Ischaemia-Reperfusion-Induced Acute and Chronic Kidney Injury. *Nephrol. Dial. Transplant.* 26 (5), 1474–1483. doi:10.1093/ndt/gfr015

Ghobadi, G., Bartelds, B., van der Veen, S. J., Dickinson, M. G., Brandenburg, S., Berger, R. M. F., et al. (2012). Lung Irradiation Induces Pulmonary Vascular Remodelling Resembling Pulmonary Arterial Hypertension. *Thorax* 67 (4), 334–341. doi:10.1136/thoraxjnl-2011-200346

Giuranno, L., Ient, J., De Ruysscher, D., and Vooijs, M. A. (2019). Radiation-Induced Lung Injury (RILI). *Front. Oncol.* 9, 877. doi:10.3389/fonc.2019.00877

Goloviznina, N. A., Verghese, S. C., Yoon, Y. m., Taratula, O., Marks, D. L., and Kurre, P. (2016). Mesenchymal Stromal Cell-Derived Extracellular Vesicles Promote Myeloid-Biased Multipotent Hematopoietic Progenitor Expansion via Toll-like Receptor Engagement. *J. Biol. Chem.* 291 (47), 24607–24617. doi:10.1074/jbc.M116.745653

Gong, W., Guo, M., Han, Z., Wang, Y., Yang, P., Xu, C., et al. (2016). Mesenchymal Stem Cells Stimulate Intestinal Stem Cells to Repair Radiation-Induced Intestinal Injury. *Cell Death Dis.* 7 (9), e2387. doi:10.1038/cddis.2016.276

Grange, C., Tritta, S., Tapparo, M., Cedrino, M., Tetta, C., Camussi, G., et al. (2019). Stem Cell-Derived Extracellular Vesicles Inhibit and Revert Fibrosis Progression in a Mouse Model of Diabetic Nephropathy. *Sci. Rep.* 9 (1), 4468. doi:10.1038/s41598-019-41100-9

Green, D. E., and Rubin, C. T. (2014). Consequences of Irradiation on Bone and Marrow Phenotypes, and its Relation to Disruption of Hematopoietic Precursors. *Bone* 63, 87–94. doi:10.1016/j.bone.2014.02.018

Guha, C., Sharma, A., Gupta, S., Alfieri, A., Gorla, G. R., Gagandeep, S., et al. (1999). Amelioration of Radiation-Induced Liver Damage in Partially Hepatectomized Rats by Hepatocyte Transplantation. *Cancer Res.* 59 (23), 5871–5874.

Hargitai, R., Kis, D., Persa, E., Szatmári, T., Sáfrány, G., and Lumniczky, K. (2021). Oxidative Stress and Gene Expression Modifications Mediated by Extracellular Vesicles: An *In Vivo* Study of the Radiation-Induced Bystander Effect. *Antioxidants* 10 (2), 156. doi:10.3390/antiox10020156

He, Y., Thummuri, D., Zheng, G., Okunieff, P., Citrin, D. E., Vujaskovic, Z., et al. (2019). Cellular Senescence and Radiation-Induced Pulmonary Fibrosis. *Translational Res.* 209, 14–21. doi:10.1016/j.trsl.2019.03.006

Herrera, M. B., Fonsato, V., Gatti, S., Deregibus, M. C., Sordi, A., Cantarella, D., et al. (2010). Human Liver Stem Cell-derived Microvesicles Accelerate Hepatic Regeneration in Hepatectomized Rats. *J. Cell Mol. Med.* 14 (6B), 1605–1618. doi:10.1111/j.1582-4934.2009.00860.x

Horton, J. A., Hudak, K. E., Chung, E. J., White, A. O., Scroggins, B. T., Burkeen, J. F., et al. (2013). Mesenchymal Stem Cells Inhibit Cutaneous Radiation-Induced Fibrosis by Suppressing Chronic Inflammation. *Stem Cells* 31 (10), 2231–2241. doi:10.1002/stem.1483

Iglesias-Bartolome, R., Patel, V., Cotrim, A., Leelahavanichkul, K., Molinolo, A. A., Mitchell, J. B., et al. (2012). mTOR Inhibition Prevents Epithelial Stem Cell Senescence and Protects from Radiation-Induced Mucositis. *Cell Stem Cell* 11 (3), 401–414. doi:10.1016/j.stem.2012.06.007

Jeyaram, A., and Jay, S. M. (2017). Preservation and Storage Stability of Extracellular Vesicles for Therapeutic Applications. *AAPS J.* 20 (1), 1. doi:10.1208/s12248-017-0160-y

Kabarriti, R., Brodin, N. P., Maron, M. I., Tomé, W. A., Halmos, B., Guha, C., et al. (2020). Extent of Prior Lung Irradiation and Mortality in COVID-19 Patients with a *Cancer* History. *Adv. Radiat. Oncol.* 5 (4), 707–710. doi:10.1016/j.adro.2020.04.028

Kabarriti, R., Zhou, H., Vainshtein, J. V., Saha, S., Hannan, R., Thawani, N., et al. (2010). Transplantation of Liver Sinusoidal Endothelial Cells Repairs HIR Induced Hepatic Endothelial Cell Damage. *Int. J. Radiat. Oncology*Biology*Physics* 78 (3), S41. doi:10.1016/j.ijrobp.2010.07.131

Kabat, M., Bobkov, I., Kumar, S., and Grumet, M. (2020). Trends in Mesenchymal Stem Cell Clinical Trials 2004-2018: Is Efficacy Optimal in a Narrow Dose Range?. *Stem Cell Transl Med* 9 (1), 17–27. doi:10.1002/sctm.19-0202

Kim, H., Wang, S. Y., Kwak, G., Yang, Y., Kwon, I. C., and Kim, S. H. (2019). Exosome-Guided Phenotypic Switch of M1 to M2 Macrophages for Cutaneous Wound Healing. *Adv. Sci.* 6 (20), 1900513. doi:10.1002/advs.201900513

Klein, D., Schmetter, A., Imsak, R., Wirsdörfer, F., Unger, K., Jastrow, H., et al. (2016). Therapy with Multipotent Mesenchymal Stromal Cells Protects Lungs from Radiation-Induced Injury and Reduces the Risk of Lung Metastasis. *Antioxid. Redox Signaling* 24 (2), 53–69. doi:10.1089/ars.2014.6183

Klein, D., Steens, J., Wiesemann, A., Schulz, F., Kaschani, F., Röck, K., et al. (2017). Mesenchymal Stem Cell Therapy Protects Lungs from Radiation-Induced Endothelial Cell Loss by Restoring Superoxide Dismutase 1 Expression. *Antioxid. Redox Signaling* 26 (11), 563–582. doi:10.1089/ars.2016.6748

Kojima, T., Kanemaru, S.-i., Hirano, S., Tateya, I., Ohno, S., Nakamura, T., et al. (2011). Regeneration of Radiation Damaged Salivary Glands with Adipose-Derived Stromal Cells. *The Laryngoscope* 121 (9), 1864–1869. doi:10.1002/lary.22080

Komaki, M., Numata, Y., Morioka, C., Honda, I., Tooi, M., Yokoyama, N., et al. (2017). Exosomes of Human Placenta-Derived Mesenchymal Stem Cells Stimulate Angiogenesis. *Stem Cel Res Ther* 8 (1), 219. doi:10.1186/s13287-017-0660-9

Kowal, J., Arras, G., Colombo, M., Jouve, M., Morath, J. P., Primdal-Bengtson, B., et al. (2016). Proteomic Comparison Defines Novel Markers to Characterize Heterogeneous Populations of Extracellular Vesicle Subtypes. *Proc. Natl. Acad. Sci. USA* 113 (8), E968–E977. doi:10.1073/pnas.1521230113

Kulkarni, S., Wang, T. C., and Guha, C. (2016). Stromal Progenitor Cells in Mitigation of Non-hematopoietic Radiation Injuries. *Curr. Pathobiol Rep.* 4 (4), 221–230. doi:10.1007/s40139-016-0114-6

Lafargue, A., Degorre, C., Corre, I., Alves-Guerra, M.-C., Gaugler, M.-H., Vallette, F., et al. (2017). Ionizing Radiation Induces Long-Term Senescence in Endothelial Cells through Mitochondrial Respiratory Complex II Dysfunction and Superoxide Generation. *Free Radic. Biol. Med.* 108, 750–759. doi:10.1016/j.freeradbiomed.2017.04.019

Leavitt, R. J., Limoli, C. L., and Baulch, J. E. (2019). miRNA-Based Therapeutic Potential of Stem Cell-Derived Extracellular Vesicles: a Safe Cell-free Treatment to Ameliorate Radiation-Induced Brain Injury. *Int. J. Radiat. Biol.* 95 (4), 427–435. doi:10.1080/09553002.2018.1522012

Lee, C., Mitsialis, S. A., Aslam, M., Vitali, S. H., Vergadi, E., Konstantinou, G., et al. (2012). Exosomes Mediate the Cytoprotective Action of Mesenchymal Stromal Cells on Hypoxia-Induced Pulmonary Hypertension. *Circulation* 126 (22), 2601–2611. doi:10.1161/CIRCULATIONAHA.112.114173

Lee, S., Lee, S.-J., and Yoon, Y.-s. (2019). Vascular Regeneration with New Sources of Endothelial Cells. *Circ. Res.* 124 (1), 29–31. doi:10.1161/circresaha.118.314195

Lei, X., He, N., Zhu, L., Zhou, M., Zhang, K., Wang, C., et al. (2020). Mesenchymal Stem Cell-Derived Extracellular Vesicles Attenuate Radiation-Induced Lung Injury via miRNA-214-3p. *Antioxid. Redox Signaling*. doi:10.1089/ars.2019.7965

Letsiou, E., and Bauer, N. (2018). Endothelial Extracellular Vesicles in Pulmonary Function and Disease. *Curr. Top. Membr.* 82, 197–256. doi:10.1016/bs.ctm.2018.09.002

Letsiou, E., Sammani, S., Zhang, W., Zhou, T., Quijada, H., Moreno-Vinasco, L., et al. (2015). Pathologic Mechanical Stress and Endotoxin Exposure Increases Lung Endothelial Microparticle Shedding. *Am. J. Respir. Cel Mol Biol* 52 (2), 193–204. doi:10.1165/rcmb.2013-0347OC

Li, M., Wang, T., Tian, H., Wei, G., Zhao, L., and Shi, Y. (2019). Macrophage-derived Exosomes Accelerate Wound Healing through Their Anti-inflammation Effects in a Diabetic Rat Model. *Artif. Cell Nanomedicine, Biotechnol.* 47 (1), 3793–3803. doi:10.1080/21691401.2019.1669617

Li, M., You, L., Xue, J., and Lu, Y. (2018). Ionizing Radiation-Induced Cellular Senescence in Normal, Non-transformed Cells and the Involved DNA Damage Response: A Mini Review. *Front. Pharmacol.* 9, 522. doi:10.3389/fphar.2018.00522

Li, T., Yan, Y., Wang, B., Qian, H., Zhang, X., Shen, L., et al. (2013). Exosomes Derived from Human Umbilical Cord Mesenchymal Stem Cells Alleviate Liver Fibrosis. *Stem Cell Development* 22 (6), 845–854. doi:10.1089/scd.2012.0395

Liao, H., Wang, H., Rong, X., Li, E., Xu, R.-H., and Peng, Y. (2017). Mesenchymal Stem Cells Attenuate Radiation-Induced Brain Injury by Inhibiting Microglia Pyroptosis. *Biomed. Res. Int.* 2017, 1–11. doi:10.1155/2017/1948985

Lim, J.-Y., Ra, J. C., Shin, I. S., Jang, Y. H., An, H.-Y., Choi, J.-S., et al. (2013). Systemic Transplantation of Human Adipose Tissue-Derived Mesenchymal Stem Cells for the Regeneration of Irradiation-Induced Salivary Gland Damage. *PLoS One* 8 (8), e71167. doi:10.1371/journal.pone.0071167

Lin, S.-L., Li, B., Rao, S., Yeo, E.-J., Hudson, T. E., Nowlin, B. T., et al. (2010). Macrophage Wnt7b Is Critical for Kidney Repair and Regeneration. *Proc. Natl. Acad. Sci.* 107 (9), 4194–4199. doi:10.1073/pnas.0912228107

Lötvall, J., Hill, A. F., Hochberg, F., Buzás, E. I., Di Vizio, D., Gardiner, C., et al. (2014). Minimal Experimental Requirements for Definition of Extracellular Vesicles and Their Functions: a Position Statement from the International Society for Extracellular Vesicles. *J. Extracellular Vesicles* 3, 26913. doi:10.3402/jev.v3.26913

Lou, G., Chen, Z., Zheng, M., and Liu, Y. (2017). Mesenchymal Stem Cell-Derived Exosomes as a New Therapeutic Strategy for Liver Diseases. *Exp. Mol. Med.* 49 (6), e346. doi:10.1038/emm.2017.63

Luan, X., Sansanaphongpricha, K., Myers, I., Chen, H., Yuan, H., and Sun, D. (2017). Engineering Exosomes as Refined Biological Nanoplatforms for Drug Delivery. *Acta Pharmacol. Sin* 38 (6), 754–763. doi:10.1038/aps.2017.12

Luo, W., Dai, Y., Chen, Z., Yue, X., Andrade-Powell, K. C., and Chang, J. (2020). Spatial and Temporal Tracking of Cardiac Exosomes in Mouse Using a Nano-Luciferase-CD63 Fusion Protein. *Commun. Biol.* 3 (1), 114. doi:10.1038/s42003-020-0830-7

Maimets, M., Rocchi, C., Bron, R., Pringle, S., Kuipers, J., Giepmans, B. N. G., et al. (2016). Long-Term *In Vitro* Expansion of Salivary Gland Stem Cells Driven by Wnt Signals. *Stem Cel Rep.* 6 (1), 150–162. doi:10.1016/j.stemcr.2015.11.009

Mandel, E. R., Uchida, C., Nwadozi, E., Makki, A., and Haas, T. L. (2017). Tissue Inhibitor of Metalloproteinase 1 Influences Vascular Adaptations to Chronic Alterations in Blood Flow. *J. Cel. Physiol.* 232 (4), 831–841. doi:10.1002/jcp.25491

Mantovani, A., Biswas, S. K., Galdiero, M. R., Sica, A., and Locati, M. (2013). Macrophage Plasticity and Polarization in Tissue Repair and Remodelling. *J. Pathol.* 229 (2), 176–185. doi:10.1002/path.4133

McBride, J. D., Rodriguez-Menocal, L., Guzman, W., Candanedo, A., Garcia-Contreras, M., and Badiavas, E. V. (2017). Bone Marrow Mesenchymal Stem Cell-Derived CD63+ Exosomes Transport Wnt3a Exteriorly and Enhance Dermal Fibroblast Proliferation, Migration, and Angiogenesis *In Vitro*. *Stem Cell Development* 26 (19), 1384–1398. doi:10.1089/scd.2017.0087

Mead, B., and Tomarev, S. (2017). Bone Marrow-Derived Mesenchymal Stem Cells-Derived Exosomes Promote Survival of Retinal Ganglion Cells through miRNA-dependent Mechanisms. *STEM CELLS Translational Med.* 6 (4), 1273–1285. doi:10.1002/sctm.16-0428

Melgar-Lesmes, P., Balcells, M., and Edelman, E. R. (2017). Implantation of Healthy Matrix-Embedded Endothelial Cells Rescues Dysfunctional Endothelium and Ischaemic Tissue in Liver Engraftment. *Gut* 66 (7), 1297–1305. doi:10.1136/gutjnl-2015-310409

Mendelson, A., and Frenette, P. S. (2014). Hematopoietic Stem Cell Niche Maintenance during Homeostasis and Regeneration. *Nat. Med.* 20 (8), 833–846. doi:10.1038/nm.3647

Misawa, T., Tanaka, Y., Okada, R., and Takahashi, A. (2020). Biology of Extracellular Vesicles Secreted from Senescent Cells as Senescence-associated Secretory Phenotype Factors. *Geriatr. Gerontol. Int.* 20 (6), 539–546. doi:10.1111/ggi.13928

Moll, G., Ankrum, J. A., Kamhieh-Milz, J., Bieback, K., Ringdén, O., Volk, H.-D., et al. (2019). Intravascular Mesenchymal Stromal/Stem Cell Therapy Product Diversification: Time for New Clinical Guidelines. *Trends Mol. Med.* 25 (2), 149–163. doi:10.1016/j.molmed.2018.12.006

Nanduri, L. S. Y., Baanstra, M., Faber, H., Rocchi, C., Zwart, E., de Haan, G., et al. (2014). Purification and Ex Vivo Expansion of Fully Functional Salivary Gland Stem Cells. *Stem Cel Rep.* 3 (6), 957–964. doi:10.1016/j.stemcr.2014.09.015

Nicolay, N. H., Lopez Perez, R., Saffrich, R., and Huber, P. E. (2015). Radio-resistant mesenchymal stem cells: mechanisms of resistance and potential implications for the clinic. *Oncotarget* 6 (23), 19366–19380. doi:10.18632/oncotarget.4358

Nolta, J. A., Galipeau, J., and Phinney, D. G. (2020). Improving Mesenchymal Stem/stromal Cell Potency and Survival. *Cytotherapy* 22 (3), 123–126. doi:10.1016/j.jcyt.2020.01.004

Orfanos, S. E., Mavrommati, I., Korovesi, I., and Roussos, C. (2004). Pulmonary Endothelium in Acute Lung Injury: from Basic Science to the Critically Ill. *Intensive Care Med.* 30 (9), 1702–1714. doi:10.1007/s00134-004-2370-x

Pacheco, R., and Stock, H. (2013). Effects of Radiation on Bone. *Curr. Osteoporos. Rep.* 11 (4), 299–304. doi:10.1007/s11914-013-0174-z

Panganiban, R. A. M., Mungunsukh, O., and Day, R. M. (2012). X-irradiation Induces ER Stress, Apoptosis, and Senescence in Pulmonary Artery Endothelial Cells. *Int. J. Radiat. Biol.* 89 (8), 656–667. doi:10.3109/09553002.2012.711502

Paris, F., Fuks, Z., Kang, A., Capodieci, P., Juan, G., Ehleiter, D., et al. (2001). Endothelial Apoptosis as the Primary Lesion Initiating Intestinal Radiation Damage in Mice. *Science* 293 (5528), 293–297. doi:10.1126/science.1060191

Peña, L. A., Fuks, Z., and Kolesnick, R. N. (2000). Radiation-induced Apoptosis of Endothelial Cells in the Murine Central Nervous System: Protection by Fibroblast Growth Factor and Sphingomyelinase Deficiency. *Cancer Res.* 60 (2), 321–327.

Peng, X., Wu, Y., Brouwer, U., van Vliet, T., Wang, B., Demaria, M., et al. (2020). Cellular Senescence Contributes to Radiation-Induced Hyposalivation by Affecting the Stem/progenitor Cell Niche. *Cel Death Dis.* 11 (10), 854. doi:10.1038/s41419-020-03074-9

Phinney, D. G., and Pittenger, M. F. (2017). Concise Review: MSC-Derived Exosomes for Cell-free Therapy. *Stem Cells* 35 (4), 851–858. doi:10.1002/stem.2575

Piryani, S. O., Jiao, Y., Kam, A. Y. F., Liu, Y., Vo-Dinh, T., Chen, B. J., et al. (2019). Endothelial Cell-Derived Extracellular Vesicles Mitigate Radiation-Induced Hematopoietic Injury. *Int. J. Radiat. Oncology*Biology*Physics* 104 (2), 291–301. doi:10.1016/j.ijrobp.2019.02.008

Pull, S. L., Doherty, J. M., Mills, J. C., Gordon, J. I., and Stappenbeck, T. S. (2005). Activated Macrophages Are an Adaptive Element of the Colonic Epithelial Progenitor Niche Necessary for Regenerative Responses to Injury. *Proc. Natl. Acad. Sci.* 102 (1), 99–104. doi:10.1073/pnas.0405979102

Rafii, S., Butler, J. M., and Ding, B.-S. (2016). Angiocrine Functions of Organ-specific Endothelial Cells. *Nature* 529 (7586), 316–325. doi:10.1038/nature17040

Rager, T. M., Olson, J. K., Zhou, Y., Wang, Y., and Besner, G. E. (2016). Exosomes Secreted from Bone Marrow-Derived Mesenchymal Stem Cells Protect the Intestines from Experimental Necrotizing Enterocolitis. *J. Pediatr. Surg.* 51 (6), 942–947. doi:10.1016/j.jpedsurg.2016.02.061

Rajendran, R. L., Gangadaran, P., Seo, C. H., Kwack, M. H., Oh, J. M., Lee, H. W., et al. (2020). Macrophage-Derived Extracellular Vesicle Promotes Hair Growth. *Cells* 9 (4), 856. doi:10.3390/cells9040856

Rana, S., Yue, S., Stadel, D., and Zöller, M. (2012). Toward Tailored Exosomes: the Exosomal Tetraspanin Web Contributes to Target Cell Selection. *Int. J. Biochem. Cel Biol.* 44 (9), 1574–1584. doi:10.1016/j.biocel.2012.06.018

Riccobono, D., Agay, D., Scherthan, H., Forcheron, F., Vivier, M., Ballester, B., et al. (2012). Application of Adipocyte-Derived Stem Cells in Treatment of Cutaneous Radiation Syndrome. *Health Phys.* 103 (2), 120–126. doi:10.1097/HP.0b013e318240595b

Rios, C., Jourdain, J.-R., and DiCarlo, A. L. (2017). Cellular Therapies for Treatment of Radiation Injury after a Mass Casualty Incident. *Radiat. Res.* 188 (2), 242–245. doi:10.1667/RR14835.1

Rocchi, C., and Emmerson, E. (2020). Mouth-Watering Results: Clinical Need, Current Approaches, and Future Directions for Salivary Gland Regeneration. *Trends Mol. Med.* 26 (7), 649–669. doi:10.1016/j.molmed.2020.03.009

Rong, X., Liu, J., Yao, X., Jiang, T., Wang, Y., and Xie, F. (2019). Human Bone Marrow Mesenchymal Stem Cells-Derived Exosomes Alleviate Liver Fibrosis through the Wnt/β-Catenin Pathway. *Stem Cel Res Ther.* 10 (1), 98. doi:10.1186/s13287-019-1204-2

Rotolo, J., Stancevic, B., Zhang, J., Hua, G., Fuller, J., Yin, X., et al. (2012). Anti-ceramide Antibody Prevents the Radiation Gastrointestinal Syndrome in Mice. *J. Clin. Invest.* 122 (5), 1786–1790. doi:10.1172/JCI59920

Royo, F., Théry, C., Falcón-Pérez, J. M., Nieuwland, R., and Witwer, K. W. (2020). Methods for Separation and Characterization of Extracellular Vesicles: Results of a Worldwide Survey Performed by the ISEV Rigor and Standardization Subcommittee. *Cells* 9 (9), 1955. doi:10.3390/cells9091955

Rühle, A., Xia, O., Perez, R. L., Trinh, T., Richter, W., Sarnowska, A., et al. (2018). The Radiation Resistance of Human Multipotent Mesenchymal Stromal Cells Is Independent of Their Tissue of Origin. *Int. J. Radiat. Oncology*Biology*Physics* 100 (5), 1259–1269. doi:10.1016/j.ijrobp.2018.01.015

Sáez, T., de Vos, P., Kuipers, J., Sobrevia, L., and Faas, M. M. (2019). Exosomes Derived from Monocytes and from Endothelial Cells Mediate Monocyte and Endothelial Cell Activation under High D-Glucose Conditions. *Immunobiology* 224 (2), 325–333. doi:10.1016/j.imbio.2019.02.004

Sáez, T., de Vos, P., Kuipers, J., Sobrevia, L., and Faas, M. M. (2018). Fetoplacental Endothelial Exosomes Modulate High D -Glucose-Induced Endothelial Dysfunction. *Placenta* 66, 26–35. doi:10.1016/j.placenta.2018.04.010

Saha, S., Aranda, E., Hayakawa, Y., Bhanja, P., Atay, S., Brodin, N. P., et al. (2016). Macrophage-derived Extracellular Vesicle-Packaged WNTs Rescue Intestinal Stem Cells and Enhance Survival after Radiation Injury. *Nat. Commun.* 7, 13096. doi:10.1038/ncomms13096

Saha, S., Bhanja, P., Kabarriti, R., Liu, L., Alfieri, A. A., and Guha, C. (2011). Bone Marrow Stromal Cell Transplantation Mitigates Radiation-Induced Gastrointestinal Syndrome in Mice. *PLoS One* 6 (9), e24072. doi:10.1371/journal.pone.0024072

Schubart, A., Anderson, K., Mainolfi, N., Sellner, H., Ehara, T., Adams, C. M., et al. (2019). Small-molecule Factor B Inhibitor for the Treatment of Complement-Mediated Diseases. *Proc. Natl. Acad. Sci. USA* 116 (16), 7926–7931. doi:10.1073/pnas.1820892116

Singh, V., Fatanmi, O., Santiago, P., Simas, M., Hanlon, B., Garcia, M., et al. (2018). Current Status of Radiation Countermeasures for Acute Radiation Syndrome under Advanced Development. *J. Radiat. Cancer Res.* 9 (1), 13. doi:10.4103/jrcr.jrcr_3_18

Singh, S., Kloss, F. R., Brunauer, R., Schimke, M., Jamnig, A., Greiderer-Kleinlercher, B., et al. (2012). Mesenchymal stem cells show radioresistance in vivo. *J. Cell. Mol. Med.* 16 (4), 877–887. doi:10.1111/j.1582-4934.2011.01383.x

Singh, V. K., and Seed, T. M. (2020). BIO 300: a Promising Radiation Countermeasure under Advanced Development for Acute Radiation Syndrome and the Delayed Effects of Acute Radiation Exposure. *Expert Opin. Investig. Drugs* 29 (5), 429–441. doi:10.1080/13543784.2020.1757648

Soria, B., Martin-Montalvo, A., Aguilera, Y., Mellado-Damas, N., López-Beas, J., Herrera-Herrera, I., et al. (2019). Human Mesenchymal Stem Cells Prevent Neurological Complications of Radiotherapy. *Front. Cel. Neurosci.* 13, 204. doi:10.3389/fncel.2019.00204

Stevens, T., Phan, S., Frid, M. G., Alvarez, D., Herzog, E., and Stenmark, K. R. (2008). Lung Vascular Cell Heterogeneity: Endothelium, Smooth Muscle, and Fibroblasts. *Proc. Am. Thorac. Soc.* 5 (7), 783–791. doi:10.1513/pats.200803-027HR

Stewart, F. A., Seemann, I., Hoving, S., and Russell, N. S. (2013). Understanding Radiation-Induced Cardiovascular Damage and Strategies for Intervention. *Clin. Oncol.* 25 (10), 617–624. doi:10.1016/j.clon.2013.06.012

Taheri, B., Soleimani, M., Fekri Aval, S., Esmaeili, E., Bazi, Z., and Zarghami, N. (2019). Induced Pluripotent Stem Cell-derived Extracellular Vesicles: A Novel Approach for Cell-free Regenerative Medicine. *J. Cel Physiol* 234 (6), 8455–8464. doi:10.1002/jcp.27775

Takeuchi, R., Katagiri, W., Endo, S., and Kobayashi, T. (2019). Exosomes from Conditioned Media of Bone Marrow-Derived Mesenchymal Stem Cells Promote Bone Regeneration by Enhancing Angiogenesis. *PLoS One* 14 (11), e0225472. doi:10.1371/journal.pone.0225472

Tan, C., Lai, R., Wong, W., Dan, Y., Lim, S.-K., and Ho, H. (2014). Mesenchymal Stem Cell-Derived Exosomes Promote Hepatic Regeneration in Drug-Induced Liver Injury Models. *Stem Cel Res. Ther.* 5 (3), 76. doi:10.1186/scrt465

Thery, C., Witwer, K. W., Aikawa, E., Alcaraz, M. J., Anderson, J. D., Andriantsitohaina, R., et al. (2018). Minimal Information for Studies of Extracellular Vesicles 2018 (MISEV2018): a Position Statement of the International Society for Extracellular Vesicles and Update of the MISEV2014 Guidelines. *J. Extracell Vesicles* 7 (1), 1535750. doi:10.1080/20013078.2018.1535750

Tomasoni, S., Longaretti, L., Rota, C., Morigi, M., Conti, S., Gotti, E., et al. (2013). Transfer of Growth Factor Receptor mRNA via Exosomes Unravels the Regenerative Effect of Mesenchymal Stem Cells. *Stem Cell Development* 22 (5), 772–780. doi:10.1089/scd.2012.0266

Tsiapalis, D., and O'Driscoll, L. (2020). Mesenchymal Stem Cell Derived Extracellular Vesicles for Tissue Engineering and Regenerative Medicine Applications. *Cells* 9 (4), 991. doi:10.3390/cells9040991

Uribe-Etxebarria, V., Luzuriaga, J., Luzuriaga, J., García-Gallastegui, P., Agliano, A., Unda, F., et al. (2017). Notch/Wnt Cross-Signalling Regulates Stemness of Dental Pulp Stem Cells through Expression of Neural Crest and Core Pluripotency Factors. *eCM* 34, 249–270. doi:10.22203/eCM.v034a16

Vakili, S., Ahooyi, T. M., Yarandi, S. S., Donadoni, M., Rappaport, J., and Sariyer, I. K. (2020). Molecular and Cellular Impact of Inflammatory Extracellular Vesicles (EVs) Derived from M1 and M2 Macrophages on Neural Action Potentials. *Brain Sci.* 10 (7), 424. doi:10.3390/brainsci10070424

van Balkom, B. W. M., Eisele, A. S., Pegtel, D. M., Bervoets, S., and Verhaar, M. C. (2015). Quantitative and Qualitative Analysis of Small RNAs in Human Endothelial Cells and Exosomes Provides Insights into Localized RNA Processing, Degradation and Sorting. *J. Extracellular Vesicles* 4, 26760. doi:10.3402/jev.v4.26760

Van Deun, J., Mestdagh, P., Mestdagh, P., Agostinis, P., Akay, Ö., Anand, S., et al. (2017). EV-TRACK: Transparent Reporting and Centralizing Knowledge in Extracellular Vesicle Research. *Nat. Methods* 14 (3), 228–232. doi:10.1038/nmeth.4185

Viñas, J. L., Spence, M., Gutsol, A., Knoll, W., Burger, D., Zimpelmann, J., et al. (2018). Receptor-Ligand Interaction Mediates Targeting of Endothelial Colony Forming Cell-Derived Exosomes to the Kidney after Ischemic Injury. *Sci. Rep.* 8 (1), 16320. doi:10.1038/s41598-018-34557-7

Viswanathan, S., Shi, Y., Galipeau, J., Krampera, M., Leblanc, K., Martin, I., et al. (2019). Mesenchymal Stem versus Stromal Cells: International Society for Cell & Gene Therapy (ISCT) Mesenchymal Stromal Cell Committee Position Statement on Nomenclature. *Cytotherapy* 21 (10), 1019–1024. doi:10.1016/j.jcyt.2019.08.002

Vrijsen, K. R., Maring, J. A., Chamuleau, S. A. J., Verhage, V., Mol, E. A., Deddens, J. C., et al. (2016). Exosomes from Cardiomyocyte Progenitor Cells and Mesenchymal Stem Cells Stimulate Angiogenesis via EMMPRIN. *Adv. Healthc. Mater.* 5 (19), 2555–2565. doi:10.1002/adhm.201600308

Walasek, M. A., van Os, R., and de Haan, G. (2012). Hematopoietic Stem Cell Expansion: Challenges and Opportunities. *Ann. N. Y Acad. Sci.* 1266, 138–150. doi:10.1111/j.1749-6632.2012.06549.x

Wallis, R., Mizen, H., and Bishop, C. L. (2020). The Bright and Dark Side of Extracellular Vesicles in the Senescence-Associated Secretory Phenotype. *Mech. Ageing Development* 189, 111263. doi:10.1016/j.mad.2020.111263

Wang, H., Zheng, R., Chen, Q., Shao, J., Yu, J., and Hu, S. (2017). Mesenchymal Stem Cells Microvesicles Stabilize Endothelial Barrier Function Partly Mediated by Hepatocyte Growth Factor (HGF). *Stem Cel Res Ther.* 8 (1), 211. doi:10.1186/s13287-017-0662-7

Wang, J., Boerma, M., Fu, Q., and HauerJensen, M. (2007). Significance of Endothelial Dysfunction in the Pathogenesis of Early and Delayed Radiation Enteropathy. *Wjg* 13 (22), 3047–3055. doi:10.3748/wjg.v13.i22.3047

Wang, L., Wei, J., Da Fonseca Ferreira, A., Wang, H., Zhang, L., Zhang, Q., et al. (2020). Rejuvenation of Senescent Endothelial Progenitor Cells by Extracellular Vesicles Derived from Mesenchymal Stromal Cells. *JACC: Basic Translational Sci.* 5 (11), 1127–1141. doi:10.1016/j.jacbts.2020.08.005

Wang, Y., Liu, L., and Zhou, D. (2011). Inhibition of P38 MAPK Attenuates Ionizing Radiation-Induced Hematopoietic Cell Senescence and Residual Bone Marrow Injury. *Radiat. Res.* 176 (6), 743–752. doi:10.1667/rr2727.1

Wang, Y., Xie, Y., Zhang, A., Wang, M., Fang, Z., and Zhang, J. (2019). Exosomes: An Emerging Factor in Atherosclerosis. *Biomed. Pharmacother.* 115, 108951. doi:10.1016/j.biopha.2019.108951

Wei, X., Yi, X., Lv, H., Sui, X., Lu, P., Li, L., et al. (2020). MicroRNA-377-3p Released by Mesenchymal Stem Cell Exosomes Ameliorates Lipopolysaccharide-Induced Acute Lung Injury by Targeting RPTOR to Induce Autophagy. *Cel Death Dis.* 11 (8), 657. doi:10.1038/s41419-020-02857-4

Wen, S., Dooner, M., Cheng, Y., Papa, E., Del Tatto, M., Pereira, M., et al. (2016). Mesenchymal Stromal Cell-Derived Extracellular Vesicles Rescue Radiation Damage to Murine Marrow Hematopoietic Cells. *Leukemia* 30 (11), 2221–2231. doi:10.1038/leu.2016.107

Wen, S., Dooner, M., Papa, E., Del Tatto, M., Pereira, M., Borgovan, T., et al. (2019). Biodistribution of Mesenchymal Stem Cell-Derived Extracellular Vesicles in a Radiation Injury Bone Marrow Murine Model. *Ijms* 20 (21), 5468. doi:10.3390/ijms20215468

Wiklander, O. P. B., Nordin, J. Z., O'Loughlin, A., Gustafsson, Y., Corso, G., Mäger, I., et al. (2015). Extracellular Vesicle In Vivo Biodistribution Is Determined by Cell Source, Route of Administration and Targeting. *J. Extracellular Vesicles* 4, 26316. doi:10.3402/jev.v4.26316

Witwer, K. W., Van Balkom, B. W. M., Bruno, S., Choo, A., Dominici, M., Gimona, M., et al. (2019). Defining Mesenchymal Stromal Cell (MSC)-derived Small Extracellular Vesicles for Therapeutic Applications. *J. Extracellular Vesicles* 8 (1), 1609206. doi:10.1080/20013078.2019.1609206

Wong, K. L., Zhang, S., Wang, M., Ren, X., Afizah, H., Lai, R. C., et al. (2020). Intra-Articular Injections of Mesenchymal Stem Cell Exosomes and Hyaluronic Acid Improve Structural and Mechanical Properties of Repaired Cartilage in a Rabbit Model. *Arthrosc. J. Arthroscopic Relat. Surg.* 36 (8), 2215–2228. doi:10.1016/j.arthro.2020.03.031

Wong, P. F., Tong, K. L., Jamal, J., Khor, E. S., Lai, S. L., and Mustafa, M. R. (2019). Senescent HUVECs-Secreted Exosomes Trigger Endothelial Barrier Dysfunction in Young Endothelial Cells. *EXCLI J.* 18, 764–776. doi:10.17179/excli2019-1505

Wynn, T. A., Chawla, A., and Pollard, J. W. (2013). Macrophage Biology in Development, Homeostasis and Disease. *Nature* 496 (7446), 445–455. doi:10.1038/nature12034

Xiao, B., Chai, Y., Lv, S., Ye, M., Wu, M., Xie, L., et al. (2017). Endothelial Cell-Derived Exosomes Protect SH-Sy5y Nerve Cells against Ischemia/reperfusion Injury. *Int. J. Mol. Med.* 40 (4), 1201–1209. doi:10.3892/ijmm.2017.3106

Xu, J., Yan, X., Gao, R., Mao, L., Cotrim, A. P., Zheng, C., et al. (2010). Effect of Irradiation on Microvascular Endothelial Cells of Parotid Glands in the Miniature Pig. *Int. J. Radiat. Oncology*Biology*Physics* 78 (3), 897–903. doi:10.1016/j.ijrobp.2010.05.048

Xu, R., Zhang, F., Chai, R., Zhou, W., Hu, M., Liu, B., et al. (2019a). Exosomes Derived from Pro-inflammatory Bone Marrow-derived Mesenchymal Stem Cells Reduce Inflammation and Myocardial Injury via Mediating Macrophage Polarization. *J. Cel Mol Med* 23 (11), 7617–7631. doi:10.1111/jcmm.14635

Xu, S., Liu, C., and Ji, H.-L. (2019b). Concise Review: Therapeutic Potential of the Mesenchymal Stem Cell Derived Secretome and Extracellular Vesicles for Radiation-Induced Lung Injury: Progress and Hypotheses. *STEM CELLS Translational Med.* 8 (4), 344–354. doi:10.1002/sctm.18-0038

Yan, K. S., Chia, L. A., Li, X., Ootani, A., Su, J., Lee, J. Y., et al. (2012). The Intestinal Stem Cell Markers Bmi1 and Lgr5 Identify Two Functionally Distinct Populations. *Proc. Natl. Acad. Sci.* 109 (2), 466–471. doi:10.1073/pnas.1118857109

Yan, W., Li, T., Yin, T., Hou, Z., Qu, K., Wang, N., et al. (2020). M2 Macrophage-Derived Exosomes Promote the C-KIT Phenotype of Vascular Smooth Muscle Cells during Vascular Tissue Repair after Intravascular Stent Implantation. *Theranostics* 10 (23), 10712–10728. doi:10.7150/thno.46143

Yang, R., Liao, Y., Wang, L., He, P., Hu, Y., Yuan, D., et al. (2019). Exosomes Derived from M2b Macrophages Attenuate DSS-Induced Colitis. *Front. Immunol.* 10, 2346. doi:10.3389/fimmu.2019.02346

Zhang, G., Zou, X., Huang, Y., Wang, F., Miao, S., Liu, G., et al. (2016). Mesenchymal Stromal Cell-Derived Extracellular Vesicles Protect against Acute Kidney Injury through Anti-oxidation by Enhancing Nrf2/ARE Activation in Rats. *Kidney Blood Press. Res.* 41 (2), 119–128. doi:10.1159/000443413

Zhang, L., Jiao, G., Ren, S., Zhang, X., Li, C., Wu, W., et al. (2020a). Exosomes from Bone Marrow Mesenchymal Stem Cells Enhance Fracture Healing through the Promotion of Osteogenesis and Angiogenesis in a Rat Model of Nonunion. *Stem Cel Res Ther.* 11 (1), 38. doi:10.1186/s13287-020-1562-9

Zhang, Y., Chopp, M., Meng, Y., Katakowski, M., Xin, H., Mahmood, A., et al. (2015). Effect of Exosomes Derived from Multipluripotent Mesenchymal Stromal Cells on Functional Recovery and Neurovascular Plasticity in Rats after Traumatic Brain Injury. *Jns* 122 (4), 856–867. doi:10.3171/2014.11.JNS14770

Zhang, Y., Jiang, X., and Ren, L. (2019). Optimization of the Adipose-Derived Mesenchymal Stem Cell Delivery Time for Radiation-Induced Lung Fibrosis Treatment in Rats. *Sci. Rep.* 9 (1), 5589. doi:10.1038/s41598-019-41576-5

Zhang, Y., Qin, Y., Chopp, M., Li, C., Kemper, A., Liu, X., et al. (2020b). Ischemic Cerebral Endothelial Cell-Derived Exosomes Promote Axonal Growth. *Stroke* 51 (12), 3701–3712. doi:10.1161/STROKEAHA.120.031728

Zheng, K., Wu, W., Yang, S., Huang, L., Chen, J., Gong, C., et al. (2016). Treatment of Radiation-Induced Acute Intestinal Injury with Bone Marrow-Derived Mesenchymal Stem Cells. *Exp. Ther. Med.* 11 (6), 2425–2431. doi:10.3892/etm.2016.3248

Zhou, Y., Li, P., Goodwin, A. J., Cook, J. A., Halushka, P. V., Chang, E., et al. (2018). Exosomes from Endothelial Progenitor Cells Improve the Outcome of a Murine Model of Sepsis. *Mol. Ther.* 26 (5), 1375–1384. doi:10.1016/j.ymthe.2018.02.020

Ziegler, V., Henninger, C., Simiantonakis, I., Buchholzer, M., Ahmadian, M. R., Budach, W., et al. (2017). Rho Inhibition by Lovastatin Affects Apoptosis and DSB Repair of Primary Human Lung Cells In Vitro and Lung Tissue In Vivo Following Fractionated Irradiation. *Cel Death Dis.* 8 (8), e2978. doi:10.1038/cddis.2017.372

Zou, L., Ma, X., Lin, S., Wu, B., Chen, Y., and Peng, C. (2019). Bone Marrow Mesenchymal Stem Cell-derived E-xosomes P-rotect against M-yocardial I-nfarction by P-romoting A-utophagy. *Exp. Ther. Med.* 18 (4), 2574–2582. doi:10.3892/etm.2019.7874

Zuo, R., Liu, M., Wang, Y., Li, J., Wang, W., Wu, J., et al. (2019). BM-MSC-derived Exosomes Alleviate Radiation-Induced Bone Loss by Restoring the Function of Recipient BM-MSCs and Activating Wnt/β-Catenin Signaling. *Stem Cel Res Ther.* 10 (1), 30. doi:10.1186/s13287-018-1121-9

Conflict of Interest: The authors declare that the research was conducted in the absence of any commercial or financial relationships that could be construed as a potential conflict of interest.

GLOSSARY

ARS Acute radiation syndrome
BMASC Bone marrow-derived adherent stromal cell
BMMSC Bone marrow mesenchymal stem cells
BMM Bone marrow macrophage
BV/TV Bone volume fraction
CCL2 Chemokine (C-C motif) ligand 2
DAMP Damage-associated molecular patterns
DEARE Delayed effects of acute radiation exposure
DSB double-strand breaks
DSS Dextran sulfate sodium
EC Endothelial cell
EC-EVs Endothelial cell-extracellular vesicles
ECFC Endothelial colony-forming cells
ERK1/2 Extracellular signal-regulated protein kinase
EM Electron microscopy
EMMPRIN Extracellular matrix metalloproteinase inducer
EV Extracellular vesicle
FDA Food and drug administration
G-CSF Granulocyte colony-stimulating factor
GM-CSF Granulocyte-macrophage colony-stimulating factor
Gy unit of radiation
Gray = 100 rads
GMP Good manufacturing practice
HSCs Hematopoietic stem cells
HUVEC Human umbilical cord vein endothelial cells
ICAM1 Intercellular adhesion molecule 1
iPSC induced pluripotent stem cells
IL Interleukin
ISC Intestinal Stem Cells
ISEV International society of extracellular vesicles
Lgr5 Leucine-rich repeat-containing G-protein coupled receptor 5
MAPK Mitogen-activated protein kinase
Mϕs Macrophages
MCM Medical countermeasure
MISEV Minimal information for studies on extracellular vesicles
MM6 Mono-Mac-6
MSC Mesenchymal Stem Cells
NF-κB nuclear factor kappa-light-chain-enhancer of activated B cells
NIH National Institute of Health
PTEN Phosphatase and Tensin Homolog
RIBE Radiation-induced bystander effect
RILD Radiation-induced liver disease
ROS reactive oxygen species
SASP Senescence-associated secreted phenotype
SH-SY5Y human neuroblastoma cells
SOD Super oxide dismutase
SSB Single strand breaks
TCF/LEF T-cell factor/lymphoid enhancer factor
TNF-α Tumor necrosis factor-alpha
TSG101 Tumor susceptibility gene 101
Plau/uPA urokinase-type plasminogen activator
VCAM1 Vascular cell adhesion molecule 1
VE-cadherin Vascular endothelial-cadherin
WBI Whole-body irradiation

frontiers in Pharmacology

REVIEW
published: 18 May 2021
doi: 10.3389/fphar.2021.643283

Acute Radiation Syndrome and the Microbiome: Impact and Review

*Brynn A. Hollingsworth, David R. Cassatt, Andrea L. DiCarlo, Carmen I. Rios, Merriline M. Satyamitra, Thomas A. Winters and Lanyn P. Taliaferro**

Radiation and Nuclear Countermeasures Program (RNCP), Division of Allergy, Immunology and Transplantation (DAIT), National Institute of Allergy and Infectious Diseases (NIAID), National Institutes of Health (NIH), Rockville, MD, United States

Study of the human microbiota has been a centuries-long endeavor, but since the inception of the National Institutes of Health (NIH) Human Microbiome Project in 2007, research has greatly expanded, including the space involving radiation injury. As acute radiation syndrome (ARS) is multisystemic, the microbiome niches across all areas of the body may be affected. This review highlights advances in radiation research examining the effect of irradiation on the microbiome and its potential use as a target for medical countermeasures or biodosimetry approaches, or as a medical countermeasure itself. The authors also address animal model considerations for designing studies, and the potential to use the microbiome as a biomarker to assess radiation exposure and predict outcome. Recent research has shown that the microbiome holds enormous potential for mitigation of radiation injury, in the context of both radiotherapy and radiological/nuclear public health emergencies. Gaps still exist, but the field is moving forward with much promise.

Keywords: radiation, microbiome, radiation medical countermeasure, radiation biodosimetry, acute radiation syndrome

OPEN ACCESS

Edited by:
Ales Tichy, University of Defence, Czechia

Reviewed by:
Harold Swartz, Dartmouth College, United States
Abdallah El-Sayed Allam, Tanta University, Egypt
Klara Kubelkova, University of Defence, Czechia

****Correspondence:***
Lanyn P. Taliaferro
lanyn.taliaferro@nih.gov

Specialty section:
This article was submitted to Translational Pharmacology, a section of the journal Frontiers in Pharmacology

Received: *17 December 2020*
Accepted: *04 March 2021*
Published: *18 May 2021*

Citation:
Hollingsworth BA, Cassatt DR, DiCarlo AL, Rios CI, Satyamitra MM, Winters TA and Taliaferro LP (2021) Acute Radiation Syndrome and the Microbiome: Impact and Review. Front. Pharmacol. 12:643283. doi: 10.3389/fphar.2021.643283

INTRODUCTION

Understanding the role of the microbiome in radiation pathogenesis, assessment of exposure, protection, and mitigation of injury following acute radiation exposure is of great interest. Such studies may help reveal new mechanisms of action, medical countermeasures (MCMs), and biomarkers for biodosimetry to be used in the event of a radiation public health emergency. Radiation exposures resulting from environmental, accidental, medical, or terrorist radiation/nuclear incidents (e.g., improvised nuclear device or radiological dispersal device) have the potential to affect the health and function of many biological systems. The possible dose ranges and radiation sources (e.g., gamma, neutron, X-ray, and mixed-field) involved in these exposures could span nearly all conceivable scenarios, from internalized radionuclides to photons and/or particulate radiation exposure, with doses from near background to high-lethal exposures (Glasstone et al., 1977; Newbold et al., 2019). The Radiation and Nuclear Countermeasures Program (RNCP) within the National Institute of Allergy and Infectious Diseases (NIAID) of the National Institutes of Health (NIH), was initiated in 2004 following a congressional mandate to fund research to develop medical-based approaches for use after a radiological or nuclear public health incident (Hafer et al., 2010; Rios et al., 2014). As of early 2021, four products have been approved by the U.S. Food and Drug Administration (FDA) to treat hematopoietic complications following acute radiation exposure—filgrastim (Neupogen®, Amgen, FDA approved March 2015) (Food and Drug Administration, 2015a), pegfilgrastim (Neulasta®, Amgen, FDA approved November 2015) (Food and Drug Administration, 2015b), sargramostim (Leukine®, Partner Therapeutics, FDA approved March 2018) (Food and Drug Administration, 2018), and romiplostim (Nplate®, Amgen,

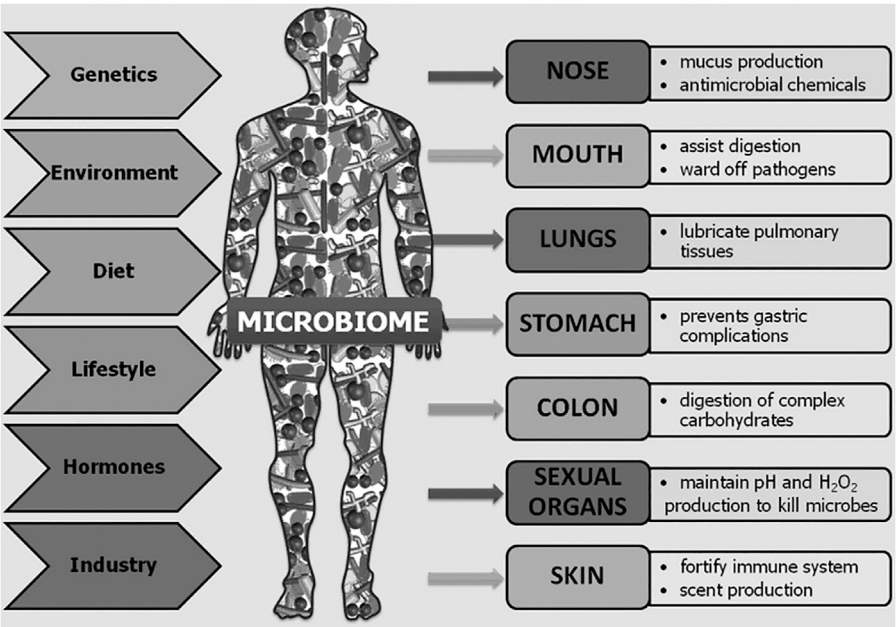

FIGURE 1 | Overview of the body areas inhabited by microbiota, their roles in those organs, and the factors contributing to their diversity among individuals and across time. Reprinted from *Human Microbes—The Power Within*, by V.D. Appanna, 2018. Springer Singapore (Appanna, 2018).

FDA approved January 2021). However, products are yet to be approved to treat other acute or delayed subsyndromes, such as gastrointestinal (GI) or lung, nor have any radiation biodosimetry tests been cleared for triage or dose assessment. It is possible that some of these gaps could be filled as researchers dig deeper into the complexities of the human microbiome and its involvement in radiation injury. This recently renewed area of research, with a focus on the acute radiation exposure setting, could lead to exciting new drug targets, MCMs, and biomarkers of radiation injury.

HISTORY OF MICROBIOME RESEARCH

It has long been known that microbes inhabit the human body alongside human cells in a symbiotic relationship. In 1886, Escherich published that *Escherichia coli* bacteria lived not only in the intestines of children with diarrheal disease but also in those of healthy children (Hayes and Sahu, 2020). Over the years, it has been determined that the human body is host to between 75 and 200 trillion microbes, similar to the total number of human cells in the body (Ursell et al., 2012; Sender et al., 2016; Sender et al., 2016; Hayes and Sahu, 2020). In 2001, Lederberg, a Nobel Prize recipient for work on microbial genetics, defined "microbiome" as "the collective genomes of all the microorganisms inhabiting a specific environment, especially that of the body" (Lederberg and McCray, 2001). Microbiota not only refers to bacteria, but encompasses all the microorganisms of the body, including archaea, fungi, protozoans, bacteria, and viruses (Lederberg and McCray, 2001; Zhu et al., 2010; Jandhyala et al., 2015). The human microbiome is incredibly diverse with an individual's microbiome so distinct that it has been proposed to be used as a differentiating biomarker in forensics (D'Angiolella et al., 2020; García et al., 2020). Not only is the microbiome diverse among individuals but also across the body and even within body areas (Roth and James, 1988; Hakansson and Molin, 2011; Seidel et al., 2020). This diverse microbiota plays a critical role in the biological function of the gut, skin, lungs, oral cavity, urogenital system, and more (**Figure 1**). The microbiota occupying the organs comprises differing types and abundance of microbial species (**Table 1**). Microbial diversity, or lack thereof, depending on the body system examined, is also an important indicator of health (Muhleisen and Herbst-Kralovetz, 2016; Buchta, 2018; Ferreira et al., 2019; Araghi, 2020).

While these microbes take their nutrients from the human body, they contribute to the health of the human host as well. Roles include outcompeting pathogenic microbes, assisting in nutrient breakdown and metabolism, and involvement in complex interactions with the immune system (Appanna, 2018). The presence of the microbiota stimulates expression of pattern recognition receptors (Brandl et al., 2007; Gallo and Nizet, 2008; Vaishnava et al., 2008; Vaishnava et al., 2011), secretion of protective proteins like mucins (Sanford and Gallo, 2013; Pickard et al., 2017; Meisel et al., 2018), as well as immune cell production, maturation, and recruitment, particularly of regulatory T-cells (Hamada et al., 2002; Kupper and Fuhlbrigge, 2004; Paulos et al., 2007; Bouskra et al., 2008). Interestingly, some immune cells are able to discriminate between pathogenic and commensal bacteria (Franchi et al., 2012; Seneschal et al., 2012; Guo et al., 2020). In addition, there are extensive and complex interactions across the distinct microbial

TABLE 1 | Dominant bacteria in microbial communities across the human body.

Body area	Bacteria	Characterization
GI (Arumugam et al., 2011; Hakansson and Molin, 2011; King et al., 2019)	Firmicutes phylum	Together with bacteroidetes makes up 80% of the gut flora
	Bacteroidetes phylum	Together with Firmicutes makes up 80% of the gut flora
	Actinobacteria phylum	Makes up ~3% of the gut flora
	Proteobacteria phylum	Makes up ~1% of the gut flora
Oral Cavity (Aas et al., 2005; Bik et al., 2010)	*Veillonella*	Predominant genus across the oral cavity, in the phylum Firmicutes
	Actinomyces	Predominant genus on the tongue and teeth, in the phylum Actinobacteria
	Neisseria	Predominant genus on the lips, palate, and cheek, in the phylum Proteobacteria
	Simonsiella	Predominant genus on the tongue, in the phylum Proteobacteria
	Eubacterium	Predominant genus on the teeth, in the phylum Firmicutes
Skin (Davis, 1996)	*Staphylococcus epidermidis*	Most abundant skin inhabitant making up 90% of the resident aerobic flora
	Micrococcus luteus	Accounts for 20–80% of the micrococci isolated from the throughout the normal skin
	Staphylococcus aureus	Common location: nose, perineum, and vulvar skin. Presence varies with age. More abundant with dermatologic disease
Lung (Charlson et al., 2011; Dickson et al., 2013; Liu et al., 2020)	*Prevotella*	Makes up 7–23% of microbes from healthy subjects' bronchoalveolar lavage, genus in the Bacteroidetes phylum
	Veillonella	Makes up 6–15% of microbes from healthy subjects' bronchoalveolar lavage, genus in the phylum Firmicutes
Naso-pharyngeal (Frank et al., 2010)	*Propionibacterium acnes*	Makes up ~42% of microbes from healthy subject nasal swabs, member of Actinobacteria phylum
	Staphylococcus epidermidis	Makes up ~10% of microbes from healthy subject nasal swabs, member of Firmicutes phylum
	Corynebacterium tuberculostearicum	Makes up ~8% of microbes from healthy subject nasal swabs, member of Actinobacteria phylum
Vaginal (Ravel et al., 2011; Muhleisen and Herbst-Kralovetz, 2016; Buchta, 2018)	*Lactobacillus iners*	Makes up 1–88% of healthy vaginal microbiota, with 34% of healthy females' vaginal microbiota dominated by this species
	Lactobacillus crispatus	Makes up 0–83% of healthy vaginal microbiota, with 27% of healthy females' vaginal microbiota dominated by this species
	Lactobacillus gasseri	Makes up 0.4–86% of healthy vaginal microbiota, with 6% of healthy females' vaginal microbiota dominated by this species
	Lactobacillus jensenii	Makes up 0.5–80% of healthy vaginal microbiota, with 5% of healthy females' vaginal microbiota dominated by this species

communities spanning the body including the so-called gut–lung axis, microbiota–gut–liver axis, and the microbiota–gut–brain axis (Keely et al., 2012; Dumas et al., 2018; Bajaj et al., 2019; Nie et al., 2020; Stavropoulou and Bezirtzoglou, 2020). Overall, the microbiome plays a vital role in human health and, in some ways, each distinct microbiota axis represents a system unto itself.

Since the initial research and visualization of cells via microscopy in the 1660s by Hooke and van Leeuwenhoek, humans have investigated microscopic organisms around and in us; and with the inception of the NIH Human Microbiome Project in 2007, research into the microbiome has exploded (Proctor et al., 2019). For most of the history of microbiome research, identification was limited to only a few hundred species that could be cultured (Lee et al., 1968; Moore and Holdeman, 1974), but with advances in whole genome sequencing, Relman and others encouraged researchers to utilize these new technologies to identify previously unrecognized, unculturable microbes that inhabit the human body (Relman, 1999; Relman, 2002). Since that time, it has been observed that 60–80% of human-colonizing bacterial species cannot be cultured with standard medical microbiology media (Suau et al., 1999). Recently, the microbial 16S ribosomal RNA (16S rRNA) gene sequencing method has been employed to conduct culture-independent investigations of microbiota composition across the body in numerous mammalian species, including humans (Muegge et al., 2011). The discovery of the 1.5-Kbp 16S rRNA gene, containing highly conserved ubiquitous sequences and regions that vary with greater or lesser frequency over evolutionary time, revolutionized culture-independent microbial determination (Lane et al., 1985; Böttger, 1989). Through this research, genus- and species-level identification and abundance across individuals and across their body regions (**Table 1**) have uncovered high inter-individual and intra-individual microbiota diversity that is impacted by co-evolutionary selection, age, diet, and geographic region (Mackie et al., 1999; Spor et al., 2011; Lozupone et al., 2012; Morgan and Huttenhower, 2012; Yatsunenko et al., 2012). While there is no core microbiome at the species level, at the phylum level, there is commonality and a broad consensus for similarities in functional gene profiles (Sekelja et al., 2011; Morgan et al., 2013; Sharpton, 2018).

Although the discovery and use of the 16S rRNA gene have greatly expanded microbiome research, it is still only bacterially selective, limiting this sequencing technique to evaluation of bacterial composition and responses to environmental changes

or challenges (Bäckhed et al., 2005). Investigation of the virome, mycobiome, and archaea components of the microbiota broadly and particularly in response to radiation has been lacking (Rosenberg and Zilber-Rosenberg, 2013; Roy and Trinchieri, 2017; Liu et al., 2021). It is possible that broader insights into the impact of nonbacterial components of the GI microbiota might be obtained through non-targeted shotgun metagenomic sequencing techniques that would be capable of assessing radiation responses in the nonbacterial compartments of the GI microbiota (Campo et al., 2020; Kaźmierczak-Siedlecka et al., 2020; Turkington et al., 2021). The current lack of studies investigating GI microbiota compartments beyond the bacteriome represents a potentially important gap in our understanding of the impact of the microbiome on radiation response.

In this review, the effect that radiation has on the microbiota of various parts of the human body is summarized. Animal models of acute radiation exposure and their use for future microbiome studies are then discussed. Given the enormous therapeutic potential of the microbiome in mitigating multiple organ damage from irradiation (e.g., the GI tract, lung, and skin), consideration of these microbial populations in research and development is necessary. A discussion of treatments and other factors that have been shown to modify the microbiome, mitigating radiation damage, is presented. These approaches can preserve organ function and health, potentially allowing the microbiome to serve as a MCM and/or biomarker for radiation injury.

To date, human microbiome studies in radiological or nuclear incidents do not exist. Thus, most radiation studies, and especially those examining the microbiome, are conducted in the context of medical treatment, primarily with respect to cancer radiotherapy. While these data are helpful for guiding future studies in the acute radiation exposure space, it is not directly comparable to an acute radiation exposure scenario. Furthermore, it is important to note that even cancer alone affects the microbiome (Nam et al., 2013), and this must be taken into consideration when extrapolating data from these studies to the context of a radiological or nuclear incident. In an effort to curate currently available data relevant to ARS, a systematic search methodology was conducted and is highlighted in **Figure 2**. In summary, related keywords were used to search PubMed, Scopus, and clinicaltrials.gov (trials referenced using the National Clinical Trial (NCT) number), followed by screens for approaches linked to high-dose radiation or radiotherapy relevant to ARS. In particular, research articles were selected based on organ systems of interest and treatment approaches that could modulate the microbiome. Certain areas of microbiome research (e.g., obesity, diabetes, ultraviolet (UV), pollution, tumors, space, and those unrelated to biology) were excluded.

THE EFFECTS OF RADIATION ON THE MICROBIOME

Gut Microbiome

The microbiota of the human GI tract is essential for metabolic and digestive function, development, and support of the gut-associated immune system, prevention of gut colonization by pathogenic microbial species, and support of epithelial integrity to prevent barrier translocation of microbes (Bäckhed et al., 2005; Hooper and MacPherson, 2010; Stecher and Hardt, 2011). Studies suggest that the human GI tract harbors more than 800 different individual bacterial species (Turnbaugh et al., 2010) with proportional representation, genus level distribution, and viable count of colony-forming units (CFUs) varying widely from the oral cavity to the rectum (Hayashi et al., 2005; Wang et al., 2005; Bik et al., 2006; Lazarevic et al., 2009; Hakansson and Molin, 2011) and changing with age, diet, and geographical location (Biagi et al., 2010; Claesson et al., 2011). The predominant phyla in the healthy gut are Firmicutes and Bacteroidetes, which typically represent up to 80% or more of the microbiota, with smaller contributions of Actinobacteria (~3%), Proteobacteria (~1%), Verrucomicrobia, and Fusobacteria (~0.1% or less) (Arumugam et al., 2011; Hakansson and Molin, 2011; King et al., 2019).

As noted above, most studies of the effect of radiation on the GI microbiome have been conducted in the context of cancer radiotherapy, and recent reviews summarize the literature in that context (Liu et al., 2021; Tonneau et al., 2021). Indeed, therapeutic abdominopelvic radiation exposure frequently results in intestinal dysfunction and dysbiosis, with acute radiation enteritis complications observed in 50% or more of abdominally irradiated cancer patients (Touchefeu et al., 2014). Radiation enteritis is associated with high morbidity and mortality, and chronic symptoms as severe as rectal hemorrhage, strictures, and fibrosis develop 3 months to 20 years after completion of radiotherapy (Packey and Ciorba, 2010; Ding et al., 2020). However, these studies can shed light on what may happen in the event of a radiological or nuclear mass casualty incident in which victims exposed to more than 6 Gy of radiation may acutely experience nausea, vomiting, diarrhea, sepsis, and death (Wojcik, 2002).

Rapidly dividing human cells are the most sensitive to the damaging and killing effects of ionizing radiation (Donnelly et al., 2010), and in particular, the GI epithelium is very sensitive to radiation, given that the GI crypt rapidly divides to shedding villi cells every 2–4 days (Novak et al., 1979; Somosy et al., 2002; Clevers, 2013; Williams et al., 2015). Radiation-induced cell death leads to loss of GI epithelial integrity and function, leading to inflammation and penetration of the GI epithelial barrier by the luminal contents and microbiota (François et al., 2013; Shukla et al., 2016). In addition, radiation damage to endothelial cells of the blood vessels within the villi can also result in vascular damage, causing further inflammation and sepsis (Paris et al., 2001). In the context of radiotherapy, most acute symptoms generally resolve within a few weeks as mucosal crypt, and villus structures are reconstituted from surviving stem cells (Umar, 2010).

A diverse and healthy commensal intestinal microbiota plays an essential role in GI homeostasis. However, it has been found that severe postirradiation enteropathy is associated with low mucosal bacterial diversity (Ferreira et al., 2019). In rodent studies, specific findings of microbiota changes in postirradiation fecal samples include increased abundance of the phylum Proteobacteria and family *Lactobacillaceae* and decreased abundance of families

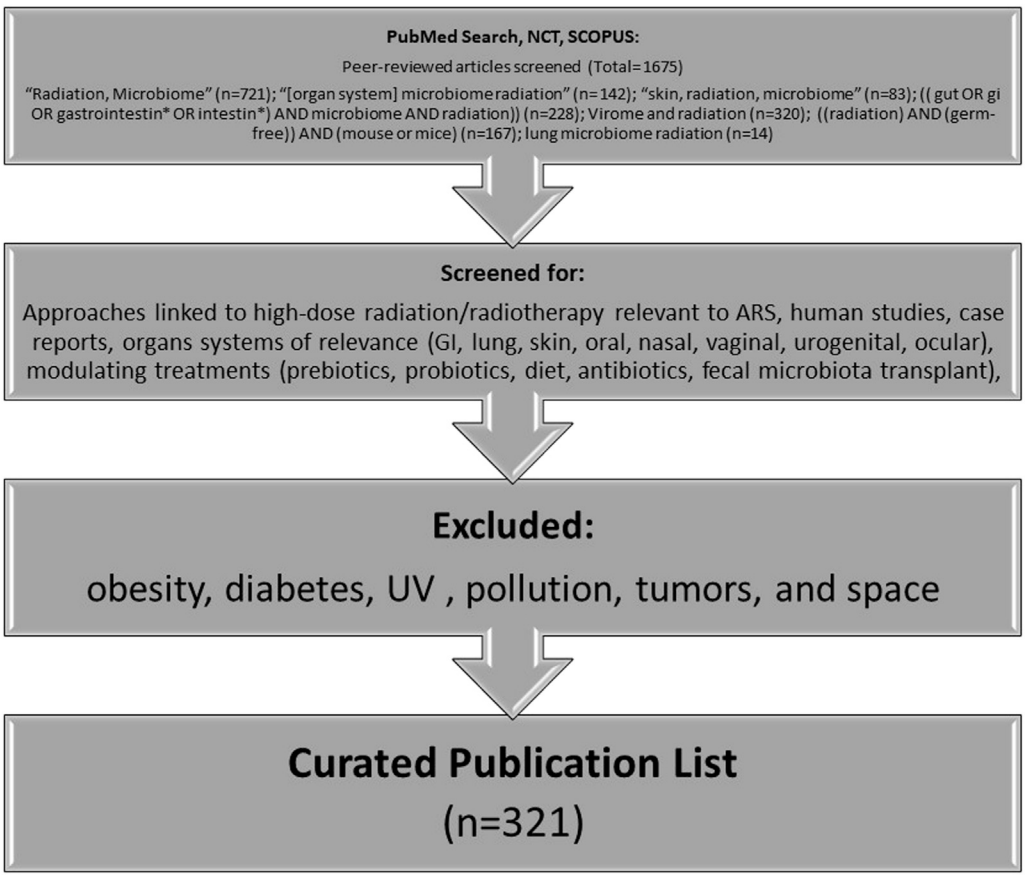

FIGURE 2 | Methodology for curation of literature for this review (*NCT: clinicaltrials.gov).

Lachnospiraceae, *Ruminococcaceae*, and *Clostridiaceae*, with some changes observed out to 10 months (Lam et al., 2012; Goudarzi et al., 2016; Zhao et al., 2019; Li et al., 2020). In humans, one prospective study of nine gynecologic cancer patients found that Firmicutes and Fusobacterium phyla were significantly decreased in fecal samples pre- versus post-pelvic irradiation (Nam et al., 2013). While there are few prospective studies that document changes in the gut microbiota postradiation, growing research interest in this area will likely fill that gap.

Oral Microbiome

The microbiota in the oral cavity has long been studied, as changes in the balance of flora in the oral cavity can lead to infections like candidiasis, also known as "thrush," first described and attributed to a fungus in 1839 by Bernhard von Langenbeck (Hellstein and Marek, 2019). Hundreds of years of interest and easy access to the oral cavity and saliva samples have facilitated extensive research on the oral microbiome and its connection to various disease processes, including responses to radiation exposure (Anjali et al., 2020; Belstrøm, 2020). In the oral cavity, there may be from 10^8 to 10^{10} CFU per gram of saliva (Lazarevic et al., 2009). It should be noted that the oral microbiota even in healthy people varies drastically across location in the oral cavity, time of day, hydration, what and when the person ate, oral hygiene, age, smoking status, and so on (Aas et al., 2005; Bik et al., 2010; Cameron et al., 2015; Leake et al., 2016; Hall et al., 2017; Belstrøm, 2020; D'Angiolella et al., 2020). In radiation exposures, oral side effects such as xerostomia (dry mouth) are seen in patients receiving external beam radiotherapy to the head and neck (Wijers et al., 2002; Dirix et al., 2006) and radioiodine therapy (Alexander et al., 1998; Solans et al., 2001; Jeong et al., 2013; Hollingsworth et al., 2016). In fact, in a follow-up Chernobyl study, 4 of 15 survivors reported experiencing xerostomia (Gottlöber et al., 2001). Salivary damage and subsequent dry mouth can lead to a variety of problems, from difficulty chewing and talking to increased dental caries, oral mucositis, osteonecrosis, and so on (Dirix et al., 2006; Gomez et al., 2011; Tolentino et al., 2011; Sroussi et al., 2017; Chen et al., 2020). While studies of the oral microbiome following a nuclear accident are limited, there are many research studies that examine the changes in the oral microbiota following head and neck radiation exposure in oncology (Anjali et al., 2020).

The oral cavity has a delicate microbiota balance that can be directly affected not only by irradiation but also from changes in saliva composition and/or volume due to radiation-induced damage of the salivary glands, which are particularly radio-sensitive organs (Kałużny et al., 2014). Since the 1970s, radiation-induced xerostomia has been known to affect the oral microbiota (Brown

et al., 1975; Brown et al., 1978; Sroussi et al., 2017; Mougeot et al., 2019; Breslin and Taylor, 2020), and it has been recently discovered that *Candida* infections in patients who received radiotherapy are often from species that are more virulent and drug-resistant (Tarapan et al., 2019). This is particularly concerning, given that *Candida* is the fourth most common cause of bloodstream infections among hospital patients in the United States and can be fatal (Hajjeh et al., 2004; Lone and Ahmad, 2019). A number of studies found increased abundance of Gram-negative and *Lactobacillus* bacterial species, as well as *Candida* fungal species following radiotherapy (Vanhoecke et al., 2015). Indeed, Nishii et al. found oral candidiasis occurred in 31% of 326 oral/oropharyngeal cancer patients who underwent radiotherapy, with oral mucositis associated with a higher incidence of oral candidiasis (Nishii et al., 2020). Researchers collected buccal swabs from oral cancer patients before and after radiotherapy, and while these patients already had altered oral microbiota with high prevalence of certain species following radiotherapy such as *Streptococcus* pathogenic *Candida albicans*, *Klebsiella*, and *Pediococcus*, with elevated *Candida* and *Pediococcus* persisting out to 6 months (Anjali et al., 2020).

Another study found *Streptococcus* and other species were predictive of high-grade oral mucositis, while *Lactobacillus* and *Staphylococcus* were only detected in patients with low- or no-grade oral mucositis in a study of 19 patients receiving fractionated radiotherapy (Vesty et al., 2020). Patients who developed more severe oral mucositis following radiotherapy had a higher abundance of *Actinobacillus* (Zhu et al., 2017), and an increase in certain microbes that coincided with the onset of severe mucositis over the course of patients' radiation treatment (Hou et al., 2018). Additionally, an *in vitro* study found ionizing radiation increased the adherence of *Streptococcus mutans* on dental restoration material and promoted the formation of biofilms (Cruz et al., 2010).

In addition to the risk of salivary and oral damage caused by prompt exposure during a radiation incident, radioactive iodine fallout can find its way into the environment and eventually into human bodies, leading to a well-documented increased risk in thyroid cancer (Robbins and Schneider, 2000; Cardis and Hatch, 2011; Thomas, 2018). Salivary glands (La Perle et al., 2013) express the sodium iodide symporter, facilitating radioiodine uptake and potential damage. Although little research on the impact of radioiodine on the oral microbiome has been conducted, given the similarities in damage and symptoms between radioiodine therapy and external beam radiotherapy, changes to the microbiota may be similar.

Skin Microbiome

With a surface area of approximately 2 m^2, the skin is the largest organ and is highly complex, with structures such as hair follicles and sweat ducts increasing its true surface area to about 25 m^2 (Gallo, 2017). The variable surface of the skin supports a vast ecosystem of distinct microorganisms, where more exposed areas tend to be drier and less populated by resident bacteria (Roth and James, 1988). However, the overall number of microorganisms present on the skin is held relatively constant under normal conditions (Davis, 1996). The commensal relationship between cutaneous tissue and the diverse community of microorganisms plays a critical role in barrier protection from invading pathogenic microorganisms, homeostasis, and the adaptive immune response (Dréno et al., 2016; Sfriso et al., 2020).

Much is still to be learned of the interplay between the skin microbiome and ionizing radiation-induced cutaneous injury. Most clinical studies focus on posttreatment inflammation, particularly dermatitis in breast cancer patients after radiotherapy (Eslami et al., 2020). As it is very likely that many individuals will have cutaneous and combined injuries following a radiation mass-casualty incident, mediating changes in the skin microbiota with preventative or mitigative treatments is of particular importance for chronic and acute wound healing outcomes and to prevent systemic complications. Combined injury, consisting of total body irradiation (TBI) followed by punch wounding resulted in early detection of bacteria in the blood, heart, and liver, although detection of bacteria was delayed in mice that received radiation alone. Only transient bacteremia occurred in mice that underwent wounding alone. Results suggest that increased levels of iNOS, cytokines, and bacterial infection triggered by combined injury may contribute to mortality in this model (Kiang et al., 2010).

Thermal and radiation burns are also likely during a radiation incident. However, standard medical management for thermal burns such as medications, wound dressings, therapy, and surgery may not be appropriate for radiation burns, which have a different damage profile with cyclic waves of inflammation and progressive lesion formation over time (DiCarlo et al., 2020). Adding to this complex scenario is the possibility of bacterial infection. Researchers have demonstrated extremophilic bacteria such as *Aeribacillus*, likely introduced during debridement of flame or scald wounds, correlated with patient comorbidities, such as pneumonia, infection, and sepsis (Plichta et al., 2017). Germ-free mice have been shown to have accelerated wound closure and scar reduction with elevated levels of anti-inflammatory cytokine IL-10, angiogenic growth factor VEGF, and angiogenesis in the germ-free wound tissue, suggesting the influence of an inflammatory component in wound healing (Canesso et al., 2014). A few case reports of mesenchymal stem cell treatment of patients with severe radiation burns also showed a resolution of inflammation (Bey et al., 2007; Bey et al., 2010). Although these studies suggest bacteria delay skin injury healing, certain bacterial species, such as *Lactobacillus plantarum*, can inhibit biofilm growth of harmful bacterial (e.g., *Pseudomonas aeruginosa*), subsequently improving tissue repair (Valdéz et al., 2005). These studies suggest it is possible to harness the beneficial power of the skin microbiome, expanding therapeutic options.

Although different from radiation injury, the microbiome research conducted for other skin injuries, such as those involving ultraviolet irradiation (Wolf et al., 2016; Patra et al., 2019; Patra et al., 2020), diabetic ulcers, and other chronic skin diseases (Wolcott et al., 2016; Johnson et al., 2018), may shed light and help guide future skin microbiome research in the context of radiation injury. Additionally, clinical strategies currently used to treat these complicated skin wounds may provide insight into identifying effective therapeutics and improving patient

outcomes. While a wealth of information can be found in the literature on processes governing wound healing, the role of the skin microbiome is less clear. Research shows that differences exist between normal and pathological microbial responses after a skin injury (Singer and Clark, 1999; Schultz et al., 2011; Johnson et al., 2018); therefore, a better understanding of the skin microbiome and its influence on the immune response has great medicinal potential with regard to radiation injuries.

Lung Microbiome

Historically, lungs have been considered sterile. When it was first reported in 2010 that the microbiome in the lower airways was comparable to the upper bowel, the phenomenon was attributed to possible contamination during the bronchoalveolar lavage (BAL) procedure (Hilty et al., 2010). Since then, the existence of a microbiome in healthy lung has been widely accepted (Kiley and Caler, 2014; Mathieu et al., 2018). The lung microbiome is situated in the lower airways of healthy lung and houses a large number of microbes, including phyla Bacteroidetes and Firmicutes (Charlson et al., 2011; Dickson et al., 2013; Liu et al., 2020). The microbiome landscape changes dramatically under disease conditions affecting the lung, such as asthma and chronic obstructive pulmonary disease (Segal et al., 2014; Evsyutina et al., 2017), through processes involving immigration, elimination, and local growth conditions (Evsyutina et al., 2017).

Microbial migration occurs via air inhalation, micro-aspiration, and direct dispersion through the respiratory tract mucosa, while microbiome elimination occurs by mucociliary clearance, cough, and immune mechanisms. Microbiome growth conditions can be influenced by pO_2, pH, blood perfusion, alveolar ventilation, temperature, lung epithelium, mucociliary clearance, and inflammatory cell activity. Furthermore, microbiome expansion is affected by bacteriostatic activity from surfactant produced in the distal alveoli. Finally, under disease conditions, the lung microbiome can be entirely destroyed and replaced with a single pathogen, as can occur during pneumonia (Araghi, 2020). Interestingly, the gut microbiota can affect general pulmonary health through a vital cross-talk between the gut microbiota and the lungs, referred to as the "gut–lung axis" (Keely et al., 2012). The gut–lung axis is bidirectional, denoting that the endotoxins and microbial metabolites released into systemic circulation by the gut can affect the lung, and if inflammation occurs in the pulmonary tissue, the gut microbiota is also affected (Dumas et al., 2018).

Though progress has been made, lung microbiome research is complicated by the difficulty in collecting biospecimens specific to the lung and lower airways. Clinically, sputum is used as a surrogate for lower airway samples; however, this process leads to contamination from microbes inhabiting the upper airways and oral cavity. Unfortunately, other than sputum, there are few reliable approaches to lower airway sampling, which is an obstacle to large-scale investigations of lung disease for studies requiring frequent sampling. Similarly, lung microbiome analysis using BAL fluid can also be contaminated by contributions from upper airway microbiota. Several studies analyzing lung tissue acquired via sterile surgical explant demonstrated that the lower respiratory tract contains a microbiome that is distinct from but related to that of the upper airways (Dickson et al., 2013).

While there are some publications related to radiotherapy and lung microbiome, there are no publications specific to the role of lung microbiome in radiation-induced lung injury at the writing of this review. One study described the prophylactic (pre-irradiation) use of heat-inactivated *Salmonella typhimurium* in ameliorating thoracic radiation-induced lung injury in mice by reducing apoptosis, inflammation, and endothelial mesenchymal remodeling of lung tissue (Kun et al., 2019). Some recent publications indicate that low-dose radiation therapy can be used in treating SARS-CoV-2–induced pneumopathy (Prasanna et al., 2020; Salomaa et al., 2020; Wilson et al., 2020); however, the relationship to the normal lung microbiome and the potential for a mitigation or biodosimetry strategy from these few studies is relatively unclear. Researchers in the radiation community can draw upon publications on the microbiome of the lung to better understand the significance of the microbiome in radiation-induced lung injury and how the microbiota are implicated in intervention strategies. These could include determining (1) whether an altered lung microbiome initiates radiation-induced disease pathogenesis, promotes chronic inflammation, or is merely a marker of injury and inflammation; (2) whether the lung microbiome can be manipulated therapeutically to change radiation-induced lung disease progression; and (3) what molecules (metabolites) generated during an inflammatory response can serve as biomarkers for pulmonary injury diagnosis and prognosis of the therapeutic interventions.

Other Microbiota Niches

The following microbiome niches are of lesser interest to the radiation emergency mission space. Radiation damage to these systems has low to no impact on lethality and no well-established animal models of injury. However, radiation exposure can still greatly damage these tissues and their resident microbiota and have been included here for completeness.

Nasopharyngeal Microbiome

Contrary to the lung, the nasopharyngeal and upper respiratory tracts are more accessible, making their microbiota easier to study. Predominant bacterial phyla in the healthy nares include Actinobacteria and Firmicutes (Frank et al., 2010). In addition, postirradiation rhinosinusitis is a well-documented side effect of radiotherapy of the nasopharyngeal, sino-nasal, or skull areas, occurring in up to 45% of patients (Huang et al., 2007; Su et al., 2014; Maxfield et al., 2017). Chronic rhinosinusitis has long been characterized by sinus microbiome dysbiosis (Cope et al., 2017), but only more recently have microbiota changes associated with chronic rhinosinusitis following radiotherapy been studied. Temporal changes in the nasopharyngeal microbiota following radiation therapy were noted in 39 nasopharyngeal carcinoma patients, which were followed for 3 months after radiation therapy (Huang et al., 2021); however, these changes were similar to findings reported in unirradiated patients with chronic rhinosinusitis (Abreu et al., 2012). Furthermore, evaluation of sino-nasal swabs of 22 patients with chronic

rhinosinusitis at an average 1.5 years after radiotherapy showed cultures dominated by many unique phyla of bacteria (Stoddard et al., 2019), which were similar to species found in unirradiated individuals with rhinosinusitis (Cope et al., 2017). This suggests that radiation can cause chronic rhinosinusitis, but the dysbiosis found is not distinct from chronic rhinosinusitis from other causes.

Urogenital Microbiome

Like the lung, the urinary tract and bladder were long thought to be a sterile environment, unless in a disease state. Only recently has more extensive research into the microbiome of the urologic system been conducted. Difficulties involved in obtaining bladder tissue samples from healthy individuals explain why its microbiome has yet to be extensively studied. A review of research done in this area discusses microbiota studies of urine and seminal fluid from prostate cancer patients, although changes in the urinary tract microbiota in response to radiation have yet to be explored (Aragón et al., 2018).

The vaginal microbiota, on the contrary, has been studied for over a century in the context of postmenopausal changes, with evidence emerging that *Lactobacillus* species dominate the microbiota and are vital for microbiota homeostasis (Ravel et al., 2011; Muhleisen and Herbst-Kralovetz, 2016; Buchta, 2018). Unlike the microbial diversity found in the healthy GI tract, the healthy vaginal microbiome is not normally phyla diverse, and an increase in bacterial diversity is an indication of vaginal dysbiosis (Muhleisen and Herbst-Kralovetz, 2016; Buchta, 2018). Indeed, one study found higher bacterial diversity in the vaginal microbiota following radiation in gynecologic cancer patients, who already had decreased lactobacilli abundance and increased diversity compared to healthy patients prior to radiotherapy (Tsementzi et al., 2020). Lactobacilli utilize glycogen and produce lactic acid which acidifies the vagina, protecting it from some infections (Buchta, 2018). Additionally, some species of lactobacilli appear to distinguish idiopathic infertile women from fertile women, indicating the vaginal microbiota is inextricably linked to reproductive health (Campisciano et al., 2017). Furthermore, low abundance of any *Lactobacillus* species has been linked to vulvovaginal atrophy which may put individuals at a higher risk of infection (Brotman et al., 2014). Changes to the vaginal microbiota have been studied in patients who received radiotherapy, which can sometimes induce menopause and subsequently decrease vaginal lubrication. Similar to the oral cavity, this change in environment alters the makeup of the microbiota and can lead to sexual and urinary organ problems, such as recurrent urinary tract infections (Portman and Gass, 2014). Specific taxa have been found to increase in abundance in the vaginal microbiota post- vs. pre-radiotherapy for gynecologic cancers including the family *Lachnospiraceae* (Tsementzi et al., 2020) and genera *Mobiluncus*, *Atopobium*, and *Prevotella* (Bai et al., 2019). Interestingly, an increase in cervical bacteria has been noted, with no difference in proportions, when culturing cervical swabs taken before and after external beam radiotherapy, suggesting the method of bacterial analysis and the location of samples affect the results (Mubangizi et al., 2014). These results suggest the microbiome may be involved in the mild reproductive and fertility effects seen in Chernobyl incident survivors (Cwikel et al., 2020) and nuclear industry workers (Doyle et al., 2001).

Ocular/Lacrimal Microbiome

The microbiota on the ocular surface, in tears and conjunctival fluid, and in lacrimal glands and ducts is only beginning to be considered. Studies among healthy patients found the genera *Corynebacterium* and *Pseudomonas* dominated the ocular microbiome (Huang et al., 2016; Suzuki et al., 2020). Studies of diseased state microbiota have been conducted in patients with dry eyes (Willis et al., 2020; Andersson et al., 2021), obstruction (Curragh et al., 2020), and Sjogren's syndrome (Trujillo-Vargas et al., 2020). Although dry eyes are a known side effect of radiotherapy (Nuzzi et al., 2020) and radioiodine treatments (da Fonseca et al., 2016), research in the area of radiation impact on the lacrimal or ocular microbiota has yet to be conducted.

Research on the microbiome, including interactions with other microbiota across the body and their human host, is ever expanding. Studies of the impact of acute radiation exposure on many areas of the microbiome are still needed, although some studies may be difficult due to access challenges, and differences between animal and human microbiomes.

ANIMAL MODELS OF RADIATION EFFECTS ON MICROBIOME

Researchers have used standard TBI or partial-body irradiation (PBI) models to study the effects of irradiation on the microbiome, and the influence of the microbiome on radiation injury. Rodent models are especially useful because researchers can build on the vast literature in rodent radiation models, and many research tools are available. These studies tend to focus on the gut microbiome and its complex interplay with the immune system.

One challenge in earlier studies that examined the effects of irradiation on acute intestinal injury (GI-ARS) is that levels of radiation necessary to cause lethal GI-ARS caused significant death from just the hematopoietic syndrome of the acute radiation syndrome (H-ARS). Although myeloablation can be ameliorated by bone marrow transplant or compensated by only looking at an earlier survival time point, more recent rodent models have employed partial body shielding, which spares enough bone marrow to allow the immune system to provide some level of protection against infection and hemorrhage, and to accelerate immune reconstitution (Booth et al., 2012; Fish et al., 2016). Shielding of 5% (or lower) of bone marrow is thought to simulate the level of shielding that would occur during an actual large-scale nuclear exposure because people will likely be indoors and thus partially shielded (Booth et al., 2012). On the contrary, localized irradiation or higher levels of shielding may be closer to the clinical experience. The various models used, and what has been learned from them are described below.

The role of infection due to bacterial translocation from the gut has long been a recognized consequence of ionizing radiation in mammals; therefore, a series of studies using mice that have no gut flora (derived and raised in germ-free environment) from the Notre Dame Lobund Laboratory's germ-free mouse colony were performed. In an initial study in mice, germ-free and conventionally housed mice were exposed to a range of radiation exposures of between 5 and 30 Gy (Wilson, 1963). In the radiation range corresponding to the hematopoietic syndrome (6–7 Gy), 30-day survival was higher in the germ-free animals. For higher radiation exposures, where all mice are expected to be dead by day 30, germ-free mice had a longer mean survival time (MST). These observations were confirmed in germ-free and conventionally housed mice as well as germ-free mice fed *E. coli* to populate the gut (McLaughlin et al., 1964).

In two subsequent articles, the MSTs and pathologies in mice receiving a range of radiation exposures were compared and described. Matsuzawa described four phases of radiation injury as radiation exposure was increased, corresponding to hematopoietic, heme/GI, GI, and CNS syndromes (Matsuzawa, 1965). Only in the last phase was no difference found in MST. Matsuzawa noted that the major difference in pathologies observed was increased septicemia in mice from the conventionally housed heme/GI group and later appearance of diarrhea in the GI group. This delay in the appearance of intestinal lesions was also observed for neutron-gamma mixed-field irradiation (Jervis et al., 1971). Further histopathological analysis of mice irradiated with 30 Gy showed differences in the epithelial cell counts of the intestinal crypts and villi, with irradiated conventionally housed mice having lower cell counts than their germ-free counterparts (Matsuzawa and Wilson, 1965).

From these studies, we can conclude that the microbiome has an influence on disease progression following radiation exposure; however, it was not until later that researchers elucidated which bacterial groups could have positive or negative influences on survival. It was found, for example, that the survival of germ-free mice reconstituted with normal human fecal bacteria had reduced survival when irradiated with 6.5 Gy compared to mice reconstituted with facultative anaerobic bacteria (Hazenberg et al., 1981). Around the same time, Onoue *et al.* found that the types of bacteria introduced into germ-free mice influenced the survival (diminishing with *Escherichia*, *Streptococcus*, *Pseudomonas*, and *Fusobacterium* or improving with *Clostridium*, *Lactobacillus*, or *Bifidobacterium* genera) when mice were exposed to 20 Gy of radiation (Onoue et al., 1981).

A subsequent study which directly examined the role of the microbiome in radiation injury also noted in a TBI model that germ-free animals were more radioresistant than those conventionally raised (Crawford and Gordon, 2005). In this study, mice were exposed to 16 Gy of radiation and given bone marrow transplants to allow them to survive H-ARS. Colonization of germ-free mice with *Bacteroides thetaiotaomicron* (obligate anaerobe) and/or *E. coli* (facultative anaerobe) prior to irradiation did not affect the relative radio-resistance of the germ-free mice, indicating that these species were not responsible for the radiation sensitivity of the mice with normal gut flora. In another study, mouse models of both TBI and fractionated total abdominal irradiation (TAI), in which 8 fractions of 4 Gy radiation was delivered to the mouse abdomen, were examined (Riehl et al., 2019). Pre-irradiation administration of lipoteichoic acid was found to protect mice given 7 or 8 fractions of radiation by 50%. Others utilized a localized rectal irradiation mouse model, which simulates pelvic radiation therapy provided in the clinic, finding a disruption in the colonic microbiome accompanied by an increase in TNFα, IL-1β, and IL-6 in the irradiated mice. These results suggest that radiation-induced disruption of the gut flora increases levels of pro-inflammatory cytokines (Gerassy-Vainberg et al., 2018). In other experiments utilizing a TBI mouse model (8.0–9.2 Gy), the role of the microbiome of "elite survivor" mice and its radioprotective effects were explored (Guo et al., 2020). This study is discussed in more detail below.

Although these models that provide information on the interplay between the gut microbiome and the immune system may mimic clinically relevant radiation exposures, they are not aligned with models currently being used to test radiation MCMs. Focal or organ-based radiation exposures do not simulate the expected situation in a mass casualty event, in which outcomes would be based on most if not all tissues being exposed to high radiation doses. Currently accepted irradiated animal models use shielding of ~2.5–5% of the bone marrow as discussed above, which provides sufficient sparing to allow for survival past the H-ARS phase (Booth et al., 2012; MacVittie et al., 2019). Therefore, studies using these relevant animal models are needed to better understand the potential impact of the microbiome in radiation exposures similar to those expected during a public health emergency.

The gut microbiome has also been studied indirectly in animal models of radiation injury by testing various antibiotic regimens. The choice of antibiotics in these rodent studies has been influenced by clinical practice and recommendations for patients from groups such as the Infectious Diseases Society of America (IDSA) (Freifeld et al., 2011). Radiation exposure leads to bone marrow myelosuppression, and the neutropenic patient is susceptible to bacteremia from gut bacteria translocation (Waselenko et al., 2004). Therefore, studies were carried out to determine if mitigation of neutropenia can affect survival and other outcomes in animal models subjected to lethal doses of radiation (Plett et al., 2012; Farese et al., 2013; Chua et al., 2014; Hankey et al., 2015; Zhong et al., 2020). These experiments showed that administration of granulocyte (G)– or granulocyte–macrophage (GM)–colony-stimulating factor (CSF) rescued animals from H-ARS and reduced bacteremia in the nonhuman primate (NHP). The use of antibiotics in treatment of radiation exposure is further discussed below.

While mouse models are frequently studied to determine involvement of the microbiome in radiation exposure outcomes, other models have been adapted to explore the relationship between radiation and the microbiome. For example, a TBI rat model (employing single or fractionated radiation exposures) has been used to examine changes in 16S rRNA gene sequences from fecal samples (Lam et al., 2012). Although the goal was to develop a predictive biomarker for gut

radiation exposure, the pattern of changes in the microbiome could not be compared to radiation-induced microbiome changes in other animal model species. Even germ-free mice that have undergone fecal microbiota transplantation (FMT) with human microbiota do not fully recapitulate the physiological human microbiota and microbiome, likely due to species microenvironmental differences (Turnbaugh et al., 2009; Nguyen et al., 2015). FMT is discussed in more detail below.

A number of large animal models of H- and GI-ARS have been developed to improve the understanding of the natural history of radiation injuries. These models include NHPs, typically Chinese rhesus macaques (*Macaca mulatta*), and Göttingen minipigs (*Sus scrofa domestica*). These models have been developed as preclinical models to more closely represent human anatomy, tissue structures, and physiology, and to predict human responses to radiation (MacVittie et al., 2012; MacVittie et al., 2012; Elliott et al., 2014). For example, researchers have examined microbiome changes following TBI in both of these larger animals (Carbonero et al., 2018; Carbonero et al., 2018). These studies suggest that the minipig microbiota may more closely reflect that of humans, with a similar distribution and response to radiation exposure. Examining 16S rRNA from pre- and postirradiation fecal samples revealed that some bacterial species normally found intracellularly, and not in the colonic lumen, were increased in postirradiation fecal samples in both minipigs and mice. Although there were some similarities in the microbiome profiles among the mouse, rhesus macaque and minipig models (Goudarzi et al., 2016; Casero et al., 2017; Carbonero et al., 2018; Carbonero et al., 2018; Gerassy-Vainberg et al., 2018), there were also notable differences. Therefore, application to the human experience should be approached with caution. In addition, the minipig model uses a higher level of shielding (55%) that would not necessarily be as applicable to a mass casualty situation (Measey et al., 2018; Measey et al., 2018). Also noteworthy is that animal care procedures can influence these results. For example, NHPs included in these studies received antibiotics for 3 days after irradiation, potentially confounding the microbiome results. These inter-species comparisons reinforce that for these animal models to be useful, they must ultimately be linked to the growing knowledge of the human microbiome and the effects of irradiation on people. Additionally, it is important to note that the nature of animal models including closely related strains of species and "well-housed environments" affect the microbiome in ways not reflective of real-world scenarios.

THE EFFECTS OF THE MICROBIOME ON THE RADIATION RESPONSE

The delicate balance between the host and its microbiota can affect patient outcomes in the areas of cancer (Liu et al., 2019), immuno- (Sivan et al., 2015; Tanoue et al., 2019), and radiotherapy (Roy and Trinchieri, 2017), as well as colorectal surgery (Chen et al., 2018). The host–microbiota interaction is a symbiotic one that needs careful consideration as potential MCMs are proposed to modulate the microbiota. Consequently, approaches such as antibiotics, probiotics, dietary modifications (including prebiotics, vitamins, and minerals), and fecal microbiota transplant could represent treatments that may alter survival outcomes after radiation exposure **(Table 2)**. Additionally, changes in the microbiota could be used as biomarkers to indicate the severity of radiation injury and/or the efficacy of treatments. Below are targeted treatments that modulate the microbiome and in turn minimize radiation injuries.

TABLE 2 | Targeted treatments that modulate the microbiome and radiation response.

Antibiotics	Doxycycline (Plett et al., 2012) Neomycin (Plett et al., 2012) Enrofloxacin (Waselenko et al., 2004) Tetracycline (Waselenko et al., 2004) Ciprofloxacin (Plett et al., 2012)
Probiotics	*Lactobacillus rhamnosus* GG (LGG; Culturelle®) (Dong et al., 1987) *Bifidobacterium longum* (Khailova et al., 2013) *Lachnospiraceae* (Guo et al., 2020) *Enterococcaceae* (Guo et al., 2020) *Lactobacillus reuteri*-producing IL-22 (Zhang et al., 2020)
Diet	Prebiotics: non-digestible dietary fibers (e.g., apple pectin) (Garcia-Peris et al., 2016; Yang et al., 2017) Hydrogen-water (Xiao et al., 2018) Omega-3 polyunsaturated fatty acids (Zhang et al., 2019) Vanillin (Li et al., 2019) Vitamins D, E, and C (Huang et al., 2019; Segers et al., 2019) Flavonoids (Turner et al., 2002) Polyphenols (Turner et al., 2002) Folic acid (Turner et al., 2002)
Fecal Microbiota Transplant	Short-chained fatty acids (Li et al., 2020; Xiao et al., 2020) Indole 3-propionic acid (Li et al., 2020; Xiao et al., 2020)
Others	4-Nitro-phenyl-piperazine pharmacophore (Micewicz et al., 2019) Phycocyanin (Lu et al., 2019)

Antibiotics

Similar to H-ARS, chemotherapy can induce myelosuppression in cancer patients, resulting in increased risk of infection. Thus, the IDSA has published guidelines recommending neutropenic cancer patients be given fluroquinolone antibiotics (Freifeld et al., 2011). As it is likely that antibiotics will be first-line therapeutics in the event of a mass casualty radiation emergency (Coleman et al., 2015), this IDSA recommendation was initially put forward as a recommendation of the Strategic National Stockpile Radiation Working Group, convened in 2002 (Waselenko et al., 2004). This guidance is supported by studies carried out in mice at various institutions. For example, in developing a model of H-ARS, investigators tested several antibiotic regimens in mice given various doses of TBI—finding MST was increased

in antibiotic-treated mice, although levofloxacin did not provide a better outcome than ciprofloxacin (Plett et al., 2012). They also found that the use of different combinations of antibiotics (e.g., doxycycline + neomycin) increased survival (Plett et al., 2012).

Additionally, iliac bacteria counts in mice exposed to 10 Gy of TBI were found to be reduced, and anaerobe repopulation was delayed (Brook et al., 1988). Anaerobic bacteria appear to be protective, as treatment with metronidazole caused a further decrease in the anaerobic population and quicker onset of mortality. A subsequent review (Brook et al., 2004) noted that administration of quinolones to mice reduced levels of Gram-negative aerobes while sparing the anaerobic population, which is in alignment with IDSA guidelines and is the preferred choice.

Researchers have long known that administration of antibiotics to irradiated animals can affect their survival, as noted above. This modification has generally been attributed to the ability of these molecules to reduce the likelihood of opportunistic infections in animals that are immunosuppressed—but what if the efficacy could also involve a more direct modification of the natural flora of the animal? Fluoroquinolones, such as enrofloxacin and tetracycline, have been shown to reduce radiation damage to hematopoietic progenitor cells grown in culture. Thus, the radiation dose-modifying effect of some antibiotics may allow them to serve as radiation mitigators in addition to their ability to slow the growth of microbes (Epperly et al., 2010). These findings were further explored in another model of GI-ARS that demonstrated that oral fluoroquinolones also led to higher survival rates in irradiated mice (Booth et al., 2012). In a mouse model of radiation combined injury, ciprofloxacin provided similar protection (Kiang et al., 2014), and in a TAI model, where radiation exposure was used to reduce the number of GI microbes, a cocktail of antibiotics given prior to radiation exposure improved bacterial regrowth in the gut (Zhao et al., 2020).

In addition, the use of acidified water, which is frequently employed in animal colonies, could mask the impact of radiation-induced GI injury. Acid water (pH 2.5–3.0) is used to prevent bacterial infections from spreading within an animal colony.[1] It is often accomplished using hydrochloric or sulfuric acid or tetracycline (Hermann et al., 1982). Its use provides protection not only primarily against *Pseudomonas aeruginosa* but also against other Gram-negative organisms (Small and Deitrich, 2007), and in mouse models, water acidification has been shown to reduce the diversity of the gut microbiome (Sofi et al., 2014). Therefore, researchers considering the use of radiation injury models to study microbiome traits should be aware of these kinds of husbandry details in their animal facilities.

Probiotics

The idea of altering the host microbiome was first introduced by Russian embryologist Elie Metchnikoff in the early 1900s (Podolsky, 2012). In the 1990s, a resurgence of probiotic research occurred and only in 2001 was the term "microbiome" used in the literature to describe the collective genome in a host. In late 2001, the Food and Agriculture Organization of the United Nations and the World Health Organization held an expert consultation in Cordoba, Argentina, to evaluate the health and nutritional properties of probiotics in food, which led to a joint report to provide assessment and safety guidelines for research in the field (Food and Agriculture Organization of the United Nations World Health Organization, 2006). Since then, many studies have demonstrated the beneficial effect that live, naturally occurring microorganisms can have on the immune system (Hardy et al., 2013; Peters et al., 2019), gut (Gourbeyre et al., 2011; Quigley, 2012), food allergies (Di Costanzo et al., 2020), colon (Pujo et al., 2020; Wang et al., 2020), skin (Friedrich et al., 2017; Patra et al., 2020), and central nervous system (Kim et al., 2020; Loniewski et al., 2020). Of particular importance for this review are the therapeutic effects of probiotics that are seen when these systems are exposed to ionizing radiation.

The Institut des Maladies de l'Appareil Digestif conducted a systematic review of six preclinical and seven clinical studies (Touchefeu et al., 2014), which found that decreases in *Bifidobacterium*, *Clostridium cluster XIVa, Faecalibacterium prausnitzii*, and increases in *Enterobacteriaceae* and *Bacteroides* after radiotherapy contributed to GI mucositis, leading to increased diarrhea and bacteremia. Many probiotic strains were investigated as preventative therapeutics, most of which led to a reduction in diarrhea or bacteremia incidence. Another systematic review considered 15 clinical trials studying varied GI pathologies (Picó-Monllor and Mingot-Ascencao, 2019). They concluded that a combination of probiotics could reduce the incidence of mucositis in chemo- or radiotherapy-treated patients. Likewise, a meta-analysis of randomized controlled trials showed that supplementation with *Lactobacillus acidophilus* plus *Bifidobacterium bifidum* had a modest effect at preventing radiation-induced diarrhea after abdominal or pelvic radiotherapy (Liu et al., 2017). Clearly, probiotics within *Lactobacillus* and *Bifidobacterium* genera were found effective in many of the trials.

Nonpathogenic bacterial species in genera such as *Lactobacillus* and *Bifidobacterium* are commonly used and have demonstrated a wide range of health benefits (Hardy et al., 2013). Understanding the role these bacteria play in the processing and biotransformation of xenobiotics or foreign compounds (e.g., drugs and antibiotics) in the host gut can lead to personalized therapeutics to avoid or circumvent antibiotic resistance (Maurice et al., 2013). In the case of a mass casualty radiation emergency, antibiotics will likely be used as first-line therapeutics (Coleman et al., 2015). Therefore, understanding this interplay will be essential to selecting the proper antibiotics. It may also be possible to co-administer a probiotic that can manage the microbial variability of the human gut.

Research on the potential for probiotics to serve as radiation MCMs is limited; however, the prophylactic use of probiotics has been explored extensively. The knowledge gained about underlying mechanisms in these kinds of studies could lead to druggable pathways and aid in the development of MCMs,

[1]https://www.avidityscience.com/media/wysiwyg/4230-MI4179_-_Drinking_Water_Acification.pdf.

specifically to address GI-ARS. For example, death was delayed for mice fed *Lactobacillus rhamnosus* GG (LGG) prior to exposure to 14 Gy of TBI (Dong et al., 1987). LGG, the first bacterial strain to be patented in 1989, has since demonstrated benefit against GI issues (Dong et al., 1987; Ciorba et al., 2012; Capurso, 2019; Riehl et al., 2019), perhaps by altering the immune system (Capurso, 2019), and protecting intestinal epithelium (Riehl et al., 2019). In another study, LGG protected the intestinal epithelium in mice that were administered the probiotic or LGG-conditioned media by oral gavage, 3 days prior to 12-Gy TBI (Ciorba et al., 2012). Researchers showed that LGG administration prior to irradiation increased the number of regenerative crypt cells and reduced epithelial cell apoptosis. This effect was observed both for mice administered LGG and mice administered LGG-conditioned media. Moreover, a head-to-head comparison of commercially available probiotics demonstrated that Culturelle offered a similar level of radioprotection to that produced by live, cultured LGG; however, protection was not provided by another non-*Lactobacillus*, commercially available probiotic (*B infantis* 35624; Align) (Ciorba et al., 2012). Administration of probiotics (LGG and *Bifidobacterium longum*) has also been shown to improve survival in pediatric mice after the onset of sepsis resulting from a cecal ligation and puncture (Khailova et al., 2013). In addition, several probiotic species were shown to be effective at displacing dangerous enteropathogens (Candela et al., 2008). Together, these studies suggest that *Lactobacillus* may be the probiotic genus of choice for ameliorating radiation-induced GI injury.

Lactobacillus is a member of the Firmicutes phylum, and another recent study found elevated Firmicutes bacteria levels in irradiated mice were associated with a survival benefit. Mice exposed to 9.2-Gy TBI that had an abundance of bacteria in the *Lachnospiraceae*, and *Enterococcaceae* families present in their gut had a significant survival advantage or were considered "elite-survivors" (Guo et al., 2020). Upon exposing germ-free mice to "elite-survivor" dirty cages or FMT via oral administration of feces, specific pathogen-free mice had significantly higher rates of survival than non-FMT controls. To substantiate these findings in humans, researchers also looked at fecal samples from 21 leukemia patients undergoing TBI as a pre-hematopoietic stem cell transplant conditioning. Patients with higher levels of *Lachnospiraceae* and *Enterococcaceae* generally had shorter bouts of diarrhea, as well as increased levels of propionate and tryptophan metabolites (Guo et al., 2020).

Second-generation probiotics are also being developed to take advantage of the natural properties of these bacteria, using microbial-mediated delivery of drugs to target the gut. Researchers have engineered probiotics that produce IL-22 (Zhang et al., 2020), a cytokine with anti-inflammatory properties known to stabilize both intestinal Paneth cells and Lgr5+ intestinal stem cells (Zha et al., 2019). In this study, C57BL/6 mice were exposed to 9.25-Gy TBI and then treated with *Lactobacillus reuteri*–producing IL-22 strains postirradiation via oral gavage. A 30% improvement in survival was noted, as compared to animals dosed only with the IL-22 protein. Time of administration of the bacteria was also examined, and a survival advantage could be seen even when dosed at 72-h postirradiation, with the highest benefit seen at 24 h (85%) and 48 h (70%) postirradiation administration (Zhang et al., 2020).

Probiotics may be therapeutic in systems beyond the GI. Oral probiotics have been found to affect microbial communities and local inflammation within these axes as well as the vaginal microbiota (Petricevic et al., 2008), skin (Eslami et al., 2020), and more. Additionally, the emerging information in the area of microbiome/gut–brain axis opens up new opportunities for the development of effective treatments for CNS disorders. Changes in the gut microbiota postirradiation have been associated with psychoneurological symptoms in cancer patients (Bai et al., 2020). Psychobiotics (bacterially mediated biotherapeutics, which include probiotics, prebiotics, and synbiotics—a combination of probiotics and prebiotics) are currently being investigated for their potential in treating neurologic disorders. Psychobiotics can be delivered through supplements, functional foods, and dietary changes (Long-Smith et al., 2020).

As the field of probiotics has continued to mature, researchers have found that synbiotics may provide a superior outcome than either one alone, by providing an optimal GI environment to allow the probiotics to survive and colonize the gut (Markowiak and Śliżewska, 2017). Another important consideration is the risk associated with certain strains of probiotics such as the *Enterococcus* genus, which can acquire antibiotic resistance and become pathogenic. To date, no enterococcal probiotics have been approved for human use, leading the European Food Safety Authority to conclude that "*Enterococci* do not meet the standard for Qualified Presumption of Safety" (Wang et al., 2020). Given these data, along with studies showing their systemic effects (Valdéz et al., 2005; Petricevic et al., 2008; Keely et al., 2012), probiotics are a promising potential treatment for GI-ARS and other radiation injuries.

Diet, Prebiotics, Vitamins, and Minerals

In considering the GI microbiome, dietary supplementation can play a major role in the composition of gut bacteria and impact of radiation exposure. For example, normal tissue injuries from administration of abdominal radiotherapy to treat gynecologic malignancies can sometimes evolve into chronic radiation enteritis. Therefore, a clinical trial (NCT01549782) was carried out to study the effect of consumption of certain prebiotics, in this case fiber and plant sugars, on stool consistency in postirradiation patients (Garcia-Peris et al., 2016). Some improvement was noted in the group that consumed the prebiotic diet (reduction in days of diarrhea), suggesting that these dietary changes could lead to improved quality of life for these patients. Although the causal role of modulating microbiome by supplements to improve radiation injury resulting from accidental exposure to large doses is not as widely published, supplements are reported to protect gamma-irradiated mice (Shimoi et al., 1994) and improve survival (Satyamitra et al., 2011; Obrador et al., 2020). However, there are conflicting reports that underscore the need for caution in the use of all supplements without supporting data. For instance, investigators reported that high-protein diet such as methionine-supplemented diet (MSD) is used to build muscle

mass in patients undergoing chemo- and/or radiotherapy; however, when this diet was fed to CBA/CaJ mice exposed to 3–8.5 Gy of TBI, the mice developed acute radiation toxicity, even at sublethal doses of 3 Gy, and demonstrated higher mortality (Miousse et al., 2020). Another study reported that MSD increased GI toxicity in abdominal irradiated CBA/CaJ mice, with a concomitant shift in gut microbiome, reduction in microbiome diversity, and significant increase in pro-inflammatory genus *Bacteroides* (Ewing et al., 2021). In addition, omega-3 polyunsaturated fatty acids were shown to reduce intestinal inflammation following radiotherapy (Zhang et al., 2019), a finding that was attributed to its ability to reduce oxidative stress in the GI tract. Similarly, consideration of the diet of astronauts has been a major source of concern, since space flight involves exposure to cosmic radiation (Turner et al., 2002). By providing extra antioxidants to the diet, in the form of vitamins such as E and C, as well as flavonoids, polyphenols, and folic acid, it may be possible to modify the composition of gut bacteria and reduce the risks associated with radiation exposure. This could be applicable to a wide range of scenarios involving radiation exposure including during space missions.

Prebiotics

The microbiome can be altered by various factors, but nondigestible dietary fibers, which serve as a food source, and can greatly influence the expansion of certain bacteria (Villéger et al., 2019). By regulating the presence or absence of key prebiotics, the microbiota can be changed, and thus, the metabolites produced by specific bacterial strains can also be enhanced to promote a positive outcome for the irradiated host (Louis et al., 2014). The addition of prebiotics has been shown to change the microbial community in the GI tract of irradiated mice and reduce intestinal permeability, leading to a decrease in the expression of inflammatory and oxidative stress markers (Cani et al., 2009). Another study showed that apple pectin could protect the terminal ileum and ameliorate radiation-induced intestinal fibrosis in mice by increasing the levels of short-chain fatty acids and altering the intestinal microbiota (Yang et al., 2017). Additionally, hydrogen-water has been associated with ameliorating radiation-induced GI toxicity by maintaining a healthier gut microbiota composition (Xiao et al., 2018). Omega-3 polyunsaturated fatty acids have been shown to reverse intestinal microbial dysbiosis by increasing beneficial bacteria such as *Lactobacillus* and *Bifidobacterium* genera after chemotherapy and radiotherapy (Zhang et al., 2019). Prebiotics offer a source of enrichment to the microbiome; thus, their use can help optimize the gut flora and thereby regulate immune function. Such dietary interventions have a demonstrated role in the control of the inflammatory response and can potentially serve as a way to regulate inflammation after exposure to ionizing radiation.

A plant compound derived from vanillin (VND3207), a flavoring agent, has also been shown to mitigate GI-ARS through its action on modifying the composition of the bacteria in the gut (Li et al., 2019). C57BL/6J mice were irradiated (9-Gy TBI) and treated orally with VND3207 either prior to or following exposure. Animals that were pretreated had the greatest improvement in survival, although those treated postirradiation also saw a statistically significant survival benefit. Researchers determined that the structures of the microbiome of the gut were modified by the radiation exposure, and treatment with VND3207 modified the relative quantities of different bacterial species back to the level of unirradiated mice.

Vitamins and Minerals

Vitamin D has received attention for its role in immunity and inflammation (Lucas et al., 2014) and can be considered a master regulator in the modulation of the host microbiome (Ghaly et al., 2019). It contains fat-soluble secosteriods, responsible for absorption of calcium, magnesium, phosphate, and other trace elements needed for healthy biological functions (Huang et al., 2019). Vitamin D has also been associated with the treatment of inflammatory bowel disease (Fletcher et al., 2019), colorectal cancer (Abrahamsson et al., 2019), radiation dermatitis (Nasser et al., 2017), and pelvic radiotherapy (Castro-Eguiluz et al., 2018). Approximately 60% of radiotherapy patients receive vitamin D supplementation, as it is thought to enhance radiation resistance of healthy tissues by multiple mechanisms that reduce tissue inflammation and help with intestinal barrier function, by way of the microbiota (Huang et al., 2019). Studies with vitamin D–deficient mice showed a depletion of *Lactobacillus* and an enhancement of enteropathogens such as *Clostridium* and *Bacteroides* genera (Jin et al., 2015). In summary, vitamin D has been shown to play a key role in radiation resistance, but the underlying molecular mechanisms of its influence on the microbiome has yet to be completely elucidated. Some of these mechanistic pathways may be potential areas of exploration for MCM discovery.

It should be noted, however, that not all dietary approaches have proven to be successful in reducing the incidence of GI complications following anti-cancer radiotherapy. For example, a clinical trial that studied oral starch supplements to reduce radiation proctitis did not meet its primary endpoint in patients irradiated for cervical cancer (Sasidharan et al., 2019). Furthermore, in a mouse model of lethal radiation exposure, mice that received dietary supplementation with methionine were found to be more sensitive to GI-ARS (Miousse et al., 2020). Carried out in a PBI (hind leg shielded) model, investigators showed a change in the gut microbiome of the supplemented animals, which progressed to leakage, bacterial translocation, decreased citrulline levels, fewer crypts, and a reduced luminal surface area.

In a recent review, it was pointed out that clinical trials investigating the use of dietary modifications to mitigate the adverse effects associated with normal tissue injuries during radiation therapy involving the pelvis have yielded contradictory results (Segers et al., 2019). Approaches such as vitamins, pre- and probiotics, and a variety of food supplements have had varying degrees of success, leading the authors to conclude that clinical trial parameters involving reinforcing the gut microbiome with natural products should involve more definitive study endpoints and greater control of quality and optimization of dosing.

Fecal Microbiota Transplant (FMT)

A novel investigative treatment is the use of FMT. Briefly, fecal material is obtained from a screened, healthy donor (or in the case of radiation exposure, an unirradiated host) followed by a dilution, homogenization, and filtration processing. The resulting preparation is then administered to the colon of the recipient, either through oral ingestion of a capsule, or via colonoscopy or enema. In preclinical studies, animals are typically fed donor feces. Initially conceived as a means of correcting the microbiome imbalance in individuals suffering from chronic GI infections, the therapy has completed a randomized, controlled clinical trial for treatment of antibiotic-resistant *Clostridium difficile* infection (Kelly et al., 2021). The therapy is believed to work by "out-competing" growth of *C. difficile* with other more protective species. Studies have shown that this treatment can mitigate infections in 80–90% of patients (van Nood et al., 2013). FMT procedures have also been studied to address a number of different disease states, such as multiple sclerosis (NCT03975413), diabetes (NCT04124211), autism (NCT03408886), AIDS (NCT02256592), and liver diseases (NCT03152188) (Lo, 2019). These findings of efficacy across multiple organ systems and disease states are not surprising, given the acknowledged role of the GI microbiome in the "gut–brain–skin axis" (Vojvodic et al., 2019) and the "gut–lung axis" (Dumas et al., 2018; Nie et al., 2020), which involve a close interplay between the systems and regulation by signaling molecules. Therefore, balance of microbes in the GI tract is important for maintenance of many conditions outside the gut.

Preclinical FMT Studies

Microbiome and FMT studies have been conducted in many animal models, including mice (Chen et al., 2020), rats (Yu et al., 2020), chickens (Metzler-Zebeli et al., 2019), pigs (McCormack et al., 2019), and NHPs (Hensley-McBain et al., 2016). There are many publications that document the potential for this unorthodox therapy (Wang et al., 2016; Cui et al., 2017; McIlroy et al., 2018; Villéger et al., 2019). For the purposes of this review, the focus will be only on its use for indications involving radiation.

The possible role of gut bacteria in the biological radiation response was suspected even as early as 1963, with the germ-free mice studies by Wilson (1963) and McLaughlin et al. (1964) discussed earlier. There have been several avenues of research that have specifically explored whether FMT could protect against high dose, TBI, or PBI exposures, which can lead to the development of the ARS. In one study, researchers noted that the composition of bacteria varied between male and female mice, a finding that correlated with the animal's radiation sensitivity (Cui et al., 2017). When provided with FMT via oral gavage for 10 days using same-sex or opposite-sex donors, C57BL/6 mice exposed to 6.5-Gy TBI had increased survival, which was found to be highest when the donor sex matched the recipient. Function and continuity of the GI tract was also found to be improved in FMT-treated animals. Earlier studies by the same group had suggested that the known circadian rhythms affecting radiation sensitivity could also be linked to different bacteria present in the guts of animals subjected to altered light/dark cycles (Cui et al., 2016). In another study carried out in irradiated germ-free mice, fecal transfer from irradiated mice exhibiting radiation-induced dysbiosis to germ-free mice transmitted inflammatory susceptibility and increased susceptibility to GI radiation injury, which appeared mediated by IL-1β (Gerassy-Vainberg et al., 2018). As mentioned earlier, researchers showed that mice who received fecal engraftment from "elite survivor" mice had higher survival following TBI (Guo et al., 2020), further supporting the prospect of utilizing FMT as a MCM.

To exploit the many microbiota and functional changes observed with animal models in response to radiation, studies have been done to evaluate the usefulness of microbiota-derived short-chain fatty acids and other metabolic products as potential MCMs, to either prevent or mitigate radiation-induced GI injury. In a study in which FMT was given to irradiated mice, analysis of fecal pellets showed that a microbial molecule—indole 3-propionic acid (IPA)—was present at high levels (Xiao et al., 2020). Believing that this molecule could be responsible for the observed radiation protection obtained with FMT, oral IPA alone was provided to another group of irradiated animals. Treated animals had decreased inflammation and improved GI function after irradiation, suggesting its possible use as an effective MCM or radiotherapy treatment. Other studies found oral gavage of IPA and microbiota-derived valeric acid (VA) provided protection against up to 7 Gy, and, in the case of VA, mitigated GI radiation injury when given post-TAI (12 Gy). VA was found to prevent intestinal inflammation and dysfunction, and maintain microbiota compositional patterns (Li et al., 2020; Xiao et al., 2020).

The potential use of FMT has also been considered as a means of mitigating late effects attributable to prior radiation exposure, including in organ systems outside the GI tract. Given the "gut–lung axis" mentioned earlier, the GI microbiome is known to play a role in lung immunity; therefore, this finding has been explored as a potential treatment for pneumonitis in lung cancer patients treated with radiation (Nie et al., 2020). To study this, C57BL/6 mice were provided antibiotics prior to irradiation. In those animals, there was higher radiation mortality and more weight loss than in control animals. In addition, higher levels of lung damage were observed. When the same animals were then treated using FMT from untreated, unirradiated animals, lung inflammation and tissue damage were decreased, along with an alteration of the bacterial colonies found in the GI tract. The authors suggested that the tissue-type plasminogen activator might be involved in the inflammatory process.

Clinical FMT Studies

To date, there are more than 380 clinical trials[2] involving FMT, many of which investigate FMT as a treatment for GI-targeted diseases such as *C. difficile* (Shogbesan et al., 2018), inflammatory bowel (Browne & Kelly, 2017), Crohn's ulcerative colitis (Paramsothy et al., 2017; Blanchaert et al., 2019), chronic constipation (Ge et al., 2017), and radiation enteritis

[2]www.clinicaltrials.gov.

(NCT03516461). In the field of cancer and radiation oncology, radiation therapy to the pelvic or abdominal area is known to lead to GI damage in up to 50% of patients (Benson 3rd et al., 2004). A 2014 review explored the published literature for evidence that the GI tract microbiome played a role in this kind of damage (Touchefeu et al., 2014). Owing to these findings, clinicians began to consider the potential of FMT in radiotherapy, where a link was made between the microbiome of the GI tract and success of stem cell transplants for leukemia (Dougé et al., 2020). Results suggested that FMT could be used to rebalance the bacterial composition of the gut, and thereby reduce posttransplant complications. In addition, FMT has been proposed as a means of addressing chronic radiation enteritis, which has major quality-of-life implications. One trial (NCT03516461) of five female patients receiving pelvic radiotherapy found that FMT could mitigate serious chronic radiation enteritis-related complications such as diarrhea, bleeding, pain, and fecal soiling, and demonstrated the procedure to be safe (Ding et al., 2020). However, results suggest that caution should be employed when considering the use of FMT. For example, one case study described the use of FMT in a female patient who had received radiotherapy localized to the cervix (30×8 Gy) for treatment of a gynecologic cancer (Harsch and Konturek, 2019). The radiation treatment led to unpleasant GI complications that included diarrhea, malabsorption, and stenosis of the sigmoid portion of the colon, which she lived with for 17 years. When other therapies, including probiotics and dietary changes, did not provide relief, FMT was considered. Several days later after the transplant, the formation of a small bowel obstruction led to emergency surgery. Given the speed with which this complication arose after the FMT, clinicians speculated that the introduction of new species into the colon could have led to "trapping of a gut segment." In summary, the use of FMT as a means of addressing radiation-induced injuries, not only to the GI tract but also to other organ systems, represents an intriguing possible treatment.

Other Treatments for Radiation Injury Targeting the Microbiome

Novel therapeutics are being developed in search of effective MCMs against ARS, including radiation mitigators that have a common 4-nitro-phenyl-piperazine pharmacophore (NPSP) (Micewicz et al., 2019). In this study, C3H mice were exposed to an $LD_{70/30}$ dose of radiation and then treated with an NPSP mitigator. To track long-term changes in the mice microbiota, fecal samples were collected from both irradiated and control mice on days 162, 214, and 442. The colonic microbiota was analyzed by 16S rDNA enrichment and sequencing, showing a consistent level of Firmicutes-to-Bacteroidetes composition in both treated and control mice until day 214. At this point, mice treated with NPSP 5355512 exhibited a decreased amount of Bacteroidetes, while the level of Firmicutes increased as compared to control mice (Micewicz et al., 2019). The Firmicutes-to-Bacteroidetes ratio is often analyzed as a marker for gut health but can fluctuate often and change with age (Mariat et al., 2009). While the significance of the change still needs to be elucidated, it is interesting to note that composition of the microbiome differed between the treated and non-treated groups.

Other therapeutics such as phycocyanin (PC), an active protein found in the genus *Arthrospira*, have been examined for efficacy against radiation-induced GI injury after radiotherapy. PC has been shown to have anti-inflammatory (Remirez et al., 2002) and antioxidant (Villegas et al., 2014) properties. In one study, C57BL/6 mice were administered PC daily for a month prior to an exposure of 12-Gy TAI (Lu et al., 2019). PC treatment provided protection against radiation-induced GI injury and maintained a healthier level of diversity in the microbiota, which is usually reduced after irradiation. In general, the levels of beneficial bacteria were increased, harmful bacteria were decreased, and inflammatory cytokines such as TNF-α and IL-6 were downregulated (Lu et al., 2019). Another drug simvastatin, commonly used to treat high cholesterol, has also been shown to alter the gut microbiota to provide a therapeutic advantage against radiation-induced injury in mice (Cui et al., 2019). Maintenance of a healthy gut microbiome appears to be essential in overcoming radiation-induced injury, as supported by studies that highlight the importance of this balance. It may be possible to repurpose existing products to modify the microbiome.

MICROBIOME BIOMARKERS AS BIODOSIMETERS

In the case of a radiation mass casualty incident, H-ARS and GI-ARS subsyndromes will pose an immediate public health risk (Donnelly et al., 2010). The mean lethal radiation dose in humans that will kill 50% of those exposed within 60 days ($LD_{50/60}$) is 3.25–4 Gy in the absence of supportive care but can be increased to 6–7 Gy with appropriate medical interventions (Waselenko et al., 2004). Consequently, effective triage of potentially exposed individuals in order to identify and separate those in need of immediate medical interventions (>2 Gy adsorbed dose) from the "worried well" (<2 Gy) requires a deployable biodosimetry method capable of making such distinctions so that limited medical resources can be used most efficiently (Dainiak, 2018).

In acute radiation exposure, it is possible that changes in microbial species, or metabolites released by them, can be used to assess dose received or the extent of radiation injury in a mass casualty scenario, particularly in easily accessible samples, such as feces or urine, but also in blood. As mentioned earlier, many bacterial species and microbiota changes in the skin (Plichta et al., 2017), vagina (Brotman et al., 2014; Bai et al., 2019), oral cavity (Vanhoecke et al., 2015; Zhu et al., 2017; Hou et al., 2018; Anjali et al., 2020; Nishii et al., 2020; Vesty et al., 2020), and GI of humans (Lam et al., 2012; Guo et al., 2020) are associated with disease severity and may even be predictive of pathogenesis. Along with the finding that some radiation-induced microbiota changes are persistent out to 6 months (Lam et al., 2012; Zhao et al., 2019; Anjali et al., 2020; Nishii et al., 2020), these data support the use of the microbiota as potentially stable biomarkers for radiation exposure and injury.

Biomarkers for triage, definitive dose, predictive biodosimetry, and/or to inform treatment decisions will be needed in a mass casualty radiation scenario. Researchers have found that microbial-derived metabolic products in fecal samples were modulated in a dose- and time-dependent manner following irradiation reflecting microbiota family-level changes in rodents (Lam et al., 2012; Goudarzi et al., 2016) and NHPs (Pannkuk et al., 2017; Pannkuk et al., 2019). The feasibility of using the GI microbiome and related metabolites as biodosimeters for early triage are currently being researched (Cai et al., 2020). More content on the state of the science for metabolomics in radiation injury have been reviewed elsewhere (Ó Broin et al., 2015; Satyamitra et al., 2020). While many promising approaches (cytogenetic and multiple "omics" approaches) are currently under investigation to identify dose-dependent biomarkers with the potential to provide rapid field-deployable biodosimetry tests, as of the writing of this review, no FDA-cleared devices are available. Although the field is in its infancy, these data suggest that the microbiome can be a powerful tool for radiation biodosimetry.

CONCLUSION

Undoubtedly, the human microbiome is complex and varies based on its location, but regardless, it is necessary to maintain organ, tissue, and immune homeostasis. When the delicate balance of commensal bacteria is disrupted, it can result in a perturbation of the resident microbiota and wreak havoc on the host. Of particular interest for this review is the effect of ionizing radiation on the GI, lung, and skin microbiomes. Radiation not only changes the flora in these and other systems but also causes a breakdown of the epithelial barrier integrity, affecting the ability of the GI tract, lung, and skin to protect the host from invasive pathogens. Given the serious impact radiation has on these environments, it is imperative that treatment options or MCMs that can restore the human microbiota or provide an advantage under these harsh conditions continue to be explored.

Understanding the essentials of what is needed to support a healthy microbiome niche can help provide insight about key metabolites and molecular signatures that could be used as predictive biomarkers or developed into drugs to restore homeostasis. This knowledge can also be harnessed to take advantage of the microbes and develop microbial-mediated drugs to target a particular niche. Overall, the wealth of knowledge about the microbiome continues to grow, and its potential as a target for development of MCMs and/or identification of biomarkers of radiation damage continue to be discovered, with many areas yet to be explored.

AUTHOR CONTRIBUTIONS

All authors listed have made a substantial, direct, and intellectual contribution to the work and approved it for publication.

REFERENCES

Aas, J. A., Paster, B. J., Stokes, L. N., Olsen, I., and Dewhirst, F. E. (2005). Defining the normal bacterial flora of the oral cavity. *J. Clin. Microbiol.* 43 (11), 5721–5732. doi:10.1128/jcm.43.11.5721-5732.2005

Abrahamsson, H., Porojnicu, A. C., Lindstrøm, J. C., Dueland, S., Flatmark, K., Hole, K. H., et al. (2019). High level of circulating vitamin D during neoadjuvant therapy may lower risk of metastatic progression in high-risk rectal cancer. *BMC Cancer* 19 (1), 488. doi:10.1186/s12885-019-5724-z

Abreu, N. A., Nagalingam, N. A., Song, Y., Roediger, F. C., Pletcher, S. D., Goldberg, A. N., et al. (2012). Sinus microbiome diversity depletion and Corynebacterium tuberculostearicum enrichment mediates rhinosinusitis. *Sci. Translational Med.* 4 (151), 151ra124. doi:10.1126/scitranslmed.3003783

Alexander, C., Bader, J. B., Schaefer, A., Finke, C., and Kirsch, C. M. (1998). Intermediate and long-term side effects of high-dose radioiodine therapy for thyroid carcinoma. *J. Nucl. Med.* 39 (9), 1551–1554.

Andersson, J., Vogt, J. K., Dalgaard, M. D., Pedersen, O., Holmgaard, K., and Heegaard, S. (2021). Ocular surface microbiota in patients with aqueous tear-deficient dry eye. *Ocul. Surf.* 19, 210. doi:10.1016/j.jtos.2020.09.003

Anjali, K., Arun, A. B., Bastian, T. S., Parthiban, R., Selvamani, M., and Adarsh, H. (2020). Oral microbial profile in oral cancer patients before and after radiation therapy in a cancer care center - a prospective study. *J. Oral Maxillofac. Pathol.* 24 (1), 117–124. doi:10.4103/jomfp.JOMFP_213_19

Appanna, V. D. (2018). The microbiome: genesis and functions. *Human microbes - the power within: health, healing and beyond*. Singapore: Springer Singapore, 37–79. doi:10.1007/978-981-10-7684-8_3

Araghi, A. (2020). The lung microbiome and pneumonia: where precision medicine meets pulmonology. *Pulmonology* 26 (6), 333–334. doi:10.1016/j.pulmoe.2020.04.005

Aragón, I. M., Herrera-Imbroda, B., Queipo-Ortuño, M. I., Castillo, E., Del Moral, J. S.-G., Gómez-Millán, J., et al. (2018). The urinary tract microbiome in health and disease. *Eur. Urol. Focus* 4 (1), 128–138. doi:10.1016/j.euf.2016.11.001

Arumugam, M., Raes, J., Raes, J., Pelletier, E., Le Paslier, D., Yamada, T., et al. (2011). Enterotypes of the human gut microbiome. *Nature* 473 (7346), 174–180. doi:10.1038/nature09944

Bäckhed, F., Ley, R. E., Sonnenburg, J. L., Peterson, D. A., and Gordon, J. I. (2005). Host-bacterial mutualism in the human intestine. *Science* 307 (5717), 1915–1920. doi:10.1126/science.1104816

Bai, J., Jhaney, I., Daniel, G., and Watkins Bruner, D. (2019). Pilot study of vaginal microbiome using QIIME 2™ in women with gynecologic cancer before and after radiation therapy. *Oncol. Nurs. Forum* 46 (2), E48–e59. doi:10.1188/19.Onf.E48-e59

Bai, J., Bruner, D. W., Fedirko, V., Beitler, J. J., Zhou, C., Gu, J., et al. (2020). Gut microbiome associated with the psychoneurological symptom cluster in patients with head and neck cancers. *Cancers* 12 (9), 2531. doi:10.3390/cancers12092531

Bajaj, J. S., Fagan, A., Gavis, E. A., Kassam, Z., Sikaroodi, M., and Gillevet, P. M. (2019). Long-term outcomes of fecal microbiota transplantation in patients with cirrhosis. *Gastroenterology* 156 (6), 1921–1923. doi:10.1053/j.gastro.2019.01.033

Belstrøm, D. (2020). The salivary microbiota in health and disease. *J. Oral Microbiol.* 12 (1), 1723975. doi:10.1080/20002297.2020.1723975

Benson, A. B., 3rd, Ajani, J. A., Catalano, R. B., Engelking, C., Kornblau, S. M., Martenson, J. A., Jr., et al. (2004). Recommended guidelines for the treatment of cancer treatment-induced diarrhea. *Jco* 22 (14), 2918–2926. doi:10.1200/jco.2004.04.132

Bey, É., Duhamel, P., Lataillade, J.-J., de Revel, T., Carsin, H., and Gourmelon, P. (2007). Irradiation aiguë localisée : chirurgie et thérapie cellulaire. A propos de deux cas. *Bull. de l'Académie Nationale de Médecine* 191 (6), 971–979. doi:10.1016/s0001-4079(19)32994-2

Bey, E., Prat, M., Duhamel, P., Benderitter, M., Brachet, M., Trompier, F. o., et al. (2010). Emerging therapy for improving wound repair of severe radiation burns

using local bone marrow-derived stem cell administrations. *Wound Repair Regen.* 18 (1), 50–58. doi:10.1111/j.1524-475X.2009.00562.x

Biagi, E., Nylund, L., Candela, M., Ostan, R., Bucci, L., Pini, E., et al. (2010). Through ageing, and beyond: gut microbiota and inflammatory status in seniors and centenarians. *PLoS ONE* 5 (5), e10667. doi:10.1371/journal.pone.0010667

Bik, E. M., Eckburg, P. B., Gill, S. R., Nelson, K. E., Purdom, E. A., Francois, F., et al. (2006). Molecular analysis of the bacterial microbiota in the human stomach. *Proc. Natl. Acad. Sci.* 103 (3), 732–737. doi:10.1073/pnas.0506655103

Bik, E. M., Long, C. D., Armitage, G. C., Loomer, P., Emerson, J., Mongodin, E. F., et al. (2010). Bacterial diversity in the oral cavity of 10 healthy individuals. *Isme j* 4 (8), 962–974. doi:10.1038/ismej.2010.30

Blanchaert, C., Strubbe, B., and Peeters, H. (2019). Fecal microbiota transplantation in ulcerative colitis. *Acta Gastroenterol. Belg.* 82 (4), 519–528.

Booth, C., Tudor, G., Tudor, J., Katz, B. P., and MacVittie, T. J. (2012). Acute gastrointestinal syndrome in high-dose irradiated mice. *Health Phys.* 103 (4), 383–399. doi:10.1097/hp.0b013e318266ee13

Böttger, E. C. (1989). Rapid determination of bacterial ribosomal RNA sequences by direct sequencing of enzymatically amplified DNA. *FEMS Microbiol. Lett.* 53 (1-2), 171–176. doi:10.1016/0378-1097(89)90386-8

Bouskra, D., Brézillon, C., Bérard, M., Werts, C., Varona, R., Boneca, I. G., et al. (2008). Lymphoid tissue genesis induced by commensals through NOD1 regulates intestinal homeostasis. *Nature* 456 (7221), 507–510. doi:10.1038/nature07450

Brandl, K., Plitas, G., Schnabl, B., DeMatteo, R. P., and Pamer, E. G. (2007). MyD88-mediated signals induce the bactericidal lectin RegIIIγ and protect mice against intestinal Listeria monocytogenes infection. *J. Exp. Med.* 204 (8), 1891–1900. doi:10.1084/jem.20070563

Breslin, M., and Taylor, C. (2020). Incidence of new carious lesions and tooth loss in head and neck cancer patients: a retrospective case series from a single unit. *Br. Dent J.* 229 (8), 539–543. doi:10.1038/s41415-020-2222-2

Brook, I., Elliott, T. B., Ledney, G. D., Shoemaker, M. O., and Knudson, G. B. (2004). Management of postirradiation infection: lessons learned from animal models. *Mil. Med.* 169 (3), 194–197. doi:10.7205/milmed.169.3.194

Brook, I., Walker, R. I., and MacVittie, T. J. (1988). Effect of antimicrobial therapy on bowel flora and bacterial infection in irradiated mice. *Int. J. Radiat. Biol.* 53 (5), 709–716. doi:10.1080/09553008814551081

Brotman, R. M., Shardell, M. D., Gajer, P., Fadrosh, D., Chang, K., Silver, M. I., et al. (2014). Association between the vaginal microbiota, menopause status, and signs of vulvovaginal atrophy. *Menopause* 21 (5), 450–458. doi:10.1097/GME.0b013e3182a4690b

Brown, L. R., Dreizen, S., Daly, T. E., Drane, J. B., Handler, S., Riggan, L. J., et al. (1978). Interrelations of oral microorganisms, immunoglobulins, and dental caries following radiotherapy. *J. Dent Res.* 57 (9-10), 882–893. doi:10.1177/00220345780570090901

Brown, L. R., Dreizen, S., Handler, S., and Johnston, D. A. (1975). Effect of radiation-induced xerostomia on human oral microflora. *J. Dent Res.* 54 (4), 740–750. doi:10.1177/00220345750540040801

Browne, A. S., and Kelly, C. R. (2017). Fecal transplant in inflammatory bowel disease. *Gastroenterol. Clin. North America* 46 (4), 825–837. doi:10.1016/j.gtc.2017.08.005

Buchta, V. (2018). Vaginal microbiome. *Ceska Gynekol* 83 (5), 371–379.

Cai, S., Zhao, T., Xie, L., Yang, Y., Li, M., and Tian, Y. (2020). A feasibility study of gut microbiome and metabolites as biodosimeters for early triage of radiation induced intestinal injury in radiological events. *Int. J. Radiat. Oncology*Biology*Physics* 108 (3), e517. doi:10.1016/j.ijrobp.2020.07.1623

Cameron, S. J. S., Huws, S. A., Hegarty, M. J., Smith, D. P. M., and Mur, L. A. J. (2015). The human salivary microbiome exhibits temporal stability in bacterial diversity. *FEMS Microbiol. Ecol.* 91 (9), fiv091. doi:10.1093/femsec/fiv091

Campisciano, G., Florian, F., D'Eustacchio, A., Stanković, D., Ricci, G., De Seta, F., et al. (2017). Subclinical alteration of the cervical-vaginal microbiome in women with idiopathic infertility. *J. Cel. Physiol.* 232 (7), 1681–1688. doi:10.1002/jcp.25806

Campo, J., Bass, D., and Keeling, P. J. (2020). The eukaryome: diversity and role of microeukaryotic organisms associated with animal hosts. *Funct. Ecol.* 34 (10), 2045–2054. doi:10.1111/1365-2435.13490

Candela, M., Perna, F., Carnevali, P., Vitali, B., Ciati, R., Gionchetti, P., et al. (2008). Interaction of probiotic Lactobacillus and Bifidobacterium strains with human intestinal epithelial cells: adhesion properties, competition against enteropathogens and modulation of IL-8 production. *Int. J. Food Microbiol.* 125 (3), 286–292. doi:10.1016/j.ijfoodmicro.2008.04.012

Canesso, M. C. C., Vieira, A. T., Castro, T. B. R., Schirmer, B. G. A., Cisalpino, D., Martins, F. S., et al. (2014). Skin wound healing is accelerated and scarless in the absence of commensal microbiota. *J.I.* 193 (10), 5171–5180. doi:10.4049/jimmunol.1400625

Cani, P. D., Possemiers, S., Van de Wiele, T., Guiot, Y., Everard, A., Rottier, O., et al. (2009). Changes in gut microbiota control inflammation in obese mice through a mechanism involving GLP-2-driven improvement of gut permeability. *Gut* 58 (8), 1091–1103. doi:10.1136/gut.2008.165886

Capurso, L. (2019). Thirty years of lactobacillus rhamnosus GG. *J. Clin. Gastroenterol.* 53 (Suppl. 1), S1–S41. doi:10.1097/MCG.0000000000001170

Carbonero, F., Mayta, A., Bolea, M., Yu, J.-Z., Lindeblad, M., Lyubimov, A., et al. (2018). Specific members of the gut microbiota are reliable biomarkers of irradiation intensity and lethality in large animal models of human health. *Radiat. Res.* 191 (1), 107–121. doi:10.1667/rr14975.1

Carbonero, F., Mayta-Apaza, A. C., Yu, J.-Z., Lindeblad, M., Lyubimov, A., Neri, F., et al. (2018). A comparative analysis of gut microbiota disturbances in the Gottingen minipig and rhesus macaque models of acute radiation syndrome following bioequivalent radiation exposures. *Radiat. Environ. Biophys.* 57 (4), 419–426. doi:10.1007/s00411-018-0759-0

Cardis, E., and Hatch, M. (2011). The chernobyl accident - an epidemiological perspective. *Clin. Oncol.* 23 (4), 251–260. doi:10.1016/j.clon.2011.01.510

Casero, D., Gill, K., Sridharan, V., Koturbash, I., Nelson, G., Hauer-Jensen, M., et al. (2017). Space-type radiation induces multimodal responses in the mouse gut microbiome and metabolome. *Microbiome* 5 (1), 105. doi:10.1186/s40168-017-0325-z

Castro-Eguiluz, D., Leyva-Islas, J. A., Luvian-Morales, J., Martínez-Roque, V., Sánchez-López, M., Trejo-Durán, G., et al. (2018). Nutrient recommendations for cancer patients treated with pelvic radiotherapy, with or without comorbidities. *Ric* 70 (3), 130–135. doi:10.24875/RIC.18002526

Charlson, E. S., Bittinger, K., Haas, A. R., Fitzgerald, A. S., Frank, I., Yadav, A., et al. (2011). Topographical continuity of bacterial populations in the healthy human respiratory tract. *Am. J. Respir. Crit. Care Med.* 184 (8), 957–963. doi:10.1164/rccm.201104-0655oc

Chen, C., Zhang, Q., Yu, W., Chang, B., and Le, A. D. (2020). Oral mucositis: an update on innate immunity and new interventional targets. *J. Dent Res.* 99 (10), 1122–1130. doi:10.1177/0022034520925421

Chen, E. B., Cason, C., Gilbert, J. A., and Ho, K. J. (2018). Current state of knowledge on implications of gut microbiome for surgical conditions. *J. Gastrointest. Surg.* 22 (6), 1112–1123. doi:10.1007/s11605-018-3755-4

Chen, X., Li, P., Liu, M., Zheng, H., He, Y., Chen, M.-X., et al. (2020). Gut dysbiosis induces the development of pre-eclampsia through bacterial translocation. *Gut* 69 (3), 513–522. doi:10.1136/gutjnl-2019-319101

Chua, H. L., Plett, P. A., Sampson, C. H., Katz, B. P., Carnathan, G. W., MacVittie, T. J., et al. (2014). Survival efficacy of the PEGylated G-CSFs Maxy-G34 and neulasta in a mouse model of lethal H-ARS, and residual bone marrow damage in treated survivors. *Health Phys.* 106 (1), 21–38. doi:10.1097/HP.0b013e3182a4df10

Ciorba, M. A., Riehl, T. E., Rao, M. S., Moon, C., Ee, X., Nava, G. M., et al. (2012). Lactobacillus probiotic protects intestinal epithelium from radiation injury in a TLR-2/cyclo-oxygenase-2-dependent manner. *Gut* 61 (6), 829–838. doi:10.1136/gutjnl-2011-300367

Claesson, M. J., Cusack, S., O'Sullivan, O., Greene-Diniz, R., De Weerd, H., Flannery, E., et al. (2011). Composition, variability, and temporal stability of the intestinal microbiota of the elderly. *Proc. Natl. Acad. Sci.* 108 (Suppl. 1), 4586–4591. doi:10.1073/pnas.1000097107

Clevers, H. (2013). The intestinal crypt, a prototype stem cell compartment. *Cell* 154 (2), 274. doi:10.1016/j.cell.2013.07.004

Coleman, C. N., Sullivan, J. M., Bader, J. L., Murrain-Hill, P., Koerner, J. F., Garrett, A. L., et al. (2015). Public health and medical preparedness for a nuclear detonation. *Health Phys.* 108 (2), 149–160. doi:10.1097/HP.0000000000000249

Cope, E. K., Goldberg, A. N., Pletcher, S. D., and Lynch, S. V. (2017). Compositionally and functionally distinct sinus microbiota in chronic rhinosinusitis patients have immunological and clinically divergent consequences. *Microbiome* 5 (1), 53. doi:10.1186/s40168-017-0266-6

Crawford, P. A., and Gordon, J. I. (2005). From the Cover: microbial regulation of intestinal radiosensitivity. *Proc. Natl. Acad. Sci.* 102 (37), 13254–13259. doi:10.1073/pnas.0504830102

Cruz, A. D. d., Cogo, K., Bergamaschi, C. d. C., Bóscolo, F. N., Groppo, F. C., and Almeida, S. M. d. (2010). Oral streptococci growth on aging and non-aging esthetic restorations after radiotherapy. *Braz. Dent. J.* 21 (4), 346–350. doi:10.1590/s0103-64402010000400010

Cui, M., Xiao, H., Li, Y., Zhang, S., Dong, J., Wang, B., et al. (2019). Sexual dimorphism of gut microbiota dictates therapeutics efficacy of radiation injuries. *Adv. Sci.* 6 (21), 1901048. doi:10.1002/advs.201901048

Cui, M., Xiao, H., Li, Y., Zhou, L., Zhao, S., Luo, D., et al. (2017). Faecal microbiota transplantation protects against radiation-induced toxicity. *EMBO Mol. Med.* 9 (4), 448–461. doi:10.15252/emmm.201606932

Cui, M., Xiao, H., Luo, D., Zhang, X., Zhao, S., Zheng, Q., et al. (2016). Circadian rhythm shapes the gut microbiota affecting host radiosensitivity. *Ijms* 17 (11), 1786. doi:10.3390/ijms17111786

Curragh, D. S., Bassiouni, A., Macias-Valle, L., Vreugde, S., Wormald, P.-J., Selva, D., et al. (2020). The microbiome of the nasolacrimal system and its role in nasolacrimal duct obstruction. *Ophthalmic Plast. Reconstr. Surg.* 36 (1), 80–85. doi:10.1097/iop.0000000000001473

Cwikel, J., Sergienko, R., Gutvirtz, G., Abramovitz, R., Slusky, D., Quastel, M., et al. (2020). Reproductive effects of exposure to low-dose ionizing radiation: a long-term follow-up of immigrant women exposed to the chernobyl accident. *Jcm* 9 (6), 1786. doi:10.3390/jcm9061786

D'Angiolella, G., Tozzo, P., Gino, S., and Caenazzo, L. (2020). Trick or treating in forensics-the challenge of the saliva microbiome: a narrative review. *Microorganisms* 8 (10). doi:10.3390/microorganisms8101501

da Fonseca, F. L., Yamanaka, P. K., Kato, J. M., and Matayoshi, S. (2016). Lacrimal system obstruction after radioiodine therapy in differentiated thyroid carcinomas: a prospective comparative study. *Thyroid* 26 (12), 1761–1767. doi:10.1089/thy.2015.0657

Dainiak, N. (2018). Medical management of acute radiation syndrome and associated infections in a high-casualty incident. *J. Radiat. Res.* 59, ii54–ii64. doi:10.1093/jrr/rry004

Davis, C. P. (1996). "Normal flora," in Medical microbiology. *Galveston (TX): university of Texas medical branch at galveston copyright © 1996*. Editor S. Baron (The University of Texas Medical Branch at Galveston).

Di Costanzo, M., Carucci, L., Berni Canani, R., and Biasucci, G. (2020). Gut microbiome modulation for preventing and treating pediatric food allergies. *Ijms* 21 (15), 5275. doi:10.3390/ijms21155275

DiCarlo, A. L., Bandremer, A. C., Hollingsworth, B. A., Kasim, S., Laniyonu, A., Todd, N. F., et al. (2020). Cutaneous radiation injuries: models, assessment and treatments. *Radiat. Res.* 194 (3), 315–344. doi:10.1667/RADE-20-00120.1

Dickson, R. P., Erb-Downward, J. R., and Huffnagle, G. B. (2013). The role of the bacterial microbiome in lung disease. *Expert Rev. Respir. Med.* 7 (3), 245–257. doi:10.1586/ers.13.24

Ding, X., Li, Q., Li, P., Chen, X., Xiang, L., Bi, L., et al. (2020). Fecal microbiota transplantation: a promising treatment for radiation enteritis? *Radiother. Oncol.* 143, 12–18. doi:10.1016/j.radonc.2020.01.011

Dirix, P., Nuyts, S., and Van den Bogaert, W. (2006). Radiation-induced xerostomia in patients with head and neck cancer. *Cancer* 107 (11), 2525–2534. doi:10.1002/cncr.22302

Dong, M.-Y., Chang, T.-W., and Gorbach, S. L. (1987). Effects of feeding lactobacillus GG on lethal irradiation in mice. *Diagn. Microbiol. Infect. Dis.* 7 (1), 1–7. doi:10.1016/0732-8893(87)90063-0

Donnelly, E. H., Nemhauser, J. B., Smith, J. M., Kazzi, Z. N., Farfán, E. B., Chang, A. S., et al. (2010). Acute radiation syndrome: assessment and management. *South. Med. J.* 103 (6), 541–546. doi:10.1097/SMJ.0b013e3181ddd571

Dougé, A., Bay, J.-O., Ravinet, A., and Scanzi, J. (2020). Microbiote intestinal et allogreffe de cellules souches hématopoïétiques. *Bull. du Cancer* 107 (1), 72–83. doi:10.1016/j.bulcan.2019.08.014

Doyle, P., Roman, E., Maconochie, N., Davies, G., Smith, P. G., and Beral, V. (2001). Primary infertility in nuclear industry employees: report from the nuclear industry family study. *Occup. Environ. Med.* 58 (8), 535–539. doi:10.1136/oem.58.8.535

Dréno, B., Araviiskaia, E., Berardesca, E., Gontijo, G., Sanchez Viera, M., Xiang, L. F., et al. (2016). Microbiome in healthy skin, update for dermatologists. *J. Eur. Acad. Dermatol. Venereol.* 30 (12), 2038–2047. doi:10.1111/jdv.13965

Dumas, A., Bernard, L., Poquet, Y., Lugo-Villarino, G., and Neyrolles, O. (2018). The role of the lung microbiota and the gut–lung axis in respiratory infectious diseases. *Cell Microbiol* 20 (12), e12966. doi:10.1111/cmi.12966

Elliott, T. B., Deutz, N. E., Gulani, J., Koch, A., Olsen, C. H., Christensen, C., et al. (2014). Gastrointestinal acute radiation syndrome in Göttingen minipigs (*Sus scrofa* domestica). *Comp. Med.* 64 (6), 456–463.

Epperly, M. W., Franicola, D., Shields, D., Rwigema, J. C., Stone, B., Zhang, X., et al. (2010). Screening of antimicrobial agents for *in vitro* radiation protection and mitigation capacity, including those used in supportive care regimens for bone marrow transplant recipients. *In Vivo* 24 (1), 9–19.

Eslami, S. Z., Majidzadeh, A. K., Halvaei, S., Babapirali, F., and Esmaeili, R. (2020). Microbiome and breast cancer: new role for an ancient population. *Front. Oncol.* 10, 120. doi:10.3389/fonc.2020.00120

Evsyutina, Y., Komkova, I., Zolnikova, O., Tkachenko, P., and Ivashkin, V. (2017). Lung microbiome in healthy and diseased individuals. *Wjr* 7 (2), 39–47. doi:10.5320/wjr.v7.i2.39

Ewing, L. E., Skinner, C. M., Pathak, R., Yee, E. U., Krager, K., Gurley, P. C., et al. (2021). Dietary methionine supplementation exacerbates gastrointestinal toxicity in a mouse model of abdominal irradiation. *Int. J. Radiat. Oncology*Biology*Physics* 109 (2), 581–593. doi:10.1016/j.ijrobp.2020.09.042

Farese, A. M., Cohen, M. V., Katz, B. P., Smith, C. P., Gibbs, A., Cohen, D. M., et al. (2013). Filgrastim improves survival in lethally irradiated nonhuman primates. *Radiat. Res.* 179 (1), 89–100. doi:10.1667/rr3049.1

Ferreira, M. R., Andreyev, H. J. N., Mohammed, K., Truelove, L., Gowan, S. M., Li, J., et al. (2019). Microbiota- and radiotherapy-induced gastrointestinal side-effects (MARS) study: a large pilot study of the microbiome in acute and late-radiation enteropathy. *Clin. Cancer Res.* 25 (21), 6487–6500. doi:10.1158/1078-0432.Ccr-19-0960

Fish, B. L., Gao, F., Narayanan, J., Bergom, C., Jacobs, E. R., Cohen, E. P., et al. (2016). Combined hydration and antibiotics with lisinopril to mitigate acute and delayed high-dose radiation injuries to multiple organs. *Health Phys.* 111 (5), 410–419. doi:10.1097/hp.0000000000000554

Fletcher, J., Cooper, S. C., Ghosh, S., and Hewison, M. (2019). The role of vitamin D in inflammatory bowel disease: mechanism to management. *Nutrients* 11 (5), 1019. doi:10.3390/nu11051019

Food and Agriculture Organization of the United Nations, World Health Organization (2006). *Probiotics in food: health and nutritional properties and guidelines for evaluation*. Rome: Food and Agriculture Organization of the United Nations : World Health Organization.

Food and Drug Administration (2015a). *FDA approves Neupogen (filgrastim) for treatment of patients with radiation-induced myelosuppression following a radiological/nuclear incident*.

Food and Drug Administration (2015b). *FDA approves sBLA for new indication of Neulasta (Pegfilgrastim) to treat adult and pediatric patients at risk of developing myelosuppression after a radiological/nuclear incident*. White Oak, MD: Health and Human Services.

Food and Drug Administration (2018). *FDA approves Leukine to increase survival of adult and pediatric patients acutely exposed to myelosuppresive of radiation (H-ARS) as could occur after a radiological/nuclear incident*. White Oak, MD: Health and Human Services.

Franchi, L., Kamada, N., Nakamura, Y., Burberry, A., Kuffa, P., Suzuki, S., et al. (2012). NLRC4-driven production of IL-1β discriminates between pathogenic and commensal bacteria and promotes host intestinal defense. *Nat. Immunol.* 13 (5), 449–456. doi:10.1038/ni.2263

Frank, D. N., Feazel, L. M., Bessesen, M. T., Price, C. S., Janoff, E. N., and Pace, N. R. (2010). The human nasal microbiota and *Staphylococcus aureus* carriage. *PLoS ONE* 5 (5), e10598. doi:10.1371/journal.pone.0010598

François, A., Milliat, F., Guipaud, O., and Benderitter, M. (2013). Inflammation and immunity in radiation damage to the gut mucosa. *Biomed. Res. Int.* 2013, 1. doi:10.1155/2013/123241

Freifeld, A. G., Bow, E. J., Sepkowitz, K. A., Boeckh, M. J., Ito, J. I., Mullen, C. A., et al. (2011). Clinical practice guideline for the use of antimicrobial agents in neutropenic patients with cancer: 2010 update by the Infectious Diseases Society of America. *Clin. Infect. Dis.* 52 (4), e56–e93. doi:10.1093/cid/cir073

Friedrich, A., Paz, M., Leoni, J., and González Maglio, D. (2017). Message in a bottle: dialog between intestine and skin modulated by probiotics. *Ijms* 18 (6), 1067. doi:10.3390/ijms18061067

Gallo, R. L. (2017). Human skin is the largest epithelial surface for interaction with microbes. *J. Invest. Dermatol.* 137 (6), 1213–1214. doi:10.1016/j.jid.2016.11.045

Gallo, R. L., and Nizet, V. (2008). Innate barriers against skin infection and associated disorders. *Drug Discov. Today Dis. Mech.* 5 (2), e145–e152. doi:10.1016/j.ddmec.2008.04.009

García, M. G., Pérez-Cárceles, M. D., Osuna, E., and Legaz, I. (2020). Impact of the human microbiome in forensic sciences: a systematic review. *Appl. Environ. Microbiol.* 86 (22). doi:10.1128/aem.01451-20

Garcia-Peris, P., Velasco, C., Hernandez, M., Lozano, M. A., Paron, L., de la Cuerda, C., et al. (2016). Effect of inulin and fructo-oligosaccharide on the prevention of acute radiation enteritis in patients with gynecological cancer and impact on quality-of-life: a randomized, double-blind, placebo-controlled trial. *Eur. J. Clin. Nutr.* 70 (2), 170–174. doi:10.1038/ejcn.2015.192

Ge, X., Zhao, W., Ding, C., Tian, H., Xu, L., Wang, H., et al. (2017). Potential role of fecal microbiota from patients with slow transit constipation in the regulation of gastrointestinal motility. *Sci. Rep.* 7 (1), 441. doi:10.1038/s41598-017-00612-y

Gerassy-Vainberg, S., Blatt, A., Danin-Poleg, Y., Gershovich, K., Sabo, E., Nevelsky, A., et al. (2018). Radiation induces proinflammatory dysbiosis: transmission of inflammatory susceptibility by host cytokine induction. *Gut* 67 (1), 97–107. doi:10.1136/gutjnl-2017-313789

Ghaly, S., Hart, P. H., and Lawrance, I. C. (2019). Inflammatory bowel diseases: interrelationships between dietary vitamin D, exposure to UV radiation and the fecal microbiome. *Expert Rev. Gastroenterol. Hepatol.* 13 (11), 1039–1048. doi:10.1080/17474124.2019.1685874

Glasstone, S., Dolan, P. J., USDo, Defense., USDo, Energy., and Agency, U. S. D. A. S. (1977). *The effects of nuclear weapons*. 3d ed. Washington: U.S. Dept. of Defense, 653.

Gomez, D. R., Estilo, C. L., Wolden, S. L., Zelefsky, M. J., Kraus, D. H., Wong, R. J., et al. (2011). Correlation of osteoradionecrosis and dental events with dosimetric parameters in intensity-modulated radiation therapy for head-and-neck cancer. *Int. J. Radiat. Oncology*Biology*Physics* 81 (4), e207–e213. doi:10.1016/j.ijrobp.2011.02.003

Gottlöber, P., Steinert, M., Weiss, M., Bebeshko, V., Belyi, D., Nadejina, N., et al. (2001). The outcome of local radiation injuries: 14 years of follow-up after the Chernobyl accident. *Radiat. Res.* 155 (3), 409–416. doi:10.1667/0033-7587(2001)155[0409:toolri]2.0.co;2

Goudarzi, M., Mak, T. D., Jacobs, J. P., Moon, B.-H., Strawn, S. J., Braun, J., et al. (2016). An integrated multi-omic approach to assess radiation injury on the host-microbiome axis. *Radiat. Res.* 186 (3), 219–234. doi:10.1667/RR14306.1

Gourbeyre, P., Denery, S., and Bodinier, M. (2011). Probiotics, prebiotics, and synbiotics: impact on the gut immune system and allergic reactions. *J. Leukoc. Biol.* 89 (5), 685–695. doi:10.1189/jlb.1109753

Guo, H., Chou, W.-C., Lai, Y., Liang, K., Tam, J. W., Brickey, W. J., et al. (2020). Multi-omics analyses of radiation survivors identify radioprotective microbes and metabolites. *Science* 370 (6516), eaay9097. doi:10.1126/science.aay9097

Guo, H., Gibson, S. A., and Ting, J. P. Y. (2020). Gut microbiota, NLR proteins, and intestinal homeostasis. *J. Exp. Med.* 217 (10), 217. doi:10.1084/jem.20181832

Hafer, N., Cassatt, D., Dicarlo, A., Ramakrishnan, N., Kaminski, J., Norman, M.-K., et al. (2010). NIAID/NIH radiation/nuclear medical countermeasures product research and development program. *Health Phys.* 98 (6), 903–905. doi:10.1097/HP.0b013e3181bbc4df

Hajjeh, R. A., Sofair, A. N., Harrison, L. H., Lyon, G. M., Arthington-Skaggs, B. A., Mirza, S. A., et al. (2004). Incidence of bloodstream infections due to *Candida* species and *in vitro* susceptibilities of isolates collected from 1998 to 2000 in a population-based active surveillance program. *J. Clin. Microbiol.* 42 (4), 1519–1527. doi:10.1128/jcm.42.4.1519-1527.2004

Hakansson, A., and Molin, G. (2011). Gut microbiota and inflammation. *Nutrients* 3 (6), 637–682. doi:10.3390/nu3060637

Hall, M. W., Singh, N., Ng, K. F., Lam, D. K., Goldberg, M. B., Tenenbaum, H. C., et al. (2017). Inter-personal diversity and temporal dynamics of dental, tongue, and salivary microbiota in the healthy oral cavity. *NPJ Biofilms Microbiomes* 3, 2. doi:10.1038/s41522-016-0011-0

Hamada, H., Hiroi, T., Nishiyama, Y., Takahashi, H., Masunaga, Y., Hachimura, S., et al. (2002). Identification of multiple isolated lymphoid follicles on the antimesenteric wall of the mouse small intestine. *J. Immunol.* 168 (1), 57–64. doi:10.4049/jimmunol.168.1.57

Hankey, K. G., Farese, A. M., Blaauw, E. C., Gibbs, A. M., Smith, C. P., Katz, B. P., et al. (2015). Pegfilgrastim improves survival of lethally irradiated nonhuman primates. *Radiat. Res.* 183 (6), 643–655. doi:10.1667/rr13940.1

Hardy, H., Harris, J., Lyon, E., Beal, J., and Foey, A. (2013). Probiotics, prebiotics and immunomodulation of gut mucosal defences: homeostasis and immunopathology. *Nutrients* 5 (6), 1869–1912. doi:10.3390/nu5061869

Harsch, I. A., and Konturek, P. C. (2019). Adhesion ileus after fecal microbiota transplantation in long-standing radiation colitis. *Case Rep. Gastrointest. Med.* 2019, 1. doi:10.1155/2019/2543808

Hayashi, H., Takahashi, R., Nishi, T., Sakamoto, M., and Benno, Y. (2005). Molecular analysis of jejunal, ileal, caecal and recto-sigmoidal human colonic microbiota using 16S rRNA gene libraries and terminal restriction fragment length polymorphism. *J. Med. Microbiol.* 54 (11), 1093–1101. doi:10.1099/jmm.0.45935-0

Hayes, W., and Sahu, S. (2020). The human microbiome: history and future. *J. Pharm. Pharm. Sci.* 23, 406–411. doi:10.18433/jpps31525

Hazenberg, M. P., Bakker, M., and Verschoor-Burggraaf, A. (1981). Effects of the human intestinal flora on germ-free mice. *J. Appl. Bacteriol.* 50 (1), 95–106. doi:10.1111/j.1365-2672.1981.tb00874.x

Hellstein, J. W., and Marek, C. L. (2019). Candidiasis: red and white manifestations in the oral cavity. *Head Neck Pathol.* 13 (1), 25–32. doi:10.1007/s12105-019-01004-6

Hensley-McBain, T., Zevin, A. S., Manuzak, J., Smith, E., Gile, J., Miller, C., et al. (2016). Effects of fecal microbial transplantation on microbiome and immunity in simian immunodeficiency virus-infected macaques. *J. Virol.* 90 (10), 4981–4989. doi:10.1128/jvi.00099-16

Hermann, L. M., White, W. J., and Lang, C. M. (1982). Prolonged exposure to acid, chlorine, or tetracycline in the drinking water: effects on delayed-type hypersensitivity, hemagglutination titers, and reticuloendothelial clearance rates in mice. *Lab. Anim. Sci.* 32 (6), 603–608.

Hilty, M., Burke, C., Pedro, H., Cardenas, P., Bush, A., Bossley, C., et al. (2010). Disordered microbial communities in asthmatic airways. *PLoS ONE* 5 (1), e8578. doi:10.1371/journal.pone.0008578

Hollingsworth, B., Senter, L., Zhang, X., Brock, G. N., Jarjour, W., Nagy, R., et al. (2016). Risk factors of 131I-induced salivary gland damage in thyroid cancer patients. *J. Clin. Endocrinol. Metab.* 101 (11), 4085–4093. doi:10.1210/jc.2016-1605

Hooper, L. V., and MacPherson, A. J. (2010). Immune adaptations that maintain homeostasis with the intestinal microbiota. *Nat. Rev. Immunol.* 10 (3), 159–169. doi:10.1038/nri2710

Hou, J., Zheng, H., Li, P., Liu, H., Zhou, H., and Yang, X. (2018). Distinct shifts in the oral microbiota are associated with the progression and aggravation of mucositis during radiotherapy. *Radiother. Oncol.* 129 (1), 44–51. doi:10.1016/j.radonc.2018.04.023

Huang, C.-C., Huang, S.-F., Lee, T.-J., Ng, S.-H., and Chang, J. T.-C. (2007). Postirradiation sinus mucosa disease in nasopharyngeal carcinoma patients. *Laryngoscope* 117 (4), 737–742. doi:10.1097/MLG.0b013e3180325b6c

Huang, R., Xiang, J., and Zhou, P. (2019). Vitamin D, gut microbiota, and radiation-related resistance: a love-hate triangle. *J. Exp. Clin. Cancer Res.* 38 (1), 493. doi:10.1186/s13046-019-1499-y

Huang, T., Debelius, J. W., Ploner, A., Xiao, X., Zhang, T., Hu, K., et al. (2021). Radiation therapy-induced changes of the nasopharyngeal commensal microbiome in nasopharyngeal carcinoma patients. *Int. J. Radiat. Oncology*Biology*Physics* 109, 145. doi:10.1016/j.ijrobp.2020.08.054

Huang, Y., Yang, B., and Li, W. (2016). Defining the normal core microbiome of conjunctival microbial communities. *Clin. Microbiol. Infect.* 22 (7), e7–e12. doi:10.1016/j.cmi.2016.04.008

Jandhyala, S. M., Talukdar, R., Subramanyam, C., Vuyyuru, H., Sasikala, M., and Reddy, D. N. (2015). Role of the normal gut microbiota. *Wjg* 21 (29), 8787–8847. doi:10.3748/wjg.v21.i29.8787

Jeong, S. Y., Kim, H. W., Lee, S.-W., Ahn, B.-C., and Lee, J. (2013). Salivary gland function 5 years after radioactive iodine ablation in patients with differentiated thyroid cancer: direct comparison of pre- and postablation scintigraphies and their relation to xerostomia symptoms. *Thyroid* 23 (5), 609–616. doi:10.1089/thy.2012.0106

Jervis, H. R., McLaughlin, M. M., and Johnson, M. C. (1971). Effect of neutron-gamma radiation on the morphology of the mucosa of the small intestine of germfree and conventional mice. *Radiat. Res.* 45 (3), 613–628. doi:10.2307/3573069

Jin, D., Wu, S., Zhang, Y.-g., Lu, R., Xia, Y., Dong, H., et al. (2015). Lack of vitamin D receptor causes dysbiosis and changes the functions of the murine intestinal microbiome. *Clin. Ther.* 37 (5), 996–1009. doi:10.1016/j.clinthera.2015.04.004

Johnson, T., Gómez, B., McIntyre, M., Dubick, M., Christy, R., Nicholson, S., et al. (2018). The cutaneous microbiome and wounds: new molecular targets to promote wound healing. *Ijms* 19 (9), 2699. doi:10.3390/ijms19092699

Kaźmierczak-Siedlecka, K., Dvořák, A., Folwarski, M., Daca, A., Przewłócka, K., and Makarewicz, W. (2020). Fungal gut microbiota dysbiosis and its role in colorectal, oral, and pancreatic carcinogenesis. *Cancers (Basel)* 12 (5). doi:10.3390/cancers12051326

Kałużny, J., Wierzbicka, M., Nogala, H., Milecki, P., and Kopeć, T. (2014). Radiotherapy induced xerostomia: mechanisms, diagnostics, prevention and treatment--evidence based up to 2013. *Otolaryngol. Pol.* 68 (1), 1–14. doi:10.1016/j.otpol.2013.09.002

Keely, S., Talley, N. J., and Hansbro, P. M. (2012). Pulmonary-intestinal cross-talk in mucosal inflammatory disease. *Mucosal Immunol.* 5 (1), 7–18. doi:10.1038/mi.2011.55

Kelly, C. R., Yen, E. F., Grinspan, A. M., Kahn, S. A., Atreja, A., Lewis, J. D., et al. (2021). Fecal microbiota transplantation is highly effective in real-world practice: initial results from the FMT national registry. *Gastroenterol.* 160, 183. doi:10.1053/j.gastro.2020.09.038

Khailova, L., Frank, D. N., Dominguez, J. A., and Wischmeyer, P. E. (2013). Probiotic administration reduces mortality and improves intestinal epithelial homeostasis in experimental sepsis. *Anesthesiol.* 119 (1), 166–177. doi:10.1097/ALN.0b013e318291c2fc

Kiang, J. G., Garrison, B. R., Smith, J. T., and Fukumoto, R. (2014). Ciprofloxacin as a potential radio-sensitizer to tumor cells and a radio-protectant for normal cells: differential effects on γ-H2AX formation, p53 phosphorylation, Bcl-2 production, and cell death. *Mol. Cel Biochem* 393 (1-2), 133–143. doi:10.1007/s11010-014-2053-z

Kiang, J. G., Jiao, W., Cary, L. H., Mog, S. R., Elliott, T. B., Pellmar, T. C., et al. (2010). Wound trauma increases radiation-induced mortality by activation of iNOS pathway and elevation of cytokine concentrations and bacterial infection. *Radiat. Res.* 173 (3), 319–332. doi:10.1667/RR1892.1

Kiley, J. P., and Caler, E. V. (2014). The lung microbiome. A new Frontier in pulmonary medicine. *Ann. ATS* 11 (Suppl. 1), S66–S70. doi:10.1513/AnnalsATS.201308-285MG

Kim, W., Lee, E. J., Bae, I. H., Myoung, K., Kim, S. T., Park, P. J., et al. (2020). Lactobacillus plantarum -derived extracellular vesicles induce anti-inflammatory M2 macrophage polarization *in vitro*. *J. Extracellular Vesicles* 9 (1), 1793514. doi:10.1080/20013078.2020.1793514

King, C. H., Desai, H., Sylvetsky, A. C., LoTempio, J., Ayanyan, S., Carrie, J., et al. (2019). Baseline human gut microbiota profile in healthy people and standard reporting template. *PLoS ONE* 14 (9), e0206484. doi:10.1371/journal.pone.0206484

Kun, C., Tao, L., Leiyuan, H., Yunhao, F., Ning, W., Zhe, L., et al. (2019). Heat-killed *Salmonella typhimurium* mitigated radiation-induced lung injury. *Clin. Exp. Pharmacol. Physiol.* 46 (12), 1084–1091. doi:10.1111/1440-1681.13135

Kupper, T. S., and Fuhlbrigge, R. C. (2004). Immune surveillance in the skin: mechanisms and clinical consequences. *Nat. Rev. Immunol.* 4 (3), 211–222. doi:10.1038/nri1310

La Perle, K. M. D., Kim, D. C., Hall, N. C., Bobbey, A., Shen, D. H., Nagy, R. S., et al. (2013). Modulation of sodium/iodide symporter expression in the salivary gland. *Thyroid* 23 (8), 1029–1036. doi:10.1089/thy.2012.0571

Lam, V., Moulder, J. E., Salzman, N. H., Dubinsky, E. A., Andersen, G. L., and Baker, J. E. (2012). Intestinal microbiota as novel biomarkers of prior radiation exposure. *Radiat. Res.* 177 (5), 573–583. doi:10.1667/rr2691.1

Lane, D. J., Pace, B., Olsen, G. J., Stahl, D. A., Sogin, M. L., and Pace, N. R. (1985). Rapid determination of 16S ribosomal RNA sequences for phylogenetic analyses. *Proc. Natl. Acad. Sci.* 82 (20), 6955–6959. doi:10.1073/pnas.82.20.6955

Lazarevic, V., Whiteson, K., Huse, S., Hernandez, D., Farinelli, L., Østerås, M., et al. (2009). Metagenomic study of the oral microbiota by Illumina high-throughput sequencing. *J. Microbiol. Methods* 79 (3), 266–271. doi:10.1016/j.mimet.2009.09.012

Leake, S. L., Pagni, M., Falquet, L., Taroni, F., and Greub, G. (2016). The salivary microbiome for differentiating individuals: proof of principle. *Microbes Infect.* 18 (6), 399–405. doi:10.1016/j.micinf.2016.03.011

Lederberg, J., and McCray, A. T. (2001). 'Ome sweet' omics-a genealogical treasury of words. *Scientist* 15 (7).

Lee, A., Gordon, J., and Dubos, R. (1968). Enumeration of the oxygen sensitive bacteria usually present in the intestine of healthy mice. *Nature* 220 (5172), 1137–1139. doi:10.1038/2201137a0

Li, M., Gu, M.-M., Lang, Y., Shi, J., Chen, B. P. C., Guan, H., et al. (2019). The vanillin derivative VND3207 protects intestine against radiation injury by modulating p53/NOXA signaling pathway and restoring the balance of gut microbiota. *Free Radic. Biol. Med.* 145, 223–236. doi:10.1016/j.freeradbiomed.2019.09.035

Li, Y., Dong, J., Xiao, H., Zhang, S., Wang, B., Cui, M., et al. (2020). Gut commensal derived-valeric acid protects against radiation injuries. *Gut Microbes* 11 (4), 789–806. doi:10.1080/19490976.2019.1709387

Li, Y., Yan, H., Zhang, Y., Li, Q., Yu, L., Li, Q., et al. (2020). Alterations of the gut microbiome composition and lipid metabolic profile in radiation enteritis. *Front. Cel. Infect. Microbiol.* 10, 541178. doi:10.3389/fcimb.2020.541178

Liu, J., Liu, C., and Yue, J. (2021). Radiotherapy and the gut microbiome: facts and fiction. *Radiat. Oncol.* 16 (1), 16. doi:10.1186/s13014-020-01735-9

Liu, M.-M., Li, S.-T., Shu, Y., and Zhan, H.-Q. (2017). Probiotics for prevention of radiation-induced diarrhea: a meta-analysis of randomized controlled trials. *PLoS ONE* 12 (6), e0178870. doi:10.1371/journal.pone.0178870

Liu, N.-N., Ma, Q., Ge, Y., Yi, C.-X., Wei, L.-Q., Tan, J.-C., et al. (2020). Microbiome dysbiosis in lung cancer: from composition to therapy. *Npj Precis. Onc.* 4 (1), 33. doi:10.1038/s41698-020-00138-z

Liu, T., Wu, Y., Wang, L., Pang, X., Zhao, L., Yuan, H., et al. (2019). A more robust gut microbiota in calorie-restricted mice is associated with attenuated intestinal injury caused by the chemotherapy drug cyclophosphamide. *mBio* 10 (2). doi:10.1128/mBio.02903-18

Lo, G.-H. (2019). The transplantation of fecal microbiota for cirrhotic patients. *Gastroenterology* 157 (3), 902. doi:10.1053/j.gastro.2019.06.040

Lone, S. A., and Ahmad, A. (2019). *Candida* auris -the growing menace to global health. *Mycoses* 62 (8), 620–637. doi:10.1111/myc.12904

Long-Smith, C., O'Riordan, K. J., Clarke, G., Stanton, C., Dinan, T. G., and Cryan, J. F. (2020). Microbiota-gut-brain axis: new therapeutic opportunities. *Annu. Rev. Pharmacol. Toxicol.* 60, 477–502. doi:10.1146/annurev-pharmtox-010919-023628

Loniewski, I., Misera, A., Skonieczna-Zydecka, K., Kaczmarczyk, M., Kazmierczak-Siedlecka, K., Misiak, B., et al. (2020). Major depressive disorder and gut microbiota - association not causation. A scoping review. *Prog. Neuropsychopharmacol. Biol. Psychiatry*, 110111. doi:10.1016/j.pnpbp.2020.110111

Louis, P., Hold, G. L., and Flint, H. J. (2014). The gut microbiota, bacterial metabolites and colorectal cancer. *Nat. Rev. Microbiol.* 12 (10), 661–672. doi:10.1038/nrmicro3344

Lozupone, C. A., Stombaugh, J. I., Gordon, J. I., Jansson, J. K., and Knight, R. (2012). Diversity, stability and resilience of the human gut microbiota. *Nature* 489 (7415), 220–230. doi:10.1038/nature11550

Lu, L., Li, W., Sun, C., Kang, S., Li, J., Luo, X., et al. (2019). Phycocyanin ameliorates radiation-induced acute intestinal toxicity by regulating the effect of the gut microbiota on the TLR4/myd88/NF-κB pathway. *JPEN J. Parenter. Enteral Nutr.* 44. 1308. doi:10.1002/jpen.1744

Lucas, R. M., Gorman, S., Geldenhuys, S., and Hart, P. H. (2014). Vitamin D and immunity. *F1000prime Rep.* 6, 118. doi:10.12703/P6-118

Mackie, R. I., Sghir, A., and Gaskins, H. R. (1999). Developmental microbial ecology of the neonatal gastrointestinal tract. *Am. J. Clin. Nutr.* 69 (5), 1035S–1045s. doi:10.1093/ajcn/69.5.1035s

MacVittie, T. J., Bennett, A., Booth, C., Garofalo, M., Tudor, G., Ward, A., et al. (2012). The prolonged gastrointestinal syndrome in rhesus macaques. *Health Phys.* 103 (4), 427–453. doi:10.1097/HP.0b013e318266eb4c

MacVittie, T. J., Farese, A. M., Bennett, A., Gelfond, D., Shea-Donohue, T., Tudor, G., et al. (2012). The acute gastrointestinal subsyndrome of the acute radiation syndrome. *Health Phys.* 103 (4), 411–426. doi:10.1097/HP.0b013e31826525f0

MacVittie, T. J., Farese, A. M., Parker, G. A., Jackson, W., 3rd, Booth, C., Tudor, G. L., et al. (2019). The gastrointestinal subsyndrome of the acute radiation syndrome in rhesus macaques: a systematic review of the lethal dose-response relationship with and without medical management. *Health Phys.* 116 (3), 305–338. doi:10.1097/hp.0000000000000903

Mariat, D., Firmesse, O., Levenez, F., Guimarães, V., Sokol, H., Doré, J., et al. (2009). The Firmicutes/Bacteroidetes ratio of the human microbiota changes with age. *BMC Microbiol.* 9, 123. doi:10.1186/1471-2180-9-123

Markowiak, P., and Śliżewska, K. (2017). Effects of probiotics, prebiotics, and synbiotics on human health. *Nutrients* 9 (9). doi:10.3390/nu9091021

Mathieu, E., Escribano-Vazquez, U., Descamps, D., Cherbuy, C., Langella, P., Riffault, S., et al. (2018). Paradigms of lung microbiota functions in health and disease, particularly, in asthma. *Front. Physiol.* 9 (1168), 9. doi:10.3389/fphys.2018.01168

Matsuzawa, T. (1965). Survival time in germfree mice after lethal whole body x-irradiation. *Tohoku J. Exp. Med.* 85, 257–263. doi:10.1620/tjem.85.257

Matsuzawa, T., and Wilson, R. (1965). The intestinal mucosa of germfree mice after whole-body x-irradiation with 3 kiloroentgens. *Radiat. Res.* 25, 15–24. doi:10.2307/3571891

Maurice, C. F., Haiser, H. J., and Turnbaugh, P. J. (2013). Xenobiotics shape the physiology and gene expression of the active human gut microbiome. *Cell* 152 (1-2), 39–50. doi:10.1016/j.cell.2012.10.052

Maxfield, A., Chambers, K., Sedaghat, A., Lin, D., and Gray, S. (2017). Mucosal thickening occurs in contralateral paranasal sinuses following sinonasal malignancy treatment. *J. Neurol. Surg. B* 78 (4), 331–336. doi:10.1055/s-0037-1598048

McCormack, U. M., Curião, T., Metzler-Zebeli, B. U., Wilkinson, T., Reyer, H., Crispie, F., et al. (2019). Improvement of feed efficiency in pigs through microbial modulation via fecal microbiota transplantation in sows and dietary supplementation of inulin in offspring. *Appl. Environ. Microbiol.* 85 (22). doi:10.1128/aem.01255-19

McIlroy, J., Ianiro, G., Mukhopadhya, I., Hansen, R., and Hold, G. L. (2018). Review article: the gut microbiome in inflammatory bowel disease-avenues for microbial management. *Aliment. Pharmacol. Ther.* 47 (1), 26–42. doi:10.1111/apt.14384

McLaughlin, M. M., Dacquisto, M. P., Jacobus, D. P., and Horowitz, R. E. (1964). Effects of the germfree state on responses of mice to whole-body irradiation. *Radiat. Res.* 23, 333–349. doi:10.2307/3571614

Measey, T. J., Pouliot, M., Wierzbicki, W., Swanson, C., Brown, D., Authier, S., et al. (2018). Pilot study of radiation-induced gastrointestinal injury in a hemi-body shielded göttingen minipig model. *Health Phys.* 114 (1), 43–57. doi:10.1097/hp.0000000000000751

Measey, T. J., Pouliot, M., Wierzbicki, W., Swanson, C., Brown, D., Stamatopoulos, J., et al. (2018). Expanded characterization of a hemi-body shielded göttingen minipig model of radiation-induced gastrointestinal injury incorporating oral dosing procedures. *Health Phys.* 114 (1), 32–42. doi:10.1097/hp.0000000000000750

Meisel, J. S., Sfyroera, G., Bartow-McKenney, C., Gimblet, C., Bugayev, J., Horwinski, J., et al. (2018). Commensal microbiota modulate gene expression in the skin. *Microbiome* 6 (1), 20. doi:10.1186/s40168-018-0404-9

Metzler-Zebeli, B. U., Siegerstetter, S.-C., Magowan, E., Lawlor, P. G., O′Connell, N. E., and Zebeli, Q. (2019). Fecal microbiota transplant from highly feed efficient donors affects cecal physiology and microbiota in low- and high-feed efficient chickens. *Front. Microbiol.* 10, 1576. doi:10.3389/fmicb.2019.01576

Micewicz, E. D., Iwamoto, K. S., Ratikan, J. A., Nguyen, C., Xie, M. W., Cheng, G., et al. (2019). The aftermath of surviving acute radiation hematopoietic syndrome and its mitigation. *Radiat. Res.* 191 (4), 323–334. doi:10.1667/RR15231.1

Miousse, I. R., Ewing, L. E., Skinner, C. M., Pathak, R., Garg, S., Kutanzi, K. R., et al. (2020). Methionine dietary supplementation potentiates ionizing radiation-induced gastrointestinal syndrome. *Am. J. Physiology-Gastrointestinal Liver Physiol.* 318 (3), G439–G450. doi:10.1152/ajpgi.00351.2019

Moore, W. E. C., and Holdeman, L. V. (1974). Human fecal flora: the normal flora of 20 Japanese-hawaiians. *APPLMICROBIOL* 27 (5), 961–979. doi:10.1128/aem.27.5.961-979.1974

Morgan, X. C., and Huttenhower, C. (2012). Chapter 12: human microbiome analysis. *Plos Comput. Biol.* 8 (12), e1002808. doi:10.1371/journal.pcbi.1002808

Morgan, X. C., Segata, N., and Huttenhower, C. (2013). Biodiversity and functional genomics in the human microbiome. *Trends Genet.* 29 (1), 51–58. doi:10.1016/j.tig.2012.09.005

Mougeot, J.-L. C., Stevens, C. B., Almon, K. G., Paster, B. J., Lalla, R. V., Brennan, M. T., et al. (2019). Caries-associated oral microbiome in head and neck cancer radiation patients: a longitudinal study. *J. Oral Microbiol.* 11 (1), 1586421. doi:10.1080/20002297.2019.1586421

Mubangizi, L., Namusoke, F., and Mutyaba, T. (2014). Aerobic cervical bacteriology and antibiotic sensitivity patterns in patients with advanced cervical cancer before and after radiotherapy at a national referral hospital in Uganda. *Int. J. Gynecol. Obstet.* 126 (1), 37–40. doi:10.1016/j.ijgo.2014.01.013

Muegge, B. D., Kuczynski, J., Knights, D., Clemente, J. C., González, A., Fontana, L., et al. (2011). Diet drives convergence in gut microbiome functions across mammalian phylogeny and within humans. *Science* 332 (6032), 970–974. doi:10.1126/science.1198719

Muhleisen, A. L., and Herbst-Kralovetz, M. M. (2016). Menopause and the vaginal microbiome. *Maturitas* 91, 42–50. doi:10.1016/j.maturitas.2016.05.015

Nam, Y.-D., Kim, H. J., Seo, J.-G., Kang, S. W., and Bae, J.-W. (2013). Impact of pelvic radiotherapy on gut microbiota of gynecological cancer patients revealed by massive pyrosequencing. *PLoS ONE* 8 (12), e82659. doi:10.1371/journal.pone.0082659

Nasser, N. J., Fenig, S., Ravid, A., Nouriel, A., Ozery, N., Gardyn, S., et al. (2017). Vitamin D ointment for prevention of radiation dermatitis in breast cancer patients. *NPJ Breast Cancer* 3, 10. doi:10.1038/s41523-017-0006-x

Newbold, L. K., Robinson, A., Rasnaca, I., Lahive, E., Soon, G. H., Lapied, E., et al. (2019). Genetic, epigenetic and microbiome characterisation of an earthworm species (Octolasion lacteum) along a radiation exposure gradient at Chernobyl. *Environ. Pollut.* 255, 113238. doi:10.1016/j.envpol.2019.113238

Nguyen, T. L. A., Vieira-Silva, S., Liston, A., and Raes, J. (2015). How informative is the mouse for human gut microbiota research?. *Dis. Models Mech.* 8 (1), 1–16. doi:10.1242/dmm.017400

Nie, X., Li, L., Yi, M., Qin, W., Zhao, W., Li, F., et al. (2020). The intestinal microbiota plays as a protective regulator against radiation pneumonitis. *Radiat. Res.* 194 (1), 52–60. doi:10.1667/RR15579.1

Nishii, M., Soutome, S., Kawakita, A., Yutori, H., Iwata, E., Akashi, M., et al. (2020). Factors associated with severe oral mucositis and candidiasis in patients undergoing radiotherapy for oral and oropharyngeal carcinomas: a retrospective multicenter study of 326 patients. *Support Care Cancer* 28 (3), 1069–1075. doi:10.1007/s00520-019-04885-z

Novak, J. M., Collins, J. T., Donowitz, M., Farman, J., Sheahan, D. G., and Spiro, H. M. (1979). Effects of radiation on the human gastrointestinal tract. *J. Clin. Gastroenterol.* 1 (1), 9–40. doi:10.1097/00004836-197903000-00003

Nuzzi, R., Trossarello, M., Bartoncini, S., Marolo, P., Franco, P., Mantovani, C., et al. (2020). Ocular complications after radiation therapy: an observational study. *Opth* 14, 3153–3166. doi:10.2147/opth.S263291

Ó Broin, P., Vaitheesvaran, B., Saha, S., Hartil, K., Chen, E. I., Goldman, D., et al. (2015). Intestinal microbiota-derived metabolomic blood plasma markers for prior radiation injury. *Int. J. Radiat. Oncol. Biol. Phys.* 91 (2), 360–367. doi:10.1016/j.ijrobp.2014.10.023

Obrador, E., Salvador, R., Villaescusa, J. I., Soriano, J. M., Estrela, J. M., and Montoro, A. (2020). Radioprotection and radiomitigation: from the bench to clinical practice. *Biomedicines* 8 (11), 461. doi:10.3390/biomedicines8110461

Onoue, M., Uchida, K., Yokokura, T., Takahashi, T., and Mutai, M. (1981). Effect of intestinal microflora on the survival time of mice exposed to lethal whole-body γ irradiation. *Radiat. Res.* 88 (3), 533–541. doi:10.2307/3575642

Packey, C. D., and Ciorba, M. A. (2010). Microbial influences on the small intestinal response to radiation injury. *Curr. Opin. Gastroenterol.* 26 (2), 88–94. doi:10.1097/MOG.0b013e3283361927

Pannkuk, E., Laiakis, E., Girgis, M., Dowd, S., Dhungana, S., Nishita, D., et al. (2019). Temporal effects on radiation responses in nonhuman primates: identification of biofluid small molecule signatures by gas chromatography-mass spectrometry metabolomics. *Metabolites* 9 (5), 98. doi:10.3390/metabo9050098

Pannkuk, E. L., Laiakis, E. C., Authier, S., Wong, K., and Fornace, A. J., Jr. (2017). Gas chromatography/mass spectrometry metabolomics of urine and serum from nonhuman primates exposed to ionizing radiation: impacts on the tricarboxylic acid cycle and protein metabolism. *J. Proteome Res.* 16 (5), 2091–2100. doi:10.1021/acs.jproteome.7b00064

Paramsothy, S., Kamm, M. A., Kaakoush, N. O., Walsh, A. J., van den Bogaerde, J., Samuel, D., et al. (2017). Multidonor intensive faecal microbiota transplantation for active ulcerative colitis: a randomised placebo-controlled trial. *The Lancet* 389 (10075), 1218–1228. doi:10.1016/s0140-6736(17)30182-4

Paris, F., Fuks, Z., Kang, A., Capodieci, P., Juan, G., Ehleiter, D., et al. (2001). Endothelial apoptosis as the primary lesion initiating intestinal radiation damage in mice. *Science* 293 (5528), 293–297. doi:10.1126/science.1060191

Patra, V., Gallais Sérézal, I., and Wolf, P. (2020). Potential of skin microbiome, pro- and/or pre-biotics to affect local cutaneous responses to uv exposure. *Nutrients* 12 (6), 1795. doi:10.3390/nu12061795

Patra, V., Wagner, K., Arulampalam, V., and Wolf, P. (2019). Skin microbiome modulates the effect of ultraviolet radiation on cellular response and immune function. *iScience* 15, 211–222. doi:10.1016/j.isci.2019.04.026

Paulos, C. M., Wrzesinski, C., Kaiser, A., Hinrichs, C. S., Chieppa, M., Cassard, L., et al. (2007). Microbial translocation augments the function of adoptively transferred self/tumor-specific CD8+ T cells via TLR4 signaling. *J. Clin. Invest.* 117 (8), 2197–2204. doi:10.1172/JCI32205

Peters, V. B. M., van de Steeg, E., van Bilsen, J., and Meijerink, M. (2019). Mechanisms and immunomodulatory properties of pre- and probiotics. *Beneficial Microbes* 10 (3), 225–236. doi:10.3920/BM2018.0066

Petricevic, L., Unger, F. M., Viernstein, H., and Kiss, H. (2008). Randomized, double-blind, placebo-controlled study of oral lactobacilli to improve the vaginal flora of postmenopausal women. *Eur. J. Obstet. Gynecol. Reprod. Biol.* 141 (1), 54–57. doi:10.1016/j.ejogrb.2008.06.003

Pickard, J. M., Zeng, M. Y., Caruso, R., and Núñez, G. (2017). Gut microbiota: role in pathogen colonization, immune responses, and inflammatory disease. *Immunol. Rev.* 279 (1), 70–89. doi:10.1111/imr.12567

Picó-Monllor, J. A., and Mingot-Ascencao, J. M. (2019). Search and selection of probiotics that improve mucositis symptoms in oncologic patients. A systematic review. *Nutrients* 11 (10), 2322. doi:10.3390/nu11102322

Plett, P. A., Sampson, C. H., Chua, H. L., Joshi, M., Booth, C., Gough, A., et al. (2012). Establishing a murine model of the hematopoietic syndrome of the acute radiation syndrome. *Health Phys.* 103 (4), 343–355. doi:10.1097/HP.0b013e3182667309

Plichta, J. K., Gao, X., Lin, H., Dong, Q., Toh, E., Nelson, D. E., et al. (2017). Cutaneous burn injury promotes shifts in the bacterial microbiome in autologous donor skin. *Shock* 48 (4), 441–448. doi:10.1097/SHK.0000000000000874

Podolsky, S. H. (2012). Metchnikoff and the microbiome. *The Lancet* 380 (9856), 1810–1811. doi:10.1016/s0140-6736(12)62018-2

Portman, D. J., and Gass, M. L. S. (2014). Genitourinary syndrome of menopause: new terminology for vulvovaginal atrophy from the international society for the study of women's sexual health and the north American menopause society. *Maturitas* 79 (3), 349–354. doi:10.1016/j.maturitas.2014.07.013

Prasanna, P. G., Woloschak, G. E., DiCarlo, A. L., Buchsbaum, J. C., Schaue, D., Chakravarti, A., et al. (2020). Low-dose radiation therapy (LDRT) for covid-19: benefits or risks?. *Radiat. Res.* 194 (5), 452–464. doi:10.1667/RADE-20-00211.1

Proctor, L., LoTempio, J., Marquitz, A., Daschner, P., Xi, D., Flores, R., et al. (2019). A review of 10 years of human microbiome research activities at the US National Institutes of Health, Fiscal Years 2007-2016. *Microbiome.* 7 (1), 31. doi:10.1186/s40168-019-0620-y

Pujo, J., Petitfils, C., Le Faouder, P., Eeckhaut, V., Payros, G., Maurel, S., et al. (2020). Bacteria-derived long chain fatty acid exhibits anti-inflammatory properties in colitis. *Gut*, gutjnl. doi:10.1136/gutjnl-2020-321173

Quigley, E. M. M. (2012). Prebiotics and probiotics. *Nutr. Clin. Pract.* 27 (2), 195–200. doi:10.1177/0884533611423926

Ravel, J., Gajer, P., Abdo, Z., Schneider, G. M., Koenig, S. S. K., McCulle, S. L., et al. (2011). Vaginal microbiome of reproductive-age women. *Proc. Natl. Acad. Sci.* 108 (Suppl 1), 4680–4687. doi:10.1073/pnas.1002611107

Relman, D. A. (2002). New technologies, human-microbe interactions, and the search for previously unrecognized pathogens. *J. Infect. Dis.* 186 (Suppl. 2), S254–S258. doi:10.1086/344935

Relman, D. A. (1999). The search for unrecognized pathogens. *Science* 284 (5418), 1308–1310. doi:10.1126/science.284.5418.1308

Remirez, D., Ledón, N., and González, R. (2002). Role of histamine in the inhibitory effects of phycocyanin in experimental models of allergic inflammatory response. *Mediators Inflamm.* 11 (2), 81–85. doi:10.1080/09629350220131926

Riehl, T. E., Alvarado, D., Ee, X., Zuckerman, A., Foster, L., Kapoor, V., et al. (2019). Lactobacillus rhamnosus GG protects the intestinal epithelium from radiation injury through release of lipoteichoic acid, macrophage activation and the migration of mesenchymal stem cells. *Gut* 68 (6), 1003–1013. doi:10.1136/gutjnl-2018-316226

Rios, C. I., Cassatt, D. R., Dicarlo, A. L., Macchiarini, F., Ramakrishnan, N., Norman, M.-K., et al. (2014). Building the strategic national stockpile through the NIAID radiation nuclear countermeasures program. *Drug Dev. Res.* 75 (1), 23–28. doi:10.1002/ddr.21163

Robbins, J., and Schneider, A. B. (2000). Thyroid cancer following exposure to radioactive iodine. *Rev. Endocr. Metab. Disord.* 1 (3), 197–203. doi:10.1023/a:1010031115233

Rosenberg, E., and Zilber-Rosenberg, I. (2013). *The hologenome concept: human, animal and plant microbiota*. Springer International Publishing, 1–178. doi:10.1007/978-3-319-04241-1

Roth, R. R., and James, W. D. (1988). Microbial ecology of the skin. *Annu. Rev. Microbiol.* 42, 441–464. doi:10.1146/annurev.mi.42.100188.002301

Roy, S., and Trinchieri, G. (2017). Microbiota: a key orchestrator of cancer therapy. *Nat. Rev. Cancer* 17 (5), 271–285. doi:10.1038/nrc.2017.13

Salomaa, S., Bouffler, S. D., Atkinson, M. J., Cardis, E., and Hamada, N. (2020). Is there any supportive evidence for low dose radiotherapy for COVID-19 pneumonia?. *Int. J. Radiat. Biol.* 96 (10), 1228–1235. doi:10.1080/09553002.2020.1786609

Sanford, J. A., and Gallo, R. L. (2013). Functions of the skin microbiota in health and disease. *Semin. Immunol.* 25 (5), 370–377. doi:10.1016/j.smim.2013.09.005

Sasidharan, B., Ramadass, B., Viswanathan, P., Samuel, P., Gowri, M., Pugazhendhi, S., et al. (2019). A phase 2 randomized controlled trial of oral resistant starch supplements in the prevention of acute radiation proctitis in patients treated for cervical cancer. *J. Can. Res. Ther.* 15 (6), 1383–1391. doi:10.4103/jcrt.JCRT_152_19

Satyamitra, M. M., Cassatt, D. R., Hollingsworth, B. A., Price, P. W., Rios, C. I., Taliaferro, L. P., et al. (2020). Metabolomics in radiation biodosimetry: current approaches and advances. *Metabolites* 10 (8), 328. doi:10.3390/metabo10080328

Satyamitra, M. M., Kulkarni, S., Ghosh, S. P., Mullaney, C. P., Condliffe, D., and Srinivasan, V. (2011). Hematopoietic recovery and amelioration of radiation-induced lethality by the vitamin E isoform δ-tocotrienol. *Radiat. Res.* 175 (6), 736–745. doi:10.1667/RR2460.1

Schultz, G. S., Chin, G. A., Moldawer, L., and Diegelmann, R. F. (2011). "Principles of wound healing," in *Mechanisms of vascular disease: a reference book for vascular specialists*. Editors R. Fitridge and M. Thompson Adelaide (AU).

Segal, L. N., Rom, W. N., and Weiden, M. D. (2014). Lung microbiome for clinicians. New discoveries about bugs in healthy and diseased lungs. *Ann. ATS* 11 (1), 108–116. doi:10.1513/AnnalsATS.201310-339FR

Segers, C., Verslegers, M., Baatout, S., Leys, N., Lebeer, S., and Mastroleo, F. (2019). Food supplements to mitigate detrimental effects of pelvic radiotherapy. *Microorganisms* 7 (4), 97. doi:10.3390/microorganisms7040097

Seidel, C. L., Gerlach, R. G., Wiedemann, P., Weider, M., Rodrian, G., Hader, M., et al. (2020). Defining metaniches in the oral cavity according to their microbial composition and cytokine profile. *Ijms* 21 (21), 8218. doi:10.3390/ijms21218218

Sekelja, M., Berget, I., Næs, T., and Rudi, K. (2011). Unveiling an abundant core microbiota in the human adult colon by a phylogroup-independent searching approach. *Isme J.* 5 (3), 519–531. doi:10.1038/ismej.2010.129

Sender, R., Fuchs, S., and Milo, R. (2016). Are we really vastly outnumbered? Revisiting the ratio of bacterial to host cells in humans. *Cell* 164 (3), 337–340. doi:10.1016/j.cell.2016.01.013

Sender, R., Fuchs, S., and Milo, R. (2016). Revised estimates for the number of human and bacteria cells in the body. *Plos Biol.* 14 (8), e1002533. doi:10.1371/journal.pbio.1002533

Seneschal, J., Clark, R. A., Gehad, A., Baecher-Allan, C. M., and Kupper, T. S. (2012). Human epidermal Langerhans cells maintain immune homeostasis in skin by activating skin resident regulatory T cells. *Immunity* 36 (5), 873–884. doi:10.1016/j.immuni.2012.03.018

Sfriso, R., Egert, M., Gempeler, M., Voegeli, R., and Campiche, R. (2020). Revealing the secret life of skin - with the microbiome you never walk alone. *Int. J. Cosmet. Sci.* 42 (2), 116–126. doi:10.1111/ics.12594

Sharpton, T. J. (2018). Role of the gut microbiome in vertebrate evolution. *mSystems* 3 (2), e00174. doi:10.1128/mSystems.00174-17

Shimoi, K., Masuda, S., Furugori, M., Esaki, S., and Kinae, N. (1994). Radioprotective effect of antioxidative flavonoids in γ-ray irradiated mice. *Carcinogenesis* 15 (11), 2669–2672. doi:10.1093/carcin/15.11.2669

Shogbesan, O., Poudel, D. R., Victor, S., Jehangir, A., Fadahunsi, O., Shogbesan, G., et al. (2018). A systematic review of the efficacy and safety of fecal microbiota transplant for clostridium *difficile* infection in immunocompromised patients. *Can. J. Gastroenterol. Hepatol.* 2018, 1. doi:10.1155/2018/1394379

Shukla, P. K., Gangwar, R., Manda, B., Meena, A. S., Yadav, N., Szabo, E., et al. (2016). Rapid disruption of intestinal epithelial tight junction and barrier dysfunction by ionizing radiation in mouse colon *in vivo*: protection by N-acetyl-L-cysteine. *Am. J. Physiology-Gastrointestinal Liver Physiol.* 310 (9), G705–G715. doi:10.1152/ajpgi.00314.2015

Singer, A. J., and Clark, R. A. F. (1999). Cutaneous wound healing. *N. Engl. J. Med.* 341 (10), 738–746. doi:10.1056/NEJM199909023411006

Sivan, A., Corrales, L., Hubert, N., Williams, J. B., Aquino-Michaels, K., Earley, Z. M., et al. (2015). Commensal Bifidobacterium promotes antitumor immunity and facilitates anti-PD-L1 efficacy. *Science* 350 (6264), 1084–1089. doi:10.1126/science.aac4255

Small, J. D., and Deitrich, R. (2007). "Environmental and equipment monitoring," in *The mouse in biomedical research*. Editors J. G. Fox, M. T. Davisson, F. W. Quimby, S. W. Barthold, C. E. Newcomer, and A. L. Smith (Burlington: Academic Press), 409–436.

Sofi, M. H., Gudi, R., Karumuthil-Melethil, S., Perez, N., Johnson, B. M., and Vasu, C. (2014). pH of drinking water influences the composition of gut microbiome and type 1 diabetes incidence. *Diabetes* 63 (2), 632–644. doi:10.2337/db13-0981

Solans, R., Bosch, J. A., Galofré, P., Porta, F., Roselló, J., Selva-O'Callagan, A., et al. (2001). Salivary and lacrimal gland dysfunction (sicca syndrome) after radioiodine therapy. *J. Nucl. Med.* 42 (5), 738–743.

Somosy, Z., Horváth, G., Telbisz, Á., Réz, G., and Pálfia, Z. (2002). Morphological aspects of ionizing radiation response of small intestine. *Micron* 33 (2), 167–178. doi:10.1016/S0968-4328(01)00013-0

Spor, A., Koren, O., and Ley, R. (2011). Unravelling the effects of the environment and host genotype on the gut microbiome. *Nat. Rev. Microbiol.* 9 (4), 279–290. doi:10.1038/nrmicro2540

Sroussi, H. Y., Epstein, J. B., Bensadoun, R.-J., Saunders, D. P., Lalla, R. V., Migliorati, C. A., et al. (2017). Common oral complications of head and neck cancer radiation therapy: mucositis, infections, saliva change, fibrosis, sensory dysfunctions, dental caries, periodontal disease, and osteoradionecrosis. *Cancer Med.* 6 (12), 2918–2931. doi:10.1002/cam4.1221

Stavropoulou, E., and Bezirtzoglou, E. (2020). Probiotics in medicine: a long debate. *Front. Immunol.* 11, 2192. doi:10.3389/fimmu.2020.02192

Stecher, B., and Hardt, W.-D. (2011). Mechanisms controlling pathogen colonization of the gut. *Curr. Opin. Microbiol.* 14 (1), 82–91. doi:10.1016/j.mib.2010.10.003

Stoddard, T. J., Varadarajan, V. V., Dziegielewski, P. T., Boyce, B. J., and Justice, J. M. (2019). Detection of microbiota in post radiation sinusitis. *Ann. Otol Rhinol Laryngol.* 128 (12), 1116–1121. doi:10.1177/0003489419862583

Su, Y.-x., Liu, L.-p., Li, L., Li, X., Cao, X.-j., Dong, W., et al. (2014). Factors influencing the incidence of sinusitis in nasopharyngeal carcinoma patients after intensity-modulated radiation therapy. *Eur. Arch. Otorhinolaryngol.* 271 (12), 3195–3201. doi:10.1007/s00405-014-3004-8

Suau, A., Bonnet, R., Sutren, M., Godon, J.-J., Gibson, G. R., Collins, M. D., et al. (1999). Direct analysis of genes encoding 16S rRNA from complex communities reveals many novel molecular species within the human gut. *Appl. Environ. Microbiol.* 65 (11), 4799–4807. doi:10.1128/aem.65.11.4799-4807.1999

Suzuki, T., Sutani, T., Nakai, H., Shirahige, K., and Kinoshita, S. (2020). The microbiome of the meibum and ocular surface in healthy subjects. *Invest. Ophthalmol. Vis. Sci.* 61 (2), 18. doi:10.1167/iovs.61.2.18

Tanoue, T., Morita, S., Plichta, D. R., Skelly, A. N., Suda, W., Sugiura, Y., et al. (2019). A defined commensal consortium elicits CD8 T cells and anti-cancer immunity. *Nature* 565 (7741), 600–605. doi:10.1038/s41586-019-0878-z

Tarapan, S., Matangkasombut, O., Trachootham, D., Sattabanasuk, V., Talungchit, S., Paemuang, W., et al. (2019). OralCandidacolonization in xerostomic postradiotherapy head and neck cancer patients. *Oral Dis.* 25 (7), 1798–1808. doi:10.1111/odi.13151

Thomas, G. (2018). Radiation and thyroid cancer-an overview. *Radiat. Prot. Dosimetry* 182 (1), 53–57. doi:10.1093/rpd/ncy146

Tolentino, E. d. S., Centurion, B. S., Ferreira, L. H. C., Souza, A. P. d., Damante, J. H., and Rubira-Bullen, I. R. F. (2011). [No title available]. *J. Appl. Oral Sci.* 19 (5), 448–454. doi:10.1590/s1678-77572011000500003

Tonneau, M., Elkrief, A., Pasquier, D., Paz Del Socorro, T., Chamaillard, M., Bahig, H., et al. (2021). The role of the gut microbiome on radiation therapy efficacy and gastrointestinal complications: a systematic review. *Radiother. Oncol.* 156, 1–9. doi:10.1016/j.radonc.2020.10.033

Touchefeu, Y., Montassier, E., Nieman, K., Gastinne, T., Potel, G., Bruley Des Varannes, S., et al. (2014). Systematic review: the role of the gut microbiota in chemotherapy- or radiation-induced gastrointestinal mucositis - current evidence and potential clinical applications. *Aliment. Pharmacol. Ther.* 40 (5), a–n. doi:10.1111/apt.12878

Trujillo-Vargas, C. M., Schaefer, L., Alam, J., Pflugfelder, S. C., Britton, R. A., and de Paiva, C. S. (2020). The gut-eye-lacrimal gland-microbiome axis in Sjögren Syndrome. *Ocul. Surf.* 18 (2), 335–344. doi:10.1016/j.jtos.2019.10.006

Tsementzi, D., Pena-Gonzalez, A., Bai, J., Hu, Y. J., Patel, P., Shelton, J., et al. (2020). Comparison of vaginal microbiota in gynecologic cancer patients pre- and post-radiation therapy and healthy women. *Cancer Med.* 9 (11), 3714–3724. doi:10.1002/cam4.3027

Turkington, C. J. R., Varadan, A. C., Grenier, S. F., and Grasis, J. A. (2021). The viral janus: viruses as aetiological agents and treatment options in colorectal cancer. *Front. Cel. Infect. Microbiol.* 10, 10. doi:10.3389/fcimb.2020.601573

Turnbaugh, P. J., Quince, C., Faith, J. J., McHardy, A. C., Yatsunenko, T., Niazi, F., et al. (2010). Organismal, genetic, and transcriptional variation in the deeply sequenced gut microbiomes of identical twins. *Proc. Natl. Acad. Sci.* 107 (16), 7503–7508. doi:10.1073/pnas.1002355107

Turnbaugh, P. J., Ridaura, V. K., Faith, J. J., Rey, F. E., Knight, R., and Gordon, J. I. (2009). The effect of diet on the human gut microbiome: a metagenomic analysis in humanized gnotobiotic mice. *Sci. Translational Med.* 1 (6), 6ra14. doi:10.1126/scitranslmed.3000322

Turner, N. D., Braby, L. A., Ford, J., and Lupton, J. R. (2002). Opportunities for nutritional amelioration of radiation-induced cellular damage. *Nutrition* 18 (10), 904–912. doi:10.1016/s0899-9007(02)00945-0

Umar, S. (2010). Intestinal stem cells. *Curr. Gastroenterol. Rep.* 12 (5), 340–348. doi:10.1007/s11894-010-0130-3

Ursell, L. K., Metcalf, J. L., Parfrey, L. W., and Knight, R. (2012). Defining the human microbiome. *Nutr. Rev.* 70 (Suppl. 1), S38–S44. doi:10.1111/j.1753-4887.2012.00493.x

Vaishnava, S., Behrendt, C. L., Ismail, A. S., Eckmann, L., and Hooper, L. V. (2008). Paneth cells directly sense gut commensals and maintain homeostasis at the intestinal host-microbial interface. *Proc. Natl. Acad. Sci.* 105 (52), 20858–20863. doi:10.1073/pnas.0808723105

Vaishnava, S., Yamamoto, M., Severson, K. M., Ruhn, K. A., Yu, X., Koren, O., et al. (2011). The antibacterial lectin RegIII promotes the spatial segregation of microbiota and host in the intestine. *Science* 334 (6053), 255–258. doi:10.1126/science.1209791

Valdéz, J. C., Peral, M. C., Rachid, M., Santana, M., and Perdigón, G. (2005). Interference of Lactobacillus plantarum with *Pseudomonas aeruginosa in vitro* and in infected burns: the potential use of probiotics in wound treatment. *Clin. Microbiol. Infect.* 11 (6), 472–479. doi:10.1111/j.1469-0691.2005.01142.x

van Nood, E., Vrieze, A., Nieuwdorp, M., Fuentes, S., Zoetendal, E. G., de Vos, W. M., et al. (2013). Duodenal infusion of donor feces for RecurrentClostridium *difficile*. *N. Engl. J. Med.* 368 (5), 407–415. doi:10.1056/NEJMoa1205037

Vanhoecke, B., De Ryck, T., Stringer, A., Van de Wiele, T., and Keefe, D. (2015). Microbiota and their role in the pathogenesis of oral mucositis. *Oral Dis.* 21 (1), 17–30. doi:10.1111/odi.12224

Vesty, A., Gear, K., Biswas, K., Mackenzie, B. W., Taylor, M. W., and Douglas, R. G. (2020). Oral microbial influences on oral mucositis during radiotherapy treatment of head and neck cancer. *Support Care Cancer* 28 (6), 2683–2691. doi:10.1007/s00520-019-05084-6

Villegas, L., Stidham, T., and Nozik-Grayck, E. (2014). Oxidative stress and therapeutic development in lung diseases. *J. Pulm. Respir. Med.* 04 (4). doi:10.4172/2161-105X.1000194

Villéger, R., Lopès, A., Carrier, G., Veziant, J., Billard, E., Barnich, N., et al. (2019). Intestinal microbiota: a novel target to improve anti-tumor treatment? *Ijms* 20 (18), 4584. doi:10.3390/ijms20184584

Vojvodic, A., Peric-Hajzler, Z., Matovic, D., Vojvodic, P., Vlaskovic-Jovicevic, T., Sijan, G., et al. (2019). Gut microbiota and the alteration of immune balance in skin diseases: from nutraceuticals to fecal transplantation. *Open Access Maced J. Med. Sci.* 7 (18), 3034–3038. doi:10.3889/oamjms.2019.827

Wang, M., AhrnÃ©, S., Jeppsson, B., and Molin, G. r. (2005). Comparison of bacterial diversity along the human intestinal tract by direct cloning and sequencing of 16S rRNA genes. *FEMS Microbiol. Ecol.* 54 (2), 219–231. doi:10.1016/j.femsec.2005.03.012

Wang, S. P., Rubio, L. A., Duncan, S. H., Donachie, G. E., Holtrop, G., Lo, G., et al. (2020). Pivotal roles for pH, lactate, and lactate-utilizing bacteria in the stability of a human colonic microbial ecosystem. *mSystems* 5 (5). doi:10.1128/mSystems.00645-20

Wang, S., Xu, M., Wang, W., Cao, X., Piao, M., Khan, S., et al. (2016). Systematic review: adverse events of fecal microbiota transplantation. *PLoS ONE* 11 (8), e0161174. doi:10.1371/journal.pone.0161174

Wang, X., Yang, Y., and Huycke, M. M. (2020). Risks associated with enterococci as probiotics. *Food Res. Int.* 129, 108788. doi:10.1016/j.foodres.2019.108788

Waselenko, J. K., MacVittie, T. J., Blakely, W. F., Pesik, N., Wiley, A. L., Dickerson, W. E., et al. (2004). Medical management of the acute radiation syndrome: recommendations of the strategic national stockpile radiation working group. *Ann. Intern. Med.* 140 (12), 1037–1051. doi:10.7326/0003-4819-140-12-200406150-00015

Wijers, O. B., Levendag, P. C., Braaksma, M. M. J., Boonzaaijer, M., Visch, L. L., and Schmitz, P. I. M. (2002). Patients with head and neck cancer cured by radiation therapy: a survey of the dry mouth syndrome in long-term survivors. *Head Neck* 24 (8), 737–747. doi:10.1002/hed.10129

Williams, J. M., Duckworth, C. A., Burkitt, M. D., Watson, A. J. M., Campbell, B. J., and Pritchard, D. M. (2015). Epithelial cell shedding and barrier function. *Vet. Pathol.* 52 (3), 445–455. doi:10.1177/0300985814559404

Willis, K. A., Postnikoff, C. K., Freeman, A., Rezonzew, G., Nichols, K., Gaggar, A., et al. (2020). The closed eye harbours a unique microbiome in dry eye disease. *Sci. Rep.* 10 (1), 12035. doi:10.1038/s41598-020-68952-w

Wilson, B. R. (1963). Survival studies of whole-body x-irradiated germfree (axenic) mice. *Radiat. Res.* 20, 477–483. doi:10.2307/3571378

Wilson, G. D., Mehta, M. P., Welsh, J. S., Chakravarti, A., Rogers, C. L., and Fontanesi, J. (2020). Investigating low-dose thoracic radiation as a treatment for COVID-19 patients to prevent respiratory failure. *Radiat. Res.* 194 (1), 1–8. doi:10.1667/RADE-20-00108.1

Wojcik, A. (2002). The medical basis for radiation-accident preparedness. The clinical care of victims, proceedings of the fourth international REACT/TS conference on the medical basis for radiation-accident preparedness. *Radiat. Res.* 158 (1), 125. doi:10.1667/0033-7587(2002)158[0125:Br]2.0.Co;2

Wolcott, R. D., Hanson, J. D., Rees, E. J., Koenig, L. D., Phillips, C. D., Wolcott, R. A., et al. (2016). Analysis of the chronic wound microbiota of 2,963 patients by 16S rDNA pyrosequencing. *Wound Rep. Reg.* 24 (1), 163–174. doi:10.1111/wrr.12370

Wolf, P., Weger, W., Patra, V., Gruber-Wackernagel, A., and Byrne, S. N. (2016). Desired response to phototherapy vs photoaggravation in psoriasis: what makes the difference?. *Exp. Dermatol.* 25 (12), 937–944. doi:10.1111/exd.13137

Xiao, H.-w., Cui, M., Li, Y., Dong, J.-l., Zhang, S.-q., Zhu, C.-c., et al. (2020). Gut microbiota-derived indole 3-propionic acid protects against radiation toxicity via retaining acyl-CoA-binding protein. *Microbiome* 8 (1), 17. doi:10.1186/s40168-020-00845-6

Xiao, H.-w., Li, Y., Luo, D., Dong, J.-l., Zhou, L.-x., Zhao, S.-y., et al. (2018). Hydrogen-water ameliorates radiation-induced gastrointestinal toxicity via MyD88's effects on the gut microbiota. *Exp. Mol. Med.* 50 (1), e433. doi:10.1038/emm.2017.246

Yang, J., Ding, C., Dai, X., Lv, T., Xie, T., Zhang, T., et al. (2017). Soluble dietary fiber ameliorates radiation-induced intestinal epithelial-to-mesenchymal transition and fibrosis. *JPEN J. Parenter. Enteral Nutr.* 41 (8), 1399–1410. doi:10.1177/0148607116671101

Yatsunenko, T., Rey, F. E., Manary, M. J., Trehan, I., Dominguez-Bello, M. G., Contreras, M., et al. (2012). Human gut microbiome viewed across age and geography. *Nature* 486 (7402), 222–227. doi:10.1038/nature11053

Yu, L., Wang, L., Yi, H., and Wu, X. (2020). Beneficial effects of LRP6-CRISPR on prevention of alcohol-related liver injury surpassed fecal microbiota transplant in a rat model. *Gut Microbes* 11 (4), 1015–1029. doi:10.1080/19490976.2020.1736457

Zha, J.-M., Li, H.-S., Lin, Q., Kuo, W.-T., Jiang, Z.-H., Tsai, P.-Y., et al. (2019). Interleukin 22 expands transit-amplifying cells while depleting Lgr5+ stem cells via inhibition of wnt and notch signaling. *Cell Mol. Gastroenterol. Hepatol.* 7 (2), 255–274. doi:10.1016/j.jcmgh.2018.09.006

Zhang, X., Fisher, R., Hou, W., Shields, D., Epperly, M. W., Wang, H., et al. (2020). Second-generation probiotics producing IL-22 increase survival of mice after total body irradiation. *In Vivo* 34 (1), 39–50. doi:10.21873/invivo.11743

Zhang, Y., Zhang, B., Dong, L., and Chang, P. (2019). Potential of omega-3 polyunsaturated fatty acids in managing chemotherapy- or radiotherapy-related intestinal microbial dysbiosis. *Adv. Nutr.* 10 (1), 133–147. doi:10.1093/advances/nmy076

Zhao, Y., Zhang, J., Han, X., and Fan, S. (2019). Total body irradiation induced mouse small intestine senescence as a late effect. *J. Radiat. Res.* 60 (4), 442–450. doi:10.1093/jrr/rrz026

Zhao, Z., Cheng, W., Qu, W., Shao, G., and Liu, S. (2020). Antibiotic alleviates radiation-induced intestinal injury by remodeling microbiota, reducing inflammation, and inhibiting fibrosis. *ACS Omega* 5 (6), 2967–2977. doi:10.1021/acsomega.9b03906

Zhong, Y., Pouliot, M., Downey, A.-M., Mockbee, C., Roychowdhury, D., Wierzbicki, W., et al. (2020). Efficacy of delayed administration of sargramostim up to 120 hours post exposure in a nonhuman primate total body radiation model. *Int. J. Radiat. Biol.*, 1–17. doi:10.1080/09553002.2019.1673499

Zhu, B., Wang, X., and Li, L. (2010). Human gut microbiome: the second genome of human body. *Protein Cell* 1 (8), 718–725. doi:10.1007/s13238-010-0093-z

Zhu, X.-X., Yang, X.-J., Chao, Y.-L., Zheng, H.-M., Sheng, H.-F., Liu, H.-Y., et al. (2017). The potential effect of oral microbiota in the prediction of mucositis during radiotherapy for nasopharyngeal carcinoma. *EBioMedicine* 18, 23–31. doi:10.1016/j.ebiom.2017.02.002

Disclaimer: The opinions contained herein are the private views of the authors and are not necessarily those of the National Institute of Allergy and Infectious Diseases, National Institutes of Health.

Conflict of Interest: The authors declare that the research was conducted in the absence of any commercial or financial relationships that could be construed as a potential conflict of interest.

frontiers in Pharmacology

REVIEW
published: 25 May 2021
doi: 10.3389/fphar.2021.640040

COVID-19-Associated Pneumonia: Radiobiological Insights

Sabine François[1], Carole Helissey[2], Sophie Cavallero[1], Michel Drouet[1], Nicolas Libert[3], Jean-Marc Cosset[4], Eric Deutsch[5,6], Lydia Meziani[5,6] and Cyrus Chargari[1,5,6]*

[1]Department of Radiation Biological Effects, French Armed Forces Biomedical Research Institute, Brétigny-sur-Orge, France, [2]Clinical Unit Research, HIA Bégin, Paris, France, [3]Percy Army Training Hospital, Clamart, France, [4]Centre de Radiothérapie Charlebourg/La Défense, Groupe Amethyst, La Garenne-Colombes, France, [5]Department of Radiation Oncology, Gustave Roussy Comprehensive Cancer Center, Villejuif, France, [6]INSERM U1030, Université Paris Saclay, Le Kremlin Bicêtre, France

The evolution of SARS-CoV-2 pneumonia to acute respiratory distress syndrome is linked to a virus-induced "cytokine storm", associated with systemic inflammation, coagulopathies, endothelial damage, thrombo-inflammation, immune system deregulation and disruption of angiotensin converting enzyme signaling pathways. To date, the most promising therapeutic approaches in COVID-19 pandemic are linked to the development of vaccines. However, the fight against COVID-19 pandemic in the short and mid-term cannot only rely on vaccines strategies, in particular given the growing proportion of more contagious and more lethal variants among exposed population (the English, South African and Brazilian variants). As long as collective immunity is still not acquired, some patients will have severe forms of the disease. Therapeutic perspectives also rely on the implementation of strategies for the prevention of secondary complications resulting from vascular endothelial damage and from immune system deregulation, which contributes to acute respiratory distress and potentially to long term irreversible tissue damage. While the anti-inflammatory effects of low dose irradiation have been exploited for a long time in the clinics, few recent physiopathological and experimental data suggested the possibility to modulate the inflammatory storm related to COVID-19 pulmonary infection by exposing patients to ionizing radiation at very low doses. Despite level of evidence is only preliminary, these preclinical findings open therapeutic perspectives and are discussed in this article.

Keywords: radiation therapy, SARS-CoV-2 pneumonia, immune system, radiation-induced cancers, radiobiology

OPEN ACCESS

Edited by:
Ales Tichy,
University of Defense, Czechia

Reviewed by:
Dimitrios Kardamakis,
University of Patras, Greece
Abdallah El-Sayed Allam,
Tanta University, Egypt

****Correspondence:***
Sabine François
sfm.francois@gmail.com

Specialty section:
This article was submitted to Translational Pharmacology, a section of the journal Frontiers in Pharmacology

Received: *10 December 2020*
Accepted: *04 March 2021*
Published: *25 May 2021*

Citation:
François S, Helissey C, Cavallero S, Drouet M, Libert N, Cosset J-M, Deutsch E, Meziani L and Chargari C (2021) COVID-19-Associated Pneumonia: Radiobiological Insights. Front. Pharmacol. 12:640040. doi: 10.3389/fphar.2021.640040

THE CONTEXT

First cases of the new coronavirus (COVID-19) were detected in Wuhan in December 2019 (Zhu et al., 2020). On January 30, 2020, the World Health Organization (WHO) officially declared the COVID-19 epidemic as a public health emergency of international concern. A year has passed and despite unprecedented health measures, the number of deaths linked to this virus is now approximately 2,412,000 worldwide, including more than 305.700, in Europe and 117,160 and in United Kingdom. COVID-19 is a potentially serious illness caused by the Coronavirus 2 of Severe Acute Respiratory Syndrome (SARS-CoV-2) (https://fr.statista.com/statistiques/1101324/morts-coronavirus-monde/).

Coronaviruses represent a large family of viruses that can cause a wide range of illnesses in humans, ranging from common cold symptoms to life-threatening SARS (Yin and Wunderink, 2018;

Malik, 2020). SARS-CoV-2 belongs to the beta-coronavirus subfamily ß-CoV and internalizes the body via the respiratory tract or through the mucosa (e.g., eyes). The virus may spread via saliva, respiratory secretions or droplets, which can be expelled into the ambient air by an infected person through coughs and/or sneezes and may remain suspended in the air for several hours. Its spread in the population is mainly through close contacts or aerosolization of viral particles into insufficiently ventilated indoor spaces (Anderson et al., 2020). When SARS-CoV-2 infects the respiratory tract, it causes pneumonia (often pauci-symptomatic) and may evolve to acute respiratory distress syndrome (ARDS) in about 15% of cases (Ragab et al., 2020).

Mortality in COVID-19 patients is linked to a virus-induced "cytokine storm" (Hu et al., 2020; Song et al., 2020). This is a continuous mechanism involving hyper-activation of immune cells, including lymphocytes and macrophages producing large amounts of pro-inflammatory cytokines such as IL-1, IL-6, IL-18, IFN-γ, and TNF- a leading to worsening of ARDS with the appearance of generalized tissue damage, potentially leading to multi-organ failure and patient death (Fara et al., 2020). Since the start of the pandemics, other clinical manifestations concomitant with pneumonia following viral infection have been described. Those include coagulopathies (activation of coagulation) and cardiac dysfunctions contributing to mortality, and even being the main cause of death in some patients who develop arrhythmias, acute coronary syndromes and venous thromboembolic events (Middeldorp et al., 2020; Nishiga et al., 2020; Ribes et al., 2020). The pathophysiology of COVID-19 cardiac disease also leads to direct myocardial lesions consecutive to viral-related cardiomyocyte damage, and is potentiated by the consequences of systemic inflammation that is a major and common mechanism responsible for cardiac damage (Bansal, 2020).

Severe forms of COVID-19 are preferentially observed in the elderly population, in people with underlying health problems such as diabetes and in those with deficit in their immune system (Shahid et al., 2020). In severe cases of COVID-19, damages can spread beyond the lungs to other organs, including the heart, kidneys, liver, brain, eyes, gastrointestinal tract, skin, and bone marrow with its stem cell compartments and hematopoietic progenitors, (Cipriano et al., 2020; Gupta et al., 2020; Khaled and Hafez, 2020). The presence of viral RNA is detected post-mortem in the endothelial cells of many organs, revealing endothelitis (Jung et al., 2020; Varga et al., 2020). Endothelial damage and thrombo-inflammation, immune system deregulation and disruption of angiotensin converting enzyme (ACE2) signaling pathways could contribute to the onset of these extra-pulmonary manifestations of COVID-19. The expression of ACE2 in the tissues facilitates the penetration of SARS-CoV-2, by enabling the virus to propagate to the cells of many organs, thereby decreasing the expression of this protein within the infected cells themselves and increasing expression of angiotensin II (Ang II) (Kuba et al., 2005; Banu et al., 2020; Bourgonje et al., 2020). Furthermore, ACE-2 expression is found in endothelial cells, smooth muscle cells and perivascular pericytes of the vast majority of organs. SARS-CoV-2, once present in the circulation, can therefore easily spread to other parts of the body (Huertas et al., 2020). ACE2 has anti-inflammatory and anti-fibrotic properties through its function of conversion of angiotensin (Ang–II) into Ang (1–7), and its decreased expression caused by the virus promotes disruption of the immune system and contribute to the development of tissue fibrosis. Combined with the activation of macrophages, such impact on ACE2 could be involved in the development of COVID-19-related fibrosis (He et al., 2006; Meng et al., 2014; Patel et al., 2016; Rodrigues Prestes et al., 2017; Smigiel and Parks, 2018; Banu et al., 2020; Pagliaro, 2020). To date, the most promising therapeutic approaches in COVID-9 pandemic are linked to the development of vaccines. However, the fight against COVID-19 pandemic in the short and mid-term cannot only rely on vaccines strategies, in particular given the growing proportion of more contagious and more lethal variants among exposed population. As long as collective immunity is still not acquired, some patients will have severe forms of the disease. Therapeutic perspectives also rely on the implementation of strategies for the prevention of secondary complications resulting from vascular endothelial damage and from immune system deregulation, which contributes to acute respiratory distress and potentially to long-term tissue fibrosis.

The C5a complement factor and its receptor (C5aR1) have key roles in the initiation and maintenance of inflammatory processes by recruiting neutrophils and monocytes, contributing to the pathophysiology of COVID-19 related acute respiratory distress syndrome. The levels of soluble C5a are increased in proportion to the severity of COVID19 infection. In animal models, inhibition of anti-C5aR1 axis prevented the C5a-mediated recruitment and activation of human myeloid cells in damaged lungs. These data open pharmacological perspectives for the modulation of COVID-19 related inflammation(Carvelli et al., 2020).

Several recent physiopathological and experimental data suggest the possibility to modulate the inflammatory storm related to COVID-19 pulmonary fsfsfs by exposing patients to ionizing radiation at very low doses. Despite level of evidence is only emerging, these preclinical findings open therapeutic perspectives and are discussed in this article.

PATHOPHYSIOLOGICAL MECHANISMS OF THE RESPIRATORY COMPLICATIONS OF COVID-19

The diagnosis of ARDS is conventionally based on well-defined parameters using the Berlin criteria, the oxygenation index and the Murray/lung Injury Score used by intensive care physicians to define the clinical, ventilatory, gasometric parameters (analysis of blood gas) and radiological criteria to establish the diagnosis of this serious pulmonary syndrome and to adapt the ventilatory management as well as possible (ARDS Definition Task Force et al., 2012; Huber et al., 2020). Respiratory physiology in patients developing COVID-19 differs from the "conventional" acute respiratory distress syndrome (ARDS) (Gattinoni et al., 2020). Indeed, there is an aberrant activation of the inflammatory system and coagulation processes, and this pattern is somewhat

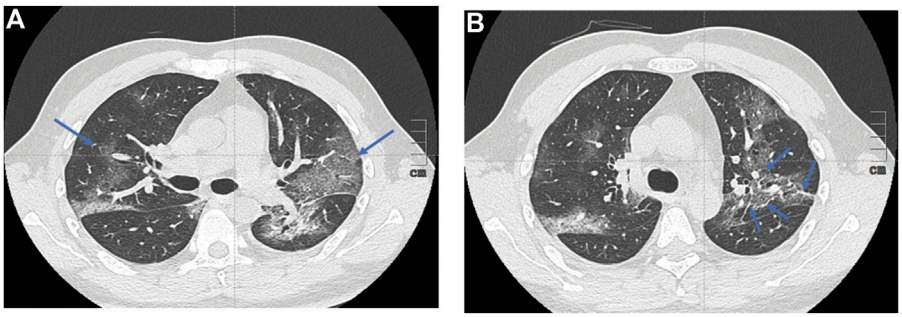

FIGURE 1 | Chest computed tomography images of patients with COVID-19 pneumonia **(A)** shows Ground-glass opacities (blue arrows) **(B)** shows confluent crazy-paving pattern and consolidation opacities: secondary appearance of intralobular reticulations (blue arrows).

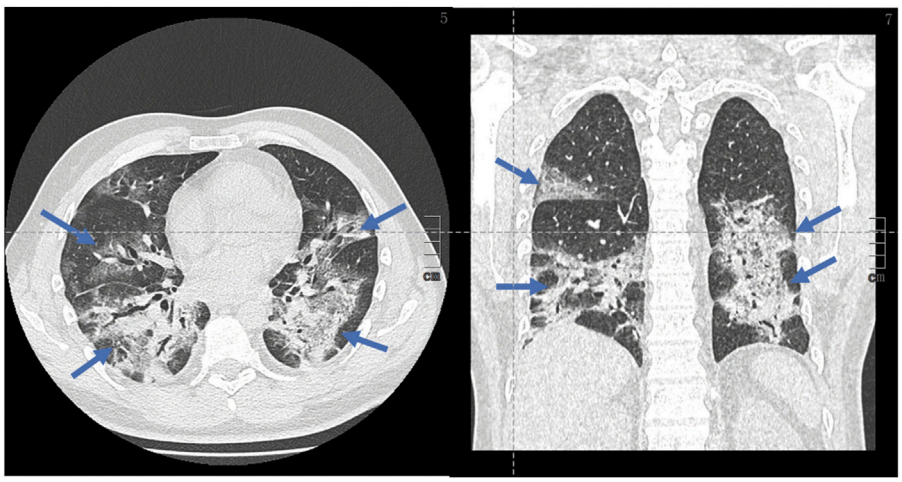

FIGURE 2 | Chest computed tomography images of patients with COVID-19 pneumonia: shows extensive abnormalities and a proportion of pulmonary condensation (blue arrows) vs. higher Ground-glass, with possible progression to pulmonary fibrosis.

characteristic of the "immuno-thrombostic" process observed in COVID-19 pneumonia (Nakazawa and Ishizu, 2020). The classical ARDS pneumonitis seen in patients infected with SARS-CoV-2 is characterized by a decrease in lung distension capability. Damages to lung tissue strongly affect the level of ventilation capability. Many unventilated areas are filled with fluid (alveolar edema) and cells. The alveolar air is replaced by a pathological product, which leads to abnormal opacities (alveolar condensations), as seen on computed tomography scans.

Chest scans are indicated to guide the management and monitoring of pulmonary symptoms in a patient with COVID-19. In addition to its use for early diagnosis, the chest scan has a prognostic role, making it possible to visually assess the extent of pulmonary lesions and monitor over time. The abnormalities observed on the CT scan are correlated to severity of clinical symptoms (Wong et al., 2003). Although radiological changes observed in the context of SARS-CoV-2 infection are not specific, those are indicative of the diagnosis in the current epidemic context. The most reported CT abnormalities are as follows: ground-glass opacities, multifocal, bilateral, and asymmetrical, with preferentially subpleural localization predominant in the basal and posterior area. The presence of bronchiolar micronodules, mediastinal lymphadenopathy and pleural effusions is also suggestive. All those characteristics may be found in pulmonary bacterial infections. At a later stage, the radiological aspects evolves toward a "crazy paving" aspect, with appearance of intralobular reticulations (peak around the 10th day) and linear condensations can be observed (**Figure 1A**) (ARDS Definition Task Force et al., 2012; Smigiel & Parks, 2018; Huber et al., 2020). In most severeforms of COVID19 pneumonia, CT scan shows extensive abnormalities and a higher proportion of pulmonary condensation vs. ground-glass opacities (**Figure 1B**). With time, weak regression of the abnormalities can be observed, often associated with so-called late fibrous sequelae (**Figure 2**).

Despite an unprecedented investment to look at therapeutic strategies, there is currently no effective treatment for COVID-19 infection. Most potential treatments have been evaluated in populations with significant heterogeneity and various levels of

symptoms severity. Several existing antiviral treatments are being tested: remdesivir, combination lopinavir/ritonavir, combination lopinavir/ritonavir/interferon beta or even hydroxychloroquine. Remdesivir did not show effect in patients presenting with severe form of the disease, as assessed per mortality probability at day 28 (Beigel et al., 2020a; Wang et al., 2020). It nevertheless has a possible beneficial effect in non-ventilated patients (Beigel et al., 2020b). Hydroxychloroquine has shown no benefit in large clinical trials (RECOVERY Collaborative Group et al., 2020b). It also exhibits significant side effects. Lopinavir/ritonavir was unsuccessful (RECOVERY Collaborative Group et al., 2020a; Cao et al., 2020). Modulation of the immune response by specific blockade of an interleukin was not effective after initially raising high expectations. Patients who received tocilizumab had fewer serious infections than patients who received placebo. In the RECOVERY trial, tocilizumab reduced death from 33 to 29%. It also reduced the chance of progressing to invasive mechanical ventilation or death from 38 to 33%. (Stone et al., 2020; RECOVERY Collaborative Group, 2021). Plasma from convalescent patients has not shown an effect in the general population (Simonovich et al., 2020). It could nevertheless be effective in patients not developing an immune response. Monoclonal antibodies targeted against the spike protein of SARS-Cov-2 (casirivimab and imdevimab) (Baum et al., 2020) have just been authorized by the FDA for patients with mild to moderate symptoms of COVID-19. In combination, monoclonal antibodies seem to reduce the probability of hospitalization or needing urgent cares. Those however did not improve the prognosis in hospitalized patients and may even make ventilated patients worse. The only specific treatment which demonstrated a decrease in mortality is corticosteroid as an anti-inflammatory therapy, dexamethasone at a dose of 6 mg/day with a modest decrease from 25.7 to 22.9% (RECOVERY Collaborative Group et al., 2020b). The disappointing results of specific therapies underline the importance of symptomatic treatment and routine supportive care, such as adapted oxygen therapy and prophylaxis of thromboembolic disease (which frequently complicates severe cases) in combination with nonspecific treatments of organs failure (Helms et al., 2020).

The long-term respiratory sequelae of COVD-19 are also a significant clinical concern. Based on data from 2003 SARS-CoV, showing that 35–60% of survivors developed pulmonary fibrosis with reduced lung function, it can be expected that at the end of this pandemic, a high number of patients surviving severe cases of Covid-19 will be severely affected by persistent respiratory complications. The true incidence of such late fibrosis in the COVID-19 context is however still uncertain (Ronald). After ARDS following SARS-CoV-2 infection, there is a progressive accumulation of the extracellular matrix potentially leading to respiratory failure. Anatomopathological examinations carried out on patients who died of COVID-19 revealed the presence of numerous lesions of alveolar epithelial cells, the formation of hyaline membranes, type II pneumocyte hyperplasia, fibroblastic proliferation with a matrix important extracellular and fibrin deposits in alveolar spaces (Carver et al., 2007; Raghu et al., 2011; Tian et al., 2020). The mechanistic phenomenon underlying the onset of lung fibrosis following COVID-19 is poorly understood, but may involve the continued presence of the immune response causing deregulation of tissue repair. The magnitude of the cytokine storm, and severity of cell alterations within the alveolar tissue, may over time accelerate the development of fibrosis in a diffuse manner across both lungs. Lung transplants have been performed to treat patients presenting with acute respiratory failure following a COVID-19 infection. Pathological examination reveals that the virus may cause an almost complete destruction of both lungs (Hu et al., 2020). Lung transplantation could be an effective curative treatment for terminal lung diseases. However, we must remain cautious about this therapeutic possibility, because the recovery of a lung transplant patient is long and very uncertain, and access to lung transplants is highly limited worldwide (Roux et al., 2019).

RATIONALE FOR LOW DOSE IRRADIATION IN THE INFLAMMATORY CONTEXT

As pointed out by Edward J Calabrese and Gaurav Dhawan, during the first half of the 20th century, radiation therapy was used a long time ago to treat pneumonia. Fifteen studies grouping together around 700 cases of pneumonia of bacterial origin (lobar and bronchopneumonia), including those unresponsive to treatment with sulfonamides, and described as being interstitial and atypical were treated effectively with low doses of X-rays, showing a decrease in clinical symptoms, and a lowering of mortality rates (Calabrese and Dhawan, 2013). Low doses of irradiations were also used for skin or articular inflammatory diseases, with most frequently high efficacy. Low doses of irradiation have been proposed as an effective treatment option in various benign inflammatory pathologies, including osteoarthritis, keloids scares, eczema, lymphatic fistulas, age-related macular degeneration, sialorrhea and suppurative hydradenitis (chronic inflammatory skin disease) (Torres Royo et al., 2020). This approach showed a beneficial effect on autoimmune diseases such as arthritis and encephalomyelitis (chronic fatigue syndrome) (Tsukimoto et al., 2008; Nakatsukasa et al., 2010). Preclinical studies on diabetes have demonstrated an antioxidant effect of low doses of irradiation (Wang et al., 2008). These clinical and preclinical investigations provided an increasing level of evidence of the effects of low doses of irradiation, with an anti-inflammatory, anti-oxidant and anti-proliferative potential, associated with high efficacy in reducing clinical symptoms in some inflammatory pathologies.

However, the empiric beneficial effect of low doses of irradiation has been debated for over 50 years, in part because of the poor knowledge on the underlying mechanistic in the context of major concerns in terms of potential radiation-induced cancers (Jaworowski, 2010). Indeed, there is a significant risk of radiation-induced cancers among survivors from a therapeutic irradiation, and epidemiological data clearly documented an increased risk for second neoplasms in cancer survivors (Chargari et al., 2016; Chargari et al., 2020). The risk is the highest among youngest patients, and seems to be organ-dependent (highest risk for the breast and the thyroid). The question of a dose threshold for this risk, as well as the

uncertainties on the shape of dose/response curve, is still unsolved. Those parameters have a major impact in the risk estimate. Anyway, the potentially carcinogenic effects of low doses of irradiation have led to almost abandon this approach to treat inflammatory diseases, and this trend was obviously accelerated by the increasing availability of highly effective non-steroidal or steroidal drugs. Scarce indications for noncancerous diseases do persist however, such as treatment of refractory keloid scares (with high efficacy and low morbidity). In Germany, approximately 50.000 patients are still referred and treated by radiotherapy for non-malignant disorders, including painful degenerative skeletal disorders, hyperproliferative disorders and symptomatic functional disorders(Seegenschmiedt et al., 2015). It should be highlighted that systemic anti-inflammatory therapies also present undesirable effects (severe bacterial complication, in particular in the case of pulmonary infection, digestive disorders such as gastritis or digestive ulcer complicated by hemorrhage, renal damage such as renal failure, necrotizing fasciitis) and a considerable number of patients do not respond correctly (Aronoff and Bloch, 2003; Rödel et al., 2007; Arenas et al., 2012; Legras et al., 2009; Arenas et al., 2012; Le Bourgeois et al., 2016; Basille et al., 2017; Voiriot et al., 2019; Point AINS.,).

An increasing number of preclinical investigations have been carried out to better understand the underlying anti-inflammatory effects of low doses of irradiation. In the light of recent radiobiological data, the putative mechanisms for the anti-inflammatory effects of low-dose irradiation are now well understood. Those include the following patterns: increased heme oxygenase, increased anti-inflammatory cytokines - interleukin-10 (IL-10), increased tumor necrosis factor -beta (TNF-β), activation of several transcription factors, such as nuclear factor kappa beta (NFkB) and protein-1 (AP-1), apoptosis promotion, transforming growth factor - beta 1 (TGFβ1) activation, and stimulation of the activity of regulatory T cells (Dhawan et al., 2020; Genard et al., 2017). As reviewed by Arenas and colleagues, the anti-inflammatory effects of low dose irradiation can also be explained by a decreased adhesion of polymorphonuclear cells to endothelial cells, decreased expression of adhesion molecules, such as selectins, ICAM, VCAM). Doses <0.7 Gy may modulate the expression of adhesion molecules and the production of cytokines, decreasing leukocytes/endothelial cells adherence. Other authors have reported a decrease in NO and ROS, and increased activation of NF-kB, and increase activator protein 1 (Ap-1) activity(Arenas et al., 2012). Doses of approximately 0.5 Gy can modify the immune microenvironment and exert an anti-inflammatory effect, by causing macrophage polarization toward anti-inflammatory macrophages (Lara et al., 2020). This anti-inflammatory effect of the low doses of irradiation was recently demonstrated in human lung macrophages (*Ex vivo*) and in a preclinical study, using a viral pneumonia model (influenza A PR8 virus (H1N1). Authors showed that low doses of irradiation decreased both lung damages and inflammation and had no effect on viral expansion (Meziani, 2020). These anti-inflammatory effects of low dose irradiation are attractive to mitigate the covid-19 related cytokine storms, though only few preclinical data tested this approach in animal models of viral pneumonia. Beneficial effect of low-dose irradiation to reprogram macrophages in anti-inflammatory M2 promoting tissue repair or slowing the progression of lung damage induced by covid 19 disease is detailed and illustrated in **Figure 3**. A recent review of radiobiological data published in 1937–1973 identified 6 studies evaluating post inoculation radiation exposure in animal models; the results were heterogeneous, with one study showing a significant increase in mortality and another showing a significant decrease associated with radiation exposure. No significant change was found in the four remaining studies. These historical preclinical results do not provide support for efficacy of post infection radiation exposure, but the added value of such old reports to the current applicability of low dose radiotherapy is uncertain (Little et al., 2020).

In spite of these limitations, several prospective trials are currently being carried out in the context of the COVID-19 pandemic, encouraged by the lack of effective alternative and the high mortality probability in most severe cases of COVID-19 pneumonia (Cosset et al., 2020; Wilson et al., 2020). In addition, the probability that such doses would result in any deterministic toxicity to healthy tissue is very low (Hanekamp et al., 2020). Most often, these studies are designed to assess the possibility to reduce the need for non-invasive or invasive ventilation by administering a very low dose of X-rays in cases of severe lung infection. To date, nine clinical studies are underway worldwide, including 3 in Spain (UTLTRA-COVID, LOWRAD-COV19), 1 study in Italy (COLOR-19) and the PREVENT study in the United States ((ongoing studies: NCT04380818, NCT04572412, NCT04534790, NCT04394182, NCT0CT044, NCT04393948, NCT04466683) (PREVENT). Preliminary results are encouraging. A clinical trial involving 5 patients over the age of 60 and hospitalized for oxygen therapy showed that a single fraction of 0.5 Gy over the entire lungs, in combination with the standard treatment then proposed, was followed by a clinical improvement in 4/5 patients (Ameri et al., 2020). In another pilot study for which only interim analysis on Day 7 is available, 5 patients with a median age of 90 years were irradiated at low doses and among them 4/5 presented a significant clinical and radiological improvement, including 3 patients within 24 h. No acute toxicity was observed and of importance, no worsening of the cytokine storm was observed in 4 of the 5 patients. As highlighted by the authors themselves, further evaluation to determine additional safety and efficacy among patients with COVID-19 pneumonia is mandatory (Hess et al., 2020). Recently, Sanmamed et al. published a preliminary report of a prospective single arm phase I-II clinical trial enrolling patients ≥50 years-old COVID-19 positive, at phase II or III with lung involvement at imaging study and oxygen requirement. Patients were exposed to 100 cGy to total lungs in a single fraction. Among nine patients included, authors observed statistically significant changes in the disease extension score and improvement of SatO2/FiO2 index 72 h and 1 week after irradiation. In parallel, they observed that LDH decreased significantly one week after RT compared with baseline. Two

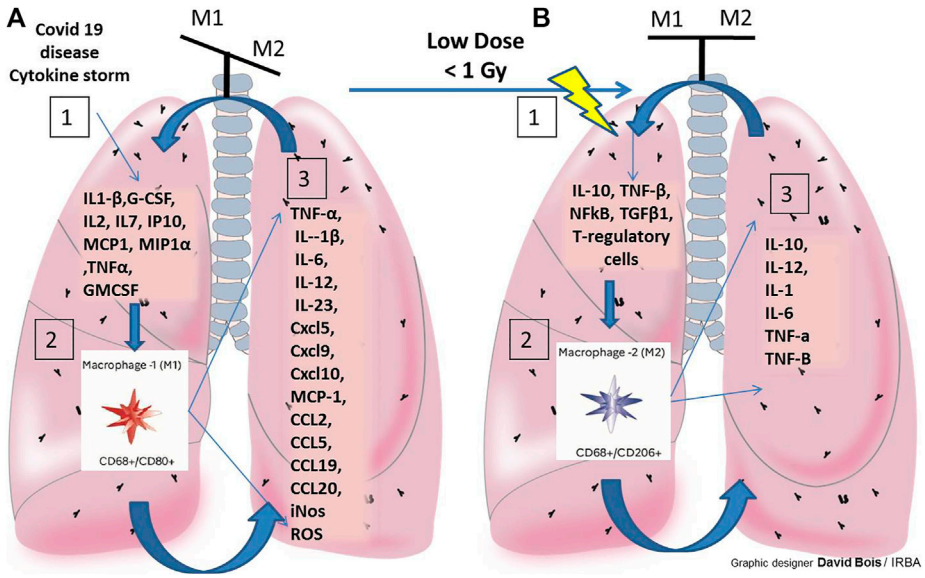

FIGURE 3 | Beneficial effect of low-dose irradiation to reprogram macrophages in anti-inflammatory M2 promoting tissue repair or slowing the progression of severe lung damage induced by covid 19 disease. Balance of M1/M2 macrophage is necessary to achieve proper tissue repair. Hyperinflammation and the severity of the lesions alter this balance (illustrated above each of the lungs **A** and **B**). **(A)**: Illustrations and details of M1 macrophage stimulation in COVID19 in the lung and their pro-inflammatory potential with very little macrophage reprogramming into anti-inflammatory M2. Depending on severity and duration inflammation (M1 persistent activation) this leads to severe lung damage by covid 19 disease. **(B)**: To generate an anti-inflammatory environment: stimulate the polarization of the M2 macrophages with low dose radiotherapy (RT). Macrophages also switch to an anti-inflammatory (M2) phenotype, leading to a wound healing phase: Maintains M1/M2 balance or slowing the progression of lung damage induced by covid 19 disease. 1/2/3 represent the 3 steps generated in case A, an M1 macrophage phenotype within the lungs of covid 19 patients, in case B, step 1 (effects of low doses of RT in lung, with ↘ NO, ROS, ↘leukocytes/endothelial cells adhesion and ↗IL-10, TNF-β, NFkB, TGF 1, AP-1 et T-regulatory cells), step 2 (stimulation of the polarization of M2 macrophages in this environment post-low dose RT) and step 3: the secretion products of M2 promoting an anti-inflammatory environment.

patients had grade 2 lymphopenia after RT and another worsened from grade 3 to grade 4. Overall, the median number of days of hospitalization was 59 days (range 26–151). After RT the median number of days in hospital was "only" 13 days (4–77). With a median follow-up after RT of 112 days, seven patients were discharged and two patients died, one due to sepsis and the other with severe baseline chronic obstructive pulmonary disease from COVID-19 pneumonia (Sanmamed et al., 2020). These results are quite encouraging, but still those are preliminary data deserving to be validated in larger-scale trials assessing the value of low-dose pulmonary irradiation in this situation with a comparative arm. Such approach could potentially improve the quality of life of post-COVID19 patients, reduce the number of deaths and reduce patients stay in intensive care (Martin, 2003; Haas et al., 2018). In addition, the duration in intensive care is not without side effects for patients who are ventilated and immobilized by sedation over a long period. Such approach, based on the anti-inflammatory properties of low dose radiation therapy, should however be extremely cautiously tested, prioritizing the patients who have the lowest risk for second cancers (elderly population) and for whom no effective treatment is available. Indeed, trials testing low dose irradiation have to take into account the theoretical risk of radiation-induced cancer, and the paucity of supportive preclinical data to treat COVID-19 pneumonia was highlighted (Chargari et al., 2016; Haas et al., 2018; Kirsch et al., 2020). Furthermore, one cannot preclude that irradiation would exacerbate an active COVID-19 infection though an increase in the cytokine storm or lead to cardiovascular morbidity. The use of low dose radiotherapy for COVID-19 pneumonia cannot be recommended outside a clinical trial. In addition, this approach should be particularly cautious in young patients (<50–60 years) -who have in most of the cases a good prognosis of their COVID-19 respiratory disease - in particular because the mammary gland and thyroid are highly sensitive to the carcinogenic effects of ionizing radiation, though the effect of such low doses remains uncertain. The risk of second cancer must be put into perspective in the context of elderly patients, frequently ineligible for invasive resuscitation or treatment with interleukin-6 inhibitors, for whom the problem of radiation-induced cancers possibly occurring 10–20 years after irradiation is not a priority concern. Thus, it is estimated that a patient who receives low-dose pulmonary radiotherapy for the treatment of COVID-19 at an age of 80 has a theoretical risk of radiation-induced cancer of less than 1% (Chargari et al., 2016; Cosset et al., 2016).

CONCLUSION

Although numerous data show that low dose radiotherapy may have anti-inflammatory properties, the evidence supporting the use of low dose radiotherapy to treat COVID-19 infection

remains preliminary. This approach could potentially have a favorable cost/effectiveness ratio, for a subgroup of COVID-19 patients for whom there is most often no therapeutic alternative and in a context of lack of access to resuscitation platforms (García-Hernández et al., 2020). A prerequisite for achieving successful development of this experimental treatment is to more accurately identify what population could get benefit, if any, from this treatment, and to better determine the optimal timing/dose/fractionation to achieve the best therapeutic index with satisfactory safety profile. The superiority of low dose radiotherapy over more conventional systemic anti-inflammatory (e.g., steroids) remains undemonstrated, and only a well-designed randomized clinical trial will provide the evidence of a benefit (if any) of low dose radiotherapy in this context. A step by step process is required, from early phase trials to larger randomized studies, to ensure that the beneficial effect of low dose radiotherapy is superior to its potential side effects.

AUTHOR CONTRIBUTIONS

All authors listed have made a substantial, direct, and intellectual contribution to the work and approved it for publication.

REFERENCES

Ameri, A., Rahnama, N., Bozorgmehr, R., Mokhtari, M., Farahbakhsh, M., Nabavi, M., et al. (2020). Low-dose whole-lung irradiation for COVID-19 pneumonia: short course results. *Int. J. Radiat. Oncology*Biology*Physics* 108 (5), 1134–1139. doi:10.1016/j.ijrobp.2020.07.026

Anderson, E. L., Turnham, P., Griffin, J. R., and Clarke, C. C. (2020). Consideration of the aerosol transmission for COVID-19 and public health. *Risk Anal.* 40 (5), 902–907. doi:10.1111/risa.13500

Arenas, M., Sabater, S., Hernández, V., Rovirosa, A., Lara, P. C., Biete, A., et al. (2012). Anti-inflammatory effects of low-dose radiotherapy. *Strahlenther Onkol* 188 (11), 975–981. doi:10.1007/s00066-012-0170-8

Aronoff, D. M., and Bloch, K. C. (2003). Assessing the relationship between the use of nonsteroidal antiinflammatory drugs and necrotizing fasciitis caused by Group A *Streptococcus*. *Medicine (Baltimore)* 82 (4), 225–235. doi:10.1097/01.md.0000085060.63483.bb

Bansal, M. (2020). Cardiovascular disease and COVID-19. *Diabetes Metab. Syndr. Clin. Res. Rev.* 14 (3), 247–250. doi:10.1016/j.dsx.2020.03.013

Banu, N., Panikar, S. S., Leal, L. R., and Leal, A. R. (2020). Protective role of ACE2 and its downregulation in SARS-CoV-2 infection leading to macrophage activation syndrome: therapeutic implications. *Life Sci.* 256, 117905. doi:10.1016/j.lfs.2020.117905

Basille, D., Plouvier, N., Trouve, C., Duhaut, P., Andrejak, C., and Jounieaux, V. (2017). Non-steroidal anti-inflammatory drugs may worsen the course of community-acquired pneumonia: a cohort study. *Lung* 195 (2), 201–208. doi:10.1007/s00408-016-9973-1

Baum, A., Fulton, B. O., Wloga, E., Copin, R., Pascal, K. E., Russo, V., et al. (2020). Antibody cocktail to SARS-CoV-2 spike protein prevents rapid mutational escape seen with individual antibodies. *Science* 369 (6506), 1014–1018. doi:10.1126/science.abd0831

Beigel, J. H., Tomashek, K. M., and Dodd, L. E. (2020a). Remdesivir for the treatment of covid-19 - preliminary report. Reply. *N. Engl. J. Med.* 383 (10), 994. doi:10.1056/NEJMc2022236

Beigel, J. H., Tomashek, K. M., Dodd, L. E., Mehta, A. K., Zingman, B. S., Kalil, A. C., et al. (2020b). Remdesivir for the treatment of covid-19 - final report. *N. Engl. J. Med.* 383 (19), 1813–1826. doi:10.1056/nejmoa2007764

Bourgonje, A. R., Abdulle, A. E., Timens, W., Hillebrands, J. L., Navis, G. J., Gordijn, S. J., et al. (2020). Angiotensin-converting enzyme 2 (ACE2), SARS-CoV -2 and the pathophysiology of coronavirus disease 2019 (COVID -19). *J. Pathol.* 251 (3), 228–248. doi:10.1002/path.5471

Calabrese, E. J., and Dhawan, G. (2013). How radiotherapy was historically used to treat pneumonia: could it Be useful today?. *Yale J. Biol. Med.* 86 (4), 555–570.

Cao, B., Wang, Y., Wen, D., Liu, W., Wang, J., Fan, G., et al. (2020). A trial of lopinavir-ritonavir in adults hospitalized with severe covid-19. *N. Engl. J. Med.* 382 (19), 1787–1799. doi:10.1056/nejmoa2001282

Carvelli, J., Demaria, O., Demaria, O., Vély, F., Batista, L., Chouaki Benmansour, N., et al. (2020). Association of COVID-19 inflammation with activation of the C5a-C5aR1 axis. *Nature* 588 (7836), 146–150. doi:10.1038/s41586-020-2600-6

Carver, J. R., Shapiro, C. L., Ng, A., Jacobs, L., Schwartz, C., Virgo, K. S., et al. (2007). American society of clinical oncology clinical evidence review on the ongoing care of adult cancer survivors: cardiac and pulmonary late effects. *Jco* 25 (25), 3991–4008. doi:10.1200/jco.2007.10.9777

Chargari, C., Goodman, K. A., Diallo, I., Guy, J.-B., Rancoule, C., Cosset, J.-M., et al. (2016). Risk of second cancers in the era of modern radiation therapy: does the risk/benefit analysis overcome theoretical models? *Cancer Metastasis Rev.* 35 (2), 277–288. doi:10.1007/s10555-016-9616-2

Chargari, C., Supiot, S., Hennequin, C., Chapel, A., and Simon, J.-M. (2020). Traitement des effets tardifs après la radiothérapie : quoi de neuf ? *Cancer/Radiothérapie* 24 (6– 7), 602–611. doi:10.1016/j.canrad.2020.06.007

Cipriano, M., Ruberti, E., and Giacalone, A. (2020). Gastrointestinal infection could Be new focus for coronavirus diagnosis. *Cureus* 12 (3), e7422, doi:10.7759/cureus.7422

Cosset, J.-M., Chargari, C., Demoor, C., Giraud, P., Helfre, S., Mornex, F., et al. (2016). Prévention des cancers radio-induits. *Cancer/Radiothérapie* 20 (Suppl. l), S61–S68. doi:10.1016/j.canrad.2016.07.030

Cosset, J.-M., Deutsch, É., Bazire, L., Mazeron, J.-J., and Chargari, C. (2020). Irradiation pulmonaire à faible dose pour l'orage de cytokines du COVID-19 : pourquoi pas ?. *Cancer/Radiothérapie* 24 (3), 179–181. doi:10.1016/j.canrad.2020.04.003

Dhawan, G., Kapoor, R., Dhawan, R., Singh, R., Monga, B., Giordano, J., et al. (2020). Low dose radiation therapy as a potential life saving treatment for COVID-19-induced acute respiratory distress syndrome (ARDS). *Radiother. Oncol.* 147, 212–216. doi:10.1016/j.radonc.2020.05.002

Fara, A., Mitrev, Z., Rosalia, R. A., and Assas, B. M. (2020). Cytokine storm and COVID-19: a chronicle of pro-inflammatory cytokines. *Open Biol.* 10 (9), 200160. doi:10.1098/rsob.200160

García-Hernández, T., Romero-Expósito, M., and Sánchez-Nieto, B. (2020). Low dose radiation therapy for COVID-19: effective dose and estimation of cancer risk. *Radiother. Oncol. J. Eur. Soc. Ther. Radiol. Oncol.* 153:289–295. doi:10.1016/j.radonc.2020.09.051

Gattinoni, L., Coppola, S., Cressoni, M., Busana, M., Rossi, S., and Chiumello, D. (2020). COVID-19 does not lead to a "typical" acute respiratory distress syndrome. *Am. J. Respir. Crit. Care Med.* 201 (10), 1299–1300. doi:10.1164/rccm.202003-0817le

Genard, G., Lucas, S., and Michiels, C. (2017). Reprogramming of tumor-associated macrophages with anticancer therapies: radiotherapy versus chemo- and immunotherapies. *Front. Immunol.* 8, 828. doi:10.3389/fimmu.2017.00828

Gupta, A., Madhavan, M. V., Sehgal, K., Nair, N., Mahajan, S., Sehrawat, T. S., et al. (2020). Extrapulmonary manifestations of COVID-19. *Nat. Med.* 26 (7), 1017–1032. doi:10.1038/s41591-020-0968-3

Haas, L. E. M., van Beusekom, I., van Dijk, D., Hamaker, M. E., Bakhshi-Raiez, F., de Lange, D. W., et al. (2018). Healthcare-related costs in very elderly intensive care patients. *Intensive Care Med.* 44 (11), 1896–1903. doi:10.1007/s00134-018-5381-8

Hanekamp, Y. N., Giordano, J., Hanekamp, J. C., Khan, M. K., Limper, M., Venema, C. S., et al. (2020). Immunomodulation through low-dose radiation for severe COVID-19: lessons from the past and new developments. *Dose-response Publ. Int. Hormesis Soc.* 18 (3), 1559325820956800. doi:10.1177/1559325820956800

He, L., Ding, Y., Zhang, Q., Che, X., He, Y., Shen, H., et al. (2006). Expression of elevated levels of pro-inflammatory cytokines in SARS-CoV-infected

ACE2+cells in SARS patients: relation to the acute lung injury and pathogenesis of SARS. *J. Pathol.* 210 (3), 288–297. doi:10.1002/path.2067

Helms, J., Tacquard, C., Tacquard, C., Severac, F., Leonard-Lorant, I., Ohana, M., et al. (2020). High risk of thrombosis in patients with severe SARS-CoV-2 infection: a multicenter prospective cohort study. *Intensive Care Med.* 46 (6), 1089–1098. doi:10.1007/s00134-020-06062-x

Hess, C. B., Buchwald, Z. S., Stokes, W., Nasti, T. H., Switchenko, J. M., Weinberg, B. D., et al. (2020). Low-dose whole-lung radiation for COVID-19 pneumonia: planned day 7 interim analysis of a registered clinical trial. *Cancer* 126 (23), 5109–5113. doi:10.1002/cncr.33130

RECOVERY Collaborative GroupHorby, P., Mafham, M., Linsell, L., Bell, J. L., Staplin, N., Emberson, J. R., et al. (2020a). Effect of hydroxychloroquine in hospitalized patients with covid-19. *N. Engl. J. Med.* 383 (21), 2030–2040. doi:10.1056/NEJMoa2022926

RECOVERY Collaborative GroupHorby, P., Lim, W. S., Emberson, J. R., Mafham, M., Bell, J. L., et al. (2020b). Dexamethasone in hospitalized patients with covid-19 - preliminary report. *N. Engl. J. Med.* 384(8):693–704. doi:10.1056/NEJMoa2021436

Hu, B., Huang, S., and Yin, L. (2020). The cytokine storm and COVID-19. *J. Med. Virol.* 93(1). 250–256. doi:10.1016/j.cytogfr.2020.08.001

Hu, C., Wang, G., Zhou, D., Wang, W., Qin, Z., Wang, Y., et al. (2020). The anesthetic management of the first lung transplant for a patient with COVID-19 respiratory failure. *J. Cardiothorac. Vasc. Anesth.* 35(3):917–920. doi:10.1053/j.jvca.2020.06.011

Huber, W., Findeisen, M., Lahmer, T., Herner, A., Rasch, S., Mayr, U., et al. (2020). Prediction of outcome in patients with ARDS: a prospective cohort study comparing ARDS-definitions and other ARDS-associated parameters, ratios and scores at intubation and over Timee0232720. *PLoS One* 15 (5). doi:10.1371/journal.pone.0232720

Huertas, A., Montani, D., Savale, L., Pichon, J., Tu, L., Parent, F., et al. (2020). Endothelial cell dysfunction: a major player in SARS-CoV-2 infection (COVID-19)?. *Eur. Respir. J.* 56 (1). doi:10.1183/13993003.01634-2020

Jaworowski, Z. (2010). Radiation hormesis - a remedy for fear. *Hum. Exp. Toxicol.* 29 (4), 263–270. doi:10.1177/0960327110363974

Jung, F., Krüger-Genge, A., Franke, R. P., Hufert, F., and Küpper, J. H. (2020). COVID-19 and the endothelium. *Clin. Hemorheol. Microcirc.* 75 (1), 7–11. doi:10.3233/CH-209007

Khaled, S. A., and Hafez, A. A. (2020). Aplastic anemia and COVID-19: how to break the vicious circuit?. *Am. J. Blood Res.* 10 (4), 60–67.

Kirsch, D. G., Diehn, M., Cucinotta, F. A., and Weichselbaum, R. (2020). Lack of supporting data make the risks of a clinical trial of radiation therapy as a treatment for COVID-19 pneumonia unacceptable. *Radiother. Oncol.* 147, 217–220. doi:10.1016/j.radonc.2020.04.060

Kuba, K., Imai, Y., Rao, S., Gao, H., Guo, F., Guan, B., et al. (2005). A crucial role of angiotensin converting enzyme 2 (ACE2) in SARS coronavirus-induced lung injury. *Nat. Med.* 11 (8), 875–879. doi:10.1038/nm1267

Lara, P. C., Burgos, J., and Macias, D. (2020). Low dose lung radiotherapy for COVID-19 pneumonia. The rationale for a cost-effective anti-inflammatory treatment. *Clin. Transl Radiat. Oncol.* 23, 27–29. doi:10.1016/j.ctro.2020.04.006eCollection 2020 Jul. PMID: 3237372

Le Bourgeois, M., Ferroni, A., Leruez-Ville, M., Varon, E., Thumerelle, C., Brémont, F., et al. (2016). Nonsteroidal anti-inflammatory drug without antibiotics for acute viral infection increases the empyema risk in children: a matched case-control study. *J. Pediatr.* 175, 47–53. doi:10.1016/j.jpeds.2016.05.025

Legras, A., Giraudeau, B., Jonville-Bera, A.-P., Camus, C., François, B., Runge, I., et al. (2009). A multicentre case-control study of nonsteroidal anti-inflammatory drugs as a risk factor for severe sepsis and septic shock. *Crit. Care* 13 (2), R43. doi:10.1186/cc7766

Little, M. P., Zhang, W., van Dusen, R., and Hamada, N. (2020). Pneumonia after bacterial or viral infection preceded or followed by radiation exposure: a reanalysis of older radiobiologic data and implications for low dose radiation therapy for coronavirus disease 2019 pneumonia. *Int. J. Radiat. Oncol. Biol. Phys.* 109(4):849–858. doi:10.1016/j.ijrobp.2020.09.052

Malik, Y. A. (2020). Properties of coronavirus and SARS-CoV-2. *Malays. J. Pathol.* 42 (1), 3–11.

Martin, P. (2003). [The cost of radiotherapy]. *Bull. Cancer* 90 (11), 969–975.

Meng, Y., Yu, C.-H., Li, W., Li, T., Luo, W., Huang, S., et al. (2014). Angiotensin-converting enzyme 2/angiotensin-(1-7)/mas *Axis* protects against lung fibrosis by inhibiting the MAPK/NF-κB pathway. *Am. J. Respir. Cel Mol. Biol.* 50 (4), 723–736. doi:10.1165/rcmb.2012-0451oc

Meziani, L., Robert, C., Classe, M., Costa, B. D., Mondini, M., Clémenson, C., et al. (2020). Low doses of radiation increase the immunosuppressive profile of lung macrophages during viral infection and pneumonia. *Int. J. Radiat. Oncol. Biol. Phys.* S0360-3016(21)00282–290. doi:10.1016/j.ijrobp.2021.03.022

Middeldorp, S., Coppens, M., Haaps, T. F., Foppen, M., Vlaar, A. P., Müller, M. C. A., et al. (2020). Incidence of venous thromboembolism in hospitalized patients with COVID-19. *J. Thromb. Haemost.* 18 (8), 1995–2002. doi:10.1111/jth.14888

Nakatsukasa, H., Tsukimoto, M., Tokunaga, A., and Kojima, S. (2010). Repeated gamma irradiation attenuates collagen-induced arthritis via up-regulation of regulatory T cells but not by damaging lymphocytes directly. *Radiat. Res.* 174 (3), 313–324. doi:10.1667/rr2121.1

Nakazawa, D., and Ishizu, A. (2020). Immunothrombosis in severe COVID-19. *EBioMedicine* 59, 102942. doi:10.1016/j.ebiom.2020.102942

Nishiga, M., Wang, D. W., Han, Y., Lewis, D. B., and Wu, J. C. (2020). COVID-19 and cardiovascular disease: from basic mechanisms to clinical perspectives. *Nat. Rev. Cardiol.* 17 (9), 543–558. doi:10.1038/s41569-020-0413-9

Pagliaro, P. (2020). Is macrophages heterogeneity important in determining COVID-19 lethality? *Med. Hypotheses* 143, 110073. doi:10.1016/j.mehy.2020.110073

Patel, V. B., Mori, J., McLean, B. A., Basu, R., Das, S. K., Ramprasath, T., et al. (2016). ACE2 deficiency worsens epicardial adipose tissue inflammation and cardiac dysfunction in response to diet-induced obesity. *Diabetes* 65 (1), 85–95. doi:10.2337/dbi15-0037

Point AINS. The French Regional Pharmacovigilance Centers (CRPVs) CRPV de Tours et CRPV d'Angers.

PREVENT. Clinicaltrials.Gov Covid 19.

Ragab, D., Salah Eldin, H., Taeimah, M., Khattab, R., and Salem, R. (2020). The COVID-19 cytokine storm; what we know so far. *Front. Immunol.* 11, 1446. doi:10.3389/fimmu.2020.01446

Raghu, G., Collard, H. R., Egan, J. J., Martinez, F. J., Behr, J., Brown, K. K., et al. (2011). An official ATS/ERS/JRS/ALAT statement: idiopathic pulmonary fibrosis: evidence-based guidelines for diagnosis and management. *Am. J. Respir. Crit. Care Med.* 183 (6), 788–824. doi:10.1164/rccm.2009-040gl

ARDS Definition Task ForceRanieri, V. M., Rubenfeld, G. D., Thompson, B. T., Ferguson, N. D., Caldwell, E., Fan, E., et al. (2012). Acute respiratory distress syndrome: the Berlin definition. *JAMA* 307 (23), 2526–2533. doi:10.1001/jama.2012.5669

RECOVERY Collaborative Group (2021). Tocilizumab in patients admitted to hospital with COVID-19 (RECOVERY): preliminary results of a randomised, controlled, open-label, platform trial. Avilable at: https://www.medrxiv.org/content/10.1101/2021.02.11.21249258v1.full.pdf (Accessed 11 February, 2021).

Ribes, A., Vardon-Bounes, F., Mémier, V., Poette, M., Au-Duong, J., Garcia, C., et al. (2020). Thromboembolic events and covid-19. *Adv. Biol. Regul.* 77, 100735. doi:10.1016/j.jbior.2020.100735

Rödel, F., Keilholz, L., Herrmann, M., Sauer, R., and Hildebrandt, G. (2007). Radiobiological mechanisms in inflammatory diseases of low-dose radiation therapy. *Int. J. Radiat. Biol.* 83 (6), 357–366. doi:10.1080/09553000701317358

Rodrigues Prestes, T. R., Rocha, N. P., Miranda, A. S., Teixeira, A. L., and Simoes-E-Silva, A. C. (2017). The anti-inflammatory potential of ACE2/angiotensin-(1-7)/mas receptor *Axis*: evidence from basic and clinical research. *Curr. Drug Targets* 18 (11), 1301–1313. doi:10.2174/1389450117666160727142401

Ronald, A. DePinho. Looming Health Crisis: Long Term Effects from Covid-19.

Roux, A., Sage, E., Cerf, C., Le Guen, M., Picard, C., Hamid, A. M., et al. (2019). [Evolution and progress of lung transplantation: an analysis of a cohort of 600 lung transplant patients at the Hospital Foch]. *Rev. Mal. Respir.* 36 (2), 142–154. doi:10.1016/j.rmr.2018.02.014

Sanmamed, N., Alcantara, P., Cerezo, E., Gaztañaga, M., Cabello, N., Gómez, S., Bustos, A., Doval, A., Corona, J., Rodriguez, G., Duffort, M., Ortuño, F., de Castro, J., Fuentes, M. E., Sanz, A., López, A., and Vazquez, M. Low-dose radiation therapy in the management of coronavirus disease 2019 (COVID-19) pneumonia (LOWRAD-Cov19): preliminary report. *Int. J. Radiat. Oncology*Biology*Physics* 2021. 109(4):880–885doi:10.1016/j.ijrobp.2020.11.049

Seegenschmiedt, M. H., Micke, O., and Muecke, R. (2015). German cooperative Group on radiotherapy for non-malignant diseases (GCG-BD). *Br. J. Radiol.* 88 (1051), 2015008–2015017. doi:10.1259/bjr.20150080

Shahid, Z., Kalayanamitra, R., McClafferty, B., Kepko, D., Ramgobin, D., Patel, R., et al. (2020). COVID -19 and older adults: what we know. *J. Am. Geriatr. Soc.* 68 (5), 926–929. doi:10.1111/jgs.16472

Simonovich, V. A., Burgos Pratx, L. D., Scibona, P., Beruto, M. V., Vallone, M. G., Vázquez, C., et al. (2020). A randomized trial of convalescent plasma in covid-19 severe pneumonia. *N. Engl. J. Med.* 384(7):619–629. doi:10.1056/NEJMoa2031304

Smigiel, K. S., and Parks, W. C. (2018). Macrophages, wound healing, and fibrosis: recent insights. *Curr. Rheumatol. Rep.* 20 (4), 17. doi:10.1007/s11926-018-0725-5

Song, P., Li, W., Xie, J., Hou, Y., and You, C. (2020). Cytokine storm induced by SARS-CoV-2. *Clinica Chim. Acta* 509, 280–287. doi:10.1016/j.cca.2020.06.017

Stone, J. H., Frigault, M. J., Serling-Boyd, N. J., Fernandes, A. D., Harvey, L., Foulkes, A. S., et al. (2020). BACC bay Tocilizumab trial investigators. Efficacy of Tocilizumab in patients hospitalized with covid-19. *N. Engl. J. Med.* 383(24): 2333–2344. doi:10.1056/NEJMoa2028836

Tian, S., Xiong, Y., Liu, H., Niu, L., Guo, J., Liao, M., et al. (2020). Pathological study of the 2019 novel coronavirus disease (COVID-19) through postmortem core biopsies. *Mod. Pathol.* 33 (6), 1007–1014. doi:10.1038/s41379-020-0536-x

Torres Royo, L., Antelo Redondo, G., Árquez Pianetta, M., and Arenas Prat, M. (2020). Low-dose radiation therapy for benign pathologies. *Rep. Pract. Oncol. Radiother.* 25 (2), 250–254. doi:10.1016/j.rpor.2020.02.004

Tsukimoto, M., Nakatsukasa, H., Sugawara, K., Yamashita, K., and Kojima, S. (2008). Repeated 0.5-gy γ irradiation attenuates experimental autoimmune encephalomyelitis with up-regulation of regulatory T cells and suppression of IL17 production. *Radiat. Res.* 170 (4), 429–436. doi:10.1667/rr1352.1

Varga, Z., Flammer, A. J., Steiger, P., Haberecker, M., Andermatt, R., Zinkernagel, A. S., et al. (2020). Endothelial cell infection and endotheliitis in COVID-19. *The Lancet* 395 (10234), 1417–1418. doi:10.1016/s0140-6736(20)30937-5

Voiriot, G., Philippot, Q., Elabbadi, A., Elbim, C., Chalumeau, M., and Fartoukh, M. (2019). Risks related to the use of non-steroidal anti-inflammatory drugs in community-acquired pneumonia in adult and pediatric patients. *J. Clin. Med.* 8 (6). doi:10.3390/jcm8060786

Wang, G.-J., Li, X.-K., Sakai, K., and Cai, L. (2008). Low-dose radiation and its clinical implications: diabetes. *Hum. Exp. Toxicol.* 27 (2), 135–142. doi:10.1177/0960327108090752

Wang, Y., Zhang, D., Du, G., Du, R., Zhao, J., Jin, Y., et al. (2020). Remdesivir in adults with severe COVID-19: a randomised, double-blind, placebo-controlled, multicentre trial. *The Lancet* 395 (10236), 1569–1578. doi:10.1016/S0140-6736(20)31022-9

Wilson, G. D., Mehta, M. P., Welsh, J. S., Chakravarti, A., Rogers, C. L., and Fontanesi, J. (2020). Investigating low-dose thoracic radiation as a treatment for COVID-19 patients to prevent respiratory failure. *Radiat. Res.* 194 (1), 1–8. doi:10.1667/rade-20-00108.1

Wong, K. T., Antonio, G. E., Hui, D. S. C., Lee, N., Yuen, E. H. Y., Wu, A., et al. (2003). Severe acute respiratory syndrome: radiographic appearances and pattern of progression in 138 patients. *Radiology* 228 (2), 401–406. doi:10.1148/radiol.2282030593

Yin, Y., and Wunderink, R. G. (2018). MERS, SARS and other coronaviruses as causes of pneumonia. *Respirology* 23 (2), 130–137. doi:10.1111/resp.13196

Zhu, N., Zhang, D., Wang, W., Li, X., Yang, B., Song, J., et al. (2020). A novel coronavirus from patients with pneumonia in China, 2019. *N. Engl. J. Med.* 382 (8), 727–733. doi:10.1056/nejmoa2001017

Conflict of Interest: The authors declare that the research was conducted in the absence of any commercial or financial relationships that could be construed as a potential conflict of interest.

frontiers | Frontiers in Pharmacology

ORIGINAL RESEARCH
published: 29 June 2022
doi: 10.3389/fphar.2022.663855

Mitigation of Ionizing Radiation-Induced Gastrointestinal Damage by Insulin-Like Growth Factor-1 in Mice

Jaroslav Pejchal[1], Ales Tichy[2], Adela Kmochova[2], Lenka Fikejzlova[1], Klara Kubelkova[3], Marcela Milanova[2], Anna Lierova[2], Alzbeta Filipova[2], Lubica Muckova[2] and Jana Cizkova[2]*

[1]Department of Toxicology and Military Pharmacy, Faculty of Military Health Sciences, University of Defence, Brno, Czechia, [2]Department of Radiobiology, Faculty of Military Health Sciences, University of Defence, Brno, Czechia, [3]Department of Molecular Pathology and Biology, Faculty of Military Health Sciences, University of Defence, Brno, Czechia

Purpose: Insulin-like growth factor-1 (IGF-1) stimulates epithelial regeneration but may also induce life-threatening hypoglycemia. In our study, we first assessed its safety. Subsequently, we examined the effect of IGF-1 administered in different dose regimens on gastrointestinal damage induced by high doses of gamma radiation.

Material and methods: First, fasting C57BL/6 mice were injected subcutaneously with IGF-1 at a single dose of 0, 0.2, 1, and 2 mg/kg to determine the maximum tolerated dose (MTD). The glycemic effect of MTD (1 mg/kg) was additionally tested in non-fasting animals. Subsequently, a survival experiment was performed. Animals were irradiated (^{60}Co; 14, 14.5, or 15 Gy; shielded head), and IGF-1 was administered subcutaneously at 1 mg/kg 1, 24, and 48 h after irradiation. Simultaneously, mice were irradiated (^{60}Co; 12, 14, or 15 Gy; shielded head), and IGF-1 was administered subcutaneously under the same regimen. Jejunum and lung damage were assessed 84 h after irradiation. Finally, we evaluated the effect of six different IGF-1 dosage regimens administered subcutaneously on gastrointestinal damage and peripheral blood changes in mice 6 days after irradiation (^{60}Co; 12 and 14 Gy; shielded head). The regimens differed in the number of doses (one to five doses) and the onset of administration (starting at 1 [five regimens] or 24 h [one regimen] after irradiation).

Results: MTD was established at 1 mg/kg. MTD mitigated lethality induced by 14 Gy and reduced jejunum and lung damage caused by 12 and 14 Gy. However, different dosing regimens showed different efficacy, with three and four doses (administered 1, 24, and 48 h and 1, 24, 48, and 72 h after irradiation, respectively) being the most effective. The three-dose regimens supported intestinal regeneration even if the administration started at 24 h after irradiation, but its potency decreased.

Conclusion: IGF-1 seems promising in the mitigation of high-dose irradiation damage. However, the selected dosage regimen affects its efficacy.

Keywords: ionizing radiation, mice, insuline-like growth factor- 1, intestine, lung, blood

Edited by:
Benny J. Chen,
Duke University, United States

Reviewed by:
Lakshman Singh,
University of Melbourne, Australia
Ana I Duarte,
University of Coimbra, Portugal

****Correspondence:***
Ales Tichy
ales.tichy@unob.cz

Specialty section:
This article was submitted to Translational Pharmacology, a section of the journal Frontiers in Pharmacology

Received: *03 February 2021*
Accepted: *08 June 2022*
Published: *29 June 2022*

Citation:
Pejchal J, Tichy A, Kmochova A, Fikejzlova L, Kubelkova K, Milanova M, Lierova A, Filipova A, Muckova L and Cizkova J (2022) Mitigation of Ionizing Radiation-Induced Gastrointestinal Damage by Insulin-Like Growth Factor-1 in Mice. Front. Pharmacol. 13:663855. doi: 10.3389/fphar.2022.663855

1 INTRODUCTION

Acute gastrointestinal radiation syndrome (GRS) is a life-threatening situation that develops after exposure of the gastrointestinal tract to high doses of ionizing radiation (IR). The pathogenesis of acute GRS is not fully understood. However, self-renewing cells at the base intestinal crypts play a crucial role, including intestine stem cells (ISCs) and daughter cells of the first few generations (Meena et al., 2022). Under physiological circumstances, ISCs self-renew, proliferate, and differentiate and thus maintain the intestinal epithelium integrity. After irradiation, these cells arrest the cell cycle and induce apoptosis (Li et al., 2021). When the number of ISCs and the production of daughter cells decrease substantially, the mucosal barrier that separates the intestinal content from the gastrointestinal tissue breaks down. This results in severe diarrhea, dehydration, electrolyte imbalance, and translocation of gastrointestinal pathogens and toxins into the body (Lu et al., 2019).

Acute GRS management is primarily symptomatic. It usually combines antiemetics, antidiarrheal drugs, rehydration, and antimicrobial prophylaxis and therapy (Lu et al., 2019). The fully developed syndrome has a poor prognosis. On the other hand, preclinical studies utilizing clinically available mitigators showed promising results. These mitigators also include different intestinotrophic substances, such as Teduglutide or Dinoprostone (Singh and Seed, 2020). Teduglutide is a dipeptidyl peptidase-resistant analog of glucagon-like peptide-2 (GLP-2). GLP-2 receptors have been localized to several intestinal cell types but not to the proliferating crypt cells. The GLP-2 actions have thus been associated with a complex network of indirect mediators activating diverse signaling pathways that enhance crypt cell proliferation and suppress apoptosis (Rowland and Brubaker, 2011). Gu et al. (2017) demonstrated that Teduglutide's subcutaneous injection in specific pathogen-free Balb/c mice for 7 days prolonged survival of animals, decreased structural damage, down-regulated radiation-induced inflammatory responses, and promoted survival of crypt cells. Dinoprostone is prostaglandin E2 (PGE_2), a lipid with pleiotropic effects. Both PGE_2 and its long-acting analog 16,16-dimethyl PGE_2 ($dmPGE_2$) act via EP receptors (Okazaki et al., 2018). When administered before irradiation, both increase ISC survival and reduce crypt damage (Hanson and Thomas, 1983; Hanson and DeLaurentiis, 1987). PGE_2 also promotes hematopoietic stem cell survival and hematopoietic recovery after radiation injury (Porter et al., 2013; Patterson et al., 2020). Patterson et al. (2020) defined a window of survival efficacy for single administration of $dmPGE_2$ as within 3 h before and 6–30 h after total-body γ irradiation.

Insulin-like growth factor 1 (IGF-1) is another pleiotropic hormone. Its synthetic analog, mecasermin (brand name Increlex), is clinically used to treat growth failure in children (Bang et al., 2022). IGF-1 receptors are present in the intestine at different cell types, including ISCs (Van Landeghem et al., 2015). Systemically administered IGF-I increases crypt cell proliferation and expression of anti-apoptotic genes, particularly in the stem cell zone, which subsequently increases mucosal mass in mice (Dahly et al., 2002). After irradiation, IGF-1 signaling stimulates crypt regeneration (Bohin et al., 2020). IGF-1 also inhibits ionizing radiation (IR)-induced apoptosis of gastrointestinal vascular endothelial cells (Qiu et al., 2010). Their damage significantly affects the response of gastrointestinal tissues after irradiation (Lu et al., 2019). Howarth et al. (1997) implanted mini-osmotic pumps infusing IGF-1 into rats before whole-body irradiation by 10 Gy and observed accelerated intestinal mucosal recovery from radiation injury. However, the maximally tolerated dose for a single subcutaneous injection has not yet been published and tested for its radiation mitigation properties when administered in different dosage regimens.

2 MATERIAL AND METHODS

2.1 Animals

All experiments were performed with female C57Bl/6 mice (age 12–16 weeks, weight 18.8–23.2 g; Velaz, Unetice, Czech Republic). Mice were housed in an accredited facility (temperature 22 ± 2°C, 50 ± 10% relative humidity, with lights from 7:00 to 19:00 h; accreditation number č. j. 69233/2015-MZE-17214; Faculty of Military Health Sciences) and allowed access to tap water and standard food DOS-2B (BIOPO spol. s.r.o., Brno, Czech Republic) *ad libitum*. The animals were acclimatized for 14 days before starting the experiments. All experiments in this study were approved by the Ethics Committee (Faculty of Military Health Sciences, Hradec Kralove, Czech Republic) and were conducted following the Animal Protection Law and Animal Protection Regulations.

2.2 Safety of IGF-1

Animals were randomly divided into four groups (n = 6). Recombinant human IGF-1 (Increlex; Ipsen Pharma, Boulogne-Billancourt, France) was administered subcutaneously (s.c.) at a dose of 0.2, 1, or 2 mg/kg to animals fasting for 12 h. Physiological saline (B Braun Melsungen AG, Melsungen, Germany) was used to dilute the growth factor and as a negative control. Blood was collected using the tail incision method at 0 (immediately before), 0.5, 1, 2, and 4 h after physiological saline or IGF-1 administration. Glucose concentration in blood was measured using SD CodeFree blood glucose monitor and SD CodeFree Plus blood glucose test strips (both from SD Biosensor, Suwon, South Korea). During the experiment, the animals were observed for clinical signs of hypoglycemia.

Clinical signs and glycemic profiles were also monitored in a group of animals (n = 6) that were not fasting before but were restricted from feeding during the experiment (4 h). The animals were administered s.c. with IGF-1 at 1 mg/kg. Glycemia was measured at 0 (immediately before), 0.5, 1, 2, and 4 h after IGF-1 administration.

All irradiation experiments were performed in non-fasting animals with free access to food during the experiments.

2.3 Source of Ionizing Radiation

The source of gamma radiation was ^{60}Co unit (Chirana, Prague, Czech Republic). The dosimetry was performed using an ionization chamber (Dosemeter PTW Unidos 1001, Serial No. 11057, with ionization chamber PTW TM 313, Serial No. 0012; RPD Inc., Albertville, MN, United States).

TABLE 1 | The experimental setup used to evaluate the different IGF-1 dosage regimens on the mitigation of ionizing radiation-induced gastrointestinal damage and peripheral blood changes.

Group	Dose (Gy)	IGF-1[a]	Group	Dose (Gy)	IGF-1[a]
1	0	-	9	0	-
2	12	-	10	14	-
3	12	1 (1 h)	11	14	1 (1 h)
4	12	2 (1, 24 h)	12	14	2 (1, 24 h)
5	12	3 (1, 24, 48 h)	13	14	3 (1, 24, 48 h)
6	12	4 (1, 24, 48, 72 h)	14	14	4 (1, 24, 48, 72 h)
7	12	5 (1, 24, 48, 72, 96 h)	15	14	5 (1, 24, 48, 72, 96 h)
8	12	3 (24, 48, 72 h)	16	14	3 (24, 48, 72 h)

[a]*Number of doses (time of administration). IGF-1, was administered subcutaneously at a dose of 1 mg/kg.*

2.4 Irradiation Procedure

Before IR treatments, animals were anesthetized using a solution of Rometar (20 mg/ml; Bioveta, Ivanovice na Hane, Czech Republic), Narketan (50 mg/ml; Vetoquinol, Prague, Czech Republic), and physiological saline in the volume ratio 1:3:12. This solution was administered intramuscularly at a dose of 10 ml/kg. The anesthetized animals were placed into a Plexiglas box (VLA JEP, Hradec Kralove, Czech Republic) and irradiated by a single dose of IR delivered from back to front at a dose rate of 0.81 Gy/min (survival experiment and assessment of jejunal and lung damage) or 0.27 Gy/min (assessment of different IGF-1 dosage regimens) with a target distance of 1 m. In both experiments, the head and neck were shielded with 10 cm thick lead bricks.

2.5 Experimental Setup of Ionizing Radiation Experiments

In survival experiments, the mice were randomly divided into 6 groups (n = 20) and irradiated by 14, 14.5, or 15 Gy. IGF-1 was administered s.c. at 1 mg/kg 1, 24, and 48 h after irradiation. Physiological saline was used to dilute the growth factor and as a negative control. The survival of animals was monitored daily.

Simultaneously, we assessed the effect of IGF-1 on IR-induced jejunum and lung damage. For this, mice were randomly divided into 6 groups (n = 8), irradiated by 12, 14, or 15 Gy, and administered s.c. with IGF-1 (1 mg/kg) 1, 24, and 48 h after irradiation. Physiological saline was used to dilute IGF-1 and for the control group. Four hours before euthanasia, animals were intraperitoneally injected with 5-bromo-2′-deoxyuridine (BrdU, 100 mg/kg; Merck, Kenilworth, NJ, United States) diluted in physiological saline. After deep narcotization in the CO_2 atmosphere at 84 h after irradiation, samples from the jejunum (5–6 cm from the pyloric ostium) and lung were collected and fixed with 10% neutral buffered formalin (Chemapol, Prague, Czech Republic).

Finally, we evaluated the effect of six different IGF-1 dosage regimens (à 1 mg/kg; single and multiple) on IR-induced gastrointestinal damage and peripheral blood changes. In this experiment, the animals were randomly divided into 16 groups (n = 6), irradiated by 12 or 14 Gy, and administered s.c. with IGF-1 according to the experimental setup presented in **Table 1**. Physiological saline was used to dilute IGF-1 and for the control group. 6 days after the irradiation, the animals were deeply narcotized in the CO_2 atmosphere, and the thorax and abdominal cavity were opened. Venous blood was collected from the right heart ventricle into heparinized tubes (Scanlab Systems, Prague, Czech Republic). Samples from the duodenum, jejunum (0.5–1 cm, 5–6 cm from the pyloric ostium, respectively), and ileum (1–2 cm from the ileocecal valve) were collected and fixed with 10% neutral buffered formalin (Chemapol, Prague, Czech Republic).

2.6 Staining of Samples

2.6.1 Hematoxylin-Eosin

According to the previously published procedure (Pejchal et al., 2012), formalin-fixed samples were processed and stained with hematoxylin and eosin (Merck).

2.6.2 Detection of BrdU Positive Cells

Dewaxed 5 μm thick sections first underwent DNA hydrolysis in 2 M HCl (Merck) for 1 h at 37°C. Subsequently, the sections were neutralized in 0.1 M sodium borate buffer (pH 8.5; Merck) for 10 min at room temperature and washed three times in phosphate-buffered saline (PBS; Merck). BrdU incorporation was then detected using a standard peroxidase technique (Pejchal et al., 2012). In short, after blocking the endogenous peroxidase activity for 20 min, the tissue sections were incubated for 1 h with rat monoclonal anti-BrdU antibody (1 μg/ml; clone BU1/75 [ICR1], Abcam, Cambridge, United Kingdom). As a secondary antibody, pre-diluted ready-to-use goat anti-rat antibody-HPR polymer (ab214882; Abcam) was applied for 20 min. Finally, 0.05% 3,3′-diaminobenzidine tetrahydrochloride-chromogen solution (Merck) in PBS containing 0.02% hydrogen peroxide was added for 10 min to visualize the antigen-antibody complex.

2.6.3 Detection of Chloroacetate Esterase-Positive Cells

Chloroacetate esterase is considered specific for cells of granulocytic lineage. To detect chloroacetate esterase-positive cells, dewaxed and hydrated 5 μm thick sections were stained using a naphthol AS-D chloroacetate esterase kit according to the manufacturer (Cat. No. 91C-1KT; Merck) instructions. The samples were mounted into an ImmunoHistoMount aqueous-based mounting medium (Merck).

TABLE 2 | A semiquantitative score of histopathological changes in the intestine.

Parameter	Score			
	0	1	2	3
loss of epithelial continuity[a]	not present	<5 microerosions	≥5 microerosions	confluent changes
edema[b]	not present	mild	moderate	severe
granulocyte infiltration[c]	<3	≥3	≥10	≥50

[a]*Evaluated in the whole cross-section.*

[b]*Number of neutrophile granulocytes per microscopic field at 400fold original magnification.*

[c]*Mild: subepithelial edema in <25% villi; moderate: subepithelial edema in ≥25% villi or cellular edema of <25% villous cells, or edema of <25% of lamina propria or submucosa; severe: cellular edema of ≥25% villous cells, or edema of ≥25% of lamina propria or submucosa.*

2.7 Evaluation of the Jejunum and Lung Damage

2.7.1 Jejunum

In the jejunum, we first performed a histopathological analysis in hematoxylin-eosin-stained samples. The samples were semiquantitatively scored for the loss of epithelial continuity, edema, and granulocyte infiltration (**Table 2**). Additionally, the number of villi per circumference, their length, number of surviving crypts per circumference, and the amount of chloroacetate esterase positive cells were scored.

A villus was judged as a villous-like structure containing at least 20 nucleated cells. The number of villi per circumference was counted in the whole cross-section of hematoxylin-eosin stained samples at ×200 magnification. Three cross-sections were evaluated for each animal, and their values were averaged.

The length of villi was assessed in the same samples using a BX-51 microscope (Olympus, Tokyo, Japan) and the ImagePro 5.1 computer image analysis system (Media Cybernetics, Bethesda, MD, United States). Lengths of 10 randomly selected villi were measured under ×160 magnification.

The amount of surviving crypts per circumference was counted in the whole cross-section of BrdU-stained samples at ×400 magnification. Only transversely sectioned crypts with ≥10 BrdU positive cells were considered as surviving. Three cross-sections were evaluated for each animal, and their values were averaged.

Chloroacetate esterase-positive cells were counted only in sub-villar mucose per microscopic field (centered in the middle of the field) to avoid the effect of different lengths of villi. Ten randomly selected microscopic fields were counted for each animal at ×400 magnification.

2.7.2 Lung

Histopathological analysis was also done in the lung, scoring cellularity, inflammation, hyperemia, and edema (**Table 3**). Subsequently, the airness of the tissue and the number of chloroacetate esterase-positive cells were measured.

The airness was assessed in hematoxylin-eosin-stained samples using a BX-51 microscope and the ImagePro 5.1 computer image analysis system. Ten microscopic fields at ×400 magnification were randomly selected from each animal. The airness of the tissue was expressed as the percentage of the bright area in the microscopic field defined in the red/green/blue scale: red 220–255, green 220–255, and blue 220–255, where 0 is black and 255 is white.

Finally, the number of chloroacetate esterase-positive cells was counted in ten randomly selected microscopic fields at ×400 magnification for each mouse.

2.8 Evaluation of Different Regimens

2.8.1 Blood

Collected venous blood was promptly analyzed using ABX Pentra 60C + hemoanalyzer (Horiba, Kyoto, Japan). All samples were measured three times, and their values were averaged.

2.8.2 Intestine

In hematoxylin-eosin-stained intestinal samples, the histopathological analysis, the number of villi per circumference, their length (all three parameters were measured similarly to the previous model), and the amount of regenerating crypts per circumference, and their length were measured.

Regenerating crypts were defined as basophilic cell clusters of ≥10 epithelial cells (excluding Paneth cells), each with a prominent nucleus and little cytoplasm, lying close together and appearing crowded (Bhat et al., 2019). The number of regenerating crypts per circumference was counted in the whole cross-section at ×400 magnification. Only transversely sectioned crypts with ≥10 epithelial cells were considered as regenerating. Three cross-sections were evaluated for each animal, and their values were averaged.

The length of crypts was assessed by BX-51 microscope and the ImagePro 5.1 computer image analysis system. Lengths of 10 randomly selected crypts were measured under ×160 magnification.

2.9 Statistical Analysis

The Kaplan-Meier Survival Analysis with post hoc Log Rank test and Mann-Whitney test by SPSS statistics version 24 (IBM, Armonk, NY, United States) were used for the statistical analysis. Graphs were produced using GraphPad Prism software (version5.04, GraphPad Software Inc., San Diego, CA). The differences were considered significant when $p \leq 0.05$.

3 RESULTS

3.1 IGF-1 Safety Assessment

In the control of fasting animals (0 mg/kg), the experimental procedure (handling and blood collection) significantly increased blood glucose levels by 16% in the 2-h interval (**Figure 1A**). The 0.2 mg/kg dose did not affect glycemia nor induced any clinical

TABLE 3 | A semiquantitative score of histopathological changes in the intestine.

Parameter	Score			
	0	1	2	3
cellularity	standard	mildly increase	moderately increased	severely increased
granulocyte infiltration[a]	0–10 per m.f	10–20 per m.f	≥20 per m.f	diffuse infiltration
edema[b]	not present	mild	moderate	severe
hyperemia	not present	mild	moderate	severe

m.f.–microscopic field.

[a]*Number of neutrophile granulocytes per microscopic field at 400fold original magnification.*

[b]*Mild: mild intraseptal edema; moderate: moderate intraseptal edema with <10% alveoly with intraalveolar edema; severe: moderate intraseptal edema with ≥10% alveoly with intraalveolar edema.*

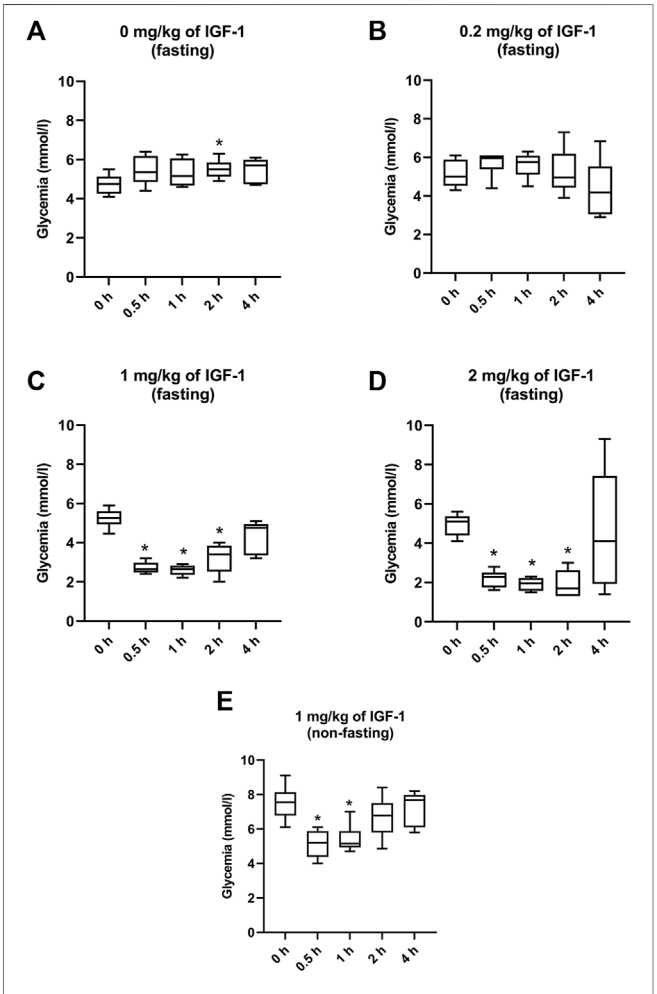

FIGURE 1 | Effect of IGF-1 on mouse glycemia. **(A)** mice fasting for 12 h before the experiment administered with physiological saline. **(B)** mice fasting for 12 h before the experiment administered with IGF-1 at a dose of 0.2 mg/kg. **(C)** mice fasting for 12 h before the experiment administered with IGF-1 at a dose of 1 mg/kg. **(D)** mice fasting for 12 h before the experiment administered with IGF-1 at a dose of 2 mg/kg. **(E)** non-fasting mice administered with IGF-1 at a dose of 1 mg/kg.

alteration (**Figure 1B**). After administration of IGF-1, the dose of 1 mg/kg significantly decreased median glycemia by 50, 50, and 36% at 0.5, 1, and 2 h, respectively (**Figure 1C**). Although acute hypoglycemia (<3 mmol/L) was recorded in 5 of 6 animals, no clinical symptoms associated with hypoglycemia were observed. The dose of 2 mg/kg decreased median glycemia by 55, 62, and 67% at 0.5, 1, and 2 h, respectively (**Figure 1D**). Mice displayed spatial segregation, hypoactivity, and decreased reactivity to external stimulation. Two mice experienced seizures. The maximum tolerated dose (MTD) was therefore established at 1 mg/kg.

In animals that were not fasting before but fasting during the experiment, 1 mg/kg of IGF-1 decreased median blood glucose levels by 31 and 32% at 0.5 and 1 h after the administration, respectively (**Figure 1E**). No clinical alterations were observed in this group.

3.2 Effect of IGF-1 on Animal Survival After Irradiation by 14, 14.5, and 15 Gy With Head and Neck Shielded

After irradiation by 14 Gy, survival significantly increased in animals administered with IGF-1 (median 176 days, 95% confidence interval [CI] = 154–198 days) when compared with control receiving only physiological saline (median = 164 days, 95% CI = 155–173 days; **Figure 2A**, **Supplementary Table S1**). We did not observe any significant differences between irradiated control receiving no treatment and IGF-1 administered groups after irradiation by 14.5 and 15 Gy (**Figures 2B,C**).

3.3 Effect of IGF-1 (MTD) on Jejunal and Lung Damage in Mice 84 h After Irradiation by 12, 14, and 15 Gy With Head and Neck Shielded

In the jejunum, IGF-1 treatment increased the length of villi and the number of surviving crypts while reducing the amount of chloroacetate esterase positive cells in the tissue at 12 Gy (by 10, 35, and 45%, respectively; **Supplementary Figure S1**). After irradiation by 14 Gy, the therapy only prolonged the villi and decreased the number of infiltrating chloroacetate esterase positive cells (by 10 and 34%, respectively; **Figure 3**). IGF-1 did not affect any histopathological parameter (**Supplementary Figure S2**) or the number of villi per circumference (**Figure 3A**).

In the lung, IGF-1 did not significantly affect any histopathological parameter (**Supplementary Figure S3**). Still, it increased airness while reducing the amount of chloroacetate esterase positive cells at 12 Gy (by 14 and 24%; **Supplementary Figure S4**) and 14 Gy (by 17 and 30%, respectively; **Figure 4**).

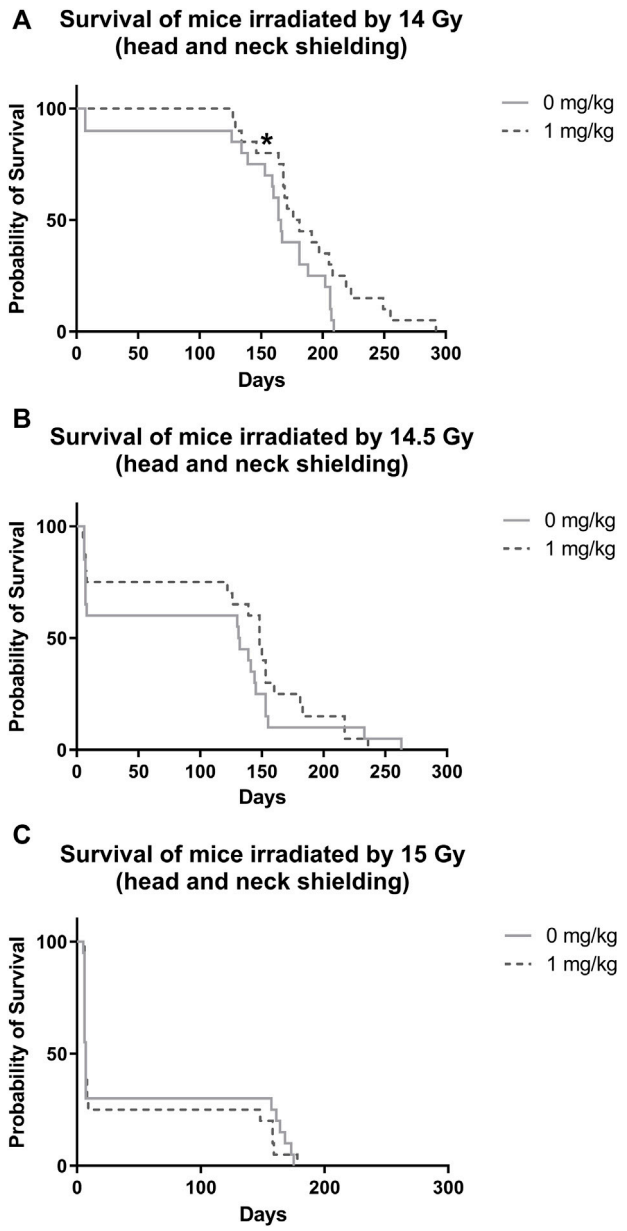

FIGURE 2 | Effect of IGF-1 at 1 mg/kg on irradiated mice's survival with shielded head and neck. **(A)** 14 Gy. **(B)** 14.5 Gy. **(C)** 15 Gy. Significantly different when compared with the solely irradiated group receiving no treatment: $^*p \leq 0.05$.

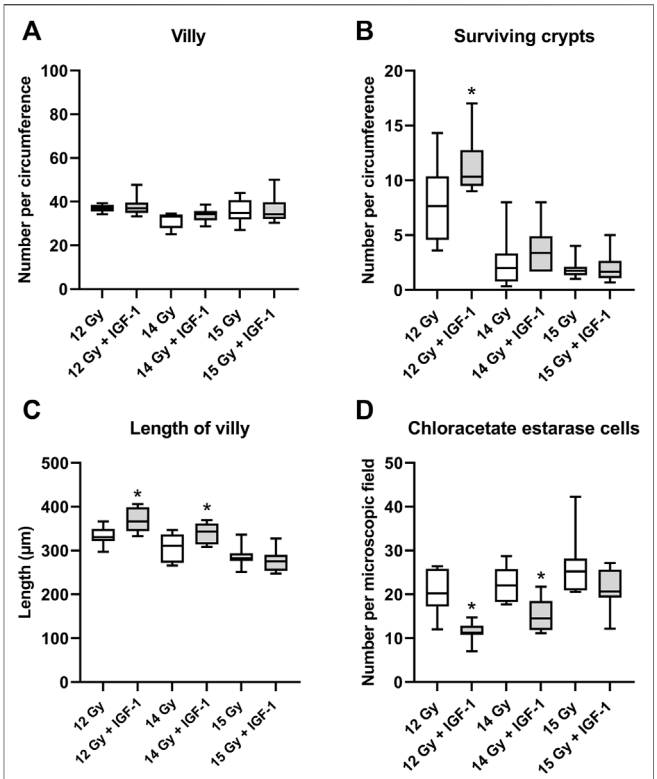

FIGURE 3 | Effect of IGF-1 at 1 mg/kg in the jejunum of mice irradiated by 12, 14, and 15 Gy with shielded head and neck. **(A)** number of villy. **(B)** number of surviving crypts. **(C)** length of villy. **(D)** chloroacetate esterase-positive cells in the subvillar mucose per centered microscopic field at ×400 magnification. Significantly different when compared with the solely irradiated group receiving no treatment: $^*p \leq 0.05$.

3.4 Effect of Different IGF-1 Therapeutical Regimens in Duodenum, Jejunum, and Ileum of Animals Irradiated Six Days After Irradiation by 12 and 14 Gy With Head and Neck Shielded

3.4.1 Histopathological Assessment

IR at 12 Gy did not induce any significant alterations. At 14 Gy, we observed edema in the duodenum, jejunum, and ileum and inflammation in the duodenum and jejunum. Compared with solely irradiated groups, IGF-1 therapy did not significantly affect the histopathological scores of IR-induced changes (**Supplementary Figures S5–S7**).

3.4.2 Number of Villy

The median amount of villy significantly decreased only in the ileum by 31% of mice irradiated by 14 Gy. Different IGF-1 regimens did not show any therapeutical effect (**Figures 5A–7A**).

3.4.3 Number of Regenerating Crypts

The median number of surviving crypts dropped by 44 and 59% in the duodenum (**Figure 5B**), by 51 and 62% in the jejunum (**Figure 6B**), and by 51 and 62% in the ileum (**Figure 7B**) after irradiation by 12 and 14 Gy, respectively. The therapeutical effect was noted only in the ileum of mice irradiated by 12 Gy. Administration of IGF-1 in 3 doses significantly increased the median value by 12%.

3.4.4 Length of Villy

In the duodenum (**Figure 5C**), the median length of villy increased by 22% after irradiation by 12 Gy. Administration of 2, 3, and 4 doses of IGF-1 and 3 doses with later onset of

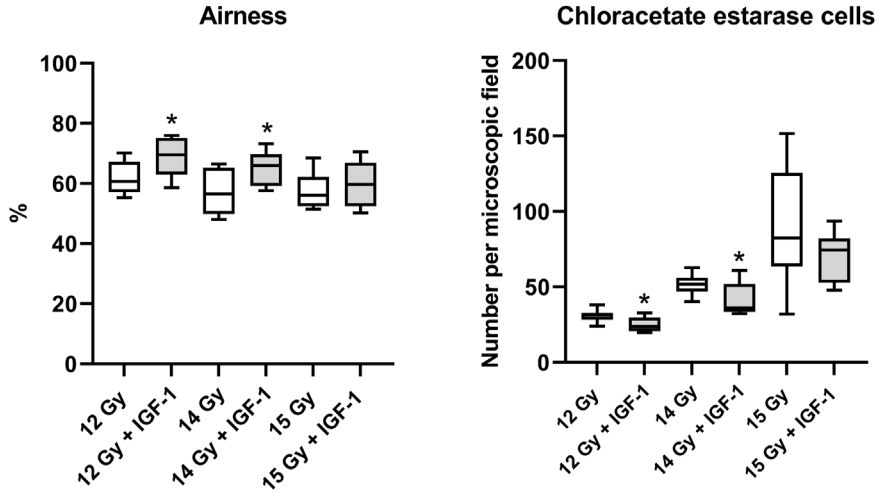

FIGURE 4 | Effect of IGF-1 at 1 mg/kg in the lung of mice irradiated by 12, 14, and 15 Gy with shielded head and neck. A: airness of the tissue. B: chloroacetate esterase-positive cells per microscopic field at ×400 magnification. Significantly different when compared with the solely irradiated group receiving no treatment: $^{*}p \leq 0.05$.

administration prolonged median villy values by 16, 17, 9, and 9%, respectively. At 14 Gy, the length of villy significantly decreased by 23% in solely irradiated animals. Compared with this group, administration of 3 and 4 doses of IGF-1 prolonged villy by 24 and 32%, respectively.

In jejunum (**Figure 6C**), the parameter increased by 10% after irradiation by 12 Gy. The administration of 1, 4 doses of IGF-1 and 3 doses with later onset of administration further prolonged villy by 12, 11, and 17%, respectively. Irradiation by 14 Gy decreased the median length of villy in the jejunum by 26%. Compared with this group, administration of 3 doses of IGF-1 significantly prolonged villy by 12%, whereas their size decreased in the group administered with 5 doses by 21%.

In the ileum after 12 Gy irradiation (**Figure 7C**), the administration of 2, 3, and 4 doses of IGF-1 and 3 doses with later onset of administration prolonged median values by 18, 26, 45, 23%, respectively. At 14 Gy, the parameter decreased by 18% in solely irradiated animals. Compared with this group, administration of 2, 3, and 4 doses of IGF-1 prolonged villy by 17, 13, and 16%, respectively. By contrast, 5 doses of IGF-1 further decreased their size by 21%.

3.4.5 The Length of Crypts

In the duodenum (**Figure 5D**), the crypts' median length increased by 50% after 12 Gy. Compared with the solely irradiated group, administration of 1, 2, 3, and 4 doses of IGF-1 further prolonged crypts by 10, 10, 14, and 13%, respectively. At 14 Gy, the length of crypts significantly increased by 45% in solely irradiated animals. In comparison with this group, administration of 3 and 4 doses of IGF-1 and 3 doses with later onset of administration prolonged crypts by 13, 18, and 19%, respectively.

In jejunum (**Figure 6D**), the median of this parameter increased by 59% at 12 Gy. The administration of 1, 3, 4, and 5 doses of IGF-1 and 3 doses with later onset of administration further prolonged crypts by 15, 25, 21, 21, and 27%, respectively. Irradiation by 14 Gy increased jejunal crypts' length by 99%. Compared with this group, administration of 2 and 3 doses of IGF-1 significantly prolonged crypts by 10 and 12%, respectively.

In the ileum (**Figure 7D**), the parameter increased by 26% after irradiation by 12 Gy. The administration of 3 and 4 doses of IGF-1 and 3 doses with later onset of administration prolonged crypts by 14, 28, and 17%, respectively. At 14 Gy, the parameter increased by 29% in solely irradiated animals. Compared with this group, administration of 2 doses of IGF-1 prolonged crypts by 10%.

3.5 Effect of Different IGF-1 Therapeutical Regimens on Blood Parameters in Animals Irradiated by 12 and 14 Gy With Head and Neck Shielded Evaluated Six Days After Irradiation

After irradiation by 12 and 14 Gy, median erythrocyte values significantly decreased by 19 and 16% (**Figure 8A**), thrombocytes by 52 and 30% (**Figure 8B**), lymphocytes by 85 and 81% (**Figure 8C**), and neutrophils by 50 and 78% (**Figure 8D**), respectively. By contrast, the monocyte median increased 3.4 fold in mice irradiated by 12 Gy (**Figure 8E**).

Compared with solely irradiated groups, IGF-1 did not affect blood parameters in animals irradiated by 12 Gy. At 14 Gy, the therapy with 3 and 4 doses of IGF-1 and 3 doses with later onset of administration increased median neutrophil values 2.0-, 1.4-, and 1.7 fold and median monocyte values 2.4-, 1.7-, and 1.6 fold, respectively. Five doses decreased the thrombocyte median by 10%.

4 DISCUSSION

Administration of IGF-1 may induce severe hypoglycemia due to its molecular structure and functional similarity with insulin (Bang et al., 2022). This response seems dose-dependent

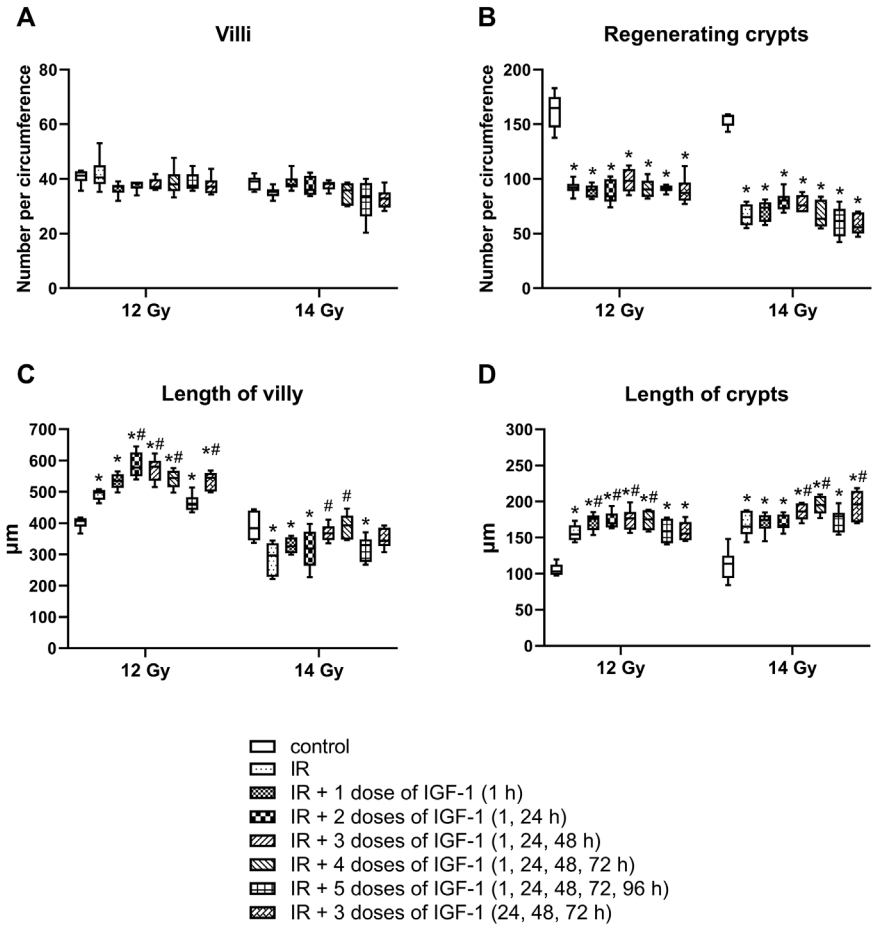

FIGURE 5 | Effect of different IGF-1 (1 mg/kg) therapeutical regimens on the duodenum of mice irradiated by 12 or 14 Gy with shielded head and neck. **(A)** number of villy. **(B)** number of surviving crypts (microcolony assay). **(C)** length of villy. **(D)** length of crypts. Significantly different when compared with the non-irradiated control: $^{*}p \leq 0.05$. Significantly different when compared with the solely irradiated group receiving no treatment: $^{\#}p \leq 0.05$.

(Woodall et al., 1991). Therefore, our study evaluated glycemic response to different single subcutaneous doses of IGF-1 in fasting female C57Bl/6J mice. The 1 mg/kg dose induced mild hypoglycemia but was clinically well tolerated. The brain is one of the first organs affected by hypoglycemia. Shortage of glucose in the brain cause prolonged reaction time, seizures, loss of consciousness, or death as the hypoglycemia progresses (Blaabjerg and Juhl, 2016). We did not observe any of these signs in this group. The 1 mg/kg dose seems even completely safe in non-fasting animals, possibly allowing further dose increase. However, due to gastrointestinal damage, diarrhea, and weight loss that develop early after high-dose irradiation, 1 mg/kg was established as the MTD under the current experimental settings.

In the next experiment, IGF-1 was tested to mitigate the lethality of mice exposed to high doses of IR with a shielded head and neck. The model spares sufficient bone marrow in the head and neck regions to prevent lethality from acute hematopoietic radiation syndrome. But still, it does not protect other regions against exposure. Besides the gastrointestinal tract, the lungs are particularly susceptible to high-dose irradiation. In female C57BL/6J mice, the lower threshold for developing lethal radiation lung injury after chest irradiation is 12 Gy (Jackson et al., 2016). Two clinical-pathological units may develop after exceeding this threshold. Acute radiation pneumonitis manifests in a dose-dependent manner 1–6 months after irradiation, while radiation fibrosis develops after 6 months. Although the two clinical-pathological units have different pathogenesis, both are associated with alveolar epithelial cell depletion (Lierova et al., 2018). By contrast, IGF-1 can stimulate the proliferation of alveolar epithelial cells type II and their differentiation into alveolar epithelial cells type I and modulates the inflammatory response of lung tissue (Zhang et al., 2022). Our study first investigated the potential of IGF-1 to affect IR-induced lethality. Since IGF-1 stimulates proliferation or cell viability in a dose-dependent manner (Yang et al., 2020; Hossain et al., 2021), the factor was administered at MTD. The initial regimen

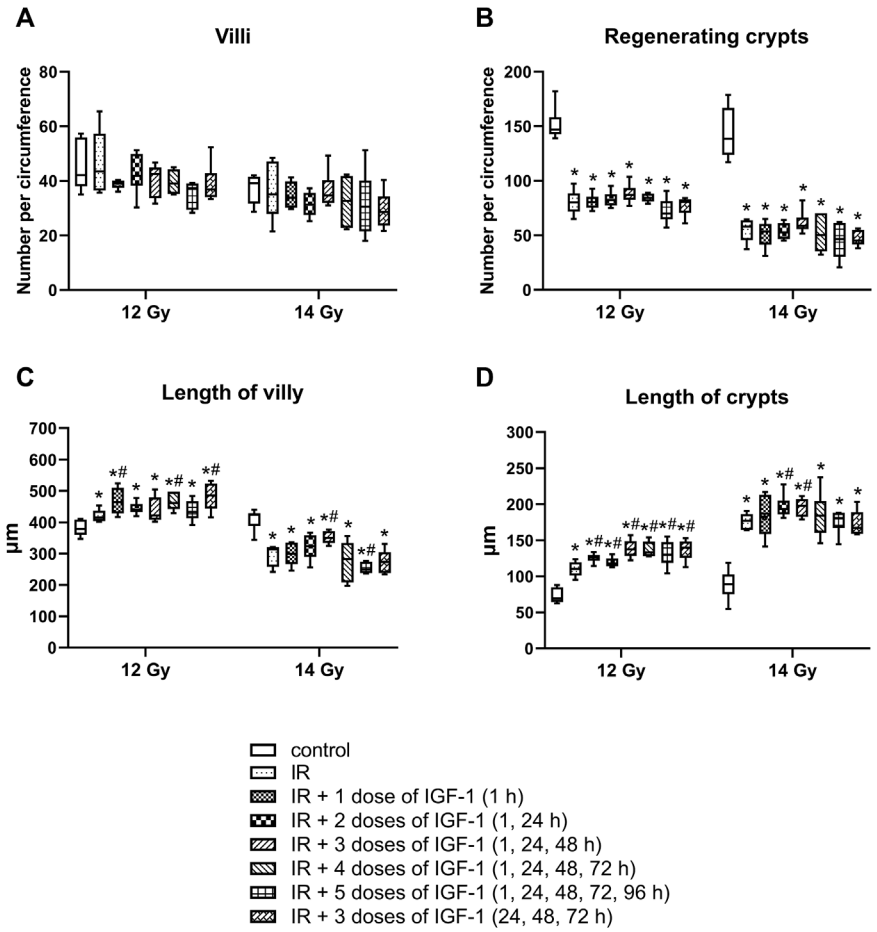

FIGURE 6 | Effect of different IGF-1 (1 mg/kg) therapeutical regimens on jejunum of mice irradiated by 12 or 14 Gy with shielded head and neck. **(A)** number of villy. **(B)** number of surviving crypts (microcolony assay). **(C)** length of villy. **(D)** length of crypts. Significantly different when compared with the non-irradiated control: $^{*}p \leq 0.05$. Significantly different when compared with the solely irradiated group receiving no treatment: $^{\#}p \leq 0.05$.

consisting of three doses followed cytokine guidelines established for other growth factors moderating epithelial tissue damage, such as KGF or EGF (Drouet and Hérodin, 2010; Pejchal et al., 2015). The results show that the therapy mitigated lethality induced by 14 Gy but could not protect against higher doses of IR. These findings corresponded with the second irradiation model. In this experiment, IGF-1 mitigated IR-induced morphological damage and inflammation in jejunum and lung after irradiation by 12 and 14 Gy but was ineffective at 15 Gy.

The final model aimed to achieve an optimal dosing regimen of the growth factor to mitigate IR-induced gastrointestinal damage. Tissue samples in this model were collected 6 days post-irradiation when signs of atrophy, inflammation, and regeneration can be observed in the gastrointestinal tract. Six different dosing regimens were tested. Five of them started at 1 h after irradiation. Potten and Grant (1998) recorded the intestine's maximum apoptotic activity during 3–6 h after radiation by 1 Gy. Thus, it is necessary to start the application as soon as possible after irradiation to save as many stem cells and early progenitors as possible. IGF-1 generally supported the mucosal renewal. The elongation of crypts and villi indicates that the growth factor administration stimulated cellular proliferation in crypts and the production of new cells into the superficial compartment. However, individual dosing regimens showed different effects, with three- and four-dose regimens being the most effective (**Table 4**). The three-dose regimens even stimulated intestinal regeneration when the administration began 24 h after irradiation, but its potency decreased. By contrast, the efficacy of the five-dose regimen significantly declined. The mechanism explaining this finding remains unknown. The theoretical explanation might lay in the selective down-regulation of IGF-1 receptors. Long-term exposure to high doses of the growth factor may reduce signaling associated with proliferation, anti-apoptotic, and anti-inflammatory action and ultimately shift the environment towards pro-inflammatory status (Kenchegowda et al., 2018).

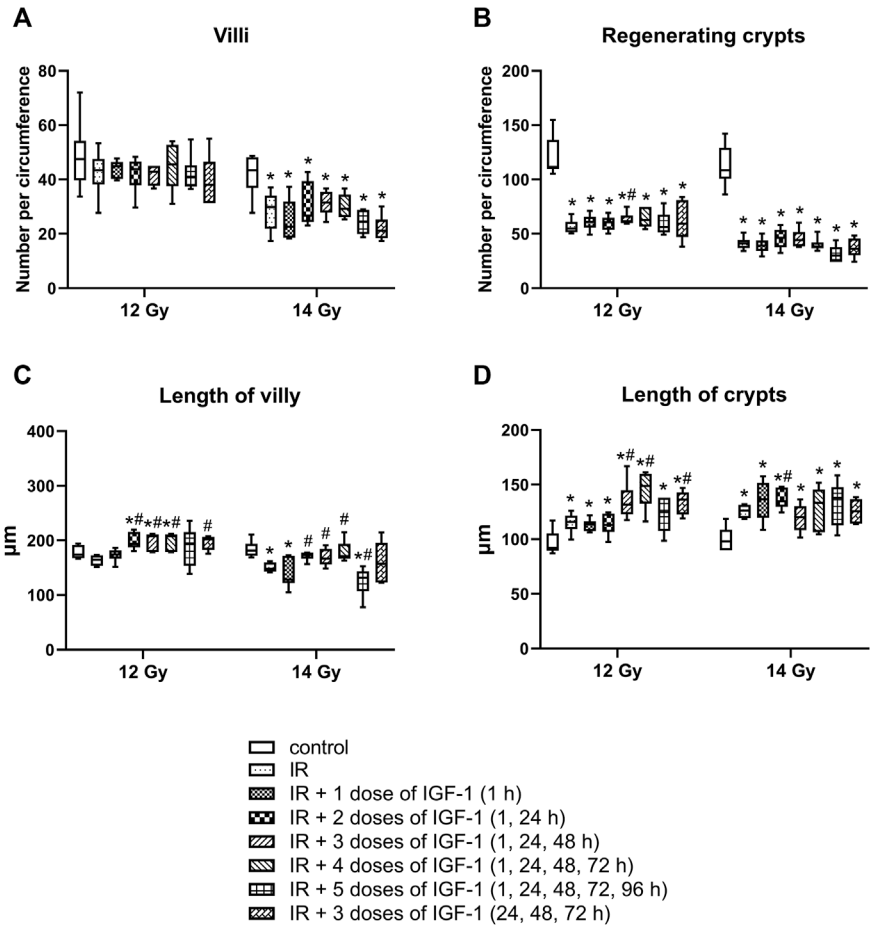

FIGURE 7 | Effect of different therapeutical regimens of IGF-1 (1 mg/kg) on ileum of mice irradiated by 12 or 14 Gy with shielded head and neck. **(A)** number of villy. **(B)** number of surviving crypts (microcolony assay). **(C)** length of villy. **(D)** length of crypts. Significantly different when compared with the non-irradiated control: $^{*}p \leq 0.05$. Significantly different when compared with the solely irradiated group receiving no treatment: $^{\#}p \leq 0.05$.

Another goal of this experimental model was to assess the effect of IGF-1 on IR-induced hematological damage. Although the head and neck were shielded with lead, a significant portion of the bone marrow was exposed to ionizing radiation, reducing counts for all three types of blood cells. IGF-1, on the other hand, enhances the survival of bone marrow stem cells and stimulates the proliferation and differentiation of progenitor cells *in vitro* (Li et al., 1997; Ratajczak et al., 1998; Miyagawa et al., 2000; Aro et al., 2002). Chen et al. (2012) injected IGF-1 subcutaneously at a dose of 100 µg/kg twice daily for 7 days to BALB/c mice after whole-body irradiation by 5 Gy. They demonstrated that IGF-1 could promote overall hematopoietic recovery, having the earliest effect on leukocytes from the seventh day. Our results did not show any changes in hematological parameters in IGF-1-treated mice after irradiation by 12 Gy. Thus, the 6-days interval seems too soon to induce any effect. In this regard, the increase in monocytes and granulocytes observed in the three- and four-dose regimens or the loss of platelets found in the five-dose regimen are most possibly associated with gastrointestinal damage.

In conclusion, IGF-1 attenuates gastrointestinal damage, but the efficacy depends on several factors, including timing, dose, and dose regimen. The dose of 1 mg/kg administered daily in three to four consecutive days post-radiation exerted the highest potency in mice. Nonetheless, there may be limitations to our study. One lies in the fact that all experiments were conducted on female animals. This choice was based on a negligible risk of inter-female aggressivity in the C57Bl/6 strain compared to males (Parmigiani et al., 1999). Intra-group aggressivity could be crucial for high-dose irradiation models and (to some extent) concurrent immunosuppression. Although sex hormones affect IGF-1 signaling, testosterone seems to potentiate IGF-1 biological roles (Li and Li, 2014; Hughes et al., 2016), implying even higher effectivity in males. The second is associated with recommended doses of Increlex for humans, ranging from 0.04 to 0.12 mg/kg (Bang et al., 2022). Administration of higher doses is not entirely ruled out. But it would require

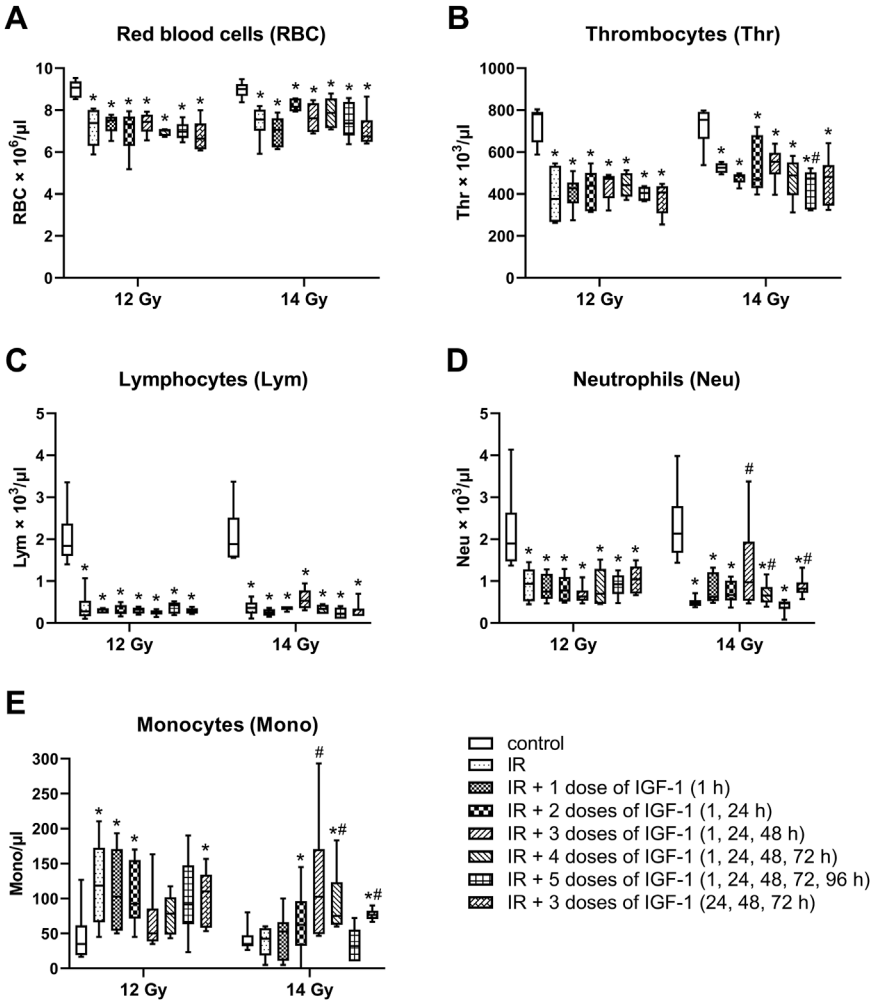

FIGURE 8 | Effect of different IGF-1 (1 mg/kg) therapeutical regimens on blood hematological parameters of mice irradiated by 12 or 14 Gy with shielded head and neck. **(A)** red blood cells. **(B)** thrombocytes. **(C)** lymphocytes. **(D)** neutrophils. **(E)** monocytes. Significantly different when compared with the non-irradiated control: $^{*}p \leq 0.05$. Significantly different when compared with the solely irradiated group receiving no treatment: $^{\#}p \leq 0.05$.

TABLE 4 | An overview of IGF-1-induced significant changes in gastrointestinal tract irradiated by 12 and 14 Gy.

Parameter		12 Gy						14 Gy					
		1 D	2 D	3 D	4 D	5 D	3 D_L	1 D	2 D	3 D	4 D	5 D	3 D_L
Villi	duodenum		+	+	+		+			+	+		
	jejunum	+			+		+			+		-	
	ileum		+	+	+		+		+	+	+	-	
Crypts	duodenum	+	+	+	+					+	+		+
	jejunum	+		+	+		+		+	+			
	ileum			+[a]	+	+	+		+				
Total		4	4	5	6	3	5	0	3	5	3	-2	1
%[b]		6	7	16	21	4	16	0	6	12	11	-7	3

+ and - represent significant changes (increase and decrease, respectively) compared with solely irradiated groups. D: dosage regimens starting at 1 h after irradiation. D_L: three-dose regimen beginning 24 h after irradiation.

[a]*To sum percentage changes in the 3 D group irradiated by 12 Gy, the length of crypts in the ileum was increased by 12% due to a significantly higher number of surviving crypts.*

[b]*Average change per compartment.*

specialized care with continuous glycemia monitoring and correction, most likely limiting the application in the field conditions. Further studies utilizing larger experimental animals seem necessary to optimize the dose and dosage regimen of IGF-1 to establish this growth factor as an effective countermeasure for large-scale radiation incidents.

DATA AVAILABILITY STATEMENT

The original contributions presented in the study are included in the article/**Supplementary Material**, further inquiries can be directed to the corresponding author.

ETHICS STATEMENT

The animal study was reviewed and approved by Ethics Committee of the Faculty of Military Health Sciences (Hradec Kralove, Czechia).

AUTHOR CONTRIBUTIONS

JP designed the experiments, participated in all the experiments, analyzed the data, wrote the manuscript, and produced figures. AT contributed to the conception and overall design of the study. AK, LF, KK, MM, AL, AF, LM, and JC helped perform the individual *in vivo* experiments. All authors contributed to the article and approved the submitted version.

FUNDING

This work was supported by the Ministry of Defense of the Czech Republic "Long Term Development Plan-Medical issues of WMD II" of the Faculty of Military Health Sciences Hradec Kralove, University of Defense, Czech Republic.

ACKNOWLEDGMENTS

We would like to thank Mrs. Šárka Průchová for her technical assistance.

SUPPLEMENTARY MATERIAL

The Supplementary Material for this article can be found online at: https://www.frontiersin.org/articles/10.3389/fphar.2022.663855/full#supplementary-material

REFERENCES

Aro, A. L., Savikko, J., Pulkkinen, V., and von Willebrand, E. (2002). Expression of Insulin-like Growth Factors IGF-I and IGF-II, and Their Receptors during the Growth and Megakaryocytic Differentiation of K562 Cells. *Leuk. Res.* 26 (9), 831–837. doi:10.1016/s0145-2126(02)00006-1

Bang, P., Polak, M., Perrot, V., Sert, C., Shaikh, H., and Woelfle, J. (2022). Pubertal Timing and Growth Dynamics in Children With Severe Primary IGF-1 Deficiency: Results from the European Increlex® Growth Forum Database Registry. *Front. Endocrinol. (Lausanne)* 13, 812568. doi:10.3389/fendo.2022.812568

Bhat, K., Duhachek-Muggy, S., Ramanathan, R., Saki, M., Alli, C., Medina, P., et al. (2019). 1-[(4-Nitrophenyl)sulfonyl]-4-phenylpiperazine Increases the Number of Peyer's Patch-Associated Regenerating Crypts in the Small Intestines after Radiation Injury. *Radiotherapy Oncol.* 132, 8–15. doi:10.1016/j.radonc.2018.11.011

Blaabjerg, L., and Juhl, C. B. (2016). Hypoglycemia-Induced Changes in the Electroencephalogram: An Overview. *J. Diabetes Sci. Technol.* 10 (6), 1259–1267. doi:10.1177/1932296816659744

Bohin, N., McGowan, K. P., Keeley, T. M., Carlson, E. A., Yan, K. S., and Samuelson, L. C. (2020). Insulin-like Growth Factor-1 and mTORC1 Signaling Promote the Intestinal Regenerative Response After Irradiation Injury. *Cell. Mol. Gastroenterology Hepatology* 10 (4), 797–810. doi:10.1016/j.jcmgh.2020.05.013

Chen, S., Xu, Y., Wang, S., Shen, M., Chen, F., Chen, M., et al. (2012). Subcutaneous Administration of rhIGF-I Post Irradiation Exposure Enhances Hematopoietic Recovery and Survival in BALB/c Mice. *J. Radiat. Res.* 53 (4), 581–587. doi:10.1093/jrr/rrs029

Dahly, E. M., Guo, Z., and Ney, D. M. (2002). Alterations in Enterocyte Proliferation and Apoptosis Accompany TPN-Induced Mucosal Hypoplasia and IGF-I-Induced Hyperplasia in Rats. *J. Nutr.* 132 (7), 2010–2014. doi:10.1093/jn/132.7.2010

Drouet, M., and Hérodin, F. (2010). Radiation Victim Management and the Haematologist in the Future: Time to Revisit Therapeutic Guidelines?. *Int. J. Radiat. Biol.* 86 (8), 636–648. doi:10.3109/09553001003789604

Gu, J., Liu, S., Mu, N., Huang, T., Zhang, W., Zhao, H., et al. (2017). A DPP-IV-Resistant Glucagon-Like Peptide-2 Dimer With Enhanced Activity Against Radiation-Induced Intestinal Injury. *J. Control. Release* 260, 32–45. doi:10.1016/j.jconrel.2017.05.020

Hanson, W. R., and DeLaurentiis, K. (1987). Comparison of *In Vivo* Murine Intestinal Radiation Protection by E-Prostaglandins. *Prostaglandins* 33 Suppl, 93–104. doi:10.1016/0090-6980(87)90052-9

Hanson, W. R., and Thomas, C. (1983). 16, 16-dimethyl Prostaglandin E2 Increases Survival of Murine Intestinal Stem Cells when Given before Photon Radiation. *Radiat. Res.* 96 (2), 393–398. doi:10.2307/3576222

Hossain, M. A., Adithan, A., Alam, M. J., Kopalli, S. R., Kim, B., Kang, C. W., et al. (2021). IGF-1 Facilitates Cartilage Reconstruction by Regulating PI3K/AKT, MAPK, and NF-kB Signaling in Rabbit Osteoarthritis. *J. Inflamm. Res.* 14, 3555–3568. doi:10.2147/JIR.S316756

Howarth, G. S., Fraser, R., Frisby, C. L., Schirmer, M. B., and Yeoh, E. K. (1997). Effects of Insulin-like Growth Factor-I Administration on Radiation Enteritis in Rats. *Scand. J. Gastroenterol.* 32 (11), 1118–1124. doi:10.3109/00365529709002990

Hughes, D. C., Stewart, C. E., Sculthorpe, N., Dugdale, H. F., Yousefian, F., Lewis, M. P., et al. (2016). Testosterone Enables Growth and Hypertrophy in Fusion Impaired Myoblasts that Display Myotube Atrophy: Deciphering the Role of Androgen and IGF-I Receptors. *Biogerontology* 17 (3), 619–639. doi:10.1007/s10522-015-9621-9

Jackson, I. L., Zhang, Y., Bentzen, S. M., Hu, J., Zhang, A., and Vujaskovic, Z. (2016). Pathophysiological Mechanisms Underlying Phenotypic Differences in Pulmonary Radioresponse. *Sci. Rep.* 6, 36579. doi:10.1038/srep36579

Kenchegowda, D., Legesse, B., Hritzo, B., Olsen, C., Aghdam, S., Kaur, A., et al. (2018). Selective Insulin-like Growth Factor Resistance Associated with Heart Hemorrhages and Poor Prognosis in a Novel Preclinical Model of the Hematopoietic Acute Radiation Syndrome. *Radiat. Res.* 190 (2), 164–175. doi:10.1667/RR14993.1

Li, W., Lin, Y., Luo, Y., Wang, Y., Lu, Y., Li, Y., et al. (2021). Vitamin D Receptor Protects against Radiation-Induced Intestinal Injury in Mice via Inhibition of Intestinal Crypt Stem/Progenitor Cell Apoptosis. *Nutrients* 13 (9), 2910. doi:10.3390/nu13092910

Li, Y., and Li, K. (2014). Osteocalcin Induces Growth Hormone/insulin-like Growth Factor-1 System by Promoting Testosterone Synthesis in Male Mice. *Horm. Metab. Res.* 46 (11), 768–773. doi:10.1055/s-0034-1371869

Li, Y. M., Schacher, D. H., Liu, Q., Arkins, S., Rebeiz, N., McCusker, R. H., et al. (1997). Regulation of Myeloid Growth and Differentiation by the Insulin-like Growth Factor I Receptor. *Endocrinology* 138 (1), 362–368. doi:10.1210/endo.138.1.4847

Lierova, A., Jelicova, M., Nemcova, M., Proksova, M., Pejchal, J., Zarybnicka, L., et al. (2018). Cytokines and Radiation-Induced Pulmonary Injuries. *J. Radiat. Res.* 59 (6), 709–753. doi:10.1093/jrr/rry067

Lu, L., Li, W., Chen, L., Su, Q., Wang, Y., Guo, Z., et al. (2019). Radiation-induced Intestinal Damage: Latest Molecular and Clinical Developments. *Future Oncol.* 15 (35), 4105–4118. doi:10.2217/fon-2019-0416

Meena, S. K., Joriya, P. R., Yadav, S. M., Kumar, R., Meena, P., and Patel, D. D. (2022). Modulation of Radiation-Induced Intestinal Injury by Radioprotective Agents: a Cellular and Molecular Perspectives. *Rev. Environ. Health*. In press. doi:10.1515/reveh-2021-0108

Miyagawa, S., Kobayashi, M., Konishi, N., Sato, T., and Ueda, K. (2000). Insulin and Insulin-like Growth Factor I Support the Proliferation of Erythroid Progenitor Cells in Bone Marrow through the Sharing of Receptors. *Br. J. Haematol.* 109 (3), 555–562. doi:10.1046/j.1365-2141.2000.02047.x

Parmigiani, S., Palanza, P., Rogers, J., and Ferrari, P. F. (1999). Selection, Evolution of Behavior and Animal Models in Behavioral Neuroscience. *Neurosci. Biobehav. Rev.* 23 (7), 957–969. doi:10.1016/s0149-7634(99)00029-9

Patterson, A. M., Liu, L., Sampson, C. H., Plett, P. A., Li, H., Singh, P., et al. (2020). A Single Radioprotective Dose of Prostaglandin E2 Blocks Irradiation-Induced Apoptotic Signaling and Early Cycling of Hematopoietic Stem Cells. *Stem Cell. Rep.* 15 (2), 358–373. doi:10.1016/j.stemcr.2020.07.004

Pejchal, J., Novotný, J., Mařák, V., Osterreicher, J., Tichý, A., Vávrová, J., et al. (2012). Activation of P38 MAPK and Expression of TGF-β1 in Rat Colon Enterocytes after Whole Body γ-irradiation. *Int. J. Radiat. Biol.* 88 (4), 348–358. doi:10.3109/09553002.2012.654044

Pejchal, J., Šinkorová, Z., Tichý, A., Kmochová, A., Ďurišová, K., Kubelková, K., et al. (2015). Attenuation of Radiation-Induced Gastrointestinal Damage by Epidermal Growth Factor and Bone Marrow Transplantation in Mice. *Int. J. Radiat. Biol.* 91 (9), 703–714. doi:10.3109/09553002.2015.1054528

Porter, R. L., Georger, M. A., Bromberg, O., McGrath, K. E., Frisch, B. J., Becker, M. W., et al. (2013). Prostaglandin E2 Increases Hematopoietic Stem Cell Survival and Accelerates Hematopoietic Recovery after Radiation Injury. *Stem Cells* 31 (2), 372–383. doi:10.1002/stem.1286

Potten, C. S., and Grant, H. K. (1998). The Relationship between Ionizing Radiation-Induced Apoptosis and Stem Cells in the Small and Large Intestine. *Br. J. Cancer* 78 (8), 993–1003. doi:10.1038/bjc.1998.618

Qiu, W., Leibowitz, B., Zhang, L., and Yu, J. (2010). Growth Factors Protect Intestinal Stem Cells from Radiation-Induced Apoptosis by Suppressing PUMA through the PI3K/AKT/p53 axis. *Oncogene* 29 (11), 1622–1632. doi:10.1038/onc.2009.451

Ratajczak, J., Zhang, Q., Pertusini, E., Wojczyk, B. S., Wasik, M. A., and Ratajczak, M. Z. (1998). The Role of Insulin (INS) and Insulin-like Growth Factor-I (IGF-I) in Regulating Human Erythropoiesis. Studies *In Vitro* under Serum-free Conditions-Ccomparison to Other Cytokines and Growth Factors. *Leukemia* 12 (3), 371–381. doi:10.1038/sj.leu.2400927

Rowland, K. J., and Brubaker, P. L. (2011). The "cryptic" Mechanism of Action of Glucagon-like Peptide-2. *Am J Physiol Gastrointest Liver PhysiolGastrointestinal Liver Physiology* 301 (1), G1–G8. doi:10.1152/ajpgi.00039.2011

Sakai, T., Hara, J., Yamamura, K., Okazaki, A., Ohkura, N., Sone, T., et al. (2018). Role of Prostaglandin I2 in the Bronchoconstriction-Triggered Cough Response in guinea Pigs. *Exp. Lung Res.* 44, 455–463. doi:10.1016/j.pupt.2017.09.00310.1080/01902148.2019.1590883

Singh, V. K., and Seed, T. M. (2020). Pharmacological Management of Ionizing Radiation Injuries: Current and Prospective Agents and Targeted Organ Systems. *Expert Opin. Pharmacother.* 21 (3), 317–337. doi:10.1080/14656566.2019.1702968

Van Landeghem, L., Santoro, M. A., Mah, A. T., Krebs, A. E., Dehmer, J. J., McNaughton, K. K., et al. (2015). IGF1 Stimulates Crypt Expansion via Differential Activation of 2 Intestinal Stem Cell Populations. *FASEB J.* 29 (7), 2828–2842. doi:10.1096/fj.14-264010

Woodall, S. M., Breier, B. H., O'Sullivan, U., and Gluckman, P. D. (1991). The Effect of the Frequency of Subcutaneous Insulin-like Growth Factor-1 Administration on Weight Gain in Growth Hormone Deficient Mice. *Horm. Metab. Res.* 23 (12), 581–584. doi:10.1055/s-2007-1003760

Yang, L., Tan, Z., Li, Y., Zhang, X., Wu, Y., Xu, B., et al. (2020). Insulin-like Growth Factor 1 Promotes Proliferation and Invasion of Papillary Thyroid Cancer through the STAT3 Pathway. *J. Clin. Laboratory Analysis* 34 (12), e23531. doi:10.1002/jcla.23531

Zhang, S., Luan, X., Li, H., and Jin, Z. (2022). Insulin-like Growth Factor-1: A Potential Target for Bronchopulmonary Dysplasia Treatment (Review). *Exp. Ther. Med.* 23 (3), 191. doi:10.3892/etm.2022.11114

Conflict of Interest: The authors declare that the research was conducted in the absence of any commercial or financial relationships that could be construed as a potential conflict of interest.

Publisher's Note: All claims expressed in this article are solely those of the authors and do not necessarily represent those of their affiliated organizations, or those of the publisher, the editors and the reviewers. Any product that may be evaluated in this article, or claim that may be made by its manufacturer, is not guaranteed or endorsed by the publisher.

Advantages of publishing in Frontiers

OPEN ACCESS
Articles are free to read for greatest visibility and readership

FAST PUBLICATION
Around 90 days from submission to decision

HIGH QUALITY PEER-REVIEW
Rigorous, collaborative, and constructive peer-review

TRANSPARENT PEER-REVIEW
Editors and reviewers acknowledged by name on published articles

Frontiers
Avenue du Tribunal-Fédéral 34
1005 Lausanne | Switzerland

Visit us: www.frontiersin.org
Contact us: frontiersin.org/about/contact

REPRODUCIBILITY OF RESEARCH
Support open data and methods to enhance research reproducibility

DIGITAL PUBLISHING
Articles designed for optimal readership across devices

FOLLOW US
@frontiersin

IMPACT METRICS
Advanced article metrics track visibility across digital media

EXTENSIVE PROMOTION
Marketing and promotion of impactful research

LOOP RESEARCH NETWORK
Our network increases your article's readership